Piezoelectric Crystals and Their Application to Ultrasonics

THEORY OF VIBRATING SYSTEMS AND SOUND. *By* IRVING B. CRANDALL.
CONTEMPORARY PHYSICS. *By* KARL K. DARROW. Second Edition.
SPEECH AND HEARING. *By* HARVEY FLETCHER.
PROBABILITY AND ITS ENGINEERING USES. *By* THORNTON C. FRY.
ELEMENTARY DIFFERENTIAL EQUATIONS. *By* THORNTON C. FRY. Second Edition.
TRANSMISSION CIRCUITS FOR TELEPHONIC COMMUNICATION. METHODS OF ANALYSIS AND DESIGN. *By* K. S. JOHNSON.
TRANSMISSION NETWORKS AND WAVE FILTERS. *By* T. E. SHEA.
ECONOMIC CONTROL OF QUALITY OF MANUFACTURED PRODUCT. *By* W. A. SHEWHART.
ELECTROMECHANICAL TRANSDUCERS AND WAVE FILTERS. *By* WARREN P. MASON. Second Edition.
RHOMBIC ANTENNA DESIGN. *By* A. E. HARPER.
POISSON'S EXPONENTIAL BINOMIAL LIMIT. *By* E. C. MOLINA.
ELECTROMAGNETIC WAVES. *By* S. A. SCHELKUNOFF.
NETWORK ANALYSIS AND FEEDBACK AMPLIFIER DESIGN. *By* HENDRIK W. BODE.
SERVOMECHANISMS. *By* LEROY A. MACCOLL.
QUARTZ CRYSTALS FOR ELECTRICAL CIRCUITS. *By* R. A. HEISING.
CAPACITORS—THEIR USE IN ELECTRONIC CIRCUITS. *By* M. BROTHERTON.
FOURIER INTEGRALS FOR PRACTICAL APPLICATIONS. *By* GEORGE A. CAMPBELL AND RONALD M. FOSTER.
VISIBLE SPEECH. *By* RALPH K. POTTER, GEORGE A. KOPP, AND HARRIET C. GREEN.
APPLIED MATHEMATICS FOR ENGINEERS AND SCIENTISTS. *By* S. A. SCHELKUNOFF.
EARTH CONDUCTION EFFECTS IN TRANSMISSION SYSTEMS. *By* ERLING D. SUNDE.
RADAR SYSTEMS AND COMPONENTS. *By* MEMBERS OF THE STAFF OF THE BELL TELEPHONE LABORATORIES; Introduction by M. J. KELLY.
THEORY AND DESIGN OF ELECTRON BEAMS. *By* J. R. PIERCE.
PIEZOELECTRIC CRYSTALS AND THEIR APPLICATION TO ULTRASONICS. *By* WARREN P. MASON.

Piezoelectric Crystals and Their Application to Ultrasonics

By

WARREN P. MASON, PH.D.

Member of the Technical Staff

BELL TELEPHONE LABORATORIES, INC.

D. VAN NOSTRAND COMPANY, INC.

TORONTO NEW YORK LONDON

NEW YORK
D. Van Nostrand Company, Inc., 250 Fourth Avenue, New York 3
TORONTO
D. Van Nostrand Company (Canada), Ltd., 228 Bloor Street, Toronto
LONDON
Macmillan & Company, Ltd., St. Martin's Street, London, W.C. 2

PRINTED IN THE UNITED STATES OF AMERICA

PREFACE

During the past thirty years Bell Laboratories has carried out a considerable program of research and development of piezoelectric crystals and their application to such communication equipment as filters, oscillators and electromechanical transducers. Starting with the work of Nicolson on rochelle salt in 1918, continuous effort has been carried on in investigating quartz, rochelle salt and a large number of water soluble synthetic piezoelectric crystals. This work has recently culminated in the discovery of two monoclinic crystals, dipotassium tartrate (DKT) and ethylene diamine tartrate (EDT) which have such favorable properties that they are replacing quartz crystals in telephone filters, the largest application of piezoelectric crystals in the telephone system. Coming at a time when quartz in large sizes was becoming increasingly difficult to obtain, they have made possible the continuation and large expansion of the high-frequency carrier systems which carry a large share of the long-distance conversations.

It is the primary purpose of this book to describe this work, particularly from the experimental and theoretical side, since the developmental phases of the quartz work have already been described in the book " Quartz Crystals for Electrical Circuits." In order to make the work intelligible, chapters have been included on crystallographic systems, stresses, strains, thermal and electric relations, as well as an appendix showing how tensors can be applied to calculating the properties of rotated systems. Hence the book can be regarded as an introduction to the study of piezoelectricity. However, no attempt has been made to introduce the subject from a historical point of view. Indeed such a development is unnecessary since Cady's monumental work " Piezoelectricity," which appeared in 1946, covers such a development very completely. The emphasis has been rather on the new subjects that have appeared since that time. These include the new crystals, ammonium dihydrogen phosphate (ADP), which was used very extensively during the war as an electromechanical transducing element in underwater sound work, potassium dihydrogen phosphate (KDP), a new ferroelectric type of crystal, DKT and EDT mentioned previously and the ceramic barium titanate which produces an electrostrictive effect comparable with the largest piezoelectric effect in any crystal. On the theoretical side a new theory of ferroelectricity in rochelle salt, KDP and barium titanite, which has been developed by the writer, is more completely presented here than in any other place.

Piezoelectric crystals supply the electromechanical transducing element that makes possible another experimental science, ultrasonics. By means of the longitudinal and shear waves set up in gases, liquids and solids, considerable information can be obtained about the properties and molecular processes existing in these forms of matter. The last three chapters of the book are devoted to a description of the methods of producing and measuring such waves and to a description of the knowledge obtained from such measurements.

The author wishes to acknowledge many helpful comments and suggestions received from his associates at Bell Laboratories. On the theoretical side parts of the book have been read by Drs. J. Bardeen, C. Kittel and J. M. Richardson. Many suggestions for improvement in the order and readability of various sections have been received from W. L. Bond, G. C. Danielson, S. O. Morgan, L. C. Peterson, R. A. Sykes, G. W. Willard, and Mrs. E. A. Wood. In particular, Sykes, who is head of the apparatus department dealing with the application of piezoelectric crystals, has suggested a chapter ordering system which has improved the readability of the book. The writer wishes also to thank the members of the out-of-hours class who listened to a presentation of a preliminary form of the book and who contributed to the elimination of errors and the more obscure parts of the book.

WARREN P. MASON

Murray Hill, N.J.
February 1949

CONTENTS

LIST OF SYMBOLS EMPLOYED

a, b, c = crystallographic axes
a_{ij} = direction cosines
A = free energy, ferroelectric constant for symmetrical bond
ΔA = free energy barrier
A' = ferroelectric constant for assymmetrical bond
$A + jB$ = attenuation and phase shift
A_λ = attenuation per wave length
A_∞ = attenuation at an infinite frequency
C = capacitance, compliance
C_s = shear compliance
C_p = specific heat at constant pressure or stress
C_v = specific heat at constant volume or strain
C_{vi} = specific heat of vibrational modes at constant volume
c_{ij} = elastic stiffness constants
C, S, V, D, T, O = Schönflies symbols
d_{ij} = piezoelectric constants relating strain to electric field
d_0 = tangential displacement
D = electric displacement, heat diffusion constant
e = electronic charge
e_{ij} = piezoelectric constants relating stress to electric field
E = electric field
f = frequency, Δf = change in frequency
f_c = relaxation frequency
f_A = antiresonant frequency
f_R = resonant frequency
F = force, internal field
g_{ij} = piezoelectric constant relating open circuit voltage to stress
G = Gibbs potential function
h = Planck's constant
h_{ij} = piezoelectric constants relating open circuit voltage to strain
h, k, i, l = Miller and Bravais-Miller symbols
i = current
I = moment of inertia
$j = \sqrt{-1}$

J_0, J_1 = Bessel's functions
k = coefficient of electromechanical coupling, Boltzmann's constant
k_i = reaction rate constant
K = heat conductivity
l = length, l_w = width, l_t = thickness
l, m, n = direction cosines
L = inductance
m = root of flexure equation
M = molecular volume, molecular weight, figure of merit of crystal
M_l = mass current tensor
n = number, order of overtone
N = number of molecules per cubic centimeter
N_A = Avogadro's number = 6.06×10^{23}
o = index number
O_{ijk} = electrooptic tensor
p = pressure
p_0 = static pressure
p_i, q_i = pyroelectric constants
P = electric polarization
P_d = dipole polarization
P_s = spontaneous polarization
PI = performance index of crystal
Q = charge per unit area, ratio of reactance to resistance, heat energy
Q_{ijkl} = electrostrictive tensor
r = ratio of capacities, radius
R = electrical or mechanical resistance, gas constant per mole
R_g, R_p = grid and plate resistance of vacuum tube
R_M = mechanical resistance per square centimeter
s_{ij} or s_{ijkl} = elastic compliance constants
S = area
S_{ij} = strain tensor
S_i = strain matrix
t = time
T = absolute temperature, taper constant
T_0 = Curie temperature
T_{sij}, T_{cij} = temperature coefficients of elastic constants
T_f = temperature coefficient of frequency
T_{ij} = stress tensor

T_i = stress matrix
u = displacement
U = internal energy
ΔU = activation energy barrier
v = velocity of propagation
v_d = dilational velocity
v_s = shear velocity
v_0 = velocity at zero frequencies
v_∞ = velocity at infinite frequency
V = electric potential
W = energy per square centimeter, activation energy barrier
x, y, z = rectangular axes
dx, dy, dz = distances along the axes
X = electrical or mechanical reactance
X_M = mechanical reactance per square centimeter
Y = admittance
Y_0 = Young's modulus
Z = electrical and mechanical impedance
Z_d = impedance of dipole arm
Z_0 = image impedance
Z_R = reflector impedance
$1, \bar{1}, m, n/m$ = Hermann-Mauguin symbols
α = temperature expansion coefficient
α_{ij} = transition probability
β = dielectric impermeability, Lorentz factor, complex factor in feedback path
β^I = isothermal compressibility
γ = ratio of specific heat, polarizability per unit volume
$\delta_i = D_i/4\pi$ = electric displacement divided by 4π
δ = distance separating potential wells or molecules
Δ = determinant, half of dissymmetry between two potential wells
$\Delta^{m,n}$ = minor of determinant
ϵ = dielectric constant
κ = bulk modulus; $\Delta\kappa$ = change in bulk modulus
κ_1 = difference between high-frequency and low-frequency compressibility
λ = temperature stress constant, Lamé elastic constant
λ_s = acoustic wave length
λ_l = light wave length
λ' = hysteresis constant
Γ = reaction rate constant, propagation constant

μ = dipole moment, shear elastic constant
η = shear viscosity
η_l = enhanced solvent viscosity
η_M = molecular viscosity
ξ, η, ζ = displacements along x, y, and z axes
φ = transformation ratio
χ = compressional viscosity
ν = frequency
ρ = density
ρ_c = density of crystal
σ = entropy, Poisson's ratio
σ_n = ratio of currents
θ, φ, ψ = angles
Θ = absolute temperature
τ = relaxation time
ω = angular rotation, 2π times the frequency
ω_R = 2π times resonant frequency
ω_A = 2π times antiresonant frequency

CHAPTER I

Introduction

1.1 *Nature of Piezoelectric Effect*

A plate cut from a piezoelectric crystal with electrodes attached serves not only as a capacitor for storing electrical energy but also as a motor for turning electrical into mechanical energy and as a generator for turning mechanical energy into electrical energy. Piezo is derived from a Greek word meaning to press, and piezoelectricity is pressure electricity. Piezoelectricity appears only in insulating solids. Although piezoelectricity can be generated in waxes which are solidified under an applied field, crystalline materials are, by far, the largest group of materials showing piezoelectricity. Piezoelectricity is distinguished from electrostriction, which is another effect which causes a solid dielectric to change shape on the application of a voltage, in that a reversal of the voltage reverses the sign of the resulting strain, whereas for electrostriction the strain is an even function of the applied voltage, and the strain does not reverse sign when the voltage is reversed. Electrostrictive effects are usually very feeble compared to piezoelectric effects but in the case of the ferroelectric materials, rochelle salt and barium titanate, they may be quite large.

All crystalline materials are anisotropic and do not have the same properties in all directions as do isotropic materials. Crystals can be divided into 32 classes on the basis of the symmetry they possess and, of these 32 classes, 20 possess the property of piezoelectricity and 12 do not. The criterion that determines whether a crystal is piezoelectric or not is its possession of a center of symmetry. A crystal possessing a center of symmetry cannot be piezoelectric because no combination of uniform stresses will produce a separation of the centers of gravity of the positive and negative charges and produce an induced dipole moment which is necessary for the production of polarization by stresses. Since a crystal is at once an electrical motor and an electrical generator, we have to consider the elastic and dielectric constants of the crystal as well as the piezoelectric constants. A crystal with no symmetry at all will have 21 elastic constants, 18 piezoelectric constants, and 6 dielectric constants. As the symmetry increases, the number of possible constants decreases, until the most symmetrical type of crystal, a cubic crystal, has only 3 elastic constants, 1 piezoelectric constant and 1 dielectric constant.

1.2 *Historical*

The piezoelectric effect was discovered experimentally by the brothers Pierre and Jacques Curie in the year 1880. By placing a weight on the surface of a crystal they produced a charge, measurable with an electrometer, which was proportional to the applied weight and hence discovered the direct effect. They found this effect in a considerable number of crystals including quartz, rochelle salt and tourmaline—crystals that are among those most used today. The converse piezoelectric effect, which deals with the motor property of the crystal, namely, producing a displacement when a voltage is applied, was predicted theoretically by Lippman in the following year 1881 and was verified by the Curies. Among the early investigators was Lord Kelvin, who suggested a molecular theory and produced a mechanical model of piezoelectricity; Pöckels, who made many determinations and contributed especially to the theory of the electro-optic effect in crystals; Duhem, whose formulation of piezoelectric principles was of fundamental importance; and finally Voigt, who systematized the work of his predecessors and whose monumental work, *Lehrbuch der Kristallphysik*, contained most of what was known about piezoelectricity up to World War I.

The connection of piezoelectricity with atomic structure, while well established on a general basis, is in its infancy regarding predictions of magnitudes of piezoelectric constants and their connection with chemical composition. Among the more important contributions are those of R. E. Gibbs and Max Born, who predicted respectively piezoelectric constants for quartz and zinc blende that are within factors of 10 of the experimental values.

The piezoelectric effect remained more or less a scientific curiosity up to the time of World War I. During the war Prof. Langevin in Paris was requested by the French government to devise some way of detecting submarines. After trying several devices he finally found that piezoelectric quartz plates could be used for this purpose. His device consisted essentially of a mosaic of quartz glued between steel plates. This device has the property that, when a voltage is applied, the crystal will expand and send out a longitudinal wave. Similarly, when a wave strikes it, it will set the quartz in vibration and generate a voltage which can be detected by vacuum tube devices. Langevin did not get his device perfected until after the end of the war, but it has been used extensively as a sonic depth finder, and similar devices were used in the present war for detecting submarines.

In 1917, A. M. Nicolson at Bell Telephone Laboratories was experimenting with rochelle salt and he constructed and demonstrated loudspeakers, microphones and phonograph pickups using this crystal. He

also controlled an oscillator by means of a crystal — in this case rochelle salt — and he has the primary crystal oscillator patent. In 1921, Cady at Wesleyan University showed that quartz crystals could be used to control oscillators and that much more stable oscillators can be obtained in this fashion. This use was a forerunner of the very wide application of crystals to control the frequency of military communication equipment which resulted in the use of more than 30,000,000 crystals in a single year. Quartz crystal oscillators using the GT crystal described in Chapter VI, produce the most stable oscillators and the best time-keeping systems that can be obtained. Both the Greenwich Observatory in England and the Bureau of Standards in Washington use such crystals in their primary standards.

Another large use for piezoelectric crystals is in producing very selective filter circuits. On account of the very high Q such crystals possess, they can be incorporated in filter circuits along with coils and condensers to give very discriminating filters. Such filters are used in all the high-frequency carrier systems and in the coaxial system for separating the simultaneous conversations that go over one pair of wires. For this purpose quartz was originally used, but a new synthetic crystal, ethylene diamine tartrate (EDT), has been developed which has low enough temperature coefficients and high enough stabilities to replace quartz for this application.

1.3 *Crystal Systems, Crystal Constants, and Motor Generator Effects*

Crystals are classified into 7 crystal systems and 32 crystal classes. The systems, as discussed in Chapter II, are determined by the shapes and dimensions of the smallest unit cells that surround a molecular configuration in such a manner that a simple translation of the unit cell along one of its axes by one unit length will cause it to surround a similar molecular configuration to that contained by the first cell. The edges of the unit cell are parallel to the crystallographic axes a, b and c, and the relative dimensions of the cell are the unit distances along these axes. The 32 crystal classes are determined by the elements of symmetry that are obtained in arranging the molecules within the seven elementary unit cells.

The most unsymmetrical type of system is the triclinic system, all three of whose crystallographic axes make oblique angles, and the lengths of the unit cells on the three axes are all unequal. In calculating the elastic constants of a triclinic crystal, as discussed in the appendix, it is more convenient to use a right-angled system of coordinates, rather than the crystallographic axes, and the question arises as to how these coordinates are to be related to the a-, b- and c-axes of the crystallographer. This question has been discussed by the Piezoelectric Crystal Committee of the

Institute of Radio Engineers under the chairmanship of Prof. W. G. Cady, and the system shown by Fig. 2.1 has been adopted. Here the z rectangular axis lies along the c crystallographic axis, the x rectangular axis lies in the plane of the a and c crystallographic axes and at right angles to the $c = z$ axis, while the y-axis is at right angles to the x- and z-axes in a right-handed system of coordinates. All the other systems are special cases of the most general case, as discussed in detail in Chapter II.

Depending on the crystal symmetries, crystals can have from 3 to 21 elastic constants, 0 to 18 piezoelectric constants and 1 to 6 dielectric constants. These are the constants referred to the x, y and z rectangular axes. If we wish to investigate the properties of crystals cut at oblique angles with respect to these axes, transformation equations, such as those discussed in the appendix, exist by means of which new elastic, piezoelectric, and dielectric constants can be calculated in terms of the constants for the new axes. These new constants are linear combinations of the fundamental constants. Conversely, in measuring the fundamental constants, it is often convenient to measure the properties of the oblique cuts and calculate the fundamental constants from the measured results. Oblique cuts are often of interest in themselves since special properties, such as low temperature coefficients, high electromechanical couplings, and freedom from secondary modes of motion, may often be obtained more easily in the oblique cuts than in cuts lying along the crystallographic axes.

Since a crystal is a motor generator, the constants of the crystal are going to vary depending upon the mechanical load attached to the crystal. For example, if the dielectric constant of a crystal is measured when it is clamped so hard that it cannot move, one obtains the so-called clamped dielectric constant of the crystal. If now the clamp has some compliance, some additional energy can be stored in the crystal in mechanical form and this results in an increase in the dielectric constant. The effect is greatest when the crystal is free to move, and one obtains the so-called "free" dielectric constant. The difference between the free and the clamped constant is determined by the electromechanical coupling factor for that crystal. This is defined as the square root of the ratio of the energy stored in mechanical form, for a given type of displacement, to the total input electrical energy obtained from the input battery. It is shown in Chapter V that this factor for a given mode of motion is equal to

$$k = \frac{d}{\sqrt{\frac{\epsilon^T}{4\pi} s^E}} \tag{1.1}$$

where d is the piezoelectric constant measuring the ratio of strain to field,

ϵ the dielectric constant and s the elastic compliance. In a converse manner, the elastic constant depends on the electrical condition obtained when the ratio of strain to stress is measured. If the electrical terminals are open-circuited, one obtains the elastic constant corresponding to a zero electric displacement (except for a minor class of crystals for which the direction of the electric displacement does not lie along the field), while if the terminals are short-circuited, one measures the constants for zero field. The ratio of these two constants and also the two dielectric constants are

$$\frac{s^E}{s^D} = \frac{\epsilon^T}{\epsilon^S} = \frac{1}{1 - k^2} \tag{1.2}$$

where ϵ^T is the constant stress (free) dielectric constant and ϵ^S the constant strain (clamped) dielectric constant. For most crystals with couplings, under 10 per cent, the difference is only about 1 per cent and is not too important. For ferroelectric crystals such as rochelle salt and potassium dihydrogen phosphate, however, the coupling may reach 90 per cent and the difference may be 5 to 1. Under these conditions it is essential to understand and measure the difference between these two types of constants.

1.4 *The Crystal Resonator and Transducer*

All of the applications of the piezoelectric effect depend on this motor generator action of the crystal. In the crystal resonator, the action drives the crystal itself in mechanical vibration and the mechanical vibration reacts back to control the electrical impedance of the crystal. As an electromechanical transducer the mechanical stress set up by the piezoelectric effect drives not only the mechanical elements of the crystal but also any other mechanical elements attached to the crystal surface. Phonograph pickups, headphones, loudspeakers, and in particular ultrasonic transducers are examples of this use. In the frequency range above about 10 kilocycles, piezoelectric crystals form the best means of transferring electrical into mechanical energy, and the last three chapters of the book are devoted to a description of these methods and results that have been obtained with them.

In analyzing the performance of a crystal for these functions, it is very convenient to obtain an equivalent electrical circuit which represents the electrical and mechanical properties of the crystal. For a crystal that is free on one end and drives a load on the other, a circuit which represents the performance of such a crystal near its resonant frequency is shown by Fig. 1.1A. Here C_0 is the static capacity of the crystal, 1 to φ is a constant that measures the force exerted by the crystal for a given applied voltage,

C_1 a compliance equal to $8/\pi^2$ times the static compliance of the crystal, M_1 a mass equal to $\frac{1}{8}$ the total mass of the crystal, C_2 a compliance equal to $\frac{1}{2}$ the static compliance of the crystal, and M_2 a mass equal to $2/\pi^2$ times the total mass of the crystal. With these values the two networks resonate at the natural resonant frequency of the crystal given by

$$\frac{\omega l}{V} = \pi \quad \text{or} \quad f = \frac{v}{2l} = \frac{1}{2l}\sqrt{\frac{1}{M_0 C_0}} = \frac{1}{2\sqrt{MC}} \tag{1.3}$$

where M_0 and C_0 are the mass and compliance per unit length and M and C the total mass and compliance of the crystal. Using this simple circuit the effect of adding mechanical units on the driving end of the crystal is easily analyzed.

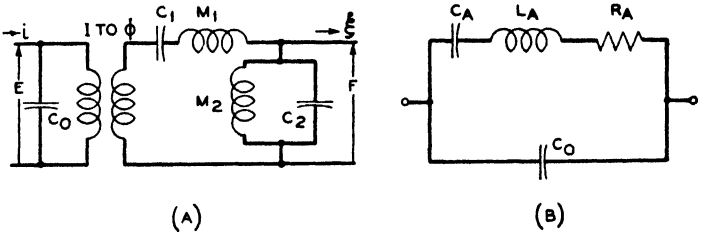

FIG. 1.1. Equivalent electromechanical and electrical circuits for a piezoelectric crystal.

If the crystal is free on both ends, the driving end of Fig. 1.1A can be short-circuited and the equivalent circuit of Fig. 1.1B results. The performance of a crystal resonator in an oscillator or filter can be analyzed by inserting this network in the place of the crystal. In quartz resonators the inductance L_A varies from the order of 0.1 henry with crystals vibrating at 2500 kc to 100 henries or more with low-frequency resonators. The synthetic crystals ADP and EDT have considerably lower values of inductance for the same size and frequency crystals, on account of the much higher electromechanical coupling. The capacitance C_A is usually in the order of a few tenths to 10 micromicrofarads. It is this enormous ratio of L_A to C_A together with the very low value of R (high Q) that gives the crystal its ability to control the frequency of an oscillator within narrow limits. The Q of a crystal in laboratory experiments[1] has been measured as high as 6,000,000 and, even in commercially mounted crystals which have to be securely held in order to stand extraneous knocks, Q's in the order of several hundred thousand are common.

[1] Van Dyke, K. S., "Vibrational Modes of Low Decrement for a Quartz Ring," *Phys. Rev.*, Vol. 53, p. 943, 1938.

In every piezoelectric oscillator circuit, the crystal acts fundamentally as a resonator. It does not generate energy, but by the electrical reactions of its vibrations it determines the alternating potential on the grid of the oscillator and controls it over a narrow frequency range. The equivalent circuit of the crystal has a frequency of resonance for which the impedance is low and a frequency of anti-resonance for which the impedance is high.

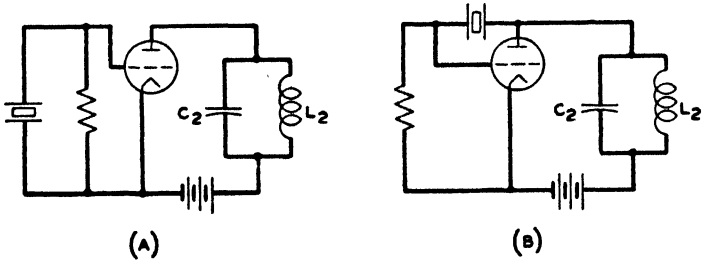

FIG. 1.2. Pierce-Miller and Pierce circuits for crystal oscillators.

In the more common form of oscillators, such as the Pierce circuits illustrated by Fig. 1.2, the frequency of oscillation comes between the resonance and anti-resonance frequency, although nearer the resonance. In later oscillators, such as the Meacham bridge oscillator, the frequency of oscillation coincides with the natural resonance frequency of the crystal.

1.5 *Important Piezoelectric Crystals*

In all, probably over five hundred crystals have been tested and a fair share of them have piezoelectric responses. Of these, however, only a few have come into practical use. Before World War II the only crystals that were at all widely used were quartz, rochelle salt and tourmaline. Quartz was used in all oscillator and filter applications, rochelle salt in most low-frequency transducer applications and tourmaline was used solely for measuring hydrostatic pressures. Stimulated by the need for a piezoelectric transducer for underwater sound applications that was more stable and less temperature sensitive than rochelle salt, considerable work was done during World War II in searching for new piezoelectric crystals. This resulted in the discovery and application of ammonium dihydrogen phosphate (ADP) to underwater sound transducers. On account of its freedom from water of crystallization (and hence dehydration), the higher temperature it will stand (up to 100°C), and the greater mechanical stability, this crystal largely displaced rochelle salt and even other types of electromechanical transducers for underwater sound applications. It

appears likely that it may replace rochelle salt for a number of peacetime applications as well.

Up to the present time quartz has been practically the only crystal suitable for the precise control of frequency in transmitting, monitoring, and receiving circuits, and in the production of very selective circuits. Quartz, which is the most abundant of natural crystals, is chemically stable at all ordinary temperatures and has very low internal losses. Furthermore, by cutting the crystal at various oblique orientations with respect to the crystallographic axes, it is possible to make resonators with very low temperature coefficients of frequency, and freedom from effects of other modes of motion. These characteristics of quartz have led to its exclusive use for primary frequency standards and as a means for obtaining very selective filters.

In the latter use, fairly large-sized crystals up to 5 centimeters in length are required. As the war progressed and more and more quartz was used in producing oscillator crystals, large-sized crystals became more difficult to obtain. With the end of the war the supply of large-sized crystals became insufficient to satisfy the needs of the telephone systems. Fortunately a study of the properties of synthetic crystals carried out during the last ten years at Bell Laboratories had resulted in discovering two new crystals which were capable of meeting the requirements necessary for filter crystals. These were two monoclinic sphenoidal crystals, ethylene diamine tartrate (EDT) and dipotassium tartrate (DKT). Low-temperature cuts in both crystals and higher electromechanical couplings are possible than exist in quartz. Of these crystals EDT has no water of crystallization, will stand a temperature of 120°C, and is easier to grow than DKT. The Western Electric Company has established a growing and processing plant for this crystal in Allentown, Pa., and it is planned to incorporate them in the high-frequency carrier and coaxial filters of the long-distance telephone systems. The properties of these crystals are described in Chapter IX.

Rochelle salt ($NaKC_4H_4O_6$-$4H_2O$) is the most strongly piezoelectric crystal at room temperatures. This is due to the fact that it becomes ferroelectric in the temperature range from -18°C to $+24$°C. Its dielectric properties are strikingly analogous to the ferromagnetic properties of iron. Below a certain temperature, which is called the Curie temperature, it exhibits dielectric hysteresis and has a dielectric constant that becomes very large for weak fields, at the Curie points. Unlike ferromagnetic materials, rochelle salt has a lower Curie temperature as well as an upper one. Potassium dihydrogen phosphate (KDP) is another ferroelectric type crystal that has only one Curie temperature, 121°K, above which it is non-ferroelectric and below which it is ferroelectric.

These two cases are discussed in Chapter XI and it is there suggested that both effects are due to a hydrogen bond dipole caused by the displacement of the hydrogen nucleus from the midpoint between the two oxygens. KDP has a symmetrical bond and, when a factor

$$A = \frac{N\mu^2\beta}{kT\left(1 - \frac{4\pi}{3}\gamma\right)} \tag{1.4}$$

becomes greater than one, the crystal becomes ferroelectric. In this equation N is the number of dipoles per cc, μ the dipole moment, β the Lorentz factor connecting the polarization with the internal field, k Boltzmann's constant, T the absolute temperature, and γ the polarizability in the absence of the hydrogen dipole. Rochelle salt has two sets of dissymmetrical bonds, and the lower Curie temperature is caused by the hydrogen nucleus freezing in the lower potential wells as the temperature is lowered. Although these effects are interesting scientifically, they detract from the usability of the crystal since the elements are so field and temperature sensitive. Considering this and the fact that rochelle salt tends to become dehydrated and that it disintegrates at 55°C, one can understand the need for a new crystal for transducer use that is free from these defects. This need is largely filled by ADP ($NH_4H_2PO_4$), as mentioned previously.

1.6 *Miscellaneous Applications*

In addition to the use of piezoelectric crystals in resonators and transducers, two second-order effects have recently become of importance. These are the electro-optical and piezo-optical effects which are caused respectively by the change in dielectric constant due to an applied voltage and the change in dielectric constant due to an applied stress. These effects were first investigated theoretically and experimentally by Pöckels. It was not, however, until the advent of ADP and KDP that any crystal with large enough electro-optical and piezo-optical constants to be of interest, were available. With these crystals light modulators can be obtained which work on voltages of 1000 volts or less. Furthermore, since the electro-optical effect depends on a change in the dielectric constant with voltage and the dielectric constant is known to be independent of frequency up to at least 10^{10} cycles, it appears likely that the electro-optical constant should also be independent of frequency up to this value.

Billings[2] has recently proposed the use of the electro-optical effect of an

[2] Billings, B. H., "A tunable narrow band optical filter," J. Opt. Soc. Amer. Vol. 37, No. 10, Oct. 1947.

ADP crystal to produce a variable band-pass optical filter, the position of whose band can be controlled by an applied voltage.

1.7 *Use of Piezoelectric Crystals in the Production of Power*

Since a crystal acts as a motor generator, the question arises as to whether it can be used in the production of electrical power. In most oscillator, filter and transducer applications, the amount of power converted is rather small; however, in underwater sound transducers considerable amounts of power are converted from electrical into mechanical energy.

For 60-cycle non-resonant operation the efficiency of conversion from mechanical to electrical power is poor, and the amount of power that can be converted by a given size structure is small. However, if one operates at the crystal resonance and tunes out the electrical capacitance of the crystals by suitable electrical coils, the efficiency of conversion can be raised to 90 per cent and the amount of power per square centimeter of area may increase to 5 to 10 watts. Such units require vibration type motors to drive them and the frequency has to be raised to 10 kc to 100 kc. Hence it appears possible that piezoelectric crystals could be used in the production of power.

CHAPTER II

Crystal Systems, Classes and Symmetries

The type of stresses set up in a crystal by an applied electric field depends on the symmetries existing in this crystal. As an example, if one wishes to find a crystal that will produce a voltage when subject to a hydrostatic pressure, he finds that not every crystal class can be used, but only 10 of the possible 32 crystal classes. Hence in order to understand the actions of piezoelectric crystals, it is necessary to consider the crystal systems, the classes and the symmetries that exist in crystals. It is the purpose of this chapter to consider briefly such relationships.

Crystals are classified into 7 crystal systems and 32 crystal classes. The ideal crystal is referred to identical unit cells, any one of which can be made to coincide with one of its neighbors by a simple translation, and the ensemble of unit cells forms the crystal lattice. The unit cell is usually chosen as the smallest parallelepiped out of which the crystal can be constructed. The edges of the unit cells are parallel to the crystallographic axes, a, b and c and their relative dimensions are the unit distances along these axes.

Bravais showed that the number of types of polyhedron that will completely fill all space is seven. He also found that when face-centered and body-centered polyhedra are considered, the number of space lattices was increased to 14. Each polyhedron is a unit cell. From these simple lattices are evolved the seven crystal systems. The edges of the polyhedron are the crystallographic axes and the faces are the pinacoids of the crystal. The seven crystal systems evolved from the Bravais lattices are the triclinic system, the monoclinic system, the orthorhombic system, the tetragonal system, the trigonal system, the hexagonal system and the cubic (or isometric) system.

All these systems can be specified in terms of the directions of the crystallographic axes a, b and c with respect to each other and the length of the unit cell measured along these three axes. For example, for the most unsymmetrical system, the triclinic, all three axes make oblique angles and the lengths of the unit cell on the three axes are all unequal. In calculating the elastic constants pertaining to a general crystal, such as discussed in Chapter III, it is much more convenient to use a right-angled system of coordinates and the question arises as to how these coordinates

are to be related to the a-, b- and c-axes of the crystallographer. This question has been discussed by the Piezoelectric Committee of the Institute of Radio Engineers under the chairmanship of Prof. W. G. Cady, and the system shown by Fig. 2.1 has been proposed. Here the z rectangular axis lies along the c crystallographic axis, the x rectangular axis lies in the plane of the a and c crystallographic axes and at right angles to the $c = z$-axis, while the y-axis is at right angles to the x- and z-axes in a right-handed

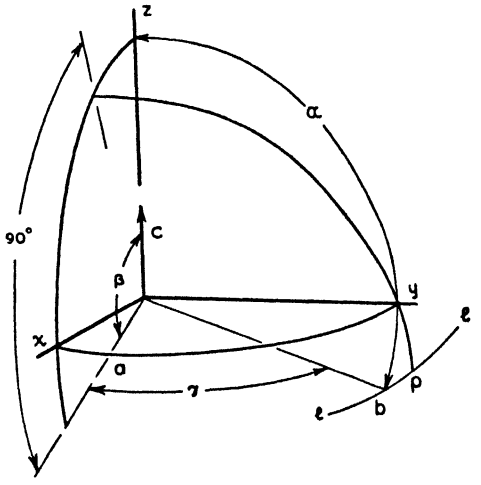

FIG. 2.1. Method for relating the crystallographic axes of a triclinic crystal to a set of rectangular axes.

system of coordinates. Certain conventions have been followed by the crystallographer in selecting the a-, b- and c-axes of the unit cell. Although these have not been universally observed, the following rules are in common use.

(1) In the triclinic system the choice of axes is based on the lengths of the sides of the unit cell. The axes are chosen so that $c < a < b$.

(2) In the monoclinic system the rule is abandoned and b is chosen parallel to the symmetry axis and normal to the symmetry plane, if any.

(3) In the orthorhombic system the three axes are chosen parallel to the three symmetry axes or, where there is only one, lying in the two symmetry planes. The axes are chosen so that $c < a < b$.

(4) In the tetragonal system the unique symmetry axis (fourfold) is taken as the c-axis and the two perpendicular equivalent secondary axes are a_1 and a_2.

(5) In the hexagonal system (including the rhombohedral division or the " trigonal system ") the unique symmetry axis (six- or threefold) is chosen as c and the three perpendicular, equivalent secondary axes are a_1, a_2 and a_3.

(6) In the isometric or cubic system the three equivalent mutually perpendicular symmetry axes are called a_1, a_2 and a_3.

The monoclinic system is characterized by having one axis, which the crystallographer has taken as the b-axis, perpendicular to the a- and c-axes which do not form a right angle. The positive directions of the a- and c-axes are outward from the obtuse angle between them, while the positive direction of the b-axis is such as to make a right-handed system with the a- and c-axes. The lengths of the unit cell on all three axes are unequal. By referring to the general case of a triclinic crystal shown by Fig. 2.1, we see that for a monoclinic crystal, the z rectangular axis will lie along c, the y rectangular axis will lie along b, and the x-axis will lie in the ac-plane and above a since the angle between a and c is an obtuse angle. More crystals belong to this system than to any other.

The orthorhombic system is characterized by three crystallographic axes all at right angles and a unit cell that has unequal intercepts along all three axes. The x, y, z rectangular axes coincide with the a, b, c crystallographic axes.

The tetragonal system is characterized by three crystallographic axes all at right angles and a unit cell that has equal intercepts along the a- and b-axes. For this reason the three axes are sometimes designated as a_1, a_2 and c. The x, y and z rectangular axes coincide with the a, b and c crystallographic axes, respectively, although there is no distinction between a and b or x and y.

The trigonal system or rhombohedral division of the hexagonal system may be characterized by three axes that form a rhombohedron. More often, however, it is referred to the axes of a hexagonal system. The way of relating the rhombohedral axes to the right-angled x, y, z system is shown by Fig. 2.2. OZ is a line making equal angles with all three equal crystallographic axes a_1, a_2, a_3. If we extend the axes a_1, a_2, a_3 down to a plane perpendicular to OZ, the intersection points M_1, M_2, M_3 form an equilateral triangle. If in this triangle we inscribe a hexagon $BCDEFG$, the x-axis is taken as OG (or OC or OE). The y-axis being perpendicular to this, is perpendicular to one of the lines, M_2M_3, M_3M_1, or M_1M_2. In quartz terminology, it is more common to refer to the x, y, z rectangular axes than the a_1, a_2, a_3 crystallographic axes.

The hexagonal system has a crystallographic axis that is an axis of sixfold symmetry. Four crystallographic axes are used, the c-axis, which corresponds to the z-axis of Fig. 2.2, and three axes a_1, a_2, a_3, 120° apart

which are normal to the c-axis. On Fig. 2.2 these correspond to the three x-axes OG, OC, and OE. The y-axis is taken at right angles to z and x and forms a right-handed system.

The cubic or isometric system is characterized by three mutually perpendicular crystallographic axes with a unit cell having equal intercepts on all three axes.

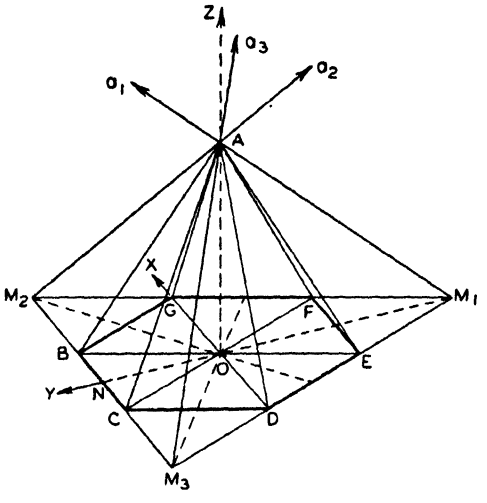

FIG. 2.2. Crystallographic axes of a hexagonal or trigonal crystal.

Crystal faces for these systems are specified in terms of the intercepts of the face or plane on the three crystallographic axes. If a, b, c are the intercepts of the unit cell along the a-, b- and c-axes, respectively, the unit plane, or 1, 1, 1 plane, is a plane passing through these three points, or is one parallel to it. Any plane drawn through three points having the coordinates a/h, b/k, c/l, where h, k, l are integers (including zero), is parallel to a net plane of the lattice and hence to a geometrically possible crystal face. The integers (h, k, l) used in specifying a plane or face, are known as the Miller indices. The symbols h, k, l are taken in the order of the a-, b-, c-axes and they are usually small positive or negative integers including zero. For example, the 001 face is one perpendicular to the c-axis at its positive end and the $00\bar{1}$ face is the corresponding face at the negative end of the c-axis. The face $\bar{3}1\bar{2}$ has the intercepts $-a/3$, b and $-c/2$. Of great physical significance is the possession by many crystals of a polar axis, which may be defined as an axis which has different properties for the two ends of the axis. For the trigonal and hexagonal systems which can be specified by four Bravais axes of Fig. 2.2, it is common to

use the Bravais-Miller symbols h, k, i, l which are the intercepts of a plane on all four axes. Since the sum of $h + k + i = 0$, it is common practice to write the symbol as $(hk \cdot l)$, the dot signifying that $i = -(h + k)$.

In general, the points that form the space lattices do not represent the positions of the atoms but merely serve to define the unit cell within which the atoms may be situated in a definite number of configurations. The space groups define the symmetry of the arrangement of atoms throughout the unit cell. The evolution of the space groups out of the Bravais space lattices consists essentially in inserting points in the unit cell of the space lattice, such that the pattern can be made to repeat itself by a combination of rotation and translation (screw axes), or of a reflection in a plane and translation (glide planes), in addition to the cyclic axes of symmetry and reflection planes that characterize the Bravais lattices. Crystallographers have shown that there are a total of 230 possible space groups or ways that the atoms can be arranged in the seven types of unit cells.

In order to determine what elastic or piezoelectric constants a crystal can have, it is not necessary to know to what space group the crystal belongs but rather what point group. It has been shown that there are 32 possible point groups which are the same as the 32 classes of the crystallographer. Any property of a body may be symmetrical with respect to a point, a line, a plane, or any combination of these. If symmetrical with respect to a point, the body is centrosymmetrical and can possess no polar properties such as piezoelectricity. With one exception, all classes devoid of a center of symmetry are piezoelectric. This exception, class 29 (Schönflies symbol O), although it has no center of symmetry, nevertheless has other symmetry elements that combine to exclude the piezoelectric property. Symmetry with respect to a line is called axial symmetry and the line is an axis of symmetry. A plane of symmetry produces a type of symmetry seen in a mirror; that is, a plane passed through the crystal divides the crystal in such a way that to each face on one side of the plane there corresponds a possible face on the other side which is a mirror image of the first face.

All these types of symmetry can exist separately or together in the various crystal classes. A set of symbols was devised by Schönflies to describe the various types of symmetries and these are shown in Table I. A later set of symbols has also been devised by Hermann and modified by Mauguin. In this system two-, three-, four- and sixfold rotation axes of symmetry are represented by the numbers 2, 3, 4 and 6, while three-, four- and sixfold inversion axes have the symbols $\bar{3}$, $\bar{4}$ and $\bar{6}$. Asymmetry is represented in the symbol 1, while a center of symmetry (or inversion through a point) has a symbol $\bar{1}$. A plane of symmetry is represented by a letter m (mirror). The first number denotes the principal axis. If a plane of symmetry is

TABLE I

SCHÖNFLIES SYMBOLS

Symbol	Meaning
C_n	A cyclic axis of symmetry, *i.e.*, an axis such that rotation about it through an angle of $2\pi/n$ radians results in a repetition of the figure. $n = 1, 2, 3, 4$ or 6. $n = 1$ means no symmetry at all.
C_{nh}	An n-fold cyclic axis with a plane of symmetry normal to it.
C_{ni}	An n-fold cyclic axis with a center of symmetry.
C_{nv}	An n-fold cyclic axis to which n planes of symmetry are parallel.
$S_2 = C_i$	Every direction is a onefold cyclic axis of rotary inversion. The crystal has a center of symmetry and nothing else.
$C_{4i} = S_4$	A fourfold cyclic axis of rotary inversion. There is no center of symmetry.
$V = D_2$	3 mutually perpendicular twofold cyclic axes.
$V_h = D_{2h}$	Symmetry V with addition of a plane of symmetry normal to each of the 3 axes.
$V_d = D_{2d}$	Symmetry V with 2 planes of symmetry containing the principal axis, and at 45° to the other 2 axes.
D_n	Axis C_n (principal axis) with n twofold axes (secondary axes) normal to it ($n = 3, 4$ or 6).
D_{nd}	Symmetry D_n with n planes of symmetry containing the C_n axis and bisecting the angles between the secondary (twofold) axes.
D_{nh}	Symmetry D_n with a plane of symmetry normal to the C_n (principal) axis and therefore n planes of symmetry, each containing the principal and 1 secondary axis.
T	3 orthogonal twofold axes and 4 threefold axes (the tetrahedral group).
T_h	Symmetry T with a plane of symmetry normal to each of the twofold axes.
T_d	Symmetry T with 6 planes of symmetry each containing 2 of the threefold axes.
O	3 orthogonal fourfold axes, 6 twofold axes and 4 threefold axes (the octahedral group).
O_h	Symmetry O with the planes of symmetry of both T_d and T_h.

perpendicular to an axis, this is represented by n/m. Then follow the symbols for the secondary axes, if any, and then any other symmetry planes. The Hermann-Mauguin system is simpler than the Schönflies system and is largely replacing it.

Although the type of crystal is determined by its symmetries, there are a number of different systems for naming and numbering such crystal classes. The name and numbering system followed here is that due to Von Groth and is followed since Von Groth's five volumes on synthetic crystals represent the most comprehensive source of information on the properties of synthetic crystals. However, the names and class numbers are not as

fundamental as the symmetry symbols, which are also shown. The 32 classes have been divided into the seven crystallographic systems and are listed in Table II.

TABLE II

CRYSTAL CLASSES

Class No. According to Von Groth	Names of classes according to Von Groth	Symmetry Symbols Schönflies	Hermann-Mauguin
	TRICLINIC SYSTEM		
1	Triclinic asymmetric	C_1	1
2	Triclinic pinacoidal	$S_2 = C_i$	$\bar{1}$
	MONOCLINIC SYSTEM		
3	Monoclinic sphenoidal	C_2	2
4	Monoclinic domatic	$C_{1h} = C_s$	$m = \bar{2}$
5	Monoclinic prismatic	C_{2h}	$\frac{2}{m}$
	ORTHORHOMBIC SYSTEM		
6	Orthorhombic disphenoidal	$V = D_2$	222
7	Orthorhombic pyramidal	C_{2v}	$2mm$
8	Orthorhombic dipyramidal	$V_h = D_{2h}$	$\frac{2}{m}\frac{2}{m}\frac{2}{m} = mmm$
	TETRAGONAL SYSTEM		
9	Tetragonal disphenoidal	S_4	$\bar{4}$
10	Tetragonal pyramidal	C_4	4
11	Tetragonal scalenohedral	$V_d = D_{2d}$	$\bar{4}2m$
12	Tetragonal trapezohedral	D_4	422
13	Tetragonal dipyramidal	C_{4h}	$\frac{4}{m}$
14	Ditetragonal-pyramidal	C_{4v}	$4mm$
15	Ditetragonal-dipyramidal	D_{4h}	$\frac{4}{m}mm = \frac{4}{m}\frac{2}{m}\frac{2}{m}$
	TRIGONAL SYSTEM		
16	Trigonal pyramidal	C_3	3
17	Trigonal rhombohedral	C_{3i}	$\bar{3}$
18	Trigonal trapezohedral	D_3	32
20	Ditrigonal-pyramidal	C_{3v}	$3m$
21	Ditrigonal-scalenohedral	D_{3d}	$\bar{3}\frac{2}{m}$

TABLE II—*Continued.*

Class No. According to Von Groth	Names of classes according to Von Groth	Symmetry Symbols Schönflies	Hermann-Mauguin
	HEXAGONAL SYSTEM		
19	Trigonal dipyramidal	C_{3h}	$\bar{6}$
22	Ditrigonal-dipyramidal	D_{3h}	$\bar{6}m2$
23	Hexagonal pyramidal	C_6	6
24	Hexagonal trapezohedral	D_6	622
25	Hexagonal dipyramidal	C_{6h}	$\frac{6}{m}$
26	Dihexagonal-pyramidal	C_{6v}	$6mm$
27	Dihexagonal-dipyramidal	D_{6h}	$\frac{6}{m}mm = \frac{6}{m}\frac{2}{m}\frac{2}{m}$
	CUBIC SYSTEM		
28	Cubic tetrahedral-pentagonal-dodecahedral	T	23
29	Cubic pentagonal icosi-tetrahedral	O	432
30	Cubic dyakis-dodecahedral	T_h	$\frac{2}{m}\bar{3} = m3$
31	Cubic hexakis-tetrahedral	T_d	$\bar{4}3m$
32	Cubic hexakis-octahedral	O_h	$\frac{4}{m}\bar{3}\frac{2}{m} = m3m$

When the symmetry of a crystal is known, it follows from *Neuman's principle* that there is a correspondence between the geometrical form and the physical properties of the crystal. According to this principle, when the elements of symmetry that characterize the outward form of the crystal are known, the symmetry of the physical properties can be predicted. Any given property such as density, thermal expansion, piezoelectricity, or elasticity may be of higher symmetry than that of the crystal form (approaching more closely that of an isotropic body) but it cannot be of lower symmetry.

The mathematical method for relating the symmetry properties of the crystal to the physical properties is discussed in Chapter III.

CHAPTER III

Elastic, Piezoelectric and Dielectric Relations in Crystals

Since a piezoelectric crystal is at once a condenser, a motor and a generator, we have to consider three sets of constants to specify its action completely. These are the dielectric, the elastic and the piezoelectric constants if only adiabatic relations are to be used, which is the normal case. As discussed in detail in this chapter, these are second partial derivatives, respectively, of one of the thermodynamic potentials with respect to the electric fields, the stresses, and the mixed derivative of the two. Because of the wide diversity of symbols used for the variables and constants, the I.R.E. Piezoelectric Committee has proposed a system of nomenclature that is used throughout this book. A suitable notation for the quantities of interest in piezoelectricity should provide a single symbol for each quantity with the various components designated by a subscript to permit the use of either matrix or tensor methods of writing the equations. This requirement prevents the adoption of either of the two most widely used notations for stresses or strains. Piezoelectric notation is further complicated by the fact that, in general, the electrical, mechanical and sometimes thermal conditions of measurement must be specified before a unique meaning can be given to the constants of the material. It is therefore desirable to provided a notation where the boundary conditions can be specified in the symbol.

The fundamental variables specified and the two most widely used systems of units are shown by the following Table III. The definition of each unit is given in the cgs electrostatic system and in the rationalized mks system, and a conversion factor is given for multiplying the number of units in the cgs system to obtain the number of units in the mks system.

Most of the data on piezoelectricity and practically all the data on elasticity have been expressed in the cgs system of units and hence this practice is followed in the present work. The equivalent mks units are sometimes given and in any case can be obtained by using the conversion factors of Table III.

3.1 *Stress and Strain Relations in Aeolotropic Crystals*

3.11 *Specification of Stress*

The stresses exerted on any elementary cube of material with its edges along the three rectangular axes x, y and z can be specified by considering

TABLE III

Variable	Symbol	Definition in cgs units	Conversion factor	Definition in mks units
Force	F	dyne	10^{-5}	Newton
Potential	V	stat-volt	300	volt
Charge	Q	stat-coulomb	3.33×10^{-10}	coulomb
Electric field	E	stat-volt/cm	3×10^{4}	volt/meter
Electric displacement	D	$\frac{4\pi \text{ stat-coulomb}}{\text{cm}^2}$	2.65×10^{-7}	coulomb/meter^2
Stress	T	dyne/cm^2	10^{-1}	Newton/meter^2
Strain	S	cm/cm	1	meter/meter
Elastic displacement	u	centimeter	10^{-2}	meter
Elastic compliance	s	cm^2/dyne	10	meter^2/Newton
Elastic stiffness	c	dyne/cm^2	10^{-1}	Newton/meter^2
Permittivity	ϵ	$\frac{\text{stat-farad}}{\text{cm}}$	8.85×10^{-12}	farad/meter
Dielectric impermeability	β	$\frac{\text{cm}}{\text{stat-farad}}$	1.13×10^{11}	meter/farad
Piezoelectric constant	d	$\frac{\text{stat-coulomb}}{\text{dyne}}$	3.33×10^{-5}	coulomb/Newton
Piezoelectric constant	e	$\frac{\text{stat-coulomb}}{\text{cm}^2}$	3.33×10^{-6}	coulomb/meter^2
Piezoelectric constant	g	$\frac{\text{cm}^2}{\text{stat-coulomb}}$	3×10^{5}	meter^2/Newton
Piezoelectric constant	h	$\frac{\text{dyne}}{\text{stat-coulomb}}$	3×10^{4}	Newton/coulomb
Temperature	Θ	degrees Kelvin, °K	1	degrees Kelvin, °K
Entropy	σ	$\frac{\text{ergs}}{\text{cm}^3 \times {}^\circ\text{K}}$	10^{-1}	$\frac{\text{Joules}}{\text{meter}^3 \times {}^\circ\text{K}}$

the stresses on each face of the cube illustrated by Fig. 3.1. The total stress acting on the face ABCD normal to the x-axis can be represented by a resultant force R, with its center of application at the center of the face, plus a couple which takes account of the variation of the stress across the face. The force R is directed outward, since a stress is considered positive if it exerts a tension. As the face is shrunk in size, the force R will be proportional to the area of the face, while the couple will vary as the cube of

the dimension. Hence in the limit the couple can be neglected with respect to the force R. The stress (force per unit area) due to R can be resolved into three components along the three axes to which we give the designation

$$T_{xx_2}, \quad T_{yx_2}, \quad T_{zx_2}. \tag{3.1}$$

Here the first letter designates the direction of the stress component and the second letter x_2 denotes the second face of the cube normal to the x-axis.

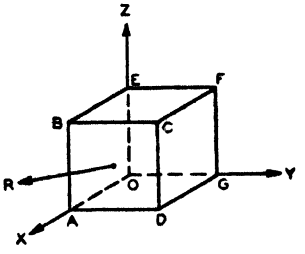

FIG. 3.1. Cube showing method for specifying stresses.

Similarly for the first x face OEFG, the stress resultant can be resolved into the components T_{xx_1}, T_{yx_1}, T_{zx_1}, which are oppositely directed to those of the second face. The remaining stress components on the other four faces have the designation

$$\begin{aligned} \text{Face OABE} \quad & T_{xy_1}, \quad T_{yy_1}, \quad T_{zy_1} \\ \text{CFGD} \quad & T_{xy_2}, \quad T_{yy_2}, \quad T_{zy_2} \\ \text{OADG} \quad & T_{xz_1}, \quad T_{yz_1}, \quad T_{zz_1} \\ \text{BCFE} \quad & T_{xz_2}, \quad T_{yz_2}, \quad T_{zz_2}. \end{aligned} \tag{3.2}$$

The resultant force in the x direction is obtained by summing all the forces with components in the x direction or

$$F_x = (T_{xx_2} + T_{xx_1})\,dy\,dz + (T_{xy_2} + T_{xy_1})\,dx\,dz + (T_{xz_2} + T_{xz_1})\,dx\,dy. \tag{3.3}$$

But

$$T_{xx_2} = -T_{xx_1} + \frac{\partial T_{xx}}{\partial x}\,dx;$$

$$T_{xy_2} = -T_{xy_1} + \frac{\partial T_{xy}}{\partial y}\,dy; \qquad T_{xz_2} = -T_{xz_1} + \frac{\partial T_{xz}}{\partial z}\,dz \tag{3.4}$$

and equation (3.3) can be written in the form

$$F_x = +\left(\frac{\partial T_{xx}}{\partial x} + \frac{\partial T_{xy}}{\partial y} + \frac{\partial T_{xz}}{\partial z}\right) dx\, dy\, dz. \tag{3.5}$$

Similarly the resultant forces in the other directions are

$$\begin{aligned} F_y &= +\left(\frac{\partial T_{yx}}{\partial x} + \frac{\partial T_{yy}}{\partial y} + \frac{\partial T_{yz}}{\partial z}\right) dx\, dy\, dz \\ F_z &= +\left(\frac{\partial T_{zx}}{\partial x} + \frac{\partial T_{zy}}{\partial y} + \frac{\partial T_{zz}}{\partial z}\right) dx\, dy\, dz. \end{aligned} \tag{3.6}$$

We call the components

$$\begin{vmatrix} T_{xx}, & T_{xy}, & T_{xz} \\ T_{yx}, & T_{yy}, & T_{yz} \\ T_{zx}, & T_{zy}, & T_{zz} \end{vmatrix} = \begin{vmatrix} T_{11}, & T_{12}, & T_{13} \\ T_{21}, & T_{22}, & T_{23} \\ T_{31}, & T_{32}, & T_{33} \end{vmatrix} \tag{3.7}$$

the stress components exerted on the elementary cube which tend to deform it. The rate of change of these stresses determines the resultant force on

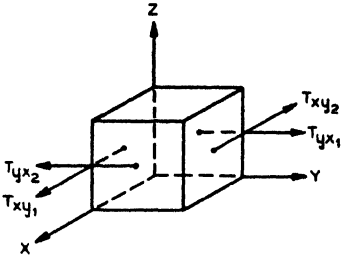

FIG. 3.2. Shearing stresses exerted on a cube.

the cube. The second form of (3.7) is commonly used when the stresses are considered as a second-rank tensor.

It can be shown that there is a relation between 3 pairs of these components, namely

$$T_{xy} = T_{yx}; \qquad T_{xz} = T_{zx}; \qquad T_{yz} = T_{zy}. \tag{3.8}$$

To show this, consider Fig. 3.2, which shows the stresses tending to rotate the elementary cube about the z-axis. The stresses T_{yx_2} and T_{yx_1} tend to rotate the cube about the z-axis by producing the couple

$$\frac{T_{yx}\, dx\, dy\, dz}{2}. \tag{3.9}$$

The stresses T_{xy_1} and T_{xy_2} produce a couple tending to cause a rotation in

the opposite direction so that

$$\tfrac{1}{2}(T_{yx} - T_{xy})\,dx\,dy\,dz = \text{couple} = I\ddot{\omega}_z \tag{3.10}$$

is the total couple tending to produce a rotation around the z-axis. But from dynamics, it is known that this couple is equal to the product of the moment of inertia of the section times the angular acceleration. This moment of inertia of the section is proportional to the fourth power of the cube edge and the angular acceleration is finite. Hence as the cube edge approaches zero, the right-hand side of (3.10) is one order smaller than the left-hand side and hence

$$T_{yx} = T_{xy}. \tag{3.11}$$

The same argument applies to the other terms. Hence the stress components of (3.7) can be written in the symmetrical form

$$\begin{vmatrix} T_{xx}, & T_{xy}, & T_{xz} \\ T_{xy}, & T_{yy}, & T_{yz} \\ T_{xz}, & T_{yz}, & T_{zz} \end{vmatrix} = \begin{vmatrix} T_{11}, & T_{12}, & T_{13} \\ T_{12}, & T_{22}, & T_{23} \\ T_{13}, & T_{23}, & T_{33} \end{vmatrix} = \begin{vmatrix} T_1, & T_6, & T_5 \\ T_6, & T_2, & T_4 \\ T_5, & T_4, & T_3 \end{vmatrix}. \tag{3.12}$$

The last form is a short-hand method for reducing the number of indices in the stress tensor. The reduced indices 1 to 6, correspond to the tensor indices if we replace

11 by 1; 22 by 2; 33 by 3; 23 by 4; 13 by 5; 12 by 6.

This last method is the most common way for writing the stresses.

3.12 *Strain Components*

The types of strain present in a body can be specified by considering two points P and Q of a medium, and calculating their separation in the strained condition. Let us consider the point P at the origin of coordinates and the point Q having the coordinates x, y and z as shown by Fig. 3.3. Upon straining the body, the points change to the positions P', Q'. In order to specify the strains, we have to calculate the difference in length after straining, or have to evaluate the distance $P'Q'-PQ$. After the material has stretched, the point P' will have the coordinates ξ_1, η_1, ζ_1, while Q' will have the coordinates $x + \xi_2$; $y + \eta_2$; $z + \zeta_2$. But the displacement is a continuous function of the coordinates x, y and z, so that we have

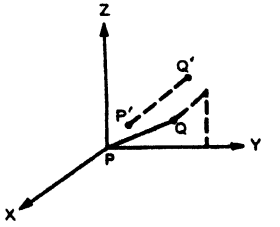

FIG. 3.3. Change in length and position of a line due to strain in a solid body.

$$\xi_2 = \xi_1 + \frac{\partial \xi}{\partial x}x + \frac{\partial \xi}{\partial y}y + \frac{\partial \xi}{\partial z}z.$$

Similarly

$$\eta_2 = \eta_1 + \frac{\partial \eta}{\partial x}x + \frac{\partial \eta}{\partial y}y + \frac{\partial \eta}{\partial z}z$$
$$\zeta_2 = \zeta_1 + \frac{\partial \zeta}{\partial x}x + \frac{\partial \zeta}{\partial y}y + \frac{\partial \zeta}{\partial z}z. \tag{3.13}$$

Hence subtracting the two lengths, we find that the increases in separation in the three directions are

$$\delta_x = x\frac{\partial \xi}{\partial x} + y\frac{\partial \xi}{\partial y} + z\frac{\partial \xi}{\partial z}$$
$$\delta_y = x\frac{\partial \eta}{\partial x} + y\frac{\partial \eta}{\partial y} + z\frac{\partial \eta}{\partial z} \tag{3.14}$$
$$\delta_z = x\frac{\partial \zeta}{\partial x} + y\frac{\partial \zeta}{\partial y} + z\frac{\partial \zeta}{\partial z}.$$

The net elongation of the line in the x direction is $x\dfrac{\partial \xi}{\partial x}$ and the elongation per unit length is $\dfrac{\partial \xi}{\partial x}$ which is defined as the linear strain in the x direction. We have therefore that the linear strains in the x, y and z directions are

$$S_1 = \frac{\partial \xi}{\partial x}; \qquad S_2 = \frac{\partial \eta}{\partial y}; \qquad S_3 = \frac{\partial \zeta}{\partial z}. \tag{3.15}$$

The remaining strain coefficients are usually defined as

$$S_4 = \frac{\partial \zeta}{\partial y} + \frac{\partial \eta}{\partial z}; \qquad S_5 = \frac{\partial \xi}{\partial z} + \frac{\partial \zeta}{\partial x}; \qquad S_6 = \frac{\partial \eta}{\partial x} + \frac{\partial \xi}{\partial y} \tag{3.16}$$

and the rotation coefficients by the equations

$$\omega_x = \frac{\partial \zeta}{\partial y} - \frac{\partial \eta}{\partial z}; \qquad \omega_y = \frac{\partial \xi}{\partial z} - \frac{\partial \zeta}{\partial x}; \qquad \omega_z = \frac{\partial \eta}{\partial x} - \frac{\partial \xi}{\partial y}. \tag{3.17}$$

Hence the relative displacement of any two points can be expressed as

$$\delta_x = xS_1 + y\left(\frac{S_6 - \omega_z}{2}\right) + z\left(\frac{S_5 + \omega_y}{2}\right)$$
$$\delta_y = x\left(\frac{S_6 + \omega_z}{2}\right) + yS_2 + z\left(\frac{S_4 - \omega_x}{2}\right) \tag{3.18}$$
$$\delta_z = x\left(\frac{S_5 - \omega_y}{2}\right) + y\left(\frac{S_4 + \omega_x}{2}\right) + zS_3$$

which represents the most general type of displacement that the line PQ can undergo.

As discussed in the appendix the definition of the shearing strains given by equation (3.16) does not allow them to be represented as part of a tensor. If, however, we defined the shearing strains as

$$2S_{23} = S_4 = \frac{\partial \zeta}{\partial y} + \frac{\partial \eta}{\partial z};$$

$$2S_{13} = S_5 = \frac{\partial \xi}{\partial z} + \frac{\partial \zeta}{\partial x}; \qquad 2S_{12} = S_6 = \frac{\partial \eta}{\partial x} + \frac{\partial \xi}{\partial y}$$

they can be expressed in the form of a symmetrical tensor

$$\begin{vmatrix} S_{11} & S_{12} & S_{13} \\ S_{12} & S_{22} & S_{23} \\ S_{13} & S_{23} & S_{33} \end{vmatrix} = \begin{vmatrix} S_1 & \frac{S_6}{2} & \frac{S_5}{2} \\ \frac{S_6}{2} & S_2 & \frac{S_4}{2} \\ \frac{S_5}{2} & \frac{S_4}{2} & S_3 \end{vmatrix}. \tag{3.19}$$

For an element suffering a shearing strain $S_6 = 2S_{12}$ only, the displacement along x is proportional to y, while the displacement along y is proportional to the x dimension. A cubic element of volume will be strained into

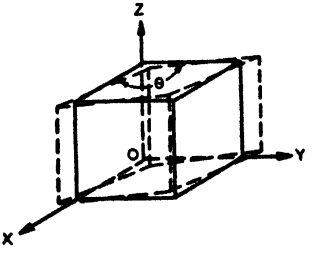

FIG. 3.4. Distortion due to a shearing strain.

a rhombic form, as shown by Fig. 3.4, and the cosine of the resulting angle θ measures the shearing deformation. For an element suffering a rotation ω_z only, the displacement along x is proportional to y and in the negative y direction, while the displacement along y is in the positive x direction. Hence, a rectangle has the displacement shown by Fig. 3.5, which is a pure rotation of the body without change of form, about the z-axis.

In general, S_1 to S_6 cannot be given arbitrarily as functions of x, y and z but are subject to restrictions imposed upon them by the definitions

of equations (3.15), (3.16) and (3.17). On substitution from these definitions it is found that six equations have to be satisfied identically. These equations, known as the conditions of compatibility, are

$$\begin{aligned}
&\frac{\partial^2 S_2}{\partial z^2} + \frac{\partial^2 S_3}{\partial y^2} = \frac{\partial^2 S_4}{\partial y\,\partial z}; \qquad 2\frac{\partial^2 S_1}{\partial y\,\partial z} = \frac{\partial}{\partial x}\left(\frac{\partial S_4}{\partial x} + \frac{\partial S_5}{\partial y} + \frac{\partial S_6}{\partial z}\right)\\
&\frac{\partial^2 S_3}{\partial x^2} + \frac{\partial^2 S_1}{\partial z^2} = \frac{\partial^2 S_5}{\partial z\,\partial x}; \qquad 2\frac{\partial^2 S_2}{\partial z\,\partial x} = \frac{\partial}{\partial y}\left(\frac{\partial S_4}{\partial x} - \frac{\partial S_5}{\partial y} + \frac{\partial S_6}{\partial z}\right) \qquad (3.20)\\
&\frac{\partial^2 S_1}{\partial y^2} + \frac{\partial^2 S_2}{\partial x^2} = \frac{\partial^2 S_6}{\partial x\,\partial y}; \qquad 2\frac{\partial^2 S_3}{\partial x\,\partial y} = \frac{\partial}{\partial z}\left(\frac{\partial S_4}{\partial x} + \frac{\partial S_5}{\partial y} - \frac{\partial S_6}{\partial z}\right)
\end{aligned}$$

These conditions are necessary and sufficient to insure the existence of the quantities ξ, η, ζ connected with the strains by the defining formulae of equation (3.15), (3.16) and (3.17).

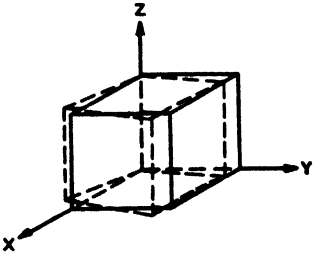

FIG. 3.5. A rotation of a solid body.

The total internal energy stored in a general distortion can be calculated as the sum of the energies due to the distortion of the various modes. For example, in expanding the cube in the x direction by an amount $\frac{\partial \xi}{\partial x}\,dx = S_1\,dx$, the work done is the force times the displacement. The force will be the force $T_1\,dy\,dz$. Hence the internal energy stored in this distortion is

$$T_1\,dS_1\,dx\,dy\,dz.$$

For a shearing stress T_6 of the type shown by Fig. 3.4, the displacement $\frac{dS_6\,dx}{2}$ times the force $T_6\,dy\,dz$ and the displacement $\frac{dS_6\,dy}{2}$ times the force $T_6\,dx\,dz$ equals the stored energy or

$$\Delta U = \tfrac{1}{2}(dS_6T_6 + dS_6T_6)\,dx\,dy\,dz = dS_6T_6\,dx\,dy\,dz.$$

Hence for all modes of motion the stored internal energy is equal to

$$\Delta U = [T_1\,dS_1 + T_2\,dS_2 + T_3\,dS_3 + T_4\,dS_4 + T_5\,dS_5 + T_6\,dS_6]\,dx\,dy\,dz. \qquad (3.21)$$

3.13 *Generalized Hooke's Law*

Having specified stresses and strains, we next consider the relationship between them. For small displacements, it is a consequence of Hooke's Law that the stresses are proportional to the strains. For the most unsymmetrical medium, this proportionality can be written in the form

$$\begin{aligned}
T_1 &= c_{11}S_1 + c_{12}S_2 + c_{13}S_3 + c_{14}S_4 + c_{15}S_5 + c_{16}S_6 \\
T_2 &= c_{21}S_1 + c_{22}S_2 + c_{23}S_3 + c_{24}S_4 + c_{25}S_5 + c_{26}S_6 \\
T_3 &= c_{31}S_1 + c_{32}S_2 + c_{33}S_3 + c_{34}S_4 + c_{35}S_5 + c_{36}S_6 \\
T_4 &= c_{41}S_1 + c_{42}S_2 + c_{43}S_3 + c_{44}S_4 + c_{45}S_5 + c_{46}S_6 \\
T_5 &= c_{51}S_1 + c_{52}S_2 + c_{53}S_3 + c_{54}S_4 + c_{55}S_5 + c_{56}S_6 \\
T_6 &= c_{61}S_1 + c_{62}S_2 + c_{63}S_3 + c_{64}S_4 + c_{65}S_5 + c_{66}S_6
\end{aligned} \tag{3.22}$$

where c_{11}, for example, is an elastic constant expressing the proportionality between the S_1 strain and the T_1 stress in the absence of any other strains. By employing the Einstein convention that a repeated suffix represents a summation with respect to this suffix, these equations can be written in the simple form

$$T_i = c_{ij}S_j \qquad i,j = 1 \text{ to } 6 \tag{3.23}$$

It follows from the fact that the internal energy ΔU is a perfect differential that

$$c_{ij} = c_{ji}$$

To show this we note that

$$T_i = \frac{\partial U}{\partial S_i} \qquad \text{and} \qquad c_{ij} = \frac{\partial T_i}{\partial S_i} = \frac{\partial^2 U}{\partial S_i \, \partial S_j}$$

Hence, since the order of the differentiation makes no difference

$$c_{ij} = \frac{\partial^2 U}{\partial S_i \, \partial S_j} = \frac{\partial^2 U}{\partial S_j \, \partial S_i} = c_{ji}$$

This reduces the number of independent elastic constants for the most unsymmetrical medium to 21. As shown in section 3.33, any symmetry existing in the crystal will reduce the possible number of elastic constants and simplify the stress strain relationship of equation (3.22).

Introducing the values of the stresses from (3.22) in the expression for the internal energy (3.21), this can be written in the form

$$\begin{aligned} 2\Delta U = {} & c_{11}S_1^2 + 2c_{12}S_1S_2 + 2c_{13}S_1S_3 + 2c_{14}S_1S_4 + 2c_{15}S_1S_5 + 2c_{16}S_1S_6 \\ & + c_{22}S_2^2 + 2c_{23}S_2S_3 + 2c_{24}S_2S_4 + 2c_{25}S_2S_5 + 2c_{26}S_2S_6 \\ & + c_{33}S_3^2 + 2c_{34}S_3S_4 + 2c_{35}S_3S_5 + 2c_{36}S_3S_6 \\ & + c_{44}S_4^2 + 2c_{45}S_4S_5 + 2c_{46}S_4S_6 \\ & + c_{55}S_5^2 + 2c_{56}S_5S_6 \\ & + c_{66}S_6^2 = c_{ij}S_iS_j. \end{aligned} \tag{3.24}$$

The relations (3.22) thus can be obtained by differentiating the internal energy according to the relation

$$T_1 = \frac{\partial U}{\partial S_1}; \qquad \cdots; \qquad T_6 = \frac{\partial U}{\partial S_6}. \tag{3.25}$$

It is sometimes advantageous to express the strains in terms of the stresses. This can be done by solving the equations (3.22) simultaneously for the strains, resulting in the equations

$$\begin{aligned} S_1 &= s_{11}T_1 + s_{12}T_2 + s_{13}T_3 + s_{14}T_4 + s_{15}T_5 + s_{16}T_6 \\ S_2 &= s_{21}T_1 + s_{22}T_2 + s_{23}T_3 + s_{24}T_4 + s_{25}T_5 + s_{26}T_6 \\ S_3 &= s_{31}T_1 + s_{32}T_2 + s_{33}T_3 + s_{34}T_4 + s_{35}T_5 + s_{36}T_6 \\ S_4 &= s_{41}T_1 + s_{42}T_2 + s_{43}T_3 + s_{44}T_4 + s_{45}T_5 + s_{46}T_6 \\ S_5 &= s_{51}T_1 + s_{52}T_2 + s_{53}T_3 + s_{54}T_4 + s_{55}T_5 + s_{56}T_6 \\ S_6 &= s_{61}T_1 + s_{62}T_2 + s_{63}T_3 + s_{64}T_4 + s_{65}T_5 + s_{66}T_6 \end{aligned} \tag{3.26}$$

or

$$S_j = s_{ji}T_i$$

where

$$s_{ij} = \frac{(-1)^{i+j}\Delta_{ij}^c}{\Delta^c} \tag{3.27}$$

for which Δ^c is the determinant of the c_{ij} terms of (3.28) and Δ_{ij}^c the minor obtained by suppressing the ith row and jth column

$$\Delta^c = \begin{vmatrix} c_{11} & c_{12} & c_{13} & c_{14} & c_{15} & c_{16} \\ c_{12} & c_{22} & c_{23} & c_{24} & c_{25} & c_{26} \\ c_{13} & c_{23} & c_{33} & c_{34} & c_{35} & c_{36} \\ c_{14} & c_{24} & c_{34} & c_{44} & c_{45} & c_{46} \\ c_{15} & c_{25} & c_{35} & c_{45} & c_{55} & c_{56} \\ c_{16} & c_{26} & c_{36} & c_{46} & c_{56} & c_{66} \end{vmatrix} \tag{3.28}$$

To derive equations (3.26) from a fundamental thermodynamic potential,

we make use of the Gibbs function G defined as

$$G = U - T_i S_i$$

Since $dU = T_i\, dS_i$, we have

$$dG = T_i\, dS_i - T_i\, dS_i - S_i\, dT_i = -S_i\, dT_i$$

Hence

$$S_i = -\frac{\partial G}{\partial T_i}$$

and

$$s_{ij} = -\frac{\partial G}{\partial T_i\, \partial T_j} = -\frac{\partial G}{\partial T_j\, \partial T_i} = s_{ji} \tag{3.29}$$

Using equations (3.26), the internal energy can be expressed in the form

$$\begin{aligned} 2\Delta U = {} & s_{11}T_1 + 2s_{12}T_1T_2 + 2s_{13}T_1T_3 + 2s_{14}T_1T_4 + 2s_{15}T_1T_5 + 2s_{16}T_1T_6 \\ & + s_{22}T_2^2 + 2s_{23}T_2T_3 + 2s_{24}T_2T_4 + 2s_{25}T_2T_5 + 2s_{26}T_2T_6 \\ & + s_{33}T_3^2 + 2s_{34}T_3T_4 + 2s_{35}T_3T_5 + 2s_{36}T_3T_6 \\ & + s_{44}T_4^2 + 2s_{45}T_4T_5 + 2s_{46}T_4T_6 \\ & + s_{55}T_5^2 + 2s_{56}T_5T_6 \\ & + s_{66}T_6^2 = s_{ij}T_iT_j. \end{aligned} \tag{3.30}$$

3.14 *Isothermal and Adiabatic Elastic Constants*

We have so far considered only the elastic relations that can be measured statically at a constant temperature. The elastic constants are then the isothermal constants. For a rapidly vibrating body, however, there is no chance for heat to equalize and consequently the elastic constants operative are the adiabatic constants determined by the fact that no heat is added or subtracted from any elemental volume. For gases there is a marked difference between the adiabatic and the isothermal constants, but for piezoelectric crystals the difference is small and can usually be neglected.

To investigate the relation existing we can write from the first and second laws of thermodynamics, the relations

$$\begin{aligned} dU = {} & [T_1\, dS_1 + T_2\, dS_2 + T_3\, dS_3 \\ & + T_4\, dS_4 + T_5\, dS_5 + T_6\, dS_6] + \Theta\, d\sigma \end{aligned} \tag{3.31}$$

which expresses the fact that the change in the total energy U is equal to the change in the potential energy plus the added heat energy $dQ = \Theta\, d\sigma$ where Θ is the temperature and σ the entropy.

To express the strains in terms of the stresses and temperature, we make

use of the Gibbs function defined for this case as

$$G = U - T_i S_i - \Theta\sigma \quad \text{or} \quad dG = -S_i\, dT_i - \sigma\, d\Theta$$

Then

$$S_i = -\frac{\partial G}{\partial T_i}; \qquad \sigma = -\frac{\partial G}{\partial \Theta}$$

Developing the strains and entropy in terms of the partial differentials of the stresses and temperature, we have

$$dS_1 = \frac{\partial S_1}{\partial T_1} dT_1 + \frac{\partial S_1}{\partial T_2} dT_2 + \frac{\partial S_1}{\partial T_3} dT_3 + \frac{\partial S_1}{\partial T_4} dT_4 + \frac{\partial S_1}{\partial T_5} dT_5 + \frac{\partial S_1}{\partial T_6} dT_6 + \frac{\partial S_1}{\partial \Theta} d\Theta$$

. . . . . .

$$dS_6 = \frac{\partial S_6}{\partial T_1} dT_1 + \frac{\partial S_6}{\partial T_2} dT_2 + \frac{\partial S_6}{\partial T_3} dT_3 + \frac{\partial S_6}{\partial T_4} dT_4 + \frac{\partial S_6}{\partial T_5} dT_5 + \frac{\partial S_6}{\partial T_6} dT_6 + \frac{\partial S_6}{\partial \Theta} d\Theta \qquad (3.32)$$

$$d\sigma = \frac{\partial \sigma}{\partial T_1} dT_1 + \frac{\partial \sigma}{\partial T_2} dT_2 + \frac{\partial \sigma}{\partial T_3} dT_3 + \frac{\partial \sigma}{\partial T_4} dT_4 + \frac{\partial \sigma}{\partial T_5} dT_5 + \frac{\partial \sigma}{\partial T_6} dT_6 + \frac{\partial \sigma}{\partial \Theta} d\Theta.$$

The partial derivatives of the strains with regard to the stresses are readily seen to be the isothermal elastic compliances. The partial derivatives of the strains by the temperatures are the six temperature coefficients of expansion, or

$$\frac{\partial S_1}{\partial \Theta} = \alpha_1; \qquad \cdots; \qquad \frac{\partial S_6}{\partial \Theta} = \alpha_6. \qquad (3.33)$$

To evaluate the partial derivatives of the entropy with respect to the stresses, we make use of the fact that G is a perfect differential so that

$$\frac{\partial S_i}{\partial \Theta} = -\frac{\partial^2 G}{\partial \Theta\, \partial T_i} = -\frac{\partial^2 G}{\partial T_i\, \partial \Theta} = \frac{\partial \sigma}{\partial T_i} = \alpha_i \qquad (3.34)$$

Finally multiplying the last of equations (3.32) by Θ, and noting that since there are no residual strains or stresses

$$
\begin{aligned}
dS_i &= S_i,\ dT_i = T_i \\
S_1 &= s^{\Theta}_{11}T_1 + s^{\Theta}_{12}T_2 + s^{\Theta}_{13}T_3 + s^{\Theta}_{14}T_4 + s^{\Theta}_{15}T_5 + s^{\Theta}_{16}T_6 + \alpha_1\, d\Theta \\
&\cdots\cdots\cdots\cdots\cdots\cdots\cdots\cdots\cdots\cdots\cdots\cdots\cdots\cdots\cdots\cdots\cdots\cdots\cdots\cdots \\
S_6 &= s^{\Theta}_{16}T_1 + s^{\Theta}_{26}T_2 + s^{\Theta}_{36}T_3 + s^{\Theta}_{46}T_4 + s^{\Theta}_{56}T_5 + s^{\Theta}_{66}T_6 + \alpha_6\, d\Theta \qquad (3.35) \\
dQ &= \Theta\, d\sigma = \Theta[\alpha_1 T_1 + \alpha_2 T_2 + \alpha_3 T_3 + \alpha_4 T_4 + \alpha_5 T_5 + \alpha_6 T_6] \\
&\qquad + \rho C_p\, d\Theta
\end{aligned}
$$

since $\Theta \dfrac{\partial \sigma}{\partial \Theta}$ is the total heat capacity of the unit volume at constant stress, which is equal to ρC_p, where ρ is the density and C_p the heat capacity at constant stress per gram of the material.

To get the adiabatic elastic constants which correspond to no heat loss from the element, or $dQ = 0$, $d\Theta$ can be eliminated from (3.35) giving

$$
\begin{aligned}
S_1 &= s^{\sigma}_{11}T_1 + s^{\sigma}_{12}T_2 + s^{\sigma}_{13}T_3 + s^{\sigma}_{14}T_4 + s^{\sigma}_{15}T_5 + s^{\sigma}_{16}T_6 + (\alpha_1/\rho C_p)\, dQ \\
&\cdots\cdots\cdots\cdots\cdots\cdots\cdots\cdots\cdots\cdots\cdots\cdots\cdots\cdots\cdots\cdots\cdots\cdots\cdots\cdots \qquad (3.36) \\
S_6 &= s^{\sigma}_{16}T_1 + s^{\sigma}_{26}T_2 + s^{\sigma}_{36}T_3 + s^{\sigma}_{46}T_4 + s^{\sigma}_{56}T_5 + s^{\sigma}_{66}T_6 + (\alpha_6/\rho C_p)\, dQ
\end{aligned}
$$

where

$$
s^{\sigma}_{ij} = s^{\Theta}_{ij} - \frac{\alpha_i \alpha_j \Theta}{\rho C_p}. \qquad (3.37)
$$

For example for quartz, the expansion coefficients are

$$
\alpha_1 = 14.3 \times 10^{-6}/°\text{C}; \qquad \alpha_2 = 14.3 \times 10^{-6}/°\text{C}; \qquad \alpha_3 = 7.8 \times 10^{-6}/°\text{C};
$$

$$
\alpha_4 = \alpha_5 = \alpha_6 = 0
$$

The density and specific heat at constant pressure are

$$
\rho = 2.65 \text{ grams/cm}^3; \qquad C_p = 7.37 \times 10^6 \text{ ergs/gram.}
$$

Hence the only constants that differ for adiabatic and isothermal values are

$$
s_{11} = s_{22}; \qquad s_{12}; \qquad s_{13}; \qquad s_{33}.
$$

Taking these values as[1]

$$
s^{\sigma}_{11} = 127.9 \times 10^{-14} \text{ cm}^2/\text{dyne}; \qquad s^{\sigma}_{12} = -15.35 \times 10^{-14};
$$

$$
s^{\sigma}_{13} = 11.0 \times 10^{-14}; \qquad s^{\sigma}_{33} = 95.6 \times 10^{-14}.
$$

We find that the corresponding isothermal values are

$$
s^{\Theta}_{11} = 128.2 \times 10^{-14}; \qquad s^{\Theta}_{12} = -15.04 \times 10^{-14};
$$

$$
s^{\Theta}_{13} = 10.83 \times 10^{-14}; \qquad s^{\Theta}_{33} = 95.7 \times 10^{-14} \text{ cm}^2/\text{dyne}
$$

[1] Mason, W. P., "Quartz Crystal Applications," *B.S.T.J.*, Vol. 22, No. 2, July, 1943; *Quartz Crystals for Electrical Circuits*, Chapter II, D. Van Nostrand Company, Inc., 1946, or Chapter VI of this book.

at 25°C or 298° absolute. These differences are probably smaller than the accuracy of the measured constants.

If we express the stresses in terms of the strains by solving equation (3.35) simultaneously, we find for the stresses

$$\begin{aligned} T_1 &= c_{11}^{\Theta} S_1 + c_{12}^{\Theta} S_2 + c_{13}^{\Theta} S_3 + c_{14}^{\Theta} S_4 + c_{15}^{\Theta} S_5 + c_{16}^{\Theta} S_6 - \lambda_1 \, d\Theta \\ &\cdots\cdots\cdots\cdots\cdots\cdots\cdots\cdots\cdots\cdots\cdots\cdots\cdots\cdots\cdots\cdots \\ T_6 &= c_{16}^{\Theta} S_1 + c_{26}^{\Theta} S_2 + c_{36}^{\Theta} S_3 + c_{46}^{\Theta} S_4 + c_{56}^{\Theta} S_5 + c_{66}^{\Theta} S_6 - \lambda_6 \, d\Theta \end{aligned} \tag{3.38}$$

where

$$\begin{aligned} \lambda_1 &= \alpha_1 c_{11}^{\Theta} + \alpha_2 c_{12}^{\Theta} + \alpha_3 c_{13}^{\Theta} + \alpha_4 c_{14}^{\Theta} + \alpha_5 c_{15}^{\Theta} + \alpha_6 c_{16}^{\Theta} \\ &\cdots\cdots\cdots\cdots\cdots\cdots\cdots\cdots\cdots\cdots\cdots\cdots\cdots\cdots\cdots\cdots \\ \lambda_6 &= \alpha_1 c_{16}^{\Theta} + \alpha_2 c_{26}^{\Theta} + \alpha_3 c_{36}^{\Theta} + \alpha_4 c_{46}^{\Theta} + \alpha_5 c_{56}^{\Theta} + \alpha_6 c_{66}^{\Theta}. \end{aligned}$$

The λ's represent the temperature coefficients of stress when all the strains are zero. The negative sign indicates that a negative stress (a compression) has to be applied to keep the strains zero. If we substitute equations (3.38) in the last of equations (3.35), the relation between increments of heat and temperature, we have

$$\begin{aligned} dQ = \Theta \, d\sigma &= \Theta[\lambda_1 S_1 + \lambda_2 S_2 + \lambda_3 S_3 + \lambda_4 S_4 + \lambda_5 S_5 + \lambda_6 S_6] \\ &+ [\rho C_p - \Theta(\alpha_1 \lambda_1 + \alpha_2 \lambda_2 + \alpha_3 \lambda_3 + \alpha_4 \lambda_4 + \alpha_5 \lambda_5 + \alpha_6 \lambda_6)] \, d\Theta. \end{aligned} \tag{3.39}$$

If we set the strains equal to zero, the size of the element does not change, and hence the ratio between dQ and $d\Theta$ should equal ρ times the specific heat at constant volume C_v. We have therefore the relation

$$\rho[C_p - C_v] = \Theta[\alpha_1 \lambda_1 + \alpha_2 \lambda_2 + \alpha_3 \lambda_3 + \alpha_4 \lambda_4 + \alpha_5 \lambda_5 + \alpha_6 \lambda_6]. \tag{3.40}$$

The relation between the adiabatic and isothermal elastic constants c_{ij} thus becomes

$$c_{ij}^{\sigma} = c_{ij}^{\Theta} + \frac{\lambda_i \lambda_j \Theta}{\rho C_v}. \tag{3.41}$$

Since the difference between the adiabatic and isothermal constants is so small, no differentiation will be made between them in the following sections.

3.2 *Expression for The Elastic, Piezoelectric, Pyroelectric and Dielectric Relations of a Piezoelectric Crystal*

When a crystal is piezoelectric, an internal energy is stored in the crystal when a voltage is applied to the crystal. Hence the energy expressions of (3.31) requires additional terms to represent the increment of

energy dU. If we employ cgs units which have so far been most widely used, as applied to piezoelectric crystals, the energy stored in any unit volume of the crystal is

$$dU = T_1\,dS_1 + T_2\,dS_2 + T_3\,dS_3 + T_4\,dS_4 + T_5\,dS_5 + T_6\,dS_6 + E_1\frac{dD_1}{4\pi} + E_2\frac{dD_2}{4\pi} + E_3\frac{dD_3}{4\pi} + \Theta\,d\sigma \qquad (3.42)$$

where E_1, E_2 and E_3 are the components of the field existing in the crystal and D_1, D_2 and D_3 the components of the electric displacement. In order to avoid using the factor $1/4\pi$ we make the substitution

$$\frac{D}{4\pi} = \delta. \qquad (3.43)$$

The normal component of δ at any bounding surface is δ_0 the surface charge. On the other hand if we employ the mks system of units, the energy of any component is given by $E_n dD_n$ directly and in the following formulation δ can be replaced by D.

There are two logical methods of writing the elastic, piezoelectric, pyroelectric and dielectric relations. One considers the independent variables as the stresses, fields, and temperature, and the dependent variables as the strains, displacements and entropy. The other system considers the strains, displacements and entropy as the fundamental independent variables, and the stresses, fields and temperature as the dependent variables. The second system appears to be more fundamental for ferroelectric types of crystals.

As first pointed out by Mueller,[2] these systems and any others involving three sets of the six variables, can be derived by using the eight thermodynamic potentials given in the following Table IV.

For the second system described above, the proper function is the internal energy function U. From Table IV

$$dU = T_i\,dS_i + E_m\delta_m + \Theta\,d\sigma$$

Then

$$T_i = \frac{\partial U}{\partial S_i}; \qquad E_m = \frac{\partial U}{\partial \delta_m}; \qquad d\Theta = \frac{\partial U}{\partial \sigma} \qquad (3.44)$$

If we develop the stresses, fields and temperature in terms of their

[2] Letter to Piezoelectric Committee.

TABLE IV

Thermodynamic Function	Independent Variables	Differential Relations
Energy, U	S_i, D_m, σ	$dU = T_i\,dS_i + E_m\frac{dD_m}{4\pi} + \Theta\,d\sigma$
Free energy, $A = U - \sigma\Theta$	S_i, D_m, Θ	$dA = T_i\,dS_i + E_m\frac{dD_m}{4\pi} - \sigma\,d\Theta$
Enthalpy, $H = U - S_iT_i - E_m\frac{D_m}{4\pi}$	T_i, E_m, σ	$dH = -S_i\,dT_i - \frac{D_m}{4\pi}dE_m + \Theta\,d\sigma$
Elastic enthalpy, $H_1 = U - S_iT_i$	T_i, D_m, σ	$dH_1 = -S_i\,dT_i + E_m\frac{dD_m}{4\pi} + \Theta\,d\sigma$
Electric enthalpy, $H_2 = U - E_m\frac{D_m}{4\pi}$	S_i, E_m, σ	$dH_2 = T_i\,dS_i - \frac{D_m}{4\pi}dE_m + \Theta\,d\sigma$
Gibbs function, $G = U - S_iT_i - \frac{E_mD_m}{4\pi} - \sigma\Theta$	T_i, E_m, Θ	$dG = -S_i\,dT_i - \frac{D_m}{4\pi}dE_m - \sigma\,d\Theta$
Elastic Gibbs function, $G_1 = U - S_iT_i - \sigma\Theta$	T_i, D_m, Θ	$dG_1 = -S_i\,dT_i + E_m\frac{dD_m}{4\pi} - \sigma\,d\Theta$
Electric Gibbs function, $G_2 = U - E_m\frac{D_m}{4\pi} - \sigma\Theta$	S_i, E_m, Θ	$dG_2 = T_i\,dS_i - \frac{D_m}{4\pi}dE_m - \sigma\,d\Theta$

On occasion all eight sets are of value.

partial derivatives, we can write

$$T_1 = \left(\frac{\partial T_1}{\partial S_1}\right)_{D,\sigma} dS_1 + \left(\frac{\partial T_1}{\partial S_2}\right)_{D,\sigma} dS_2 + \left(\frac{\partial T_1}{\partial S_3}\right)_{D,\sigma} dS_3 + \left(\frac{\partial T_1}{\partial S_4}\right)_{D,\sigma} dS_4 + \left(\frac{\partial T_1}{\partial S_5}\right)_{D,\sigma} dS_5 + \left(\frac{\partial T_1}{\partial S_6}\right)_{D,\sigma} dS_6 + \left(\frac{\partial T_1}{\partial \delta_1}\right)_{S,\sigma} d\delta_1 + \left(\frac{\partial T_1}{\partial \delta_2}\right)_{S,\sigma} d\delta_2 + \left(\frac{\partial T_1}{\partial \delta_3}\right)_{S,\sigma} d\delta_3 + \left(\frac{\partial T_1}{\partial \sigma}\right)_{S,D} d\sigma$$

. . . . . (3.45A)

$$T_6 = \left(\frac{\partial T_6}{\partial S_1}\right)_{D,\sigma} dS_1 + \left(\frac{\partial T_6}{\partial S_2}\right)_{D,\sigma} dS_2 + \left(\frac{\partial T_6}{\partial S_3}\right)_{D,\sigma} dS_3 + \left(\frac{\partial T_6}{\partial S_4}\right)_{D,\sigma} dS_4$$

$$+\frac{\partial T_6}{\partial S_5}\Big)_{D,\sigma} dS_5 + \frac{\partial T_6}{\partial S_6}\Big)_{D,\sigma} dS_6 + \frac{\partial T_6}{\partial \delta_1}\Big)_{S,\sigma} d\delta_1 + \frac{\partial T_6}{\partial \delta_2}\Big)_{S,\sigma} d\delta_2$$
$$+\frac{\partial T_6}{\partial \delta_3}\Big)_{S,\sigma} d\delta_3 + \frac{\partial T_6}{\partial \sigma}\Big)_{S,D} d\sigma$$

$$E_x = E_1 = \frac{\partial E_1}{\partial S_1}\Big)_{D,\sigma} dS_1 + \frac{\partial E_1}{\partial S_2}\Big)_{D,\sigma} dS_2 + \frac{\partial E_1}{\partial S_3}\Big)_{D,\sigma} dS_3 + \frac{\partial E_1}{\partial S_4}\Big)_{D,\sigma} dS_4$$
$$+\frac{\partial E_1}{\partial S_5}\Big)_{D,\sigma} dS_5 + \frac{\partial E_1}{\partial S_6}\Big)_{D,\sigma} dS_6 + \frac{\partial E_1}{\partial \delta_1}\Big)_{S,\sigma} d\delta_1 + \frac{\partial E_1}{\partial \delta_2}\Big)_{S,\sigma} d\delta_2$$
$$+\frac{\partial E_1}{\partial \delta_3}\Big)_{S,\sigma} d\delta_3 + \frac{\partial E_1}{\partial \sigma}\Big)_{S,D} d\sigma$$

. . . . . .

$$E_z = E_3 = \frac{\partial E_3}{\partial S_1}\Big)_{D,\sigma} dS_1 + \frac{\partial E_3}{\partial S_2}\Big)_{D,\sigma} dS_2 + \frac{\partial E_3}{\partial S_3}\Big)_{D,\sigma} dS_3 + \frac{\partial E_3}{\partial S_4}\Big)_{D,\sigma} dS_4$$
$$+\frac{\partial E_3}{\partial S_5}\Big)_{D,\sigma} dS_5 + \frac{\partial E_3}{\partial S_6}\Big)_{D,\sigma} dS_6 + \frac{\partial E_3}{\partial \delta_1}\Big)_{S,\sigma} d\delta_1 + \frac{\partial E_3}{\partial \delta_2}\Big)_{S,\sigma} d\delta_2$$
$$+\frac{\partial E_3}{\partial \delta_3}\Big)_{S,\sigma} d\delta_3 + \frac{\partial E_3}{\partial \sigma}\Big)_{S,D} d\sigma \qquad (3.45B)$$

$$d\Theta = \frac{\partial \Theta}{\partial S_1}\Big)_{D,\sigma} dS_1 + \frac{\partial \Theta}{\partial S_2}\Big)_{D,\sigma} dS_2 + \frac{\partial \Theta}{\partial S_3}\Big)_{D,\sigma} dS_3 + \frac{\partial \Theta}{\partial S_4}\Big)_{D,\sigma} dS_4$$
$$+\frac{\partial \Theta}{\partial S_5}\Big)_{D,\sigma} dS_5 + \frac{\partial \Theta}{\partial S_6}\Big)_{D,\sigma} dS_6 + \frac{\partial \Theta}{\partial \delta_1}\Big)_{S,\sigma} d\delta_1 + \frac{\partial \Theta}{\partial \delta_2}\Big)_{S,\sigma} d\delta_2$$
$$+\frac{\partial \Theta}{\partial \delta_3}\Big)_{S,\sigma} d\delta_3 + \frac{\partial \Theta}{\partial \sigma}\Big)_{S,D} d\sigma.$$

The subscripts under the partial derivatives indicate the quantities kept constant. Subscript D indicates that the electric displacement is held constant, subscript σ indicates that the entropy is held constant, while subscript S indicates that the strains are held constant.

Examining the first equation, we see that the partial derivatives of the stress T_1 by the strains are the elastic constants c_{ij} which determine the ratios between the stress T_1 and the appropriate strain with all other strains equal to zero. To indicate the conditions for the partial derivatives, the superscripts D and σ are given to the elastic constants and they are written $c_{ij}^{D,\sigma}$. The partial derivatives of the stresses by $\delta = D/4\pi$ are the piezoelectric constants h_{ij} which measure the increases in stress necessary to hold the crystal free from strain in the presence of a displacement. Since if the crystal tends to expand on the application of a displacement,

the stress to keep it from expanding has to be a compression or negative stress, the negative sign is given to the h_{ij}^{σ} constants. As the only meaning of the h constants is obtained by measuring the ratio of the stress to $\delta = D/4\pi$ at constant strains, no superscript S is added. However, there is a difference between isothermal and adiabatic piezoelectric constants in general, so that these piezoelectric constants are written h_{ij}^{σ}. Finally the last partial derivatives of the stresses by the entropy σ can be written

$$\frac{\partial T_n}{\partial \sigma}\Big)_{S,D} d\sigma = \frac{1}{\Theta}\frac{\partial T_n}{\partial \sigma}\Big)_{S,D} \Theta\, d\sigma = \frac{1}{\Theta}\frac{\partial T_n}{\partial \sigma}\Big)_{S,D} dQ = -\gamma_n^{S,D}\, dQ$$

where dQ is the added heat. We designate $1/\Theta$ times the partial derivative as $-\gamma_n^{S,D}$ and note that it determines the negative stress (compression) necessary to put on the crystal to keep it from expanding when an increment of heat dQ is added to the crystal. The electric displacement is held constant, and hence the superscripts S and D are used. The first six equations then can be written in the form

$$T_j = c_{j1}^{D,\sigma} S_1 + c_{j2}^{D,\sigma} S_2 + c_{j3}^{D,\sigma} S_3 + c_{j4}^{D,\sigma} S_4 + c_{j5}^{D,\sigma} S_5 + c_{j6}^{D,\sigma} S_6 - h_{1j}^{\sigma}\delta_1 - h_{2j}^{\sigma}\delta_2 - h_{3j}^{\sigma}\delta_3 - \gamma_j^{S,D}\, dQ. \quad (3.46)$$

To evaluate the next three equations involving the fields, we make use of the fact that the expression for dU in equation (3.44) is a perfect differential. As a consequence there are relations between the partial derivatives, namely

$$\frac{\partial T_j}{\partial \delta_n} = \frac{\partial E_n}{\partial S_j}; \qquad \frac{\partial T_j}{\partial \sigma} = \frac{\partial \Theta}{\partial S_j}; \qquad \frac{\partial E_n}{\partial \sigma} = \frac{\partial \Theta}{\partial \delta_n}. \quad (3.47)$$

We note also that

$$\frac{\partial E_m}{\partial \delta_n}\Big)_{S,\sigma} = 4\pi\beta_{mn}^{S,\sigma} \quad (3.48)$$

where β is the so-called "impermeability" matrix obtained from the dielectric matrix ϵ_{nm} by means of the equation

$$\beta_{mn} = \frac{(-1)^{m+n}\Delta^{m,n}}{\Delta} \quad (3.49)$$

where Δ is the determinant

$$\Delta = \begin{vmatrix} \epsilon_{11}, \epsilon_{12}, \epsilon_{13} \\ \epsilon_{12}, \epsilon_{22}, \epsilon_{23} \\ \epsilon_{13}, \epsilon_{23}, \epsilon_{33} \end{vmatrix} \quad (3.50)$$

and $\Delta^{m,n}$ the minor obtained by suppressing the mth row and nth column.

The partial derivatives of the fields by the entropy can be written

$$\frac{\partial E_m}{\partial \sigma}\Big)_{S,D} d\sigma = \frac{1}{\Theta}\frac{\partial E_m}{\partial \sigma}\Big)_{S,D} \Theta\, \delta\sigma = \frac{1}{\Theta}\frac{\partial E_m}{\partial \sigma}\Big)_{S,D} dQ = -q_m^{S,D}\, dQ \quad (3.51)$$

where $q_m^{S,D}$ is a pyroelectric constant measuring the increase in field required to produce a zero charge on the surface when a heat dQ is added to the crystal. Since the voltage will be of opposite sign to the charge generated on the surface of the crystal in the absence of this counter voltage, a negative sign is given to $q_m^{S,D}$.

Finally the last partial derivative

$$\frac{\partial \Theta}{\partial \sigma}\Big)_{S,D} d\sigma = \frac{1}{\Theta}\frac{\partial \Theta}{\partial \sigma}\Big)_{S,D} \Theta\, d\sigma = \frac{1}{\Theta}\frac{\partial \Theta}{\partial \sigma}\Big)_{S,D} dQ = \frac{dQ}{\rho C_v^D} \quad (3.52)$$

represents the ratio of the increase in temperature due to the added amount of heat dQ when the strains and electric displacements are held constant. It is therefore the inverse of the specific heat at constant volume and constant electric displacement per gram of material times the density ρ. Hence the ten equations of equation (3.45) can be written in the generalized forms

$$\begin{aligned}
T_j &= c_{j1}^{D,\sigma} S_1 + c_{j2}^{D,\sigma} S_2 + c_{j3}^{D,\sigma} S_3 + c_{j4}^{D,\sigma} S_4 + c_{j5}^{D,\sigma} S_5 + c_{j6}^{D,\sigma} S_6 \\
&\qquad - h_{1j}^{\sigma}\delta_1 - h_{2j}^{\sigma}\delta_2 - h_{3j}^{\sigma}\delta_3 - \gamma_j^{S,D} dQ \\
E_m &= -h_{m1}^{\sigma} S_1 - h_{m2}^{\sigma} S_2 - h_{m3}^{\sigma} S_3 - h_{m4}^{\sigma} S_4 - h_{m5}^{\sigma} S_5 - h_{m6}^{\sigma} S_6 \\
&\qquad + 4\pi\beta_{m1}^{S,\sigma}\delta_1 + 4\pi\beta_{m2}^{S,\sigma}\delta_2 + 4\pi\beta_{m3}^{S,\sigma}\delta_3 - q_m^{S,D} dQ \qquad (3.53) \\
d\Theta &= -\Theta[\gamma_1^{S,D} S_1 + \gamma_2^{S,D} S_2 + \gamma_3^{S,D} S_3 + \gamma_4^{S,D} S_4 + \gamma_5^{S,D} S_5 + \gamma_6^{S,D} S_6] \\
&\qquad - \Theta[q_1^{S,D}\delta_1 + q_2^{S,D}\delta_2 + q_3^{S,D}\delta_3] + \frac{dQ}{\rho C_v^D}.
\end{aligned}$$

$$n = 1 \text{ to } 6; \qquad m = 1 \text{ to } 3$$

If, as is usually the case with vibrating crystals, the vibration occurs with no interchange of heat between adjacent elements, $dQ = 0$ and the ten equations reduce to the usual nine given by the general forms

$$\begin{aligned}
T_j &= c_{j1}^{D} S_1 + c_{j2}^{D} S_2 + c_{j3}^{D} S_3 + c_{j4}^{D} S_4 + c_{j5}^{D} S_5 + c_{j6}^{D} S_6 \\
&\qquad - h_{1j}\delta_1 - h_{2j}\delta_2 - h_{3j}\delta_3 \qquad (3.54) \\
E_m &= -h_{m1} S_1 - h_{m2} S_2 - h_{m3} S_3 - h_{m4} S_4 - h_{m5} S_5 - h_{m6} S_6 \\
&\qquad + 4\pi\beta_{m1}^{S}\delta_1 + 4\pi\beta_{m2}^{S}\delta_2 + 4\pi\beta_{m3}^{S}\delta_3.
\end{aligned}$$

In these equations the superscript σ has been dropped since the ordinary constants are adiabatic. The tenth equation of (3.53) determines the

increase in temperature caused by the strains and displacements in the absence of any flow of heat.

The other form for writing the elastic, piezoelectric, pyroelectric and dielectric relations is to take the strains, displacements, and entropy as the fundamental variables and the stresses, fields and temperature increments as the dependent variables. These can be developed from the thermodynamic variable G of Table IV by employing the relation

$$S_i = -\frac{\partial G}{\partial T_i}; \qquad E_m = -\frac{\partial G}{\partial E_m}; \qquad d\sigma = -\frac{\partial G}{\partial \Theta} \tag{3.55}$$

If we develop S_i, E_m and $d\sigma$ in terms of their partial derivatives, and use the relations between the partial derivatives shown by equation (3.56) (which follow from the fact that G is a perfect differential)

$$\frac{\partial \delta_m}{\partial T_j} = \frac{\partial S_j}{\partial E_m}; \qquad \frac{\partial S_j}{\partial \Theta} = \frac{\partial \sigma}{\partial T_j}; \qquad \frac{\partial \delta_m}{\partial \Theta} = \frac{\partial \sigma}{\partial E_m} \tag{3.56}$$

and substitute for the partial derivatives their equivalent elastic, piezoelectric, pyroelectric, temperature expansions, dielectric and specific heat constants, there are 10 equations of the form

$$\begin{aligned} S_i = {} & s_{i1}^{E,\Theta} T_1 + s_{i2}^{E,\Theta} T_2 + s_{i3}^{E,\Theta} T_3 + s_{i4}^{E,\Theta} T_4 + s_{i5}^{E,\Theta} T_5 + s_{i6}^{E,\Theta} T_6 + d_{1i}^{\Theta} E_1 \\ & + d_{2i}^{\Theta} E_2 + d_{3i}^{\Theta} E_3 + \alpha_i^E \, d\Theta \end{aligned}$$

$$\begin{aligned} \delta_m = {} & d_{m1}^{\Theta} T_1 + d_{m2}^{\Theta} T_2 + d_{m3}^{\Theta} T_3 + d_{m4}^{\Theta} T_4 + d_{m5}^{\Theta} T_5 + d_{m6}^{\Theta} T_6 \\ & + \frac{\epsilon_{m1}^{T,\Theta}}{4\pi} E_1 + \frac{\epsilon_{m2}^{T,\Theta}}{4\pi} E_2 + \frac{\epsilon_{m3}^{T,\Theta}}{4\pi} E_3 + p_m^T \, d\Theta \end{aligned} \tag{3.57}$$

$$\begin{aligned} dQ = \Theta \, d\sigma = {} & \Theta[\alpha_1^E T_1 + \alpha_2^E T_2 + \alpha_3^E T_3 + \alpha_4^E T_4 + \alpha_5^E T_5 + \alpha_6^E T_6] \\ & + \Theta[p_1^T E_1 + p_2^T E_2 + p_3^T E_3] + \rho C_p^E \, d\Theta. \end{aligned}$$

$$n = 1 \text{ to } 6, \qquad m = 1 \text{ to } 3$$

The superscripts E, Θ, and T indicate respectively constant field, constant temperature and constant stress for the measurements of the respective constants. It will be noted that the elastic compliance and the piezoelectric constants d_{mn} are for isothermal conditions. The α^E constants are the temperature expansion constants measured at constant field, while the p^T constants are the pyroelectric constants relating the ratio of $\delta = D/4\pi$ to increase in temperature $d\Theta$, measured at constant stress. Since there is constant stress, these constants take into account not only the " true " pyroelectric effect which is the ratio of $\delta = D/4\pi$ to the temperature at constant volume, but also the so-called " false " pyroelectric effect of the first kind which is the polarization caused by the temperature expansion of

the crystal. This appears to be a misnomer. A better designation for the two effects is the pyroelectric effect at constant strain and the pyroelectric effect at constant stress. C_p^E is the specific heat at constant pressure and constant field.

The adiabatic equations holding for a rapidly vibrating crystal can be obtained by setting dQ equal to zero in the last of equations (3.57) and eliminating $d\Theta$ from the other nine equations. The resulting equations are

$$\begin{aligned} S_i &= s_{i1}^E T_1 + s_{i2}^E T_2 + s_{i3}^E T_3 + s_{i4}^E T_4 \\ &\quad + s_{i5}^E T_5 + s_{i6}^E T_6 + d_{1i} E_1 + d_{2i} E_2 + d_{3i} E_3 \\ \delta_m &= d_{m1} T_1 + d_{m2} T_2 + d_{m3} T_3 + d_{m4} T_4 \\ &\quad + d_{m5} T_5 + d_{m6} T_6 + \frac{\epsilon_{m1}^T}{4\pi} E_1 + \frac{\epsilon_{m2}^T}{4\pi} E_2 + \frac{\epsilon_{m3}^T}{4\pi} E_3 \end{aligned} \tag{3.58}$$

where the symbol σ for adiabatic is understood and where the relations between the isothermal and adiabatic constants are given by

$$s_{ij}^{E,\sigma} = s_{ij}^{E,\Theta} - \frac{\alpha_i^E \alpha_j^E \Theta}{\rho C_p^E}; \qquad d_{im}^{\sigma} = d_{im}^{\Theta} - \frac{\alpha_i^E p_m^T \Theta}{\rho C_p^E}; \qquad \frac{\epsilon_{mn}^{T,\sigma}}{4\pi} = \frac{\epsilon_{mn}^{T,\Theta}}{4\pi} - \frac{p_m^T p_n^T \Theta}{\rho C_p^E}. \tag{3.59}$$

Hence the piezoelectric and dielectric constants are identical for isothermal and adiabatic conditions provided the crystal is not pyroelectric, but differ if the crystal is pyroelectric. The difference between the adiabatic and isothermal elastic compliances was discussed in section (3.14) and was shown to be small. Hence the equations in the form (3.58) are generally used in discussing piezoelectric crystals.

Two other forms of the piezoelectric equations are also used. For adiabatic conditions they can be developed by employing the thermodynamic potentials H_2 and H_1 of Table IV and can be written in the form

$$\begin{aligned} T_j &= c_{ij}^E S_i - e_{mj} E_m \\ \frac{D_n}{4\pi} = \delta_n &= e_{ni} S_i + \frac{\epsilon_{mn}^S}{4\pi} E_m \end{aligned} \tag{3.60}$$

$$\begin{aligned} S_i &= s_{ij}^D T_j + g_{ni} \delta_n \\ E_m &= 4\pi \beta_{mn}^T \delta_n - g_{mj} T_j \end{aligned} \tag{3.61}$$

The four piezoelectric constants d, e, g and h thus defined are all related, but each represents a different aspect of the piezoelectric relationship and is useful for a particular set of conditions. For example, d measures the strain in a free crystal for a given applied field, e the stress developed by a given field when the crystal is clamped, g the open-circuit voltage for a

given stress, and h the open-circuit voltage for a given strain. As shown in the appendix, there are relationships between them that can be written in the form

$$\begin{aligned} d_{nj} &= \frac{\epsilon^T_{mn}}{4\pi} g_{mj} = e_{ni} s^E_{ij} \\ e_{nj} &= \frac{\epsilon^S_{mn}}{4\pi} h_{mj} = d_{ni} c^E_{ij} \qquad \begin{matrix} m, n = 1 \text{ to } 3 \\ i, j = 1 \text{ to } 6 \end{matrix} \\ g_{nj} &= 4\pi \beta^T_{mn} d_{mj} = h_{ni} s^D_{ij} \\ h_{nj} &= 4\pi \beta^S_{mn} e_{mj} = g_{ni} c^D_{ij} \end{aligned} \tag{3.62}$$

where as before a repeated suffix indicates a summation.

In general, equations of the form (3.58) and (3.60) are more convenient for nonferroelectric type crystals, while equations of the form (3.54) and (3.61) are more convenient for ferroelectric types of crystals.

3.3 *Effect of Symmetry on the Dielectric Piezoelectric and Elastic Constants of Crystals*

All crystals can be divided into 32 classes depending on the type of symmetry. These groups can be divided into seven general classifications depending on how the axes are related and furthermore all 32 classes can be built out of symmetries based on twofold (binary) axes, threefold (trigonal) axes, fourfold axes of symmetry, sixfold axes of symmetry, planes of reflection symmetry and combinations of axis reflection symmetry besides a simple symmetry through the center. Each of these types of symmetry result in a reduction of the number of dielectric, piezoelectric, and elastic constants.

Since the tensor method discussed in the appendix lends itself most easily to a transformation from one system of axes to another, the effect of symmetries in reducing the number of fundamental constants and providing relationships between others is dealt with there. The results of these transformations for the various crystal classes are given in the following equations.

3.31 *Second Rank Tensors for Crystal Classes*

The symmetry relations have been calculated for all classes of crystals. For a second-rank tensor such as ϵ_{ij}, the following forms are required

Triclinic

$$\begin{vmatrix} \epsilon_{11}, \epsilon_{12}, \epsilon_{13} \\ \epsilon_{12}, \epsilon_{22}, \epsilon_{23} \\ \epsilon_{13}, \epsilon_{23}, \epsilon_{33} \end{vmatrix} \tag{3.63}$$

Monoclinic	$\begin{vmatrix} \epsilon_{11}, 0, \epsilon_{13} \\ 0, \epsilon_{22}, 0 \\ \epsilon_{13}, 0, \epsilon_{33} \end{vmatrix}$
Orthorhombic	$\begin{vmatrix} \epsilon_{11}, 0, 0 \\ 0, \epsilon_{22}, 0 \\ 0, 0, \epsilon_{33} \end{vmatrix}$
Tetragonal, Trigonal Hexagonal	$\begin{vmatrix} \epsilon_{11}, 0, 0 \\ 0, \epsilon_{11}, 0 \\ 0, 0, \epsilon_{33} \end{vmatrix}$
Cubic	$\begin{vmatrix} \epsilon_{11}, 0, 0 \\ 0, \epsilon_{11}, 0 \\ 0, 0, \epsilon_{11} \end{vmatrix}$
Transverse isotropy z an axis of rotary symmetry $C_n = n$ where $n = \infty$	$\begin{vmatrix} \epsilon_{11}, 0, 0 \\ 0, \epsilon_{11}, 0 \\ 0, 0, \epsilon_{33} \end{vmatrix}$

(3.63)

3.32 *Third Rank Tensors of the Piezoelectric Type for the Crystal Classes*

Triclinic asymmetric (Class 1) No Symmetry $C_1 = 1$	$\begin{vmatrix} h_{11}, h_{12}, h_{13}, h_{14}, h_{15}, h_{16} \\ h_{21}, h_{22}, h_{23}, h_{24}, h_{25}, h_{26} \\ h_{31}, h_{32}, h_{33}, h_{34}, h_{35}, h_{36} \end{vmatrix}$

Triclinic pinacoidal (center of symmetry) $h = 0$ (Class 2) $S_2 = C_i$ or $\bar{1}$

Monoclinic sphenoidal (Class 3) y is binary axis $C_2 = 2$	$\begin{vmatrix} 0, 0, 0, h_{14}, 0, h_{16} \\ h_{21}, h_{22}, h_{23}, 0, h_{25}, 0 \\ 0, 0, 0, h_{34}, 0, h_{36} \end{vmatrix}$
Monoclinic domatic (Class 4) y plane is plane of symmetry $C_s = m = \bar{2}$	$\begin{vmatrix} h_{11}, h_{12}, h_{13}, 0, h_{15}, 0 \\ 0, 0, 0, h_{24}, 0, h_{26} \\ h_{31}, h_{32}, h_{33}, 0, h_{35}, 0 \end{vmatrix}$

Monoclinic prismatic (center of symmetry) $h = 0$ (Class 5) $C_{2h} = \dfrac{2}{m}$

(3.64)

Orthorhombic disphenoidal (Class 6) x, y, z binary axes $V = D_2$ or 222	$\begin{vmatrix} 0, 0, 0, h_{14}, 0, 0 \\ 0, 0, 0, 0, h_{25}, 0 \\ 0, 0, 0, 0, 0, h_{36} \end{vmatrix}$
Orthorhombic pyramidal (Class 7) z binary, x, y, planes of symmetry $C_{2v} = 2mm$	$\begin{vmatrix} 0, 0, 0, 0, h_{15}, 0 \\ 0, 0, 0, h_{24}, 0, 0 \\ h_{31}, h_{32}, h_{33}, 0, 0, 0 \end{vmatrix}$

Orthorhombic dipyramidal (center of symmetry) $h = 0$ (Class 8)
$V_h = D_{2h}$ or $\frac{2}{m}\frac{2}{m}\frac{2}{m} = mmm$

Tetragonal disphenoidal (Class 9) z is quaternary alternating $S_4 = \bar{4}$	$\begin{matrix} 0, & 0, & 0, & h_{14}, & h_{15}, & 0 \\ 0, & 0, & 0, & -h_{15}, & h_{14}, & 0 \\ h_{31}, & -h_{31}, & 0, & 0, & 0, & h_{36} \end{matrix}$
Tetragonal pyramidal (Class 10) z is quaternary $C_4 = 4$	$\begin{matrix} 0, & 0, & 0, & h_{14}, & h_{15}, & 0 \\ 0, & 0, & 0, & h_{15}, & -h_{14}, & 0 \\ h_{31}, & h_{31}, & h_{33}, & 0, & 0, & 0 \end{matrix}$
Tetragonal scalenohedral (Class 11) z quaternary, x and y binary $V_d = D_{2d} = \bar{4}2m$	$\begin{matrix} 0, & 0, & 0, & h_{14}, & 0, & 0 \\ 0, & 0, & 0, & 0, & h_{14}, & 0 \\ 0, & 0, & 0, & 0, & 0, & h_{36} \end{matrix}$
Tetragonal trapezohedral (Class 12) z quaternary, x and y binary $D_4 = 422$	$\begin{matrix} 0, & 0, & 0, & h_{14}, & 0, & 0 \\ 0, & 0, & 0, & 0, & -h_{14}, & 0 \\ 0, & 0, & 0, & 0, & 0, & 0 \end{matrix}$

Tetragonal dipyramidal (center of symmetry) $h = 0$ (Class 13) $C_{4h} = \frac{4}{m}$

Ditetragonal pyramidal (Class 14) z quaternary, x and y planes of symmetry $C_{4v} = 4mm$	$\begin{matrix} 0, & 0, & 0, & 0, & h_{15}, & 0 \\ 0, & 0, & 0, & h_{15}, & 0, & 0 \\ h_{31}, & h_{31}, & h_{33}, & 0, & 0, & 0 \end{matrix}$ (3.64)

Ditetragonal dipyramidal (center of symmetry) $h = 0$ (Class 15)
$D_{4h} = \frac{4}{m}\,mm = \frac{4}{m}\frac{2}{m}\frac{2}{m}$

Trigonal pyramidal (Class 16) z trigonal axis $C_3 = 3$	$\begin{matrix} h_{11}, & -h_{11}, & 0, & h_{14}, & h_{15}, & -h_{22} \\ -h_{22}, & h_{22}, & 0, & h_{15}, & -h_{14}, & -h_{11} \\ h_{31}, & h_{31}, & h_{33}, & 0, & 0, & 0 \end{matrix}$

Trigonal rhombohedral (Class 17) center of symmetry, $h = 0$, $C_{3i} = \bar{3}$

Trigonal trapezohedral (Class 18), z trigonal, x binary $D_3 = 32$	$\begin{matrix} h_{11}, & -h_{11}, & 0, & h_{14}, & 0, & 0 \\ 0, & 0, & 0, & 0, & -h_{14}, & -h_{11} \\ 0, & 0, & 0, & 0, & 0, & 0 \end{matrix}$
Trigonal dipyramidal (Class 19), z trigonal, plane of symmetry $C_{3h} = \bar{6}$	$\begin{matrix} h_{11}, & -h_{11}, & 0, & 0, & 0, & -h_{22} \\ -h_{22}, & h_{22}, & 0, & 0, & 0, & -h_{11} \\ 0, & 0, & 0, & 0, & 0, & 0 \end{matrix}$

Ditrigonal pyramidal (Class 20) z trigonal, y plane of symmetry
$C_{3v} = 3m$

$$\begin{vmatrix} 0, & 0, 0, 0, & h_{15}, & -h_{22} \\ -h_{22}, & h_{22}, 0, & h_{15}, & 0, & 0 \\ h_{31}, & h_{31}, h_{33}, 0, & 0, & 0 \end{vmatrix}$$

Ditrigonal scalenohedral (Class 21) center of symmetry, $h = 0, \bar{3}\frac{2}{m} = D_{3d}$

Ditrigonal dipyramidal (Class 22) z trigonal, z plane of symmetry and y plane of symmetry
$D_{3h} = \bar{6}m2$

$$\begin{vmatrix} h_{11}, & -h_{11}, 0, 0, & 0, & 0 \\ 0, & 0, 0, 0, & 0, & -h_{11} \\ 0, & 0, 0, 0, & 0, & 0 \end{vmatrix}$$

Hexagonal pyramidal (Class 23) z hexagonal
$C_6 = 6$

$$\begin{vmatrix} 0, & 0, 0, h_{14}, & h_{15}, & 0 \\ 0, & 0, 0, h_{15}, & -h_{14}, & 0 \\ h_{31}, & h_{31}, h_{33}, 0, & 0, & 0 \end{vmatrix}$$

Hexagonal trapezohedral (Class 24) z hexagonal, x binary
$D_6 = 622$

$$\begin{vmatrix} 0, & 0, 0, h_{14}, & 0, & 0 \\ 0, & 0, 0, 0, & -h_{14}, & 0 \\ 0, & 0, 0, 0, & 0, & 0 \end{vmatrix} \tag{3.64}$$

Hexagonal dipyramidal (Class 25) center of symmetry, $h = 0$, $C_{6h} = \frac{6}{m}$

Dihexagonal pyramidal (Class 26) x hexagonal y plane of symmetry
$C_{6v} = 6mm$

$$\begin{vmatrix} 0, 0, 0, 0, & h_{15}, & 0 \\ 0, 0, 0, & h_{15}, & 0, 0 \\ h_{31}, & h_{31}, h_{33}, & 0, 0, 0 \end{vmatrix}$$

Dihexagonal dipyramidal (Class 27) center of symmetry, $h = 0, D_{6h} = \frac{6}{m}mm$

Cubic tetrahedral-pentagonal-dodecahedral (Class 28) x, y, z binary
$T = 23$

$$\begin{vmatrix} 0, 0, 0, h_{14}, & 0, & 0 \\ 0, 0, 0, 0, & h_{14}, & 0 \\ 0, 0, 0, 0, & 0, & h_{14} \end{vmatrix}$$

Cubic pentagonal-icosi-tetrahedral (Class 29) $h = 0$; $0 = 432$

Cubic, dyakis-dodecahedral (Class 30) center of symmetry, $h = 0$; $T_h = \frac{2}{m}\bar{3} = m3$

Cubic, hexakis-tetrahedral (Class 31) x, y, z quaternary alternating
$T_d = \bar{4}3m$

$$\begin{vmatrix} 0, 0, 0, h_{14}, & 0, & 0 \\ 0, 0, 0, 0, & h_{14}, & 0 \\ 0, 0, 0, 0, & 0, & h_{14} \end{vmatrix}$$

Cubic, hexakis-octahedral (Class 32) center of symmetry, $h = 0$; $O_h = \frac{4}{m}\bar{3}\frac{2}{m}(m3m)$

Transverse isotropy
z an axis of rotary symmetry
$C_n = n$ where $n = \infty$

$$\begin{vmatrix} 0 & 0 & 0 & 0 & h_{15} & 0 \\ 0 & 0 & 0 & h_{15} & 0 & 0 \\ h_{31} & h_{31} & h_{33} & 0 & 0 & 0 \end{vmatrix}$$

These matrices hold for the e and h piezoelectric constants. Because of the definition of shearing strain adopted, the d and g relations for classes 16, 18, 19 and 22 will be somewhat different than for the h symbols given above. In these classes, the d and g matrices will be

Class 16
$$\begin{vmatrix} d_{11} & -d_{11} & 0 & d_{14} & d_{15} & -2d_{22} \\ -d_{22} & d_{22} & 0 & d_{15} & -d_{14} & -2d_{11} \\ d_{31} & d_{31} & d_{33} & 0 & 0 & 0 \end{vmatrix}$$

Class 18
$$\begin{vmatrix} d_{11} & -d_{11} & 0 & d_{14} & 0 & 0 \\ 0 & 0 & 0 & 0 & -d_{14} & -2d_{11} \\ 0 & 0 & 0 & 0 & 0 & 0 \end{vmatrix} \qquad (3.65)$$

Class 19
$$\begin{vmatrix} d_{11} & -d_{11} & 0 & 0 & 0 & -2d_{22} \\ -d_{22} & d_{22} & 0 & 0 & 0 & -2d_{11} \\ 0 & 0 & 0 & 0 & 0 & 0 \end{vmatrix}$$

Class 22
$$\begin{vmatrix} d_{11} & -d_{11} & 0 & 0 & 0 & 0 \\ 0 & 0 & 0 & 0 & 0 & -2d_{11} \\ 0 & 0 & 0 & 0 & 0 & 0 \end{vmatrix}$$

3.33 *Fourth Rank Tensors of the Elastic Type for the Crystal Classes*

Triclinic system (Classes 1 and 2) 21 moduli

$$\begin{vmatrix} c_{11} & c_{12} & c_{13} & c_{14} & c_{15} & c_{16} \\ c_{12} & c_{22} & c_{23} & c_{24} & c_{25} & c_{26} \\ c_{13} & c_{23} & c_{33} & c_{34} & c_{35} & c_{36} \\ c_{14} & c_{24} & c_{34} & c_{44} & c_{45} & c_{46} \\ c_{15} & c_{25} & c_{35} & c_{45} & c_{55} & c_{56} \\ c_{16} & c_{26} & c_{36} & c_{46} & c_{56} & c_{66} \end{vmatrix}$$

The s tensor is entirely analogous (3.66)

Monoclinic system (Classes 3, 4 and 5) 13 moduli

$$\begin{vmatrix} c_{11} & c_{12} & c_{13} & 0 & c_{15} & 0 \\ c_{12} & c_{22} & c_{23} & 0 & c_{25} & 0 \\ c_{13} & c_{23} & c_{33} & 0 & c_{35} & 0 \\ 0 & 0 & 0 & c_{44} & 0 & c_{46} \\ c_{15} & c_{25} & c_{35} & 0 & c_{55} & 0 \\ 0 & 0 & 0 & c_{46} & 0 & c_{66} \end{vmatrix}$$

The s tensor is entirely analogous

Rhombic system (Classes 6, 7 and 8) 9 moduli	c_{11}	c_{12}	c_{13}	0	0	0	The s tensor is entirely analogous
	c_{12}	c_{22}	c_{23}	0	0	0	
	c_{13}	c_{23}	c_{33}	0	0	0	
	0	0	0	c_{44}	0	0	
	0	0	0	0	c_{55}	0	
	0	0	0	0	0	c_{66}	
Tetragonal system, z a fourfold axis (Classes 9, 10, 13) 7 moduli	c_{11}	c_{12}	c_{13}	0	0	c_{16}	The s tensor is entirely analogous
	c_{12}	c_{11}	c_{13}	0	0	$-c_{16}$	
	c_{13}	c_{13}	c_{33}	0	0	0	
	0	0	0	c_{44}	0	0	
	0	0	0	0	c_{44}	0	
	c_{16}	$-c_{16}$	0	0	0	c_{66}	
Tetragonal system, z a fourfold axis, x a twofold axis (Classes 11, 12, 14, 15) 6 moduli	c_{11}	c_{12}	c_{13}	0	0	0	The s tensor is entirely analogous (3.66)
	c_{12}	c_{11}	c_{13}	0	0	0	
	c_{13}	c_{13}	c_{33}	0	0	0	
	0	0	0	c_{44}	0	0	
	0	0	0	0	c_{44}	0	
	0	0	0	0	0	c_{66}	
Trigonal system, z a twofold axis, (Classes 16, 17) 7 moduli	c_{11}	c_{12}	c_{13}	c_{14}	$-c_{25}$	0	The s tensor is analogous except that $s_{46} = 2s_{25}$, $s_{56} = 2s_{14}$, $s_{66} = 2(s_{11} - s_{12})$
	c_{12}	c_{11}	c_{13}	$-c_{14}$	c_{25}	0	
	c_{13}	c_{13}	c_{33}	0	0	0	
	c_{14}	$-c_{14}$	0	c_{44}	0	c_{25}	
	$-c_{25}$	c_{25}	0	0	c_{44}	c_{14}	
	0	0	0	c_{25}	c_{14}	$\frac{c_{11}-c_{12}}{2}$	
Trigonal system, z a trigonal axis, x a binary axis (Classes 18, 20, 21) 6 moduli	c_{11}	c_{12}	c_{13}	c_{14}	0	0	The s tensor is analogous except that $s_{56} = 2s_{14}$, $s_{66} = 2(s_{11} - s_{12})$
	c_{12}	c_{11}	c_{13}	$-c_{14}$	0	0	
	c_{13}	c_{13}	c_{33}	0	0	0	
	c_{14}	$-c_{14}$	0	c_{44}	0	0	
	0	0	0	0	c_{44}	c_{14}	
	0	0	0	0	c_{14}	$\frac{c_{11}-c_{12}}{2}$	
Hexagonal system, z a sixfold axis, x a twofold axis (Classes 19, 22, 23, 24, 25, 26, 27) 5 moduli	c_{11}	c_{12}	c_{13}	0	0	0	The s tensor is analogous except $s_{66} = 2(s_{11} - s_{12})$
	c_{12}	c_{11}	c_{13}	0	0	0	
	c_{13}	c_{13}	c_{33}	0	0	0	
	0	0	0	c_{44}	0	0	
	0	0	0	0	c_{44}	0	
	0	0	0	0	0	$\frac{c_{11}-c_{12}}{2}$	

Cubic system (Classes 28, 29, 30, 31, 32) 3 moduli	c_{11}	c_{12}	c_{12}	0	0	0	The s tensor is entirely analogous
	c_{12}	c_{11}	c_{12}	0	0	0	
	c_{12}	c_{12}	c_{11}	0	0	0	
	0	0	0	c_{44}	0	0	
	0	0	0	0	c_{44}	0	
	0	0	0	0	0	c_{44}	(3.66)
Isotropic bodies, 2 moduli	c_{11}	c_{12}	c_{12}	0	0	0	The s tensor analogous except last three diagonal terms are $2(s_{11}-s_{12})$
	c_{12}	c_{11}	c_{12}	0	0	0	
	c_{12}	c_{12}	c_{11}	0	0	0	
	0	0	0	$\frac{c_{11}-c_{12}}{2}$	0	0	
	0	0	0	0	$\frac{c_{11}-c_{12}}{2}$	0	
	0	0	0	0	0	$\frac{c_{11}-c_{12}}{2}$	
Transverse isotropy $C_n = n$ where $n = \infty$	c_{11}	c_{12}	c_{13}	0	0	0	The s tensor is analogous except $s_{66} = 2(s_{11}-s_{12})$
	c_{12}	c_{11}	c_{13}	0	0	0	
	c_{13}	c_{13}	c_{33}	0	0	0	
	0	0	0	c_{44}	0	0	
	0	0	0	0	c_{44}	0	
	0	0	0	0	0	$\frac{c_{11}-c_{12}}{2}$	

CHAPTER IV

Properties of Crystals Determinable from Small Sizes

A program for measuring the properties of synthetic piezoelectric crystals has been under way at the Bell Laboratories for the last ten years or more and has resulted in a number of publications and produced crystals of interest for the war effort. This search also resulted in the ethylene diamine tartrate (EDT) and di potassium tartrate (DKT) crystals described in Chapter IX. These crystals are finding considerable use in electrical wave filters in place of quartz crystals. It is the purpose of this chapter to describe the methods used for the search and to present data on a number of crystals that have been investigated. While these crystals have not been completely measured, the data for them may find use in predicting the chemical and atomic properties necessary for obtaining the best crystals for meeting definite requirements.

4.1 *Methods for Measuring Small-Sized Crystals*

Since the time and effort necessary to measure and grow large-sized piezoelectric crystals are very considerable, and since special growing techniques are often required for specific crystals, it is a matter of some importance to obtain a method for eliminating non-promising crystals in the small-grain size state, since these are rather easily grown in beakers by spontaneous seeding. Two methods have been used for this purpose, the Giebe and Scheibe click method and a balanced-bridge method first proposed by the writer.

For the Giebe and Scheibe method, a number of grains of the substance are inserted between two electrodes which are placed across the plates of an oscillator, constructed as shown by Fig. 4.1. The frequency of the oscillator is changed by changing the tuning condenser C_1 and if a resonance of one of the piezoelectric crystals occurs near the oscillator frequency, the frequency of the oscillator will be briefly controlled by the crystal resonance. As the condenser is turned further, the natural frequency of the oscillator becomes far enough away from the crystal resonance so that it cannot control the oscillator frequency, and a jump occurs from the crystal frequency to a different frequency controlled by the oscillator constants. This jump in frequency is accompanied by a change in the plate current, so that if a pair of headphones or a loud speaker is attached to the plate

circuit of the oscillator, a click is heard. By changing the oscillator frequency over a wide range, a number of possible resonances will be crossed and a series of clicks obtained. This is entirely a qualitative

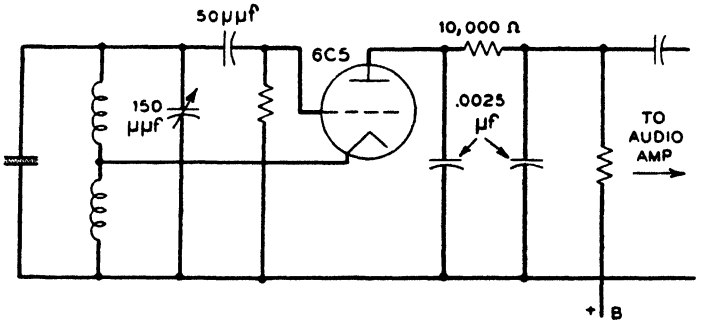

FIG. 4.1. Giebe-Scheibe type oscillator for obtaining indications of piezoelectricity from a crystalline powder.

method since the loudness of the clicks cannot be related to the coupling in the crystal or the crystal Q. It will, however, determine whether a

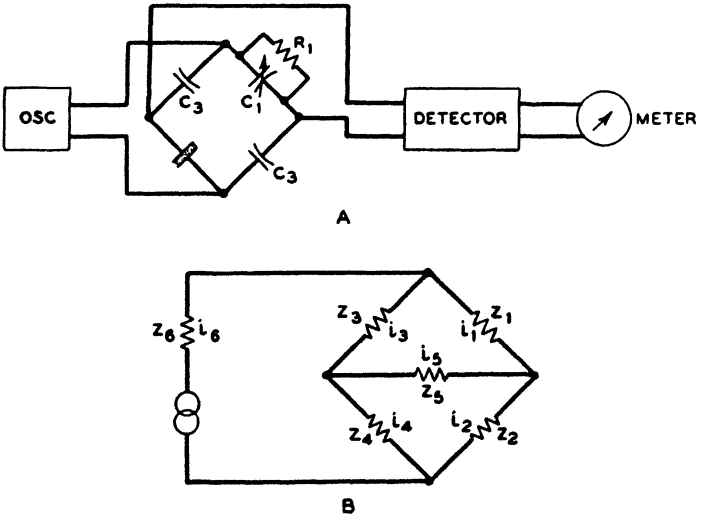

FIG. 4.2. Bridge circuit for obtaining semi-quantitative measurements of piezoelectricity.

crystal is piezoelectric, or not, down to a very small coupling for the crystal.

The bridge method on the other hand is semiquantitative, even for very small-sized crystals. The circuit for the bridge is shown by Fig. 4.2.

Here crystal grains are placed between two electrodes which are placed in one arm of a capacity bridge. An oscillator is connected to the input and a sensitive detector to the output of the bridge. The capacity C_1 is balanced outside the crystal resonance range so that a minimum of current occurs in the detector. As the frequency is changed, the bridge becomes unbalanced as a crystal resonance is approached and the amount of unbalance determines the ratio of the crystal Q to the ratio of capacitances existing for the crystal. For a bridge as shown by Fig. 4.2B, the current in the output is given in terms of the input voltage by the equation

$$i_0 = \frac{E_0[Z_2Z_3 - Z_1Z_4]}{H} \quad \text{where} \quad \begin{aligned} H = {} & (Z_1 + Z_2)Z_3Z_4 \\ & + (Z_3 + Z_4)Z_1Z_2 \\ & + Z_5[(Z_1 + Z_2)(Z_3 + Z_4)] \\ & + Z_6[(Z_1 + Z_3)(Z_2 + Z_4)] \\ & + Z_5Z_6[Z_1 + Z_2 + Z_3 + Z_4] \end{aligned} \tag{4.1}$$

If we let

$$Z_1 = -\frac{j}{\omega C_1}; \qquad Z_2 = Z_3 = -\frac{j}{\omega C_3};$$

$$Z_4 = \frac{-j}{\omega(C_0 + C_2)} \frac{\left[1 - \frac{f^2}{f_R^2} + \frac{jf}{f_R Q}\right]}{\left[1 - \frac{f^2}{f_A^2} + \frac{jf}{f_A Q}\right]} \tag{4.2}$$

where $f_R = \frac{1}{2\pi\sqrt{L_2C_2}}$; $\quad f_A = \frac{1}{2\pi\sqrt{L_2\frac{C_0C_2}{C_0 + C_2}}}$; $\quad Q = \frac{1}{2\pi f_R R}$,

we have the equations for a capacity bridge with a crystal in one arm. Suppose now that C_1, C_3 and $(C_0 + C_2)$ are approximately equal and that the input and output impedances Z_5 and Z_6 are low compared to the impedances of the bridge. Then the current in the detector will be

$$i_0 = E_0 \left[1 - \frac{\left[1 - \frac{f^2}{f_R^2} + \frac{jf}{f_R Q}\right]}{\left[1 - \frac{f^2}{f_A^2} + \frac{jf}{f_A Q}\right]}\right] \Bigg/ \frac{-j}{\omega(C_0 + C_2)} \left[3\frac{\left[1 - \frac{f^2}{f_R^2} + \frac{jf}{f_R Q}\right]}{\left[1 - \frac{f^2}{f_A^2} + \frac{jf}{f_A Q}\right]} - 1\right] \tag{4.3}$$

$$= jE_0\omega(C_0 + C_2)\left[\frac{f^2[f_A^2 - f_R^2] - j\frac{f}{Q}[f_A - f_R]f_A f_R}{2f_A^2 f_R^2 - f^2[3f_R^2 - f_A^2] + \frac{jf}{Q}[3f_A - f_R]f_R f_A}\right].$$

When
$$f^2 = \frac{2f_A^2 f_R^2}{3f_R^2 - f_A^2} \tag{4.4}$$

the denominator nearly vanishes, if the value of Q for the crystal is high, and a large current results. The value of this current at resonance is equal very nearly to

$$i_0 = \frac{E_0}{2}\omega_R(C_0 + C_2)\left[\frac{f_A^2 - f_R^2}{f_R^2}\right]Q = E_0\omega_R(C_0 + C_2)\frac{Q}{2r} \tag{4.5}$$

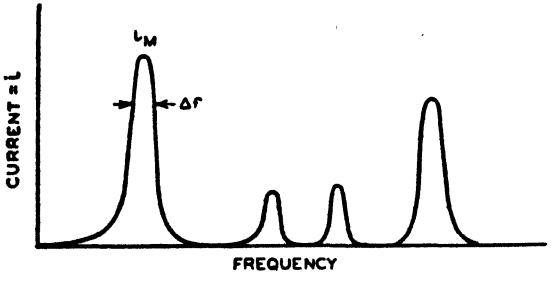

FIG. 4.3. Current in bridge circuit as a function of frequency.

where r is the ratio of capacitances existing for the crystal, which ratio is related to the electromechanical coupling k by the equation

$$r = \frac{\pi^2}{8}\left(\frac{1 - k^2}{k^2}\right) \tag{4.6}$$

The current will vary over a frequency range as shown by Fig. 4.3. The maximum current is proportional to $Q/2r$, and the rapidity with which it decreases from the maximum value is determined by the value of Q for the crystal. This can be measured by determining the frequency separation of the two frequencies 3 db down (or a current ratio of $1/\sqrt{2}$) from the maximum value, with the Q being

$$Q = \frac{f_R}{\Delta f} \tag{4.7}$$

Hence both the Q and the electromechanical coupling could be obtained from this measurement if the orientation and field applied to the crystal

were known. Since small grains are commonly used, these last two factors are not known, and only a qualitative measure of the coupling is possible. If a number of grains of different orientation are present, it is thought that the coupling can be judged within a factor of 3 to 1.

It has become customary to rate the coupling in four categories: zero, weak, moderately strong and strong. From measurements on larger-sized crystals, it has been determined that these categories correspond approximately to the coupling ranges

Zero	Weak	Moderately Strong	Strong
< 1%	1 to 7%	5 to 15%	8% to 30% or higher

A program of selecting and growing promising chemical materials into crystal form has been carried out by A. N. Holden. These have been measured and classified into coupling groups by the writer. The following tables show these classifications for a large number of materials for which the measurements have been completed.

TABLE V

STRONG COUPLING

No.	
1	Acetamide *d*-tartrate
2	Aminoethyl-ethanolamine hydrogen tartrate
3	Ammonium hydrogen tartrate
4	Ammonium hydrogen *dl*-malate
5	Ammonium hydrogen *d*-tartrate-*l*-malate
6	Ammonium arsonyl *d*-tartrate hemihydrate
7	Ammonium lithium *d*-tartrate monohydrate
8	Ammonium oxalate hydrate
9	Benzil
10	1, 3-diaminobutane arsonyl tartrate
11	Dextrose sodium iodide
12	Ethylene diamine arsonyl tartrate
13	Ethylene diamine chromate
14	Ethylene diamine tartrate
15	Ethylene diamine *d*-tartrate
16	Ethylene diamine antimonyl *d*-tartrate
17	Ethylene diamine hydrogen *l*-malate
18	Iodic acid
19	*l*-tyrosine hydrobromide
20	*l*-propylene diamine arsonyl tartrate
21	*l*-tyrosine hydrochloride
22	*l*-hystidine dihydrochloride

TABLE V—*Continued.*

STRONG COUPLING

No.	
23	Lithium thallium tartrate hydrate
24	Lithium rubidium tartrate
25	Methylamine arsonyl tartrate
26	Methylamine hydrogen tartrate
27	Nickel hydrogen *l*-malate dihydrate
28	Nickel selenate hexahydrate
29	Potassium bromate
30	Potassium lithium *d*-tartrate monohydrate
31	Potassium thiochromate
32	Piperidine-acetic acid hydrate
33	Rubidium dihydrogen arsenate
34	Rubidium dihydrogen phosphate
35	Sodium ammonium tartrate
36	Sodium tartrate dihydrate
37	Sodium dihydrogen phosphate dihydrate
38	Sodium rubidium tartrate tetrahydrate
39	Sucrose sodium iodide
40	Tartaric acid
41	Thallium hydrogen tartrate

TABLE VI

MODERATELY STRONG COUPLING

No.	
1	Ammonium tartrate
2	Ammonium pentaborate
3	*d*-mandelic acid
4	*d*-propylene diamine arsonyl tartrate
5	Dextrose sodium chloride
6	Ethylene diamine antimonyl tartrate
7	Ethanolymine hydrogen tartrate
8	Isopropylamine arsonyl tartrate
9	*l*-benzoylalamine
10	*l*-asparagine
11	*l*-tyrosine hydroiodide
12	Methylalamine
13	Morpholine acetic acid
14	Methyl morpholine antimonyl tartrate
15	Potassium pentaborate
16	Rubidium tartrate
17	Silver tartrate thiourea
18	Sodium hydrogen tartrate
19	Urea

TABLE VII

Weak Coupling

No.	
1	Aminoacetic acid
2	Acetamide hydrogen tartrate
3	Ammonium hydrogen *l*-malate
4	Ammonium dimolybdomalate
5	Aminoethyl morpholine arsonyl tartrate
6	Aminoethyl ethanolamine arsonyl tartrate
7	Ammonium iodate
8	Benzophenone
9	Barium nitrate
10	Coumarin
11	Calcium hydrogen *l*-malate hexahydrate
12	Diethylamine hydrogen tartrate
13	Diphenylguanidine tartrate
14	*dl*-alpha-phenylethylamine hydrogen *dl*-malate
15	*d*-alpha-phenylethylamine *l*-malate
16	2, 3-dibromopropylamine hydrogen tartrate
17	Diethylamine arsonyl tartrate
18	1, 3-diaminobutane arsonyl tartrate
19	Dimethylamine hydroiodide
20	Ethylene diamine sulphate
21	Ethanolamine arsonyl tartrate
22	Ethyl propyl piperidinium iodide
23	Guanidine carbonate
24	Hexamethylene tetramine
25	Hippuric acid
26	Hexamethylene tetramine mandelate
27	Hydroxyethyl morpholine arsonyl tartrate
28	Isobutylamine antimonyl tartrate
29	*l*-leucine
30	*l*-histidine monohydrochloride
31	*l*-tyrosine sulphate
32	*m*-nitrobromobenzene
33	Morpholine hydrogen tartrate
34	Morpholine antimonyl tartrate
35	Methylmorpholine hydrogen tartrate
36	Magnesium lead propinate
37	*m*-nitrochlorbenzene
38	Morpholine mandelate
39	Magnesium *l*-malate
40	Morpholine piperidine arsonyl tartrate
41	*n*-butylamine arsonyl tartrate
42	Phthalic anhydride

TABLE VII—*Continued.*

WEAK COUPLING

No.	
43	Potassium antimonyl tartrate-sodium sulphate
44	Potassium antimonyl tartrate-lithium nitrate
45	Piperidine hydrogen tartrate
46	Piperazine tartrate
47	Potassium hydrogen tartrate
48	Piperazine antimonyl tartrate
49	Piperazine hydrogen tartrate
50	Phenyl-*n*-propylamine hydrogen tartrate
51	Propylene diamine hydrogen tartrate
52	Potassium hydrogen *d*-saccharate
53	Piperazine arsonyl tartrate
54	Rubidium hydrogen tartrate
55	Resorcin
56	Silver nitrate succinononitrile
57	Tribenzylamine nitrate
58	Triethylene tetramine hydrobromide
59	Tetramethyl-pyrazine hydrogen tartrate
60	Trans-dimethyl piperazine tartrate
61	Xylose

TABLE VIII

ZERO COUPLING

No.	
1	Aminoethyl-morpholine tartrate
2	Aminoethyl-morpholine mandelate
3	Ammonium antimonyl tartrate hydrate
4	Ammonium hydrogen *o*-sulfobenzoate
5	Acetamide oxalate
6	Acetylphenyl hydrazine
7	Barium thiosulfate-acetate dihydrate
8	Calcium tartrate tetrahydrate
9	Diammonium citrate
10	Diphenyl trisiloxane
11	Diphenyl iodonium chloride
12	*d*-6-6′-dinitro diphenic acid
13	Dimethylamine antimonyl tartrate
14	Dimethylamine arsonyl tartrate
15	*d*-arginine monohydrochloride
16	Dimethyl piperazine
17	Dimethyl piperazine mercurichloride
18	1, 2-Dimorpholino propane dihydrobromide
19	1, 3-Dimorpholino propane dihydrobromide
20	1, 3-Dipperidino propane dihydrobromide

TABLE VIII—*Continued.*

ZERO COUPLING

No.	
21	Dimethyl morpolinium iodide
22	Ethylene diamine thiosulphate acetate
23	Ethyl morpholine hydrogen tartrate
24	Ethylene diamine ethylene diamine tetra acetate
25	Ethylene diamine selanate
26	Ethylene diamine iodate
27	Ethylene diamine primary arsenate
28	Ethylene diamine tetracetic acid hydrochloride
29	Ethyl morpholine arsonyl tartrate
30	Ethyl-α-picolinium iodide
31	Ethylene diamine succinate
32	Ethylene diamine hydrogen *dl*-malate
33	Glycine hydrochloride
34	Glycine tartrate
35	Guanidine aluminum sulphate hexahydrate
36	Hexamethylene tetramine hydrobromide
37	Hydroxyethyl morpholine hydrogen tartrate
38	Hydrazine sulphate
39	Isobutylamine arsonyl tartrate
40	Methylethyl morpholinium iodide
41	Methylamine antimonyl tartrate
42	Methyl-α-picolinium iodide
43	Methylhydroxyethyl morpholinium iodide
44	Methylhydroxyethyl morpholinium arsonyl tartrate
45	Magnesium tartrate pentahydrate
46	Magnesium 2, 5 dichlorbenzol sulfonate octohydrate
47	5-Nitrosalicylic acid
48	5-Nitro 2, 3 di(trichloromethyl) dihydrocoumarone
49	Potassium zinc cyanide
50	Potassium tetraoxalate dihydrate
51	Potassium hydrogen succinate dihydrate
52	*P*-Toluidine hydrochloride
53	*P*-Aminohippuric acid
54	*P*-Chloroacetanilide
55	Phenylthiosemicarbazide
56	Propylene diamine mandelate
57	Piperidine mandelate
58	Potassium amino acetate
59	Phenyltrimethyl ammonium iodide
60	Potassium dibromoacetate
61	Propylene diamine arsonyl racemate
62	Potassium iodate
63	Phenolphthalein diacetate
64	*P*-Nitrobenzoyl piperidine

TABLE VIII—*Continued.*

ZERO COUPLING

No.	
65	Sodium dihydrogen arsenate dihydrate
66	Strontium nitrate-acetate hemitrihydrate
67	Thiomalic acid
68	Triphenyl guanidine hydrogen tartrate
69	Trimethyl sulfonium iodide
70	Tetraethanolammonium hydrogen arsenate perchlorate
71	Tetraethanolammonium hydrogen sulphate
72	Tetra-*p*-tolyl silane
73	Triphenyl methanone
74	Urea nitrate
75	Zinc 2, 5 dichlorbenzolsulfonate octohydrate

4.2 *Properties Determined from Three Small Oriented Plates*

It has been thought worth-while to investigate the properties of all piezoelectric crystals having an electromechanical coupling of 12 to 15 per cent or higher. This is a rather arbitrary division point which was chosen on the basis that since quartz has a 10 per cent coupling, it would require unusually good mechanical properties for a synthetic crystal to compete with quartz; whereas a coupling of 15 per cent or higher would be of interest for types of applications other than these usually satisfied by quartz.

Since the powder method has a probable spread of 3 to 1 in the indicated coupling, it was thought worth-while to interpose an intermediate screening test between the powder test and the measurement of properties of large-scale crystals. This test consists in growing crystals from the powder size up to a size of 3 to 4 millimeters for all dimensions. This size is large enough to cut and handle in a practical manner. W. L. Bond has devised a method of determining the orientation of crystal cuts by means of the optic axes of the crystals. Triclinic, monoclinic, and orthorhombic crystals have two optic axes making an acute angle with respect to each other. By taking three plates perpendicular to the bisectrix of these two axes, parallel to the bisectrix and perpendicular to the plane of the optic axes, three mutually perpendicular sets of plates can be obtained, from which more accurate coupling data can be obtained. For crystals of tetragonal, hexagonal, and trigonal classes, there is one optic axis and crystals cut parallel to this and two other orientations perpendicular to the optic axis at directions determined by the crystal faces, will provide a set of three mutually perpendicular plates which can be used for coupling measurements. While no assurance exists that by measuring the couplings of these mutually perpendicular plates, one obtains the maximum coupling, experience has shown that couplings measured in this way will usually be within 50 per cent of the couplings measured for larger-sized crystals.

TABLE IX

APPROXIMATE MEASURE OF STRONGEST COUPLING

	Material	Crystal System	Strongest Coupling *Per cent*
1	Ammonium tartrate	monoclinic	11.3
2	Ammonium pentaborate	orthorhombic	7.0
3	Ammonium hydrogen-*dl*-malate	orthorhombic	6.1
4	Ammonium hydrogen-*d*-tartrate-*l*-malate	monoclinic	8.6
5	Ammonium oxalate monohydrate	orthorhombic	10.25
6	Ammonium arsonyl-*d*-tartrate hemihydrate	orthorhombic	9.0
7	Aminoethyl ethanolamine hydrogen tartrate	triclinic	16.0
8	*d*-propylene diamine arsonyl tartrate	monoclinic	7.1
9	1, 3-diamine butane arsonyl tartrate	orthorhombic	7.0
10	Dextrose sodium chloride	trigonal trapezohedral	9.0
11	Ethylene diamine antimonyl *d*-tartrate	orthorhombic	8.0
12	Ethylene diamine arsonyl tartrate	orthorhombic	15.4
13	Iodic acid	orthorhombic	25.0
14	Isopropylamine arsonyl tartrate	orthorhombic	11.7
15	Lithium rubidium tartrate	orthorhombic	11.7
16	*l*-asparagine	orthorhombic	12.5
17	*l*-tyrosene hydrochloride	monoclinic	13.2
18	*l*-tyrosene hydrobromide	monoclinic	16.0
19	Lithium thallium tartrate hydrate	orthorhombic	15.8
20	Methylalamine	orthorhombic	6.0
21	Methyl morpholine antimonyl tartrate	orthorhombic	16.0
22	Neutral acetamide tartrate	orthorhombic	8.4
23	Potassium pentaborate	orthorhombic	11.8
24	Piperidine acetic acid hydrate	orthorhombic	9.0
25	Rubidium tartrate	trigonal trapezohedral	6.5
26	Rubidium dihydrogen arsenate	tetragonal	16.4
27	Rubidium dihydrogen phosphate	tetragonal	16.0
28	Sodium dihydrogen phosphate	orthorhombic	5.5
29	Sodium rubidium tartrate	orthorhombic	19.5
30	Sodium ammonium tartrate	orthorhombic	22.7
31	Silver tartrate thiourea	monoclinic	6.2
32	Sodium hydrogen tartrate	monoclinic	11.5
33	Tartaric acid	monoclinic	17.5
34	Thallium hydrogen tartrate	orthorhombic	24.0

For monoclinic and triclinic crystals, measurements of thickness modes are made as well as those for contour modes measured for the other crystal classes.

These measurements have been made by cutting square slabs, evaporating gold over the surface, putting the crystals in a well-shielded holder with all the stray capacitances tied to ground across a low input and output impedance circuit. The resonance and anti-resonance, the static capacitance, and the equivalent resistance of the crystal at resonance, are all measured. From these, the dielectric constant, the ratio of capacitances and the electromechanical coupling can be obtained from the formula

$$\epsilon = \frac{4\pi C_0 \times 9 \times 10^{11} l_c}{A}; \qquad r = \frac{1}{\frac{f_A^2}{f_R^2} - 1}; \qquad k = \frac{1}{\sqrt{1 + \frac{8}{\pi^2} r}}$$

where C_0 is the measured capacitance in farads, l_c the thickness, A the cross-sectional area of the crystal, f_R the resonance frequency, and f_A the anti-resonant frequency. Table IX on page 57 shows measurements of the value of the strongest coupling found for the three mutually perpendicular plates for a number of the strong coupling materials of Tables IV and V.

CHAPTER V

Resonant Measurement of the Properties of Large-Size Crystals

When crystals of a large size are available, the elastic, piezoelectric and dielectric constants can be determined by measuring the electrical impedances of the crystal over a wide frequency range. These constants are measured by cutting out a specified number of crystal plates at various orientations with respect to the natural crystal and measuring the capacitance of the plates at low frequencies, the resonant, and the anti-resonant frequencies. These determine the "free" dielectric constant, the frequency constant and the ratio of capacitances of the crystal. Knowing the density of the crystal, one can calculate the elastic constant pertaining to the mode of motion. By measuring the resistance of the crystal at resonance, a measure of the "Q" is obtained. This is an indication of the internal dissipation of a crystal, if this is high enough to override other sources of dissipation. For most crystals measured, however, it is the mounting losses and the acoustic radiation losses that predominate and determine the crystal Q. Since the application of a crystal depends to quite an extent on the temperature coefficient of frequency and the temperature coefficient of the piezoelectric and dielectric constants, these properties are usually measured over a wide temperature range. Such measurements also provide an indication of the type of dipole operative in the piezoelectric effect, as discussed in section 10.6, Chapter X.

The mode of motion that can be related most easily to the fundamental elastic and piezoelectric constants of the crystal is the longitudinal mode of motion. This follows from the fact that the resonant frequency of a long, thin bar is controlled by the Young's modulus of the bar, and the ratio of capacitances is simply related to the piezoelectric constant, the dielectric constant and the elastic constant. Other simple modes that can be related to the elastic constants are flexure modes and torsional modes, but these require complicated plating arrangements for driving them and hence cannot be used for measuring piezoelectric and dielectric constants. As shown in section 5.2, longitudinal-mode crystals can be used to evaluate all the elastic constants except the shear constants and can be used to evaluate all of the dielectric constants and all of the piezoelectric constants. For evaluating the shear elastic constants, we have a choice of

using face-shear modes or thickness-shear modes. The face-shear mode has been used exclusively for these measurements on account of the greater ease of dimensioning such crystals and because no corrections have to be made for piezoelectric coupling effects. An alternate method for measuring the elastic constants is by using harmonics of thickness modes. This method[1] has been made the basis of an optical method for measuring elastic constants, which consists in using the standing-wave pattern as an optical diffraction grating. From the position of the diffracted light spots, taken for three orientations of the crystal, all of the elastic constants can be determined.

Another method[2] used recently for measuring crystal elasticities is the pulsing ultrasonic method discussed in section 16.3. By sending shear and longitudinal waves down various oriented crystal cuts, all of the elastic constants of a crystal can be calculated. As shown by Huntington,[2] these measurements result in the constant field elastic constants, which, for a ferroelectric type of crystal, vary considerably near the Curie temperature. By means of this method, an indication of the size of a domain can be obtained for a ferroelectric type crystal, such as rochelle salt. This follows from the fact that when a crystal becomes ferroelectric, it breaks up into domains of definite sizes that act as sound-scattering centers; for example, just as metal grains do in aluminum. The data of Fig. A.4 taken at 100 kilocycles, show that the Q of a 45° X-cut rochelle salt crystal drops from 9,000 to 3,000 in the Curie region, due to the sound-scattering power of the domain. This corresponds to an attenuation of 2.5×10^{-4} nepers per centimeter due to sound scattering. From equation (16.49), assuming that the non-homogeneity constant is within the limits 0.001 to 0.1, this results in a domain size within the limits of 0.01 to 1 cubic centimeter. This is about the same size as found by Mueller by an electrostatic method.

The last two methods, the optical diffraction method and the ultrasonic pulse method, give only the elastic constants and do not evaluate the piezoelectric and the dielectric constant. Hence the measurement of the resonant and anti-resonant frequencies of specially oriented crystals still appears to be the best method for obtaining the constants of a piezoelectric crystal, although it may be supplemented by other methods.

5.1 *Calculation of the Resonance and Anti-Resonance Frequencies of a Piezoelectric Crystal in Terms of the Fundamental Constants*

In order to determine the fundamental elastic, piezoelectric and dielectric constants from measurements of capacitances, and the resonance and

[1] Bergman, L., Dr. Ultraschall, J. W. Edwards, 1942.

[2] Huntington, H. B., "Measurements of Crystal Elasticities by a Pulse Method," *Phys. Rev.*, Vol. 72, No. 4, pp. 321–332, August 15, 1947.

anti-resonance frequencies, a calculation of these quantities is made from the fundamental relationships given in Chapter III. For a plated crystal, the type of equation that satisfies the boundary conditions best is the Voigt type expressed in terms of the electrical field. This follows because for a plated crystal the tangential electric fields vanish and the only component left is the normal component. It is the purpose of this section to calculate these quantities for longitudinal and face-shear modes.

5.11 *Longitudinally Vibrating Piezoelectric Crystals*

In obtaining the elastic and piezoelectric constants of a crystal, it is necessary to vibrate the crystal in a simple mode of motion and determine the constants, from the measured resonant and anti-resonant frequencies and the capacitance of the crystal measured at low frequencies. The simplest mode of motion, and the one most easily related to the crystal constants, is the simple longitudinal mode. According to a recent convention in specifying crystal cuts, the thickness is taken along the z- or x_3-axis of the crystal, the length along the x- or x_1-axis, while the width lies along the y- or x_2-axis. If we take z as the thickness direction and apply plating to the surfaces normal to this axis, the only value of surface charge different from zero will be δ_3, since no electric connections are made to the other surfaces. Since z is assumed small, the voltage gradient $\partial E_3/\partial z$ will be a constant throughout the thickness of the crystal. Also, since the plating is an equipotential surface, E_3 will not vary with x or y directions and

$$\frac{\partial E_3}{\partial x} = \frac{\partial E_3}{\partial y} = 0 \tag{5.1}$$

For sides normal to the thickness, the stresses on the surface are zero. Using the matrix notation of Chapter III, this is expressed by setting the stresses

$$T_3 = T_4 = T_5 = 0 \tag{5.2}$$

Since the thickness is taken as small and all the stresses are zero on the two surfaces normal to z, these stresses cannot differ appreciably from zero in the interior and hence we can set

$$T_3 = T_4 = T_5 = 0 \tag{5.3}$$

for all elements of the crystal. Similarly, since the width is considered very small, the stresses

$$T_2 = T_4 = T_6 = 0 \tag{5.4}$$

For the length, the only finite dimension, the stresses on the surface are

$$T_1, \quad T_5, \quad T_6 \tag{5.5}$$

of these T_5 and T_6 have already been found to be zero so that the only stress different from zero in the interior is T_1.

The equation of motion for such a bar can be derived from Newton's law of motion, and the piezoelectric relation of equation (3.1). In vector form, Newton's law can be written

$$\rho \frac{\partial^2 \xi_k}{\partial t^2} dx\, dy\, dz = F_k \tag{5.6}$$

where ξ_k are the displacements of the elementary cube $dx\ dy\ dz$ in the directions x, y and z, F_k are the components of force in these directions exerted on the elementary cube, and ρ is the density of the material in the cube. From elastic theory as discussed in Chapter III, equations (3.5) and (3.6), we have that the total resultant force along the x direction is the partial derivative of the stresses or

$$F_1 = \left[\frac{\partial T_1}{\partial x} + \frac{\partial T_6}{\partial y} + \frac{\partial T_5}{\partial z}\right] dx\, dy\, dz \tag{5.7}$$

Similarly, for the other two directions,

$$\begin{aligned} F_2 &= \left[\frac{\partial T_6}{\partial x} + \frac{\partial T_2}{\partial y} + \frac{\partial T_4}{\partial z}\right] dx\, dy\, dz, \\ F_3 &= \left[\frac{\partial T_5}{\partial x} + \frac{\partial T_4}{\partial y} + \frac{\partial T_3}{\partial z}\right] dx\, dy\, dz \end{aligned} \tag{5.8}$$

These can be expressed in the general tensor form

$$F_k = \frac{\partial T_{kl}}{\partial x_k} dx_k \tag{5.9}$$

Hence the equations of motion become

$$\rho \frac{\partial^2 \xi_k}{\partial t^2} = \frac{\partial T_{kl}}{\partial x_k} \tag{5.10}$$

For the longitudinal bar with its length along x, the only stress different from zero is T_1, and hence the only equation of motion for this bar is

$$\rho \frac{\partial^2 \xi_1}{\partial t^2} = \frac{\partial T_1}{\partial y} \tag{5.11}$$

Since T_1 is the only stress, the corresponding strains are given by equation (3.58), the first part. For the case of interest here $j = 1$ and since a charge is developed only in the z direction, $n = 3$. Hence we have

$$S_1 = s_{11}^E T_1 + d_{31} E_3$$

In particular, the stress T_1 can be specified by a single strain, all the other strains being related dependently on this one. Taking the strain S_1, since it is simply related to the displacement ξ_1, we can write

$$S_1 = s_{11}^E T_1 + d_{31} E_3$$

or

$$T_1 = \frac{S_1}{s_{11}^E} - \frac{d_{31} E_3}{s_{11}^E} \tag{5.13}$$

The electrical relations of equation (3.58) reduce to the form

$$\delta_n = \frac{\epsilon_{n3}^T}{4\pi} E_3 + d_{n1} T_1 = \left(\frac{\epsilon_{n3}^T}{4\pi} - \frac{d_{n1} d_{31}}{s_{11}^E} \right) E_3 + \frac{d_{n1}}{s_{11}^E} S, \tag{5.14}$$

The only charge of interest is the one in the z direction, which is the direction of the applied field. Hence

$$\delta_3 = \left[\frac{\epsilon_{33}^T}{4\pi} - \frac{d_{31}^2}{s_{11}^E} \right] E_3 + \frac{d_{31}}{s_{11}^E} S_1 \tag{5.15}$$

Finally, we call the expression

$$\frac{\epsilon_{33}^T}{4\pi} - \frac{d_{31}^2}{s_{11}^E} = \frac{\epsilon_{33}^{LC}}{4\pi} = \frac{\epsilon_{33}^{S_1}}{4\pi} \tag{5.16}$$

indicating that it is the longitudinally clamped dielectric constant which relates the potential and surface charge when the crystal is clamped so that S_1 disappears.

In terms of the two index symbols, the two piezoelectric and elastic relations can be written

$$\begin{aligned} \rho \frac{\partial^2 \xi_1}{\partial t^2} &= \frac{1}{s_{11}^E} \frac{\partial^2 \xi_1}{\partial x^2} + \frac{d_{31}}{s_{11}^E} \frac{\partial E_3}{\partial x} \\ \delta_3 &= \frac{\epsilon_{33}^{LC}}{4\pi} E_3 + \frac{d_{31}}{s_{11}^E} \frac{\partial \xi_1}{\partial x} \end{aligned} \tag{5.17}$$

To solve this equation, we note that E_3 is a constant independent of x since the plating forms an equipotential surface. Hence the equation of motion becomes

$$\rho \frac{\partial^2 \xi_1}{\partial t^2} = \frac{1}{s_{11}^E} \frac{\partial^2 \xi_1}{\partial x^2} \tag{5.18}$$

For simple harmonic motion, the variation of ξ_1 with time can be written in the usual form

$$\xi_1 = \xi e^{j\omega t} \tag{5.19}$$

so that for simple harmonic motion equation (5.18) becomes

$$\frac{d^2\xi}{dx^2} - \omega^2 \rho s_{11}^E \xi = \frac{d^2\xi}{dx^2} - \frac{\omega^2}{v^2}\xi = 0 \tag{5.20}$$

where v, the velocity of a plated crystal, is given by the formula

$$v^2 = 1/\rho s_{11}^E \tag{5.21}$$

A solution of equation (5.20) with two arbitrary boundary conditions is

$$\xi = A \cos \frac{\omega x}{v} + B \sin \frac{\omega x}{v} \tag{5.22}$$

To determine the constants A and B, use is made of equation (5.13). Differentiating equation (5.22)

$$\frac{d\xi}{dx} = S_1 = \frac{\omega}{v}\left[-A \sin \frac{\omega x}{v} + B \cos \frac{\omega x}{v} \right] = s_{11}^E T_1 + d_{31} E_3 \tag{5.23}$$

When $x = 0$ and $x = l$ the crystal length, for a free crystal, the stress

$$T_1 = 0 \tag{5.24}$$

Under these conditions

$$\frac{\omega}{v} B = d_{31} E_3 \text{ and } \frac{\omega}{v}\left[-A \sin \frac{\omega l}{v} + B \cos \frac{\omega l}{v} \right] = d_{31} E_3 \tag{5.25}$$

Solving for the constants A and B and substituting in equation (5.23),

$$\begin{aligned} S_1 &= d_{31} E_3 \left[\cos \frac{\omega x}{v} + \frac{\left(1 - \cos \frac{\omega l}{v}\right)}{\sin \frac{\omega l}{v}} \sin \frac{\omega x}{v} \right] \\ &= d_{31} E_3 \left[\frac{\sin \frac{\omega (l - x)}{v} + \sin \frac{\omega x}{v}}{\sin \frac{\omega l}{v}} \right] \end{aligned} \tag{5.26}$$

The electrical impedance measured at the terminals of the plated crystal is then determined by substituting the value of $S_1 = \partial \xi_1 / \partial x$ in the last of equations (5.17). This gives $\delta_3 = D_3/4\pi$, where D_3 is the electric displacement in the z direction. Since the normal component of the displacement $/4\pi$ equals the surface charge, δ_3 then represents the charge on the surface of the crystal. The current into the crystal is the rate of change

of the surface charge with time, and for a simple harmonic voltage is given by

$$i = j\omega \int \delta_3 \, dS = j\omega l_w \int_0^l \delta_3 \, dx = j\omega l_w \int_0^l \left[\frac{\epsilon_{33}^{LC}}{4\pi} E_3 + \frac{d_{31}}{s_{11}^E} S_1 \right] dx \quad (5.27)$$

Introducing the value of S_1 from (5.26) and integrating from 0 to l, we have

$$i = j\omega l_w l \left[\frac{\epsilon_{33}^{LC}}{4\pi} + \frac{d_{31}^2}{s_{11}^E} \left(\frac{\tan \dfrac{\omega l}{2v}}{\dfrac{\omega l}{2v}} \right) \right] E_3 \quad (5.28)$$

The admittance of the free crystal is then

$$\frac{1}{Z} = \frac{i}{E} = \frac{i}{E_3 l_t} = \frac{j\omega l_w l \epsilon_{33}^{LC}}{4\pi l_t} \left[1 + \frac{4\pi d_{31}^2}{\epsilon_{33}^{LC} s_{11}^E} \left(\frac{\tan \omega l/2v}{\omega l/2v} \right) \right] \quad (5.29)$$

At very low frequencies this admittance reduces to the capacitative reactance

$$\frac{j\omega l_w l}{4\pi l_t} \left[\epsilon_{33}^{LC} + \frac{4\pi d_{31}^2}{s_{11}^E} \right] = \frac{j\omega l_w l \epsilon_{33}^T}{4\pi l_t} = j\omega C \quad (5.30)$$

so that the low-frequency measurement of the capacitance C determines the free dielectric constant ϵ_{33}^T. When the tangent

$$\tan \frac{\omega l}{2v} = \infty \quad \text{or} \quad \frac{\omega l}{2v} = \frac{\pi}{2}$$
$$f_R = \frac{v}{2l} = \frac{1}{2l\sqrt{\rho s_{11}^E}} \quad (5.31)$$

A resonant frequency is obtained whose value is determined by the elastic compliance s_{11}^E, the density ρ, and the length of the crystal.

The anti-resonance occurs when the expression in brackets of equation (5.29) equals zero or when

$$1 + \frac{4\pi d_{31}^2}{\epsilon_{33}^{LC} s_{11}^E} \left(\frac{\tan \omega_A l/2v}{\omega_A l/2v} \right) = 0$$

or (5.32)

$$\frac{\omega_A l}{2v} \cot \frac{\omega_A l}{2v} = -\frac{4\pi d_{31}^2}{\epsilon_{33}^{LC} s_{11}^E}$$

Defining the coefficient of electromechanical coupling as

$$k = \frac{d_{31}}{\sqrt{\frac{\epsilon_{33}^{T}}{4\pi} s_{11}^{E}}} \tag{5.33}$$

and substituting in the value of ϵ_{33}^{LC} from equation (5.19), equation (5.32) becomes

$$\frac{\omega_A l}{2v} \cot \frac{\omega_A l}{2v} = -\left(\frac{k^2}{1 - k^2}\right) \tag{5.34}$$

Defined in this way, the electromechanical coupling factor represents the percentage of the total electrical energy applied to the crystal at zero frequency, that is stored in mechanical form.

We wish now to obtain an expression for evaluating the coupling factor k in terms of the measured resonant and anti-resonant frequencies f_R and f_A. Their difference is usually small so that we can write

$$f_A = f_R + \Delta f; \qquad \omega_A = \omega_R + 2\pi\Delta f \tag{5.35}$$

Inserting these values in (5.34) and noting that

$$\cot (A + B) = \frac{\cot A \cot B - 1}{\cot A + \cot B}$$

we have, since $\frac{\omega_R l}{2v} = \frac{\pi}{2}$ for the lowest resonance

$$\frac{\pi}{2}\left(1 + \frac{\Delta f}{f_R}\right) \frac{\left(\cot \frac{\pi}{2} \cot \frac{\pi}{2} \frac{\Delta f}{f_R} - 1\right)}{\left(\cot \frac{\pi}{2} + \cot \frac{\pi \Delta f}{2 f_R}\right)} = -\frac{\frac{\pi}{2}\left(1 + \frac{\Delta f}{f_R}\right)}{\cot \frac{\pi}{2} \frac{\Delta f}{f_R}} = -\left(\frac{k^2}{1 - k^2}\right)$$

Expanding $\tan \frac{\pi}{2} \frac{\Delta f}{f_R}$ into the power series

$$\tan \frac{\pi}{2} \frac{\Delta f}{f_R} = \frac{1}{\cot \frac{\pi}{2} \frac{\Delta f}{f_R}} = \frac{\pi}{2} \frac{\Delta f}{f_R} + \frac{\left(\frac{\pi}{2} \frac{\Delta f}{f_R}\right)^3}{3} +$$

and solving for k^2 we have

$$k^2 = \frac{\pi^2}{4} \frac{\Delta f}{f_R}\left[1 + \left(\frac{4 - \pi^2}{4}\right) \frac{\Delta f}{f_R} + \left(\frac{\pi^2 - 4}{4}\right)\left(\frac{\pi^2}{4}\right)\left(\frac{\Delta f}{f_R}\right)^2 + \cdots\right] \tag{5.36}$$

Hence, when the frequency difference between resonance and anti-resonance

is measured, the coupling coefficient k can be obtained by substituting in the above formula. Usually the first term is sufficient. Having the coupling the elastic constant s_{11}^{E}, which can be calculated from the resonant frequency, and ϵ_{33}^{T}, which is obtained from low-frequency capacitance measurements, the piezoelectric constant d_{31} can be evaluated. By using these constants for rotated cuts, all the independent elastic constants not involving pure shear, all of the piezoelectric constants, and all of the dielectric constants can be evaluated.

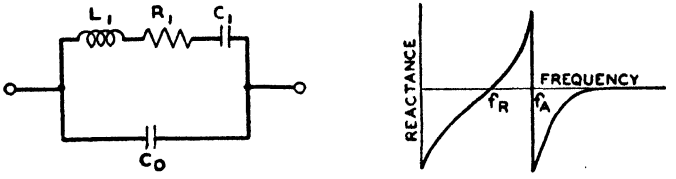

FIG. 5.1. Equivalent electrical circuit of a piezoelectric crystal and a plot of its reactance against the frequency.

The equivalent circuit of the crystal[3] can be evaluated from equations (5.33) and (5.36) and is shown by Fig. 5.1. From network equations, the resonant frequency and the separation of resonance and anti-resonance frequencies are given in terms of the elements of Fig. 5.1 by the equations

$$f_R = \frac{1}{2\pi\sqrt{L_1 C_1}}; \qquad \frac{f_A - f_R}{f_R} = \frac{C_1}{2C_0} = \frac{1}{2r} \tag{5.37}$$

From equation (5.29), the capacity C_0 is given by

$$C_0 = \frac{\epsilon_{33}^{LC} ll_w \times 1.11 \times 10^{-12}}{4\pi l_t} \text{ farads}$$

$$\text{Hence} \quad C_1 = 2C_0\left[\frac{f_A - f_R}{f_R}\right] = 2C_0\left(\frac{\Delta f}{f_R}\right)$$

$$= \frac{8}{\pi^2}\left(\frac{k^2}{1-k^2}\right) C_0 = \frac{8}{\pi^2}\frac{d_{31}^2}{s_{11}^{E}}\frac{ll_w}{l_t} \times \tag{5.38A}$$

$$(1.11 \times 10^{-12}) \text{ farads}$$

[3] The equivalent electrical circuit of a crystal was first derived by K. S. Van Dyke, *Phys. Rev.*, Vol. 25, p. 895, 1925; *Proc. I.R.E.*, Vol. 16, pp. 742–764, 1928.

From the resonant-frequency equation

$$L_1 = \frac{1}{4\pi^2 f_R^2 C_1} = \frac{9 \times 10^{11}}{4\pi^2 \left[\left(\frac{1}{4l^2 \rho s_{11}^E}\right)\left(\frac{8}{\pi^2}\frac{d_{31}^2}{s_{11}^E}\frac{ll_w}{l_t}\right)\right]} \tag{5.38B}$$

It is interesting to note that if the same process is carried out for an overtone mode, the same value of C_0 and L_1 result but C_1 has to be multiplied by a factor $1/n^2$ where n is the order of the overtone.

5.12 *Evaluation of Shearing Constants From Face-Shear Vibrations*

A measurement of various orientations of the crystal in longitudinal vibration will evaluate all of the elastic constants except the shear constants. To measure the shearing elastic constants requires setting up a vibration in which a pure shear is the predominant motion. A choice can be made of a thickness-shear mode or a face-shear mode and the latter was chosen since the mode is simpler and is more easily dimensioned and because the fundamental constants can be measured directly by a single orientation. Also, with a face-shear mode the motion is normal to the direction of the applied field and hence no correction has to be made for field distortion due to piezoelectric displacements, as will occur when the motion is along the direction of the applied field.

The face-shear mode is a more complicated contour mode than the longitudinal mode and involves satisfying boundary conditions along four edges. We consider crystals cut normal to the z- or x_3-axis and assume that the thickness is so small that the stresses determined by the x_3 direction can be set equal to zero. Hence

$$T_3 = T_4 = T_5 = 0 \tag{5.39}$$

The remaining stresses, T_1, T_2 and T_6, are all finite throughout the crystal but vanish at the edges. The vanishing of the stresses in equation (5.39) simplifies the equation of motion for it results in only three independent strains, *i.e.* the other three strains have a definite ratio to the independent strains. Since the field E is parallel to the z-axis at the surface, and the thickness is assumed small, the only component of the field will be E_3. Then equation (3.58) can be written

$$\begin{aligned}
S_{11} &= S_1 = s_{11}^E T_1 + s_{12}^E T_2 + s_{16}^E T_6 + d_{31} E_3 \\
2S_{12} &= S_6 = s_{16}^E T_1 + s_{26}^E T_2 + s_{66}^E T_6 + d_{36} E_3 \\
S_{22} &= S_2 = s_{12}^E T_1 + s_{22}^E T_2 + s_{26}^E T_6 + d_{32} E_3 \\
\delta_3 &= \frac{\epsilon_{33}^T}{4\pi} E_3 + d_{31} T_1 + d_{32} T_2 + d_{36} T_6
\end{aligned} \tag{5.40}$$

All the other stresses disappear by virtue of (5.39). While the other components of the electric displacement do not disappear, the only one of interest is δ_3 since the surface charge is equal to the normal component of the electric displacement divided by 4π and this is given by δ_3.

For inserting in the equation of motion, it is desirable to express the stress in terms of the strain. This can be done by solving equations (5.40) simultaneously, giving

$$\begin{aligned} T_1 &= c_{11}^{c,E} S_1 + c_{12}^{c,E} S_2 + c_{16}^{c,E} S_6 - e_{31}^{c} E_3 \\ T_2 &= c_{12}^{c,E} S_1 + c_{22}^{c,E} S_2 + c_{26}^{c,E} S_6 - e_{32}^{c} E_3 \\ T_6 &= c_{16}^{c,E} S_1 + c_{26}^{c,E} S_2 + c_{66}^{c,E} S_6 - e_{36}^{c} E_3 \\ \delta_3 &= E_3 \left[\frac{\epsilon_{33}^{T}}{4\pi} - (d_{31} e_{31}^{c} + d_{32} e_{32}^{c} + d_{36} e_{36}^{c}) \right] + e_{31}^{c} S_1 + e_{32}^{c} S_2 + e_{36}^{c} S_6 \end{aligned} \tag{5.41}$$

In these equations $c_{ij}^{c,E}$ designates the field, contour, elastic constants that apply when a contour mode occurs for a very thin crystal. These constants are given in terms of the elastic compliances at constant field by the formula

$$c_{ij}^{c,E} = \frac{(-1)^{k+l} \Delta^{kl}}{\Delta} ; \qquad k, l = 1, 2, 3 \tag{5.42}$$

where Δ is the determinant

$$\Delta = \begin{vmatrix} s_{11}^{E}, s_{12}^{E}, s_{16}^{E} \\ s_{12}^{E}, s_{22}^{E}, s_{26}^{E} \\ s_{16}^{E}, s_{26}^{E}, s_{66}^{E} \end{vmatrix} \tag{5.43}$$

and Δ^{kl} is the minor obtained by suppressing the k^{th} row and l^{th} column. The piezoelectric moduli applying to a contour mode of motion are given by

$$\begin{aligned} e_{31}^{c} &= d_{31} c_{11}^{c,E} + d_{32} c_{12}^{c,E} + d_{36} c_{16}^{c,E} \\ e_{32}^{c} &= d_{31} c_{12}^{c,E} + d_{32} c_{22}^{c,E} + d_{36} c_{26}^{c,E} \\ e_{36}^{c} &= d_{31} c_{16}^{c,E} + d_{32} c_{26}^{c,E} + d_{36} c_{66}^{c,E} \end{aligned} \tag{5.44}$$

while the contour clamped dielectric constant is given by the equation

$$\epsilon_{33}^{c,S} = \epsilon_{33}^{T} - (d_{31} e_{31}^{c} + d_{32} e_{32}^{c} + d_{36} e_{36}^{c}) 4\pi \tag{5.45}$$

The superscripts c,S indicate that this is the dielectric constant if the crystal is free from contour strain, but not from thickness strain.

Inserting equation (5.41) in the equations of motion (5.10), noting that

$$\frac{\partial E_3}{\partial x} = \frac{\partial E_3}{\partial y} = 0$$

since the plating is an equipotential surface, the equations of motion become

$$\rho \frac{\partial^2 \xi_1}{\partial t^2} = c_{11}^{c,E} \frac{\partial^2 \xi_1}{\partial x^2} + 2c_{16}^{c,E} \frac{\partial^2 \xi_1}{\partial x \partial y} + c_{66}^{c,E} \frac{\partial^2 \xi_1}{\partial y^2} + c_{16}^{c,E} \frac{\partial^2 \xi_2}{\partial x^2} + (c_{12}^{c,E} + c_{66}^{c,E}) \frac{\partial^2 \xi_2}{\partial x \partial y} + c_{26}^{c,E} \frac{\partial^2 \xi_2}{\partial y^2} \tag{5.46}$$

$$\rho \frac{\partial^2 \xi_2}{\partial t^2} = c_{16}^{c,E} \frac{\partial^2 \xi_1}{\partial x^2} + (c_{12}^{c,E} + c_{66}^{c,E}) \frac{\partial^2 \xi_1}{\partial x \partial y} + c_{26}^{c,E} \frac{\partial^2 \xi_1}{\partial y^2} + c_{66}^{c,E} \frac{\partial^2 \xi_2}{\partial x^2} + 2c_{26}^{c,E} \frac{\partial^2 \xi_2}{\partial x \partial y} + c_{22}^{c,E} \frac{\partial^2 \xi_2}{\partial y^2}$$

For simple harmonic motion, equations (5.46) reduce to the form

$$c_{11} \frac{\partial^2 \xi_1}{\partial x^2} + 2c_{16} \frac{\partial^2 \xi_1}{\partial x \partial y} + c_{66} \frac{\partial^2 \xi_1}{\partial y^2} + c_{16} \frac{\partial^2 \xi_2}{\partial x^2} + (c_{12} + c_{66}) \frac{\partial^2 \xi_2}{\partial x \partial y} + c_{26} \frac{\partial^2 \xi_2}{\partial y^2} + \omega^2 \rho \xi_1 = 0 \tag{5.47}$$

$$c_{16} \frac{\partial^2 \xi_1}{\partial x^2} + (c_{12} + c_{66}) \frac{\partial^2 \xi_1}{\partial x \partial y} + c_{26} \frac{\partial^2 \xi_1}{\partial y^2} + c_{66} \frac{\partial^2 \xi_2}{\partial x^2} + 2c_{26} \frac{\partial^2 \xi_2}{\partial x \partial y} + c_{22} \frac{\partial^2 \xi_2}{\partial y^2} + \omega^2 \rho \xi_2 = 0$$

where the elastic constants are understood to be the contour, field constants.

For experimental purposes it is found that the best measurements are obtained when the crystal is long compared to its width or thickness. This is further accentuated by taking a high harmonic of the mode which in effect makes the unit cell longer compared to its width. Hence the solution is one where the crystal is infinitely long in the x direction and with a finite width in the y direction. For an infinitely long crystal, there should be no variation of the displacements ξ_1 and ξ_2 along the length of the crystal and hence

$$\frac{\partial^2 \xi_1}{\partial x^2} = \frac{\partial^2 \xi_1}{\partial x \partial y} = \frac{\partial^2 \xi_2}{\partial y^2} = \frac{\partial^2 \xi_2}{\partial x \partial y} = 0 \tag{5.48}$$

This leaves only the terms

$$c_{66} \frac{\partial^2 \xi_1}{\partial y^2} + c_{26} \frac{\partial^2 \xi_2}{\partial y^2} + \omega^2 \rho \xi_1 = 0; \quad c_{26} \frac{\partial^2 \xi_1}{\partial y^2} + c_{22} \frac{\partial^2 \xi_2}{\partial y^2} + \omega^2 \rho \xi_2 = 0 \tag{5.49}$$

The solution of these equations represents two coupled modes controlled by the y dimension, *i.e.* the width. If $c_{26} = 0$, these two motions are a shear vibration and a longitudinal vibration existing independently, but with c_{26} finite, the shear and the longitudinal motions are coupled so that there is no pure shear or pure longitudinal motion. To show this we eliminate ξ_2 from the above equation and obtain one fourth-order equation

$$\frac{\partial^4 \xi_1}{\partial y^4} + \omega^2 \rho \left[\frac{c_{22} + c_{66}}{c_{22}c_{66} - c_{26}^2} \right] \frac{\partial^2 \xi_1}{\partial y^2} + \frac{\omega^4 \rho^2 \xi_1}{c_{22}c_{66} - c_{26}^2} = 0 \tag{5.50}$$

A solution of this equation is

$$\xi_1 = A \cos \alpha y + B \sin \alpha y + C \cos \beta y + D \sin \beta y$$

where

$$\begin{aligned} \alpha &= \omega \sqrt{\frac{(c_{22} + c_{66})\rho}{2(c_{22}c_{66} - c_{26}^2)}} \sqrt{1 + \sqrt{\frac{(c_{22} - c_{66})^2 + 4c_{26}^2}{(c_{22} + c_{66})^2}}} \\ \beta &= \omega \sqrt{\frac{(c_{22} + c_{66})\rho}{2(c_{22}c_{66} - c_{26}^2)}} \sqrt{1 - \sqrt{\frac{(c_{22} - c_{66})^2 + 4c_{26}^2}{(c_{22} + c_{66})^2}}} \end{aligned} \tag{5.51}$$

If $c_{26} = 0$

$$\alpha = \omega \sqrt{\frac{\rho}{c_{66}}}; \quad \beta = \omega \sqrt{\frac{\rho}{c_{22}}}$$

and the two vibrations would exist independently.

The value of ξ_2 is obtained by a substitution of the value of ξ_1 in the last of equations (5.49) and is

$$\begin{aligned} \xi_2 = &\left(\frac{\alpha^2 c_{26}}{\omega^2 \rho - \alpha^2 c_{22}} \right) [A \cos \alpha y + B \sin \alpha y] \\ &+ \left(\frac{\beta^2 c_{26}}{\omega^2 \rho - \beta^2 c_{22}} \right) [C \cos \beta y + D \sin \beta y] \end{aligned} \tag{5.52}$$

The boundary conditions to be satisfied are

$$T_2 = c_{22} \frac{\partial \xi_2}{\partial y} + c_{26} \frac{\partial \xi_1}{\partial y} - e_{31}^c E_3 = 0 \text{ when } y = 0 \text{ and } y = l_w \tag{5.53}$$

$$T_6 = c_{26} \frac{\partial \xi_2}{\partial y} + c_{66} \frac{\partial \xi_1}{\partial y} - e_{36}^c E_3 = 0 \text{ when } y = 0 \text{ and } y = l_w$$

where l_w is the width of the crystal. These conditions determine the four

independent constants A, B, C and D. In terms of E_3, these constants are

$$A = -\left[\frac{(\omega^2\rho - \alpha^2 c_{22}) \tan \alpha l_w/2}{\alpha(\beta^2 - \alpha^2)(c_{22}c_{66} - c_{26}^2)}\right] \times \left\{e_{36}^c E_3 - e_{32}^c E_3 \left[\frac{\omega^2\rho c_{66} - \beta^2(c_{22}c_{66} - c_{26}^2)}{\omega^2 \rho c_{26}}\right]\right\}$$

$$B = \left[\frac{(\omega^2\rho - \alpha^2 c_{22})}{\alpha(\beta^2 - \alpha^2)(c_{22}c_{66} - c_{26}^2)}\right] \times \left\{e_{36}^c E_3 - e_{32}^c E_3 \left[\frac{\omega^2\rho c_{66} - \beta^2(c_{22}c_{66} - c_{26}^2)}{\omega^2 \rho c_{26}}\right]\right\} \quad (5.54)$$

$$C = \left[\frac{(\omega^2\rho - \beta^2 c_{22}) \tan \beta l_w/2}{\beta(\beta^2 - \alpha^2)(c_{22}c_{66} - c_{26}^2)}\right] \times \left\{e_{36}^c E_3 - e_{32}^c E_3 \left[\frac{\omega^2\rho c_{66} - \alpha^2(c_{22}c_{66} - c_{26}^2)}{\omega^2 \rho c_{26}}\right]\right\}$$

$$D = -\left[\frac{(\omega^2\rho - \beta^2 c_{22})}{\beta(\beta^2 - \alpha^2)(c_{22}c_{66} - c_{26}^2)}\right] \times \left\{e_{36}^c E_3 - e_{32}^c E_3 \left[\frac{\omega^2\rho c_{66} - \alpha^2(c_{22}c_{66} - c_{26}^2)}{\omega^2 \rho c_{26}}\right]\right\}$$

To obtain the electrical admittance of the crystal, we make use of the last of equations (5.40), which for this limiting case becomes

$$\delta_3 = \frac{E_3 \epsilon_{33}^{c,S}}{4\pi} + e_{22}^c \frac{\partial \xi_2}{\partial y} + e_{36}^c \frac{\partial \xi_1}{\partial y} \quad (5.55)$$

Integrating this equation over the length and width of the crystal, noting that E_3 does not vary over the surface of the crystal, and ξ_2 and ξ_1 are not functions of x, we have

$$Q = \frac{E_3 l_w l \epsilon_{33}^{c,S}}{4\pi} + e_{32}^c l[\xi_{2_2} - \xi_{2_1}] + e_{36}^c l[\xi_{1_2} - \xi_{1_1}] \quad (5.56)$$

where the displacements are the displacements at the two edges and Q is the total charge on the surface. Introducing the displacements from (5.51), (5.52) and (5.54), and noting that the current to enter the crystal is $j\omega Q$, the admittance of the crystal becomes

$$\frac{i}{E} = \frac{j\omega l l_w \epsilon_{33}^{c,S}}{4\pi l_t}\left\{1 - \frac{e_{32}^2 4\pi}{\epsilon_{33}^{c,S}}\left[\frac{\alpha^2[\omega^2\rho c_{66} - \beta^2(c_{22}c_{66} - c_{26}^2)]}{(\beta^2 - \alpha^2)(c_{22}c_{66} - c_{26}^2)\omega\rho^2}\left(\frac{\tan \alpha l_w/2}{\alpha l_w/2}\right)\right.\right.$$
$$\left.\left. - \beta^2\left[\frac{\omega^2\rho c_{66} - \alpha^2(c_{22}c_{66} - c_{26}^2)}{(\beta^2 - \alpha^2)(c_{22}c_{66} - c_{26}^2)\omega^2\rho}\right]\frac{\tan \beta l_w/2}{\beta l_w/2}\right] \quad (5.57)$$

$$+\frac{4\pi e_{36}^{c2}}{\epsilon_{33}^{c,S}}\left[\left[\frac{(\omega^2\rho-\alpha^2c_{22})\left(\frac{\tan\alpha l_w/2}{\alpha l_w/2}\right)}{(\beta^2-\alpha^2)(c_{22}c_{66}-c_{26}^2)}\right]\right.$$
$$\left.-\left[\frac{(\omega^2\rho-\beta^2c_{22})\left(\frac{\tan\beta l_w/2}{\beta l_w/2}\right)}{(\beta^2-\alpha^2)(c_{22}c_{66}-c_{26}^2)}\right]\right] \tag{5.57}$$
$$-\frac{4\pi e_{32}^{c}e_{36}^{c}}{\epsilon_{33}^{c,S}}\left[\left[\frac{c_{66}(\omega^2\rho-\alpha^2c_{22})(\omega^2\rho-\beta^2c_{22})-\alpha^2\beta^2c_{22}c_{26}^2}{(\beta^2-\alpha^2)(c_{22}c_{66}-c_{26}^2)\omega^2\rho c_{26}}\right]\right.$$
$$\times\left[\frac{\tan\alpha l_w/2}{\alpha l_w/2}-\frac{\tan\beta l_w/2}{\beta l_w/2}\right]$$
$$\left.+\left[\frac{c_{26}}{c_{22}c_{66}-c_{26}^2}\right]\left[\frac{\tan\alpha l_w/2}{\alpha l_w/2}+\frac{\tan\beta l_w/2}{\beta l_w/2}\right]\right]\Bigg\}$$

At low frequencies

$$\frac{\tan\alpha l_w/2}{\alpha l_w/2}\longrightarrow\frac{\tan\beta l_w/2}{\beta l_w/2}\longrightarrow 1 \tag{5.58}$$

and the admittance is a capacitance

$$C=\frac{ll_w\epsilon_{33}^{c,S}}{4\pi l_t}\left[1+\frac{4\pi e_{32}^{c2}}{\epsilon_{33}^{c,S}}\left(\frac{c_{66}}{c_{22}c_{66}-c_{26}^2}\right)+\frac{4\pi e_{36}^{c2}}{\epsilon_{33}^{c,S}}\left(\frac{c_{22}}{c_{22}c_{66}-c_{26}^2}\right)\right.$$
$$\left.-\frac{4\pi e_{32}^{c}e_{36}^{c}}{\epsilon_{33}^{c,S}}\left(\frac{2c_{26}}{c_{22}c_{66}-c_{26}^2}\right)\right] \tag{5.59}$$

This capacitance is determined by the free dielectric constant of the crystal.

If $c_{26}=0$, the impedance reduces to that for two uncoupled modes, and is

$$\frac{i}{E}=\frac{j\omega ll_w\epsilon_{33}^{c,S}}{4\pi l_t}\left[1+\frac{4\pi e_{32}^{c2}}{c_{22}\epsilon_{33}^{c,S}}\left(\frac{\tan\omega\sqrt{\frac{\rho}{c_{22}}}\frac{l_w}{2}}{\omega\sqrt{\frac{\rho}{c_{22}}}\frac{l_w}{2}}\right)+\frac{4\pi e_{36}^{c2}}{c_{66}\epsilon_{33}^{c,S}}\left(\frac{\tan\omega\sqrt{\frac{\rho}{c_{66}}}\frac{l_w}{2}}{\omega\sqrt{\frac{\rho}{c_{66}}}\frac{l_w}{2}}\right)\right] \tag{5.60}$$

For such a case a measurement of the resonant and anti-resonant frequencies of the shear mode will determine the contour elastic constant c_{66} and the contour piezoelectric constant e_{36}^{c}. Since the shear piezoelectric constant is more easily determined from longitudinal crystals, the elastic constant c_{66}, determined by the resonant frequency, is the usual objective for shear measurements.

For the general case when c_{26} is not zero, equation (5.57) is the admit-

tance of two coupled modes. The resonant frequencies occur when the admittance is infinite (impedance zero) and hence occur when

$$\tan \alpha l_w/2 = \infty \qquad \text{or} \qquad \tan \beta l_w/2 = \infty \tag{5.61}$$

These are satisfied for the first modes when

$$\begin{aligned} f_1 &= \frac{1}{2l_w}\sqrt{\frac{(c_{22}+c_{66}) - \sqrt{(c_{22}-c_{66})^2 + 4c_{26}^2}}{2\rho}} \\ f_2 &= \frac{1}{2l_w}\sqrt{\frac{(c_{22}+c_{66}) + \sqrt{(c_{22}-c_{66})^2 + 4c_{26}^2}}{2\rho}} \end{aligned} \tag{5.62}$$

Since the frequency f is equal to the velocity of propagation $v/2l_w$, we find that the two values of the velocity satisfy the determinant

$$\begin{vmatrix} \rho v^2 - c_{22}, & c_{26} \\ c_{26}, & \rho v^2 - c_{66} \end{vmatrix} \tag{5.63}$$

Measurements of the two resonant frequencies will give two relations for calculating c_{26}, c_{22} and c_{66}. Other relations are obtainable from longitudinal measurements. In all crystals except monoclinic and triclinic crystals, the longitudinal and the shear mode occur without coupling and can be used directly to determine c_{22} and c_{66}.

5.2 *Elastic, Piezoelectric, and Dielectric Constants of Rotated Crystals*

We have so far calculated the resonant and anti-resonant frequencies of longitudinal and shear crystals cut normal to the z-axis, with their lengths along the x-axis and their widths along the y-axis. To measure all the properties of a crystal requires a number of different orientations for both longitudinal and shear vibrations. To make the solutions given previously hold for any of these oriented cuts, we use a system of rotated axes which are rotated from the reference axes by three rotations for the most general case.

Starting with the x, y and z rectangular axes as defined in Chapter II as the reference axes, the elastic constants for any rotated cuts are given by the general tensor formula

$$s'_{ijkl} = \frac{\partial x'_i}{\partial x_m}\frac{\partial x'_j}{\partial x_n}\frac{\partial x'_k}{\partial x_o}\frac{\partial x'_l}{\partial x_p} s_{mnop} \tag{5.64}$$

as shown by the Appendix Section A–4, where the partial derivatives are

the direction cosines defined by the equation

$$\frac{\partial x_i'}{\partial x_m} = \begin{vmatrix} \frac{\partial x_1'}{\partial x_1} & \frac{\partial x_1'}{\partial x_2} & \frac{\partial x_1'}{\partial x_3} \\ \frac{\partial x_2'}{\partial x_1} & \frac{\partial x_2'}{\partial x_2} & \frac{\partial x_2'}{\partial x_3} \\ \frac{\partial x_3'}{\partial x_1} & \frac{\partial x_3'}{\partial x_2} & \frac{\partial x_3'}{\partial x_3} \end{vmatrix} = \begin{array}{c|ccc} & x_1 & x_2 & x_3 \\ \hline x_1' & l_1 & m_1 & n_1 \\ x_2' & l_2 & m_2 & n_2 \\ x_3' & l_3 & m_3 & n_3 \end{array} \tag{5.65}$$

In a similar manner the piezoelectric and dielectric tensors are given by the formulae

$$\begin{aligned} d'_{ijk} &= \frac{\partial x_i'}{\partial x_l}\frac{\partial x_j'}{\partial x_m}\frac{\partial x_k'}{\partial x_n} d_{lmn} \\ \epsilon'_{ij} &= \frac{\partial x_i'}{\partial x_k}\frac{\partial x_j'}{\partial x_l}\epsilon_{kl} \end{aligned} \tag{5.66}$$

The constants of interest for longitudinal vibrations are the s'_{1111} elastic constant, the d'_{311} piezoelectric constant, and the ϵ'_{33} dielectric constant. Applying the tensor transformation formulae and expressing in terms of two index symbols, these quantities become for any orientation

$$\begin{aligned} s_{11}^{E'} &= s_{11}^E l_1^4 + (2s_{12}^E + s_{66}^E) l_1^2 m_1^2 + (2s_{13}^E + s_{55}^E) l_1^2 n_1^2 \\ &\quad + (2s_{14}^E + 2s_{56}^E) l_1^2 m_1 n_1 + 2s_{15}^E l_1^3 n_1 + 2s_{16}^E l_1^3 m_1 + s_{22}^E m_1^4 \\ &\quad + (2s_{23}^E + s_{44}^E) m_1^2 n_1^2 + 2s_{24}^E m_1^3 n_1 + (2s_{25}^E + 2s_{46}^E) m_1^2 l_1 n_1 + 2s_{26}^E m_1^3 l_1 \\ &\quad + s_{33}^E n_1^4 + 2s_{34}^E n_1^3 m_1 + 2s_{35}^E n_1^3 l_1 + 2(s_{36}^E + s_{45}^E) n_1^2 l_1 m_1 \end{aligned} \tag{5.67}$$

$$\begin{aligned} d'_{31} &= d_{11} l_3 l_1^2 + d_{12} l_3 m_1^2 + d_{13} l_3 n_1^2 + d_{14} l_3 m_1 n_1 + d_{15} l_3 l_1 n_1 \\ &\quad + d_{16} l_3 l_1 m_1 + d_{21} m_3 l_1^2 + d_{22} m_3 m_1^2 + d_{23} m_3 n_1^2 + d_{24} m_3 m_1 n_1 \\ &\quad + d_{25} m_3 l_1 n_1 + d_{26} m_3 l_1 m_1 + d_{31} n_3 l_1^2 + d_{32} n_3 m_1^2 + d_{33} n_3 n_1^2 \\ &\quad + d_{34} n_3 m_1 n_1 + d_{35} n_3 l_1 n_1 + d_{36} n_3 l_1 m_1 \end{aligned}$$

$$\epsilon_{33}^{T'} = \epsilon_{11}^T l_3^2 + 2\epsilon_{12}^T l_3 m_3 + 2\epsilon_{13}^T l_3 n_3 + \epsilon_{22}^T m_3^2 + 2\epsilon_{23}^T m_3 n_3 + \epsilon_{33}^T n_3^2$$

For shear vibrations in order to calculate the contour elastic constants in terms of the fundamental elastic compliances, we need to know $s_{11}^{E'}$, $s_{12}^{E'}$, $s_{16}^{E'}$, $s_{22}^{E'}$, $s_{26}^{E'}$ and $s_{66}^{E'}$ as a function of a general orientation. $s_{11}^{E'}$ is given by (5.67). The other five equations are

$$
\begin{aligned}
s_{12}^{E'} &= s_{11}^{E} l_1^2 l_2^2 + s_{12}^{E}[m_1^2 l_2^2 + l_1^2 m_2^2] + s_{13}^{E}[l_2^2 n_1^2 + l_1^2 n_2^2] \\
&+ s_{14}^{E}[m_1 n_1 l_2^2 + l_1^2 m_2 n_2] + s_{15}^{E}[l_2^2 n_1 l_1 + l_1^2 n_2 l_2] \\
&+ s_{16}^{E}[l_1 m_1 l_2^2 + l_1^2 l_2 m_2] + s_{22}^{E} m_1^2 m_2^2 + s_{23}^{E}[n_1^2 m_2^2 + m_1^2 n_2^2] \\
&+ s_{24}^{E}[m_1 n_1 m_2^2 + m_1^2 m_2 n_2] + s_{25}^{E}[n_1 l_1 m_2^2 + m_1^2 n_2 l_2] \\
&+ s_{26}^{E}[l_1 m_1 n_2^2 + m_1^2 l_2 m_2] + s_{33}^{E}[n_1^2 n_2^2] + s_{34}^{E}[m_1 n_1 n_2^2 + n_1^2 m_2 n_2] \\
&+ s_{35}^{E}[n_1 l_1 n_2^2 + n_1^2 n_2 l_2] + s_{36}^{E}[l_1 m_1 n_2^2 + n_1^2 l_2 m_2] + s_{44}^{E}[m_1 n_1 m_2 n_2] \\
&+ s_{45}^{E}[n_1 l_1 m_2 n_2 + m_1 n_1 n_2 l_2] + s_{46}^{E}[l_1 m_1 m_2 n_2 + m_1 n_1 l_2 m_2] \\
&+ s_{55}^{E}[n_1 l_1 n_2 l_2] + s_{56}^{E}[l_1 m_1 n_2 l_2 + n_1 l_1 l_2 m_2] + s_{66}^{E}[l_1 m_1 l_2 m_2]
\end{aligned} \tag{5.68}
$$

$$
\begin{aligned}
s_{16}^{E'} &= s_{11}^{E} 2 l_1^3 l_2 + 2 s_{12}^{E}[m_1 l_1 (m_1 l_2 + m_2 l_1)] + 2 s_{13}^{E} l_1 n_1 [l_2 n_1 + l_1 n_2] \\
&+ s_{14}^{E}[2 m_1 n_1 l_1 l_2 + l_1^2 (m_1 n_2 + n_1 m_2)] + s_{15}^{E}[3 l_1^2 l_2 n_1 + l_1^3 n_2] \\
&+ s_{16}^{E}[3 l_1^2 m_1 l_2 + l_1^3 m_2] + 2 s_{22}^{E} m_1^3 m_2 + 2 s_{23}^{E}[m_1 m_2 n_1^2 + n_1 n_2 m_1^2] \\
&+ s_{24}^{E}[3 m_1^2 n_1 n_2 + m_1^3 n_2] + s_{25}^{E}[2 m_1 m_2 n_1 l_1 + m_1^2 (l_1 n_2 + n_1 l_2)] \\
&+ s_{26}^{E}[3 m_1^2 l_1 m_2 + m_1^3 l_2] + 2 s_{33}^{E} n_1^3 n_2 + s_{34}^{E}[3 m_1 n_1^2 n_2 + n_1^3 m_2] \\
&+ s_{35}^{E}[3 n_1^2 l_1 n_2 + n_1^3 l_2] + s_{36}^{E}[2 l_1 m_1 n_1 n_2 + n_1^2 (l_1 m_2 + m_1 l_2)] \\
&+ s_{44}^{E} m_1 n_1 (m_1 n_2 + n_1 m_2) + s_{45}^{E}[2 n_1 l_1 m_1 n_2 + n_1^2 (l_1 m_2 + m_1 l_2)] \\
&+ s_{46}^{E}[l_1 m_1 (m_1 n_2 + n_1 m_2) + m_1 n_1 (l_1 m_2 + m_1 l_2)] \\
&+ s_{55}^{E}[n_1 l_1 (l_1 n_2 + n_1 l_2)] + s_{56}^{E}[2 l_1 n_1 l_2 m_1 + l_1^2 (n_1 m_2 + m_1 n_2)] \\
&+ s_{66}^{E} l_1 m_1 (l_1 m_2 + m_1 l_2)
\end{aligned} \tag{5.69}
$$

$$
\begin{aligned}
s_{22}^{E'} &= s_{11}^{E} l_2^4 + (2 s_{12}^{E} + s_{66}^{E}) l_2^2 m_2^2 + (2 s_{13}^{E} + s_{55}^{E}) l_2^2 n_2^2 \\
&+ (2 s_{14}^{E} + 2 s_{56}^{E}) l_2^2 m_2 n_2 + 2 s_{15}^{E} l_2^3 n_2 + 2 s_{16}^{E} l_2^3 m_2 + s_{22}^{E} m_2^4 \\
&+ (2 s_{23}^{E} + s_{44}^{E}) m_2^2 n_2^2 + 2 s_{24}^{E} m_2^3 n_2 + (2 s_{25}^{E} + 2 s_{46}^{E}) l_2 m_2^2 n_2 \\
&+ 2 s_{26}^{E} l_2 m_2^3 + s_{33}^{E} n_2^4 + 2 s_{34}^{E} m_2 n_2^3 + 2 s_{35}^{E} l_2 n_2^3 + 2 (s_{36}^{E} + s_{46}^{E}) l_2 m_2 n_2^2
\end{aligned} \tag{5.70}
$$

$$
\begin{aligned}
s_{26}^{E'} &= s_{11}^{E} 2 l_1 l_2^3 + 2 s_{12}^{E} l_2 m_2 (l_1 m_2 + m_1 l_2) + 2 s_{13}^{E} l_2 n_2 [l_1 n_2 + n_1 l_2] \\
&+ s_{14}^{E}[2 l_1 l_2 m_2 n_2 + l_2^2 (m_1 n_2 + n_1 m_2)] + s_{15}^{E}[3 l_1 l_2^2 n_2 + l_2^3 n_1] \\
&+ s_{16}^{E}[3 l_1 l_2^2 m_2 + l_2^3 m_1] + 2 s_{22}^{E} m_1 m_2^3 + 2 s_{23}^{E} m_2 n_2 [m_1 n_2 + n_1 m_2] \\
&+ s_{24}^{E}[3 m_1 m_2^2 n_2 + m_2^3 n_1] + s_{25}^{E}[2 m_1 m_2 n_2 l_2 + m_1^2 (l_1 n_2 + n_1 l_2)] \\
&+ s_{26}^{E}[3 l_2 m_2^2 m_1 + m_2^3 l_1] + 2 s_{33}^{E} n_1 n_2^3 + s_{34}^{E}[3 n_1 n_2^2 m_2 + m_1 n_2^3]
\end{aligned} \tag{5.71}
$$

$$
\begin{aligned}
&+ s_{35}^{E}[3n_1n_2^2l_2 + l_1n_2^3] + s_{36}^{E}[2n_1n_2l_2m_2 + n_2^2(l_1m_2 + m_1l_2)] \\
&+ s_{44}^{E}m_2n_2(m_1n_2 + n_1m_2) \\
&+ s_{45}^{E}[n_2l_2(m_1n_2 + n_1m_2) + m_2n_2(l_1n_2 + n_1l_2)] \\
&+ s_{46}^{E}[l_2m_2(m_1n_2 + n_1m_2) + m_2n_2(l_1m_2 + m_1l_2)] \qquad (5.71) \\
&+ s_{55}^{E}n_2l_2[l_1n_2 + n_1l_2] \\
&+ s_{56}^{E}[l_2m_2(l_1n_2 + n_1l_2) + n_2l_2(l_1m_2 + m_1l_2)] \\
&+ s_{66}^{E}l_2m_2(l_1m_2 + m_1l_2)
\end{aligned}
$$

$$
\begin{aligned}
s_{66}^{E'} &= 4s_{11}^{E}l_1^2l_2^2 + 8s_{12}^{E}l_1l_2m_1m_2 + 8s_{13}^{E}l_1l_2n_1n_2 \\
&+ 4s_{14}^{E}l_1l_2(m_1n_2 + n_1m_2) + 4s_{15}^{E}l_1l_2(l_1n_2 + l_2n_1) \\
&+ 4s_{16}^{E}l_1l_2(l_1m_2 + m_1l_2) + 4s_{22}^{E}m_1^2m_2^2 + 8s_{23}^{E}m_1m_2n_1n_2 \\
&+ 4s_{24}^{E}m_1m_2(m_1n_2 + m_2n_1) + 4s_{25}^{E}m_1m_2(l_1n_2 + l_2n_1) \\
&+ 4s_{26}^{E}m_1m_2(l_1m_2 + m_1l_2) + 4s_{33}^{E}n_1^2n_2^2 + 4s_{34}^{E}n_1n_2(m_1n_2 + n_1m_2) \qquad (5.72) \\
&+ 4s_{35}^{E}n_1n_2[l_1n_2 + n_1l_2] + 4s_{36}^{E}n_1n_2(l_1m_2 + m_1l_2) \\
&+ s_{44}^{E}(m_1n_2 + n_1m_2)^2 + 2s_{45}^{E}(l_1n_2 + l_2n_1)(m_1n_2 + n_1m_2) \\
&+ 2s_{46}^{E}(l_1m_2 + m_1l_2)(m_1n_2 + n_1m_2) + s_{55}^{E}(l_1n_2 + n_1l_2)^2 \\
&+ 2s_{56}^{E}(l_1m_2 + m_1l_2)(l_1n_2 + n_1l_2) + s_{66}^{E}(l_1m_2 + m_1l_2)^2.
\end{aligned}
$$

From these rotational equations and the relations of Chapter III, all the elastic, piezoelectric and dielectric constants can be determined as illustrated by specific crystals discussed in Chapter X.

Equations (5.67) show that all of the piezoelectric and dielectric constants can be evaluated from measurements on longitudinal crystals, while 9 elastic constants and 6 relations between the other 12 elastic constants can be evaluated from measurements for longitudinal crystals. For the most general case, the triclinic crystal, all of these measurements can be obtained from 18 oriented cuts. To obtain the remaining 6 independent relations, 6 face-shear crystals cut for various orientations can be used. Alternately, all the elastic constants can be obtained from 21 independently oriented crystal cuts vibrating in a face-shear mode, but this is not as easily done as for the longitudinal modes.

The data of Chapter X illustrate the cuts required for particular crystal classes.

CHAPTER VI

Properties and Uses of Quartz Crystals

Quartz crystals were the first piezoelectric crystals to receive wide application and because of their excellent mechanical properties they are still the most widely applied piezoelectric crystals. Although they were originally used in underwater sound transducers, quartz crystals are now almost restricted to uses for which their very stable mechanical properties are essential. These uses are principally in the control of the frequency of oscillators and in the production of very selective filters.

Stable quartz crystal oscillators grew out of the original work of Professor W. G. Cady of Wesleyan University. These have been applied to controlling the frequency of broadcasting stations and radio transmitters in general. Quartz-crystal units, using some one of the low-temperature coefficient crystals described in this chapter, produce the most stable oscillators and the best time-keeping systems that can be obtained. The use of crystals to stabilize oscillators was so prevalent during World War II that over 30,000,000 crystals were produced in a single year for this purpose.

Another use of quartz crystals has been in producing very selective filters. Because of the high Q existing in crystals they can practically eliminate the effect of dissipation in filter structures. Such filters have been applied widely in the long-distance telephone lines and in single side-band transatlantic radio telephone systems. Narrow-band crystal filters have been used in picking off single frequencies and narrow bands of frequencies for control and analyzing purposes. For this application quartz crystals have been most widely used. However, it appears that the requirements are lenient enough to allow some of the synthetic crystals, such as dipotassium tartrate (DKT) and ethylene diamine tartrate (EDT), to be employed, and their use is discussed in Chapter IX.

Besides producing and detecting sound in liquids, quartz crystals have been used to produce and detect vibrations in gases and solids. Because of their high mechanical and electrical impedances, crystals are somewhat at a disadvantage in coupling to low mechanical impedance air waves. However, for solids and liquids, they are well-suited to generate and measure sound waves and are largely used in ultra-sonic interferometers and in generating shear and longitudinal waves in solids. Uses and results of employing such devices are discussed in Chapters XIII, XIV, and

XV. For most of these high-frequency applications quartz crystals are employed since they can be ground very thin and can be used to produce high frequencies. *X*-cut quartz is used to set up longitudinal vibrations and *Y*-cut quartz to produce shear vibrations. Such high-frequency sound waves have been used for testing steel castings and other solid materials for flaws.[1]

It is the purpose of this chapter to describe the properties of quartz crystals and the special orientations that have found applications in the oscillator, filter and ultra-sonic applications.

6.1 *Physical Properties of Quartz*

Quartz is described by the chemist as silicon dioxide SiO_2, and crystallizes in the trigonal trapezohedral class. The z or optic axis is an axis of threefold symmetry, *i.e.*, if one measures any property of the crystal at a definite position in the crystal, this property will be repeated at angles of $\pm 120°$ rotation about the z-axis. The melting point of quartz is 1750°C, the density 2.65, and the hardness is 7 on the Mohs' scale. Under atmospheric pressure, α or low-temperature quartz transforms into β or high-temperature quartz at 573°C. Under stress, this transformation temperature is lowered. α quartz is insoluble in ordinary acids, but is decomposed in hydrofluoric acid and in hot alkalis. Quartz is soluble to some extent in water at high pressures and temperatures and to a much larger extent if sodium hydroxide is present.

Quartz is mined principally in Brazil in several different types of deposits.[2] The preponderance of the crystals mined is in the lower weight class as shown by Table X on page 80. Most of the clear quartz has recognizable natural faces, but some, particularly river quartz, has no natural faces.

Quartz occurs in optical, right-hand and left-hand forms, *i.e.*, the crystals will rotate the plane of polarization of polarized light passing along the z or optic axis counterclockwise (left-handed) or clockwise (right-handed) from the point of view of the observer facing the source of light. Most crystals have sections with both handedness. In general, the middle section is likely to be all of one hand while the outside sections may have parts of each handedness. A conoscope[3] may be used to locate the optic

[1] Firestone, F. A., "The Supersonic Reflectoscope," *J.A.S.A.*, Vol. 17, No. 3, Jan., 1946.

[2] Stoiber, Tolman and Butler, "Geology of Quartz Crystal Deposits," *Amer. Min.*, Vol. 30; pp. 245–268, 1945.

[3] Bond, W. L., "Method for Specifying Quartz Crystal Orientations and Their Determinations by Optical Means," *B.S.T.J.*, July, 1943; *Quartz Crystals for Electrical Circuits*, Chapter II, D. Van Nostrand Company, Inc., 1946.

TABLE X

Crystal Weight Groups Weight in Grams	Percentage of the Total Number of Crystals which were in Each Weight Group
200– 300	55.5
300– 500	29.5
500– 700	10.4
700– 1,000	2.1
1,000– 2,000	1.8
2,000– 3,000	0.5
3,000– 4,000	0.2
4,000– 5,000	<0.1
5,000– 7,000	<0.1
7,000–10,000	<0.1

axis and will also show the handedness and position of any optical twinning. The principle of the conoscope is shown by Fig. 6.1. Light from the source is sent through a polarizer and through the converging lens L_1. This lens sends converging or conical beams through the crystal, which are gathered by the second lens, focused, and sent through the analyzer. In

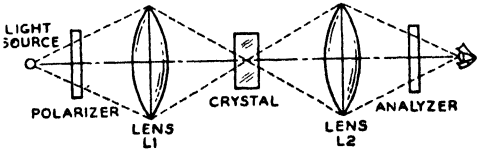

FIG. 6.1. Principle of coniscope.

practice, the lenses and crystal are immersed in a liquid which has the same index of refraction as does the crystal along its optic axis. Such liquids may be mixtures of Decalin and Dowtherm or dimethylphthalate and α-monochlornaphthalene. The crystal breaks up all rays not parallel to the optic axis into two components which travel with different velocities. Hence the analyzer is not able to extinguish the light that has traversed the crystal except at angles for which the two rays are in opposite phase, and one sees a series of rings in the conoscope when the direction of the z-axis is along the line between the source and the eye. Due to the rotation of the plane of polarization in the crystal, one finds that the rings either expand or contract for a right- or left-handed crystal, respectively, for a clockwise rotation of the analyzer. This gives a method of determining the handedness of the crystal. Optical twinning also shows up in a viewing system of this type for it deforms the ring pattern. If plane rays rather

than conical rays are used and a source of white light is used, color effects also show the position of the optical twinning.

Another type of twinning exists in quartz, the Dauphine or electrical type of twinning. This results from a 180° change in the direction of the crystal atomic arrangements. As shown by Fig. 6.2, bottom figure, the silicon atoms normal to the z-axis are arranged in near hexagons all pointing

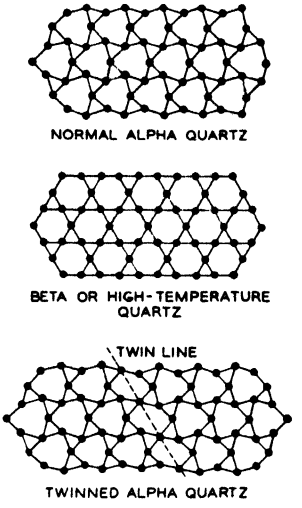

FIG. 6.2. Arrangement of Silicon Atoms in planes Normal to z. Top-normal untwinned α quartz. Middle-high temperature β quartz. Bottom-electrically twinned α quartz.

in one direction. If the temperature is raised above 573°C, a change in the arrangement to the hexagonal pattern shown in the middle occurs. As the temperature is decreased below 573°, the crystal may return to the form at the bottom, or part of it may return to this form and part to the form in which the near hexagons point in the opposite direction. If both forms exist, the crystal is said to have electrical twinning. The best method of detecting electrical twinning is by etching the surface with hydrofluoric acid.[4] This dissolves the crystal at rates which depend on the orientation of the crystal surface. Since the two twinned areas will develop etch pits that are different in orientation or shape, grazing light will cause one part to reflect brightly while the other reflects diffusely, and hence one can see the parts that have different regions of electrical twinning. Since

[4] Willard, G. W., "Raw Quartz, Its Imperfections and Inspection," *B.S.T.J.*, Oct., 1943; *Quartz Crystals for Electrical Circuits*, Chapter IV, D. Van Nostrand Company, Inc., 1946.

the piezoelectric effect is opposite for the two twinned areas, it is necessary to have only one region in a useful crystal. Electrical twinning usually occurs in an untwinned plate, if it is taken above the inversion point. It may also occur at lower temperatures, if stress is applied. Such twinning has been observed when a hot soldering iron is pressed against a crystal and may even occur when it is sawed. The Woosters[5] have recently found that the electrical twinning can be removed by exerting a definite stress on the crystal and taking it up in temperature nearly to the inversion temperature. Under this condition, the two twinned areas will store different amounts of potential energy and under high-temperature conditions the crystal tends to change in the direction of the twin which will store the larger energy. For a torque applied to the crystal, the twin cut in the direction of the *BT* cut will have the highest shear compliance and hence a *BT* crystal can be detwinned by applying a torque. An *AT*, on the other hand, tends to detwin in the *BT* directions and hence cannot be detwinned by using a torque. However, since the s'_{33} elastic compliance is larger for the *AT* cut at $+35°$ than for a cut at $-35°$, the *AT* can be detwinned by applying an elongation along z' or a bending which excites the same elastic constant.

Other defects[4] in quartz crystals are:

(1) " Bubbles ": bubble-like cavities that can be fine or large.
(2) Veils, heavy or fine, which are more or less continuous sheets of small, bubble-like cavities.
(3) Clouds or haze: aggregates of fine bubble-like cavities.
(4) Ghosts or phantoms: outlines of earlier growths within the crystal, usually marking what were once edges of adjoining faces which become visible when a beam of light is reflected from the minute fractures or parting planes which outline them.
(5) Fractures.

These imperfections can be observed by directing a strong light through the crystal at right angles to the direction of observation. The crystal is usually immersed in an inspection tank, which is filled with a liquid having the same index of refraction as the crystal. Opinions differ on how many inclusions or bubbles of a small size can be tolerated in the finished crystal.

Inspection and orienting instruments, as well as the method of sawing and preparing crystals, are well-described in a recent book[6] and in the May–June 1945 issue of the American Mineralogist.[2]

[5] *Nature*, Vol. 157, No. 3987, March 30, 1946. This criterion also derived independently by Dr. C. J. Davisson and Mrs. E. A. Wood.

[6] Heising, R. A., *Quartz Crystals for Electrical Circuits*, D. Van Nostrand Company, Inc., 1946.

6.2 *Elastic, Piezoelectric and Dielectric Equations for Quartz*

The modes of motion and the properties of these modes depend markedly on how crystal plates are oriented with respect to the natural crystal structure. Fig. 6.3 shows a quartz crystal with idealized natural faces,

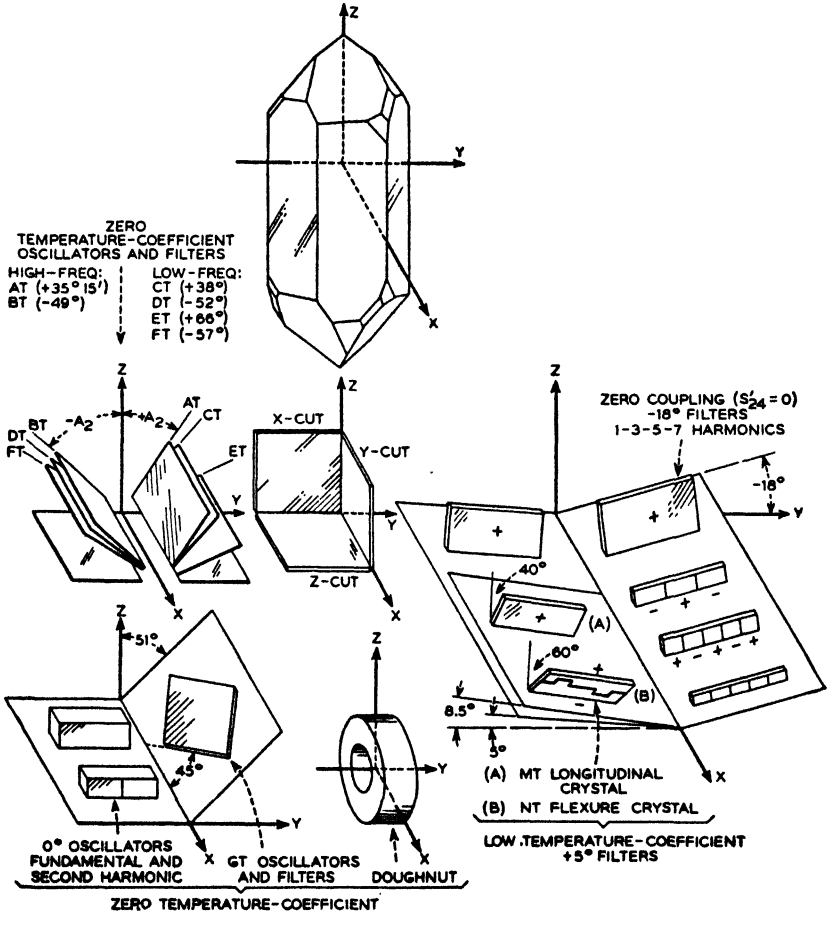

FIG. 6.3. Quartz crystal and principal cuts.

the three crystallographic axes, and some of the more important special cuts that have found use in the radio and telephone art. The axes as shown are in accordance with the 1945 IRE standard. In order to agree with general crystallographic nomenclature, the signs of the positive x- and y-axes have recently been reversed by the IRE piezoelectric committee. At the same time the sign of a counterclockwise angle is made

positive so that the angles for the new standard are the same as for Fig. 6.3. The z or optic axis of the crystal is parallel to the long direction of the crystal, the x-axis lies through one of the apexes of the hexagon, and the y-axis is normal to the other two in a right-handed system. The piezoelectric, elastic and dielectric constants of quartz take the form

$$\begin{aligned}
S_1 &= s_{11}^E T_1 + s_{12}^E T_2 + s_{13} T_3 + s_{14}^E T_4 + d_{11} E_x \\
S_2 &= s_{12}^E T_1 + s_{11}^E T_2 + s_{13} T_3 - s_{14}^E T_4 - d_{11} E_x \\
S_3 &= s_{13} T_1 + s_{13} T_2 + s_{33} T_3 \\
S_4 &= s_{14}^E T_1 - s_{14}^E T_2 + s_{44}^E T_4 - d_{14} E_x \\
S_5 &= s_{44}^E T_5 + 2 s_{14}^E T_6 - d_{14} E_y \\
S_6 &= 2 s_{14}^E T_5 + 2(s_{11}^E - s_{12}^E) T_6 - 2 d_{11} E_y \\
\delta_x &= \frac{D_x}{4\pi} = d_{11} T_1 - d_{11} T_2 + d_{14} T_4 + \frac{\epsilon_1^T}{4\pi} E_x \\
\delta_y &= \frac{D_y}{4\pi} = -d_{14} T_5 - 2 d_{11} T_6 + \frac{\epsilon_1^T}{4\pi} E_y \\
\delta_z &= \frac{D_z}{4\pi} = \frac{\epsilon_3}{4\pi} E_z
\end{aligned} \tag{6.1}$$

where S_1, S_2, S_3 are the three elongation strains along the x, y and z-axis, respectively, S_4, S_5 and S_6 the three shearing strains, T_1, T_2, T_3 the three tensional stresses, T_4, T_5 and T_6 the three shearing stresses, E_x, E_y, E_z the three fields, D_x, D_y, D_z the three electrical displacements which at the outer surfaces are equal to the surface charges $4\pi\delta_x$, $4\pi\delta_y$ and $4\pi\delta_z$. The method of defining these quantities is discussed in Chapter III. In cgs units, the elastic, piezoelectric and dielectric constants have the values.[7]

$$\begin{aligned}
s_{11}^E &= 127.9 \times 10^{-14} \times \text{cm}^2/\text{dyne} & c_{11}^E &= 86.05 \times 10^{10} \text{ dyne/cm}^2 \\
s_{12}^E &= -15.35 & c_{12}^E &= 4.85 \\
s_{13}^E &= -11.0 & c_{13}^E &= 10.45 \\
s_{14}^E &= -44.6 & c_{14}^E &= 18.25 \\
s_{33} &= 95.6 & c_{33}^E &= 107.1 \\
s_{44}^E &= 197.8 & c_{44}^E &= 58.65
\end{aligned} \tag{6.2}$$

[7] Mason, W. P., "Quartz Crystal Applications," *B.S.T.J.*, Vol. 22, No. 2, July, 1943.

$$s_{66}^E = 2(s_{11}^E - s_{12}^E) = 286.5 \times 10^{-14} \qquad c_{66}^E = \frac{c_{11}^E - c_{12}^E}{2} = 40.5$$

$$d_{11} = -6.76 \times 10^{-8} \text{ statcoulombs/dyne} \qquad \epsilon_1^T = 4.58 \left(\frac{4\pi \text{ statcoulombs}}{\text{stat volt}} \right)$$

$$d_{14} = 2.56 \times 10^{-8} \qquad \epsilon_3 = 4.70$$

For the mks system, the elastic compliances are multiplied by 10, the piezoelectric constants divided by 30,000, and the dielectric constants multiplied by the factor 8.85×10^{-12}.

6.3 *Modes of Motion Excited in Quartz Crystals*

The various modes of motion that can be excited in quartz crystals can be obtained from equation 6.1. It is the purpose of this section to describe the simplest modes of motion and the methods for exciting them. Formulae for their frequency are given when these can be obtained in simple form.

6.31 *Longitudinal Mode*

The simplest mode of motion which can be produced in quartz is the longitudinal. This can be produced by cutting a bar out of the crystal in such a direction that a d_{31}' piezoelectric constant exists for the cut, and covering both of the major faces with metal electrodes. In practice,[8] such crystals are usually supported by soldering headed wires to the surface and these wires also serve as electrical contacts to the crystal surfaces. When the crystal is long and thin, it is shown in Chapter V that the frequency of such a crystal is given by

$$f_R = \frac{1}{2l\sqrt{\rho s_{11}^{E'}}} \tag{6.3}$$

where l is the length of the crystal, ρ the density, and $s_{11}^{E'}$, the inverse of Young's modulus along the length of the crystal. The resonant frequency is the frequency of lowest impedance. It is shown in Chapter V that the impedance of such a crystal is similar to that of two condensers, a coil and a resistance, as shown by Fig. 5.1A. The impedance of such a network, neglecting the resistance, is a reactance as shown in Fig. 5.1B having a resonant frequency f_R, an anti-resonant frequency f_A, and ending up as a capacitative reactance. The resonant frequency and the anti-resonant

[8] Heising, R. A., *Quartz Crystals for Electrical Circuits*, Chapter VIII, D. Van Nostrand Company, Inc., 1946.

frequency are given by the formulae

$$f_R = \frac{1}{2\pi\sqrt{L_1 C_1}}; \qquad f_A = \frac{1}{2\pi}\sqrt{\frac{C_0 + C_1}{L_1 C_1 C_0}} \tag{6.4}$$

Taking the ratio

$$\frac{f_A^2}{f_R^2} = \frac{C_0 + C_1}{C_0} \quad \text{or} \quad \frac{f_A^2 - f_R^2}{f_R^2} = \frac{C_1}{C_0} = \frac{1}{r} \tag{6.5}$$

where r is the ratio of C_0 the capacitance due to the longitudinally clamped dielectric constant to the capacitance C_1 due to the motional capacitance. A measurement at low frequencies gives the sum of the capacitances $C_0 + C_1$. From the solution for $\Delta f = f_A - f_R$ given in equations (5.36) and (5.33), we can evaluate all the constants of the equivalent circuit in terms of the piezoelectric constant d'_{31}, the free dielectric constant ϵ_{33}^{T}, and the inverse of Young's modulus along the lengths of the crystal $s_{11}^{E'}$. In terms of these quantities

$$\begin{aligned} C_0 &= \frac{\epsilon_{33}^{LC} l l_w \times 1.11 \times 10^{-12}}{4\pi l_t} \text{ farads} \\ C_1 &= \frac{8}{\pi^2}\frac{d_{31}'^2}{s_{11}^{E'}}\left(\frac{l l_w}{l_t}\right) \times 1.11 \times 10^{-12} \text{ farads} \\ L_1 &= \left(\frac{\rho l_t l_w l}{8}\right)\left(\frac{s_{11}^{E'}}{l_w d_{31}}\right)^2 \times 9 \times 10^{11} \text{ henries} \end{aligned} \tag{6.6}$$

where

$$\epsilon_{33}^{LC} = \epsilon_{33}^{T}(1 - k^2) = \epsilon_{33}^{T} - \frac{4\pi d_{31}'^2}{s_{11}^{E}} \tag{6.7}$$

l = length of crystal in centimeters, l_w width of crystal, and l_t the thickness of the crystal, ρ is the density.

As the width of the crystal gets larger, the frequency gets lower due to a sidewise coupling to a width motion through the Poisson's ratio of the crystal. For a crystalline material such as quartz, a coupling to a face-shear mode can also occur through the elastic constant s_{24} (for an x-cut crystal with its length along y), for a stress along the length produces a shear which distorts the face of the crystal from a rectangle to a rhombus. This face-shear mode is coupled to a flexure mode as shown by the resonant frequency of an x-cut crystal with its length along the y-axis, published in a former paper[9] and shown in Fig. 6.4. The width of the cross-hatched

[9] Mason, W. P., "Electrical Wave Filters Employing Quartz Crystals as Elements," *B.S.T.J.*, July, 1934.

region is proportional to the separation of resonance and anti-resonance frequency, while the lower part of the curve is the frequency of resonance. The main longitudinal resonance is the one marked *C*. *A* is the width mode and *B* the face-shear mode. At a ratio of width to length of 0.8 to 1.0, the face-shear mode is split into two parts due to coupling with some other mode, probably a thickness flexure. The curve labeled *D* shows

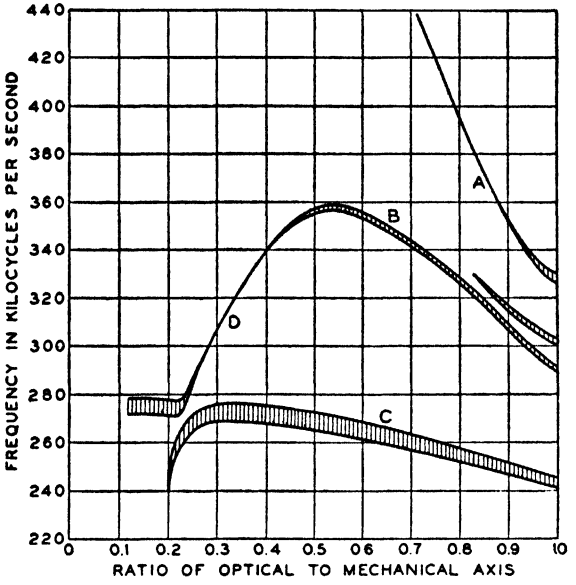

FIG. 6.4. Resonances of an *X*-cut quartz crystal with its length along the *y*-axis.

that the face-shear mode can drive the second flexural mode weakly, but when the frequency coincides with that of the longitudinal mode it is relatively strongly coupled and makes the crystal useless for that ratio of width to length. By orienting the crystal so that its length comes at an angle of 18.5° from *y* in the direction of the minimum value of Young's modulus, it can be shown that the s'_{24} elastic constant disappears. The resulting frequency spectrum for this crystal known as the $-18.5°$ *X*-cut is shown by Fig. 6.5. As can be seen, the shear and second flexure are very weakly driven and are of such a small order of magnitude that they do not interfere with the use of the crystal in a filter.

Longitudinal crystals are usually mounted at their nodal lines by soldering headed wires to silver spots baked on the surface, and these heads serve both as a support and as the electrically conducting connection. The details of these mountings are described in reference 8.

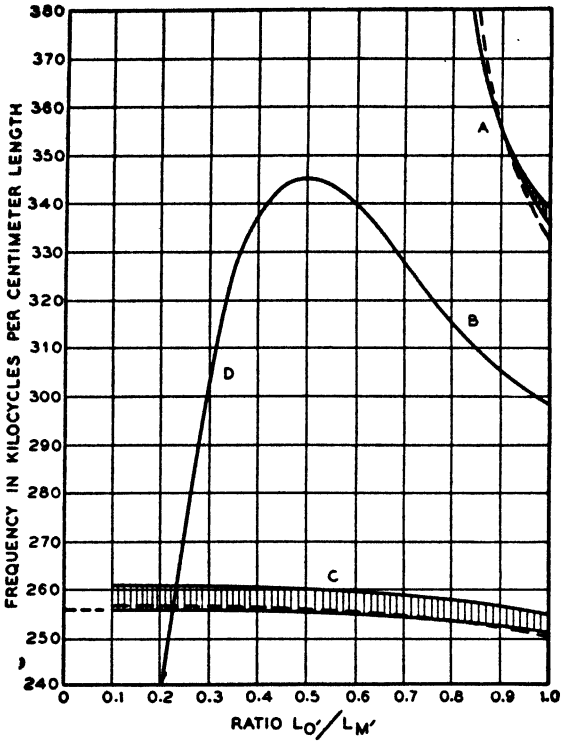

FIG. 6.5. Resonances of a $-18°$ X-cut crystal.

6.32 *Flexure Crystals*

Another simple mode of motion which has received use in the low-frequency range is the flexure crystal. Two varieties are in use, the width flexure mode and the thickness flexure or bimorph type.

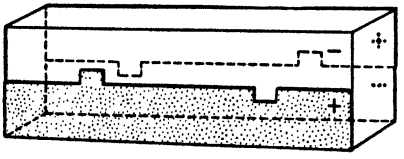

FIG. 6.6. Method for plating a longitudinal crystal to obtain a flexure mode.

The width mode is driven by putting on two sets of electrodes, as shown by Fig. 6.6. The frequency of a long, thin bar is given by the equation

$$f = \frac{m^2 l_w}{2\pi\sqrt{12}\, l^2 \sqrt{s'_{22\rho}}} \tag{6.8}$$

where l_w is the width of the crystal, l its length in centimeters, s'_{22} the inverse of Young's modulus along the length, ρ the density and m a root of a transcendental equation. For a long, narrow crystal plate free on both ends, as is usually the case, the values of m for the successive overtones are

$$m_1 = 4.37; \qquad m_2 = 7.85; \qquad m_3 = 11.00 \tag{6.9}$$

As the ratio of width to length becomes larger, rotary inertia plays a more important part and changes the value of m. It was shown in a former[10]

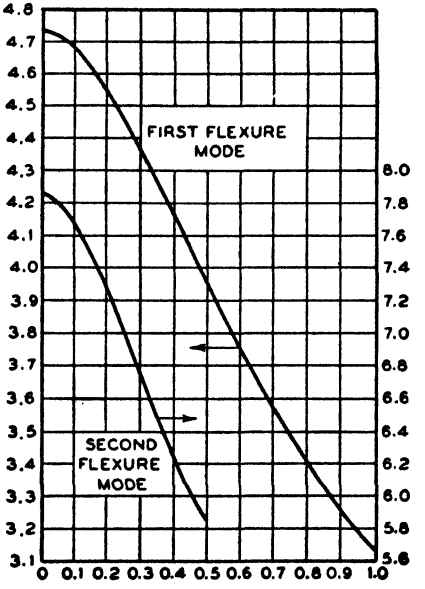

FIG. 6.7. Values of m for a flexure crystal as a ratio of width to length.

paper that the effect of rotary inertia is to change the value of m according to the curves of Fig. 6.7. Figure 6.8 shows the frequency constant of an NT-cut crystal as described in the next section plotted as a ratio of width to length. As the ratio gets large, the frequency becomes asymptotic to that of a shear crystal.

Flexure crystals are mounted by four wires attached to the nodal points, which occur at a distance of 0.224 times the length from each end

[10] Mason, W. P., "The Motion of a Bar Vibrating in Flexure, Including the Effects of Rotary and Lateral Inertia," *J.A.S.A.*, Vol. 6, 1935; W. P. Mason, *Electromechanical Transducers and Wave Filters*, Appendix A, D. Van Nostrand Company, Inc., 1942, 2nd edition, 1948.

of the crystal. The ratio of capacitances[11] is somewhat larger than that for the same crystal driven longitudinally by a factor of $128/9\pi^2$. They are used in the frequency range from 10 kc to 50 kc for narrow-band pilot filters and other similar filters.

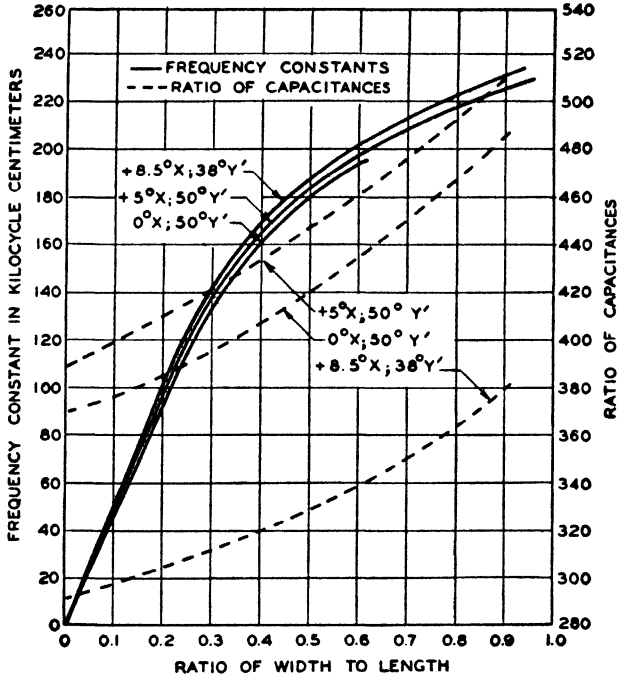

FIG. 6.8. Frequency constant and ratio of capacitances of an *MT* flexure crystal.

Thickness flexure crystals[12] are used in the form of two thin plates soldered together to produce a bimorph-type crystal. These have been made as low in frequency as 900 cycles and have been used to control rotating devices. By constructing them from +5° *X*-cut crystals, their temperature coefficient can be made low and such crystals produce stable low-frequency oscillators.

6.33 *Torsional Crystals*

Another simple mode that can be excited in quartz is a torsional mode whose frequency is controlled by the shear elastic constant of the crystal.

[11] Mason, W. P., *Electromechanical Transducers and Wave Filters*, p. 215, D. Van Nostrand Company, Inc., 1942, 2nd edition, 1948.

[12] Lane, C. E., "Duplex Crystals," *Bell Lab. Rec.*, Vol. 24, No. 2, pp. 59–62, Feb., 1946.

By using a cylindrical crystal, as shown by Fig. 6.9, its length along the x-axis and with 4 electrodes whose central lines make angles of 45° with respect to the y-axis, with opposite pairs connected together, a torsional mode can be generated in the crystal. The field in one direction along the y-axis as shown, generates an x_y or S_6 face shear, which moves the top

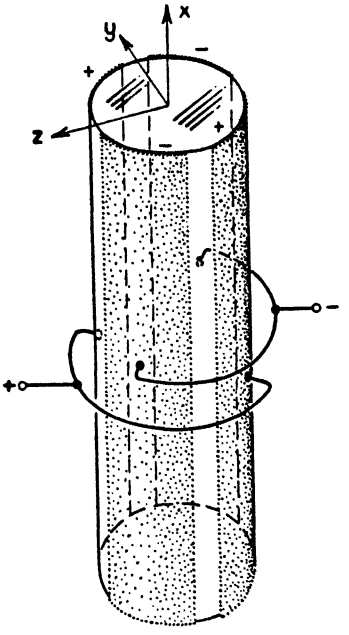

FIG. 6.9. Method for obtaining a torsional crystal from quartz.

plane with respect to the bottom plane. The other set of electrodes has the reverse field and hence the reverse shear is generated in the other half of the crystal. This combination rotates the top plane with respect to a plane lower in the crystal and produces a torsional motion. The frequency of such a crystal is given by the expression

$$f = \frac{1}{2l}\sqrt{\frac{\mu}{\rho}} = \frac{1}{2l}\sqrt{\frac{c_{66}}{\rho}} \tag{6.10}$$

where μ is the shear elastic constant for an isotropic body and c_{66} is the corresponding shear elastic constant for shears around the z-axis. Inserting the value given by equation (6.2)

$$c_{66} = 40.5 \times 10^{10}$$

the resonant frequency for a crystal 1 centimeter long is

$$f_R = 1.95 \times 10^5 \text{ cycles} \tag{6.11}$$

This mode has not been used appreciably except to measure the shear constants of solid materials, but may be of importance in measuring shear viscosities and shear elasticities of liquids, as described in Chapter XIV.

6.34 *Face-Shear Mode of Motion*

A more complicated mode of motion which has received considerable use, is the face-shear mode. The *CT* and *DT* crystals described in section 6.42 have this mode of motion. This is a complicated contour mode and no exact solution has been obtained for its frequency. When the crystal is long compared to its width, it is shown in Chapter V that the frequency is given by

$$f_R = \frac{1}{2l_w}\sqrt{\frac{c'_{66}}{\rho}} \tag{6.12}$$

for a crystal cut normal to the z or z′ rotated axis, where l_w is the width of the crystal and c'_{66} is the contour elastic constant of the crystal. This mode has been used in evaluating the shear elastic constants of many crystals. Figure 6.10 shows a measurement of the frequency spectrum of a *Y*-cut quartz crystal plotted as a ratio of width to length. It is evident that the principal shear mode is coupled to even-order flexures. By dimensioning the crystal so that the main shear mode lies half way between two coupled flexure modes, a good agreement is obtained with the frequency of equation (6.12).

An approximate formula derived by the writer[13] for an uncoupled face-shear mode takes the form

$$f = \frac{1}{2}\sqrt{\frac{c_{66}}{\rho}}\sqrt{\frac{m^2}{a^2} + \frac{n^2}{b^2}} \tag{6.13}$$

where m and n are integers, a the length along the x-axis, and b the length along the y-axis, assuming that the field is applied along z. The principal mode is given by $m = 1$, $n = 1$, and as shown by the dotted line of Fig. 6.10, this agrees reasonably well with the " uncoupled " frequency of the shear mode. The shear mode is coupled to even-order flexures, as shown by the coupled mode frequencies. This coupling probably occurs through the stress conditions at the boundary.

[13] Mason, W. P., " Electrical Wave Filters Employing Quartz Crystals as Elements," *B.S.T.J.*, Vol. 13, pp. 405–452, July, 1934.

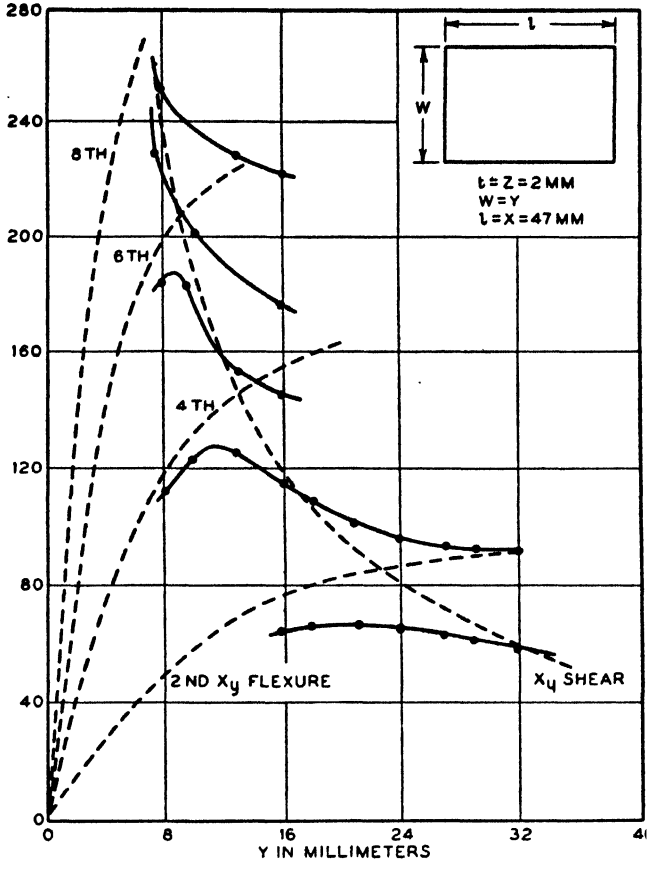

FIG. 6.10. Spectrum of a *Y*-cut shear quartz crystal plotted as a function of width to length.

6.35 *Thickness-Shear Modes*

The thickness-shear mode is used very extensively for obtaining high-frequency vibrating crystals of the *AT* and *BT* type, as described in section 6.42. Here again the only exact solution obtained is for a plate with infinitely large widths and lengths compared with the thickness. This theory is due to Christoffel,[14] who showed that if *l*, *m* and *n* are the direction cosines between the direction of propagation and the *x*-, *y*- and *z*-axes, that there are in general three different waves that can be propagated, whose velocities of propagation can be obtained from the

[14] Love, A. E. H., *Theory of Elasticity*, fourth edition, p. 298.

determinant

$$\begin{vmatrix} \lambda_{11} - \rho v^2 & \lambda_{12} & \lambda_{13} \\ \lambda_{12} & \lambda_{22} - \rho v^2 & \lambda_{23} \\ \lambda_{13} & \lambda_{23} & \lambda_{33} - \rho v^2 \end{vmatrix} = 0 \tag{6.14}$$

where ρ = the density, v the velocity and the λ's are related to the elastic constants of the crystal by the formulae

$$\begin{aligned}
\lambda_{11} &= c_{11}l^2 + c_{66}m^2 + c_{55}n^2 + 2c_{56}mn + 2c_{15}nl + 2c_{16}lm \\
\lambda_{12} &= c_{16}l^2 + c_{26}m^2 + c_{45}n^2 + (c_{46} + c_{25})mn + (c_{14} + c_{56})nl \\
&\quad + (c_{12} + c_{66})lm \\
\lambda_{13} &= c_{15}l^2 + c_{46}m^2 + c_{35}n^2 + (c_{45} + c_{36})mn + (c_{13} + c_{55})nl \\
&\quad + (c_{14} + c_{56})lm \\
\lambda_{23} &= c_{56}l^2 + c_{24}m^2 + c_{35}n^2 + (c_{44} + c_{23})mn + (c_{36} + c_{45})nl \\
&\quad + (c_{25} + c_{46})lm \\
\lambda_{22} &= c_{66}l^2 + c_{22}m^2 + c_{44}n^2 + 2c_{24}mn + 2c_{46}nl + 2c_{26}lm \\
\lambda_{33} &= c_{55}l^2 + c_{44}m^2 + c_{33}n^2 + 2c_{34}mn + 2c_{35}nl + 2c_{45}lm
\end{aligned} \tag{6.15}$$

For quartz

$$c_{22} = c_{11};\quad c_{24} = -c_{14};\quad c_{55} = c_{44};\quad c_{56} = c_{14};\quad c_{66} = \frac{(c_{11} - c_{12})}{2}$$

and

$$c_{15} = c_{16} = c_{25} = c_{26} = c_{34} = c_{35} = c_{36} = c_{45} = c_{46} = 0$$

For the rotated crystals containing the AT and BT crystals, which occur for a rotation about the x-axis, $l = 0$, $m = \cos\theta$; $n = -\sin\theta$. Then for these crystals

$$\begin{aligned}
\lambda_{11} &= c_{66}\cos^2\theta + c_{44}\sin^2\theta - 2c_{14}\sin\theta\cos\theta = c'_{66} \\
\lambda_{23} &= -c_{14}\cos^2\theta - (c_{44} + c_{23})\sin\theta\cos\theta \\
\lambda_{22} &= c_{22}\cos^2\theta + c_{44}\sin^2\theta + 2c_{14}\sin\theta\cos\theta \\
\lambda_{33} &= c_{44}\cos^2\theta + c_{33}\sin^2\theta \\
\lambda_{12} &= \lambda_{13} = 0
\end{aligned} \tag{6.16}$$

With these values of λ, the three solutions of equation (6.14) become

$$\begin{aligned}
v_1 &= \sqrt{\frac{\lambda_{11}}{\rho}} \\
v_{2,3} &= \sqrt{\frac{1}{2}\left[\frac{\lambda_{22}}{\rho} + \frac{\lambda_{33}}{\rho} \pm \sqrt{\left(\frac{\lambda_{22}}{\rho} - \frac{\lambda_{33}}{\rho}\right)^2 + \frac{4\lambda_{23}^2}{\rho^2}}\right]}
\end{aligned} \tag{6.17}$$

The first solution corresponds to the high-frequency shear mode and hence the frequency of such a plate is given by

$$f = \frac{v_1}{2t} = \frac{1}{2t}\sqrt{\frac{c_{66}\cos^2\theta + c_{44}\sin^2\theta - 2c_{14}\sin\theta\cos\theta}{\rho}}$$

$$= \frac{1}{2t}\sqrt{\frac{c'_{66}}{\rho}} \tag{6.18}$$

where t is the thickness of the plate.

This solution for the infinite plate agrees fairly well with the most prominent frequency but does not show any of the other shear modes or the coupled flexure modes. An approximate solution for the finite plate has been made by McSkimin[15] which results in the formula

$$f = \frac{1}{2}\sqrt{\frac{c_{11}}{\rho}\frac{n^2}{l^2} + \frac{c_{66}}{\rho}\frac{m^2}{t^2} + \frac{c_{55}p^2}{w^2}} \tag{6.19}$$

where n, m and p are integers and l, t and w the length, width and thickness of the crystal. If l and w are infinite, this reduces to (6.18). Experimentally, the upper modes predicted by (6.19) are present, but the elastic constants used do not give too good an agreement with experiment and Sykes[16] has proposed a formula

$$f = \frac{1}{2}\sqrt{\frac{c'_{66}}{\rho}}\sqrt{\frac{m^2}{t^2} + \frac{kn^2}{l^2} + \frac{k_1(p-1)^2}{w^2}} \tag{6.20}$$

where k and k_1 are experimentally determined constants.

In addition to these shear modes, coupling is found to all the even-order flexure modes. A number of experimental results are shown by Sykes.[16] The dimensioning of a crystal to avoid all of these resonances is a complex study and has to be carried out largely by experimental techniques.

6.4 *Useful Orientations for Quartz Crystals*

By cutting out crystals at specified orientations with respect to the crystallographic axes, these modes can be excited with such desirable characteristics as low temperature coefficients of frequency, freedom from coupling to secondary modes of motion and high electromechanical coupling factors. It is the purpose of this section to describe these specific cuts.

[15] Heising, R. A., *Quartz Crystals for Electrical Circuits*, Chapter VII, D. Van Nostrand Company, Inc., 1946.

[16] Heising, R. A., *Quartz Crystals for Electrical Circuits*, Chapter VI, D. Van Nostrand Company, Inc., 1946.

6.41 *X-cut Plates*

Equations (6.1) are useful in predicting the type of motion that will be generated in a given type of cut and the magnitude of the electromechanical coupling. For example, the first equation of equations (6.1) shows that a strain S_1, which is an elongation along the x-axis, will be generated by a field applied along the x-axis. The applied field will then generate a thickness longitudinal mode since the motion is in the same direction as the applied field. If the thickness is made small, this type of crystal can produce a very high frequency and it was originally used to control oscillators. Due to the poor temperature coefficient of the X-cut plates, they have largely been replaced in the control of oscillators by AT and BT thickness shear-mode cuts, which have much better properties. X-cut plates are used, however, in producing ultra-sonic vibrations in solids, liquids and gases. Such waves have been used to study the properties of these materials and have also been used in flaw detectors[1] which determine whether any cracks or irregularities occur in metal castings. For this purpose it is desirable to transform as much input electrical energy as possible into mechanical energy. A measure of the efficiency of this conversion for statically or slowly varying applied fields is the electromechanical coupling factor k, which is defined by the equation

$$k = d_{11}\sqrt{\frac{4\pi c_{11}^{E}}{\epsilon_1^{T}}} = .095 \tag{6.21}$$

where c_{11}^{E} is the effective elastic constant for a thickness mode. This is equal to

$$c_{11}^{E} = 8.60 \times 10^{11} \text{ dynes/cm}^2 \tag{6.22}$$

Inserting the values given in equation (6.21), we find that the coupling is about 9.5 per cent. This means that for a static field, the square of k is about 1 per cent, and about 1 per cent of the input energy is stored in mechanical form. For alternating fields near the resonance of the crystal, a considerably larger part, in fact nearly all, can be converted into mechanical energy if the shunt capacity is tuned by a coil, but nevertheless, the coupling is a measure of the width of the frequency range for which this conversion can be done efficiently. If f_B is the highest frequency and f_A the lowest frequency for which the loss is not more than 50 per cent, it has been shown that[17]

$$\frac{f_B}{f_A} = \sqrt{\frac{1+k}{1-k}} \tag{6.23}$$

[17] Mason, W. P., *Electromechanical Transducers and Wave Filters*, Chapter VI, Equation 6, D. Van Nostrand Company, Inc., 1942.

Some synthetic crystals such as lithium sulphate and *L*-cut rochelle salt have coupling factors of .35 to .4 and are to be preferred when it is desired to radiate a wide band of frequencies, but for high frequencies, *X*-cut quartz is commonly used because of its excellent mechanical properties.

The second equation of (6.1) shows that a strain S_2, which is an elongation along the *y*-axis, is excited when a field is applied along the *x*-axis. Since the length of the crystal is taken along this direction, this mode of motion is called a length longitudinal mode. It has been used to some extent to produce low-frequency oscillations in gases, liquids and solids. Two modifications of this cut have received considerable use in the construction of quartz crystal filters. These cuts are the $-18°$ *X*-cut crystal and the $+5°$ *X*-cut crystal, shown by Fig. 6.3. The $-18°$ cut is used because it produces a very pure frequency spectrum giving only a single resonance over a frequency range of three to one.[18] The $+5°$ *X*-cut crystal is used because it is the best orientation of the *X*-cuts for giving a low temperature coefficient of frequency. By putting a divided plating on the crystal as shown by Fig. 6.6, this crystal can be driven in a flexure mode at much lower frequencies than can be realized with a longitudinal mode. It has been used for selecting single-frequency pilot channels for controlling the gain of a carrier system.

The temperature coefficient of the $+5°$ *X*-cut used for both longitudinal and flexure modes, can be improved by rotating the thickness around the length of the crystal. This results in the *MT* and *NT* crystals, shown by Fig. 6.3. These have temperature coefficients under one part in a million per degree centigrade, but a smaller coupling than the equivalent $+5°$ *X*-cut crystals.[19]

6.42 *Y-Cut Crystals*

When a field E_y is applied along the *y*-axis, equations (6.1) show that there are two types of strain generated, S_5 and S_6. Both of these strains are shearing strains which distort a square in the crystal into a rhombus, as shown by Fig. 6.11. The S_5 strain, which is shown in Fig. 6.11, distorts the crystal in the *xz*-plane, while the S_6 strain distorts the crystal in the *xy*-plane. Since the field is applied along the thickness, which is the *y* direction, the first strain S_5 is called a face-shear strain and S_6 a thickness-shear strain. The frequency of a face-shear mode is controlled by the contour dimensions and hence will be relatively low. The frequency of the

[18] Mason, W. P., "Electrical Wave Filters Employing Quartz Crystals as Elements," *B.S.T.J.*, Vol. 13, July, 1934.

[19] Mason, W. P. and R. A. Sykes, "Low Frequency Quartz Crystal Cuts Having Low Temperature Coefficients," *Proc. I.R.E.*, Vol. 32, No. 4, April, 1944. This also appears in reference 6, Chapter XVII.

thickness-shear mode is controlled by the thickness dimension, which can be made very small, resulting in a high frequency.

The Y-cut crystal was first used in the control of high-frequency oscillators but because of its high temperature coefficient, has largely been displaced by the AT and BT crystals, which are modified Y-cut crystals.

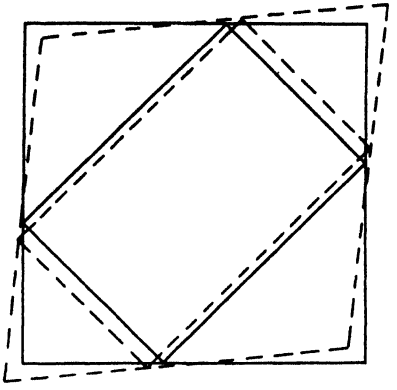

FIG. 6.11. Distortion for a shear crystal and method for obtaining a longitudinal mode.

The Y-cut crystal is still used to generate shear vibrations in solids. For this purpose it has a higher coupling than does the X-cut, since the coupling for the shear thickness mode is

$$k = 2d_{11}\sqrt{\frac{4\pi c_{66}^{E}}{\epsilon_1^{T}}} = .142 \tag{6.24}$$

Rotations of the thickness direction around the x-axis have resulted in rotated Y-cuts that have very favorable properties. Investigations made by Lack, Willard, Fair, Mason, Sykes, Koga, Bechmann, and Straubel have shown how the properties of the thickness-shear mode varied with angle of cut. As shown by Fig. 6.3, all the orientations resulting in useful crystals have their length along the x-axis and their thickness makes an angle θ with the y-axis. Figure 6.12 shows the frequency constant (kilocycles for a crystal one millimeter thick) as a function of the angle of rotation. At an angle of rotation of $+31°$ and $-59°$, the frequency is minimum and maximum respectively. At these two angles the mechanical coupling between the thickness-shear mode and the face-shear mode and its overtones becomes zero, and a crystal is obtained which is much freer from extraneous modes of motion than is the Y-cut. Figure 6.13 shows a plot of temperature coefficient against the orientation angle and at $35° - 15'$ and $-49°$, crystals are obtained which have zero temperature coefficients.

These cuts are known as the *AT* and *BT* crystals respectively, and they have been very widely used to control high-frequency oscillators. Frequencies as high as 15 megacycles are used for fundamental control and by using mechanical harmonics, frequencies as high as 197 megacycles have been obtained.[20]

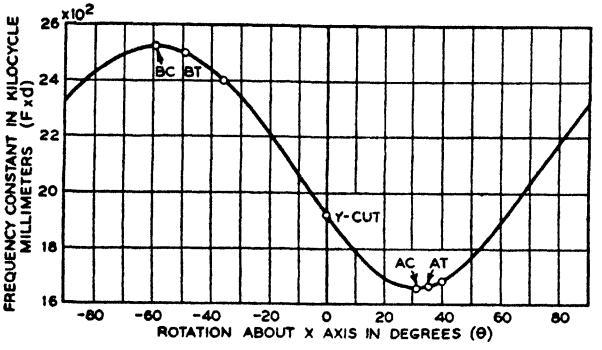

FIG. 6.12. Frequency constant in kilocycle millimeters for a rotated *Y*-cut crystal.

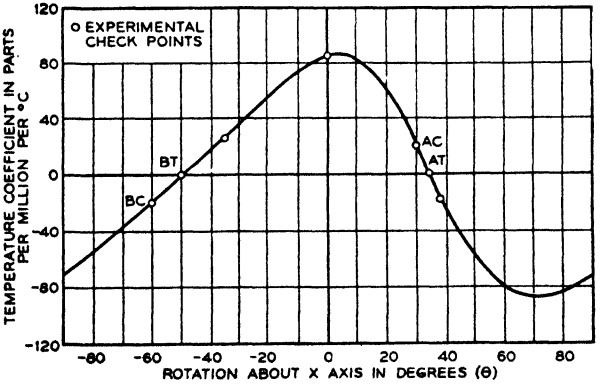

FIG. 6.13. Temperature coefficients for rotated *Y*-cut crystals.

Since the *AT* and *BT* are relatively near in angle to the *AC* and *BC* cuts, they have a good frequency spectrum. Strong couplings still exist to flexure modes of motion. By measuring the modes of motion as a function of the length, width and thickness, dimensional ratios can be obtained for which only the main mode exists for a large frequency range on either side

[20] Mason, W. P. and I. E. Fair, "A New Direct Crystal Controlled Oscillator," *Proc. I.R.E.*, Vol. 30, pp. 464–472, Oct., 1942.

of the main frequency.[21] By maintaining these ratios fixed as the thickness is changed, a good crystal free from resonances over a wide temperature range is obtained. Crystals produced by the process of grinding to a set of predetermined dimensions are called predimensioned crystals and usually result in a higher activity crystal and one which has a smooth temperature-frequency curve over a wide temperature range. Another manufacturing process called the edge-grinding process, is sometimes employed. This consists in controlling the thickness dimension only, and removing troublesome couplings by grinding the edges of the crystal until the crystal has a high activity over a specified temperature range. This process has been used for crystals that do not have to satisfy stringent activity and temperature requirements, but is not likely to produce as satisfactory crystals as the predimensioning process.

Thickness-vibrating crystals may either be ground or etched to frequency. On account of an aging which appears to be due to loosely bound and misoriented layers of quartz on the surface caused by sawing and lapping processes, it has become customary to etch crystal surfaces to frequency since this process removes the loosely bound material and leaves a surface that does not age appreciably. Aging appears to be caused by the effects of water vapor on the strained surface which results in either loosening or removing the strained material. The first process causes a lowering of the Q of the crystal (ratio of reactance to resistance) and a consequent lowering of the activity of the oscillator controlled by the crystal, while the second process causes an increase in the frequency of the crystal. Aging can be prevented by etching the crystal surface or by hermetically sealing the crystal.

Two other methods of adjusting the frequency of crystals have recently been employed. One[22] uses a crystal whose frequency is etched above the desired frequency by a predetermined number of kilocycles and then lowered by plating of a metal by an evaporation process. The metal is evaporated by an amount necessary to load the crystal down to its desired frequency. By this method the frequency can be very accurately controlled in the final mounting that the crystal uses. The other method employs the recently discovered fact that exposure to X-ray irradiation lowers the elastic constant of BT and AT crystals and hence lowers their frequency of oscillation.[23] The effect is produced by electrons being

[21] Sykes, R. A., "Modes of Motion in Quartz Crystals," *B.S.T.J.*, Vol. 23, No. 1, Jan., 1944. This also appears in reference 6, Chapter VI.

[22] Sykes, R. A., "High Frequency Plated Quartz Crystal Units for Control of Communications Equipment," *Proc. I.R.E.*, Vol. 34, No. 2, p. 92W Feb., 1946; *Proc. I.R.E.*, Vol. 36, No. 1, pp. 4–7, Jan., 1948.

[23] Frondel, C., "Effect of Radiation on the Elasticity of Quartz," *Amer. Min.*, Vol. 30, May, 1945.

expelled from orbits around silicon atoms in the quartz and causing a lower energy of binding between molecules and hence a slightly lower elastic constant. This effect amounts to one-tenth of one per cent frequency change at the most and varies by considerable factors from crystal to crystal, presumably due to the amount of their impurity content. Exposure to X-rays causes a darkening of the crystal and the amount of darkening appears to be correlated with the amount of frequency change. Because of the variability of the effect, this process has not had a wide use.

Two other rotated Y-cut crystals that have a zero temperature coefficient are the CT and DT face-shear cuts.[24] These are nearly at right angles to the AT and BT cuts and use the same shearing moduli in the face-shear mode that the AT and BT do in the thickness-shear mode. The CT cut at $+38°$ orientation, as shown by Fig. 6.3, has a frequency constant of 308 kilocycles centimeters for a square crystal and has been used in frequency-modulated oscillators in the frequency range from 300 kc to 1000 kc. The DT crystal is smaller for the same frequency and is used in the frequency range from 200 to 500 kilocycles. The CT crystal received wide use in frequency-modulated oscillators for tank and artillery radio circuits during the past war.

The final rotated Y-cut crystal that has been used considerably for controlling very precise oscillators for time standards and for use in the Loran navigation system, is the GT crystal.[25] This crystal is produced, as shown by Fig. 6.3, by rotating the plane by $51° - 7.5'$ from y and by rotating the length $45°$ from the x-axis. It has been found that the frequencies of all the zero coefficient crystals can be represented by an equation of the type

$$f = f_0[1 + a_2(T - T_0)^2 + a_3(T - T_0)^3 \cdots] \qquad (6.25)$$

where the successive constants decrease very rapidly and T_0 is the temperature of the zero coefficient. Most zero temperature coefficient crystals have a parabolic temperature variation about T_0 with a curvature determined by the constant a_2, as shown by Fig. 6.14. An exception to this rule is the AT cut for which a_2 is zero and the frequency change is determined by a_3. To obtain the value plotted, the angle of orientation has to be very closely $35° - 17'$. If the angle is 3 minutes smaller, a positive temperature coefficient of 1 part in a million per degree centigrade is superposed on this characteristic, while a 3 minute increase in orientation introduces a negative coefficient of the same order of magnitude. This characteristic is much more favorable for a wide temperature range than

[24] Willard, G. W. and S. C. Hight, *Proc. I.R.E.*, Vol. 25, pp. 549–563, 1937.

[25] Mason, W. P., "A New Crystal Plate Designated the 'GT'," *Proc. I.R.E.*, Vol. 28, pp. 220–223, May, 1940.

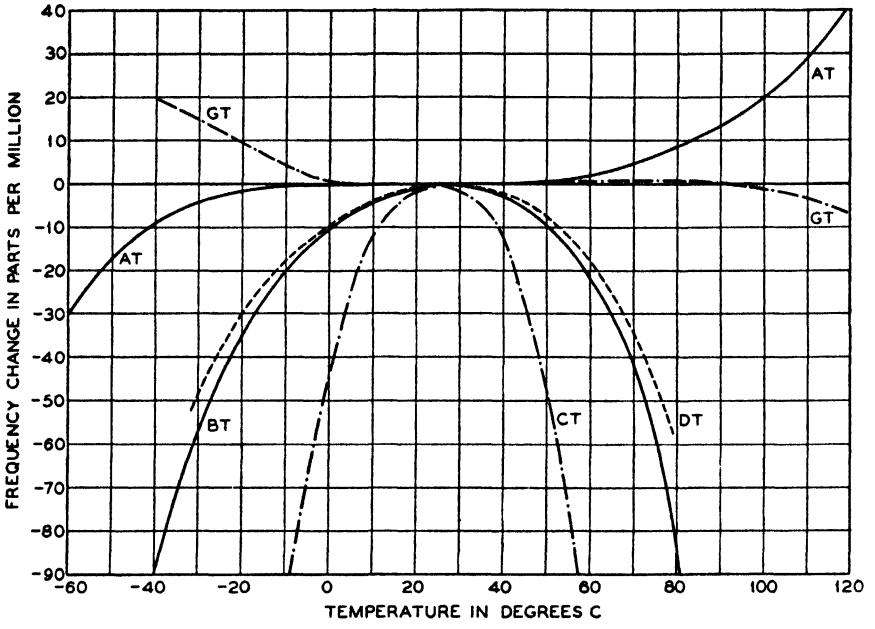

FIG. 6.14. Temperature frequency characteristics of zero temperature coefficient quartz crystals.

the *BT*; hence *AT* crystals are used where close tolerances over a wide temperature range are required.

The *GT* crystal has a similar freedom from a parabolic variation of frequency with temperature. The *GT* is a coupled-mode type of vibration and by adjusting the ratio of width to length, a positive or negative temperature coefficient can be superposed on the temperature curve of Fig. 6.14. Using a crystal mounted by means of several wires soldered to the crystal surface,[26] a very stable unit is obtained which is little-affected by shocks and which ages very little over a long period of time. This has resulted in an oscillator that maintains its frequency to 1 part in 10^9 or better, over long periods of time and has made possible the precise timing necessary in the Loran system and in very stable time standards.[27]

6.43 *Generalized Low-Temperature Coefficient Crystals*

In addition to the single- and double-orientation crystals described previously, whole families of triple-orientation crystals can be obtained

[26] Greenidge, R. M. C., "Mounting and Fabrication of Plated Quartz Crystal Units," *B.S.T.J.*, Vol. 23, p. 234, July, 1944. This also appears in reference 6, Chapter XII.

[27] Jones, H. Spencer, *Endeavor*, Vol. 4, No. 16, Oct., 1945.

with zero temperature coefficients. While none of these have come into practical use, it appears worth-while to point out their existence and method for analyzing their location. By knowing the elastic constants of the crystal, their temperature coefficients, and how these vary with orientation, regions of low coefficients can be analyzed by calculation.

Several measurements have been made of the temperature coefficients of quartz. The latest determination[28] of the writer's, which agrees within a few per cent with determinations of Bechmann and Atanasoff and Hart, are given in equation (6.26) expressed in terms of changes in parts per million per degree centigrade.

$$\begin{aligned}
Ts_{11}^E &= +\ 11.8 & Ts_{44}^E &= +\ 195 & Tc_{14}^E &= +\ 90 \\
Ts_{12}^E &= -1350 & Ts_{66}^E &= -\ 134 & Tc_{33} &= -\ 205 \\
Ts_{13}^E &= -\ 295 & Tc_{11}^E &= -\ 46.5 & Tc_{44}^E &= -\ 166 \\
Ts_{14}^E &= +\ 120 & Tc_{12}^E &= -3300 & Tc_{66}^E &= +\ 164 \\
Ts_{33} &= +\ 182 & Tc_{13}^E &= -\ 700
\end{aligned} \tag{6.26}$$

These coefficients, with the elastic constants of quartz given by equations (6.2) and the temperature coefficients of expansion which are

$$\alpha_3 = 7.8 \times 10^{-6}, \quad \alpha_1 = \alpha_2 = 14.3 \times 10^{-6} \tag{6.27}$$

are sufficient to determine the temperature coefficient of any mode of motion whose frequency can be given in terms of the elastic constants.

For example, the temperature coefficient of frequency of a longitudinal mode can be calculated from the frequency equation

$$f = \frac{1}{2l\sqrt{\rho s_{11}^{E'}}} \tag{6.3}$$

The equation fits the elastic compliance of a rotated cut and the above temperature coefficients. The variation of $s_{11}^{E'}$, which is the inverse of Young's modulus, as a function of orientation is investigated in Chapter V, and in terms of the IRE orientation system shown by Fig. 6.15, the oriented modulus is

$$\begin{aligned}
s_{11}^{E'} = {} & s_{11}^E (\cos^2\theta \cos^2\psi + \sin^2\psi)^2 \\
& + (2s_{13} + s_{44}^E) \sin^2\theta \cos^2\psi (\cos^2\theta \cos^2\psi + \sin^2\psi) \\
& + s_{33} \sin^4\theta \cos^2\psi - 2s_{14}^E \sin\theta \sin\psi \cos\psi \\
& \times [3 (\cos\varphi \cos\theta \cos\psi - \sin\varphi \sin\psi)^2 \\
& - (\sin\varphi \cos\theta \cos\psi - \cos\varphi \sin\psi)^2]
\end{aligned} \tag{6.28}$$

[28] Mason, W. P., "Quartz Crystal Applications," *B.S.T.J.*, July, 1943.

Differentiating equation (6.3) with respect to θ, the temperature, we have

$$\frac{df}{d\theta} = -\frac{1}{2l}\sqrt{\frac{1}{\rho s_{11}^{E'}}}\left[\frac{\frac{dl}{d\theta}}{l} + \frac{1}{2}\left(\frac{\frac{d\rho}{d\theta}}{\rho} + \frac{\frac{ds_{11}^{E'}}{d\theta}}{s_{11}^{E'}}\right)\right]$$

or

$$\frac{\frac{df}{d\theta}}{f} = T_f = -\alpha_l - \frac{1}{2}[T_\rho + Ts_{11}^{E'}] \tag{6.29}$$

where T_A, the temperature coefficient of the quantity A is defined as the rate of change of A with temperature divided by the value of A. For a

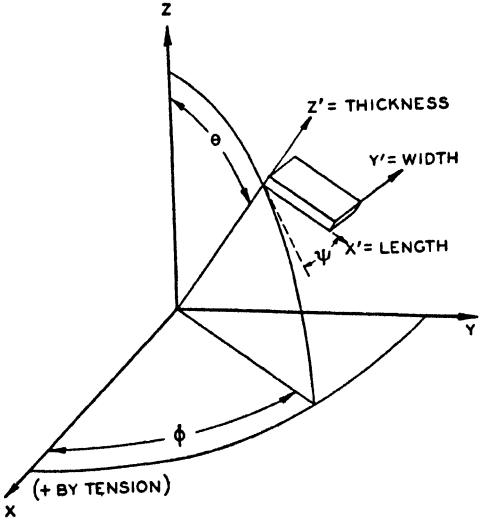

FIG. 6.15. I.R.E. orientation system.

general orientation, the temperature coefficient of the length α_l' varies as

$$\alpha_l' = 14.3 - 6.5\,(\sin^2\theta\cos^2\psi) \tag{6.30}$$

Since the total mass is the same when the crystal expands, the temperature coefficient of the density is the negative of the sum of the coefficients of the three axes or

$$T_\rho = -36.4 \tag{6.31}$$

Hence the temperature coefficient of frequency becomes

$$T_f = 3.9 + 6.5\sin^2\theta\cos^2\psi - \frac{1}{2}\left(\frac{\frac{ds_{11}^{E'}}{d\theta}}{s_{11}^{E'}}\right) \tag{6.32}$$

Differentiating equations (6.28), we have the temperature coefficient for a general orientation

$$T_f = 3.9 + 6.5 \sin^2\theta \cos^2\psi$$

$$-\frac{1}{2}\left[\frac{\begin{array}{c} s_{11}^E T s_{11}^E (\cos^2\theta\cos^2\psi + \sin^2\psi)^2 \\ + (2s_{13}Ts_{13} + s_{44}^E Ts_{44}^E)\sin^2\theta\cos^2\psi(\cos^2\theta\cos^2\psi + \sin^2\psi) \\ + s_{33}Ts_{33}\sin^4\theta\cos^4\psi - 2s_{14}^E Ts_{14}^E \sin\theta \\ \times \sin\psi\cos\psi[3(\cos\theta\cos\varphi\cos\psi - \sin\varphi\sin\psi)^2 \\ - (\sin\varphi\cos\theta\cos\psi + \cos\varphi\sin\psi)^2] \end{array}}{\begin{array}{c} s_{11}^E(\cos^2\theta\cos^2\psi + \sin^2\psi)^2 + (2s_{13} + s_{44}^E)\sin^2\theta\cos^2\psi \\ \times (\cos^2\theta\cos^2\psi + \sin^2\psi) + s_{33}\sin^4\theta\cos^4\psi \\ - 2s_{14}^E \sin\theta\sin\psi\cos\psi[3(\cos\varphi\cos\theta\cos\psi - \sin\varphi\sin\psi)^2 \\ - (\sin\varphi\cos\theta\cos\psi + \cos\varphi\sin\psi)^2] \end{array}}\right] \tag{6.33}$$

Introducing the values of the elastic constants from (6.2) and the temperature coefficients from (6.26), equation (6.34) takes the numerical values

$$T_f = 3.9 + 6.5 \sin^2\theta \cos^2\psi$$

$$-\left[\frac{\begin{array}{c} 755(\cos^2\theta\cos^2\psi + \sin^2\psi)^2 + 22{,}565\sin^2\theta\cos^2\psi \\ \times (\cos^2\theta\cos^2\psi + \sin^2\psi) + 8700\sin^4\theta\cos^4\psi \\ + 5310\sin\theta\sin\psi\cos\psi[3(\cos\varphi\cos\theta\cos\psi - \sin\varphi\sin\psi)^2 \\ - (\sin\varphi\cos\theta\cos\psi + \cos\varphi\sin\psi)^2] \end{array}}{\begin{array}{c} 127.9(\cos^2\theta\cos^2\psi + \sin^2\psi)^2 + 175.8\sin^2\theta\cos^2\psi \\ \times (\cos^2\theta\cos^2\psi + \sin^2\psi) + 95.6\sin^4\theta\cos^4\psi \\ + 89.2\sin\theta\sin\psi\cos\psi[3(\cos\varphi\cos\theta\cos\psi - \sin\varphi\sin\psi)^2 \\ - (\sin\varphi\cos\theta\cos\psi + \cos\varphi\sin\psi)^2] \end{array}}\right] \tag{6.34}$$

The only regions of low-temperature coefficients are the regions for which the two, big middle terms are small, which requires that $\theta \to 0$, or $\psi \to 90°$. The first region would be a Z-cut crystal with its length somewhere in the xy-plane and would result in a temperature coefficient of two parts per million negative. Such a crystal is not of much interest since there is no piezoelectric constant for driving it. The other region $\psi \to 90°$ also results in the length being near the xy crystallographic plane, but would allow the major surface to be made perpendicular to the x-axis and hence would allow the crystal to be driven piezoelectrically. By allowing ψ to be slightly greater than 90°, the fourth term in the numerator can be made slightly negative and of a value greater than the two positive

terms. This results in the $+5°$ X-cut crystal having nearly a zero coefficient and this is the most favorable one for a low coefficient longitudinal mode of motion. All other directions have a negative temperature coefficient.

The temperature coefficients of many other modes of motions can be derived in a similar manner, but since none of them have come into practical use, they will not be considered further.

6.5 *Quartz Crystal Applications*

As mentioned in the introduction, the principal uses for quartz crystals are in the control of radio-frequency oscillators, the production of very selective filters, and as high-frequency electromechanical transducers for producing and measuring mechanical vibrations in gases, liquids and solids. It is the purpose of this section to discuss briefly the uses of quartz crystals in oscillators and filters. The last three chapters are devoted to the use of crystal transducers in measuring the properties of gases, liquids and solids.

6.51 *Use of Quartz Crystals in the Control of Oscillators of the Pierce Type*

A vacuum-tube oscillator is a device for producing and maintaining a source of power having a definite frequency of oscillation. It involves the use of a vacuum-tube amplifier for producing a gain and a feedback circuit which produces a phase shift of $2n\pi$ radians (n an integer, usually one) at the frequency of oscillation. Hence, when the oscillator is started, a transient in the circuit (which will have a wide range of frequencies) will be amplified, but it is only the frequency that comes back in the same phase that will continue to build up. This frequency will build up until it is limited by the non-linear elements of the vacuum-tube amplifier. Hence, the condition for determining the frequency and amplitude of oscillation are that the gain through the complete feedback path must be equal to zero and the phase shift through the feedback loop must be equal to 2π radians or some integral multiple of this. This criterion is often written in the form

$$\mu\beta = 1 \tag{6.35}$$

where μ is the complex amplification factor of the tube (*i.e.*, the ratio of the output plate voltage to the input grid voltage) and β is the same factor for the feedback path.

Since non-linear parameters are involved in the vacuum-tube amplifier, the solution for the stability is rather complex. The general conditions for determining the frequency stability of an oscillator has been given by

Llewellyn[29] and solutions for crystal oscillators have been given by Terry, Wright, Vigoureux, Koga, Heegner, Boella and Fair.[30] Since these are summarized by I. E. Fair in Chapter XII of the book *Quartz Crystals for Electrical Circuits*, they will not be discussed further. It is there shown that an approximate idea of the conditions for frequency stability can be obtained by representing the feedback circuit by the three reactances X_1, X_2 and X_3 of Fig. 6.16 and the tube parameter by a plate resistance R_p, a grid resistance R_G and a source of voltage μV_g where V_g is the voltage across the grid resistance R_g, and μ is the amplification factor of the tube. For circuits of the Pierce type, shown by Fig. 1.2, X_1 is the reactance of the tuning condenser and coil in the plate of the tube, X_3 the reactance feedback

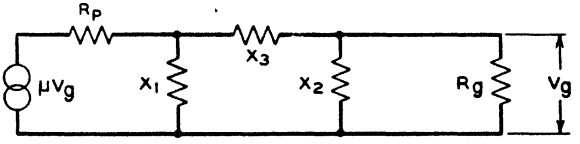

FIG. 6.16. Equivalent circuit for analyzing performance of an oscillator.

from plate to grid, and X_2 the reactance from grid to cathode. For a single tube, the sign of the amplification factor μ is negative, since a positive grid voltage will produce a reduction in the voltage across the plate.

Crystal oscillators can be divided into two classes, those in which the oscillator frequency is modified by the presence of the crystal, and those in which the oscillator will not oscillate unless the crystal is present. An example of the first class is shown by the Giebe, Scheibe click oscillator of Fig. 4.1, for which the oscillator frequency is controlled by the crystal, if the adjustment of the coil and condenser is such that the oscillator frequency, as controlled by them, is in the neighborhood of the crystal frequency. If the frequency of the coil condenser oscillator alone is far from the crystal frequency, the crystal acts as a simple capacitance and has no effect on the oscillator frequency. Examples of the crystal-controlled oscillator are the Pierce-Miller circuits of Fig. 1.2A and the Pierce circuit of Fig. 1.2B. If the crystal of either of these circuits becomes broken or loses its activity, the oscillator will stop oscillating.

These two circuits are probably the most widely used crystal-oscillator circuits. In the Pierce-Miller circuit of Fig. 1.2A, the crystal is in the grid circuit and feedback is obtained through the grid-plate capacitance or

[29] Llewellyn, F. B., "Constant Frequency Oscillators," *Proc. I.R.E.*, Vol. 19, p. 2063, Dec., 1931.

[30] These solutions are discussed by I. E. Fair in Chapter XII of *Quartz Crystals for Electrical Circuits*, D. Van Nostrand Company, Inc., 1946.

through an external capacitance sometimes added. For the Pierce circuit, feedback is obtained through the crystal itself and the grid-cathode capacitance is the source of the reactance X_2. If the oscillator is not driven so hard that the grid goes positive and grid current is drawn, the grid resistance R_g becomes very high and can be neglected. Under these circumstances it can be shown that the frequency occurs very nearly when

$$X_1 + X_2 + X_3 = A \doteq 0 \tag{6.36}$$

where A is a small quantity, determined by the tube constants, and is nearly zero for a high-gain tube. This condition is determined by the fact that the three reactances have to produce a 180°-phase shift and if the amplification factor μ is high, their sum is nearly zero to produce a zero gain. Furthermore, it can be shown[31] that the conditions of oscillation are not satisfied unless the crystal reactance is positive. Hence, in these circuits, the oscillating frequency is always between the resonant and anti-resonant frequencies of the crystal.

By tuning the plate circuit by the variable condenser, X_1 will vary and hence in order to satisfy equation (6.36), the frequency of the oscillator will vary. However, since the change in reactance with frequency (as shown by Fig. 5.1) is so sharp, the amount of frequency change that can be obtained by tuning is small and can be made smaller by letting f_A approach f_R. This can be accomplished by using a crystal with small coupling or by shunting capacitance around the crystal. Due, however, to the fact that the crystal has some dissipation, this process cannot be carried too far or the loss in the feedback circuit will become too large for the tube amplification to overcome. As shown by Mason and Fair[31] a figure of merit M for such crystals is given by

$$M = \frac{Q}{r} \tag{6.37}$$

where r is the ratio of capacitances (C_0/C_1 of Fig. 5.1) for the crystal and where Q is the ratio of reactance of one of the series elements L_1 or C_1 of Fig. 5.1 to the resistance R_1. If this figure of merit is greater than 2, the reactance of the crystal becomes positive and by employing enough gain the crystal can always be made to oscillate. To maintain oscillations within a narrow limit of frequency, the ratio of capacitances of the crystal must be high, and to maintain oscillations for a high ratio of capacitances, the Q of the crystal must be high. The same considerations apply to the change of frequency due to change in tube parameters caused by fluctuation of plate current, change of tubes, etc. These change the factor A of

[31] Mason, W. P. and I. E. Fair, "A New Direct Crystal-Controlled Oscillator for Ultra-Short Wave Frequencies," *Proc. I.R.E.*, Vol. 30, p. 464, Oct., 1943.

equation (6.36) and cause a slight change in frequency in order that the reactances shall balance (6.36). However, if the ratio of capacitances and the Q of the crystal are high, this results in a very small change of frequency.

It has been shown by Fair[30] that a quantity which determines the activity and frequency stability of a given crystal in a definite oscillator circuit, is the performance index PI of the crystal and circuit. When this factor is known, the frequency stability and the oscillator activity can be uniquely determined. In terms of the figure of merit M, the static capacitance of the crystal C_0 and C_t, the total input grid capacitance of the circuit, PI is

$$\text{PI} = \frac{M}{\omega C_0 \left(1 + \frac{C_t}{C_0}\right)^2} \tag{6.38}$$

Methods for measuring the PI of a crystal for a given circuit are discussed by C. W. Harrison in Chapter XV of "Quartz Crystals for Electrical Circuits."

Circuits of the Pierce and Pierce-Miller type are capable of maintaining the frequency of a crystal oscillator within a few parts in a million and can be changed in frequency by about 200 parts in a million by a tuning of the plate condenser. They are the most widely used oscillator circuits.

6.52 *Oscillators of the Bridge Type*

Oscillators of the Pierce type satisfy the requirements for most crystal oscillators where a moderate amount of frequency stability is satisfactory. For very precise oscillators, however, the Pierce type is not the most stable type. This is obvious from Fig. 6.16, for if the coupling circuit between plate and grid can be made of pure resistances, then a change in the plate and grid resistances due to voltage fluctuation will not involve any frequency change. Also in the Pierce circuits there is no way to limit or control the amplitude of the crystal, which is an important matter if very precise frequencies are to be obtained.

Both of these limitations are removed in the resistance bridge circuit devised by Meacham,[32] which is shown schematically by Fig. 6.17. With this circuit a transformer is used to reverse the phase of the output voltage and the feedback circuit has to produce a zero phase shift in order to establish the conditions for oscillation. The crystal is one arm of a resistance bridge and in order to produce a zero phase shift in the bridge, the crystal has to work at its resonance frequency. The control of amplitude is obtained by using a small resistance lamp or thermistor as another

[32] Meacham, L. A., "The Bridge Stabilized Oscillator," *Proc. I.R.E.*, Vol. 26, pp. 1278–1294, 1938; *B.S.T.J.*, Vol. 17, pp. 574–591, 1938.

arm of the bridge. As the amplitude builds up, the resistance of this element gets less and the bridge tends to become balanced. This increases the loss of the bridge circuit and cuts down the amplitude. Hence, a stable amplitude is quickly reached which depends on the thermal element rather than the non-linear tube parameters. The thermal element is usually chosen so that the crystal amplitude is very small, and since the amplitude is maintained at a constant value, no frequency fluctuation due to amplitude variations occur. The Meacham bridge oscillator is used in all of the very constant frequency oscillators of the Bell System, Bureau of Standards and the Greenwich Observatory.

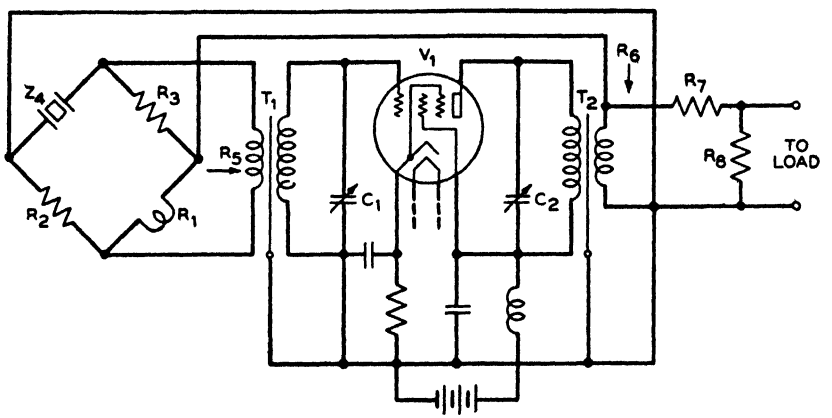

FIG. 6.17. Meacham bridge oscillator.

Another limitation of the Pierce type circuit is that the crystal has to have a positive reactance in order that oscillation can be produced. This limits the use of the Pierce oscillator circuit in driving the crystal at a high overtone frequency. To obtain a positive reactance the figure of merit M has to be greater than 2. It can be shown from equation (5.34) that the ratio of capacitances of a crystal increases as the square of the overtone order. For example, a BT crystal having a ratio of capacitances of 1000 for the fundamental and a Q of 100,000, will have a figure of merit $M = 4$ for the fifth overtone frequency, that is, five times the fundamental. In practice it is found that the fifth overtone frequency is as high as can be consistently driven by an oscillator circuit of the Pierce type.

To get around this difficulty, the writer and Fair[31] proposed the use of a bridge-type circuit in the feedback path, the arms of which are the crystal and three capacitances. Various forms of the circuit are possible and a self-contained bridge was also constructed. The capacitance of the crystal is balanced out by the bridge capacitances and the limitation that

the crystal has to have a positive reactance is removed. With this arrangement, the 23rd overtone of an 8.56-megacycle *AT* crystal was driven and frequencies as high as 197 megacycles were controlled. The crystals had to be ground very flat to be active in this high-frequency range and commercially the 9th overtone of a 10-megacycle plate is about as high as has been used.

6.53 *Use of Crystals in Filters*

The largest use of crystals in the telephone industry is their use in the very selective band-pass filters of the broad-band carrier frequency systems. For this purpose quartz crystals have been largely used, but as discussed in Chapter IX, they are being replaced by a new synthetic crystal, ethylene diamine tartrate. Since the use of crystals in filters is fully discussed in Chapter VIII of "Electromechanical Transducers and Wave Filters" by the writer, only a brief summary will be given here.

The crystal element of Fig. 5.1 is equivalent to a combination of coils and condensers of high Q having the reactance characteristic of Fig. 5.1B. Due to the fundamental limitation of about 10 per cent electromechanical coupling obtainable in a quartz crystal, the separation of resonance and anti-resonance is from equation (5.36) equal to

$$\frac{\Delta f}{f_R} \doteq \frac{4}{\pi^2} k^2 \doteq .004 \tag{6.39}$$

or about 0.4 per cent of the resonant frequency f_R. Hence, if we deal only with combinations of crystals, it can be shown that the widest pass bands obtainable are twice this or 0.8 per cent. This is too narrow for most communication bands, but narrow band filters of this type have been used for essentially single-frequency pilot channel filters and for analyzing the spectrum of noise and speech. Such crystals can be combined into T and π networks and in lattice networks. The filter circuits and their design formulae are discussed in the above reference.

For the wider band filters needed for passing voice channels, it is necessary to employ coils as well as condensers and crystals. Since the ratio of reactance to resistance of the best coils mounted in a reasonable space does not exceed 400, attention must be given to the effect of dissipation.

In a filter the effect of dissipation is twofold. It may add a constant loss to the insertion loss characteristic of the filter, and it may cause a loss varying with frequency in the transmitting band of the filter. The second effect is much more serious since the additive loss can be overcome by the use of vacuum-tube amplifiers, whereas the second effect limits the slope of the insertion-loss frequency curve. Hence, if the dissipation in the coils

needed to widen the band of the filter produce only an additive loss, a satisfactory result is obtained.

By using only series or shunt coils on the ends of the filters, this result can be accomplished, for the coil resistances can be made part of the terminating resistances and add only a constant loss independent of frequency. Figure 6.18 shows the most common filter configuration[33] employing coils, crystals and condensers. In this configuration two divided plate crystals form the four arms of the lattice. The two halves of the crystal Q_1 form the series arms of the lattice while the two sets of plates on Q_2 form the crossarms. The two small condensers C_B are used for the adjustment of the frequencies of the attenuation peaks. The condensers C_A on the ends of the bridge serve to adjust the band width of the filters

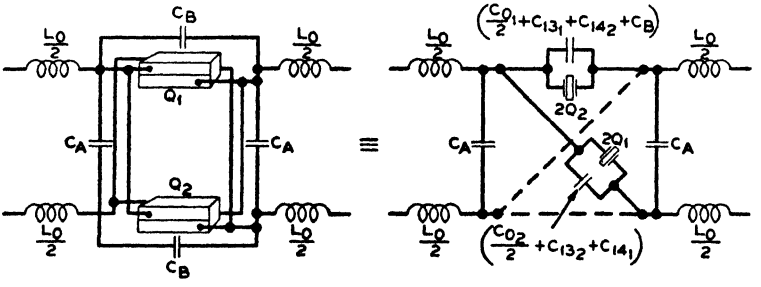

FIG. 6.18. Crystal filter using a lattice of crystals and series coils.

together with the coils L_0. Each end coil consists of two balanced windings, each of which form the two coils $L_0/2$. The equivalent electrical circuit for the divided plate crystals are shown on the right side of the figure, where $2Q_1$ and $2Q_2$ indicate the equivalent electrical circuit of a crystal (shown by Fig. 5.1) of twice the impedance of the fully plated crystal.

It is shown[34] that the attenuation of such a filter section is equal to the sum of three "m" derived type band filter sections. With the coils on the end of the sections, one of these sections is of the type having an infinite loss at an infinite frequency. The frequency of infinite loss of the other two sections is adjustable and is controlled by the relative impedances and frequencies of the two crystals Q_1 and Q_2. The formulae for designing these crystals are discussed in reference.[34]

This filter section can be generalized by the addition of crystals to the series or crossarms of the lattice. If one crystal is taken out and a condenser substituted, the attenuation corresponds to two simple filter sec-

[33] This configuration is covered in U. S. Pat. No. 2,045,991, issued to the writer.

[34] Mason, W. P., *Electromechanical Transducers and Wave Filters*, Chapter VIII, D. Van Nostrand Company, Inc., 1942, 2nd edition, 1948.

tions. The addition of a crystal in either the series or crossarms adds the equivalent of a simple filter section. The use of two divided plate crystals in both the series and the crossarms forms the basis of the 219-type quartz crystal filters[35] and in this filter the equivalent of five simple band-pass filters is obtained in a single lattice configuration. This filter provides sufficient attenuation to meet the requirements of the broad-band carrier filters. By using other configurations[34] of coils, crystals and condensers low-pass, high-pass, band-elimination filters, and all pass-phase networks are possible.

[35] Willis, E. S., "A New Crystal Channel Filter for Broad Band Carrier System," *Elec. Eng. Trans. Sec.*, March, 1946.

CHAPTER VII

Properties and Uses of Rochelle Salt

7.1 *Introduction*

Rochelle salt was first produced in 1672 by an apothecary of LaRochelle by the name of Pierre de la Seignette. While the medical and chemical properties of rochelle salt became well-known, it was not until 1880 that anything remarkable was discovered about its physical properties. In that year the Curie brothers included it in their pioneer researches on the piezoelectric effect and found it to be strongly piezoelectric.

The first quantitative measurements of the piezoelectric effect in rochelle salt were made by Pöckels in 1894. In the course of his experiments, Pöckels also discovered the Kerr effect in rochelle salt as well as the anomalous dielectric behavior in the directions of the *a* or *x* crystallographic axis.

The first descriptions of technical applications of rochelle salt crystals were made by A. M. Nicolson[1] in 1919. Nicolson described the application of rochelle salt in obtaining piezoelectric microphones, receivers, loudspeakers, etc., and also used rochelle salt crystals in controlling the frequency of the first piezoelectric crystal-controlled oscillator.[2]

These early investigations were followed a few years later by a series of important papers by J. Valesek, in which the piezoelectric and dielectric properties of the crystal were thoroughly investigated. His most important work was on the analogy between the dielectric properties of rochelle salt and ferromagnetism, which is the source of the description of the properties of rochelle salt as being ferroelectric.

Widespread interest in the structural theory of rochelle salt started in 1929 with the work of the Russians, Shulvas-Sorokina and I. Kurchatov and his collaborators. This has been followed by many investigations, both theoretical and experimental, outstanding among which are those of Scherrer and his associates in Zurich; Fowler, Beevers and Hughes, and Ubbelohde and Woodward in England; and Cady, Mueller and the writer in this country. Theories of the action of rochelle salt have been given

[1] Nicolson, A. M., "The Piezoelectric Effect in the Composite Rochelle Salt Crystal," *Trans. A.I.E.E.*, Vol. 38, pp. 1467–1485, 1919; *Proc. A.I.E.E.*, Vol. 38, pp. 1315–1333, 1919.

[2] U. S. Pat. No. 2,212,845, filed April 10, 1918, issued August 27, 1940.

by Fowler, Cady, Mueller and Busch. Since they are described in detail in Cady's " Piezoelectricity," they are not discussed here. A theoretical treatment of the ferroelectric effect for rochelle salt and KDP due to the writer, is given in Chapter XI. This is similar in structure to Mueller's " internal field " theory, but an attempt has been made to associate the theory with the hydrogen bonds occurring in the structures. It is the purpose of the present chapter to describe briefly some of the physical and chemical properties of the crystal.

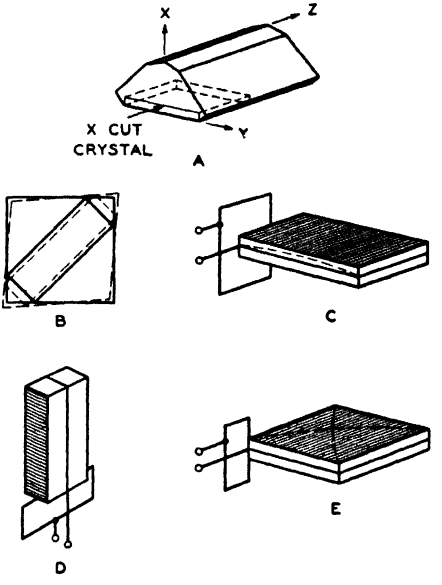

FIG. 7.1. Rochelle salt crystal and principal cuts.

7.11 *General Properties of Rochelle Salt*

Rochelle salt is sodium potassium tartrate with four molecules of water of crystallization ($NaKC_4H_4O_6$—$4H_2O$) and forms in the orthorhombic bisphenoidal class. The usual form of the crystal is shown by Fig. 7.1A, which shows the direction of the *x*-, *y*- and *z*-axes which coincide with the *a*, *b* and *c* crystallographic axes of the crystal. Although this crystal can occur in enantiomorphic forms, it is generally true that all the tartaric acid obtained from the grape industry is of the dextro form and only dextro or *d*-rochelle salt crystals are found. The molecular weight of rochelle salt is 282.184 and the density, as measured by W. L. Bond, is 1.775 ± 0.003 at 25°C. This determination agrees very well with that determined from the X-ray structure of the cell which, as shown by Beevers and

Hughes,[3] has a cell dimension of 11.93Å along the x-axis, 14.3Å along y and 6.17Å along z. Since there are four molecules per unit cell, this gives 3.81×10^{21} molecules per cubic centimeter. Dividing this number by Avogadro's number 6.06×10^{23} and multiplying by the molecular weight 282.184, one obtains a density of 1.77. The solubility, per liter of water, at 0°C is 1.50 moles (420 g.) and at 30°C it is 4.90 moles (1,390 g.). The most common method for growing rochelle salt, and in fact most water soluble

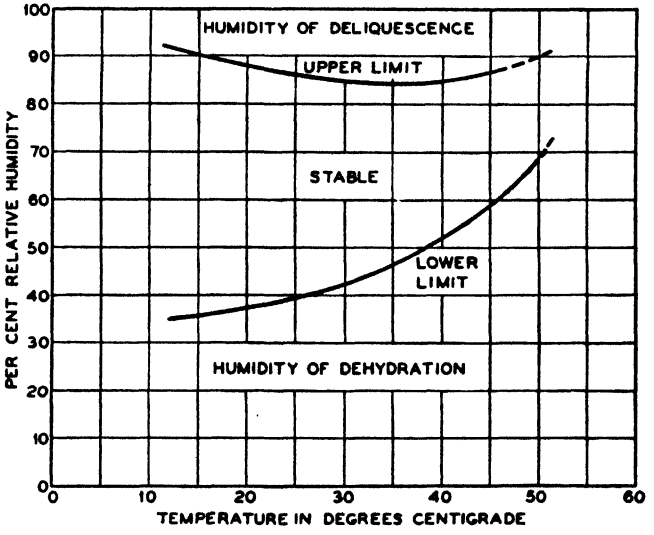

FIG. 7.2. Stable humidity limits for rochelle salt.

crystals, makes use of this solubility temperature relation. Seed bars are placed in a rocking or rotating tank which contains a supersaturated solution at about 40°C. Salt comes out of solution and is deposited on the seed bar surface, thus reducing the degree of supersaturation. To maintain it in a growing condition, the temperature is reduced a certain fraction of a degree per day, the degree of supersaturation is maintained and the crystal continues to grow. When it has reached room temperature or some convenient temperature it is removed from the tank and the process is repeated. The Brush Company of Cleveland, Ohio, are the largest growers of rochelle salt.

Since the crystal has water of crystallization, it has an appreciable vapor pressure. As shown in Fig. 7.2 lower line, if the humidity of the surround-

[3] Beevers, C. A. and W. Hughes, "The Crystal Structure of Rochelle Salt (Sodium Potassium Tartrate Tetrahydrate $NaKC_4H_4O_6—4H_2O$)," *Proc. Roy. Soc.*, Vol. 177, pp. 251–259, 1941.

ing atmosphere is below 35 per cent at 25°C, the water vapor pressure of the crystal is greater than the vapor pressure of water in the surrounding atmosphere and the crystal will lose water and dehydrate. This causes a white powder of dehydrated material to form on the outside of the crystal, which will ruin the operation of the crystal if it becomes too large. The crystal is stable between 35 and 85 per cent relative humidity at room temperature. Above 85 per cent humidity, the crystal will absorb water from the atmosphere on its surface and will slowly dissolve if kept in such an atmosphere. To minimize these humidity effects, the crystals are often coated with waxes. These retard rather than prevent the dehydration of the crystal. If the crystal can be hermetically sealed in a container, it can be made to last indefinitely by putting powdered crystalline rochelle salt and dehydrated rochelle salt in the container. The former will give up water if the temperature rises, while the latter will take up water if the temperature lowers, and the two will maintain a humidity that approximates the lower curve as a function of temperature.

At a temperature of 55°C (130°F) the crystal breaks up into sodium tartrate and potassium tartrate with the evolution of one mole of water, which dissolves the two crystals in a liquid solution. If the solution is rapidly supercooled, it remains quite fluid for a number of minutes before it crystallizes and hardens. This " melted " rochelle salt forms a very stiff glue that has been used to glue together pieces of rochelle salt.

Rochelle salt crystals are commonly cut either with a band saw or a wet string technique. They are most easily surfaced by a milling technique using a sharp high-speed cutting tool. They can also be surfaced with a sanding belt cooled with a saturated solution of the material. The most recent and satisfactory method of applying metal electrodes to their surface is by evaporating gold in a relatively high vacuum. This process has to be completed quite rapidly, since the crystal will give off moisture in a vacuum. However, if done quickly, the loss of water is negligible and very satisfactory electrodes result.

7.2 *Physical Properties of Rochelle Salt*

7.21 *Dielectric Properties of Rochelle Salt*

Between the temperature of −18°C and +24°C, rochelle salt has ferroelectric properties. By this is meant that the salt becomes spontaneously polarized in the $\pm x$-direction, and polarization-field curves show hysteresis loops just as *B-H* curves do for a ferromagnetic material. The magnitudes of the spontaneous polarization has been measured by Mueller[4] and by

[4] Mueller, H., "The Dielectric Anomalies of Rochelle Salt," *Ann. N. Y. Acad. Sci.*, Vol. 40, p. 34, 1940.

Hablützal[5] by measuring the remanent polarization of the hysteresis loop and the results are shown by Fig. 7.3 plotted as a function of temperature. The polarization rises to a value of 740 esu/cm^2 at 3°C, the optimum temperature. The figure also shows the spontaneous polarization of heavy water rochelle salt for which the hydrogens in the water of crystallization and the hydrogens in the OH groups are replaced by heavy hydrogens. The two Curie temperatures (the temperatures for which spontaneous

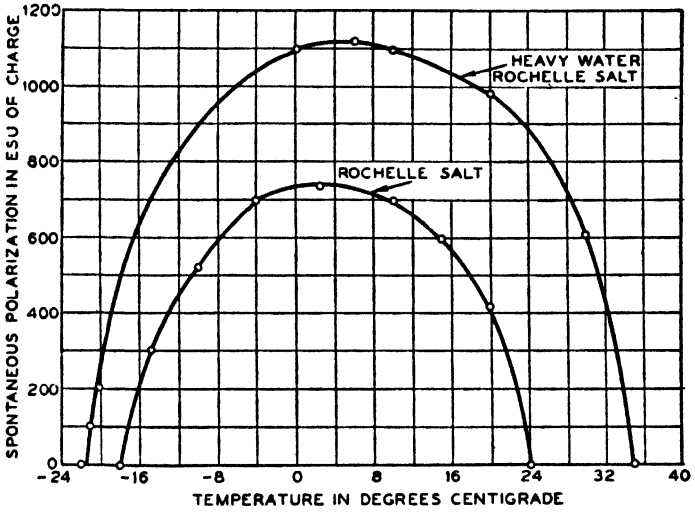

FIG. 7.3. Spontaneous polarization for rochelle and heavy water rochelle salt.

polarization occurs) are changed to −22°C and +35°C, and the spontaneous polarization increases to 1,120 esu/cm^2 at about 6°C. The Curie temperatures can also be changed by pressure. Figure 7.4 shows measurements by Bancroft[6] of the Curie temperatures of rochelle salt as a function of hydrostatic pressure. Hydrostatic pressure can raise the upper and lower Curie temperatures and cause them to separate. On the hydrogen bond theory of Chapter XI this is a result of the change with pressure of the factor

$$\frac{N\mu^2\beta}{kT\left(1-\frac{4\pi}{3}\gamma\right)}\,(1-\tanh^2\Delta/kT)$$

where the meaning of the terms is given in Chapter XI.

[5] Hablützal, J., "Dielectric Investigations of Heavy Water Rochelle Salt," *Helv. Phys. Acta*, Vol. 12, pp. 489–510, 1931.

[6] Bancroft, D., "The Effect of Hydrostatic Pressure on the Susceptibility of Rochelle Salt," *Phys. Rev.*, Vol. 53, pp. 587–590, 1938.

A typical set of hysteresis loops showing polarization versus field strength (volts per cm) for a free crystal are shown by Fig. 7.5. These are due to

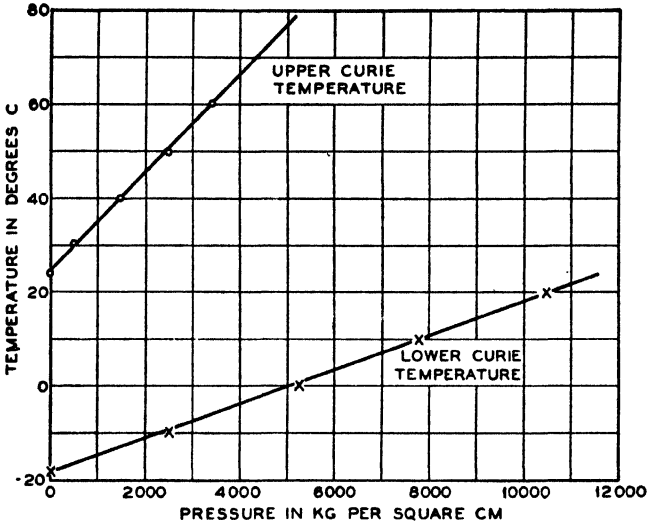

FIG. 7.4. Effect of hydrostatic pressure on upper and lower Curie temperatures.

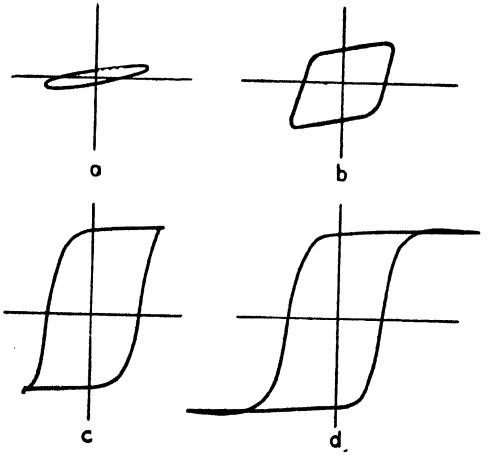

FIG. 7.5. Hysteresis loop for rochelle salt as a function of the applied voltage (after David).

David[7] and were measured at 50 cycles with the field applied along the x-axis. The curves labeled a, b, c and d are respectively for maximum

[7] David, R., "The Dependence of the Dielectric Properties of Rochelle Salt on Mechanical Conditions," *Helv. Phys. Acta*, Vol. 8, pp. 431–484, 1935.

field strengths of 30.7, 61.4, 123 and 384 volts per cm. It is obvious from these curves that the average and the instantaneous dielectric constants (which for these curves are nearly 4π times the ratio of the polarizations to the field), vary markedly depending on the field strength. The rounding off of the hysteresis loops is usually ascribed to domain structure in rochelle salt. Other evidence is the existence of a Barhausen effect,[8] the pyroelectric tests[9] with Bürker's powders, and the scattering of sound from an ultrasonic wave. From his tests Mueller concluded that the domain sizes were around 1 cm in diameter. On account of the difficulty of observing twinning in rochelle salt and KDP optically or with X-rays, not much is known about the type of twinning responsible for domain structure in these crystals. For barium titanate, on the other hand, where a 90° change in orientation of the ferroelectric axis can occur, it is definitely known that domain structure can be the result of a twinning along the 101 plane.

At low field strengths, the dielectric constant is much smaller than at high field strengths. Figures 7.6 and 7.7 show measurements[10] of the " free " dielectric constant along the x-axis plotted as a function of temperature for field strengths in the order of 5 volts per cm. The dielectric constant is about 200 midway between the Curie temperatures of $-18°C$ and $+24°C$, and increases to nearly 2000 at the Curie temperatures. Outside of the Curie region the dielectric constant falls off and at a temperature of $-157°C$, the dielectric constant decreases to a value of 7 and does not decrease farther with a lowering of the temperature. For high field strengths, the dielectric constant, as shown by Fig. 7.6, measured by the average slope of the hysteresis loop, becomes larger between the Curie points than it is at the Curie temperatures. The differential dielectric constant, represented by the instantaneous slope of the curve, may be as high as 200,000.

The dielectric constants of rochelle salt along the y- and z-axes are entirely normal and do not depend appreciably on the field strength. The dielectric constant along the y-axis ϵ_2^T, *i.e.* the " free " dielectric constant under constant stress is

$$\epsilon_2^T = 11.1 \text{ from } -10°C \text{ to } +24°C$$

and increases linearly from 11.1 to 12.5 at 45°C. The dielectric constant

[8] Mueller, H., " Properties of Rochelle Salt," *Phys. Rev.*, Vol. 47, pp. 175–191, 1935.

[9] Mueller, H., " The Dielectric Anomalies of Rochelle Salt," *Ann. N. Y. Acad. Sci.*, Vol. 40, pp. 321–356, 1940.

[10] Mason, W. P., " A Dynamic Measurement of the Elastic, Electric and Piezoelectric Constants of Rochelle Salt," *Phys. Rev.*, Vol. 55, pp. 775–789, 1939; H. Mueller, " Properties of Rochelle Salt," *Phys. Rev.*, Vol. 47, pp. 175–191, 1935.

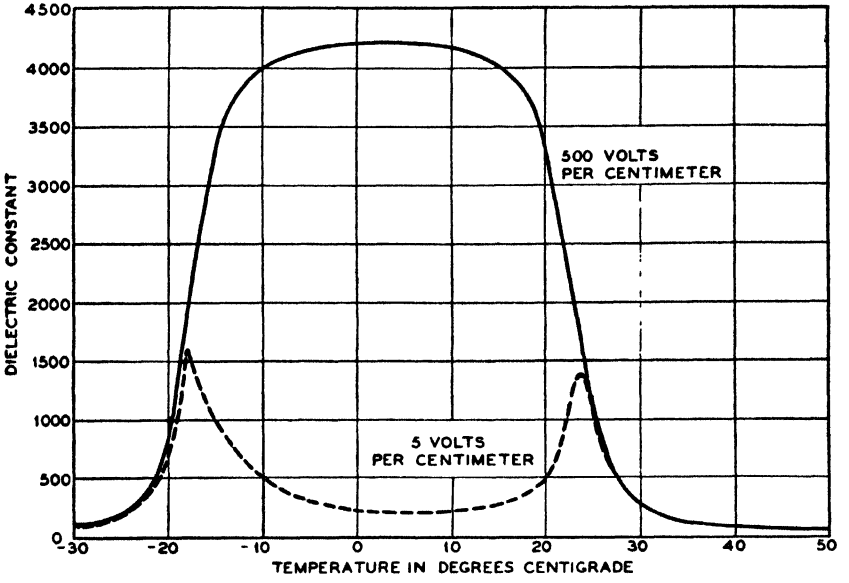

FIG. 7.6. Free dielectric constant for rochelle salt for fields of 5 and 500 volts per centimeter.

FIG. 7.7. Free inverse susceptibility of rochelle salt for temperatures below the lower Curie temperature.

normal to the z-axis is

$$\epsilon_3^T = 9.2$$

The " free " or constant stress dielectric constant determines not only the energy stored in electrical form but also that stored for a static or low-frequency voltage in mechanical form. The mechanical energy stored results from a distortion of the crystal due to the piezoelectric effect. If we clamp the crystal so that it cannot be distorted, then the only energy stored is the electrical energy and the dielectric constant corresponding to this is the clamped dielectric constant. It is difficult to clamp a crystal hard enough to prevent any mechanical distortion, but a similar result can

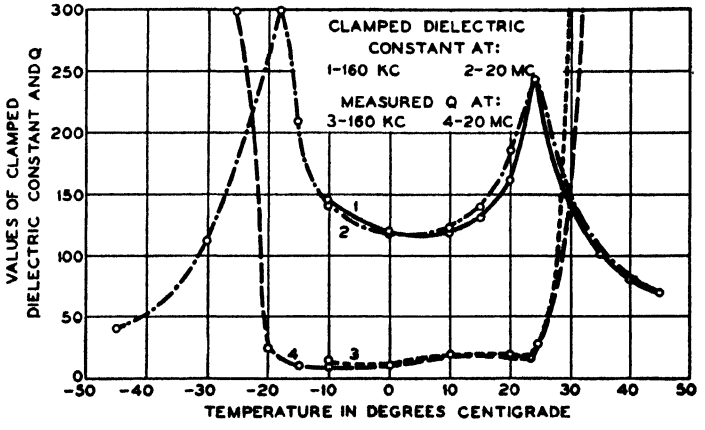

FIG. 7.8. Clamped dielectric constant for rochelle salt at low field strengths.

be obtained by measuring the crystal at a frequency so high that almost all of the natural resonances and their harmonics are lower in frequency than the value of the applied frequency. This is similar in principal to the measurement of the electronic dielectric constant of any substance. By increasing the frequency, the dipole and atomic dielectric constants fall out of the picture, because they require a motion that is too slow to follow the applied field. The clamped dielectric constant has recently been measured[11] by measuring the dielectric constant and associated resistance for a large-sized crystal ($l = 1.75$ cm; $w = 1.75$ cm; $t = 0.75$ cm) at a frequency of 20 megacycles. The result over a temperature range is shown plotted by Fig. 7.8. The dielectric constant increases to about 300 at $-18°$ and $+24°$, the two Curie temperatures. The finite value of the "clamped" dielectric

[11] Mason, W. P., "Theory of the Ferroelectric Effect and Clamped Dielectric Constant of Rochelle Salt," *Phys. Rev.*, Vol. 72, No. 9, pp. 854–865, Nov. 1, 1947.

constant and the occurrence of its maximum at the same temperature as that for the "free" dielectric constant are accounted for by the theory presented in section 11.5, Chapter XI. The solid curve labeled 1 is another measurement[12] of the constant made at a frequency of 160 kilocycles by eliminating the interaction between the mechanical and electrical energies by means of theoretical relationships of the type discussed in the next section. The two measurements agree quite closely, as do also the associated Q's of the crystal considered as a condenser.

7.22 *Piezoelectric Properties of Rochelle Salt*

When a voltage is applied to an X-cut rochelle salt crystal, a relatively large distortion occurs for the crystal. The distortion for a plain X-cut crystal is a face shear which distorts a square into a rhombus, as shown in Fig. 7.1B. To obtain a longitudinal motion, one cuts a crystal out with its length 45° from the y- and z-axis as shown by Fig. 7.1B. If one plots the ratio of the extension to the applied voltage, the ratio becomes very large near the Curie points and is much smaller at other temperatures. Also the ratio is a function of the voltage gradient. On the other hand if one plots the ratio of the extension to the charge per unit area on the surface, the ratio is nearly constant for all temperatures and does not depend on the voltage gradient. Actually, as shown in Chapter VIII and Chapter X, the most constant ratio is not the ratio of the extension to surface charge (or electric displacement, if we consider a quantity that has meaning in the interior of the crystal and is equal to the surface change (times 4π) at the surface), but is the ratio of the stress to a part of the electric displacement, namely, the dipole polarization. However, the dipole polarization is not easily measured so that it appears better to base the fundamental equations on the electric displacement, since this is easily measured and is directly related to the energy stored per unit volume of the crystal. This point of view is developed in Chapter III and it is shown that the piezoelectric, elastic and dielectric equations for an orthorhombic bisphenoidal crystal (class 6 symmetry $V = D_2$ or 222), can be written in the form

$$\begin{aligned} T_1 &= c_{11}S_1 + c_{12}S_2 + c_{13}S_3 & E_x &= \frac{D_x}{\epsilon_{11}^S} - h_{14}S_4 \\ T_2 &= c_{12}S_1 + c_{22}S_2 + c_{23}S_3 & & \\ T_3 &= c_{13}S_1 + c_{23}S_2 + c_{33}S_3 & E_y &= \frac{D_y}{\epsilon_{22}^S} - h_{25}S_5 \end{aligned} \qquad (7.1)$$

[12] "The Location of Hysteresis Phenomena in Rochelle Salt Crystals," *Phys. Rev.*, Vol. 58, pp. 744–756, Oct. 15, 1940.

$$T_4 = c_{44}^D S_4 - h_{14}\left(\frac{D_x}{4\pi}\right)$$

$$T_5 = c_{55}^D S_5 - h_{25}\left(\frac{D_y}{4\pi}\right) \qquad E_z = \frac{D_z}{\epsilon_{33}^S} - h_{36} S_6 \qquad (7.1)$$

$$T_6 = c_{66}^D S_6 - h_{36}\left(\frac{D_z}{4\pi}\right)$$

where T_1 to T_6 are the six stresses for the crystal, as defined in Chapter III, S_1 to S_6 the six strains, D_x, D_y, D_z the electric displacements along the x-, y- and z-axis, respectively, E_x, E_y, E_z the fields along the three axis, c_{11} to c_{66} the nine elastic stiffness constants, and h_{14}, h_{25}, h_{36} the three piezoelectric constants relating the stress to the electric displacement divided by 4π. The shear elastic constants have a superscript D, indicating that they are measured at constant electric displacement, while the dielectric constants along x, y and z, ϵ_{11}^S, ϵ_{22}^S, ϵ_{33}^S are measured at constant strain, *i.e.* are the clamped dielectric constants.

All the dynamic methods of measuring the piezoelectric constants of rochelle salt employ longitudinal vibrations of crystals cut with their length 45° from the crystallographic axis and with their thickness along the third axis. By using the transformation equations given in the appendix, Section A-4, it can be shown that the elastic and piezoelectric equations pertaining to a 45° X-cut crystal can be written in the form

$$T_1' = c_{11}S_1' + \left(\frac{c_{12}+c_{13}}{2}\right)S_2' + \left(\frac{c_{12}+c_{13}}{2}\right)S_3' + \left(\frac{c_{13}-c_{12}}{2}\right)S_4'$$

$$T_2' = \left(\frac{c_{12}+c_{13}}{2}\right)S_1' + \left(\frac{c_{22}+c_{33}+2c_{23}+4c_{44}^D}{4}\right)S_2'$$
$$+ \left(\frac{c_{22}+c_{33}+2c_{23}-4c_{44}^D}{4}\right)S_3' + \left(\frac{c_{33}-c_{22}}{4}\right)S_4' - h_{14}\left(\frac{D_x}{4\pi}\right)$$

$$T_3' = \left(\frac{c_{12}+c_{13}}{2}\right)S_1' + \left(\frac{c_{22}+c_{33}+2c_{23}-4c_{44}^D}{4}\right)S_2' \qquad (7.2)$$
$$+ \left(\frac{c_{22}+c_{33}+2c_{23}+4c_{44}^D}{4}\right)S_3' + \left(\frac{c_{33}-c_{22}}{4}\right)S_4' + h_{14}\left(\frac{D_x}{4\pi}\right)$$

$$T_4' = \left(\frac{c_{13}-c_{12}}{2}\right)S_1' + \left(\frac{c_{33}-c_{22}}{4}\right)S_2' + \left(\frac{c_{33}-c_{22}}{4}\right)S_3'$$
$$+ \left(\frac{c_{22}+c_{33}-2c_{23}}{4}\right)S_4'$$

$$E_x' = \frac{D_x}{\epsilon_{11}^S} - h_{14}(S_2' - S_3')$$

T_5', T_6', E_y' and E_z' do not enter into the motion of the crystal. For a long, thin crystal with its length along the y'-axis, its thickness along x, and its width along z', the only stress that differs from zero is T_2'. Setting $T_1' = T_3' = T_4' = T_5' = T_6' = 0$, the equations pertaining to this crystal are

$$T_2' = \left(\frac{4}{s_{44}^D + s_{22} + s_{33} + 2s_{23}}\right) S_2' - \frac{h_{14}}{2c_{44}^D}\left(\frac{D_x}{4\pi}\right)\left(\frac{4}{s_{44}^D + s_{22} + s_{33} + 2s_{23}}\right), \quad (7.3)$$

$$E_x = \frac{D_x}{4\pi}\left[\frac{4\pi}{\epsilon_{11}^S} - \frac{h_{14}^2}{c_{44}^D}\left(\frac{s_{22} + s_{33} + 2s_{23}}{s_{44}^D + s_{22} + s_{33} + 2s_{23}}\right)\right] - \frac{h_{14}}{2c_{44}^D}\left(\frac{4}{s_{44}^D + s_{22} + s_{33} + 2s_{23}}\right) S_2'$$

where s_{22}, s_{33}, s_{23} are the elastic compliances of the crystal which are determined from the elastic stiffnesses by the equations

$$s_{ij} = (-1)^{i+j}\Delta^c{}_{ij}/\Delta^c$$

where

$$\Delta^c = \begin{vmatrix} c_{11} & c_{12} & c_{13} \\ c_{12} & c_{22} & c_{23} \\ c_{13} & c_{23} & c_{33} \end{vmatrix}$$

and $\Delta^c{}_{ij}$, is the minor obtained from Δ^c by suppressing the ith row and jth column. $s_{44}^D = 1/c_{44}^D$. From the form of (7.3) it is obvious that

$$\frac{s_{44}^D + s_{22} + s_{33} + 2s_{23}}{4} = s_{22}^{D'} \quad (7.4)$$

which is the inverse of Young's modulus for the long, thin crystal at an angle of 45° between the y- and z-axes. Also

$$\frac{4\pi}{\epsilon_{11}^S} - \frac{h_{14}^2}{c_{44}^D}\left(\frac{s_{22} + s_{33} + 2s_{23}}{s_{44}^D + s_{22} + s_{33} + 2s_{23}}\right) = \frac{4\pi}{\epsilon_{11}^{LC}} = \frac{4\pi}{\epsilon_{11}^{S_2'}} \quad (7.5)$$

where ϵ_{11}^{LC} is the longitudinal clamped dielectric constant, *i.e.* the dielectric constant measured when the strain S_2' is zero. As discussed in a previous paper,[12] this can be measured by measuring the dielectric constant at twice the resonant frequency of the crystal. By evaluating the terms

$$\frac{h_{14}^2}{c_{44}^D}\left(\frac{s_{22} + s_{33} + 2s_{23}}{s_{44}^D + s_{22} + s_{33} + 2s_{23}}\right),$$

the clamped dielectric constant can be evaluated, and this is the source of the 160-kc clamped dielectric constant measurement of Fig. 7.8. With these simplifications, equation (7.3) can be written in the form

$$T_2' = S_2'/s_{22}^{D'} - \frac{h_{14}}{2c_{44}^{D}s_{22}^{D'}}\left(\frac{D_x}{4\pi}\right); \quad E_x = \frac{D_x}{\epsilon_{11}^{LC}} - \frac{h_{14}}{2c_{44}^{D}s_{22}^{D'}}S_2' \tag{7.6}$$

The most direct way of measuring the constant h_{14} is to determine the open-circuit voltage of a rochelle 45° X-cut for a given strain S_2'. This was done in a previous paper[12] by glueing a half-wave rochelle salt crystal onto a half-wave quartz crystal and comparing the open-circuit voltage of the quartz with that of the rochelle salt when they are both driven by a half-wave quartz driver. Knowing the relative strain in the two crystals which are in the ratios of the velocities of sound propagation for the two crystals, and the open-circuit voltage for quartz, which is given by the equation

$$E_Q = \frac{4\pi d_{12}S_2 l_t}{\epsilon_{11}^{T}s_{22}} = 1.312 \times 10^5\, l_t S_2, \tag{7.7}$$

where l_t is the thickness of the crystal, it was found that the value of h_{14} for rochelle salt was

$$h_{14} = 7.58 \times 10^4 \text{ dynes/cgs units of charge} \tag{7.8}$$

and this value was quite independent of temperature from -10°C to $+45$°C.

Another method of measuring h_{14} is to measure the resonant and anti-resonant frequencies of a plated crystal and the free dielectric constant. Figure 7.9 shows the measured resonance (Curve A), the anti-resonance (Curve B), while Curve C shows the resonance of the same crystal measured with the plating removed and the crystal in an air-gap holder with a large air gap. To use these measurements in evaluating h_{14}, one has to combine the piezoelectric equation (7.6) with Newton's law of motion for any element of the crystal which for this case can be written in the form

$$\rho\frac{\partial^2\eta}{\partial t^2} = \frac{\partial T_2'}{\partial y'} \tag{7.9}$$

where η is the displacement of the elementary volume in the direction of the length, *i.e.*, y'. Introducing the first of equations (7.6), noting that

$S_2' = \dfrac{\partial \eta}{\partial y}$, we have the equation

$$\rho \frac{\partial^2 \eta}{\partial t^2} = \frac{1}{s_{22}^{D'}} \frac{\partial^2 \eta}{\partial y'^2} - \frac{h_{14}}{2c_{44}^{D} s_{22}^{D'}} \left(\frac{\partial D_x}{\partial y'} \right) \frac{}{4\pi} \tag{7.10}$$

From the second of equation (7.6) noting that the plated surface is an

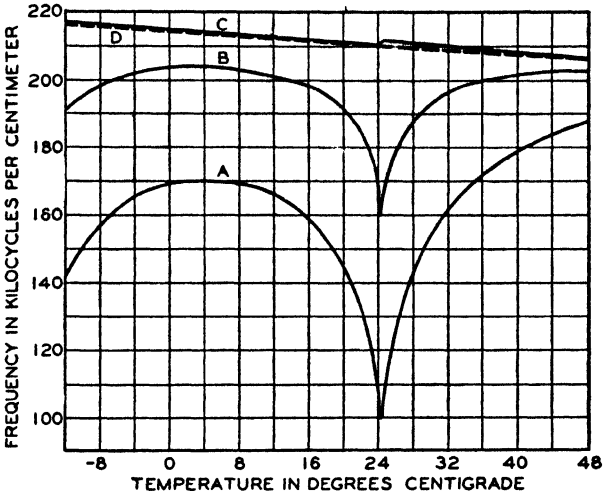

FIG. 7.9. Resonances of a rochelle salt crystal as a function of temperature. A. Resonant frequency of a plated crystal. B. Anti-resonant frequency of a plated crystal. C. Resonance of an unplated crystal in an air gap holder.

equipotential surface so that E_x is independent of y', we have

$$\frac{1}{\epsilon_{11}^{LC}} \frac{\partial D_x}{\partial y'} = \left(\frac{h_{14}}{2c_{44}^{D} s_{22}^{D'}} \right) \frac{\partial^2 \eta}{\partial y'^2} \tag{7.11}$$

Eliminating $\dfrac{\partial D_x}{\partial y'}$ from the two equations, we have

$$\rho \frac{\partial^2 \eta}{\partial t^2} = \frac{1}{s_{22}^{D'}} \frac{\partial^2 \eta}{\partial y'^2} - \left(\frac{h_{14}}{2c_{44}^{D} s_{44}^{D'}} \right)^2 \left(\frac{\epsilon_{11}^{LC}}{4\pi} \right) \frac{\partial^2 \eta}{\partial y^{2\prime}} = \frac{1}{s_{22}^{E}} \left(\frac{\partial^2 \eta}{\partial y^{2\prime}} \right)$$

where (7.12)

$$\frac{1}{s_{22}^{E}} = \frac{1}{s_{22}^{D}} \left[1 - \left(\frac{h_{14}}{2c_{44}^{D}} \right)^2 \left(\frac{\epsilon_{11}^{LC}}{4\pi s_{22}^{D'}} \right) \right] = \frac{1 - k^2}{s_{22}^{D}}$$

where k the electro-mechanical coupling factor is defined by

$$k^2 = \left(\frac{h_{14}}{2c_{44}^D}\right)^2\left(\frac{\epsilon_{11}^{LC}}{4\pi s_{22}^{D'}}\right) = \left(\frac{h_{14}}{2c_{44}^D}\right)^2\left(\frac{\epsilon_{11}^{T}}{4\pi s_{22}^{E'}}\right) = \left(\frac{d_{14}}{2}\right)^2\frac{4\pi}{\epsilon_{11}^{T}s_{22}^{E'}} \tag{7.13}$$

as can be shown from the relations in Chapter III. These follow from the equations

$$\frac{4\pi}{\epsilon_{11}^{LC}} = \frac{4\pi}{\epsilon_{11}^{S}} - \frac{h_{14}^2}{c_{44}^D}\left(\frac{4s_{22}^{D'} - s_{44}^D}{4s_{22}^{D'}}\right); \quad \frac{4\pi}{\epsilon_{11}^{S}} = \frac{4\pi}{\epsilon_{11}^{T}} + g_{14}h_{14}$$
$$g_{14} = \frac{h_{14}}{c_{44}^D}; \quad d_{14} = g_{14}\left(\frac{\epsilon_{11}^{T}}{4\pi}\right) = \left(\frac{h_{14}}{c_{44}^D}\right)\left(\frac{\epsilon_{11}^{T}}{4\pi}\right) \tag{7.14}$$

which hold for an orthorhombic bisphenoidal crystal (class of rochelle salt). In these equations d_{14} and g_{14} are other types of piezoelectric constants as defined in Chapter III. From these equations we have

$$\frac{4\pi}{\epsilon_{11}^{S}} = \frac{4\pi}{\epsilon_{11}^{LC}} + \frac{h_{14}^2}{c_{44}^D}\left(\frac{4s_{22}^{D'} - s_{44}^D}{4s_{22}^{D'}}\right) = \frac{4\pi}{\epsilon_{11}^{T}} + \frac{h_{14}^2}{c_{44}^D}$$

hence (7.15)

$$\frac{4\pi}{\epsilon_{11}^{LC}}\left[1 - \left(\frac{h_{14}}{2c_{44}^D}\right)^2\frac{\epsilon_{11}^{LC}}{4\pi s_{22}^{D'}}\right] = \frac{4\pi}{\epsilon_{11}^{LC}}(1 - k^2) = \frac{4\pi}{\epsilon_{11}^{T}}$$

and

$$\frac{\epsilon_{11}^{LC}}{4\pi s_{22}^{D'}} = \frac{\epsilon_{11}^{T}}{4\pi s_{22}^{E'}}$$

Equation (7.12) is the same equation discussed in detail in Chapter V. It is there shown that the resonant frequency is given by the equation

$$f_r = \frac{1}{2l}\frac{1}{\sqrt{\rho s_{22}^{E'}}} \tag{7.16}$$

while the electromechanical coupling defined by equation (7.13) is related to the separation Δf between the resonant and anti-resonant frequencies by the equation

$$k^2 = \frac{\pi^2}{4}\frac{\Delta f}{f_R}\left[1 + \left(\frac{4 - \pi^2}{4}\right)\frac{\Delta f}{f_R} + \left(\frac{\pi^2 - 4}{4}\right)\left(\frac{\pi^2}{4}\right)\left(\frac{\Delta f}{f_R}\right)^2 + \cdots\right] \tag{7.17}$$

From the data on the resonant and anti-resonant frequencies of Fig. 7.9, which allow one to calculate $s_{22}^{E'}$, and k the electromechanical coupling, the data of Fig. 7.6 for the free dielectric constant, and from Fig. 7.10 of the

next section which shows a measurement of c_{44}^D over a temperature range, the value of h_{14} can be evaluated and was found to be nearly a constant equal to about 7.8×10^4. There is some indication that it falls off slightly at the higher temperature which would agree with the data of Chapter X that the ratio between the piezoelectric stress and the dipole polarization is the most nearly constant ratio. Since the dielectric constant of electrons and atoms ϵ_{11}^0, *i.e.* for all sources except the dipole, is around 7, the dipole polarization represents from 92 to 99 per cent of the total value of $Dx/4\pi$ and hence the dipole polarization piezoelectric constant f_{14}, defined as the

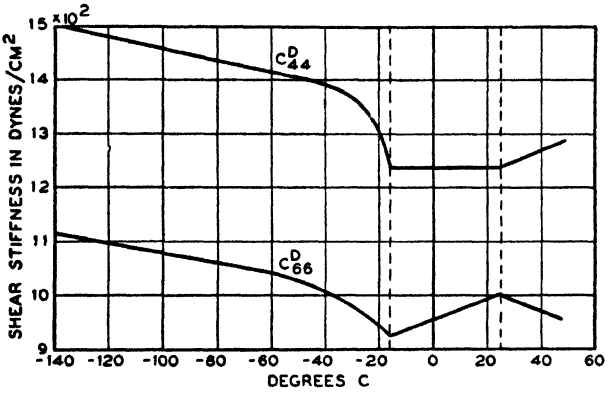

FIG. 7.10. Shear elastic constants of rochelle salt measured in air gap holder.

ratio of the piezoelectric stress to the dipole polarization for a constant strain, has a value around

$$f_{14} = \frac{\epsilon_{11}^S h_{14}}{\epsilon_{11}^S - \epsilon_{11}^0} = 7.8 \times 10^4 \tag{7.18}$$

No very exact measurements have been made for these constants for high polarizations, but theoretically they should be independent of the polarization value.

For the other two piezoelectric constants along the y- and z-axes, the writer[13] found

$$h_{25} = -5.8 \times 10^4; \qquad h_{36} = 4.81 \times 10^4 \tag{7.19}$$

As discussed in Chapter III, three other forms for writing the piezoelectric

[13] Mason, W. P., "A Dynamic Measurement of the Elastic, Electric, and Piezoelectric Constants of Rochelle Salt," *Phys. Rev.*, Vol. 55, pp. 775–789, April 15, 1939.

equations are in common use and these involve other piezoelectric constants that are related to the ones measured here by the equations

$$\begin{aligned} g_{14} &= \frac{h_{14}}{c_{44}^D}; & g_{25} &= \frac{h_{25}}{c_{55}^D}; & g_{36} &= \frac{h_{36}}{c_{66}^D} \\ e_{14} &= \frac{h_{14}\epsilon_{11}^S}{4\pi}; & e_{25} &= \frac{h_{25}\epsilon_{22}^S}{4\pi}; & e_{36} &= \frac{h_{36}\epsilon_{33}^S}{4\pi} \\ d_{14} &= \frac{h_{14}(\epsilon_{11}^T)}{c_{44}^D(4\pi)}; & d_{25} &= \frac{h_{25}(\epsilon_{22}^T)}{c_{55}^D(4\pi)}; & d_{36} &= \frac{h_{36}(\epsilon_{33}^T)}{c_{66}^D(4\pi)} \end{aligned} \tag{7.20}$$

The g constants determine the open-circuit voltage of the crystal used as a microphone for a given applied pressure, the e constants determine the stress exerted by the crystal for a given applied field, and the d constants determine the displacement of the crystal for a given applied field. From the elastic constants determined in the next section and the dielectric constants determined in the last section, these constants for room temperature (25°C) become

$$\begin{aligned} g_{14} &= 6.3 \times 10^{-7}; & g_{25} &= -19 \times 10^{-7}; & g_{36} &= 4.8 \times 10^{-7} \\ e_{14} &= 1.4 \times 10^{6}; & e_{25} &= -4.7 \times 10^{4}; & e_{36} &= 3.4 \times 10^{4} \\ d_{14} &= 7 \times 10^{-5}; & d_{25} &= -169 \times 10^{-8}; & d_{36} &= 35.5 \times 10^{-8} \end{aligned} \tag{7.21}$$

The values of e_{14} and d_{14} vary considerably with temperature and field strength while the value of g_{14} and h_{14} are relatively constant. For the y and z directions, since no ferroelectric effect exists along these axes, the values of all four constants are relatively fixed for temperature and field strength conditions.

7.23 *Elastic Constants of Rochelle Salt*

As shown by equation (7.1) there are nine elastic constants for rochelle salt. Six of them c_{11}, c_{12}, c_{13}, c_{22}, c_{23} and c_{33}, are independent of the field or electric displacement conditions while the other three depend on whether we have constant field or constant electric displacement. The relation between the constant field and constant displacement constants is discussed in the Appendix Section A–2, and it is there shown that

$$c_{44}^D = c_{44}^E + e_{14}h_{14}; \qquad c_{55}^D = c_{55}^E + e_{25}h_{25}; \qquad c_{66}^D = c_{66}^E + e_{36}h_{36} \tag{7.22}$$

The elastic compliances which occur when we write the strains in terms of the stresses are also of interest, and, in fact, are more easily measured than the elastic stiffness constants. For rochelle salt these occur in equations

of the type

$$\begin{aligned} S_1 &= s_{11}T_1 + s_{12}T_2 + s_{13}T_3 & S_6 &= s_{66}^{D}T_6 + g_{36}\frac{D_z}{4\pi} \\ S_2 &= s_{12}T_1 + s_{22}T_2 + s_{33}T_3 & E_x &= \frac{D_x}{\epsilon_{11}^{T}} - g_{14}T_4 \\ S_3 &= s_{13}T_1 + s_{23}T_2 + s_{33}T_3 & E_y &= \frac{D_y}{\epsilon_{22}^{T}} - g_{25}T_5 \\ S_4 &= s_{44}^{D}T_4 + g_{14}\frac{D_x}{4\pi} & E_z &= \frac{D_z}{\epsilon_{33}^{T}} - g_{36}T_6 \\ S_5 &= s_{55}^{D}T_5 + g_{25}\frac{D_y}{4\pi} \end{aligned} \tag{7.23}$$

The s constants s_{11} to s_{33} are related to the c_{11} to c_{33} constants by the relations

$$s_{ij} = (-1)^{i+j} \quad \Delta^{c}{}_{ij}/\Delta^{c}$$

where

$$\Delta^{c} = \begin{vmatrix} c_{11} & c_{12} & c_{13} \\ c_{12} & c_{22} & c_{23} \\ c_{13} & c_{23} & c_{33} \end{vmatrix} \tag{7.24}$$

and $\Delta^{c}{}_{ij}$ is the minor of this determinant obtained by suppressing the ith row and jth column. The three shear compliances at constant field are related to the shear compliances at constant displacement by the formulae

$$s_{44}^{D} = s_{44}^{E} - d_{14}g_{14}; \qquad s_{55}^{D} = s_{55}^{E} - d_{25}g_{25}; \qquad s_{66}^{D} = s_{66}^{E} - d_{36}g_{36} \tag{7.25}$$

The relation between shear elastic stiffness and shear elastic compliance constants can be written in the form

$$\begin{aligned} c_{44}^{D} &= \frac{1}{s_{44}^{D}}; & c_{55}^{D} &= \frac{1}{s_{55}^{D}}; & c_{66}^{D} &= \frac{1}{s_{66}^{D}}; \\ c_{44}^{E} &= \frac{1}{s_{44}^{E}}; & c_{55}^{E} &= \frac{1}{s_{55}^{E}}; & c_{66}^{E} &= \frac{1}{s_{66}^{E}} \end{aligned} \tag{7.26}$$

The nine elastic compliances have been measured by static means by Mandell and Hinz and by dynamic methods by the writer[13] and Huntington.[14] The shear constants measured by the writer were the constant displacement type measured by employing an unplated crystal in an air-gap holder. The method of separating out the various constants by using

[14] Huntington, H. B., *Phys. Rev.*, Vol. 72, No. 4, pp. 321–331, Aug. 15, 1947.

variously oriented crystals is discussed in detail in Chapter X. Huntington measured essentially the constant field constants since he employed the ultrasonic pulse method which results in the constant field constants. Table XI shows a comparison of the measurements of Hinz, Huntington and the writer. The last two agree very well except for the value of s_{13}. The last column shows the recommended values of the constants.

TABLE XI

ELASTIC CONSTANTS OF ROCHELLE SALT

	Hinz, Room Temp. Constant Field		Mason, 30°C Constant Displacement	Huntington Adiabatic	Recommended values
	Obsd.	Calc. Adiabatic	Observed Adiabatic	Constant Displacement	Constant Displacement, Adiabatic
$cm^2/dyne$	$\times 10^{-12}$	$\times 10^{-12}$	$\times 10^{-12}$	$\times 10^{-12}$	$\times 10^{-12}$
s_{11}	5.23	5.19	5.18	5.24	5.20
s_{22}	3.43	3.41	3.49	3.50	3.50
s_{33}	3.24	3.22	3.34	3.37	3.35
s_{44}	9.63	9.63	7.98	7.45	7.9
s_{55}	33.7	33.7	32.8	34.9	33.0
s_{66}	11.8	11.8	10.1	10.4	10.2
s_{12}	−2.18	−2.20	−1.53	−1.54	−1.53
s_{13}	−1.69	−1.72	−2.11	−0.98	−1.7
s_{23}	−1.34	−1.36	−1.03	−0.91	−1.0

Some values have been measured for the temperature coefficients of the elastic constants. In general these differ depending on whether the temperature range is below, between, or above the Curie temperature. Above the Curie temperature, the writer found the following values of the temperature coefficient expressed in parts per million per degree centigrade

$$Ts_{11} = 1{,}230; \quad Ts_{44}^{D} = -1{,}660; \quad Ts_{12} = 5{,}240$$

$$Ts_{22} = 1{,}330; \quad Ts_{55}^{D} = 700; \quad Ts_{13} = 2{,}710$$

$$Ts_{33} = 890; \quad Ts_{66}^{D} = 1{,}830; \quad Ts_{23} = -10{,}200$$

These are useful in only one temperature range but show the large variation of elastic constants compared to what one can obtain in quartz. Two of the shear elastic constants have been measured over a wide temperature range by measuring the face-shear modes of long, thin crystals cut with

their thickness along the x- and z-axes and with their lengths along the z- and y-axes respectively. The face-shear modes of these two crystals are determined by the c_{44}^D and c_{66}^D constants, respectively, when they are measured in an air gap holder with a large air gap. This follows from the fact that the D_x and D_z electric displacements are the only ones generated by these modes of motion, and since the normal component equals the surface charge which is zero, since no plating is on the crystal, and hence D_x and D_z are constant through the crystal and equal to zero. Figure 7.10 shows the values plotted as a function of temperature and it is obvious that the proximity of the ferroelectric temperatures exercises an effect on these two shear elastic constants.

7.3 *Useful Cuts in Rochelle Salt*

The cut most widely used is the X-cut which as shown by Fig. 7.1B, is cut with its major face normal to the x-axis. If a voltage is applied to this cut, it shears so that the square changes into a rhombus. But cutting the crystal length 45° from the crystallographic y- and z-axes, a crystal is obtained which elongates along one direction and contracts along the width. This cut, which is known as the 45° X-cut, is widely used in producing longitudinal vibrations. By combining two longitudinal crystals, as shown by Fig. 7.1C, a " bimorph " crystal is obtained which bends. This has a much lower frequency than a longitudinal crystal and is used in voice frequency apparatus for picking up and reproducing sound. Figure 7.1D shows a combination of two X-cut crystals used to produce a twisting motion. The center faces of the two crystals form one set of electrodes, and the two outside electrodes, the other pair, so that two opposing face-shears are applied to the combination. This causes the whole crystal to twist and produces a torsional motion in the pair. Finally, Fig. 7.1E shows two thin face-shear X-cut crystals which, when they are clamped on three corners, produce a large motion at the fourth corner. All three of these bimorph-type crystals have been used in such devices as phonograph pickups, microphones, headphones, loudspeakers, surface roughness analyzers, light valves and many other applications.

For a 45° X-cut crystal, the equations applicable for the extension are

$$S_l = s_{22}'^D T_l + g_l \frac{D_x}{4\pi}$$

$$E_x = -g_l T_l + \beta_1^T D_x \tag{7.27}$$

where S_l is the strain along the length, T_l the stress applied along the length, g_l the effective piezoelectric constant for the 45° axis, and β^T the

impermeability (inverse of the dielectric constant) which is measured when the crystal is free to move. In cgs units the above constants have the values

$$s_{22}^{D} = 3.16 \times 10^{-12} \text{ cm}^2/\text{dyne}; \qquad g_l = 31.5 \times 10^{-8} = \frac{g_{14}}{2} \tag{7.28}$$

while the free dielectric constant, which is the inverse of β^T, has the value shown by Fig. 7.6 for low applied fields and for high fields (500 volts per cm). Equation (7.27) can be used to predict the action of the crystal under static conditions or at frequencies much lower than the resonant frequencies of the crystal. For example, if we wish to find the response of the crystal as a microphone, the second equation states that for open-circuit conditions for which the charge on the surface, and hence the electrical displacement D_x, is zero, the potential generated for a given pressure (negative of the tension T_l) is

$$E_x = \frac{E}{l_t} = g_l T_l = 31.5 \times 10^{-8} \text{ (pressure in dynes/cm}^2\text{)} \tag{7.29}$$

Since the electrostatic unit of potential, the stat volt, is 300 volts, the volts generated per dyne per sq cm pressure are

$$E_{\text{volts}} = 31.5 \times 10^{-8} \times 300 \times l_t x p = 9.1 \times 10^{-5} \text{ volts per dyne} \tag{7.30}$$

per sq cm for a crystal 1 centimeter thick. Since the voltage generated for a given pressure is directly proportional to the g_l constant, which is one half the appropriate shear constant, equation (7.21) shows that a 45° Y-cut crystal, which will have a g_l piezoelectric constant equal to $\frac{1}{2} \times 190 \times 10^{-8} = 95 \times 10^{-8}$, will generate about 3 times the open-circuit voltage for the same pressure that a 45° X-cut crystal will. The 45° Y-cut has been used to some extent as a microphone and as a transducer in underwater sound equipment for transferring electrical energy into mechanical energy. When the crystal is used as a microphone working into a low impedance, the Y-cut will not deliver as much voltage as an X-cut crystal on account of the very low impedance (high capacity) of the X-cut crystal, but the voltage that it does deliver is not a function of the temperature as in the case of the 45° X-cut.

By eliminating D_x from equation (7.27), the strain S_l, which is the expansion per unit length, can be expressed in terms of the applied field as

$$S_l = \left(s_{22}^{D} + \frac{g_l^2 \epsilon_1^T}{4\pi}\right) T_l + \frac{g_l \epsilon_1^T}{4\pi} E_x \tag{7.31}$$

In the absence of an external stress T_l, the total free displacement for 1 volt applied is

$$d = S_l l = 1.03 \times 10^{-9} \frac{V\epsilon_1^T}{4\pi}\left(\frac{l}{l_t}\right) \tag{7.32}$$

This displacement as a function of the volts per inch applied is shown by Fig. 7.11 for several different temperatures. Outside of the Curie region the displacement is much less since the dielectric constant ϵ_1^T is so much smaller, particularly for large fields.

When two crystals are glued together to form a bimorph unit it has been shown[15] that the displacement of the component longitudinal crystals is

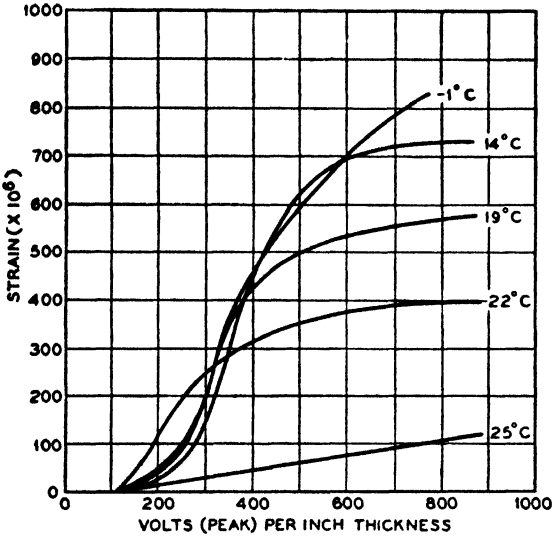

FIG. 7.11. Strain in an X-cut rochelle salt crystal as a function of the field and temperature.

multiplied by the factor $3l/l_t$ where l is the length of the crystal and l_t the total thickness of the two elements. This is a method of enhancing the total displacement of the unit at the expense of a considerable lowering of the resonant frequency of the device. Since the dielectric constants of the two crystals glued together will be less than the free dielectric constant of Fig. 7.6 and will approach the dielectric constant of the clamped crystal shown by Fig. 7.8, the very large temperature and saturation effects noted for the free crystal, will be considerably reduced for the bimorph type. However, the response may vary by a factor of 5 for a wide-temperature

[15] Mason, W. P., *Electromechanical Transducers and Wave Filters*, Chapter VI, p. 214, D. Van Nostrand Company, Inc., 1942, 2nd Edition, 1948.

range. A typical response in the ferroelectric range for a bender unit $1\frac{1}{2}$ inches long, $\frac{3}{4}$ inches wide and 0.040 inch thick is

33 volts	0.002 inch
77 volts	0.0045 inch
125 volts	0.006 inch
140 volts	0.0065 inch

The displacement for any other shape unit will vary in proportion to the factor $(l/l_t)^2$ and will be independent of the width.

When such units are used as voltage generators, as in phonograph pickup devices, the mechanical impedance of the device is very considerably lowered over what would be obtained with a clamped longitudinal device. The response can be calculated by determining how much strain is generated by a given motion and calculating the voltage from equation (7.27). A typical unit 0.030 inch thick, $\frac{11}{16}$ inch long and $\frac{7}{16}$ inch wide will give an output as high as one volt when played from a phonograph record. This response will be relatively independent of the temperature when the device is operated into the grid of a vacuum tube.

CHAPTER VIII

Properties and Uses of Ammonium Dihydrogen Phosphate (ADP) and Potassium Dihydrogen Phosphate (KDP)

During World War II a new piezoelectric crystal ammonium dihydrogen phosphate ($NH_4H_2PO_4$) was developed and was widely used[1] as the transducing element of underwater transducers and hydrophones. This crystal has no water of crystallization and hence will not dehydrate, will stand temperatures up to 100°C, and will radiate considerable amounts of acoustic power without breaking down. The properties were so favorable that ADP largely displaced rochelle salt and other types of electromechanical transducers in underwater sound applications. It appears likely that for devices that transform mechanical vibrations into electrical vibrations, such as phonograph pickups, microphones, etc. — that ADP will give superior results to rochelle salt and may eventually replace rochelle salt for such applications. For devices that have to produce a large motion for a given voltage, however, rochelle salt is still the only crystal that has a large enough d constant to be of interest.

ADP is one of a group of four isomorphous salts that have very interesting dielectric and piezoelectric properties. It was first shown by Busch[2] that ammonium dihydrogen phosphate ($NH_4H_2PO_4$), potassium dihydrogen phosphate (KH_2PO_4), potassium dihydrogen arsenate (KH_2ASO_4), and ammonium dihydrogen arsenate ($NH_4H_2ASO_4$), all exhibited phase changes at temperatures ranging from 91°K to 220°K. It was established for potassium dihydrogen phosphate and potassium dihydrogen arsenate by measuring the dielectric constant and the associated charge potential loops, that these phase changes were of the ferroelectric type. Similar measurements of ammonium dihydrogen phosphate (ADP) and ammonium dihydrogen arsenate failed to show ferroelectric properties on account of the sudden fracture of these crystals at temperatures above the ferroelectric Curie temperatures. Furthermore, by extrapolating the dielectric and piezoelectric measurements to low temperatures, it is doubtful if they would become ferroelectric down to temperatures of 0°K.

[1] Keller, A. C., "Submarine Detection by Sonar," *Trans. A.I.E.E.*, Vol. 66, pp. 1217–1230, 1937.

[2] Busch, George, "Neue Seignette Elektrika," *Helv. Phys. Acta*, Vol. 2, No. 3, 1938.

Of these crystals, ADP is the only crystal that has had technical application although the use of KDP has been suggested for use in filters by Matthias and Scherrer.[3] On account of the high temperature coefficient of frequency, however, which amounts to about 300 parts per million per degree C in the room temperature range, it is doubtful if KDP would be useful for this purpose. ADP is the crystal of the four isomorphous crystals having the largest electromechanical coupling (30 per cent) and it is the purpose of this chapter to describe its properties and applications. Since KDP has considerable theoretical interest on account of its ferroelectric transformation, its properties are also discussed.

8.1 *Physical Properties of ADP and KDP*

8.11 *General Properties of ADP and KDP*

ADP and KDP crystallize in the tetragonal scalenohedral class (symmetry $V_d = D_{2d}$ or $\bar{4}2m$ on the Hermann-Mauguin system) with the habit shown by Fig. 8.1. The c- or z-axis lies along the long direction of the crystal. This is an axis of fourfold alternating symmetry. The x- and y-axes, which lie normal to the prism faces, are axes of twofold symmetry. Since the properties of crystal plates cut normal to these two surfaces are identical, it is a matter of convention which is called x and which y. The two diagonal axes, labeled P_1 and P_2, can be distinguished by piezoelectric tests and P_1 has been taken as the axis along which a positive stress (tension) produces a positive charge at the positive (*i.e.* upper) end of the z-axis. With the z-axis vertical and the P_1-axis toward the observer's right hand, the x-axis has been taken as the axis which runs from front to back of the crystal and the y-axis from left to right. The density of ADP is 1.804 while that of KDP is 2.31.

ADP and KDP have no water of crystallization and hence will not dehydrate when the humidity becomes low. At about 93 per cent humidity the crystals will deliquesce and will pick up moisture from the atmosphere. They are usually used under oil or in a sealed container so that this property does not cause trouble. ADP can be taken up to 190°C before it melts. However, ammonia is given off from the surface at temperatures above 100°C and since this impairs the adherence of the electrodes to the crystal surface, it is desirable to keep the temperature of operation under 100°C. This allows one to use the crystal under any likely atmospheric conditions. Electrodes are usually put on by the gold-evaporation process. The crystal can be cut by an abrasive disc, cooled by a saturated solution of

[3] Matthias, B. and P. Scherrer, "Crystal Band Pass Filters," *Helv. Phys. Acta*, Vol. 16, pp. 432–434, 1943.

the material, and can be surfaced by an abrasive belt cooled by the same solution.

Due to the transmission of ions through the crystals, they have a volume leakage, which for the purest salt is shown for ADP and KDP in Fig. 8.2. The crystal structure of KDP is shown by Fig. 11.9 of Chapter XI and it is seen that the PO_4 groups are bonded to other PO_4 groups by means

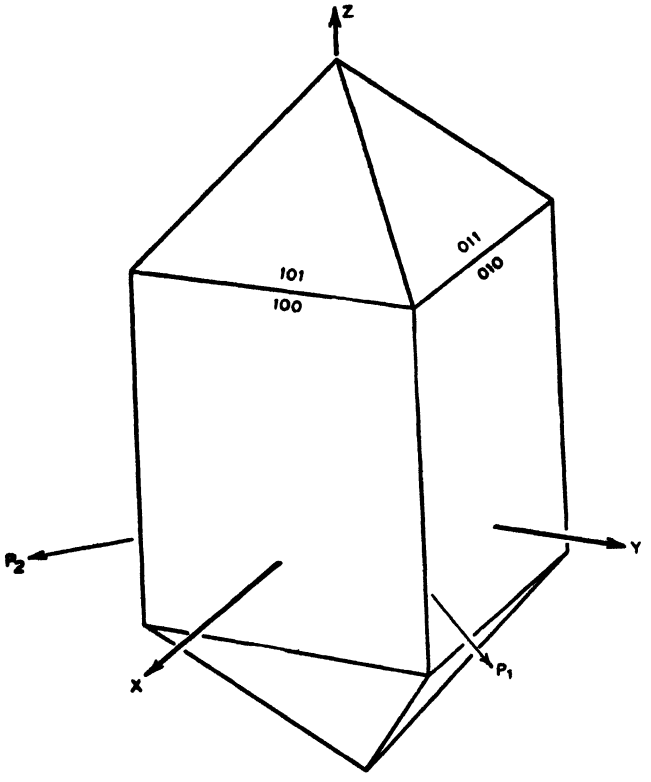

FIG. 8.1. Crystal form and crystal axes for ADP and KDP.

of hydrogen bonds. An ion containing these bonds will have less activation energy than for most crystals and a lower resistivity results. The presence of a field can cause a migration in the direction of the field which is the source of the resistivity measured and plotted in Fig. 8.2.

A rough calculation of the conductivity[4] can be made as follows. In order that a hydrogen bonded ion shall move from one position to another,

[4] This calculation follows closely that given by J. Frenkel, *Kinetic Theory of Liquids*, pp. 40–48, Oxford University Press, 1946.

enough energy must be imparted to it to break the bond. As will be seen, this bond energy is in the order of 12.6 kilocalories per mole for Z-cut KDP and 14.6 kilocalories for Z-cut ADP. The potential barrier that has to be overcome in breaking this bond will be as shown by Fig. 8.3, plotted as a function of the distance. There are two stable positions separated by a distance δ which for KDP is in the order of 4.6×10^{-8} cm

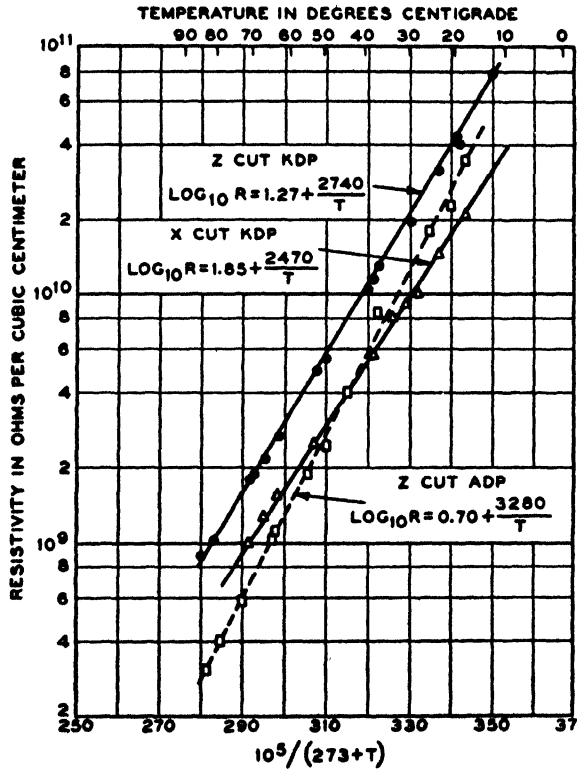

FIG. 8.2. Resistivity of ADP and KDP as a function of temperature.

on the average. The height of the potential barrier W in ergs is about 21 times the average potential energy of the ion, so that according to Maxwell's distribution law, the probability that a molecule will have enough energy to cross the barrier and become free for a single try, is

$$e^{-W/kT} \doteq e^{-21} = 0.80 \times 10^{-9} \tag{8.1}$$

for a temperature of 300°K = 27°C. Multiplying this by ν, the number of times per second that the molecule assaults the barrier, α_{12}, the number

of transitions occurring per second from potential well 1 to potential well 2, is

$$\alpha_{12} = \nu e^{-W/kT} \doteq \frac{kT}{h} e^{-W/kT} \tag{8.2}$$

According to Eyring's reaction rate theory, $\nu \doteq \frac{kT}{h}$, where k is Boltzmann's constant, h Planck's constant and T the absolute temperature.

When a field E is impressed across the crystal in the direction 1 to 2, the potential well 1 will be raised with respect to the potential maximum

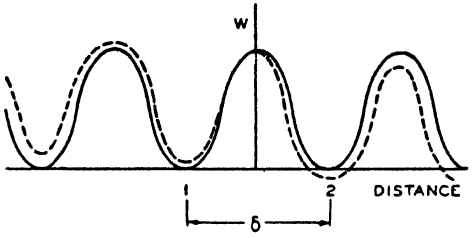

FIG. 8.3. Potential well distribution for calculating leakage resistance.

W, while the potential well 2 will be lowered, as shown by the dotted line. Then the difference between the bottom of wells 1 and 2 and the top of the potential barrier are

$$W_1 = W - \frac{Ee\delta}{2}; \qquad W_2 = W + \frac{Ee\delta}{2} \tag{8.3}$$

where δ is the potential well separation, e the charge on the nucleus, and E the field which is also the applied field, since the current flow would destroy any internal field of the Lorentz type. Hence α_{12} and α_{21}, the rates of going from potential wells 1 to 2 or vice versa, are

$$\alpha_{12} = \frac{kT}{h} e^{-(W - Ee\delta/2)/kT}; \qquad \alpha_{21} = \frac{kT}{h} e^{-(W + Ee\delta/2)/kT} \tag{8.4}$$

The net flow in the direction of the field is

$$(\alpha_{12} - \alpha_{21}) = \frac{kT}{h} e^{-W/kT} \left[e^{Ee\delta/2kT} - e^{-Ee\delta/2kT} \right]$$

$$\doteq \frac{kT}{h} \frac{Ee\delta}{kT} e^{-W/kT} = \frac{Ee\delta}{h} e^{-W/kT} \tag{8.5}$$

The leakage current will be the number of cells n per sq cm times the

charge e times the net flow $(\alpha_{12} - \alpha_{21})$ or will be

$$i = ne(\alpha_{12} - \alpha_{21}) = \frac{NEe^2\delta^2}{h} e^{-W/kT} \tag{8.6}$$

where $N = n/\delta$ is the number of molecules per cubic centimeter. The resistivity per cubic centimeter will then be the field E per centimeter divided by the current i per square centimeter or

$$R = \frac{E}{i} = \frac{he^{W/kT}}{Ne^2\delta^2} \text{ in cgs units} = \frac{h \times 9 \times 10^{11} e^{W/kT}}{Ne^2\delta^2} \text{ in ohms per cc} \tag{8.7}$$

The activation energy W can be calculated from the data of Fig. 8.2, from the resistivity as a function of temperature. By taking two temperatures T_1 and T_2

$$\frac{R_1}{R_2} = \frac{e^{W/kT_1}}{e^{W/kT_2}} = e^{\frac{W}{k}\left[\frac{1}{T_1} - \frac{1}{T_2}\right]} \tag{8.8}$$

Hence

$$\log_e \frac{R_1}{R_2} = \frac{W}{k}\left[\frac{1}{T_1} - \frac{1}{T_2}\right] \quad \text{and} \quad W = \frac{k \log_e \dfrac{R_1}{R_2}}{\left(\dfrac{1}{T_1} - \dfrac{1}{T_2}\right)} \tag{8.9}$$

The expression in calories per mole is obtained by multiplying by Avogadro's number $N_A = 6.06 \times 10^{23}$ and dividing by the mechanical equivalent of heat (4.187×10^7 ergs/cal). Hence

$$W_{\text{(cal. per mole)}} = \frac{N_A k \log_e \left(\dfrac{R_1}{R_2}\right)}{\left(\dfrac{1}{T_1} - \dfrac{1}{T_2}\right) 4.187 \times 10^7} = 12.6 \text{ kilocalories per mole for } Z\text{-cut KDP.} \tag{8.10}$$

For Z-cut ADP the activation energy is 14.6 kilocalories per mole.

The constant of (8.7) is also of some interest. From X-ray data, $N = 10^{22}$, $\delta \doteq 4.6 \times 10^{-8}$ cm and $h = 6.6 \times 10^{-27}$, $e = 4.8 \times 10^{-10}$, and $W/kT = 24.3$ at 300°K = 27°C for Z-cut ADP. This gives a calculated resistivity of 4×10^7 compared to a measured value of 2×10^{10}. This makes it appear that the conductivity is due to an impurity, having a lower activation energy than pure ADP, for which 1 molecule in 10^8 is providing an ion.

Some confirmation of this idea is furnished by the work of E. J. Murphy, who found that by taking the temperature up to 125°C a break occurred in the resistivity curve and the activation energy indicated for the higher

temperature was 20.4 kilocalories. Murphy ascribes this activation energy to the pure salt and the lower activation energy to an impurity. Further confirmation of this idea is had by introducing 0.006 molar per cent of sulphate ions (SO_4) into the crystal, which caused the activation energy to drop to 10.9 kilocalories and the resistivity to 5×10^8 ohm centimeters at 27°C = 300°K. This checks the idea that one molecule in 10^4 is contributing to the conduction with a much lower activation energy. For some applications it is necessary to specify a high resistivity and the freedom from certain ions, such as the sulphate ions, has to be good.

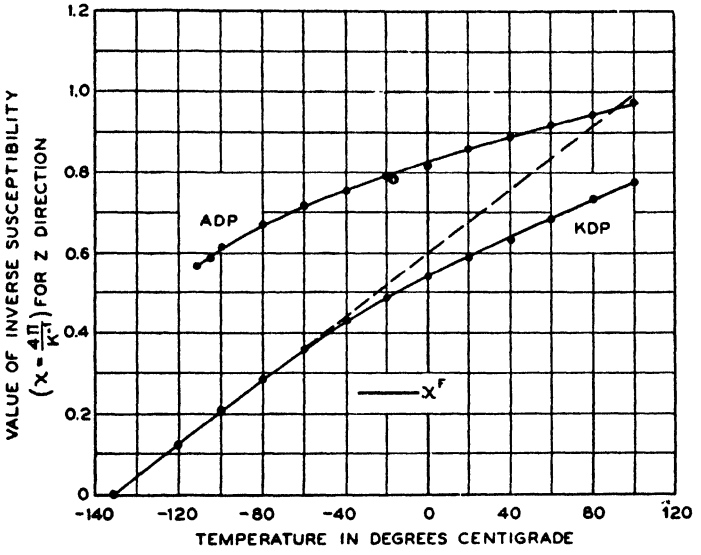

FIG. 8.4. Inverse susceptibility of ADP and KDP as a function of temperature measurements along z-axis.

8.12 *Dielectric Properties of ADP and KDP*

On account of their symmetry these two crystals have two dielectric constants $\epsilon_{11} = \epsilon_{22}$ and ϵ_{33}. These constants have been measured for the free crystal by Busch[2] and the writer.[5] The results agree quite closely and are shown by Fig. 8.4 for KDP and Fig. 8.5 for ADP. The dielectric constant along the z-axis for KDP shows the very large peak associated with a ferroelectric crystal at a temperature of 122°K and the dielectric constant, becomes as high as 30,000. Below the Curie temperature, the

[5] Mason, W. P., "The Elastic, Piezoelectric and Dielectric Constants of Potassium Dihydrogen Phosphate and Ammonium Dihydrogen Phosphate," *Phys. Rev.*, Vol. 69, pp. 173–194, March 1 and 15, 1946.

polarization exhibits hysteresis effects, and by taking the saturation value for the hysteresis loop Busch[2] finds that the spontaneous polarization as a function of temperature is shown by Fig. 8.6. The maximum polariza-

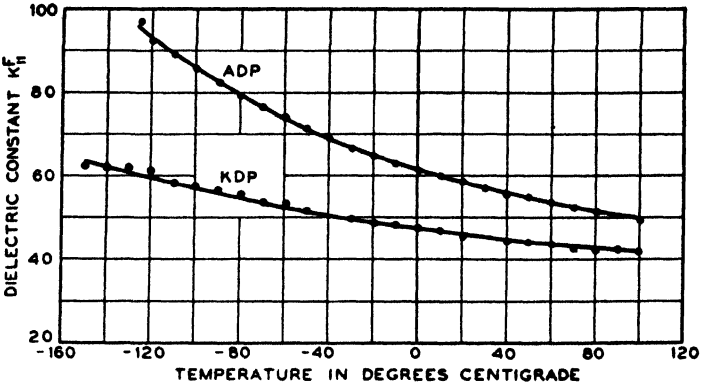

FIG. 8.5. Dielectric constant of ADP and KDP along x-axis.

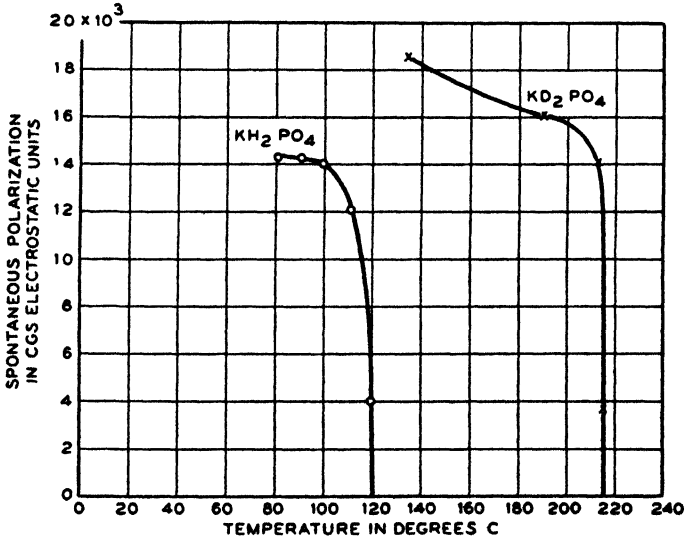

FIG. 8.6. Spontaneous polarization of potassium dihydrogen phosphate and potassium dideuterium phosphate.

tion is in the order of 14,100 esu/cm^2 compared to 740 for rochelle salt. By introducing deuterium in place of the hydrogen, Bantle[6] showed that

[6] Bantle, W., "The Specific Heat of Seignette-electric Substances. Dielectric Measurements on KD_2PO_4 Crystals," *Helv. Phys. Acta*, Vol. 15, pp. 373–404, 1942.

the Curie point could be raised to 213°K. The dotted curve of Fig. 8.6 shows the measured spontaneous polarization. By going to temperatures below 58°K for KDP and below 105°K for the deuterium salt, it was found that the hysteresis loops disappeared and the dielectric constant dropped to 40. It has been suggested that this effect is due to the freezing-in of the domains so that they cannot be reversed even by the largest applied field.

Above the Curie temperature, the " free " dielectric constant for KDP is given closely by the equation

$$\epsilon_{33}^{T} = 4.5 + 3122/(T + 151) \tag{8.11}$$

where T is expressed in degrees centigrade. This indicates that the dielectric constant is made up of a part that varies only slightly with temperature, and another, due presumably to the hydrogen bond dipoles, which varies inversely as the temperature difference. A similar equation fitting ADP is

$$\epsilon_{33}^{T} = 7.0 + 2670/(T + 287) \tag{8.12}$$

indicating that the Curie temperature due to the hydrogen bonds is in the neighborhood of absolute zero. No measurement has been made of the clamped dielectric constant, but this can be calculated from the equation

$$\epsilon_{33}^{S} = \epsilon_{33}^{T} - 4\pi(d_{36}e_{36}); \qquad \epsilon_{11}^{S} = \epsilon_{11}^{T} - 4\pi(d_{14}e_{14}) \tag{8.13}$$

and the evaluation of the piezoelectric constants given in the next section and also in Tables XII and XIII.

8.13 *Piezoelectric Properties of ADP and KDP*

For the crystal class ($V_d = D_{2d}$ or $\bar{4}2m$) the piezoelectric, elastic and dielectric equations can be written in the form

$$\begin{aligned}
T_1 &= c_{11}S_1 + c_{12}S_2 + c_{13}S_3; & T_6 &= c_{66}^{D}S_6 - h_{36}(D_{z/4\pi}) \\
T_2 &= c_{12}S_1 + c_{22}S_2 + c_{13}S_3; & E_x &= \frac{D_x}{\epsilon_{11}^{S}} - h_{14}S_4 \\
T_3 &= c_{13}S_1 + c_{13}S_2 + c_{33}S_3; & E_y &= \frac{D_y}{\epsilon_{11}^{S}} - h_{14}S_5 \\
T_4 &= c_{44}^{D}S_4 - h_{14}(Dx/4\pi); & E_z &= \frac{D_z}{\epsilon_{33}^{S}} - h_{36}S_6 \\
T_5 &= c_{44}^{D}S_5 - h_{14}(Dy/4\pi);
\end{aligned} \tag{8.14}$$

with similar forms for the other three methods for writing these equations.

The piezoelectric constant h_{36} has been measured for these crystals over a wide temperature range and has been found to decrease somewhat

as the temperature is increased. If, however, we take the ratio of the piezoelectric stress to the dipole polarization, a constant ratio f_{36} is obtained which is independent of temperature. To obtain this constant using equation (8.14), we note that

$$\frac{D_z}{4\pi} = \frac{E_z}{4\pi} + P_z + P_{zd} = \frac{E_z}{4\pi}(1 + 4\pi\kappa_{3_0}) + P_{zd} = \frac{E_z\epsilon_{3_0}}{4\pi} + P_{zd} \qquad (8.15)$$

where P_{z_0} is the polarization for electrons and atoms and P_{zd} is the dipole polarization. κ_{3_0} is the susceptibility due to electrons and atoms, and ϵ_{3_0} is the dielectric constant due to electrons and atoms, which from equations (8.11) and (8.12) are 4.5 and 7.0 for KDP and ADP respectively. Introducing (8.15) into equations (8.14), the equations for the piezoelectric effect become

$$\begin{aligned} T_6 &= c_{66}^D S_6 - h_{36}\left(\frac{E_z\epsilon_{3_0}}{4\pi} + P_{zd}\right); \\ E_z &= \frac{4\pi}{\epsilon_{33}^S}\left(\frac{E_z\epsilon_{3_0}}{4\pi} + P_{zd}\right) - h_{36}S_6 \end{aligned} \qquad (8.16)$$

Solving these equations simultaneously

$$\begin{aligned} T_6 &= \left[c_{66}^D + \frac{h_{36}\epsilon_{3_0}\epsilon_{33}^S}{4\pi(\epsilon_{33}^S - \epsilon_{3_0})}\right] S_6 - \left(\frac{h_{36}\epsilon_{33}^S}{\epsilon_{33}^S - \epsilon_{3_0}}\right) P_{zd}; \\ E_z &= \frac{4\pi P_{zd}}{\epsilon_{33}^S - \epsilon_{3_0}} - \left(\frac{h_{36}\epsilon_{33}^S}{\epsilon_{33}^S - \epsilon_{3_0}}\right) S_6 \end{aligned} \qquad (8.17)$$

Hence the piezoelectric constant f_{36} relating the stress T_6 to the dipole polarization, is

$$f_{36} = \left(\frac{h_{36}\epsilon_{33}^S}{\epsilon_{33}^S - \epsilon_{3_0}}\right) \qquad (8.18)$$

The piezoelectric constant h_{36} was measured by measuring the resonant frequency of a plated 45° Z-cut crystal and comparing that with the resonant frequency for an unplated crystal. The frequency of the plated crystal is controlled by s_{22}^E elastic compliance, while that for the unplated crystal with an air gap holder is controlled by the elastic compliance s_{22}^D. As shown by equation (7.12) of the last chapter, these are related by the equation

$$1 - k^2 = s_{22}^D/s_{22}^E \qquad (7.12)$$

where k^2, the electromechanical coupling, is equal to

$$k^2 = \left(\frac{h_{36}}{2c_{66}^D}\right)^2 \frac{\epsilon_{33}^T}{4\pi s_{33}^E} = \left(\frac{d_{36}}{2}\right)^2 \frac{4\pi}{\epsilon_{33}^T s_{22}^E} \qquad (7.13)$$

Figure 8.7 shows the measured resonance frequencies for plated and unplated crystals for KDP and Fig. 8.8 shows the same quantities for ADP. From these the electromechanical coupling constant can be calculated and

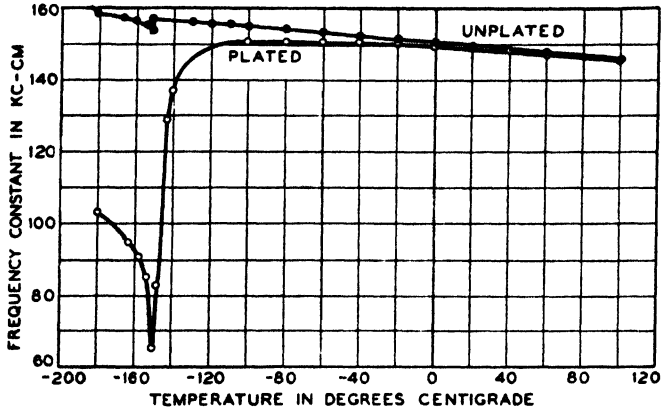

FIG. 8.7. Resonance frequencies for plated and unplated KDP crystals.

is shown plotted by Fig. 8.9 for both ADP and KDP. The curve for KDP rises to a maximum of 92 per cent at −151°C, the Curie temperature, and continues high to 80°K, the lowest temperature measured. ADP has

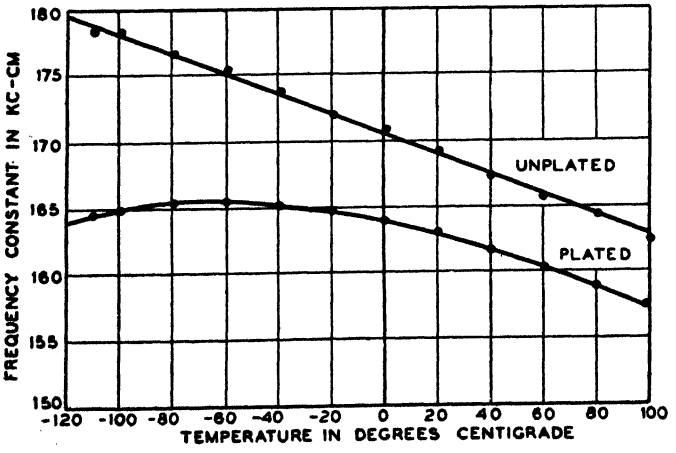

FIG. 8.8. Resonance frequencies for plated and unplated ADP crystals.

about a 30-per cent coupling at room temperature, which is the highest value for a non-ferroelectric crystal so far found. It increases to about 42 per cent at −125°C, at which temperature the crystal shatters to bits.

This temperature is not a Curie temperature, for the dielectric constant and coupling curves of Fig. 8.4 and 8.9 do not show any deviation from a smooth curve as this temperature is approached. It was surmised[5] by the writer that there was a second set of hydrogen bonds between the oxygen and the ammonia ions and that the sudden shattering at $-125°C$ is due to a first-order change in the crystal structure connected with the ammonium hydrogen bond system. The existence of this second set of hydrogen bonds has recently been confirmed by Prof. R. Pepinsky[7] by a

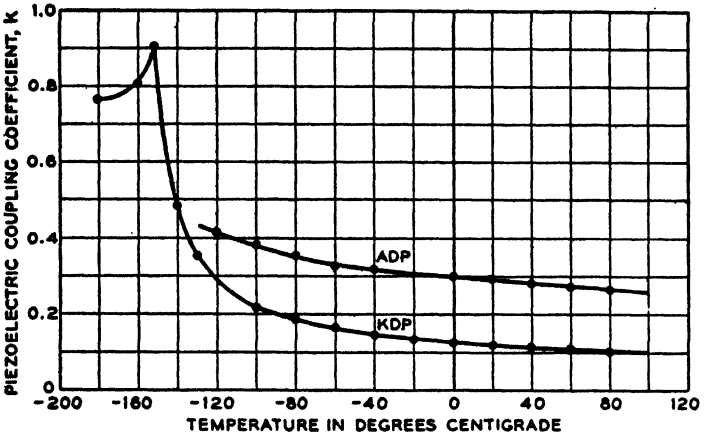

FIG. 8.9. Coefficient of coupling of ADP and KDP as a function of temperature.

structure analysis of ADP. This ammonium hydrogen bond system may explain why the coupling constant of ADP is so much larger than that of KDP, for with the close mechanical coupling between all the PO_4 ions that occur through the ammonium hydrogen bonds, one would expect a larger change in the lattice positions would be caused by a change in the H_2PO_4 dipoles than would occur in the KH_2PO_4 case, where the PO_4 ions are coupled to the K ions by central electrostatic forces.

That the fracture at $-125°C$ is not a change in the PO_4 hydrogen bond system is confirmed by the work of Bartschi,[8] Matthias, Merz and Scherrer. According to them the transition is due to the freezing of the rotation of the ammonium ion similar to what occurs in ammonium chloride. By introducing thallium in the ADP crystal, they screen the quadruple moment of NH_4 and lower the transition point to $-180°C$.

[7] Private communication, to be published shortly.

[8] Bartschi, P., B. Matthias, W. Merz, and P. Scherrer, *Helv. Phys. Acta*, Vol. 18, Fasciculus Quartus, 1945.

From these data, the data on the free dielectric constant given in Fig. 8.4 and Fig. 8.5 and the data on the elastic constant c_{66}^{D} given in the next section, all of the piezoelectric constants can be calculated and are given by Table XII for ADP and Table XIII for KDP.

TABLE XII

PIEZOELECTRIC CONSTANTS OF ADP

Temperature in °C	$d_{36} \times 10^{8}$	$e_{36} \times 10^{-4}$	$g_{36} \times 10^{8}$	$h_{36} \times 10^{-4}$	ϵ_{33}^{S}	$f_{36} \times 10^{-4}$
100	129.5	7.62	117	7.47	12.9	16.3
80	132.5	7.82	116	7.55	13.0	16.3
60	136	8.14	116	7.67	13.3	16.2
40	142	8.61	117.5	7.87	13.6	16.2
20	148	9.04	118.5	8.09	14.0	16.2
0	155	9.54	120.0	8.37	14.4	16.3
− 20	161	10.0	119	8.44	14.9	16.0
− 40	170	10.65	121	8.75	15.4	16.1
− 60	180	11.32	122	8.94	16.0	15.9
− 80	198	12.4	125	9.35	16.7	16.1
−100	207	12.9	126	9.6	17.3	16.1
−110	242	14.9	130	10.0	18.2	16.3
−120	261	15.4	132	10.2	18.6	16.3
−122	270	15.6	132	10.3	19.0	16.3

TABLE XIII

PIEZOELECTRIC CONSTANTS OF KDP

Temperature in °C	$d_{36} \times 10^{8}$	$e_{36} \times 10^{-4}$	$g_{36} \times 10^{8}$	$h_{36} \times 10^{-4}$	ϵ_{33}^{S}	$f_{36} \times 10^{-4}$
100	50.4	2.91	36.8	2.16	17.0	2.95
80	54.0	3.17	37.2	2.21	18.0	2.95
60	59.0	3.5	38.6	2.32	18.9	3.04
40	63.2	3.8	38.8	2.35	20.3	3.02
20	69.6	4.26	39.4	2.44	21.8	3.07
0	76.2	4.73	39.6	2.50	23.75	3.09
− 20	85.9	5.39	40.4	2.58	26.0	3.12
− 40	98.6	6.24	41.0	2.66	29.4	3.14
− 60	119.0	7.55	41.5	2.73	34.9	3.14
− 80	153	9.75	42.0	2.79	43.9	3.10
−100	202	12.8	42.2	2.81	57.6	3.05
−120	334	20.8	43.0	2.93	89.8	3.08
−130	480	29.0	43.2	2.97	123	3.09
−140	975	47.3	43.4	2.98	200	3.06
−145	1465	70.0	43.6	3.02	291	3.07
−150	4400	130.0	44.0	3.07	542	3.10

The first four columns of these two tables show the four standard piezoelectric constants d_{36}, e_{36}, g_{36} and h_{36}. Of these for the ferroelectric crystal, d_{36} varies by a factor of 88, e_{36} by 44.5, g_{36} by a factor 1.2, and h_{36} by a factor 1.42. Hence the constants involving the electric displacement D_z are much more constant than those involving the field. However, if we take a part of the displacement, namely, that part due to the dipole polarization, a much more constant ratio is obtained for both ADP and KDP. The fifth column shows the clamped dielectric constant and from this and the dielectric constant due to electrons and atoms which, from equations (8.11) and (8.12), are respectively 4.5 for KDP and 7.0 for ADP, one can calculate the ratio of piezoelectric stress to dipole polarization. This is shown by the last column, for the two crystals and within the experimental error is a constant equal to 16.2×10^4 for ADP and 3.1×10^4 for KDP. It is this ratio of 5 to 1 that gives ADP the larger electromechanical coupling and makes it the more useful crystal at room temperatures.

The other piezoelectric constant for these crystals is very small, and any crystal with its major face cut perpendicular to the z-axis is very weakly driven. The coupling is so small that measurements by the resonant and anti-resonant method are not too reliable. The constants were measured at one temperature by putting the crystal in an impedance bridge and measuring the equivalent shunt resistance as a function of frequency near resonance. The relation for a KDP crystal is

Frequency	102250	102270	102280	102290	102300	102310	102320	102330
Equivalent shunt resistance in ohms	1,200,000	680,000	570,000	500,000	550,000	700,000	900,000	1,180,000

the crystal being a 45° X-cut with the dimension $L = 19.56$ mm; $W = 6.10$ mm; $T = 0.90$ mm. The shunt capacity of the crystal was 54 $\mu\mu f$ agreeing with a dielectric constant of 46 shown in Fig. 8.4. By considering the equivalent circuit of a crystal, it can be shown that the equivalent shunt resistance is given by the formula

$$R_s = R_1\left[1 + \left(\frac{r}{2\pi f_R R_1 C_0}\right)^2\left(\frac{f_R}{f} - \frac{f}{f_R}\right)^2\right] \tag{8.19}$$

where R_s is the shunt resistance at resonance, C_0 the shunt capacitance of the crystal, r the ratio of C_0 to the motional capacitance C_1, and f_R the resonant frequency of the crystal. From the measurements $R_1 = 500{,}000$ ohms, $f_R = 102{,}290$ cycles; $C = 54 \times 10^{-12}$ farads. At 40 cycles from resonance, the ratio $R_s/R_1 = 2.4$. This gives enough data to solve for r,

which we find to be 26,400. The electromechanical coupling factor is related to r by the equation

$$k = \sqrt{\frac{1}{1 + \frac{8}{\pi^2} r}} \tag{8.20}$$

From the resonant frequency and the length, $s_{22}^{E'}$ is found to be 2.56×10^{-12} cm^2/dyne. Hence

$$d_{14} = 2 \times k \sqrt{\frac{\epsilon_{11}^{T} s_{22}^{E'}}{4\pi}} = 4.2 \times 10^{-8} \text{ for KDP} \tag{8.21}$$

A similar measurement for the 45° X-cut ADP crystal gives

$$d_{14} = 5 \times 10^{-8} \text{ (ADP)} \tag{8.22}$$

Hence although the dielectric constants normal to the x-axis are very large, the piezoelectric constants for this direction are very small.

8.14 *Elastic Constants for ADP and KDP*

All the elastic constants of these two crystals have been measured over a temperature range by the usual process of measuring longitudinal vibrations for 6 oriented crystals, and face-shear modes for crystals cut normal to the x- and z-axis. The constants s_{11}, s_{12}, s_{13} and s_{33} are independent of the condition of the applied field and are shown by Fig. 8.10 for ADP and Fig. 8.11 for KDP. The two shear-elastic constants do depend on the field, but since the coupling is so small for fields normal to the z-axis, no measurable difference is found for c_{44}. Figure 8.12 shows the s_{44} and s_{66} constants for ADP. The s_{66} constant is given for the two conditions of the electric field, namely, s_{66}^{E} denoting a constant field and s_{66}^{D} denoting a constant displacement. Similar measurements for KDP, plotted as $c_{44} = \frac{1}{s_{44}}$ and $c_{66} = \frac{1}{s_{66}}$, are shown by Fig. 8.13.

The temperature expansion coefficients for these two crystals are also of interest and are shown by Fig. 8.14 for ADP and Fig. 8.15 for KDP. ADP has nearly a zero temperature coefficient of expansion in the region from 20°C to 80°C.

8.2 *Useful Cuts and Applications of ADP Crystals*

8.21 *Useful Cuts for ADP Crystals*

Since the g_{36} constant is so much larger than the g_{14} constant in ADP, it is obvious that most of the useful cuts will be those that are normal or

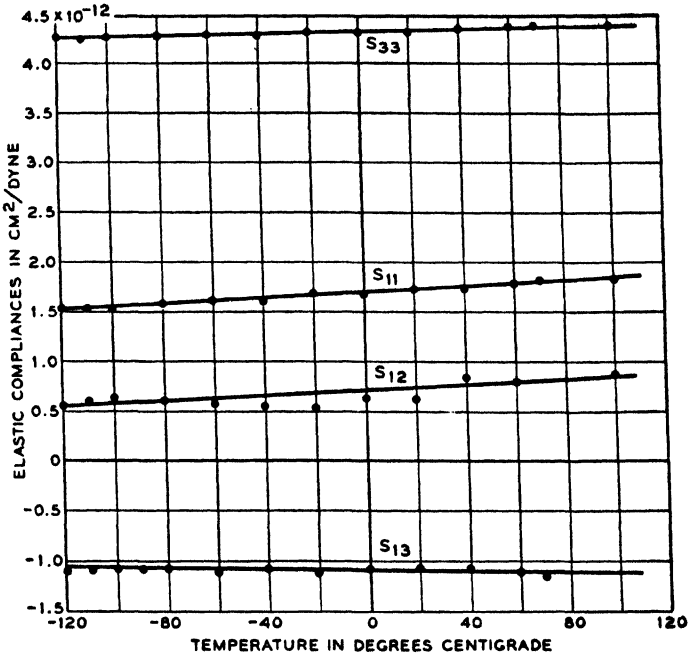

FIG. 8.10. Elastic compliances of ADP.

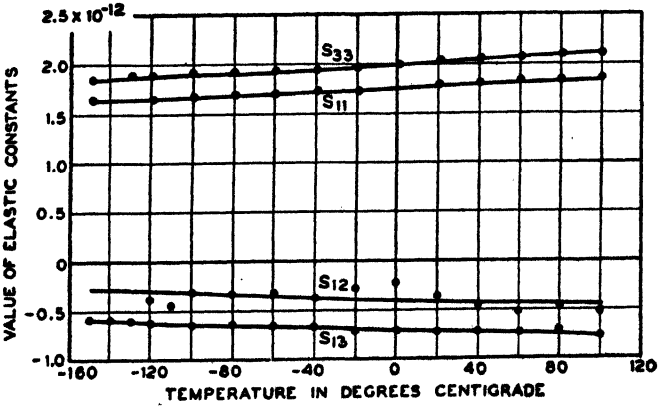

FIG. 8.11. Elastic compliances of KDP.

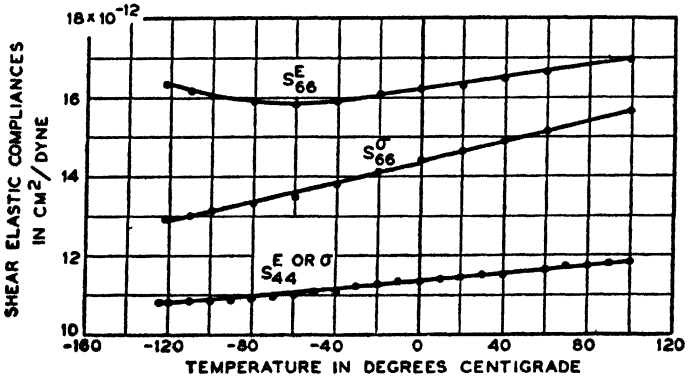

FIG. 8.12. Shear elastic compliances of ADP.

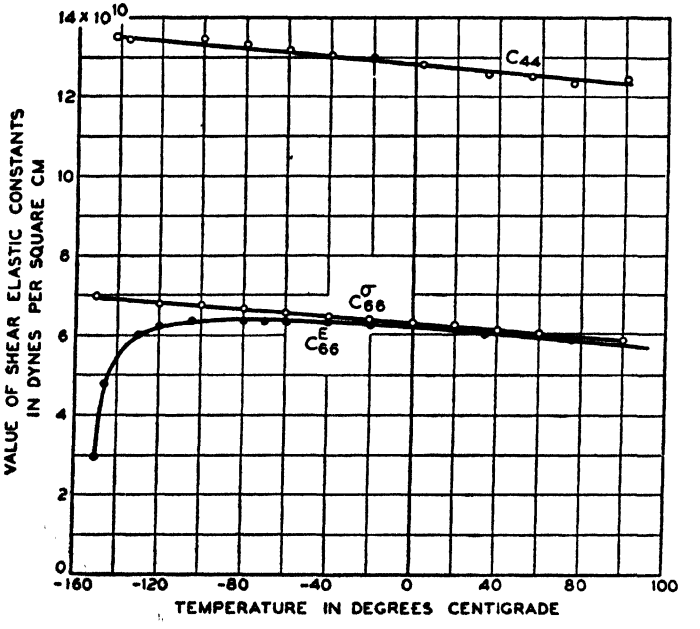

FIG. 8.13. Shear elastic stiffnesses of KDP.

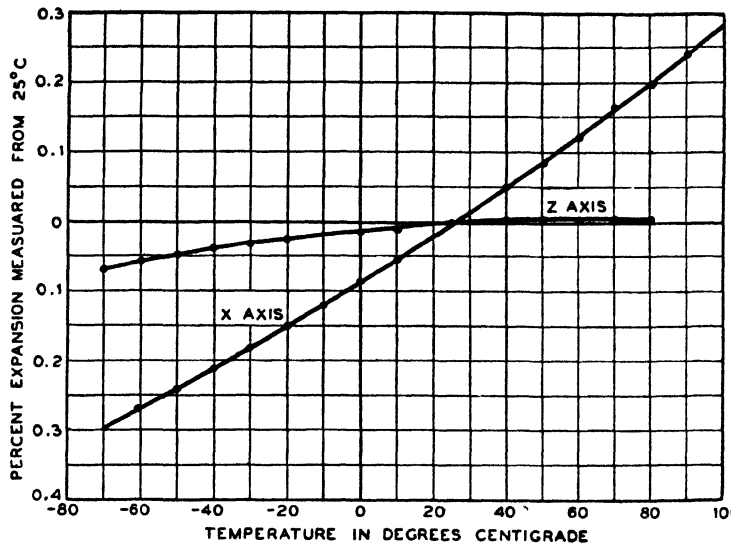

FIG. 8.14. Temperature expansions of ADP along x- and z-axes.

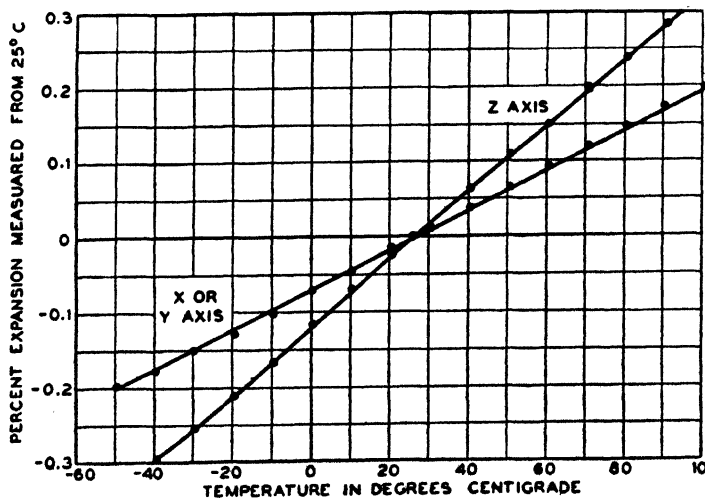

FIG. 8.15. Temperature expansions of KDP along x- and z-axes.

nearly normal to the z-axis. A crystal cut normal to the z-axis will generate a face-shear motion similar to that shown by Fig. 7.1B for rochelle salt. By cutting the length 45° from the x and y crystallographic axes, a longitudinal motion may be produced. The Z-cut and the 45° Z-cut crystals are the principal cuts used for ADP crystals. The Z-cut has been used in generating face-shear modes and in the production of torsional crystals. The 45° Z-cut crystal has been used as the transducing element in underwater sound equipment and in microphones, phonograph pickups, and in other devices for transforming mechanical energy into electrical energy. By cutting the major surface at an angle of 45° between the x- and z-axes, with the width along the y-axis, a cut is obtained which will produce a thickness-shear mode of high electromechanical coupling. Also if the normal makes equal angles with all three crystallographic axes, a plate is obtained which will generate a thickness longitudinal mode in the manner of an L-cut rochelle salt crystal.[9] The coupling is less than can be obtained in an X-cut thickness vibrating quartz crystal and therefore this cut has not been used.

The equations of motion of a 45° Z-cut take the form

$$S_l = s_{22}^{D'} T_l + g_l \frac{D_z}{4\pi}$$

$$E_x = -g_l T_l + \beta_{33}^{T} D_z \tag{8.23}$$

where $g_l = \frac{g_{36}}{2} = 59.2 \times 10^{-8}$; $\quad s_{22}^{D'} = 4.72 \times 10^{-12}$ cm^2/dyne;

$$\epsilon_{33}^{T} = \frac{1}{\beta_{33}^{T}} = 15.7$$

When used as a voltage generating device, the volts generated on open circuit per dyne per sq cm for a crystal 1 centimeter thick, are

$$E_{\text{volts}} = 1.78 \times 10^{-4} \text{ volts.} \tag{8.24}$$

This is larger than for 45° X-cut rochelle salt. Because of the lower dielectric constant this crystal has to be operated into a higher impedance than does rochelle salt to obtain the same output. Crystals of this sort are replacing rochelle salt for applications such as microphones and phonograph pickups because of their greater chemical stability and their ability to withstand wide temperature variations.

[9] The L-cut rochelle salt crystal was first described by Cady, "The Longitudinal Piezoelectric Effect in Rochelle Salt Crystals," *Proc. Phys. Soc.*, Vol. 49, pp. 645–653, 1937, and has been used to some extent in producing high-frequency longitudinal vibrations in liquids.

8.22 *Applications of ADP in Underwater Transducers*

The electromechanical coupling factor of ADP, given by the formula

$$k = \frac{g_{36}}{2}\sqrt{\frac{T'}{\epsilon_{33}}{4\pi s_{22}^{E'}}} = .3 \tag{8.25}$$

On account of this high coupling[10] these crystals can convert electrical

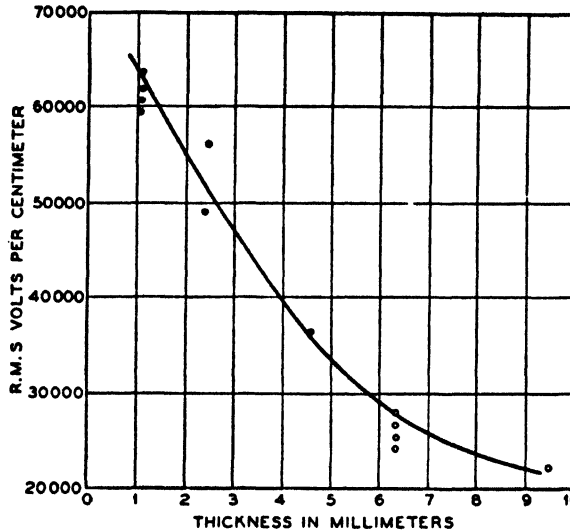

FIG. 8.16. Voltage breakdown of ADP crystals plotted as a function of crystal thickness.

into mechanical energy or vice versa, efficiently over a frequency range of

$$f_B/f_A = 1.36 \tag{8.26}$$

The crystal limitations in transferring electrical power to mechanical power are the breaking strain and the voltage gradient that the crystals will permit. Experiments with ADP crystals show that they will break if the strain exceeds from 5 to 10 $\times$ 10^{-4} cm per cm. The voltage gradient that they will stand, before a voltage puncture occurs, is a function of the thickness of the crystal. Figure 8.16 shows the voltage gradient which will produce a puncture in the average crystal when they are immersed in an insulating oil.

The two types of units commonly used are shown by Fig. 8.17. The quarter-wave unit is glued to a quarter-wave heavy metal backing plate,

[10] Mason, W. P., *Electromechanical Transducers and Wave Filters*, Chapter VI and VII, D. Van Nostrand Company, Inc., 1942, 2nd Edition, 1948.

usually with a ceramic or plastic insulator in between, and radiates its energy from its free face. A half-wave unit works into a low mechanical impedance on one end and radiates its energy from the other end. The equivalent circuit for these types of units and methods for calculating their efficiency, band widths, etc. has been discussed in the book, *Electromechanical Transducers and Wave Filters*[10] Chapter VI.

A large-scale transducer[1] using a number of quarter-wave radiators was produced during the war by Bell Laboratories and incorporated as part of QJA sonar system used by the Navy. The face plate of the transducer is shown by Fig. 8.18, which shows 52 quarter-wave transducing blocks of crystals which are glued to the same number of quarter-wave metal backing plates and the whole assembly held by a thin, metal-face plate. The

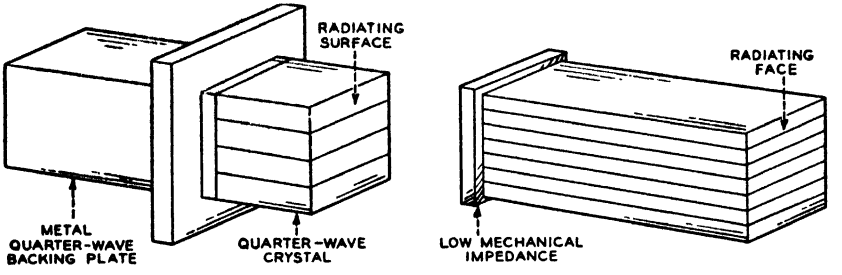

FIG. 8.17. Quarter-wave and half-wave transducers.

blocks on the outside are made of two ADP crystals, while those on the inside are made of four ADP crystals. Since the same voltage is applied across all the crystals, the inner and thinner crystals operate at an amplitude twice that of the outer crystals, which are twice the thickness of the inner crystals. The purpose of this graduation was to suppress the minor lobes that are only 13.5 db down from the main lobe if the whole unit acts like a plane piston. This has been accomplished, as shown by Fig. 8.19, which shows the measured and theoretical response of this unit plotted as a function of angle from the normal. The measured side lobes are at least 22 db down from the main lobe. The crystal groups are connected electrically into halves about a vertical line and each half is connected to the high side of a transformer; the low sides provide impedance matches to the driver amplifier and receiver amplifier circuits. The purpose of dividing the transducer in two halves is to allow a phase comparison of the received pulse on the two halves, which will locate the direction of the pulse much closer than would be possible with the directivity pattern of the transducer alone. The transformers are

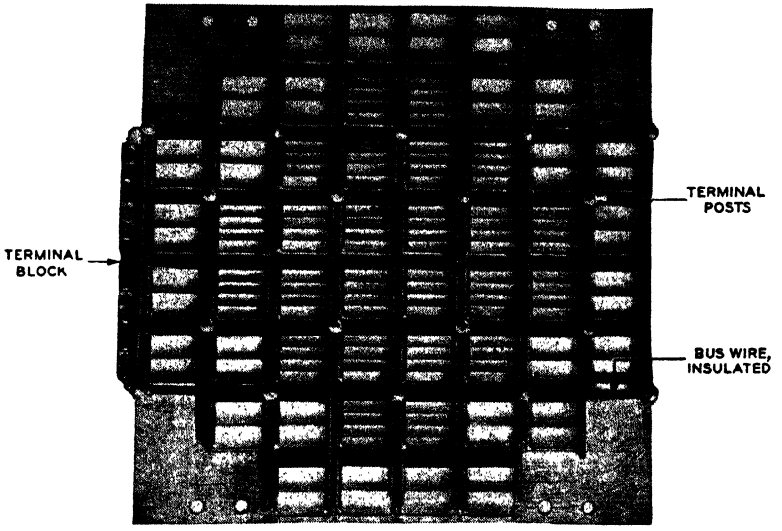

FIG. 8.18. Crystal array for QJA underwater sound transducer.

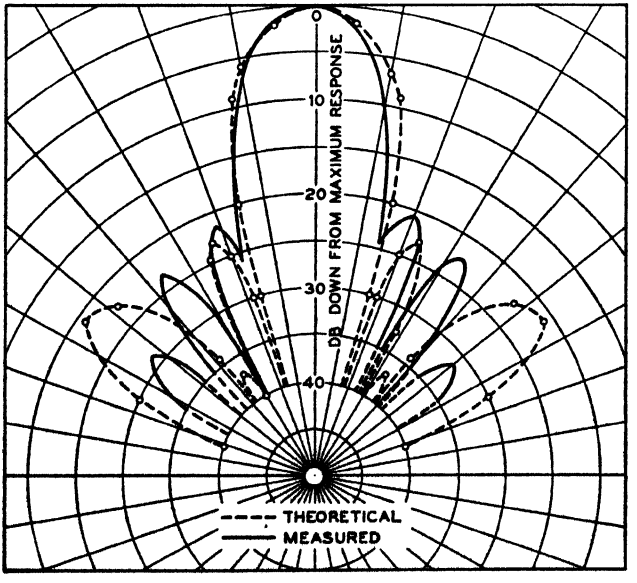

FIG. 8.19. Theoretical and measured directional pattern of QJA transducer.

mounted within the transducer case. The contacts between the crystals and their electrodes are gold to gold. Gold is evaporated on the crystals and gold-plated metal foil is later attached to the prepared crystals by glueing. This combination provides a very low interface electrical resistance and consequently minimizes heating at this point during the transmission of the high-power outgoing pulses.

The crystal array and resonator plate assembly are supported in rubber mountings inside a steel case. A rubber closure essentially sound transparent is vulcanized to the steel case forming the front face, as shown in Fig. 8.20. The case is sealed by a rubber gasketed steel cover which also serves to house the matching transformers within the cylindrical section. A sound absorbent baffle, which consists of alternate layers of 100-mesh wire cloth and expanded metal is fastened to the inside of the case directly back of the steel resonators. The function of this sound-absorbent baffle is to attenuate signals through the back of the transducer and also to reduce reflections within the case. The transducer assembly is supported by a flange at the top of the cover casting which is attached to the vertical training shaft of the retracting gear. The transducer can be rotated within a cylindrical space 12 inches in diameter. The entire transducer weighs about 200 pounds.

The inside of the transducer is vacuum filled with electrical grade castor oil from which air and water vapor have been removed by evacuation. The crystal array has an effective area of 200 sq cm so that with an electrical power input of the order of 100 to 150 watts, it corresponds to at least 0.5 watt per sq cm of crystal area. Because the conversion efficiency of the crystals is nearly perfect, better than 80 per cent of this power is converted into acoustic energy. By the time this energy has reached the front surface it has spread out so that the energy density in the water is considerably less than $\frac{1}{3}$ watt per sq cm which represents the steady-state cavitation value for sea water at atmospheric pressure. It has been found that many liquids including castor oil will support more energy density than that indicated by the calculated steady-state value based on pressure only. The cohesive pressure of the liquid and the increases observed for short pulse duration indicate that such projectors are capable of radiating considerably more power.

The transducer is mounted in a stream-lined dome and the whole unit can be drawn up into the ship by the retracting gear, shown by Fig. 8.21. The details of the stream-lined dome are shown by Fig. 8.22. The front part is a transparent .018-inch thick piece of stainless steel supported on an expanded metal frame. In the back fastened to this bulkhead is an absorbing panel and a reflecting pad to provide sound absorption for the transducer and reflection of noise coming from the propeller. The

directional pattern of the transducer within the dome is essentially the same as that outside, and the use of the streamlined dome reduces materi-

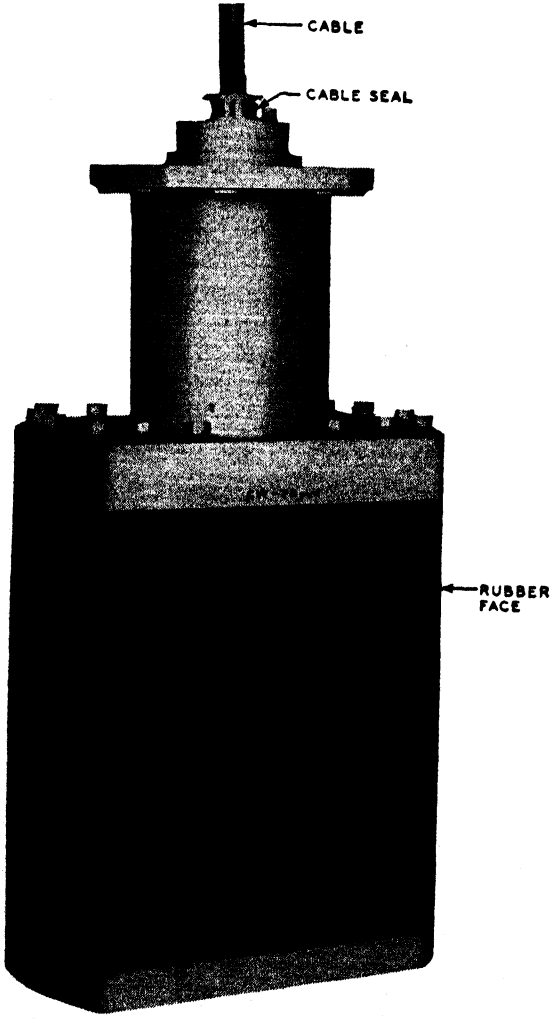

FIG. 8.20. Case and ρc rubber transparent window for QJA transducer.

ally the noise generated by moving the transducer rapidly through the sea water.

The details of the QJA system are described in the above-mentioned paper.[1] Such systems were widely used during World War II, and they

and other type systems employed ADP crystals to a very considerable amount.

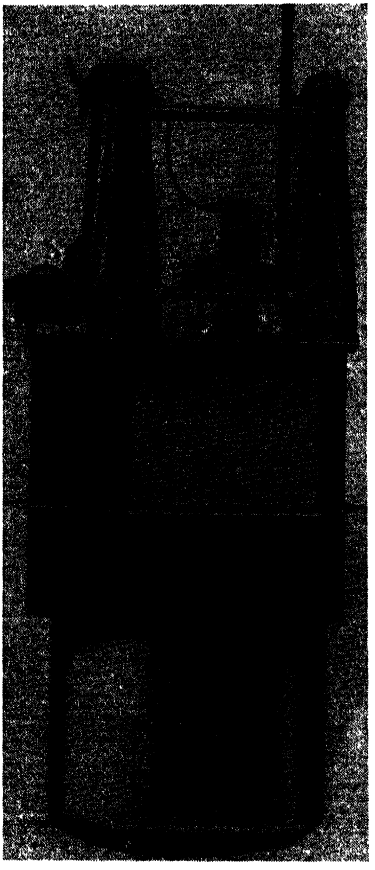

FIG. 8.21. Dome and retracting system for QJA sonar system.

8.23 *Use of ADP Crystals in Producing High Strains in Metals*

The particle velocity on the end of a quarter-wave or half-wave crystal is equal to

$$\dot{\xi} = vS_M \quad \text{or} \quad \dot{\xi} = 3.3 \times 10^5 S_M \tag{8.27}$$

where $\dot{\xi}$ is the particle velocity, v the velocity of propagation (equal to 3.3×10^5 cm per sec for a 45° Z-cut ADP crystal) and S_M is the maximum strain that the crystal will stand. This maximum strain occurs at the middle of a half-wave length unit or at the glued joint for a quarter-wave unit. Since the crystal is stronger than most of the adhesives that can be

used to attach it to high mechanical impedance solid materials, the half-wave length unit can be used to produce a higher particle velocity than the quarter-wave unit.

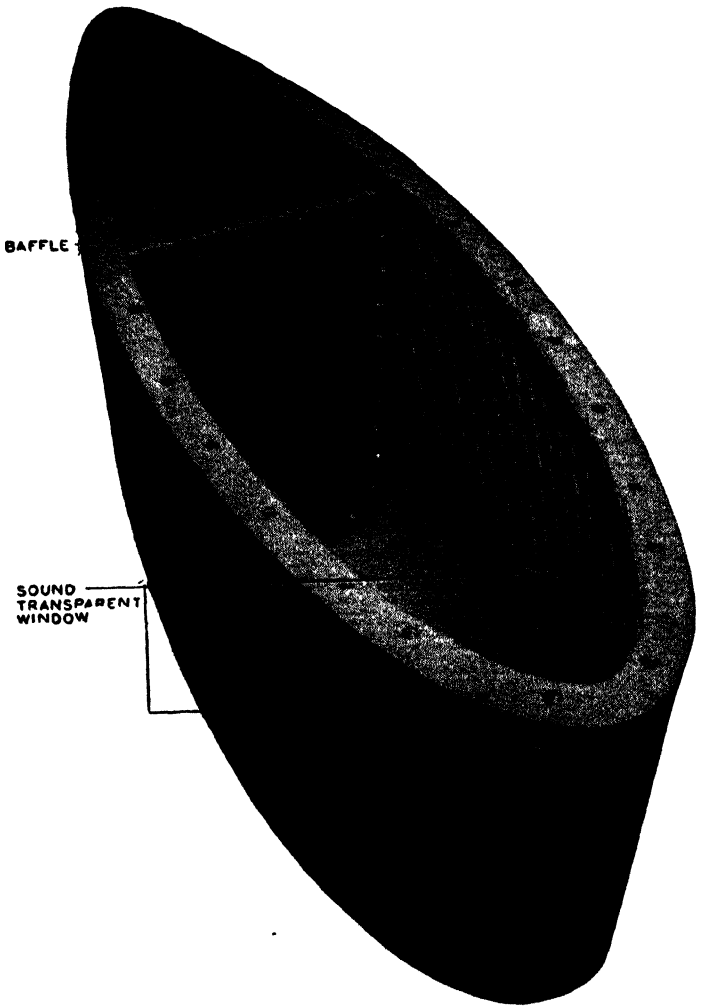

FIG. 8.22. Details of transparent dome showing absorbing baffle.

With a maximum strain of 5×10^{-4} possible for ADP or most other synthetic crystals, the limiting particle velocity is about 165 cm per sec, and hence crystals cannot be used directly to produce very high strains in metals, or terminal velocities approaching the speed of sound. If, how-

ever, a crystal mosaic is glued to a metal rod tapered exponentially like a horn, a very high strain and a very high terminal velocity can be produced at the small end. Fig. 8.23 shows a construction used for testing fatigue in metals. A crystal mosaic several inches in cross-section is glued to a steel rod which tapers from the crystal area down to a thickness of 0.05

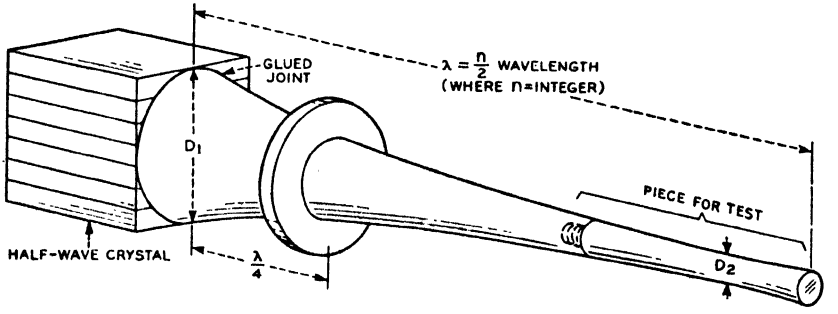

FIG. 8.23. Metal " horn " for obtaining a large strain in a metal sample.

inch, after which it increases in diameter. The taper is an exponential function of the length and must satisfy the relation.

$$T \leqq \frac{2\pi f}{v_s} \tag{8.28}$$

where the taper T is determined by the equation for the area

$$S = S_0 e^{-2Tl} \tag{8.29}$$

f is the resonant frequency of the crystal, and v_s the velocity of sound in the steel. If the total length of the steel piece is made an integral number of half-wave lengths of the crystal frequency, the glued joint will come at a loop of the motion and will not be appreciably strained. The whole system acts as a resonant system and produces a considerable motion for small applied voltages. The particle velocity of the steel section adjacent to the crystal is the same particle velocity as the crystal surface. Now it can be shown that the strain in the bar of uniform section at the nodal point (point of maximum strain), is equal to

$$S = \dot{\xi}/v_s \tag{8.30}$$

where v_s is the velocity of propagation of the wave in the steel and $\dot{\xi}$ the particle velocity at the surface. The effect of the tapered section is to increase the particle velocity in inverse proportion to the diameter. Hence, if the diameter decreases from 2 inches to .05 inch, the velocity is multiplied

by a factor of 40 and the strain at the nodal point is equal to

$$S_s = 40 \times \frac{v_c}{v_s} S_c \tag{8.31}$$

where S_s is the strain in the steel, S_c the strain in the crystal, v_c the velocity of propagation in the crystal (3.3×10^5 cm per sec) and v_s the velocity of propagation in the steel—about 5.1×10^5 cm per sec. For a strain of 4×10^{-4} in the crystal, a strain of .01 can be generated in the steel. This is sufficient to cause plastic deformation in the steel and by gradually increasing the drive on the crystal the fatigue properties of the steel can be investigated at a high rate of strain and velocity. It should be noted that for the transformer formulae to remain valid, the largest diameter of the metal horn should be less than a half-wave length for the frequency of operation.

This same system can be used to produce a high particle velocity on the small end of the steel bar. The only limitation is the strain that the metal will stand. Other uses appear to be delivering a large amount of power for a small area. By attaching a boring tool and using carborundum, a very rapid drill is obtained.

By mounting a torsional crystal on the large end of the bar a torsional vibration can be given to the bar and the properties of the material under shearing strain can be tested. An ADP crystal can be made to vibrate in torsion as discussed in Chapter XIV, by using the electrode system shown by Fig. 14.7. The inside surface is covered by one electrode while the two outside electrodes, each of which cover a 90-degree segment, are connected together and form the other electrode. The centers of the two outside electrodes are normal to the z-axis and the field is directed out from the center for both electrodes, as shown in Fig. 14.7, thus producing a shearing motion for one segment and the opposite shear on the other segment so that the whole crystal is given a torsional motion. The use of a torsional ADP crystal for measuring shear viscosity and elasticities of liquids is discussed in Chapter XIV.

CHAPTER IX

Properties and Uses of Ethylene Diamine Tartrate (EDT) and Dipotassium Tartrate (DKT) Crystals

9.1 *Introduction*

During the last 10 years or more, the properties of synthetic crystals have been investigated at Bell Laboratories with the aim of understanding the properties of such crystals and in obtaining crystals of use for the telephone plant. This search has recently resulted in two crystals of the monoclinic sphenoidal class which have cuts having zero temperature coefficients, high Q's, little or no water of crystallization, and a high electromechanical coupling. These crystals are a suitable substitute for quartz for use in electrical wave filters. The requirements for such crystals are a rather high degree of frequency and inductance stability over a temperature range from 55°F to 110°F, a good chemical stability against atmospheric humidity conditions, a low mechanical dissipation, and a long-time stability against structure changes which would produce a change or aging in frequency or electrical properties.

Fortunately, these crystals were discovered before the end of the war, for due to the large number of quartz crystals used in communication equipment, a shortage of large-sized quartz crystals had developed. During the war, quartz crystals to the number of 30,000,000 per year, were used in the communication equipment of the services for the purpose of stabilizing the frequencies of oscillators. As the war progressed, it became difficult to obtain large-sized crystals and toward the end of the war most manufacturers were using crystals whose original weights were under 100 grams. With the end of the war, it has become difficult to obtain natural crystals of sufficient size to supply blanks for filters which may run in size up to 2 inches long. With these synthetic crystals, it is possible to grow natural crystals of any desired size and hence the filter crystal supply problem can be met.

These crystals are ethylene diamine tartrate[1] ($C_6H_{14}N_2O_6$) and dipotassium tartrate[1] ($K_2C_4H_4O_6—\frac{1}{2}H_2O$). The first has been given the

[1] The properties of EDT are described in a paper "New Low Coefficient Synthetic Piezoelectric Crystals for Use in Filters and Oscillators," W. P. Mason, *Proc. I.R.E.*, Vol. 35, No. 10, p. 1005, 1947, while the properties of DKT are described in a paper "Properties of Monoclinic Crystals," *Phys. Rev.*, Vol. 80, pp. 705–728, Nov., 1946.

designation EDT and the second DKT. EDT has no water of crystallization and hence will not dehydrate. It will deliquesce or collect water at humidities above 93 per cent, but since it is fabricated in low-humidity rooms and mounted in sealed glass containers, this introduces no handicaps. DKT has one molecule of water of crystallization for each two of potassium tartrate, but this is tightly bound and tests show that no dehydration takes place up to 80°C. The crystal deliquesces somewhat lower in humidity — around 80 per cent — than does EDT. Of these two crystals, DKT is more stable with temperature, but is harder to grow and requires more careful handling than does EDT. Accordingly, the first commercial application has been made using the EDT crystal. The Western Electric Company has established a growing plant for this crystal at Allentown, Pa., and is producing finished crystals of this material for filters.

As discussed in a recent paper by Walker and Kohman,[2] these crystals are not grown by the rocking-tank method which has been used for rochelle salt and ADP, because of the much greater tendency to crystallize from solution spontaneously as compared with the other two crystals. Instead, a rotary method has been used in which crystal seeds are mounted on a spider rotated with a reciprocating motion through the saturated solution. This motion keeps a constant saturated solution at the growing face of the crystal. Experience has shown that if motion is stopped for a period of several hours, the interfacial solution becomes less saturated, thus starving the crystal and causing the formation of a veil. The rotary motion also tends to sweep out spurious seeds, permitting them to settle on the bottom of the tank, where an unsaturated zone is maintained because of the proximity of the tank bottom to the heating element located at the base of the apparatus. The crystals can be grown by either starting with a saturated solution at a high temperature and gradually lowering the temperature, or by using a constant temperature and replenishing the salt by a continuous process. The constant-temperature method is used at the Western Electric plant at Allentown. The temperature is set at 43°C, for it has recently been found that a hydrate of EDT is more stable below 41°C, and trouble has been experienced in growing this as a contaminant when the temperature is lower than 43°C. The early process of growing involves a capping operation in which the formation of natural faces occurs on a cut plate of the proper cross-section, and a bar growth in which clear material is grown on the capped plate. The capping operation can be dispensed with if the growing end of the crystal is used as a capped plate. The crystal has peculiar growing habits and will grow only on one end of the *y* or *b* crystallographic axis.

[2] Walker, A. C. and G. T. Kohman, "Growing Crystals of Ethylenediamine Tartrate," *Trans. A.I.E.E.*, Vol. 67, 1948.

The study of the methods of fabricating, mounting, methods for eliminating interfering modes of motion, and testing, has been carried out under the direction of R. A. Sykes. Part of this work is described in a paper by Pennell and Griffin.[3] The bars used are up to 7 inches of clear growth having a cross-sectional area of from 2 to 4 square inches. The cutting and wafering is performed by a wet-string type of saw which cuts by dissolving the material locally along the cutting line. This machine is shown by Fig. 9.1. The string saw consists of one or more endless strings running over pulleys to give a taut vertical section similar to a ganged band saw. Following cutting, the wafers are rough ground to give a flat face and a straight edge and are X-ray corrected for face and edge orientation. They are then ground to size on a wet-belt sander equipped with accurate ways and holding fixtures. To prevent local heating, a liquid coolant is used.

Processing of the plates into finished crystal units now begins. The first steps consist of etching the plates in a solution of alcohol and water to remove any surface cracks, and attaching of four headed terminal wires by a cementing process. These wires are only 8 mil inches in diameter, yet can withstand loads of 7 to 8 pounds. They are located in pairs on opposite sides near the center of the plate. The plate, with the wires attached, is then coated to a thickness of a few hundred thousandths of an inch with gold by an evaporation process and the plating on each major surface is divided into halves by a sand-blasting process.

Frequency adjustment is accomplished by reducing the length of the crystal by grinding the end with a fine abrasive paper. After adjustment, the crystal is mounted in a cage and sealed in an evacuated glass container, as shown by Fig. 9.2. Tests on the long-time stability of these plates have been made over a considerable period. These measurements show that a typical EDT crystal unit will frequency age about +40 parts in a million over the first year. This aging rate is rapid at first, but diminishes to almost zero at the end of the year. The same general sort of thing occurs for the dissipation factor, the resistance decreasing to 50 per cent of its initial level and becoming asymptotic within a year. In frequency aging, the dispersion is low enough so that the ultimate frequency can be predicted and provided for during final adjustment. In comparing the characteristics of the new EDT synthetic crystal units to the more commonly used cuts of quartz for network applications in the low-frequency ranges, it may be said that EDT is superior with regard to inductance and ratio of capacitances, that it is approximately equal or superior in temperature coefficient, physical size, and aging characteristics,

[3] Griffin, J. P. and E. S. Pennell, "Design and Performance of Ethylene Diamine Tartrate Crystal Units," *Trans. A.I.E.E.*, Vol. 67, 1948. Presented before A.I.E.E., Jan. 26–30, 1948.

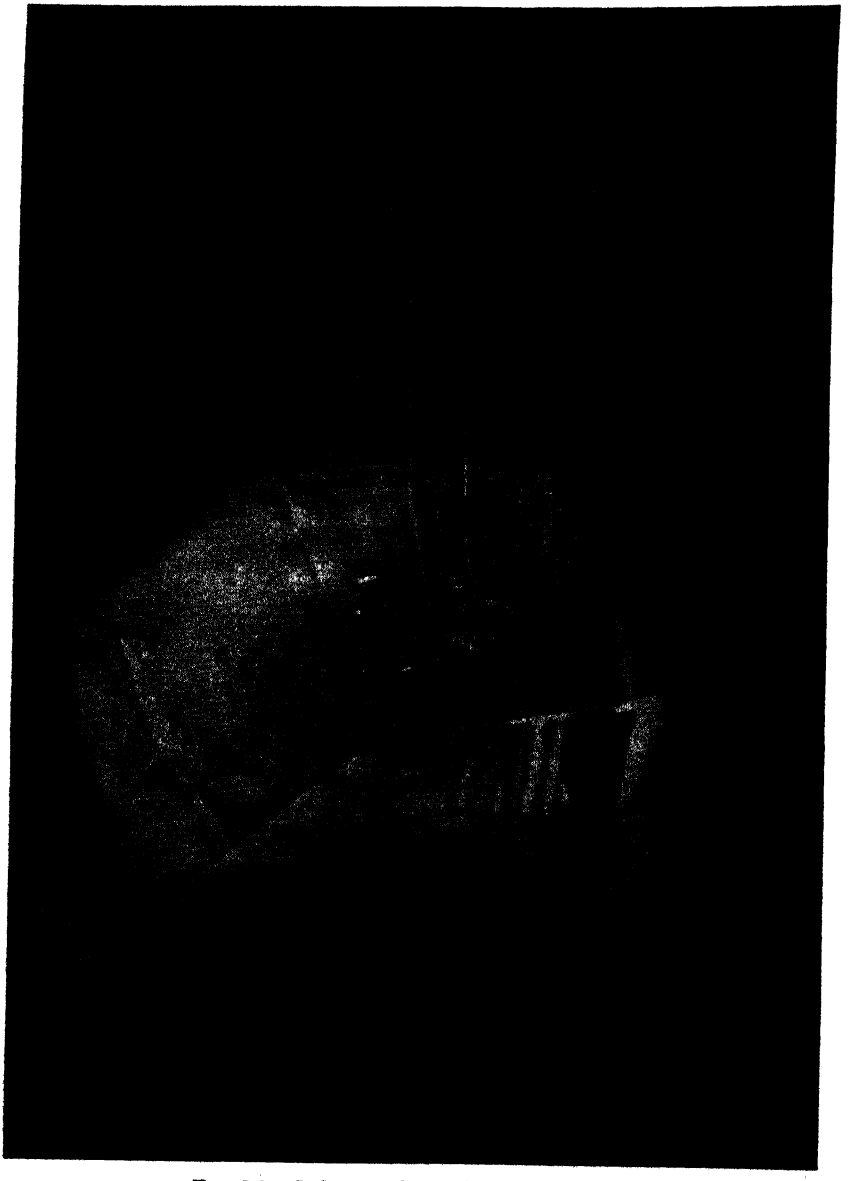

FIG. 9.1. String saw for cutting EDT crystals.

but that it is inferior in regard to mechanical strength and dissipation factor. However, Q's as high as 30,000 are regularly obtained with the mounted crystal and this is sufficient to meet the band-pass filter requirements for the high-frequency carrier systems.

The application of these crystal units to filters has been carried out under the direction of A. R. D'Heedene and some of the work is described in a paper by E. S. Willis.[4] The crystals have been applied in the 56-kc

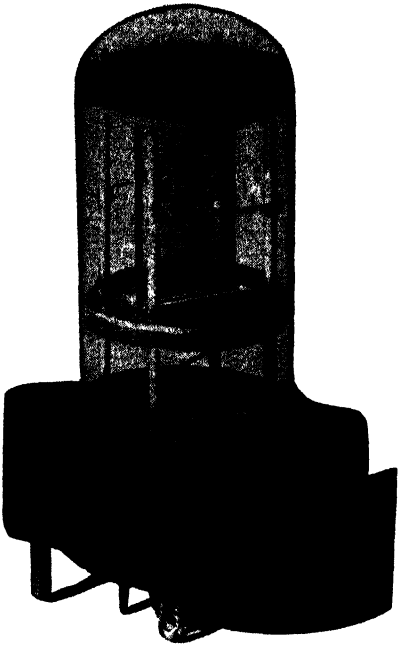

FIG. 9.2. Mounted EDT crystal for filter uses.

pilot channel filters and in the 12-channel bank of the high-frequency carrier systems, which provide very flat filter bands utilizing about 3300 cycles of a total frequency spacing of 4000 cycles for transmission of speech. All the filters for the cable and open-wire carrier and the coaxial systems use the same bank of filters which lie in the frequency region from 60 to 108 kc. The need for these new crystals arising out of the large growth of the carrier systems and the dwindling supply of quartz, is summarized in this paper. After considering alternate means for supplying these filters it was decided, in the interest of manufacturing effort and office space

[4] Willis, E. S., "Crystal Filters Using Ethylene Diamine Tartrate in Place of Quartz," *Trans. A.I.E.E.*, Vol. 67, 1948. Presented before A.I.E.E., Jan. 26–30, 1948.

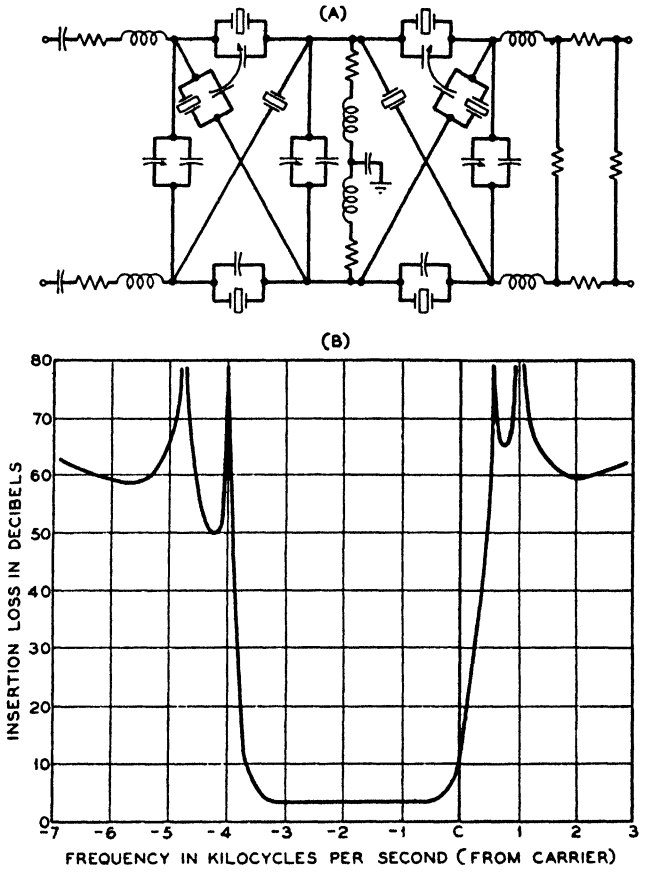

FIG. 9.3. Crystal filter circuit and resulting attenuation characteristic.

required, to develop the EDT crystal units. These not only maintained the same operating frequency range as the present circuits, but also provided the following advantages:

1. The EDT filters can be designed to meet practically the same electrical requirements as the quartz filters, thereby requiring only minor systems circuit changes.
2. The EDT filters occupy the same mounting space as the quartz-crystal filters, eliminating the need for extensive equipment design changes.
3. An independent source of piezo-active material is provided so that growth of the long-distance facilities in the future will not be restricted by the inability to import sufficient quartz.

The initial application was for the pilot-channel filter used for picking off a control frequency for adjusting the gain of the amplifiers of the system. A ladder network was used with three shunt condensers and two series crystals. The A type EDT crystal, described in section 9.3, was used because of its greater temperature stability and smaller size.

The channel filters in the form of a bank of 12 ranging in frequency from 60 kc to 108 kc, require about 75 per cent of all the crystals used for filters.

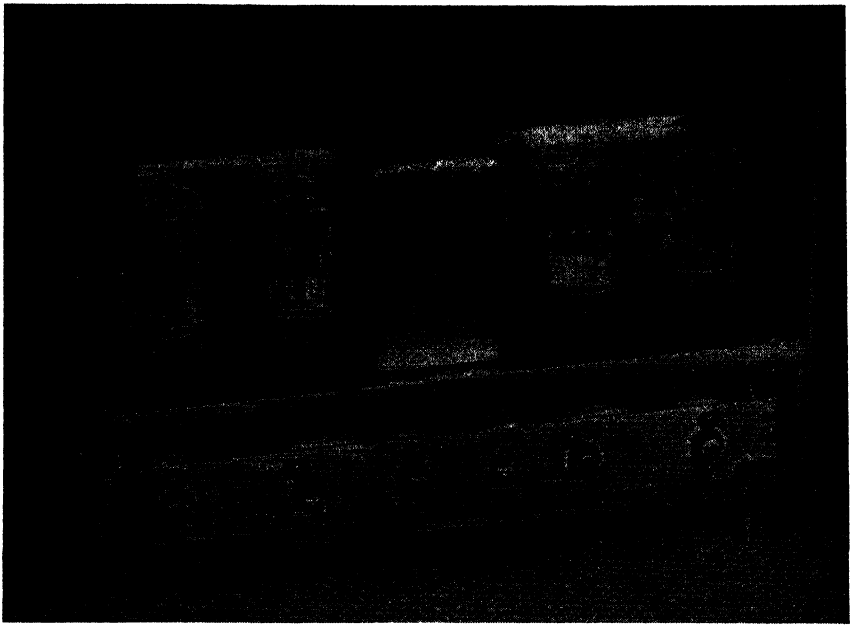

FIG. 9.4. Finished filter assembly.

The type of circuit utilized, as shown by Fig. 9.3A, is similar to the quartz crystal section described in Chapter VI, except that a shunt coil is used between the two balanced lattice sections rather than series coils. For the first six channel filters, ranging in frequency from 60 kc to 84 kc, the *Y*-cut crystal described in section 9.3 is used. This crystal is used on account of its high electromechanical coupling, which allows the impedances of the associated coils and condensers to be maintained at a reasonable value. The frequency stability of this cut over a temperature range from 55°F to 110°F, is about four times as good as that of the $-18°$ *X*-cut quartz crystal, which has heretofore been used in this type of filter. For the upper six channels, the electromechanical coupling of the *Y*-cut is too high and the ($yxlt \pm 20°/-5°$) cut of Fig. 9.19 (which has been given the

designation of *B*-cut), will probably be used. Fixed resistances are used with these filters in order to equalize the losses over the frequency range. The three coils are made with powdered-iron-dust cores having a good temperature stability and a high Q. A typical filter loss frequency curve is shown by Fig. 9.3B. The completed assembly is shown by Fig. 9.4, which shows the four crystals mounted in glass sealed tubes, the three coils, and the variable condensers. The fixed condensers and the resistances are in the chassis under the base plate.

9.2 *Properties of Ethylene Diamine Tartrate (EDT) Crystals*

Monoclinic crystals are characterized by having two crystallographic axes a and c not at right angles to each other, and a third axis b that is perpendicular to the other two. The c-axis is along the shortest distance

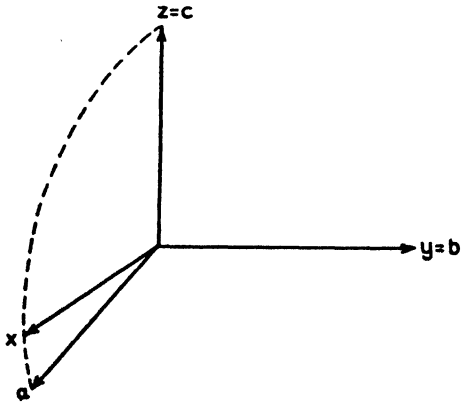

FIG. 9.5. Method for relating rectangular axes to the crystallographic axes of a monoclinic crystal.

of the unit cell while the b-axis is the axis of twofold symmetry. In measuring the properties of a crystal, the calculations come out much more simply for a right-angled system of coordinates. As shown by Fig. 9.5, the method chosen for relating the right-angled x-, y-, z-systems of axes to the a, b, c crystallographic axes of the crystallographer, is to make z coincide with c, y with b, and to have the x-axis lie in the plane perpendicular to the b-axis and at an angle of $51'$ above the a-axis for DKT. For EDT the angle between x and a is much larger, *i.e.* $15°30'$.

The x-, y-, z-axes form a right-handed system of axes. Since $b = y$ is a binary axis, it is necessary to have a convention for specifying which end of the axis is positive. This can be done by locating the two optic axes of the crystal. A monoclinic crystal is a biaxial crystal and the plane that

contains these two axes must be either perpendicular or parallel to the b or y crystallographic axis. As shown by Fig. 9.6, for these two crystals the optic axes lie in a plane parallel to the b-axis and at an angle of 21° in a clockwise direction from the c or z crystallographic axis for DKT and at an angle of 25° for EDT. Since $+x$ lies at a counterclockwise angle of 90° from c, and $+b = +y$ makes a right-handed system of coordinates with the x- and z-axes, the measurement determines the positive direction of all three axes.

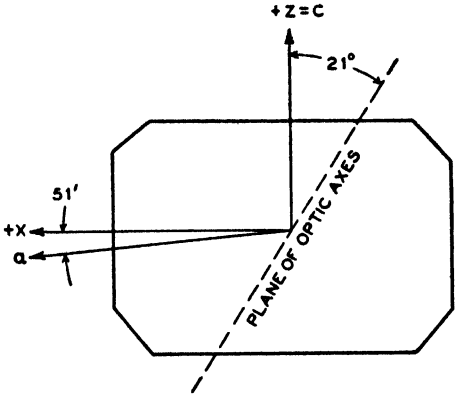

FIG. 9.6. Plane of optic axes with respect to the a and c crystallographic axes.

DKT has two cleavage planes lying along planes determined by the three crystallographic axes. EDT has one cleavage plane which is the 001 plane, *i.e.*, the plane containing the a and b crystallographic axes. None of these cleavages are sufficiently bad to prevent lapping and grinding these crystals by ordinary procedures. The density of EDT is 1.538 while that of DKT is 1.988.

Since not all directions in the crystal are equivalent, useful cuts occur in certain materials and modes at motion at definite orientations with respect to the crystallographic axes. The quickest method for finding the locations of these cuts in a suitable crystal substance is by determining the values and temperature coefficients of the fundamental elastic, piezoelectric, and dielectric constants of the crystal. From these fundamental constants, the properties of any other orientation can be calculated by applying mathematical formulae for transferring from the set of crystallographic x-, y-, z-axes to a rotated x', y', z' system of axes. Hence, if the fundamental constants are known, the location can be calculated, in a properly selected material and mode of vibration, of all crystal cuts having such desirable properties as low temperature coefficients and high electromechanical couplings.

For a plated, non-ferroelectric type crystal such as these, the most useful method of expressing the piezoelectric constants is that originally due to Voigt, who expressed the six strains S_1 to S_6 in terms of the six stresses T_1 to T_6 and the three electric fields E_x, E_y, E_z. The strains S_1, S_2, S_3 are the elongation per unit length along the x-, y-, z-axes respectively, while the strains S_4, S_5 and S_6 represent the shearing strains around the axes x, y, and z, respectively, as discussed in Chapter III. The stresses T_1, T_2, T_3 similarly represent the stresses tending to produce elongations along the x-, y-, z-axes, respectively, while T_4, T_5, T_6 represent the shearing stresses tending to produce shearing strains around the x-, y-, z-axes respectively. The fields E_x, E_y, E_z are the potential gradients (or the potentials divided by the distance over which they are applied) existing along the x-, y-, z-axes respectively. This relation shown by Equation (9.1) is Voigt's method of expressing the inverse piezoelectric effect. For a monoclinic sphenoidal crystal, these equations take the form

$$\begin{aligned}
S_1 &= s_{11}^E T_1 + s_{12}^E T_2 + s_{13}^E T_3 + s_{15}^E T_5 + d_{21} E_y \\
S_2 &= s_{12}^E T_1 + s_{22}^E T_2 + s_{23}^E T_3 + s_{25}^E T_5 + d_{22} E_y \\
S_3 &= s_{13}^E T_1 + s_{23}^E T_2 + s_{33}^E T_3 + s_{35}^E T_5 + d_{23} E_y \\
S_4 &= s_{44}^E T_4 + s_{46}^E T_6 + d_{14} E_x + d_{34} E_z \\
S_5 &= s_{15}^E T_1 + s_{25}^E T_2 + s_{35}^E T_3 + s_{55}^E T_5 + d_{25} E_y \\
S_6 &= s_{46}^E T_4 + s_{66}^E T_6 + d_{16} E_x + d_{36} E_z
\end{aligned} \tag{9.1}$$

The s_{11}^E to s_{66}^E are the 13 elastic compliances of the crystal which are the ratios of the strains to the appropriate stress when all other stresses and the field are held constant, and d_{14} to d_{36} the eight piezoelectric constants, which are the ratios of the strains to the appropriate applied field when all the stresses are held constant. The superscript E over the s^E, s indicates that the fields are held constant for the compliance measurements.

The direct piezoelectric equations express the electric displacement generated in the medium along the three axes in terms of the applied stresses and the applied fields. These become

$$\begin{aligned}
\frac{D_x}{4\pi} &= \frac{\epsilon_{11}^T E_x}{4\pi} + \frac{\epsilon_{13}^T E_z}{4\pi} + d_{14} T_4 + d_{16} T_6 \\
\frac{D_y}{4\pi} &= \frac{\epsilon_{22}^T E_y}{4\pi} + d_{21} T_1 + d_{22} T_2 + d_{23} T_3 + d_{25} T_5 \\
\frac{D_z}{4\pi} &= \frac{\epsilon_{13}^T E_z}{4\pi} + \frac{\epsilon_{33}^T E_z}{4\pi} + d_{34} T_4 + d_{36} T_6
\end{aligned} \tag{9.2}$$

where ϵ_{11}^{T} etc., are the dielectric constants measured at constant stress T, and D_x, D_y, D_z, the electric displacement along the three axes.

As discussed in Chapter X all of these constants can be measured by measuring the resonant frequency, anti-resonant frequency, and the capaci-

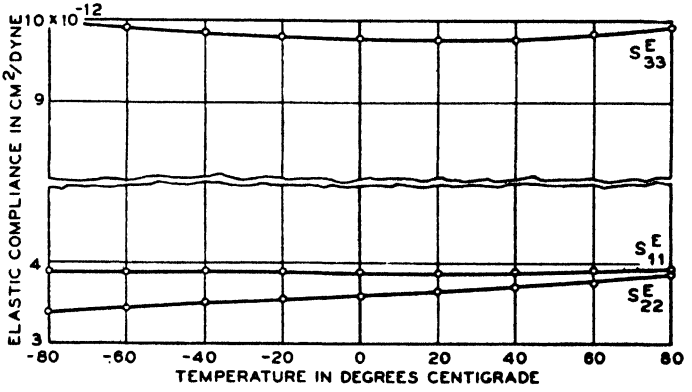

FIG. 9.7. Longitudinal elastic compliances of EDT plotted as a function of temperature.

tance at low frequencies of 18 oriented cuts. This process is described and illustrated for several crystals in Chapter X and has been employed for the EDT crystal, the resulting constants expressed in cgs units are shown

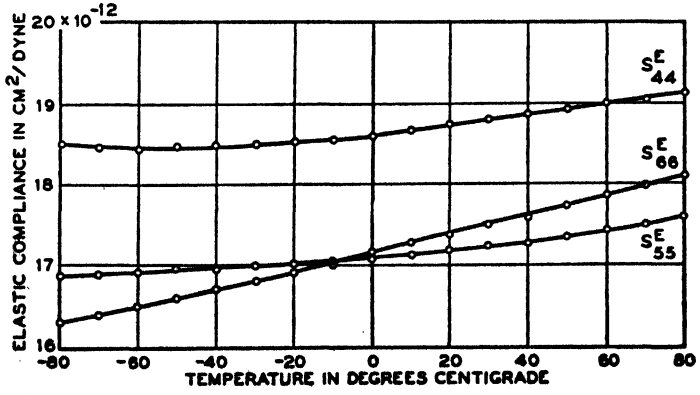

FIG. 9.8. Shear elastic compliances of EDT plotted as a function of temperature.

by Figs. 9.7, 9.8, 9.9, 9.10 and 9.11. Fig. 9.7 shows the longitudinal elastic compliances, Fig. 9.8 the shear elastic compliances, Fig. 9.9 the cross coupling elastic compliances, Fig. 9.10 the eight piezoelectric constants and Fig. 9.11 the four dielectric constants — all plotted as a function of

temperature. In deriving the elastic constants as a function of temperature, use has to be made of the temperature expansion coefficient in the various directions, in order to eliminate the change in length and the change in density. Measurements made by Mrs. E. A. Wood of the expansion co-

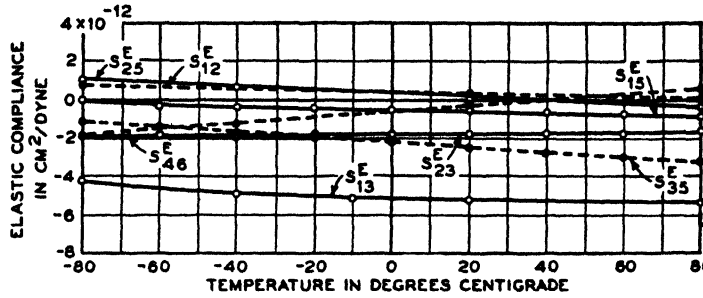

FIG. 9.9. Cross coupling elastic compliances plotted as a function of temperature.

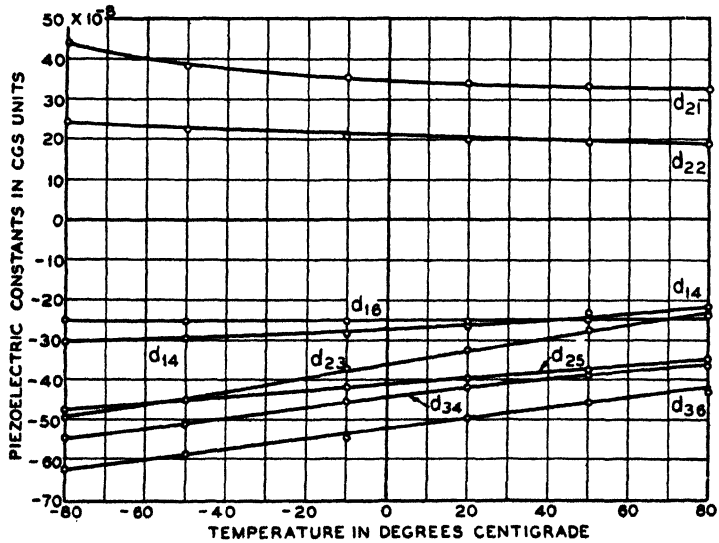

FIG. 9.10 Piezoelectric constants of EDT plotted as a function of temperature.

efficient in the x, z plane are shown by Fig. 9.12 and the coefficient along the y-axis is $+20.3$ parts per million per degree centigrade. From these values the four temperature coefficients become

$$\alpha_{11} = 0; \qquad \alpha_{22} = +20.3 \times 10^{-6}; \qquad \alpha_{33} = 80 \times 10^{-6}$$
$$\alpha_{13} = -32 \times 10^{-6} \tag{9.3}$$

This crystal has a rather remarkable temperature expansion characteristic, since it has a very high positive expansion in one direction (+90 parts in 10^6 per °C) and a small negative coefficient (−12 parts in 10^6 per °C) in a direction perpendicular to the large coefficient. This temperature expansion property is the source of some trouble in handling, since the crystal is likely to fracture if subject to sudden uneven heating or cooling. This property also limits the rapidity with which a change in temperature can be made in measuring temperature coefficients and is the source of some trouble in cementing wires to the surface.

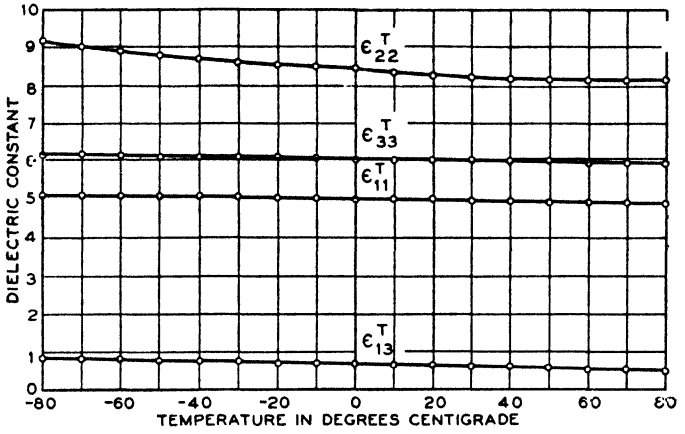

FIG. 9.11. Free dielectric constants plotted as a function of temperature.

9.3 *Useful Filter Cuts in EDT Crystals*

For use in filters one of the requirements is that a single mode be obtained which is separated in frequency from other interfering modes by a considerable amount. This requirement can usually be met by utilizing a longitudinal-mode crystal with its length two to three times the width. By observing the data of Fig. 9.7, it is noted that both the elastic compliances s_{11}^E and s_{33}^E of EDT have minimum points at 20°C and hence crystals cut with their lengths along either the x-axis or the z-axis will have zero temperature frequency values at about 20°C. Furthermore, these two modes can be driven by applying a field along the y-axis, since as shown by Fig. 9.10, there are values for d_{21} and d_{23} equal respectively at 20°C to

$$d_{21} = +34 \times 10^{-8} \frac{\text{cgs units of charge}}{\text{dyne per sq cm}}; \qquad d_{23} = -31 \times 10^{-8} \quad (9.4)$$

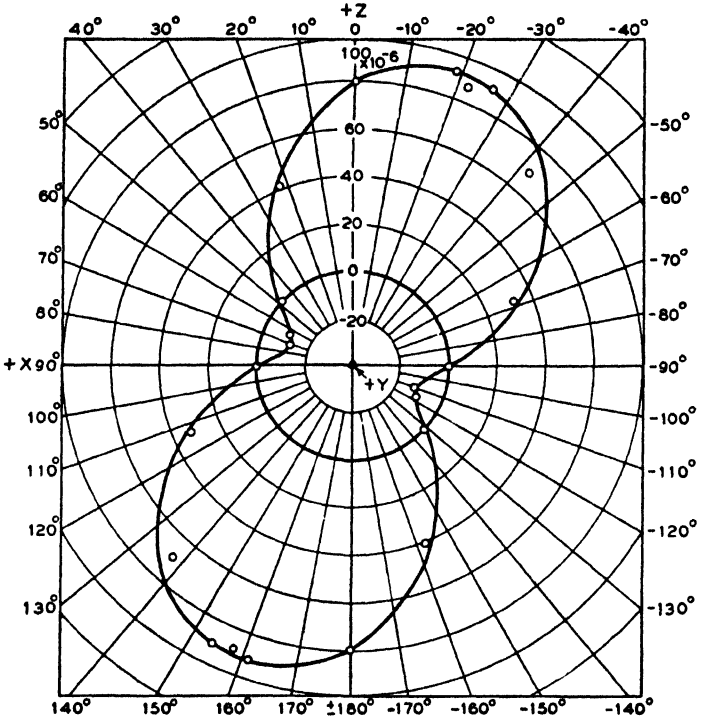

FIG. 9.12. Temperature expansion coefficients of EDT in xz plane.

The elastic compliances for these two cuts are

$$s_{11}^E = 3.88 \times 10^{-12}; \qquad s_{33}^E = 9.8 \times 10^{-12} \tag{9.5}$$

and the free dielectric constant for both cuts is

$$\epsilon_{22}^T = 8.22 \tag{9.6}$$

It has been shown that the electromechanical coupling factor k, and the ratio of capacitances r for a longitudinal crystal are given by the formulae

$$k = d_{21}\sqrt{\frac{4\pi}{\epsilon_{22}^T s_{22}^E}}; \qquad r = \frac{\pi^2}{8}\left(\frac{1 - k^2}{k^2}\right) \tag{9.7}$$

Hence, for these two crystals, y-cut, length along x, and y-cut, length along z, the constants are respectively

$$k = .215; \quad r = 25.5 \text{ length along } x,$$
$$k = .126; \quad r = 76.5 \text{ length along } z \tag{9.8}$$

The first cut, the 0°Y-cut with its length along x, has a high coupling and low ratio of capacitance, a relatively small change of frequency about the point of zero temperature coefficient, and a small change of coupling with temperature. It is one of the most important filter cuts. On the other hand, the 90°Y-cut, with its length along z, has a low coupling, a large change in frequency about its zero temperature coefficient, and a large change of coupling with temperature and hence has not found any practical applications.

By combining the elastic constants according to the equation for a rotated system of axes,[5] which takes the form

$$s_{11}^{E'} = l_1^4 s_{11}^E + l_1^2 m_1^2 (2s_{12}^E + s_{66}^E) + l_1^2 n_1^2 (2s_{13}^E + s_{55}^E) + 2l_1^3 n_1 s_{15}^E + m_1^4 s_{22}^E$$
$$+ m_1^2 n_1^2 (2s_{23}^E + s_{44}^E) + 2n_1^3 l_1 s_{35}^E + n_1^4 s_{33}^E + m_1^2 l_1 n_1 (2s_{25}^E + 2s_{46}^E), \tag{9.9}$$

where the directions cosines l_1 to n_3 for the rotated system are related to the crystallographic axes x, y, z by the relation

	x	y	z
x'	l_1	m_1	n_1
y'	l_2	m_2	n_2
z'	l_3	m_3	n_3

(9.10)

it can be shown that there is another region for which zero-temperature-coefficient crystals can be obtained. This region, as shown by Fig. 9.13, is obtained by starting with a crystal whose thickness is along y and whose length is along z, rotating the direction of the length by a counterclockwise angle of 45° about the thickness, then rotating the crystal about its width by a counterclockwise angle of 63°. According to a system of notation proposed by W. L. Bond and adopted by the Committee on Piezoelectric Crystals of the I.R.E., this crystal is designated as the (*yztw*, 45°, 63°) crystal. The first letter indicates the direction of the thickness before rotation; the second letter represents the direction of the length before rotation; the third letter and the first number represent respectively the axis of the first rotation, and the value of the angle measured in a counterclockwise direction, and the fourth letter and second number represent respectively the second axis of rotation and the angle of rotation measured in a counterclockwise direction.

[5] See transformation equation of Chapter V, equation 5.69.

For this crystal the direction cosines between the new rotated axes and the crystallographic axes, assuming that z' lies along the thickness of the crystal, x' along the length, and y' along the width (in a right-handed coordinate system), are given by the equations

$$\begin{aligned} l_1 &= \sin\varphi\cos\theta; & m_1 &= -\sin\theta; & n_1 &= \cos\theta\cos\varphi \\ l_2 &= \cos\varphi; & m_2 &= 0; & n_2 &= -\sin\varphi \\ l_3 &= \sin\theta\sin\varphi; & m_3 &= \cos\theta; & n_3 &= \sin\theta\cos\varphi \end{aligned} \tag{9.11}$$

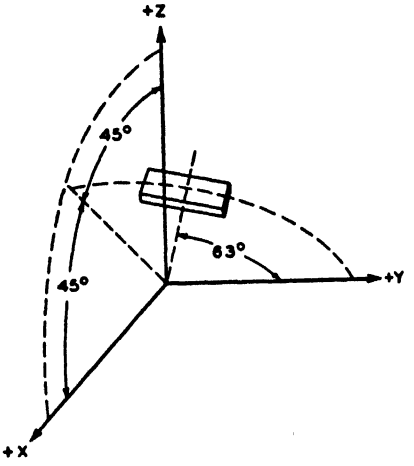

FIG. 9.13. Orientation of A-cut crystal.

With these values, the piezoelectric constants of the rotated crystals become

$$\begin{aligned} d'_{12} = {} & \cos^3\theta\,[d_{21}\sin^2\varphi + d_{23}\cos^2\varphi + d_{25}\sin\varphi\cos\varphi] \\ & + \sin^2\theta\cos\theta\,\{d_{22} - [(d_{14} + d_{36})\sin\varphi\cos\varphi \\ & + d_{16}\sin^2\varphi + d_{34}\cos^2\varphi]\} \end{aligned} \tag{9.12}$$

while the elastic and dielectric constants are given by

$$\begin{aligned} s'^{E}_{11} = {} & s^E_{11}\sin^4\varphi\cos^4\theta + (2s^E_{12} + s^E_{66})\sin^2\theta\cos^2\theta\sin^2\varphi \\ & + (2s^E_{13} + s^E_{55})\cos^4\theta\sin^2\varphi\cos^2\varphi \\ & + 2s^E_{15}\cos^4\theta\sin^3\varphi\cos\varphi + s^E_{22}\sin^4\theta \\ & + (2s^E_{23} + s^E_{44})\sin^2\theta\cos^2\theta\cos^2\varphi \\ & + 2s^E_{35}(\cos^4\theta\cos^3\varphi\sin\varphi) + s^E_{33}\cos^4\theta\cos^4\varphi \\ & + 2(s^E_{25} + s^E_{46})\sin^2\theta\cos^2\theta\sin\varphi\cos\varphi \\ \epsilon'^{T}_{33} = {} & \epsilon^T_{11}\sin^2\theta\sin^2\varphi + 2\epsilon^T_{13}\sin^2\theta\sin\varphi\cos\varphi \\ & + \epsilon^T_{22}\cos^2\theta + \epsilon^T_{33}\sin^2\theta\cos^2\varphi \end{aligned} \tag{9.13}$$

With these equations the constants for the (*yztw*, 45°, 63°) crystal, which has been given the designation *A*-cut, become

$$d'_{12} = +31.0 \times 10^{-8}; \qquad s_{11}^{E'} = 5.55 \times 10^{-12}; \qquad \epsilon_{11}^{T'} = 6.50 \qquad (9.14)$$

Furthermore, by determining the elastic constant $s_{11}^{E'}$ as a function of temperature, we find that the variation is very small.

The characteristics of a crystal in which the filter designer is interested are the change in resonant frequency with temperature, the ratio of capacitances in the equivalent circuit of the crystal, and the dielectric constant. All the elements of the equivalent circuit (Fig. 9.14) can be calculated from these values. Figure 9.15 shows these values as a function

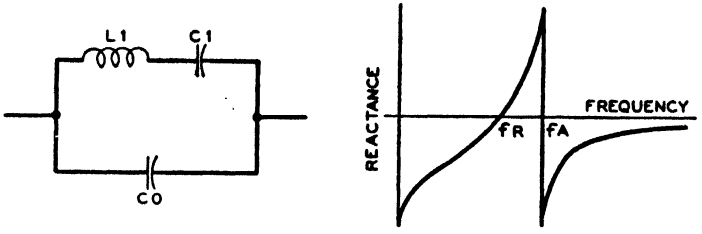

FIG. 9.14. Equivalent circuit and reactance frequency characteristic of piezoelectric crystal.

of temperature for temperatures from −80°C to +80°C. Similar quantities for the *Y*-cut crystal are shown by Fig. 9.16.

The *A*-cut crystal has a higher ratio of capacitances (lower electromechanical coupling) than the *Y*, but has a considerably flatter temperature-frequency characteristic and hence is used in such applications as pilot channels, where a higher stability and a lower coupling are required. The *Y*-cut crystal has been used in applications where a high coupling and a moderate temperature stability are required.

A monoclinic crystal has the advantage that with the large number of elastic constants existing, a greater probability exists in balancing the temperature coefficients of one constant against those of the other constants and obtaining a zero temperature coefficient, but, it has the disadvantage that with the large number of cross coupling elastic constants, the chances of obtaining disturbing interfering modes is also larger. This is illustrated by Fig. 9.17, which shows the frequency spectrum of a *Y*-cut EDT crystal plotted as a ratio of width to length. The lower solid line represents the resonant frequency of the main mode and the numbers on the figure are the ratios of capacitance at 25°C. The top solid line is the coupled width mode, which has relatively strong resonances. The first dotted line above the main mode is the second flexure, which is coupled to the main longitudinal mode through the shear coupling as in quartz. This becomes so

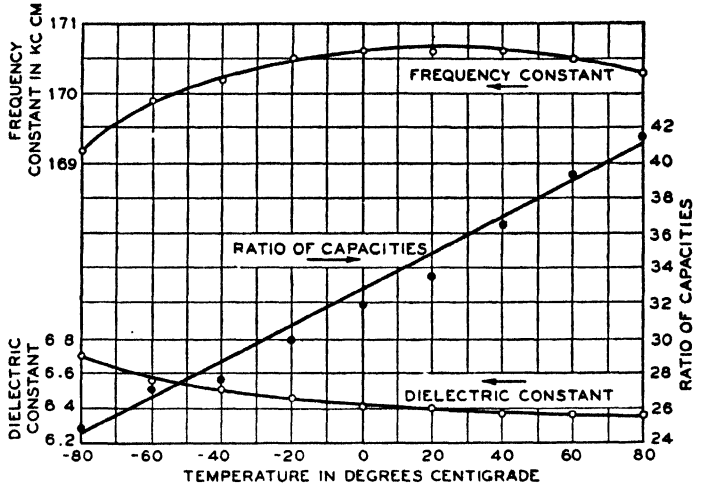

FIG. 9.15. Frequency constant, ratio of capacities, and dielectric constant of *A*-cut plotted as a function of temperature.

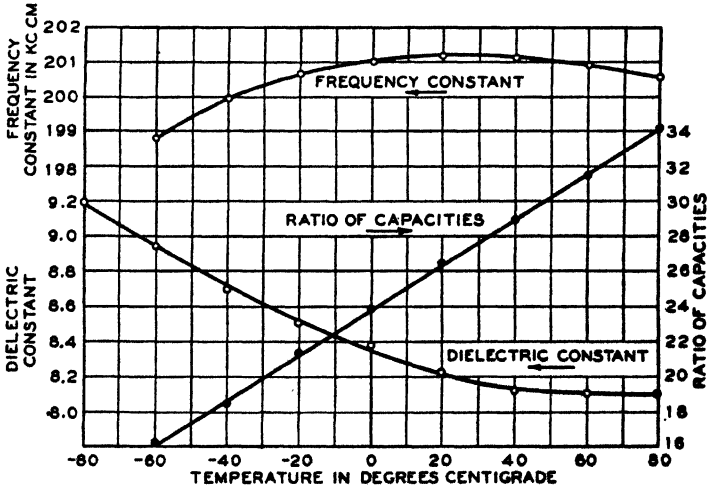

FIG. 9.16. Frequency constant, ratio of capacities, and dielectric constant of *Y*-cut plotted as a function of temperature.

strong at low ratios of width to length that it makes the crystal unusable for ratios of width to length less than 0.31 and greater than 0.5. The second dotted line represents another mode that causes a small interfering effect. In addition to these modes, there exists a coupling to a thickness flexure which makes certain ratios of thickness to length unusable.

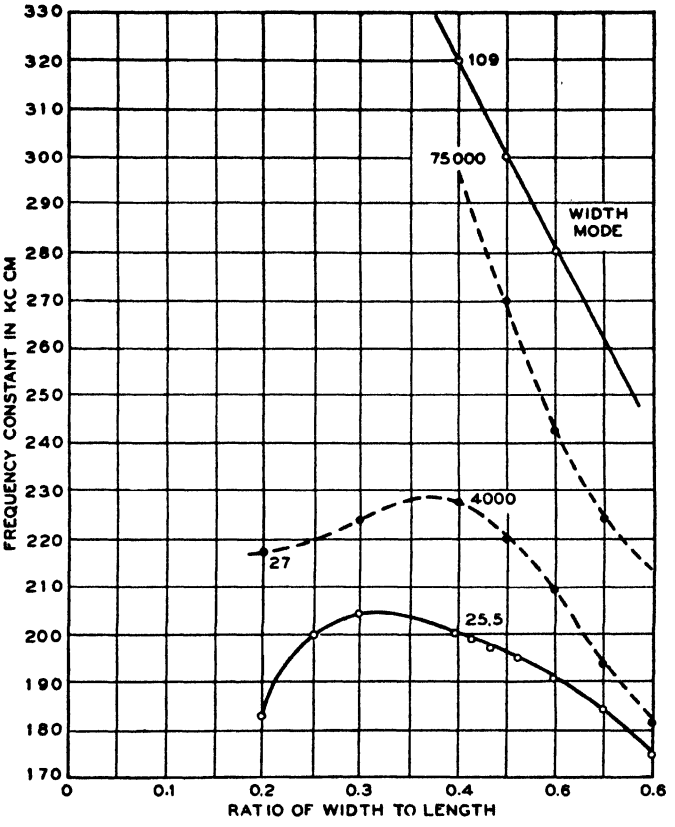

FIG. 9.17. Frequency spectrum of Y-cut crystal.

With all these limitations, the constants of the elements in the equivalent circuit for a crystal shown by Fig. 9.14 cannot be obtained by varying the width and thickness over wide ranges as can be done with quartz crystals. To get all of these variations it has been found necessary to employ more complicated orientations, which vary the fundamental constants of the crystal without changing the temperature stability. Since most of the crystals require a coupling greater than can be obtained in the A-cut but less than in the Y-cut, we look for modifications in orientations surrounding the Y-cut.

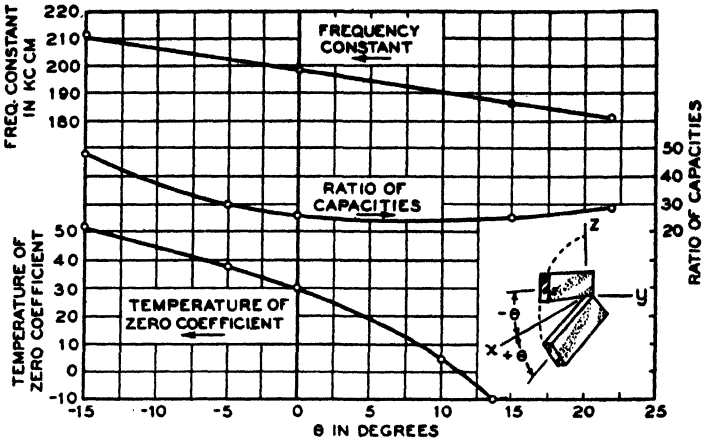

FIG. 9.18. Effect of a rotation about y on the frequency constant, ratio of capacities, and temperature of the zero coefficient for a Y-cut EDT crystal.

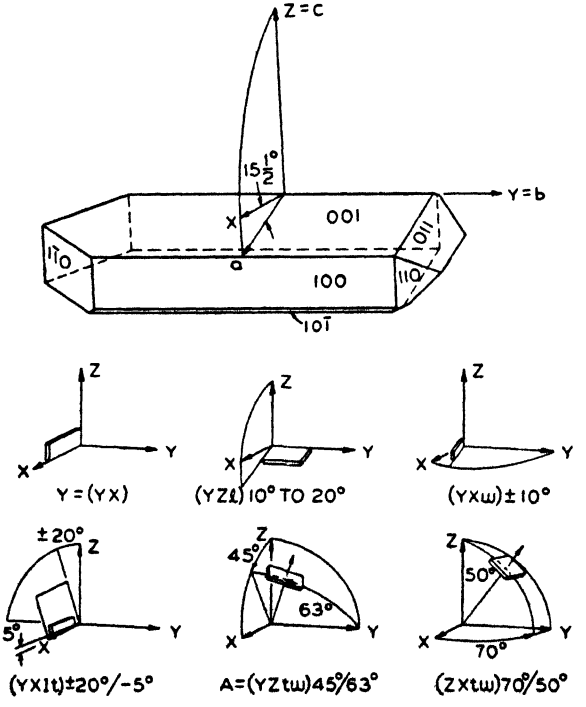

FIG. 9.19. Useful cuts found for EDT crystals.

The simplest orientation to employ is a rotation about the thickness, causing the length to vary from the x direction by $\pm\theta°$. The effect of this rotation is to change the constants of the crystal, as shown by Fig. 9.18. The top curve shows the frequency constant, at 25°C, of a crystal whose ratio of width to length is 0.4. This increases for negative angles and decreases for positive. The second curve shows the ratio of capacitances as a function of angle, and the bottom curve shows the temperature for which the temperature coefficient becomes zero. This increases for negative angles and decreases for positive angles.

Two other rotations are also possible: rotations about the width and rotations about the length. As shown by Fig. 9.19, which shows the principal filter orientations, so far found useful, an orientation of $\pm 10°$ about the width was found and this has very similar characteristics to the Y-cut crystal. A rotation around the length has also been tried and by rotating $\pm 20°$ about the length and $-5°$ about the resulting thickness, an orientation, having a zero temperature coefficient, relative freedom from unwanted modes of motion, and a relative inductance in the equivalent circuit of Fig. 9.14, about 50 per cent larger than that for the Y-cut has been found. This is shown on Fig. 9.19 as the ($yxlt$ $\pm 20°$, $-5°$) crystal and it appears likely that this cut may be used for the higher channel band-pass filters. It has been given the designation B-cut.

9.4 *Properties of Dipotassium Tartrate (DKT) Crystals*

The constants of DKT crystals are given in Table XIV.

TABLE XIV

CONSTANTS OF DKT CRYSTALS

Piezoelectric Constants	Elastic Compliances	Dielectric Constants	Temperature Expansion Constants
$d_{14} = -25.0 \times 10^{-8}$	$s_{11} = +2.24 \times 10^{-12}$ cm^2/dyne	$\epsilon_{11} = 6.44$	$\alpha_{11} = +12.0 \times 10^{-6}$/°C
$d_{16} = +6.5$	$s_{12} = -0.08$	$\epsilon_{22} = 5.80$	$\alpha_{22} = +44.8$
$d_{21} = -2.2$	$s_{13} = -1.64$	$\epsilon_{33} = 6.49$	$\alpha_{33} = +32.0$
$d_{22} = +8.5$	$s_{15} = -0.64$	$\epsilon_{13} = .005$	$\alpha_{13} = -12.0$
$d_{23} = -10.4$	$s_{22} = +3.37$	$\rho = 1.988$	
$d_{25} = -22.5$	$s_{23} = -1.05$		
$d_{34} = +29.4$	$s_{25} = -0.57$		
$d_{36} = -66.0$	$s_{33} = +3.86$		
	$s_{35} = +0.90$		
	$s_{44} = +11.90$		
	$s_{46} = +0.57$		
	$s_{55} = +8.15$		
	$s_{66} = +10.41$		

Using these constants, some interesting cuts for DKT crystals have also been found. Figure 9.20 shows two longitudinal cuts, the (*zxt* 45°) cut and the (*zxt* 37.5°) cut, and one face-shear cut, all of which have zero temperature coefficients of frequency around room temperature. Figure 9.21 shows how the resonant frequency and ratio of capacitances of the 45° *z*-cut crystal vary over a wide temperature range. Comparing this with the

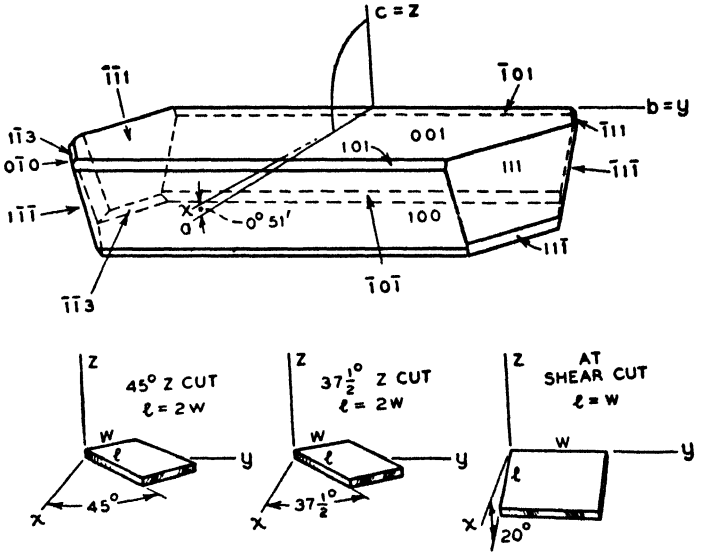

FIG. 9.20. Form of DKT crystal and useful zero temperature coefficient cuts.

data of Fig. 9.16 for a *Y*-cut EDT crystal, we see that the DKT crystal has a higher coupling (lower ratio of capacitances) than does the *Y*-cut EDT crystal and a frequency variation that is only about one third that for the EDT crystal. It appears likely that when growing and processing methods are further investigated, this crystal may have uses in apparatus for which a large electromechanical coupling and a low temperature coefficient are required.

The higher coupling existing in EDT and DKT crystals over what can be obtained in quartz, also open up interesting possibilities. With this coupling, band-pass filters having the channel band widths of 3300 cycles, are possible at frequencies as low as 20 kilocycles. Also with the high coupling, it may be possible to dispense with coils entirely in the high-frequency range for voice channels and reduce the size and cost of such filters. These possibilities have not yet been explored.

9.5 *Application of EDT Crystals in the Control of High-Frequency Oscillators*

A high-frequency shear mode has also been found in EDT crystals which has a zero temperature coefficient at room temperature. This crystal, as shown by Fig. 9.19, has its major plane, the 001 crystallographic axis, *i.e.*, the plane determined by the *a* and *b* crystallographic axes. Figure 9.22 shows a measurement of a crystal having the dimension *l* along *y* = 1.737

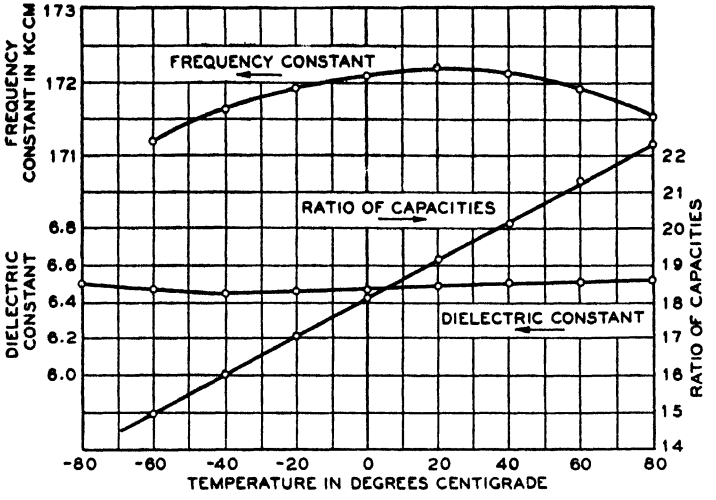

FIG. 9.21. Frequency constant, ratio of capacities, and dielectric constant of 45° Z-cut DKT crystal as a function of temperature.

cm; *w* along *a* = 0.922 cm; *t* = 0.874 mm. The resonance frequency f_R shown by the curve has a frequency that is given by the equation for a crystal 1 mm thick

$$f_R = f_0[1 - a_2(T - T_0)^2] = 904{,}000[1 - 1.21 \times 10^{-6}(T - 10°)^2] \quad (9.15)$$

where *T* is the temperature in degrees centigrade.

This is a rather large curvature constant a_2 compared to what can be obtained with a quartz crystal. For example, the curvature constant a_2 for *BT* quartz, which is one of the cuts most widely used for high-frequency oscillators, is

$$a_2 = .042 \times 10^{-6} \quad (9.16)$$

Hence, for a given temperature range on either side of the zero coefficient temperature, the EDT crystal would have around 29 times as much frequency change as the quartz crystal. Another way of expressing the relation is that for a given frequency tolerance, the EDT crystal could

cover only $1/\sqrt{29} = .185$ times the temperature range that the quartz crystal could. This larger curvature appears to be possessed by all synthetic crystals so far examined.

However, for the very wide temperature range required for military application ($-50°C$ to $+90°C$), a quartz crystal may not give all the accuracy required and hence a moderate temperature control is often required. If a temperature control is used, it requires one only five times as good to hold the frequency of an EDT crystal to the same variation as a quartz crystal. For example, an accuracy of .01 per cent in frequency

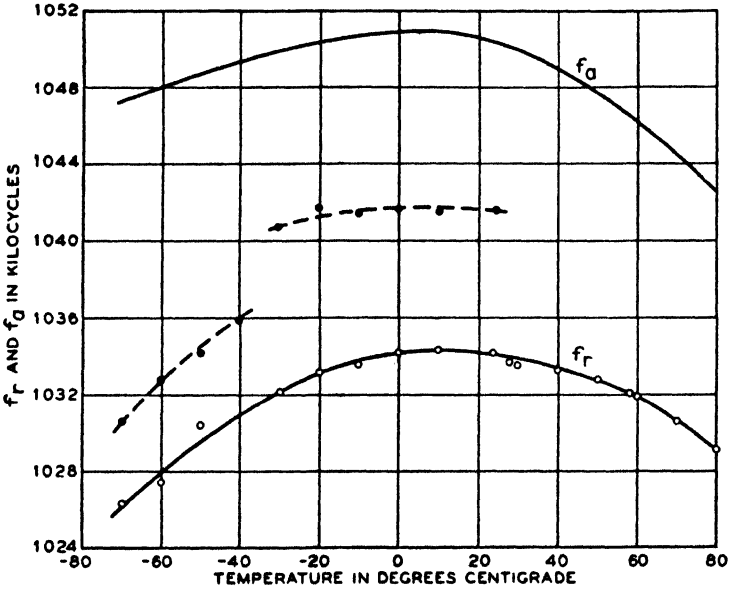

FIG. 9.22. Resonant and anti-resonant frequencies of thickness vibrating EDT crystal.

could be met by holding the temperature constant to $\pm 9°C$ and this is easily held by even a snap-switch thermostat. Hence an EDT thickness vibrating crystal has uses in controlling oscillators.

For a temperature-controlled crystal, it is desirable to have the temperature of zero coefficient up around 70°C to 90°C in order that the thermostat will operate under all ambient conditions. This can be obtained with an EDT crystal by increasing the rotation angle about y. Figure 9.23 shows measured values of this temperature in degrees centigrade as a function of the angle of rotation of the normal from z. The ratio of capacitances curve and the frequency constant plotted in kilocycle millimeters are also shown. For high angles of rotation, the coupling gets quite large and hence there

is a large separation between resonant and anti-resonant frequencies. This property of the crystal is of considerable use in a frequency-modulated oscillator, for it allows a wide percentage swing of the resonant frequency. By temperature controlling the crystal, the average frequency can be held quite constant and the frequency swing made quite large, so that these crystals have applications in frequency-modulated oscillators.

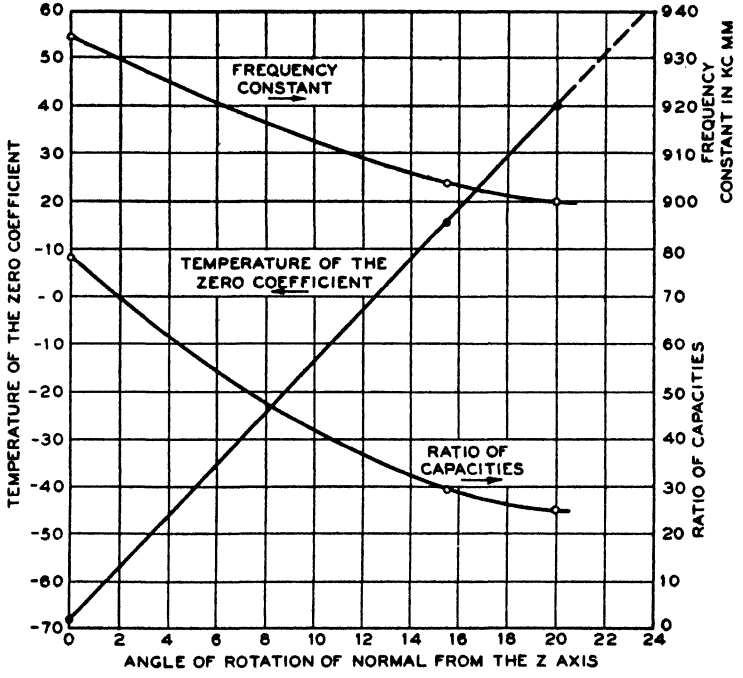

FIG. 9.23. Frequency constant, ratio of capacities, and temperature of zero coefficient of thickness vibrating EDT crystal plotted as a function of orientation.

The thickness of the crystal can be easily lapped down to one-third of a millimeter, which will give a frequency of about 2.7 megacycles. On account of the large electromechanical coupling, the third and fifth harmonics are strongly driven and hence it should be possible to reach frequencies as high as 13.5 megacycles. Hence for certain purposes the use of EDT crystals to control oscillators is a distinct possibility.

CHAPTER X

Measurements of the Properties of a Number of Piezoelectric Crystals

In the program for measuring the properties of promising piezoelectric crystals, the complete or partial properties of a number of crystals, particularly if they appeared to have specific applications, have been published. However, a number of crystals for which partial determinations have been made, or for which there did not appear to be any specific uses, have not been published. It appears worth-while to record all the measured properties, since from them indications may be obtained of the effects of chemical substitutions and of the types of molecular structure that result in high piezoelectric couplings, low temperature coefficients, or related quantities.

The crystals are grouped according to crystal classes, since similar measuring methods are applicable to all members of a particular class.

10.1 *Measurements of the Properties of the Cubic Crystals, Sodium Chlorate and Sodium Bromate*

Two crystals of the cubic tetrahedral class (symmetry T or 23) have been measured[1] rather extensively since their crystal structure is well known and measurements of their properties throw some light on the molecular mechanism of piezoelectricity. These two crystals are sodium chlorate and sodium bromate.

Measurements of the piezoelectric constant of sodium chlorate were made as early as 1893 by Pöckels, who obtained a value of 4.84×10^{-8} cgs units for the piezoelectric constant d_{14}.[2] Voigt[3] measured the elastic constants and came to the conclusion that the crystal had a negative Poisson's ratio; *i.e.*, the crystal would expand sidewise as it elongates lengthwise. The measurements made here do not confirm this conclusion and they have recently been checked by Bhagavantam and Surganarayon[4] who used a piezoelectric wedge to measure the elastic constants.

[1] Mason, W. P., "Elastic, Piezoelectric and Dielectric Properties of Sodium Chlorate and Sodium Bromate," *Phys. Rev.*, Vol. 70, pp. 529–537, Oct., 1946.

[2] Voigt, W., *Lehrbuch der Kristallphysik*, B. Teubner, p. 873.

[3] *Ibid.*, p. 741.

[4] Bhagavantam, S. and D. Surganarayon, "Elastic Constants of Sodium Chlorate," *Phys. Rev.*, Vol. 71, No. 8, p. 553, April 15, 1947.

X-ray crystal structure studies[5] show that sodium chlorate has four molecules per unit cell. Each molecule consists of three oxygen atoms arranged in the form of an equilateral triangle with a separation of 2.38Å between oxygen centers, as shown by Fig. 10.1. The chlorine is located at a distance of 0.48Å above the plane of the oxygen atoms in a line through the center of gravity of the oxygens. The sodium lies above the chlorine

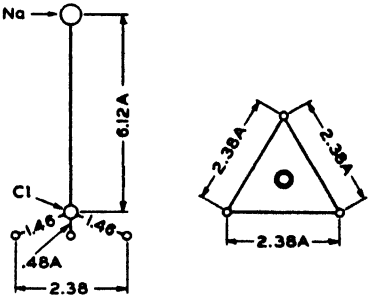

FIG. 10.1. Positions of sodium, chlorine, and three oxygens in sodium chlorate.

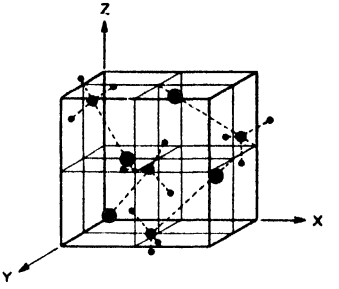

FIG. 10.2. Location of molecules in unit cell for sodium chlorate.

at a distance of 6.12Å. On account of the large separation of the sodium from the chlorate ion, it is probably the latter which acts as the dipole in the temperature variable part of the dielectric constant. The dipole is formed by the positive charge on the chlorine reacting with the center of gravity of the negative oxygens. The evidence from the temperature measurements is that this is a rotating dipole formed by an actual turning through a very small angle of the plane of the three oxygen atoms and the chlorine. The dipole moves very little at low temperatures, but becomes more free to move at higher temperatures and at the melting point is approaching the state of a ferroelectric crystal.

All of the properties of this crystal can be measured by employing three oriented cuts. This follows from the piezoelectric equations for a cubic crystal,

$$
\begin{aligned}
S_1 &= s_{11}T_1 + s_{12}T_2 + s_{12}T_3 & S_6 &= s_{44}^E T_6 + d_{14}E_z \\
S_2 &= s_{12}T_1 + s_{11}T_2 + s_{12}T_3 & \delta_x &= \frac{D_x}{4\pi} = \frac{E_x\epsilon_{11}^T}{4\pi} + d_{14}T_4 \\
S_3 &= s_{12}T_1 + s_{12}T_2 + s_{11}T_3 & \delta_y &= \frac{D_y}{4\pi} = \frac{E_y\epsilon_{11}^T}{4\pi} + d_{14}T_5 \qquad (10.1) \\
S_4 &= s_{44}^E T_4 + d_{14}E_x & \delta_z &= \frac{D_z}{4\pi} = \frac{E_z\epsilon_{11}^T}{4\pi} + d_{14}T_6 \\
S_5 &= s_{44}^E T_5 + d_{14}E_y
\end{aligned}
$$

[5] Wyckoff, R. W. G., *The Structure of Crystals*, p. 276, Chemical Catalogue Co., New York.

There are three elastic constants, one piezoelectric constant, and one dielectric constant.

All cuts are taken normal to one of the three equivalent crystallographic axes, which for convenience will be designated the z-axis. One cut has its length 45° from the other two axes, one cut has its length 22.5° from one of the axes, and the third with its length along one of the crystallographic axes. The first two cuts are driven in their lowest longitudinal mode and their length is made long compared to their width or thickness so that the uncorrected compliance $s_{11}^{E'}$ is determined. Since the direction cosines for these two cuts are

	x	y	z
x'	$l_1 = \cos\theta;$	$m_1 = \sin\theta;$	$n_1 = 0$
y'	$l_2 = -\sin\theta;$	$m_2 = \cos\theta;$	$n_2 = 0$
z'	$l_3 = 0;$	$m_3 = 0;$	$n_3 = 1$

(10.2)

we have from equation (5.67) that the elastic compliance s_{11}^{E} and the piezoelectric constant d_{31}' are given by the equations

$$s_{11}^{E'} = s_{11}(\cos^4\theta + \sin^4\theta) + (2s_{12} + s_{44}^{E})\sin^2\theta\cos^2\theta$$

$$d_{31}' = d_{36}\sin\theta\cos\theta = d_{14}\sin\theta\cos\theta, \text{ since } d_{36} = d_{14}$$

The third cut with its length along x, thickness along z and width along y, determines the shear-elastic constant s_{44}. This crystal was about 6 times as long as its width, and by measuring the fundamental and high harmonics of the shear mode, the elastic constant s_{44} is determined according to the equation

$$s_{44}^{E} = \frac{1}{(2l_w f_R)^2\rho} \tag{10.3}$$

where l_w is the width, f_R the resonant frequency (which is most accurately obtained by taking a high harmonic and dividing the resonant frequency by the harmonic order), and ρ the density.

The measured values of the resonant frequency f_R, the separation of resonant f_R and anti-resonant frequency f_A (*i.e.*, $\Delta f = f_A - f_R$) divided by the resonant frequency, and the dielectric constant measured at 1000 cycles, are shown in Table XV.

From these data and the density $\rho = 2.49$ at 25°C, one can calculate the elastic and piezoelectric constants at a temperature of 28°C. Since the resonant frequency of a longitudinal mode is given by

$$f_R = \frac{1}{2l\sqrt{\rho s_{11}^{E'}}} \tag{10.4}$$

TABLE XV

MEASURED PROPERTIES OF SODIUM CHLORATE

Temperature in Degrees C	Z-cut $L = 22.5°$ from X $L = 20.13$ mm $W = 2.69$ mm $T = 1.00$ mm	Z-cut, $L = 45°$ from X $L = 20.38$ mm $W = 2.71$ mm $T = 1.01$ mm	0° Z-cut, L along X $L = 29.90$ mm $W = 6.02$ mm $T = 1.04$ mm	$\Delta f/f_R$ for 45° Z-cut	Free Dielectric Constant ϵ_{11}^T
28	193.2 kc cm	181.8 kc cm	108.6	0.000281	5.76
40	192.2	180.9	108.3	0.000317	5.8
75	190.2	179.3	108.2	0.000393	5.94
100	187.2	177.2	106.2	0.000465	6.05
130	183.4	173.5	104.2	0.000584	6.21
140	182.3	172.5	103.8	0.00065	6.27
150	181.3	171.3	103.1	0.000725	6.34
160		170.3	102.5	0.000807	6.41
170	178.6	169.2	102.0	0.000894	6.49
180	177.5	168.3	101.2	0.00098	6.57
190	176.1	167.1	100.4	0.00115	6.70
200	175.1	166.2	99.9	0.00134	6.81
210	173.1	164.5	99.1		
220	172.2	163.3	98.3		
230	170.3	161.3	97.2		
240	168.5	160.2	96.2		

where l is the length of the crystal, which has been assumed long and thin, the values are

$$s_{11}^{E'} \text{ at } 22.5° = 2.69 \times 10^{-12} \text{ cm}^2/\text{dyne};$$
$$s_{11}^{E'} \text{ at } 45° = 3.045 \times 10^{-12} \tag{10.5}$$

Now since

$$s_{11}^{E'} \text{ at } 22.5° = s_{11}[\cos^4\theta + \sin^4\theta] + (2s_{12} + s_{44}^E)\sin^2\theta\cos^2\theta$$

where $\theta = 22.5°$ we have

$$\begin{aligned} s_{1122.5°}^{E'} &= .75s_{11} + .125(2s_{12} + s_{44}^E) \\ s_{1145°}^{E'} &= .5s_{11} + .25(2s_{12} + s_{44}^E) \end{aligned} \tag{10.6}$$

Solving for s_{11} and $(2s_{12} + s_{44}^E)$, we find

$$\begin{aligned} s_{11} &= 2s_{1122.5°}^{E'} - s_{1145°}^{E'} = 2.335 \times 10^{-12} \text{ cm}^2/\text{dyne} \\ (2s_{12} + s_{44}^E) &= 6s_{1145°}^{E'} - 4s_{1122.5°}^{E'} = 7.51 \times 10^{-12} \text{ cm}^2/\text{dyne} \end{aligned} \tag{10.7}$$

The value of s_{44}^E can be obtained from the data on the 0°Z-cut and equation (8.3). These give

$$s_{44}^E = \frac{1}{(2 \times 108{,}600)^2 \times 2.49} = 8.54 \times 10^{-12} \text{ cm}^2/\text{dyne} \quad (10.8)$$

Hence, we have

$$s_{12}^E = \frac{(7.51 - 8.54) \times 10^{-12}}{2} = -0.515 \times 10^{-12} \text{ cm}^2/\text{dyne} \quad (10.9)$$

Since the value of Poisson's ratio is equal to

$$\sigma = -\frac{s_{12}}{s_{11}} = \frac{.515}{2.335} = .22 \quad (10.10)$$

the value is positive and has an ordinary value contrary to Voigt's measurement indicating a negative value of -0.51.

The value of the piezoelectric constant can be obtained from the measurement of the dielectric constant, the elastic constant of the 45°-cut crystal and the separation of resonant and anti-resonant frequencies. From equation (5.33), the coefficient of electromechanical coupling defined by the equation

$$k = \frac{d_{31}}{\sqrt{\frac{\epsilon_{33}^T s_{11}^E}{4\pi}}}$$

can be calculated from the separation of $(f_A - f_R)/f_R = \Delta f/f_R$ given in the fourth column of Table XI. From the equation

$$k^2 = .000694; \quad k = .0264; \quad \epsilon_{33}^T = 5.76; \quad s_{11_{45°}}^{E'} = 3.045 \times 10^{-12} \quad (10.11)$$

hence

$$d_{31} = \frac{d_{14}}{2} = 3.05 \times 10^{-8} \text{ in cgs units}; \qquad d_{14} = 6.1 \times 10^{-8} \quad (10.12)$$

This is slightly larger than Pöckel's measured value of 4.84×10^{-8}.

As the temperature increases, both the length and density change so if an accurate measurement of the elastic constants is to be obtained over a wide temperature range, account has to be taken of the temperature-expansion coefficient of the crystal. These have been measured over a range of temperatures by using an optometer mounted on a frame of fused quartz. The expansion coefficient is measured[6] by determining the change in length of the specimen compared to the length of a similar section of

[6] This measurement was made by Mrs. Elizabeth A. Wood.

fused quartz as the temperature changes. The results for sodium chlorate and sodium bromate are shown by Fig. 10.3. Since the frequency of a crystal is given by the equation

$$f_R = \frac{1}{2l\sqrt{\rho s_{11}^{E'}}}$$

SUBSTANCE	COEF. OF THERMAL EXPANSION ($10^6 \times \Delta l/l$ PER DEGREE C)			$\Delta l/l = a(t-25) + b(t-25)^2$	
	-40° TO 0°	0° TO 50°	50° TO 90°	$10^5 \times a$	$10^8 \times b$
S.B.	37.5	39.2	41.7	3.94	1.0
S.C.	40.8	43.4	45.2	4.36	3.6

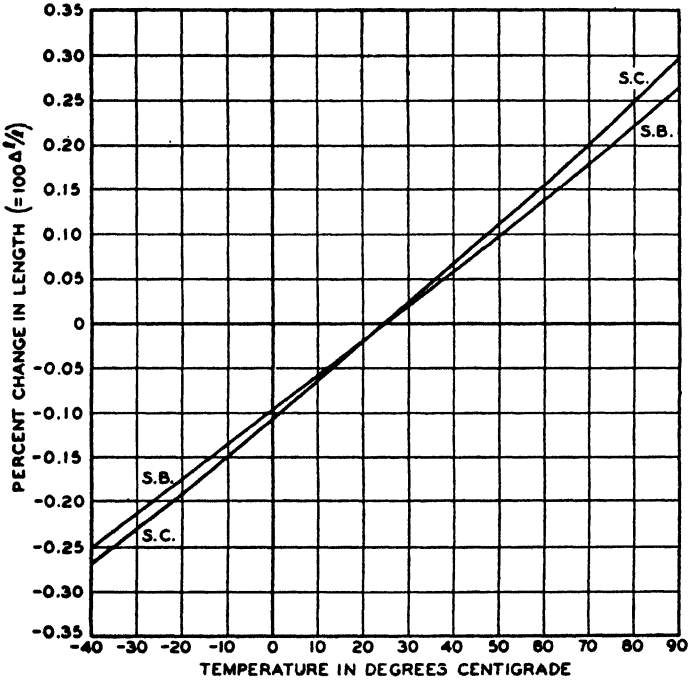

FIG. 10.3. Temperature expansion curves for sodium chlorate and sodium bromate.

and the frequency constant $f_c = f_R l_0$, where l_0 is measured at 25°C, the elastic constant $s_{11}^{E'}$ is given by the formula

$$s_{11}^{E'} = \frac{1}{\left(2f_c \frac{l}{l_0}\right)^2 \rho} = \frac{1}{\{2f_0[1 + \alpha(\Theta - 25)]\}^2} \Big/ \frac{\rho_0}{[1 + \alpha(\Theta - 25)]^3}$$

$$= \frac{1 + \alpha(\Theta - 25)}{(2f_0)^2 \rho_0} \tag{10.13}$$

where α is the temperature expansion coefficient of length which is the same for all directions of a cubic crystal and Θ is the temperature in degrees C. Taking account of this correction, the elastic compliances of sodium chlorate are shown plotted by Fig. 10.4. As the melting point of 264°C is approached, the elastic compliances, in particular the shear compliance, increases more rapidly with temperature. Similar curves for

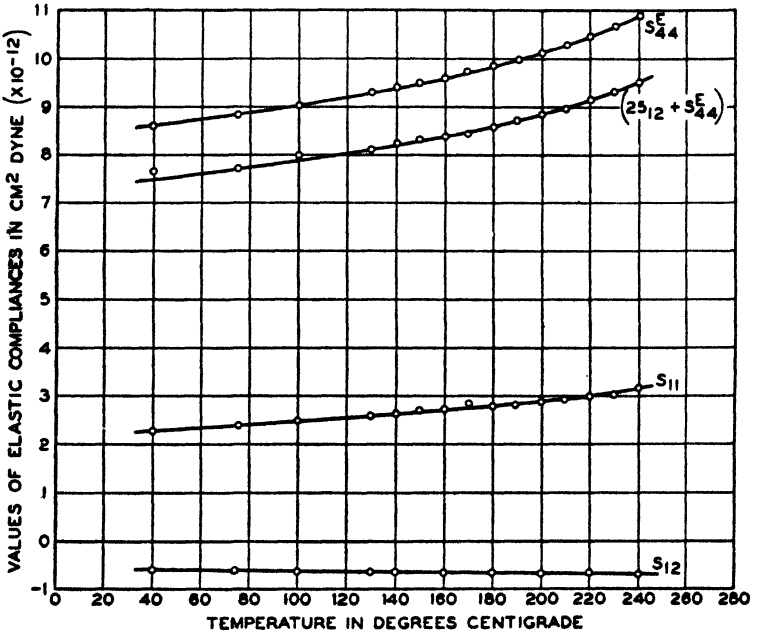

FIG. 10.4. Elastic compliances of sodium chlorate.

sodium bromate are shown plotted on Fig. 10.5. Since the melting point of this crystal is around 420°C, the elastic compliances of this crystal are very linear with temperature up to 200°C and it has been suggested that this crystal could be used as a thermometer by comparing the frequency of an oscillator controlled by a sodium bromate crystal with the frequency of an oscillator controlled by a quartz crystal.

As the temperature increased, it was found that the dielectric and piezoelectric constants also increased. At 200°C the leakage resistance of the crystal became noticeable and became low enough at 210°C and higher to make the measurement of the dielectric constant and the anti-resonant frequency unreliable. The resistivity curve as a function of temperature is shown plotted by Fig. 10.6. At 245°C the resistivity was low enough so that no appreciable piezoelectric response was obtained, and at the melting

point of 263°C, the resistivity was less than 1000 ohms per cubic centimeter. This indicates that as the crystal approaches its melting point, it becomes highly ionized with the chlorate ion separating from the sodium ion for a large number of molecules. This behavior is usual for an " ionic crystal." The logarithmic plot of resistance versus inverse temperature, which is usual for crystals, is explained as a defect phenomenon in the crystal lattice. Holes exist in the lattice and ions in the crystal can migrate through the crystal by jumping into empty holes, leaving holes in the structure behind them. In jumping from one position to a free hole, the ion has to surmount a potential barrier of energy W. The applied field is not sufficiently

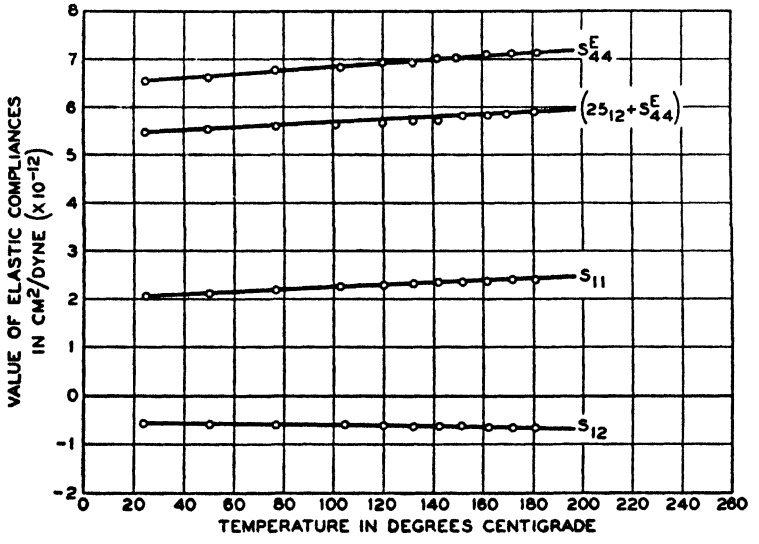

FIG. 10.5. Elastic compliances of sodium bromate.

strong to accomplish this and it requires an accumulation of thermal energy to cause the ion to move from one position to another. The probability of changing positions under no external field is

$$\alpha = Ce^{W/kT} \tag{10.14}$$

where W is the value of the potential barrier, called the activation energy, k Boltzmann's constant, and T the absolute temperature. When a field is applied more movement occurs in the direction of the field than against it, and this average flow times the amount of charge carried by the ions, results in the leakage current as discussed in Chapter VIII. The fact that there are usually two slopes is accounted for by two different mechanisms having different activation energies and different multiplying constants C.

Table XV shows the ratio of $\Delta f/f_R$ for the 45° cut and the free dielectric constant measured at 1000 cycles as a function of temperature. The

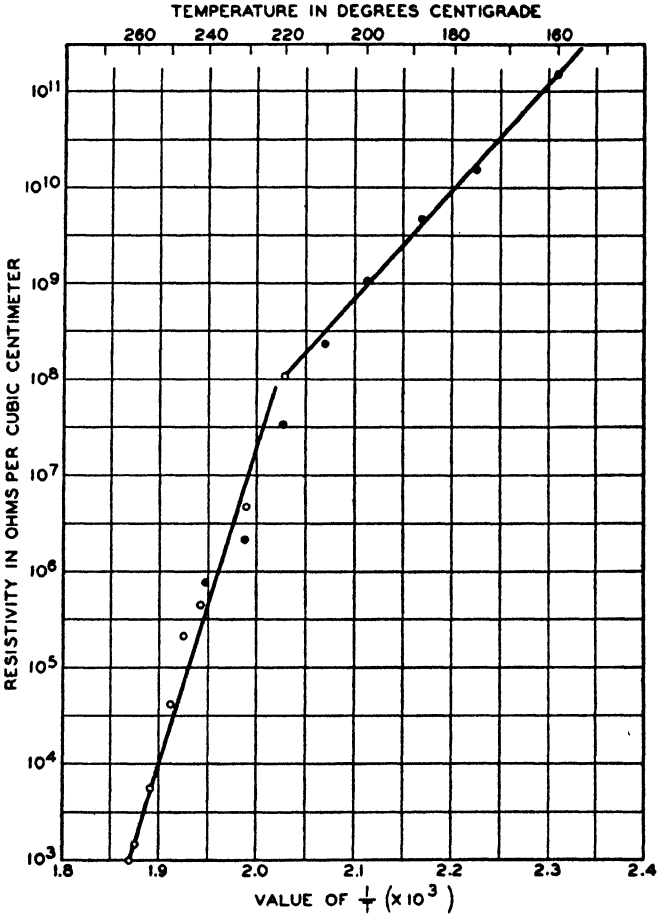

FIG. 10.6. Resistivity of sodium chlorate plotted against $1/T$.

dielectric constants of sodium chlorate and sodium bromate as a function of temperature are shown plotted on Fig. 10.7. The dielectric constant of sodium chlorate can be expressed as a function of temperature by the empirical equation

$$\epsilon = 4.7 + \frac{310}{320 - \Theta} - \frac{6750}{(320 - \Theta)^2} \tag{10.15}$$

where Θ is the temperature in degrees centigrade. This indicates that

there is a part equal to 4.7 that is independent of temperature and another part that varies with temperature and becomes large for temperatures approaching 320°C. The first part is caused by the electronic and ionic polarizabilities, while the temperature variable part is caused by changes of the dipoles. For sodium bromate, since the measured values are taken

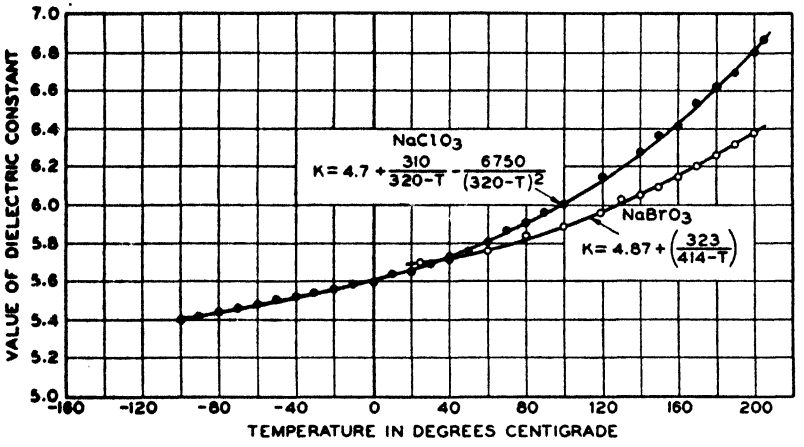

FIG. 10.7. Dielectric constants of sodium chlorate and sodium bromate plotted as a function of temperature.

considerably below the transition point, a single term is sufficient to fit the curve and we have

$$\epsilon = 4.87 + \frac{323}{(414 - \Theta)} \tag{10.16}$$

From the data of Table XV on $\Delta f/f_R$, the elastic compliance for a 45° cut and the free dielectric constant, the piezoelectric constant of sodium chlorate can be determined as a function of temperature. This is shown plotted by Fig. 10.8 as is also the d_{14} values for sodium bromate. If we plot $1/d_{14}$ for these two crystals, the values lie on a straight line, as shown in the dashed lines of Fig. 10.8. The sodium chlorate curve, if we extend it, has a zero value of $1/d_{14}$ (infinity value for d_{14}) at about 320°C, while for sodium bromate this temperature occurs at about 415°C. As discussed in Chapters VII and VIII, the high value of the d_{14} piezoelectric constant indicates that the crystal is approaching a Curie temperature for which the dipoles are sufficiently free so that they can aid each other in orienting themselves and would produce a spontaneous polarization. These temperatures are somewhat above the melting points where the ions are free translationally and indicate that the dipoles are due to an actual turning

of the chlorate ion, since otherwise there is no reason why the Curie temperature should be so closely related to the melting temperature.

The large variation of piezoelectric and dielectric constant with temperature allows one to make some calculations about the cause of the piezoelectric effect. By employing the transformation equations between the various systems for writing piezoelectric equations, one can relate the

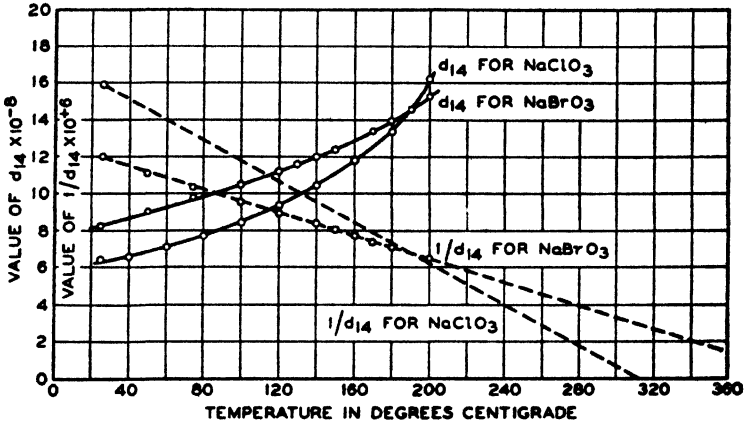

FIG. 10.8. Piezoelectric constant d_{14} for sodium chlorate and sodium bromate.

piezoelectric stresses to the electric field or the electric displacement D, or can relate the piezoelectric strain to the electric field or the electric displacement. These equations are for a cubic crystal

$$S_6 = s_{66}^E T_6 + d_{36}E_z; \quad S_6 = s_{66}^D T_6 + g_{36}\delta_z; \quad T_6 = c_{66}^E S_6 - e_{36}E_z;$$

$$T_6 = c_{66}^E S_6 - h_{36}\delta_z \quad \text{where} \quad \delta_z = \frac{D_z}{4\pi} \quad \text{and} \quad g_{36} = \frac{4\pi d_{36}}{\epsilon_{33}^T}; \tag{10.17}$$

$$e_{36} = d_{36}c_{66}^E; \quad h_{36} = \frac{4\pi d_{36}}{\epsilon_{33}^T} c_{66}^D; \quad c_{66}^E = \frac{1}{s_{66}^E}; \quad c_{66}^D = \frac{1}{s_{66}^D};$$

$$c_{66}^D = \frac{c_{66}^E}{\left(1 - \dfrac{4\pi d_{36}^2 c_{66}^E}{\epsilon_{33}^T}\right)}$$

If we calculate the constants d_{14}, e_{14}, g_{14} or h_{14} which relate respectively the piezoelectric strain to the electric field, the piezoelectric stress to the electric field, the piezoelectric strain to the electric displacement, and the piezoelectric stress to the electric displacement, we find that none of these quantities are a constant over the temperature range. The one that is most constant is the ratio h_{14} of piezoelectric stress to electric displacement.

If, however, we segregate out a part of the electric displacement, namely the dipole polarization, and calculate the ratio of piezoelectric stress to dipole polarization, we obtain a ratio denoted by f_{14} which is a constant within experimental error for both sodium chlorate and sodium bromate. The electric displacement is equal to

$$\frac{D_z}{4\pi} = \delta_z = \frac{E_z}{4\pi} + P_{z_0} + P_{z_d} \tag{10.18}$$

where P_{z_0} is the polarization due to electrons and ions, and P_{z_d} the polarization due to dipoles. Since the polarization P_{z_0} is independent of temperature and stress and is proportional to the field, we can write

$$\frac{D_z}{4\pi} = \delta_z = \frac{E_z}{4\pi}[1 + 4\pi\kappa_0] + P_{z_d} = \frac{E_z\epsilon_0}{4\pi} + P_{z_d} \tag{10.19}$$

where ϵ_0 is the temperature and strain independent part of the dielectric constant. Introducing this expression into equation (10.17), we have for the form relating piezoelectric stress to electric displacement

$$T_6 = c_{66}^{*}S_6 - f_{14}P_{z_d} \quad \text{where} \quad c_{66}^{*} = c_{66}^{D} + \frac{h_{14}^2\epsilon_0\epsilon_{33}^{S}}{4\pi(\epsilon_{33}^{S} - \epsilon_0)}$$

and

$$f_{14} = \frac{h_{14}\epsilon_{33}^{S}}{\epsilon_{33}^{S} - \epsilon_0} \tag{10.20}$$

Calculating f_{14} for sodium chlorate and sodium bromate, we find that it is a constant within experimental error equal to 9×10^4 for sodium chlorate and 18×10^4 for sodium bromate. The constancy of this quantity indicates that when the dipole turns through a small angle (which is proportional to the dipole polarization), this produces a stress on the crystal lattice which distorts it and produces a piezoelectric strain. Since the compliance is a function of temperature, the resultant strain dipole polarization ratio is not as constant as the stress dipole polarization ratio.

By using the dipole piezoelectric constant, an equivalent circuit can be obtained which takes account of the dielectric constant ϵ_0, the dielectric constant for dipoles ϵ_d^S, the coupling between the dipole polarization and the piezoelectric stress, and the elastic compliance. At low frequencies, this network is shown by Fig. 10.9. $(\epsilon_0/4\pi)$ represents the capacitance of a crystal one cubic centimeter due to electrons and atoms, while $(\epsilon_d/4\pi)$ represents the capacitance of the crystal of one cubic centimeter due to dipoles. The combination of three mutual compliances C_M, of which two are positive and one negative, represents the coupling between the electrical and mechanical properties of the crystal. Since the charge on the condenser $(\epsilon_d/4\pi)$ represents the dipole polarization when the crystal is

clamped so that no displacement can occur in the mechanical arm, the dielectric constant is the clamped dielectric constant ϵ_d^S. The mechanical elastic constant represented by the condenser C_E is the ratio between the applied stress T_1 and the strain when the dipole polarization P_{zd} is suppressed. By writing equation (10.20) in the form for a longitudinal crystal, we have

$$T_1 = c_{11}^* S_1 - f_{31} P_{zd}; \qquad E_z = \frac{4\pi}{(\epsilon_3^S - \epsilon_0)} P_{zd} - f_{31} S_1 \tag{10.21}$$

where $$c_{11}^* = c_{11}^D + \frac{h_{31}\epsilon_0\epsilon_3^S}{4\pi(\epsilon_3^S - \epsilon_0)}; \qquad f_{31} = \frac{h_{31}\epsilon_3^S}{\epsilon_3^S - \epsilon_0}$$

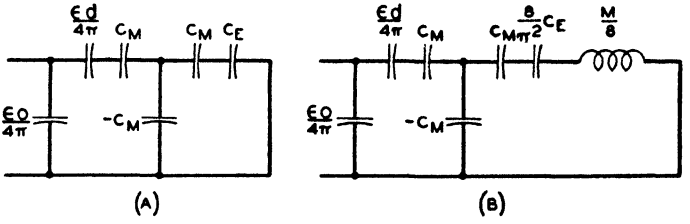

FIG. 10.9. Equivalent circuit of crystal showing effect of dipole coupling.

For the 45° cut, $h_{31} = h_{14}$ and $f_{31} = f_{14}$. When the crystal is clamped so that no displacement occurs in the mechanical compliance $C_E = 1/c_{11}^*$, the force applied by the mutual compliance capacitance C_M is

$$(j\omega P_{zd})\left(-\frac{j}{\omega C_M}\right) = \frac{P_{zd}}{C_M} = P_{zd} f_{31} \therefore \frac{1}{C_M} = f_{31} \tag{10.22}$$

The final arm containing C_E is the mechanical arm and the charge on C_E, if T_1 is set equal to zero, represents the strain in the crystal due to the applied field. If T_1 is zero, the total capacitance as measured from the electrical side is

$$C = \frac{\epsilon_0}{4\pi} + \frac{\epsilon_d^S}{4\pi}\left[\frac{1}{1 - \dfrac{\epsilon_d^S f_{31}^2}{4\pi c_{11}^*}}\right] = \frac{\epsilon_0}{4\pi} + \frac{\epsilon_d^S}{4\pi(1 - k_d^2)} = \frac{\epsilon_0}{4\pi} + \frac{\epsilon_d^T}{4\pi} \tag{10.23}$$

where $$k_d = f_{31}\sqrt{\frac{\epsilon_d^S}{4\pi c_{11}^*}}$$

is the dipole coupling constant, and represents the percentage of the electrical energy in the dipole arm stored in a mechanical form. The dipole dielectric constant for zero stress is the dipole dielectric constant for constant strain divided by $(1 - k_d^2)$.

If we define the square of the electromechanical coupling constant as the ratio of the total input energy that is stored in mechanical form for a static applied voltage, the electromechanical coupling is given by the equation

$$k^2 = \frac{\epsilon_d^S k_d^2}{\epsilon^S - \epsilon_0 k_d^2} \qquad \text{where} \qquad \epsilon^s = \epsilon_0 + \epsilon_d^S \tag{10.24}$$

If the dipole dielectric constant is small compared to the dielectric constant for electrons and atoms, the electromechanical coupling is small compared to the dipole coupling constant. These quantities have been evaluated for four crystals and the results are shown in Table XVI.

TABLE XVI

Material	f_{31}	c_{11}^*	ϵ_d^S	k_d	ϵ^S	k
KH_2PO_4(KDP)	3.2×10^4	1.70×10^{11}	17.4	.114	21.9	.105
$NH_4H_2PO_4$(ADP)	16×10^4	1.85×10^{11}	9.7	.332	15.7	.285
$NaClO_3$	9×10^4	4.3×10^{11}	1.0	.039	5.70	.017
$NaBrO_3$	18×10^4	4.2×10^{11}	0.83	.072	5.70	.028

This table shows that the dipole constant f_{31} varies for different crystals by a factor of 6 to 1, being highest for sodium bromate and lowest for potassium dihydrogen phosphate. The last column shows the value of the electromechanical coupling which is a measure of the amount of the total applied electrical energy that appears in mechanical form under static conditions. An examination of the data shows that this is low for sodium chlorate and sodium bromate, because the electronic and ionic polarization is large compared to the dipole polarization and hence only a small fraction of the total input electrical energy goes into orienting the dipoles. KDP, which has a smaller dipole piezoelectric constant, has a larger electromechanical coupling because of the fact that the dipole polarization represents about three fourths of the total polarization, whereas for sodium chlorate it is only 0.2 of the total. Ammonium dihydrogen phosphate obtains its large coupling because of the fact that over fifty per cent of the total polarization is dipole polarization and in addition the dipole piezoelectric constant is large.

To complete the equivalent circuit of Fig. 10.9 for high frequencies, one adds a mass equal to $\frac{1}{8}$ the mass of the crystal, for a crystal vibrating freely on both ends, and multiplies the compliance C_E by a factor $8/\pi^2$ to take account of the variation of compliance with frequency. The factor $8/\pi^2$ holds for frequencies near the first resonance. This equivalent circuit is shown by Fig. 10.9B.

10.2 *Measurements of the Properties of Trigonal and Hexagonal Crystals*

10.21 *Properties of Dextrose Sodium Chloride, Bromide and Iodide*

The crystals of dextrose sodium chloride, dextrose sodium bromide and dextrose sodium iodide all crystallize in the quartz class and hence are of some interest in answering the question of whether crystals of similar classes will have the same types of properties, such as, for example, temperature coefficient of frequency. For quartz, the low and zero temperature coefficients of frequency are made possible by the fact that the c_{66} shear-elastic constant has a positive temperature coefficient and by various orientation processes, the positive coefficient can be made to annul the usual negative temperature coefficients of frequency.

Measurements made for these crystals show that the shear temperature coefficient of frequency is highly negative and hence crystals belonging to the same crystal class do not always have the same types of temperature coefficients. The piezoelectric constants are of the same order as quartz, the elastic constants all have high negative coefficients of frequency and the values of Q are relatively low. Hence it does not appear that these crystals will be of practical use.

The method of measuring these crystals is to take four oriented cuts with their thickness direction along the x-axis, and with their lengths at orientation from $-30°$ to $+60°$ with respect to the y crystallographic axes of the crystal, and to measure a Y-cut crystal in its face-shear mode and its thickness-shear mode. These data are sufficient to determine the six elastic constants, the two piezoelectric constants and one dielectric constant. To determine the other dielectric constant, a crystal is cut normal to the z-axis. Since no piezoelectric motion is excited by a field along z, only the dielectric constant can be measured for this orientation.

Since these crystals belong to the quartz class, the elastic, dielectric and piezoelectric equations are the same as those given by equation (6.1). For the series of four oriented cuts all with their thicknesses along the x-axes, the equations of motion for a long, thin crystal take the form

$$S_2' = s_{22}^E T_2' + d_{12}' E_x; \qquad \delta_x = \frac{D_x}{4\pi} = \frac{\epsilon_1^T}{4\pi} E_x + d_{12}' T_2' \tag{10.25}$$

since all the stresses except T_2' are equal to zero for a long, thin crystal. For crystals rotated by positive or negative angles of θ with respect to the y crystallographic axes

$$s_{22}^{E'} = s_{11}^E \cos^4\theta + s_{33} \sin^4\theta - 2s_{14}^E \cos^3\theta \sin\theta + (2s_{13} + s_{44}^E) \sin^2\theta \cos^2\theta$$

$$d_{12}' = \left[\frac{-d_{11}(1 + \cos 2\theta) + d_{14} \sin 2\theta}{2}\right] \tag{10.26}$$

These equations follow from equations (5.67) by taking the direction cosines

	x	y	z
x'	$l_1 = 0;$	$m_1 = \cos\theta;$	$n_1 = \sin\theta$
y'	$l_2 = 0;$	$m_2 = -\sin\theta;$	$n_2 = \cos\theta$
z'	$l_3 = 1;$	$m_3 = 0;$	$n_3 = 0$

(10.27)

and noting that for crystals of this class $s_{22} = s_{11}$; $s_{23} = s_{13}$; $s_{24} = -s_{14}$; $d_{12} = -d_{11}$. In this equation θ is the angle between the length and the y crystallographic axis measured in a counterclockwise direction.

The data for dextrose sodium bromide are shown by Table XVII.

TABLE XVII

Cut	Dimension in mm l	w	t	Resonant Frequency f_R	Anti-Resonant Frequency f_A	Ratio of Capacitances r	Coefficient of Coupling k	Capacitance of Crystal $\mu\mu f$	Dielectric Constant ϵ_{11}^T
−30° X-cut	4.38	1.28	0.96	371,280	—	—	—	—	—
0° X-cut	9.13	2.95	0.975	177,500	178,990	182.5	.082	1.0	4.1
+30° X-cut	9.89	2.70	0.99	158,600	158,972	213.0	.0765	1.0	4.0
+60° X-cut	9.98	2.95	1.01	163,240	163,338	832.0	.0385	1.1	4.0

Cut	Resistance at Resonance R	Value of Q	Frequency Constant f_k	Elastic Compliance s'_{22}	Piezoelectric Constant d'_{11}	Temperature Coefficient of Frequency
−30° X-cut	—	—	162.5	5.62×10^{-12}	—	−186 in 10^6/°C
0° X-cut	38,000	3,900	161.5	5.69×10^{-12}	11.0×10^{-8}	−328
+30° X-cut	100,000	5,280	156.5	6.06×10^{-12}	10.62	−285
+60° X-cut	115,000	5,500	163.1	5.56×10^{-12}	5.13	−210

From these data, equations (10.26), and the density $\rho = 1.69$, part of the elastic constants and the piezoelectric constants can be determined. The value of s_{11}^E is determined directly from the 0° X-cut and is $s_{11}^E = 5.69 \times 10^{-12}$. Since the term in s_{14} reverses sign on going from positive to negative angles, we have

$$s_{14} = \frac{s_{22-30^\circ} - s_{22+30^\circ}}{1.3} = 0.34 \times 10^{-12} \tag{10.28}$$

The remaining two constants of equation (10.26) can be solved from the remaining data and are given by the equations

$$s_{33} = s_{11} + .43s_{14} + s'_{22_{60°}} - \left(\frac{s_{22_{30°}} + s_{22_{-30°}}}{2}\right) = 5.23 \times 10^{-12} \tag{10.29}$$

$$(2s_{13} + s_{44}) = 3(s_{22_{30°}} + s_{22_{-30°}}) - .662s_{22_{60°}} - 3.31s_{11} - .142s_{14}$$
$$= 12.6 \times 10^{-12}$$

From the values of d'_{12} given in Table XVII and in the equations (10.26) we find

$$d_{11} = -11.0 \times 10^{-8}; \qquad d_{14} = -5.4 \times 10^{-8} \tag{10.30}$$

These values are slightly larger than in quartz, but due to the much larger compliance, the coupling factor k is even lower than in quartz.

To obtain the remaining elastic constants we have to evaluate the shear elastic compliances. These can both be obtained from a Y-cut crystal by measuring the thickness shear and the face shear, both of which are driven for this type of crystal. To obtain the high-frequency shear mode, a square crystal was cut and the contour dimensions were decreased until a good resonance free from interfering modes was obtained. The data then were taken and are shown by Table XVIII. The same crystal was then ground down till its length was six times its width and the face-shear frequency was measured. The results are given in Table XXXII.

TABLE XVIII

Mode	Dimension in mm l	w	t	Resonant Frequency	Temperature Coefficient	Dielectric Constant	Shearing Constant
High Freq. Shear	7.04	7.04	1.05	1,017,820	−320 parts in 10^6/°C	4.0	$c_{66} = 7.66 \times 10^{10}$
Low Freq. Shear	7.04	1.6	1.05	601,000	−240 parts in 10^6/°C	4.0	$c_{44} = 6.34 \times 10^{10}$

To obtain the s constants from the c constants, we have to make use of the relation derived in the Appendix Table XXXII, which can be written

$$s_{ij} = (-1)^{i+j}\Delta^{cij}/\Delta^c \tag{10.31}$$

where

$$\Delta^e = \begin{vmatrix} c_{11} & c_{12} & c_{13} & c_{14} & 0 & 0 \\ c_{12} & c_{11} & c_{13} & -c_{14} & 0 & 0 \\ c_{13} & c_{13} & c_{33} & 0 & 0 & 0 \\ c_{14} & -c_{14} & 0 & c_{44} & 0 & 0 \\ 0 & 0 & 0 & 0 & c_{44} & c_{14} \\ 0 & 0 & 0 & 0 & c_{14} & \frac{c_{11} - c_{12}}{2} \end{vmatrix}$$

and Δ^{eij} is the determinant obtained from this by suppressing the ith row and jth column. Solving these, we have

$$2s_{11} = \frac{c_{33}}{\alpha'} + \frac{c_{44}}{\beta'}; \qquad 2s_{12} = \frac{c_{33}}{\alpha'} - \frac{c_{44}}{\beta'}; \qquad s_{13} = \frac{-c_{13}}{\alpha'};$$

$$s_{14} = \frac{-c_{14}}{\beta'}; \qquad s_{33} = \frac{c_{11} + c_{12}}{\alpha'}; \qquad s_{44} = \frac{c_{11} - c_{12}}{\beta'};$$

$$s_{66} = 2(s_{11} - s_{12}) = \frac{2c_{44}}{\beta'} \tag{10.32}$$

where $\alpha' = c_{33}(c_{11} + c_{12}) - 2c_{13}^2$; $\beta' = c_{44}(c_{11} - c_{12}) - 2c_{14}^2$. Conversely, we can also write

$$2c_{11} = \frac{s_{33}}{\alpha} + \frac{s_{44}}{\beta}; \qquad 2c_{12} = \frac{s_{33}}{\alpha} - \frac{s_{44}}{\beta}; \qquad c_{13} = \frac{-s_{13}}{\alpha}; \qquad c_{14} = \frac{-s_{14}}{\beta};$$

$$c_{33} = \frac{s_{11} + s_{12}}{\alpha}; \qquad c_{44} = \frac{s_{11} - s_{12}}{\beta}; \qquad c_{66} = \frac{c_{11} - c_{12}}{2} = \frac{s_{44}}{2\beta} \tag{10.33}$$

where $\alpha = s_{33}(s_{11} + s_{12}) - 2s_{13}^2$; $\beta = s_{44}(s_{11} - s_{12}) - 2s_{14}^2$.

The above measurements give some elastic compliances, and some elastic stiffness constants. Since c_{44} and c_{66} are measured, we find on solving the expression for c_{44} and c_{66} that

$$(s_{11} - s_{12}) = \frac{1}{4c_{66}} + \sqrt{\frac{1}{(4c_{66})^2} + \frac{s_{14}^2 c_{44}}{c_{66}}};$$

$$s_{44} = \frac{1}{c_{44}} + \frac{2s_{14}^2}{\frac{1}{4c_{66}} + \sqrt{\frac{1}{(4c_{66})^2} + \frac{s_{14}^2 c_{44}}{c_{66}}}} \tag{10.34}$$

Hence with the measured values

$$s_{44}^E = 15.8 \times 10^{-12}; \qquad s_{11}^E = +s_{22}^E = 6.55 \times 10^{-12}$$

and hence $$s_{12}^E = -0.86 \times 10^{-12} \tag{10.35}$$

Hence all the constants are determined and are when collected together

$$\begin{aligned} s_{11}^E &= 5.69 \times 10^{-12} & s_{33} &= 5.23 \times 10^{-12} & d_{11} &= -11.0 \times 10^{-8} \\ s_{12}^E &= -0.86 \times 10^{-12} & s_{14}^E &= -0.34 \times 10^{-12} & d_{14} &= -5.4 \times 10^{-8} \\ s_{13} &= -1.60 \times 10^{-12} & s_{44}^E &= 15.8 \times 10^{-12} & \epsilon_{11}^T &= 4.0 \\ & & \epsilon_{33} &\text{ not measured} & & \end{aligned} \tag{10.36}$$

The temperature coefficients of frequency of all of the crystal cuts were measured and are shown by Tables XVII and XVIII. They are all found to have high negative temperature coefficients. Hence there exists no possibility of obtaining zero or positive temperature coefficients with this crystal. This shows that crystals of the same class do not all have the same type of temperature-coefficient response.

The other two crystals of this class, dextrose sodium chloride and dextrose sodium iodide, have also been measured and the results are shown by equations (10.37) and (10.38). Here also all the temperature coefficients are highly negative and no zero temperature coefficients are possible. In dextrose sodium chloride

$$\begin{aligned} s_{11}^E &= 6.38 \times 10^{-12} & s_{33} &= 7.02 \times 10^{-12} & d_{11} &= -20.9 \times 10^{-8} \\ s_{12}^E &= -2.61 \times 10^{-12} & s_{14}^E &= +0.36 \times 10^{-12} & d_{14} &= +1.0 \times 10^{-8} \\ s_{13} &= -1.6 \times 10^{-12} & s_{44}^E &= 13.0 \times 10^{-12} & \epsilon_{11} &= 4.25 \\ & & \rho &= 1.564 & & \end{aligned} \tag{10.37}$$

For dextrose sodium iodide

$$\begin{aligned} s_{11}^E &= 6.02 \times 10^{-12} & s_{33} &= 5.16 \times 10^{-12} & d_{11} &= -11.4 \times 10^{-8} \\ s_{12}^E &= -3.43 \times 10^{-12} & s_{14}^E &= +0.38 \times 10^{-12} & d_{14} &= +2.2 \times 10^{-8} \\ s_{13} &= -0.62 \times 10^{-12} & s_{44}^E &= 13.0 \times 10^{-12} & \epsilon_{11}^T &= 4.6 \\ & & \rho &= 1.864 & & \end{aligned} \tag{10.38}$$

Another crystal in the quartz class, aluminum phosphate $AlPO_4$, has been measured. This crystal has a melting point of 1500°C, is nearly insoluble in water, and has a density of 2.566. The measured constants are

$$\begin{aligned} s_{11}^E &= 1.61 \times 10^{-12}\ \text{cm}^2/\text{dyne} & s_{44}^E &= 5.3 \times 10^{-12} \\ s_{12}^E &= -.01 \times 10^{-12} & s_{66}^E &= 3.22 \times 10^{-12} \\ s_{13}^E &= -0.83 \times 10^{-12} & d_{11} &= \pm 10.0 \times 10^{-8} \\ s_{14}^E &= +0.89 \times 10^{-12} & d_{14} &= \mp 4.65 \times 10^{-8} \\ s_{33}^E &= +1.61 \times 10^{-12} & \epsilon_{11}^T &= 6.05 \end{aligned}$$

This crystal has all negative temperature coefficients in the room-temperature range. The crystal having the lowest frequency temperature coefficient is the Y-cut thickness-shear mode and at $-40°C$ the temperature coefficient is zero.

10.22 *Properties of Crystals in the Tourmaline Class*

Tourmaline belongs to the ditrigonal-pyramidal class (20) having the symmetry c_{3v} or $3m$, which means that the z-axis is a threefold axis and that there are three planes of symmetry for the crystal parallel to z. Its piezoelectric and elastic constants have been measured by Voigt[7] but previously no measurements have been made of the temperature coefficients of the crystal for various orientations. Measurements have been made and are discussed in this section. It appears that the temperature coefficients for all the modes of motions are negative and hence no possibilities exist for zero temperature coefficient cuts.

Tourmaline has the same set of elastic constants as quartz but a different set of piezoelectric constants. This necessitates a different set of crystal orientations to obtain all the elastic and piezoelectric constants, since, for example, a crystal cut normal to the x-axis cannot be driven in a longitudinal mode. To obtain the set of crystals with lengths in the yz plane as was done for quartz, we take a set whose thickness directions also lie in the yz plane, as shown by Fig. 10.10. This series of four crystals having lengths along the y-axis and at angles of 22.5°, 45° and 67.5° with y, have the direction cosines given by equation (10.39) when the length of the crystal is taken along the x'-axis, the width y' lies along the negative x-axis and the thickness lies along z'.

$$\begin{array}{cccc} & x & y & z \\ x' & l_1 = 0 & m_1 = \cos\theta & n_1 = \sin\theta \\ y' & l_2 = -1 & m_2 = 0 & n_2 = 0 \\ z' & l_3 = 0 & m_3 = -\sin\theta & n_3 = \cos\theta \end{array} \tag{10.39}$$

Inserting these direction cosines in equations (5.67), the inverse of Young's modulus for the crystal length and the piezoelectric constant driving the crystal become

$$\begin{aligned} s'^{E}_{11} &= s^{E}_{11}\cos^4\theta + (2s^{E}_{13} + s^{E}_{44})\sin^2\theta\cos^2\theta - 2s^{E}_{14}\sin\theta\cos^3\theta + s^{E}_{33}\sin^4\theta \\ d'_{31} &= d_{31}\cos^3\theta + (d_{33} - d_{15})\sin^2\theta\cos\theta - d_{22}\sin\theta\cos^2\theta \end{aligned} \tag{10.40}$$

Crystals were obtained with the orientations shown by Fig. 10.10, and the

[7] Voigt, W., *Lehrbuch der Kristallphysik*, p. 753, B. Teubner, 1910.

measured and calculated results are shown by Table XIX. The orientation in the first column is specified by a method adopted by the Piezoelectric Standardization Committee of the I.R.E. The first letter denotes the direction of the thickness in the unrotated position, the second letter denotes the direction of the length, the third letter denotes the axis of rotation of the rotated cut and the angle given denotes the angle of rotation

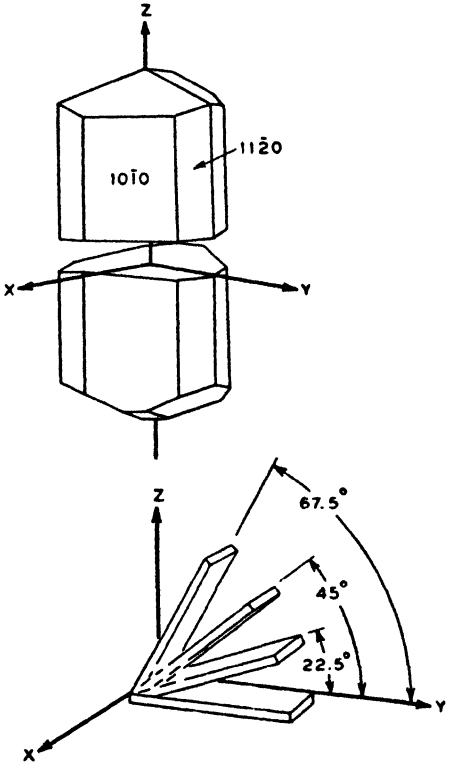

FIG. 10.10. Set of crystals for measuring piezoelectric constants of tourmaline.

measured in a counterclockwise direction. The orientations used were rotated in a counterclockwise direction from the y-axis. The second, third and fourth columns denote the dimensions in millimeters; the fifth column is the resonant frequency in cycles; the sixth column is the separation in frequency Δf between the resonant and anti-resonant frequencies; the seventh column is the frequency constant, *i.e.* the product of the frequency by the length of the crystal; the eighth column is the temperature coefficient of the resonant frequency measured from $-50°C$ to $+50°C$ given in parts per million per degree centigrade. The ninth column is the free

TABLE XIX

Orientation	Dimensions in mm l	w	t	f_R	Δf	f_M kc cm	T_K parts in 10^6	ϵ^T	$s_{11}^{E'} \times 10^{12}$	r	k	$d_{31}' \times 10^8$
zy	12.95	1.89	0.85	355,100	66	459	−57.7	7.5	.385	2,680	.0214	1.03
$zyw + 22.5°$	10.25	1.61	0.99	420,580	—	431	−61.0	7.6	.435	>10,000	<.011	<.5
$zyw + 45°$	9.32	1.45	1.02	403,715	150	375	−51.2	7.85	.575	1,340	.0304	1.82
$zyw + 67.5°$	8.09	1.21	1.01	439,195	140	355	−41.4	8.1	.64	1,570	.028	1.7
yx	10.54	1.61	1.01	435,500	70	459	−58	8.2	.385	3,100	.02	1.0

dielectric constant measured at 1000 cycles. The other four columns are data calculated from the measured values in the other columns. $s_{11}^{E'}$ is the inverse of Young's modulus along the length of the crystal calculated from the frequency constant and the density $\rho = 3.1$ from the formula

$$f_M = \frac{1}{2\sqrt{s_{11}^{E'}\rho}} \tag{10.41}$$

The next column is the ratio of the capacitances of the crystal given by

$$r = \frac{f_R}{2\Delta f} \tag{10.42}$$

The electromechanical coupling can be calculated from equation (5.36) and is plotted in the next to the last column, while the piezoelectric constant d'_{31} can be calculated from the data of the table by using equation (5.33). One extra crystal, the Y-cut crystal with its length along x, is also used since the piezoelectric constant d_{21}, which from equation (3.64), class 20, of Chapter III, is equal to d_{22}, can be directly evaluated from the d constant and from Table XV has the numerical value of 1×10^{-8}. From equation (10.40) we also see that the first crystal of the table gives the numerical value of $d_{31} = 1.03 \times 10^{-8}$. There remain then the values of d_{15} and d_{33} to determine as well as the signs of the other two constants. Squeeze tests by W. L. Bond show that the signs of these constants are negative.

By using the piezoelectric constants for a rotated crystal given by equation (10.40), we find that to fit the measured values of the last column of Table XIX, we have to have

$$\begin{gathered} d_{31} = -1.03 \times 10^{-8}; \qquad d_{22} = -1.0 \times 10^{-8}; \\ (d_{33} - d_{15}) = +5.4 \times 10^{-8} \end{gathered} \tag{10.43}$$

The data for $s_{11}^{E'}$ given in the tenth column of Table XIX, will determine three of the elastic compliances and one relation between the remaining constants. $s_{11}^{E'}$ is given directly by the first or last crystals and is

$$s_{11}^{E'} = 0.385 \times 10^{-12} \text{ cm}^2/\text{dyne} \tag{10.44}$$

To obtain the other three values in (10.40), we have three equations with three unknowns for the three different angles. For these negative angle orientations we find on solving these equations that

$$\begin{aligned} s_{33} &= 1.79 s_{11_{67.5°}} + .74 s_{11_{22.5°}} - 1.265 s_{11_{45°}} - .265 s_{11} \\ s_{14} &= -3.05 s_{11_{22.5°}} - 0.53 s_{11_{67.5°}} + 1.79 s_{11_{45°}} + 1.79 s_{11} \\ (2s_{13} + s_{44}) &= 8.85 s_{11_{45°}} - 6.85 s_{11_{22.5°}} - 2.85 s_{11_{67.5°}} + 2.85 s_{11} \end{aligned} \tag{10.45}$$

where $s_{11_{22.5°}}$ is the value of s_{11} at the positive angle of 22.5° from y, etc. and s_{11} is the value along y given in (10.44). Substituting in the values from Table XIX, we find

$$\begin{aligned} s_{11}^{E'} &= 0.385 \times 10^{-12}; \quad & s_{33}^{E'} &= 0.636 \times 10^{-12}; \\ (2s_{13}^{E} + s_{44}^{E}) &= 1.402 \times 10^{-12}; \quad & s_{14}^{E} &= +.045 \times 10^{-12} \end{aligned} \tag{10.46}$$

All of these values agree quite well with those measured by Voigt, shown by equation (10.47).

$$\begin{aligned} &s_{11} = s_{22} = 0.398 \times 10^{-12} && c_{11} = c_{22} = 270 \times 10^{10}\ \text{dynes/cm}^2 && \\ &s_{33} = 0.625 && c_{33} = 161 && d_{15} = 11.0 \times 10^{-8} \\ &s_{44} = s_{55} = 1.51 && c_{44} = c_{55} = 67 && d_{22} = -0.94 \\ &s_{12} = -0.103 && c_{12} = 69 && d_{31} = 0.96 \\ &s_{13} = s_{23} = -0.016 && c_{13} = c_{23} = 8.8 && d_{33} = 5.4 \\ &s_{14} = -s_{24} = s_{56/2} = +0.058 && c_{14} = -c_{24} = c_{56} = -7.8 && \end{aligned} \tag{10.47}$$

The last column shows the piezoelectric constants measured by Voigt and Röntgen, with the preferred values selected.[8]

To complete the measurements of the elastic and piezoelectric constants, we need to measure two shear vibrating crystals. Since it is not possible to obtain face-shear modes in this class for crystals cut along the crystallographic axes, two thickness-shear modes, both driven by the piezoelectric constants $d_{15} = d_{24}$, are used and the measured results are shown by Table XX.

From these measurements we have directly that

$$\begin{aligned} c_{44} &= 65 \times 10^{10}\ \text{dynes/cm}^2; \quad & c_{66} &= 95 \times 10^{10}; \\ & & d_{15} &= \pm 10.9 \times 10^{-8} \end{aligned} \tag{10.48}$$

Using equations (10.34) of the last section, which applies to this crystal class also, all the constants can be evaluated and are

$$\begin{aligned} &s_{11} = 0.385 \times 10^{-12} && c_{11} = 272 \times 10^{10}\ \text{dynes/cm}^2 && d_{15} = -10.9 \times 10^{-8} \\ &s_{12} = -0.048 \times 10^{-12} && c_{12} = 40 \times 10^{10} && d_{22} = -1.0 \times 10^{-8} \\ &s_{13} = -0.071 \times 10^{-12} && c_{13} = 35 \times 10^{10} && d_{31} = -1.03 \times 10^{-8} \\ &s_{33} = 0.636 \times 10^{-12} && c_{33} = 165 \times 10^{10} && d_{33} = -5.5 \times 10^{-8} \\ &s_{44} = 1.54 \times 10^{-12} && c_{44} = 65 \times 10^{10} && \epsilon_{11}^{T} = \epsilon_{22}^{T} = 8.2 \\ &s_{14} = +0.045 \times 10^{-12} && c_{14} = -6.8 \times 10^{10} && \epsilon_{33}^{T} = 7.5 \end{aligned} \tag{10.49}$$

[8] Cady, W. G., *Piezoelectricity*, p. 227, McGraw-Hill Book Co., Inc., 1946.

TABLE XX

Orientation	Dimensions mm l	w	t	f_R	Δf	f_M kc mm	T_K parts in 10^6/°C	ϵ^T	$c \times 10^{-10}$	r	k	$d_{15} \times 10^8$
yz	8.97	8.95	1.002	2,285,120	11,130	2289.5	−40.0	8.2	65	103	.1085	10.9
xy	5.02	5.02	1.01	2,743,000	19,000	2270	−50.0	8.2	95	71	.131	10.9

These signs of the piezoelectric constant are opposite from those given by Voigt on account of a different choice of the +z-axis. All the temperature coefficients are uniformly negative, of values from −40 to −60 parts in a million per degree C and hence no possibility exists of obtaining zero temperature coefficient of frequency cuts.

Two other crystals of the tourmaline class, lithium trisodium chromate and lithium trisodium molybdate have been partially measured. Since they dehydrate rapidly, it was not thought worth-while to make complete measurements. The results obtained for these two crystals are given by equations (10.50) and (10.51).

LITHIUM TRISODIUM CHROMATE HEXAHYDRATE

$$\begin{aligned} s_{11} &= 7.87 \times 10^{-12} & Ts_{11} &= +7.5 \times 10^{-4}/°\text{C} \\ s_{33} &= 3.5 \times 10^{-12} & Ts_{33} &= +7.0 \times 10^{-4} \\ (2s_{13} + s_{44}) &= 0.9 \times 10^{-12} & (2Ts_{13} + Ts_{44}) &= +19 \times 10^{-4} \\ d_{22} &= \pm 8.6 \times 10^{-8} & & \\ \epsilon_{11}^{T} &= 8.0 & & \\ \rho &= 2.11 & & \end{aligned} \tag{10.50}$$

LITHIUM TRISODIUM MOLYBDATE HEXAHYDRATE

$$\begin{aligned} s_{11} &= 2.95 \times 10^{-12} & Ts_{11} &= +7.3 \times 10^{-4}/°\text{C} \\ s_{33} &= 2.71 \times 10^{-12} & Ts_{33} &= +5.9 \times 10^{-4} \\ (2s_{13} + s_{44}) &= 7.05 \times 10^{-12} & (2Ts_{13} + Ts_{44}) &= +4.0 \times 10^{-4} \\ d_{22} &= \pm 7.45 \times 10^{-8} & \epsilon_{11}^{T} &= 6.7 \\ d_{31} &= \pm 4.0 \times 10^{-8} & \epsilon_{33}^{T} &= 5.3 \\ d_{33} &= \pm 5.8 \times 10^{-8} & \rho &= 2.43 \end{aligned} \tag{10.51}$$

10.3 *Measurements of Properties of Crystals in the Tetragonal Class*

Three crystals of the tetragonal class have been measured, ammonium dihydrogen phosphate (ADP) and potassium dihydrogen phosphate (KDP), whose constants were given in Chapter VIII, and nickel sulphate hexahydrate. The first two belong to the tetragonal scalenohedral class (11), (symmetry V_d; $\bar{4}2m$) while nickel sulphate hexahydrate belongs to the tetragonal trapezohedral class (12) (symmetry D_4 or 422). The process of measuring crystals of class 11 is to take a set of four crystals perpendicular to the $a = x$ crystallographic axis and another set perpendicular

to the $c = z$ crystallographic axis. One of each set has its length along one of the crystallographic axes, and the other three angles of 22.5°, 45° and 67.5° with this axis. The crystal with its axis along the crystallographic axis, is driven in a face-shear mode, while the other three are driven in longitudinal modes. For crystals cut perpendicular to x, the longitudinal modes are controlled by the elastic and piezoelectric constants

$$d'_{31} = \frac{d_{14}}{2} \sin 2\theta \tag{10.52}$$

$$s_{11}^{E'} = s_{11} \cos^4 \theta + (2s_{13} + s_{44}^{E}) \sin^2 \theta \cos^2 \theta + s_{33} \sin^4 \theta$$

where θ is the angle between the length and the y crystallographic axes. Hence determining the elastic constants from the resonant frequency by the equation

$$s_{11}^{E'} = \frac{1}{(2lf_R)^2 \rho} \tag{10.53}$$

the three moduli are determined by the equations

$$\begin{aligned} s_{11} &= 1.707 s_{22.5°}^{E'} - s_{45°}^{E'} + .293 s_{67.5°}^{E'} \\ s_{33} &= 1.707 s_{67.5°}^{E'} - s_{45°}^{E'} + .293 s_{22.5°}^{E'} \\ (2s_{13} + s_{44}^{E}) &= 6s_{45°}^{E'} - 2s_{22.5°}^{E'} - 2s_{67.5°}^{E'} \end{aligned} \tag{10.54}$$

For crystals cut perpendicular to the z-axis

$$d'_{31} = \frac{d_{36}}{2} \sin^2 \theta \tag{10.55}$$

$$s_{11}^{E'} = s_{11} (\sin^4 \theta + \cos^4 \theta) + (2s_{12} + s_{66}^{E}) \sin^2 \theta \cos^2 \theta$$

and the equations for determining the constants become

$$s_{11} = (s_{22.5°}^{E'} + s_{67.5°}^{E'}) - s_{45°}^{E'}; \qquad (2s_{12} + s_{66}^{E}) = 6s_{45°}^{E'} - 2(s_{22.5°}^{E'} + s_{67.5°}^{E'}) \tag{10.56}$$

The face-shear mode perpendicular to the x-axis is controlled by the shear-elastic constant c_{44}^{E}, while the shear mode perpendicular to the z-axis determines the shear constants c_{66}^{E}. This process was followed for ADP and KDP and the results are given in Chapter VIII.

For crystals of class (12), however, there is no piezoelectric constant d_{36} and hence crystals cut perpendicularly to the z-axis will not be driven piezoelectrically. To get around this difficulty, one crystal is cut as shown by Fig. 10.11 with its length 45° from the z-axis in a plane 45° from the x- and y-axes and with its thickness in the xy plane. This crystal has a

TABLE XXI

Orientation	Dimension mm l	w	t	f_R	Δf	$f_M$kc cm	Parts T_f in ^{6}/°C	ϵ^T	$s \times 10^{12}$	r	k	d
xzt − 22.5°	16.97	2.48	1.04	106,700	120	181.0	-3.9×10^{-4}	6.2	3.68	444	.053	7.1×10^{-8}
xzt − 45°	17.55	2.59	1.05	92,895	150	162.5	-5.2×10^{-4}	6.2	4.56	310	.0629	9.4
xzt − 67.5°	20.0	2.91	1.0	71,900	60	143.5	-3.9×10^{-4}	6.2	5.84	600	.045	7.4
xzt − 0°	18.47	2.72	1.0	435,795	827	118	-5.3×10^{-4}	6.2	8.65	264	.0685	14.1
zwy 45°	19.93	3.0	1.0	443,380	260	132.5	-4.3×10^{-4}	6.5	6.8	852	.0379	7.1
yxwt 45°, 45°	19.93	3.02	1.02	96,330	—	191.5	-4.0×10^{-4}	6.2	3.30	—	—	—

piezoelectric driving constant, and an elastic constant

$$d'_{31} = \frac{d_{14}}{2}; \quad s_{11}^{E'} = \frac{1}{4}\left[\frac{s_{11}}{2} + \frac{(2s_{12} + s_{66}^{E})}{2} + (2s_{13} + s_{44}^{E}) + s_{33}\right] \tag{10.57}$$

and allows one to evaluate the sum $(2s_{12} + s_{66}^{E})$. The other crystal, as shown by Fig. 10.11, is cut with its width along x and its length and

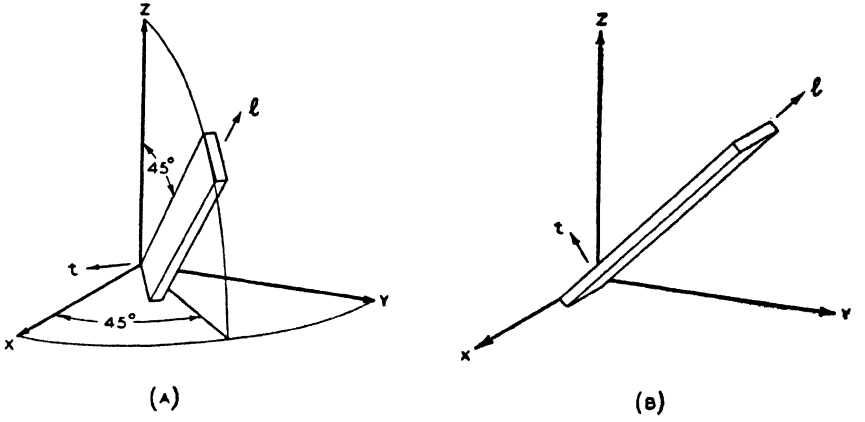

FIG. 10.11. Crystal orientations for measuring constants of nickel sulphate.

thickness 45° between the y- and z-axes. This crystal has piezoelectric and elastic constants equal to

$$\frac{d_{14}}{2} \quad \text{and} \quad \frac{c_{44}^{E} + c_{66}^{E}}{2} \tag{10.58}$$

and hence can be used to determine c_{66}^{E}.

Table XXI on p. 217 shows measurements for these 6 orientations for nickel sulphate hexahydrate. From these measurements the constants can be evaluated and are given by equations (10.59). The temperature coefficients of all modes of motions are negative and no zero temperature coefficients are possible.

$$\begin{aligned} s_{11} &= 6.5 \times 10^{-12} & d_{14} &= \pm 18.0 \times 10^{-8} \text{ (9)} \\ s_{12} &= -4.68 \times 10^{-12} & \epsilon_{11}^{T} &= 6.2 \\ s_{13} &= -0.13 \times 10^{-12} & \epsilon_{33}^{T} &= 6.8 \\ s_{33} &= 3.43 \times 10^{-12} & \rho &= 2.07 \\ s_{44}^{E} &= 8.65 \times 10^{-12} & & \\ s_{66}^{E} &= 5.62 \times 10^{-12} & & \end{aligned} \tag{10.59}$$

[9] It has recently been found that the piezoelectric constants of a number of crystals were measured by Frederich Spitzer for his thesis at Goettingen in 1938. He

10.4 *Measurements of Crystals in the Orthorhombic Class*

Six crystals of the orthorhombic class have been measured, all of them belonging to the orthorhombic bisphenoidal class 6 (symmetry $V = D_2$, or 222) which is the class of rochelle salt. The method of measurement is very similar to that of tetragonal crystals except that the process is repeated for all three axes since the properties of all three axes are different. The equations for the inverse of Young's modulus and the longitudinal piezoelectric constants for the x-, y- and z-axes are given by equations (10.60), (10.61) and (10.62).

$$s_{11}^{E'} = s_{22}\cos^4\theta + (2s_{23} + s_{44}^{E})\sin^2\theta\cos^2\theta + s_{33}\sin^4\theta$$

$$d_{31}' = \frac{d_{14}}{2}\sin 2\theta \tag{10.60}$$

$$s_{11}^{E'} = s_{11}\cos^4\theta + (2s_{13} + s_{55}^{E})\sin^2\theta\cos^2\theta + s_{33}\sin^4\theta$$

$$d_{31}' = \frac{d_{25}}{2}\sin 2\theta \tag{10.61}$$

$$s_{11}^{E'} = s_{11}\cos^4\theta + (2s_{12} + s_{66}^{E})\sin^2\theta\cos^2\theta + s_{22}\sin^4\theta$$

$$d_{31}' = \frac{d_{36}}{2}\sin 2\theta \tag{10.62}$$

Hence from measurements of three crystals, whose lengths are 22.5°, 45° and 67.5° from one of the crystallographic axes and whose thickness lies along another axis, the elastic constants of these equations can be derived. The equations for evaluating the constants from the measurements are similar to (10.54). The face-shear modes for crystals cut perpendicular to the x-, y- and z-axes are controlled by the elastic constants

$$c_{44}^{E} = \frac{1}{s_{44}^{E}}; \qquad c_{55}^{E} = \frac{1}{s_{55}^{E}}; \qquad c_{66}^{E} = \frac{1}{s_{66}^{E}} \tag{10.63}$$

Hence twelve cuts in sets of four perpendicular to the three crystallographic axes will determine the nine elastic constants and give checks on the s_{11}, s_{22} and s_{33} elastic constants. The three 45° cuts will determine the three

---

measured the constants of sodium chlorate, sodium bromate, nickel sulphate hexahydrate, ADP, KDP; magnesium sulphate, lithium sulphate monohydrate, DKT and ammonium tartrate. The values agree closely with the data presented in this book and for nickel sulphate hexahydrate the value of d_{14} found by Spitzer was -15.9×10^{-8}.

piezoelectric constants, and low-frequency measurements of the capacitances of any of the crystals perpendicular to the x-, y- and z-axes, will determine the dielectric constants ϵ_{11}^T, ϵ_{22}^T and ϵ_{33}^T.

The six crystals measured were lithium ammonium tartrate monohydrate, lithium potassium tartrate monohydrate, strontium formate dihydrate, barium formate, iodic acid, and sodium ammonium tartrate. The first two are isomorphic crystals and lithium ammonium tartrate has one orientation having a zero temperature coefficient of frequency. Since, however, the coupling is smaller than in ethylene diamine tartrate and the curvature of the frequency with temperature is larger, this crystal has not come into practical use. Perpendicular to the y-axis, the dielectric constant and the piezoelectric constant get larger as the temperature is reduced and some possibility exists that ferroelectric effects may occur at low temperatures. This question is discussed further in section 10.6. Strontium formate with two moles of water is fairly strongly coupled but dehydrates badly and does not appear useful. Barium formate has no water of crystallization but has a small coupling and all of its frequency temperature coefficients are negative. The fact that iodic acid (HIO_3) has large piezoelectric coupling coefficients was pointed out by the Naval Research Laboratories[10] and independent measurements have been made by them of the fundamental constants. Sodium ammonium tartrate tetrahydrate is isomorphous with rochelle salt. In spite of the rather large piezoelectric constants, it is not likely to be used practically on account of the very bad dehydration properties which are considerably worse than those of rochelle salt.

By employing these methods of measurements it is found that the elastic, piezoelectric and dielectric constants of lithium ammonium tartrate at 25°C are

$$\begin{array}{lll} s_{11} = 3.0 \times 10^{-12}\ \text{cm}^2/\text{dyne} & s_{12} = -0.82 \times 10^{-12} & \epsilon_{11}^T = 7.2 \\ s_{22} = 2.56 & s_{13} = -0.27 \times 10^{-12} & \epsilon_{22}^T = 8.0 \\ s_{33} = 3.5 & s_{23} = -1.22 \times 10^{-12} & \epsilon_{33}^T = 6.9 \\ s_{44}^E = 8.4 & d_{14} = \pm 13.2 \times 10^{-8} & \rho = 1.71 \\ s_{55}^E = 15.0 & d_{25} = \pm 19.6 \times 10^{-8} & \\ s_{66}^E = 4.3 & d_{36} = \pm 14.8 \times 10^{-8} & \end{array} \qquad (10.64)$$

[10] Burstein, Elias, "Approximate Determination of the Piezoelectric Properties of Small Crystals," *Rev. Sc. Inst.*, Vol. 18, No. 5, May, 1947.

The temperature coefficients of these quantities have also been measured and between $-30°$ and $+80°C$ have the following values.

$$
\begin{aligned}
Ts_{11} &= +8.8 \times 10^{-4} \text{ per } °C & Ts_{23} &= +6.0 \times 10^{-4} \\
Ts_{22} &= +6.2 \times 10^{-4} & Td_{14} &= +3.9 \times 10^{-3} \\
Ts_{33} &= +6.1 \times 10^{-4} & Td_{25} &= -5.0 \times 10^{-3} \\
Ts_{44}^{E} &= +6.7 \times 10^{-4} & Td_{36} &= +3.1 \times 10^{-3} \\
Ts_{55}^{E} &= -8.3 \times 10^{-4} & T\epsilon_{11} &= +1.9 \times 10^{-4} \\
Ts_{66}^{E} &= +10.9 \times 10^{-4} & T\epsilon_{22} &= -2.7 \times 10^{-4} \\
Ts_{12} &= +4.5 \times 10^{-4} & T\epsilon_{33} &= -0.4 \times 10^{-4} \\
Ts_{13} &= +74.0 \times 10^{-4}
\end{aligned}
\tag{10.65}
$$

As with quartz, the zero temperature coefficient crystals are made possible by the negative temperature coefficients of one of the shear elastic compliances, in this case s_{55}^{E}. However, the curvature of this constant is so high that the temperature characteristic is very curved. The properties of the crystals cut normal to the y-axis are discussed further in section 10.6.

Only the three 45° cuts have been measured for lithium potassium tartrate, since the results did not appear promising. From these the following data are obtained.

Normal to x

$$
\begin{aligned}
s_{1145°}^{E'} &= 2.8 \times 10^{-12} & Ts_{1145°}^{E'} &= +5.4 \times 10^{-4} \\
d_{14} &= \pm 9.6 \times 10^{-8} & \epsilon_{11}^{T} &= 5.84
\end{aligned}
$$

Normal to y

$$
\begin{aligned}
s_{1145°}^{E'} &= 5.72 \times 10^{-12} & Ts_{1145°}^{E'} &= +1.3 \times 10^{-4} \\
d_{25} &= \pm 33.6 \times 10^{-8} & \epsilon_{22}^{T} &= 7.32
\end{aligned}
\tag{10.66}
$$

Normal to z

$$
\begin{aligned}
s_{1145°}^{E'} &= 2.56 \times 10^{-12} & Ts_{1145°}^{E'} &= +7.3 \times 10^{-4} \\
d_{36} &= \pm 22.8 \times 10^{-8} & \epsilon_{33}^{T} &= 7.4
\end{aligned}
$$

$$\rho = 1.61$$

The data for strontium formate dihydrate are given by equation (10.67) and (10.68)

$$
\begin{aligned}
s_{11} &= 2.84 \times 10^{-12}\ \text{cm}^2/\text{dyne} & s_{23} &= -0.2 \times 10^{-12} \\
s_{22} &= 3.1 & d_{14} &= \pm 25.6 \times 10^{-8} \\
s_{33} &= 3.1 & d_{25} &= \pm 34.6 \\
s_{44}^E &= 6.5 & d_{36} &= \pm 7.0 \\
s_{55}^E &= 9.3 & \epsilon_{11}^T &= 6.1 \\
s_{66}^E &= 5.8 & \epsilon_{22}^T &= 6.4 \\
s_{12} &= -0.8 \times 10^{-12} & \epsilon_{33}^T &= 6.0 \\
s_{13} &= +1.1 & \rho &= 2.25
\end{aligned}
\qquad (10.67)
$$

The temperature coefficients for these quantities have been measured and are shown by equation (10.68)

$$
\begin{aligned}
Ts_{11} &= +10 \times 10^{-4}/°\text{C} & Ts_{23} &= +42 \times 10^{-4} \\
Ts_{22} &= +5.5 \times 10^{-4} & Td_{14} &= -8 \times 10^{-4} \\
Ts_{33} &= +5.95 \times 10^{-4} & Td_{25} &= -3.8 \times 10^{-4} \\
Ts_{44}^E &= +4.6 \times 10^{-4} & Td_{36} &= -14.7 \times 10^{-4} \\
Ts_{55}^E &= +3.2 \times 10^{-4} & T\epsilon_{11} &= -0.8 \times 10^{-4} \\
Ts_{66}^E &= +4.7 \times 10^{-4} & T\epsilon_{22} &= -1.3 \times 10^{-4} \\
Ts_{12} &= +10.4 \times 10^{-4} & T\epsilon_{33} &= +5.7 \times 10^{-4} \\
Ts_{13} &= 0
\end{aligned}
\qquad (10.68)
$$

On account of the low coupling only the face-shear modes have been measured for barium formate. These yield the following data:

$$
\begin{aligned}
s_{44}^E &= 7.85 \times 10^{-12}\ \text{cm}^2/\text{dyne} & d_{14} &= \pm 12 \times 10^{-8} \\
s_{55}^E &= 6.0 \times 10^{-12} & d_{25} &= \pm 8 \times 10^{-8} \\
s_{66}^E &= 8.25 \times 10^{-12} & d_{36} &= \pm 14 \times 10^{-8} \\
Ts_{44}^E &= +3.2 \times 10^{-4}/°\text{C} & \epsilon_{11}^T &= 7.9 \\
Ts_{55}^E &= +3.2 \times 10^{-4} & \epsilon_{22}^T &= 5.9 \\
Ts_{66} &= +3.9 \times 10^{-4} & \epsilon_{33}^T &= 7.5
\end{aligned}
\qquad (10.69)
$$

$$\rho = 3.261$$

The data for iodic acid yield the following constants and temperature coefficients:

$$\begin{aligned}
s_{11} &= 3.98 \times 10^{-12} & s_{12} &= -0.775 \times 10^{-12} & \epsilon_{11} &= 7.5 \\
s_{22} &= 2.01 \times 10^{-12} & s_{13} &= -0.97 \times 10^{-12} & \epsilon_{22} &= 12.4 \\
s_{33} &= 2.56 \times 10^{-12} & s_{23} &= -0.045 \times 10^{-12} & \epsilon_{33} &= 8.1 \\
s_{44}^{E} &= 5.45 \times 10^{-12} & d_{14} &= \pm 56.8 \times 10^{-8} & \rho &= 4.63 \\
s_{55}^{E} &= 4.56 \times 10^{-12} & d_{25} &= \pm 46 \times 10^{-8} & & \\
s_{66}^{E} &= 5.76 \times 10^{-12} & d_{36} &= \pm 70.5 \times 10^{-8} & &
\end{aligned} \tag{10.70}$$

For the temperature coefficients all of them are positive and no possibility exists for obtaining a zero temperature coefficient crystal.

$$\begin{aligned}
Ts_{11} &= +7.0 \times 10^{-4}/°\text{C} & Ts_{12} &= +9.3 \times 10^{-4} \\
Ts_{22} &= +6.0 \times 10^{-4} & Ts_{13} &= +11.0 \times 10^{-4} \\
Ts_{33} &= +12.0 \times 10^{-4} & Ts_{23} &= +1.7 \times 10^{-2} \\
Ts_{44}^{E} &= +7.5 \times 10^{-4} & Td_{14} &= +3.5 \times 10^{-4} \\
Ts_{55}^{E} &= +7.0 \times 10^{-4} & Td_{25} &= -3.5 \times 10^{-4} \\
Ts_{66}^{E} &= +6.5 \times 10^{-4} & Td_{36} &= -0.9 \times 10^{-4}
\end{aligned} \tag{10.71}$$

Measurements have been made of sodium ammonium tartrate tetrahydrate that is isomorphous with rochelle salt. It is found that one of the shear elastic constants s_{55}^{E} has a negative temperature coefficient and hence a series of zero temperature coefficient of frequency cuts are possible. However, since, the crystal dehydrates so badly it does not appear likely that this crystal will be of any practical use, although the piezoelectric constant along the y direction is rather large and increases with a lowering of the temperature. The temperature coefficient of d_{25} is too low to indicate any ferroelectric properties above absolute zero in temperature. The measured constants are given in equation (10.72) while the temperature coefficients of these properties are shown by equation (10.73).

$$\begin{aligned}
s_{11} &= 5.70 \times 10^{-12} & s_{12} &= -1.55 \times 10^{-12} & \epsilon_{11}^{T} &= 9.0 \\
s_{22} &= 3.85 \times 10^{-12} & s_{13} &= -2.2 \times 10^{-12} & \epsilon_{22}^{T} &= 8.9 \\
s_{33} &= 4.0 \times 10^{-12} & s_{23} &= -1.55 \times 10^{-12} & \epsilon_{33}^{T} &= 10.0 \\
s_{44}^{E} &= 9.45 \times 10^{-12} & d_{14} &= \pm 57.0 \times 10^{-8} & \rho &= 1.587 \\
s_{55}^{E} &= 33.0 \times 10^{-12} & d_{25} &= \pm 95.0 \times 10^{-8} & & \\
s_{66}^{E} &= 11.5 \times 10^{-12} & d_{36} &= \pm 31.0 \times 10^{-8} & &
\end{aligned} \tag{10.72}$$

For the temperature coefficients, we find

$$
\begin{aligned}
Ts_{11} &= +9.0 \times 10^{-4}/°C & Ts_{23} &= -4.8 \times 10^{-4} \\
Ts_{22} &= +10.5 \times 10^{-4} & Td_{14} &= +2.1 \times 10^{-4} \\
Ts_{33} &= +11.4 \times 10^{-4} & Td_{25} &= -1.9 \times 10^{-3} \\
Ts^{E}_{44} &= +4.4 \times 10^{-4} & Td_{36} &= +12.1 \times 10^{-4} \\
Ts^{E}_{55} &= -18.5 \times 10^{-4} & T\epsilon^{T}_{11} &= +1.0 \times 10^{-4} \\
Ts^{E}_{66} &= +4.6 \times 10^{-4} & T\epsilon^{T}_{22} &= +3.0 \times 10^{-4} \\
Ts_{12} &= +4.8 \times 10^{-4} & T\epsilon^{T}_{33} &= +3.8 \times 10^{-4} \\
Ts_{13} &= +5 \times 10^{-4}
\end{aligned}
\qquad (10.73)
$$

The elastic and piezoelectric constants agree quite well with those measured by Mandell.[11]

10.5 *Crystals of Monoclinic Class*

A total of five crystals, all of the monoclinic sphenoidal class (symmetry C_2 or 2), have been measured. Two of these, the ethylene diamine tartrate (EDT) and dipotassium tartrate (DKT), have already been discussed in Chapter IX. The other three crystals are lithium sulphate monohydrate ($LiSO_4$–H_2O), tartaric acid ($C_4H_6O_6$) and ammonium tartrate ($N_2C_4H_{12}O_6$). Of these crystals lithium sulphate is shown by the International Critical Tables to have the largest pyroelectric constant. It has been pointed out by Dr. Hans Jaffe of the Brush Development Co., that lithium sulphate has one of the highest electromechanical couplings (about 35 per cent) for a thickness longitudinal mode of any non-ferroelectric crystal. This property may be of use in creating high power ultrasonic waves in liquids. Another use of crystals of this class is in obtaining hydrophones or other indicators of static or low-frequency hydrostatic pressure. Up to the present time tourmaline has been the crystal most widely used, but lithium sulphate and tartaric acid are more sensitive than tourmaline. The open-circuit voltage for a hydrostatic pressure is proportional to the ratio

$$V_0 = K \frac{(d_{21} + d_{22} + d_{23})}{\epsilon^{T}_{22}} \qquad (10.74)$$

for these crystals, while for tourmaline the open-circuit voltage normal to

[11] Mandell, W., *Proc. Roy. Soc.*, Vol. 121, pp. 130–140, 1928; *Proc. Roy. Soc.*, Vol. 165, pp. 414–431, 1938.

the z-axis is

$$V_0 = K\left(\frac{d_{31} + d_{33}}{\epsilon_{33}^T}\right) = K\left(\frac{5.5 + 1.03}{5.3}\right) \times 10^{-8}$$
$$= K(1.23 \times 10^{-8}) \tag{10.75}$$

For lithium sulphate and tartaric acid the ratios are respectively

$$(LiSO_4\text{–}H_2O) = K\left(\frac{45.0 + 5.5 - 11.6}{10.3}\right) = K(3.7 \times 10^{-8});$$
$$(C_4H_6O_6) = K\left(\frac{2.3 + 6.3 + 6.5}{4.3}\right) = K(3.5 \times 10^{-8}) \tag{10.76}$$

Hence these crystals are about three times as sensitive as tourmaline and provide an acceptable substitute for this relatively expensive material.

Crystals of this class have 13 elastic constants, 8 piezoelectric constants and 4 dielectric constants. The process of measuring these constants is described completely in a recent paper[12] and was illustrated for the crystal dipotassium tartrate (DKT). The process consists of measuring the properties of four long, thin, oriented crystals cut normal to the x-axis, four cut normal to the z-axis, five cut normal to the y-axis (which is the axis of diagonal symmetry) and four doubly oriented cuts as described below. The equations for the crystals cut normal to the x- and z-axes are the same as for the orthorhombic crystals given by equation (10.60) and (10.62) and from these one can determine

$$s_{11},\ s_{22},\ s_{33},\ s_{44},\ s_{66},\ s_{12},\ s_{23},\ \pm d_{14},\ \pm d_{36},\ \epsilon_{11}^T,\ \epsilon_{33}^T \tag{10.77}$$

by the process described in section 10.4. Crystals cut normal to the y-axis have Young's moduli $1/s_{11}'$ and piezoelectric constants d_{31}' defined by the equations

$$s_{11}^{E'} = s_{33}^E \cos^4\theta + 2s_{35}^E \cos^3\theta \sin\theta + (2s_{13}^E + s_{55}^E) \sin^2\theta \cos^2\theta$$
$$+ 2s_{15}^E \sin^3\theta \cos\theta + s_{11}^E \sin^4\theta \tag{10.78}$$
$$d_{31}' = d_{21} \sin^2\theta + d_{23} \cos^2\theta + d_{25} \sin\theta \cos\theta$$

where θ is the angle between the crystal length and the $+z$-axis measured in a counterclockwise direction. Since there are five constants in the compliance equation, five crystals are cut with their lengths respectively along z, 22.5° from z, 45° from z, 67.5° from z, and along x. The first and last crystals respectively determine s_{33}^E and s_{11}^E and give a check on the values determined from the x- and z-cut crystals. The other three crystals

[12] Mason, W. P., "Properties of Monoclinic Crystals," *Phys. Rev.*, Vol. 70, pp. 705–728, Nov., 1946.

determine s_{15}^E, s_{35}^E and $(2s_{13}^E + s_{55}^E)$ according to the equation

$$\begin{aligned} s_{15}^E &= 3.407 s_{67.5°}^E + 1.414 s_{22.5°}^E - 2.407 s_{45°}^E - .5 s_{33}^E - 1.914 s_{11}^E \\ s_{35}^E &= 3.407 s_{22.5°}^E + 1.414 s_{67.5°}^E - 2.407 s_{45°}^E - .5 s_{11}^E - 1.914 s_{33}^E \\ (2s_{13}^E + s_{55}^E) &= 13.628 s_{45}^E - 9.642(s_{22.5°}^E + s_{67.5°}^E) + 3.828(s_{11}^E + s_{33}^E) \end{aligned} \tag{10.79}$$

where $s_{22.5°}^E$, $s_{45°}^E$, $s_{67.5°}^E$ denote respectively the elastic compliances along the direction 22.5°, 45° and 67.5° from z measured in a counterclockwise direc-

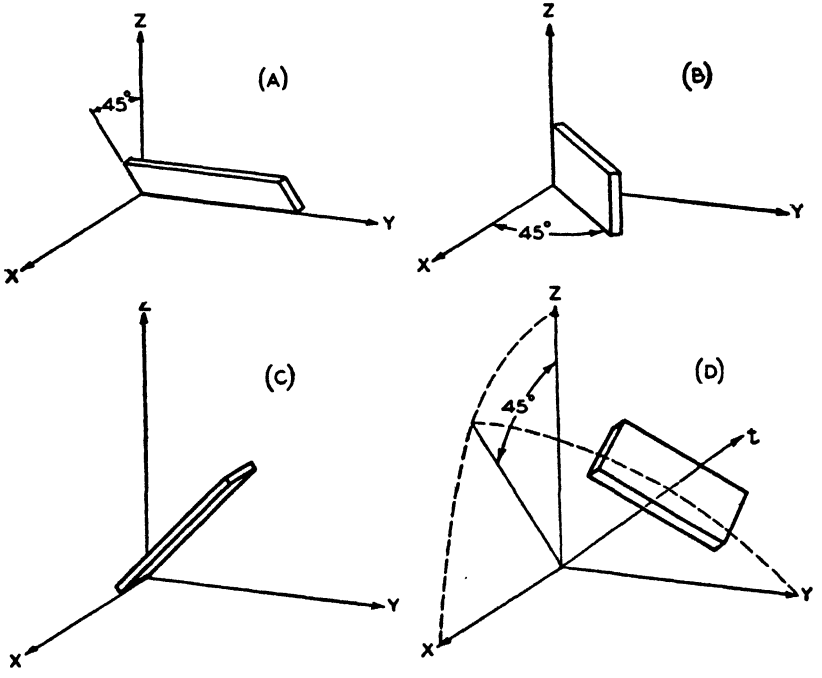

FIG. 10.12. Crystal orientations for measuring constants of monoclinic crystals.

tion. The value of the piezoelectric coupling for the crystals, with its length along x and with its length along z, determines respectively the magnitude of d_{21} and d_{23}. The crystal cut at 45° between x and z, together with the other two, will determine d_{25} according to the equation

$$d_{25} = d_{45°} - (d_{21} + d_{23}) \tag{10.80}$$

The values throughout the entire orientation allow one to determine the signs of d_{23} and d_{25} with respect to d_{21}. To determine an absolute sign, one can resort to squeeze tests which will tell the polarity of the charge on

the surface for a given distortion. The convention is adopted that a positive d constant is one which gives a positive charge along the positive axis when a positive strain (an extension in the case of a longitudinal motion) is exerted on the crystal. Crystals cut normal to the three crystallographic axes and vibrated in longitudinal and face-shear modes will determine 11 of the elastic constants, 5 of the piezoelectric constants and 3 of the 4 dielectric constants. To determine the remaining constants requires four more crystals which are rotated with respect to the crystallographic axes. The ones chosen are (1), a crystal with its length along the y crystallographic axis and its width 45° between the positive x- and y-axes, vibrating in a face-shear mode; (2) a crystal with its width parallel to z and its length 45° between the $+x$- and $+y$-axes vibrating in a longitudinal mode; (3) a crystal with its width parallel to x and its length 45° from $+y$ and $+z$ vibrating in a longitudinal mode, and (4) a double orientation crystal, as shown by Figure 10.12D, $a(y, z, t, w, 45°\ 45°$ crystal) vibrating in a longitudinal mode. By introducing the appropriate direction cosines in equations (5.67), (5.68), (5.69) and (5.72), it can be shown that the elastic, piezoelectric and dielectric constants for these four oblique cuts are

$$\mathrm{O}(x, y, l, +45°) \qquad d'_{14} = \frac{d_{14} + d_{16} - d_{34} - d_{36}}{2}, \qquad \epsilon'^{T}_{11} = \frac{\epsilon^{T}_{11} + 2\epsilon^{T}_{13} + \epsilon^{T}_{33}}{2},$$

$$s^{E'}_{66} = \frac{s^{E}_{66} - 2s^{E}_{46} + s^{E}_{44}}{2} \tag{10.81}$$

$$\mathrm{O}_{-}(y, x, w, +45°), \qquad d'_{31} = -0.3535[d_{21} + d_{22} - d_{16}], \qquad \epsilon'^{T}_{33} = \frac{\epsilon^{T}_{11} + \epsilon^{T}_{22}}{2},$$

$$s'_{11} = \frac{s^{E}_{11} + s^{E}_{22} + 2s^{E}_{12} + s^{E}_{66}}{4} \tag{10.82}$$

$$\mathrm{O}_3(z, y, w, +45°), \qquad d'_{31} = +0.3535[d_{23} + d_{22} - d_{34}], \qquad \epsilon'^{T}_{33} = \frac{\epsilon^{T}_{22} + \epsilon^{T}_{33}}{2}$$

$$s'_{11} = \frac{s^{E}_{22} + s^{E}_{33} + 2s^{E}_{23} + s^{E}_{44}}{4} \tag{10.83}$$

$\mathrm{O}_4(y, z, t, w, +45°, +45°)$,

$$d'_{31} = 0.1768[d_{21} + d_{23} + d_{25} + 2d_{22} - (d_{14} + d_{16} + d_{34} + d_{36})] \tag{10.84}$$

$$\epsilon'^{T}_{33} = \frac{\epsilon^{T}_{11} + \epsilon^{T}_{33} + 2(\epsilon^{T}_{22} + \epsilon^{T}_{13})}{4}; \qquad s'^{E}_{11} = \tfrac{1}{16}[s^{E}_{11} + s^{E}_{33} + (2s^{E}_{13} + s^{E}_{55})]$$

$$+ \tfrac{1}{8}[s^{E}_{15} + s^{E}_{35} + (2s^{E}_{23} + s^{E}_{44}) + (2s^{E}_{12} + s^{E}_{66})] + \tfrac{1}{4}[s^{E}_{22} + s^{E}_{25} + s^{E}_{46}] \tag{10.85}$$

The first crystal allows one to determine ϵ_{13}^{T}, s_{46}^{E} and gives one relation between four of the piezoelectric constants. The second crystal does not give any new dielectric or elastic data, but gives a second relation between three of the piezoelectric constants d_{21}, d_{22} and d_{16}. The third gives a third piezoelectric relation between d_{23}, d_{22} and d_{34}, while the fourth determines the elastic constant s_{25}^{E} and gives a fourth relation between the piezoelectric constants. To complete the piezoelectric constant determination, one thickness mode has to be measured, and usually the longitudinal thickness mode along y is chosen on account of its interest for producing high-frequency vibrations. This determines the magnitude of d_{22}. Squeeze tests are then used to determine the sign, the test consisting of compressing a crystal in the y direction, one side of which is connected to the grid of an electrometer tube. By the direction in which the plate current changed, the sign of the charge on the surface touching the grid is determined. By pressing this same crystal along the x- and z-axes, the signs of the constants d_{21} and d_{23} can be determined.

The measurements on these 14 crystals cut normal to the crystallographic axes and the four oblique cuts, together with the squeeze tests, determine uniquely all of the constants of the crystal. However, one of these crystals, the crystal cut normal to y and vibrated in a face-shear mode, is a coupled-mode type of vibration. As shown in Chapter V, equation (5.62), with the axes rotated to correspond to a Y-cut crystal with its length along x, the elastic constant controlling the resonant frequency of the face-shear mode is

$$f_R = \frac{1}{2l_w}\sqrt{\frac{c_{11}^{C,E} + c_{55}^{C,E} - \sqrt{(c_{11}^{C,E} - c_{55}^{C,E})^2 + 4c_{15}^{C,E^2}}}{2\rho}} \tag{10.86}$$

where $c_{11}^{C,E}$, $c_{55}^{C,E}$ and $c_{15}^{C,E}$ are the contour clamped elastic constants. These are related to s_{ij}^{E} constants by the equation

$$c_{ij}^{C,E} = \frac{(-1)^{k+l}\Delta^{kl}}{\Delta} \quad (k, l = 1, 2, 3) \tag{10.87}$$

where Δ is the determinant

$$\Delta = \begin{vmatrix} s_{11}^{E} & s_{13}^{E} & s_{15}^{E} \\ s_{13}^{E} & s_{33}^{E} & s_{35}^{E} \\ s_{15}^{E} & s_{35}^{E} & s_{55}^{E} \end{vmatrix}$$

and Δ^{kl} is the determinant obtained from Δ by suppressing the kth row and lth column. Since all the s_{ij}^{E} values have been determined but s_{55}^{E}, the two relations can be solved simultaneously for s_{55}^{E} and all of the elastic constants can be determined.

The constants measured at 25°C for lithium sulphate monohydrate ($LiSO_4$–H_2O) are, for a left-handed crystal, $\rho = 2.06$, dielectric constants and temperature coefficients

$$\begin{aligned}
\epsilon_{11}^T &= 5.6 & T\epsilon_{11}^T &= +7.8 \times 10^{-4}/°C \\
\epsilon_{33}^T &= 6.5 & T\epsilon_{33}^T &= +1.6 \times 10^{-4} \\
\epsilon_{22}^T &= 10.3 & T\epsilon_{33}^T &= +4.7 \times 10^{-4} \\
\epsilon_{13}^T &= .07 & T\epsilon_{13}^T &= -4.0 \times 10^{-3}
\end{aligned} \tag{10.88}$$

PIEZOELECTRIC CONSTANTS AND TEMPERATURE COEFFICIENTS

$$\begin{aligned}
d_{14} &= +14.0 \times 10^{-8} & Td_{14} &= +3.6 \times 10^{-3}/°C \\
d_{16} &= -12.5 \times 10^{-8} & Td_{16} &= +4.5 \times 10^{-4} \\
d_{21} &= +11.6 \times 10^{-8} & Td_{21} &= +3.2 \times 10^{-3} \\
d_{22} &= -45.0 \times 10^{-8} & Td_{22} &= -1.5 \times 10^{-4} \\
d_{23} &= -5.5 \times 10^{-8} & Td_{23} &= -6.1 \times 10^{-4} \\
d_{25} &= +16.5 \times 10^{-8} & Td_{25} &= -2.2 \times 10^{-3} \\
d_{34} &= -26.4 \times 10^{-8} & Td_{34} &= -0.4 \times 10^{-4} \\
d_{36} &= +10.0 \times 10^{-8} & Td_{36} &= +3.6 \times 10^{-3}
\end{aligned} \tag{10.89}$$

ELASTIC CONSTANTS AND TEMPERATURE COEFFICIENTS

$$\begin{aligned}
s_{11}^E &= 2.39 \times 10^{-12}\ \text{cm}^2/\text{dyne} & Ts_{11}^E &= +7.2 \times 10^{-4}/°C \\
s_{22}^E &= 2.13 \times 10^{-12} & Ts_{22}^E &= +5.2 \times 10^{-4} \\
s_{33}^E &= 2.31 \times 10^{-12} & Ts_{33}^E &= -0.24 \times 10^{-4} \\
s_{44}^E &= 3.69 \times 10^{-12} & Ts_{44}^E &= +2.5 \times 10^{-4} \\
s_{55}^E &= 4.1 \times 10^{-12} & Ts_{55}^E &= +5.0 \times 10^{-4} \\
s_{66}^E &= 7.40 \times 10^{-12} & Ts_{66}^E &= +4.2 \times 10^{-4} \\
s_{12}^E &= -0.95 \times 10^{-12} & Ts_{12}^E &= +1.6 \times 10^{-3} \\
s_{13}^E &= -0.5 \times 10^{-12} & Ts_{13}^E &= +5.0 \times 10^{-4} \\
s_{23}^E &= -0.36 \times 10^{-12} & Ts_{23}^E &= 0 \\
s_{15}^E &= +0.71 \times 10^{-12} & Ts_{15}^E &= -1.5 \times 10^{-4} \\
s_{25}^E &= -1.20 \times 10^{-12} & Ts_{25}^E &= -6.0 \times 10^{-4} \\
s_{35}^E &= +0.05 \times 10^{-12} & Ts_{35}^E &= -1.0 \times 10^{-2} \\
s_{46}^E &= -0.41 \times 10^{-12} & Ts_{46}^E &= -8.0 \times 10^{-4}
\end{aligned} \tag{10.90}$$

For tartaric acid ($C_4H_6O_6$) the measured constants and temperature coefficients become

$$\rho = 1.760$$

DIELECTRIC CONSTANTS AND TEMPERATURE COEFFICIENTS

$$\begin{aligned} \epsilon_{11}^T &= 4.3 & T\epsilon_{11}^T &= +2.6 \times 10^{-4}/°C \\ \epsilon_{22}^T &= 4.3 & T\epsilon_{22}^T &= +2.6 \times 10^{-4} \\ \epsilon_{33}^T &= 4.5 & T\epsilon_{33}^T &= +1.9 \times 10^{-4} \\ \epsilon_{13}^T &= 0.55 & T\epsilon_{13}^T &= +12.0 \times 10^{-4} \end{aligned} \tag{10.91}$$

PIEZOELECTRIC CONSTANTS AND TEMPERATURE COEFFICIENTS

$$\begin{aligned} d_{14} &= +24 \times 10^{-8} & Td_{14} &= -6.0 \times 10^{-4}/°C \\ d_{16} &= +15.8 \times 10^{-8} & Td_{16} &= -5.0 \times 10^{-4} \\ d_{21} &= -2.3 \times 10^{-8} & Td_{21} &= +9.6 \times 10^{-4} \\ d_{22} &= -6.5 \times 10^{-8} & Td_{22} &= +2 \times 10^{-4} \\ d_{23} &= -6.3 \times 10^{-8} & Td_{23} &= +5.3 \times 10^{-4} \\ d_{25} &= +1.1 \times 10^{-8} & Td_{25} &= +2.5 \times 10^{-4} \\ d_{34} &= -32.4 \times 10^{-8} & Td_{34} &= +1.0 \times 10^{-4} \\ d_{36} &= +35.0 \times 10^{-8} & Td_{36} &= -0.65 \times 10^{-4} \end{aligned} \tag{10.92}$$

ELASTIC CONSTANTS AND TEMPERATURE COEFFICIENTS

$$\begin{aligned} s_{11}^E &= 2.16 \times 10^{-12} & s_{25}^E &= +2.76 \times 10^{-12} \\ s_{22}^E &= 7.7 \times 10^{-12} & s_{35}^E &= -2.9 \times 10^{-12} \\ s_{33}^E &= 3.85 \times 10^{-12} & s_{46}^E &= -1.64 \times 10^{-12} \\ s_{44}^E &= 12.6 \times 10^{-12} & Ts_{11}^E &= +3.9 \times 10^{-4}/°C \\ s_{55}^E &= 17.5 \times 10^{-12} & Ts_{22}^E &= +10.8 \times 10^{-4} \\ s_{66}^E &= 9.62 \times 10^{-12} & Ts_{33}^E &= +6.7 \times 10^{-4} \\ s_{12}^E &= -0.61 \times 10^{-12} & Ts_{44}^E &= +5.3 \times 10^{-4} \\ s_{13}^E &= -1.5 \times 10^{-12} & Ts_{55}^E &= +1.5 \times 10^{-4} \\ s_{23}^E &= -1.8 \times 10^{-12} & Ts_{66}^E &= +4.1 \times 10^{-4} \\ s_{15}^E &= +2.8 \times 10^{-12} & Ts_{12}^E &= +0.9 \times 10^{-4} \end{aligned} \tag{10.93}$$

$$
\begin{aligned}
Ts_{13}^E &= -4 \times 10^{-3} & Ts_{25}^E &= +3.0 \times 10^{-3} \\
Ts_{23}^E &= +3.8 \times 10^{-3} & Ts_{35}^E &= -5.2 \times 10^{-4} \\
Ts_{13}^E &= +2.6 \times 10^{-3} & Ts_{46}^E &= +3.2 \times 10^{-3}
\end{aligned} \tag{10.93}
$$

For ammonium tartrate ($N_2C_4H_{12}O_6$) only partial determinations have been made since the measured couplings were small. Only the crystals cut normal to the three crystallographic axes were made and these determine the values

$$\rho = 1.601$$

DIELECTRIC CONSTANTS AND TEMPERATURE COEFFICIENTS

$$
\begin{aligned}
\epsilon_{11}^T &= 6.45 & T\epsilon_{11}^T &= +3.5 \times 10^{-4}/°C \\
\epsilon_{22}^T &= 6.8 & T\epsilon_{22}^T &= +7.4 \times 10^{-4} \\
\epsilon_{33}^T &= 6.0 & T\epsilon_{33}^T &= +2.8 \times 10^{-4}
\end{aligned} \tag{10.94}
$$

PIEZOELECTRIC CONSTANTS AND TEMPERATURE COEFFICIENTS[13]

$$
\begin{aligned}
d_{14} &= \pm 14.6 \times 10^{-8} & Td_{14} &= -5 \times 10^{-4}/°C \\
d_{23} &= +17.5 \times 10^{-8} & Td_{23} &= +5.6 \times 10^{-4} \\
d_{21} &= +2.0 \times 10^{-8} & Td_{21} &= -3.2 \times 10^{-3} \\
d_{25} &= -3.0 \times 10^{-8} & Td_{25} &= -2.3 \times 10^{-3} \\
d_{36} &= \pm 8.8 \times 10^{-8} & Td_{36} &= -6.10^{-4}
\end{aligned} \tag{10.95}
$$

ELASTIC CONSTANTS AND TEMPERATURE COEFFICIENTS

$$
\begin{aligned}
s_{11}^E &= 3.60 \times 10^{-12} & Ts_{11}^E &= +7.4 \times 10^{-4}/°C \\
s_{22}^E &= 3.71 \times 10^{-12} & Ts_{22}^E &= +3.5 \times 10^{-4} \\
s_{33}^E &= 3.50 \times 10^{-12} & Ts_{33}^E &= +4.6 \times 10^{-4} \\
s_{44}^E &= 18.5 \times 10^{-12} & Ts_{44}^E &= +9.0 \times 10^{-4} \\
s_{66}^E &= 8.50 \times 10^{-12} & Ts_{66}^E &= +6.5 \times 10^{-4} \\
s_{12}^E &= -1.2 \times 10^{-12} & Ts_{12}^E &= +6.8 \times 10^{-4} \\
s_{23}^E &= +0.35 \times 10^{-12} & Ts_{23}^E &= -4.2 \times 10^{-3}
\end{aligned} \tag{10.96}
$$

[13] Piezoelectric constants of these three monoclinic crystals are given in reference 9, and the piezoelectric constants and part of the elastic constants have been measured by Dr. Hans Jaffe, Bruch Co. report No. W-28-003 to U. S. Signal Corps. All three sets of piezoelectric constants agree closely and for ammonium tartrate Spitzer and Jaffe have shown that the largest piezoelectric constant is d_{22} having a value of $+26.0 \times 10^{-8}$. This results in an electromechanical coupling factor of 20 percent for a thickness Y-cut crystal.

10.6 *Possible Ferroelectric Properties in Crystals Measured*

Of the crystals measured over a wide temperature range, the only ones (besides rochelle salt and KDP) that have high enough temperature coefficients of piezoelectric constants to indicate possible ferroelectric effects above absolute zero, or below the transition temperatures of the crystals, are sodium chlorate and bromate (investigated in section 10.1),

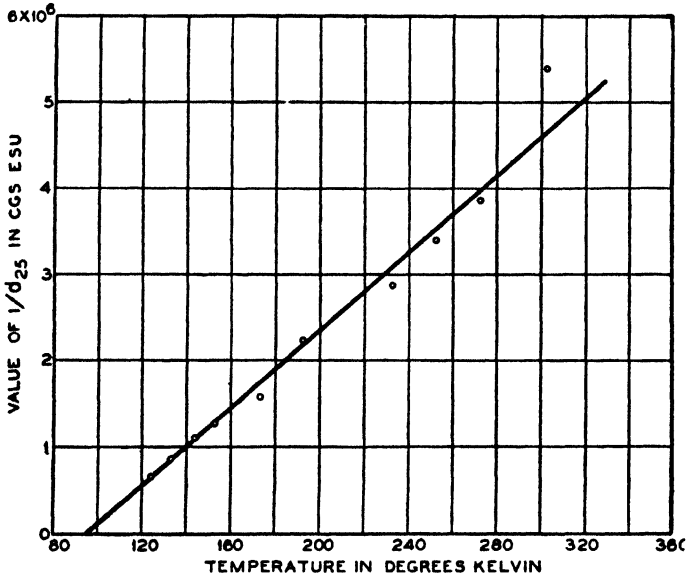

FIG. 10.13. Value of $1/d_{25}$ plotted against temperature for lithium ammonium tartrate.

ethylene diamine tartrate (EDT) and lithium ammonium tartrate. For the latter two the piezoelectric constants d_{21} and d_{25} respectively increase markedly as the temperature is lowered.

In searching for ferroelectric properties in crystals, the two most prominent characteristics are large variations with temperature of the dielectric constants and the piezoelectric constants d_{ij}. As shown in the next chapter, the clamped dielectric constant and hence also the "free" dielectric constant for a ferroelectric crystal, outside of its ferroelectric region, satisfies approximately a Curie-Weiss law of the type

$$\epsilon = \epsilon_0 + \frac{C}{T - T_0} \tag{10.97}$$

where T_0 is a Curie temperature, *i.e.* a temperature for which the dielectric

constant becomes very large and for which a spontaneous polarization occurs.

Since the d piezoelectric constants satisfy the tensor equation

$$d_{nkl} = g_{mkl} \frac{\epsilon^T_{mn}}{4\pi} \tag{10.98}$$

and since the g piezoelectric constants have been found to change only very slightly with temperature, it is obvious that the d piezoelectric constants will become large in the neighborhood of a Curie temperature.

If we plot $1/d_{25}$ for lithium ammonium tartrate as a function of temperature, the curves of Fig. 10.13 result. The curve for EDT has been taken down to the temperature of 120°K, and if we extrapolate the curve down to absolute zero, it does not appear that EDT would become ferroelectric. However, the curve for lithium ammonium tartrate is quite straight over the range −150° to 80° (123°K to 353°K) and if extended down would indicate a Curie temperature or some transition effect at about 94°K. No further measurements have been made for this crystal at lower temperatures since the systems available did not give a lower temperature.

CHAPTER XI

Theory of Ferroelectric Crystals

A ferroelectric type of a crystal is one which exhibits a spontaneous polarization in one or more directions of the crystal over a definite temperature range. The phenomena associated with a ferroelectric crystal are a polarization field curve that occurs in the form of a hysteresis loop, a strain field curve that also occurs in a loop, and a wide variation of the principal properties of the crystal as a function of temperature.

Considerable progress has been made in the last few years in analyzing the properties of ferroelectric types of crystals and in locating the causes of the ferroelectric anomalies. As shown by the data of Chapters VII, VIII, and X, if we plot the piezoelectric stress or strain of the crystal as a function of the electric displacement or the polarization of the crystal, a single-valued function results, or in other words, the strain was a double-valued function of the field because the electric displacement and polarization were double-valued functions of the field. In particular, it has been found that if one plots the piezoelectric stress as a function of the dipole polarization, a constant ratio f_{ij} is obtained. Not much progress has been made in calculating the ratio f_{ij} from the atomic arraignments of the crystal lattice. The only attempt is that of Born[1] and the results do not agree with experiment closer than a factor of about 10.

If, however, we determine the piezoelectric constant h_{ij} (or f_{ij}) experimentally, considerable progress can be made in determining the remaining properties and relating them to the atomic structure. For example, the "free" dielectric constant measured at low frequencies is the sum of the "clamped" dielectric constant, *i.e.*, the dielectric constant when no strain exists in the crystal, plus a dielectric constant which represents the energy stored in the mechanical strain of the crystal. By measuring the piezoelectric constants and the elastic constants of the crystal, the dielectric constant due to mechanical strain can be evaluated and the clamped dielectric constant can be determined uniquely. Another method for determining the clamped dielectric constant is to measure the dielectric constant at frequencies much higher than the fundamental resonances and their

[1] Born, Max, "Atomtheorie des festen Zustandes," B. G. Teubner, Leipzig and Berlin, 1923.

principal harmonics. At these frequencies no energy can be stored in mechanical vibrations, since such vibrations cannot be excited and, as shown by Fig. 7.8, the " clamped " dielectric constants determined by these two methods agree quite well.

All the anomalies of a ferroelectric crystal reside in the clamped dielectric constant. This is shown by the fact that the piezoelectric constant f_{14}, which measures the ratio of the piezoelectric stress to the dipole polarization, does not show any change at the ferroelectric temperatures nor do the elastic constants measured at constant electric displacement (except for a minute change discussed in the appendix, which can be related to a second order effect). Furthermore, as shown by Fig. 7.8, the " clamped " dielectric constant as measured at high frequencies, has a maximum at the Curie temperature of the " free " dielectric constant. One can still change the " clamped " dielectric constant by putting on a steady stress such as a hydrostatic pressure, but this corresponds to a new grouping of the molecules. For the new state, the " free " dielectric constant Curie temperatures measured at low frequencies and the temperature of the maximum value of the " clamped " dielectric constant measured at very high frequencies should still coincide. Hence, in order to understand the properties of a ferroelectric type of crystal, one has to understand the clamped dielectric constant of the crystal. It is possible to incorporate all of the properties in a single theory, as discussed in Section 11.5, but it is more instructive to consider first the clamped dielectric constant.

There are three separate types of ferroelectric crystals that have so far been found — the rochelle salt type, the potassium dihydrogen phosphate, and the barium titanate type. The rochelle salt type has a range of temperatures for which it is ferroelectric and upper and lower Curie points that mark the separation temperatures between the ferroelectric regions and the non-ferroelectric regions. Potassium dihydrogen phosphate on the other hand has a single Curie temperature. The crystal is ferroelectric from absolute zero up to a temperature of 121°K, above which it becomes non-ferroelectric. Barium titanate is another ferroelectric crystal which is capable of becoming ferroelectric in any one of three directions. It has an upper Curie temperature at 120°C and has two transitions between this temperature and absolute zero, as shown[2] by the X-ray measurements of Miss Megaw, and the dielectric constant measurements. These transitions are due to the crystal becoming ferroelectric in two and three directions, simultaneously.

Using a crystal structure determination of rochelle salt made by Beevers and Hughes, a theory of the ferroelectric effect and the clamped dielectric

[2] Megaw, H. D., *Proc. Roy. Soc.*, Vol. 189, pp. 261–283, April, 1947.

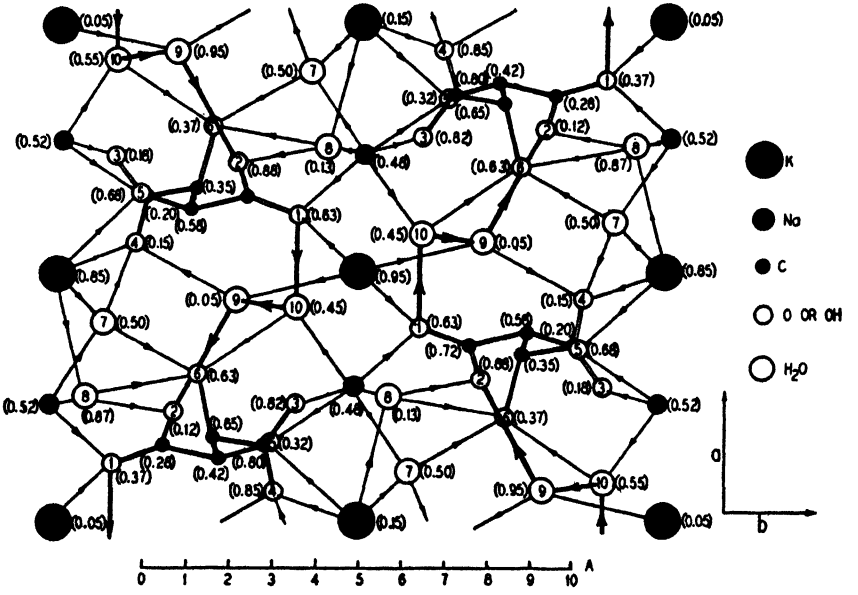

FIG. 11.1. Projection on (001) plane, of the structure of rochelle salt. The bonds involved in the 1-2-9-10 chains are drawn thick, so that the chains can be picked out.

Table of Coordinates

		$x = a$	$y = b$	$z = c$
2K on (a)		0.00	0.00	0.05
2K on (b)		0.00	0.50	0.15
4Na on		0.23	0.99	0.52
4O on	(1)	0.12	0.10	0.37
4O on	(2)	0.22	0.20	0.12
4O on	(3)	0.23	0.40	0.82
4O on	(4)	0.06	0.37	0.85
4OH on	(5)	0.16	0.36	0.32
4OH on	(6)	0.29	0.24	0.63
$4H_2O$ on	(7)	0.40	0.08	0.50
$4H_2O$ on	(8)	0.25	0.05	0.87
$4H_2O$ on	(9)	0.44	0.30	0.05
$4H_2O$ on	(10)	0.42	0.40	0.45
4C on		0.15	0.18	0.28
4C on		0.12	0.28	0.42
4C on		0.17	0.27	0.65
4C on		0.15	0.35	0.80

constant of rochelle salt has been developed by the writer[3] which appears to account quantitatively for the principal properties of rochelle salt. This is discussed in section 11.1. For potassium dihydrogen phosphate, the connection with the crystal structure appears to be as given in a theory of Slater as modified by Bardeen. For both cases the ferroelectric dipole is one associated with the motion of the hydrogen nucleus along a hydrogen bond. For barium titanate, a three dimensional structure involving 6 equilibrium positions for the titanium nucleus, appears to be responsible for the ferroelectric effect.

The structure of rochelle salt according to Beevers and Hughes[4,5] is shown by Fig. 11.1. There are three possible hydrogen bonds in the structure, between the oxygen molecule 1 and the water molecule 10, between the water molecule 10 and the water molecule 9, and between the water molecule 9 and the oxygen 2. The distance between the successive molecules are 1 to 10, 2.59Å; 9 to 10 is 2.86Å; and 9 to 2 = 3.02Å. The bond with the shortest distance is 1 to 10 (2.59Å) and it is the motion of the hydrogen nucleus along this bond that causes the ferroelectric effect in rochelle salt. This bond lies nearly along the x-axis (x-coordinate = 2.35Å, y-coordinate = 0; z-coordinate = 1.09Å) which is the ferroelectric axis of the crystal. The theory discussed in the next section is based on the action of this hydrogen bond and leads to a ferroelectric effect having the right value of spontaneous polarization, two Curie temperatures, a good quantitative agreement with the measured values of the clamped dielectric constant, and agrees well with recent measurements which show that the dipole dielectric constant is relaxed at a frequency of about 5×10^8 cycles.

11.1 *Ferroelectric Effect in Rochelle Salt*

According to the present theory, the ferroelectric effect is due to the motions of the hydrogen neuclei in the 1–10 hydrogen bonds. Since this is a bond between a water molecule and an oxygen ion, there is no reason to expect that the bond is symmetric and hence we assume a potential field of the type shown by Fig. 11.2B. Two of the 1–10 bonds are directed

[3] "Theory of the Ferroelectric Effect and Clamped Dielectric Constant of Rochelle Salt," *Phys. Rev.*, Vol. 72, No. 9, Nov. 1, 1947, and letter to editor, *Phys. Rev.*, Vol. 72, No. 10, Nov. 15, 1947.

[4] Beevers, C. A., and W. Hughes, "The Crystal Structure of Rochelle Salt, Sodium Potassium Tartrate Tetrahydrate ($NaKC_4H_4O_6$–$4H_2O$)," *Proc. Royal Soc.*, Vol. 177, pp. 251–259, 1941.

[5] Ubbelohde, A. R., and I. Woodward, "Structure and Thermal Properties of Crystals, VI, The Role of Hydrogen Bonds in Rochelle Salt," *Proc. Roy. Soc.*, Vol. 185, pp. 448–465, 1946.

in one direction from 10 to 1 along the plus x-axis, and will be referred to as bonds of type 1, while the other two are directed from 1 to 10 along the minus x-axis and will be referred to as bonds of type 2. This results in having two sets of potential wells, as shown in Fig. 11.2B. The dissymmetry between the two potential minima is called 2Δ; the height of the potential barrier from the mid-position is called ΔU, and the separation between the two potential minima is called δ. Now according to ele-

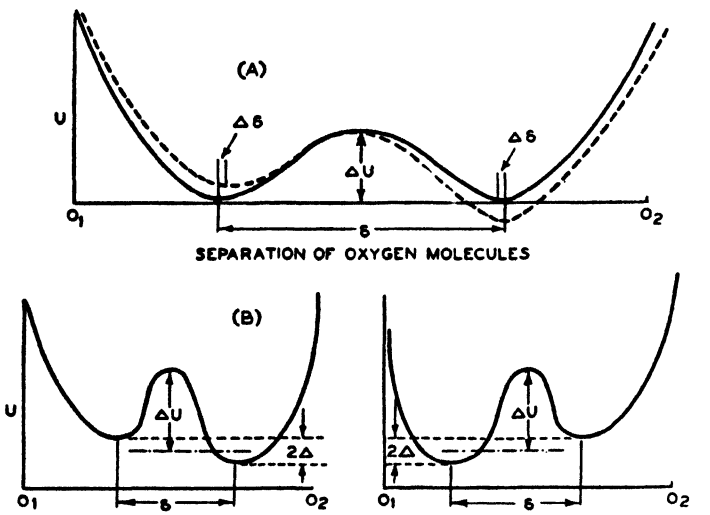

FIG. 11.2. Possible potential well distributions on 1–10 bond. A. Potential well distribution if 1 and 10 are equivalent. B. Potential well distributions if 1 and 10 are not equivalent.

mentary kinetic theory, the probability of a nucleus in one potential well jumping to the other potential well per unit of time is

$$\alpha = \Gamma e^{-\Delta U/kT} \tag{11.1}$$

where Γ is a constant. (In Eyring's reaction rate theory Γ is an infrared frequency substantially equal to kT/h.) Let α_{12} be the probability of a particle jumping in the plus x direction per unit of time and α_{21} the probability of its jumping in the negative direction. For the first bond, N_1 is the population in the first minimum per cc, and N_2 that in the second. For the first bond we have the relation:

$$N_1 + N_2 = \frac{N}{2}; \qquad P_{d_1} = [-N_1 + N_2]\mu \tag{11.2}$$

where μ is the dipole moment per molecule. If the hydrogen nucleus is in the center between the two oxygens, the bond is neutral and no dipole

moment exists. If the nucleus is moved a distance $\delta/2$ from the center, the dipole moment is $e\delta/2$ where e is the electronic charge 4.80×10^{-10} esu and this has been taken as the dipole moment of each molecule. (Actually the dipole moment is probably less than this due to opposing polarization induced in the oxygens, but this effect is neglected.) Since the bond is at an angle of 25° from the x-axis, $\mu = \frac{e\delta}{2} \cos 25°$.

The rate at which the dipole polarization changes with time in the first bond is

$$\frac{dP_{d_1}}{dt} = [N_1\alpha_{12} - N_2\alpha_{21}]\mu = \frac{N\mu}{4}[\alpha_{12} - \alpha_{21}] - \frac{P_{d_1}}{2}[\alpha_{12} + \alpha_{21}] \quad (11.3)$$

upon introducing the results of equation (11.2). Hence the rate of change of polarization is the number of molecules in the wells along the negative direction times their probability of jumping to the positive wells minus the reverse reaction, all multiplied by the dipole moment μ. Now suppose that we put on a field E. This is going to change the potential wells, as shown by the dotted line of Fig. 11.2. There is a change $\Delta\delta$, in the position of the minima and a change in the potential barriers that the molecules have to surmount to reach the other potential minima. The changes in the positions of the potential minima do not depend on temperature and the polarization caused by them can be combined with that caused by displacements of atoms and electrons. The dipole polarization which results from the passage of the hydrogen nuclei over the potential barriers is controlled by the height of the barriers

$$\Delta U - \Delta - \tfrac{1}{2}Fe\delta \quad \text{and} \quad \Delta U + \Delta + \tfrac{1}{2}Fe\delta \quad (11.4)$$

where F is the internal field, e the electronic charge, and δ the separation of the two wells. When we establish a field E and change the polarization, there will be an internal field of the Lorentz type given by the equation

$$F = E + \beta P$$

where β is $4\pi/3$ for an isotropic medium, but may differ from $4\pi/3$ for a crystal. It has long been recognized that this equation is only a very rough approximation since the contributions to a field from various portions in the unit cell are not going to be the same. Slater[6] in his discussion of potassium dihydrogen phosphate allows F to be proportional to E with a factor of proportionality that varies with position in the unit cell. Busch[7]

[6] Slater, J. C., "Theory of the Transition in KH_2PO_4," *J. Chem. Phys.*, Vol. 9, 1633 (1941).

[7] Busch, George, "Neue Seignette Elektrika," *Helv. Phys. Acta*, Vol. II, No. 3 (1938).

on the other hand regards the total polarization as the most constant quantity, and says that the local field may be different when it is acting on the electronic and atomic polarization P_E, than it is when acting on dipole polarization P_d. Busch's two equations are then

$$F_E = E + \beta_e P; \quad F_d = E + \beta_d P$$

A more plausible case can be made out for considering that the local field is the sum of a contribution due to the electronic and atomic polarization and a contribution due to the dipole polarization, as in the equation used in discussing solutions.[8] Hence

$$F = E + \beta_e P_E + \beta_d P_d$$

The electronic and atomic polarization can be considered as randomly distributed so that β_e should equal $4\pi/3$. However, the dipole polarization is not randomly distributed and its effect on the local field may be less than $4\pi/3$ due to shielding by neighboring oxygens.

Letting $\beta_e = 4\pi/3$ and $\beta_d = \beta$ a constant that may vary from crystal to crystal and in all cases will be less than $4\pi/3$, and setting P_E proportional to the local field

$$F = E + \frac{4\pi}{3} P_E + \beta P_d = E + \frac{4\pi}{3} \gamma F + \beta P_d \text{ or } F = \frac{E + \beta P_d}{1 - \frac{4\pi}{3}\gamma} \quad (11.5)$$

where γ is the polarizability per unit volume due to all polarization except that of the hydrogen dipoles. The value of γ can be determined by measuring the dielectric constant at absolute zero for then the dipole polarization is equal to zero. Then

$$P_E = \gamma F = \frac{\gamma E}{1 - \frac{4\pi}{3}\gamma}$$

The dielectric constant ϵ_0 for this case is the ratio of electric displacement to field or

$$\epsilon_0 = \frac{D}{E} = \frac{4\pi P_E + E}{E} = 1 + \frac{4\pi\gamma}{1 - \frac{4\pi}{3}\gamma}$$

Hence

$$\frac{\epsilon_0 - 1}{4\pi} = \frac{\gamma}{1 - \frac{4\pi}{3}\gamma}. \quad (11.6)$$

[8] VanVleck, J. H., "The Theory of Electric and Magnetic Susceptibilities," Oxford Univ. Press, 1932, page 57.

The total polarization is

$$P = P_E + P_d = \frac{\gamma[E + \beta P_d]}{1 - \frac{4\pi}{3}\gamma} + P_d = \frac{(\epsilon_0 - 1)}{4\pi} E + P_d \left[1 + \frac{\gamma\beta}{1 - \frac{4\pi}{3}\gamma} \right]$$

This shows that any measured dipole polarization, such for example that determined by a hysteresis loop, is the internal dipole polarization enhanced by the electronic polarization caused by the dipole polarization. The measured dipole polarization is equal to

$$P_d' = P_d \left[1 + \beta \left(\frac{\epsilon_0 - 1}{4\pi} \right) \right] \tag{11.7}$$

The dielectric constant then is given by

$$\epsilon = \frac{D}{E} = \epsilon_0 + \frac{4\pi P_d}{E} \left[1 + \beta \left(\frac{\epsilon_0 - 1}{4\pi} \right) \right] \tag{11.8}$$

To determine the internal dipole polarization, one can substitute the value of F in the expression for the potential barriers (11.4) and have

$$\begin{aligned} \alpha_{12} &= \Gamma e^{-\left[\Delta U - \Delta - \frac{e\delta \cos 25^\circ}{2[1-(4\pi/3)\gamma]}(E+\beta P_d)\right]/kT} \\ \alpha_{21} &= \Gamma e^{-\left[\Delta U + \Delta + \frac{e\delta \cos 25^\circ}{2[1-(4\pi/3)\gamma]}(E+\beta P_d)\right]/kT} \end{aligned} \tag{11.9}$$

Introducing these values in equations (11.3) and employing the abbreviation

$$A = \frac{e^2\delta^2\beta N \cos^2 25^\circ}{4kT\left[1 - \frac{4\pi}{3}\gamma\right]} = \frac{\mu^2\beta N}{kT\left[1 - \frac{4\pi}{3}\gamma\right]} \tag{11.10}$$

the equations for the dipole polarization of the first set of bonds becomes:

$$\frac{1}{\Gamma}\frac{dP_{d_1}}{dt} e^{\Delta U/kT} = \frac{N\mu}{2} \sinh\left[\frac{\Delta}{kT} + A\left(\frac{E + \beta P_d}{\beta N\mu}\right)\right] - P_{d_1} \cosh\left[\frac{\Delta}{kT} + A\left(\frac{E + \beta P_d}{\beta N\mu}\right)\right]$$

In a similar manner the equation for the second set is:

$$\frac{1}{\Gamma}\frac{dP_{d_2}}{dt} e^{\Delta U/kT} = \frac{N\mu}{2} \sinh\left[-\frac{\Delta}{kT} + A\left(\frac{E + \beta P_d}{\beta N\mu}\right)\right] - P_{d_2} \cosh\left[\frac{-\Delta}{kT} + A\left(\frac{E + \beta P_d}{\beta N\mu}\right)\right] \tag{11.11}$$

These two equations determine all the ferroelectric and dielectric properties of the crystal.

For static conditions, we can set $dP_1/dt = dP_2/dt = 0$ and solve directly for P_{d_1} and P_{d_2}. Adding these

$$P_d = P_{d_1} + P_{d_2} = \frac{N\mu}{2}\left\{\tanh\left[\frac{\Delta}{kT} + A\left(\frac{E + \beta P_d}{\beta N\mu}\right)\right] + \tanh\left[\frac{-\Delta}{kT} + A\left(\frac{E + \beta P_d}{\beta N\mu}\right)\right]\right\} \quad (11.12)$$

Combining these by the formulae for the addition of hyperbolic functions, this can be reduced to

$$P_d = N\mu\left\{\frac{\sinh A\left(\frac{E + \beta P_d}{\beta N\mu}\right)\cosh A\left(\frac{E + \beta P_d}{\beta N\mu}\right)}{\cosh^2\frac{\Delta}{kT} + \sinh^2\left[A\left(\frac{E + \beta P_d}{\beta N\mu}\right)\right]}\right\} \quad (11.13)$$

Setting the field E equal to zero, this equation becomes

$$\frac{P_d}{N\mu} = \frac{\sinh\frac{AP_d}{N\mu}\cosh\frac{AP_d}{N\mu}}{\cosh^2\frac{\Delta}{kT} + \sinh^2\frac{AP_d}{N\mu}} \quad (11.14)$$

The easiest case to discuss, and one which applies for KDP described in the next section, is the one where Δ the dissymmetry is equal to zero. For this case equation (11.14) reduces to the simple form

$$\frac{P_d}{N\mu} = \tanh\frac{AP_d}{N\mu} \quad (11.15)$$

If the factor A is greater than 1, this equation will have real positive and negative solutions other than zero, representing spontaneous polarization along the $+x$ or $-x$ directions. For values of A slightly greater than unity, we can replace $\tanh(AP_d/N\mu)$ by the first two terms of the expressions, or

$$P_d/N\mu = A(P_d/N\mu) - \frac{A^3(P_d/N\mu)^3}{3}$$

Solving for $P_d/N\mu$, we have (11.16)

$$P_d/N\mu = \sqrt{\frac{3(A-1)}{A^3}}$$

A plot of this equation is given by Fig. 11.3, solid line. The effect of the dissymmetry is principally to change the value of A for which the ferroelectric effect can occur. Very close to the ferroelectric temperature,

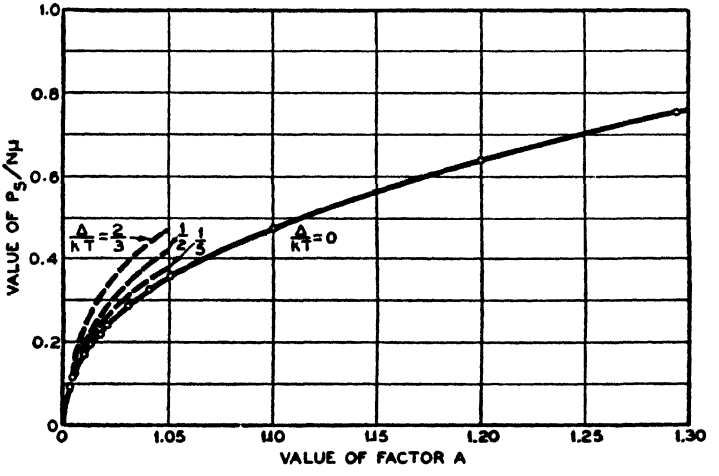

FIG. 11.3. Ratio of spontaneous polarization P_s to maximum dipole polarization $N\mu$ as a function of A and A'.

$P_d/N\mu$ is going to be small and $\cosh \frac{AP_d}{N\mu} \to 1$, $\sinh^2 \frac{AP_d}{N\mu} \to \left(\frac{AP_d}{N\mu}\right)^2$ and equation (11.14) reduces to

$$\frac{P_d}{N\mu} = \left(1 - \tanh^2 \frac{\Delta}{kT}\right)\frac{AP_d}{N\mu}\left\{1 - A^2\left(\frac{P_d}{N\mu}\right)^2\left[\tfrac{1}{3} - \tanh^2\left(\frac{\Delta}{kT}\right)\right]\right\} \quad (11.17)$$

Hence for this case the product

$$A' = A\left(1 - \tanh^2 \frac{\Delta}{kT}\right) = \frac{e^2\delta^2 N\beta \cos^2 25°}{4kT\left(1 - \frac{4\pi}{3}\gamma\right)}\left(1 - \tanh^2 \frac{\Delta}{kT}\right) \quad (11.18)$$

has to be equal to or greater than unity before a ferroelectric effect can occur. The dotted lines of Fig. 11.3 show the values of $\frac{\Delta}{kT} = \frac{1}{3}$; $\frac{\Delta}{kT} = \frac{1}{2}$; and $\frac{\Delta}{kT} = \frac{2}{3}$; and $P_d/N\mu$ is plotted against A'. These result in an increase in polarization for the same value of A'.

In order to calculate A we have to know how the separation δ depends on the separation of the oxygens 1 to 10. The greatest value of separation

would result if we assume that the hydrogen nucleus maintains its distance of 0.99Å (observed for water) for all values of oxygen separations. This would result in the straight-line relationship shown by the top full line of Fig. 11.4. Another calculation of δ has been made by Huggins[9] by adding two Morse potential curves as the separation of the oxygens are varied. The results of this calculation adjusted to give the same separation as for water, are shown by the bottom solid line. This calculation also yields a value for the height of the potential well ΔU. Some confirmation of this

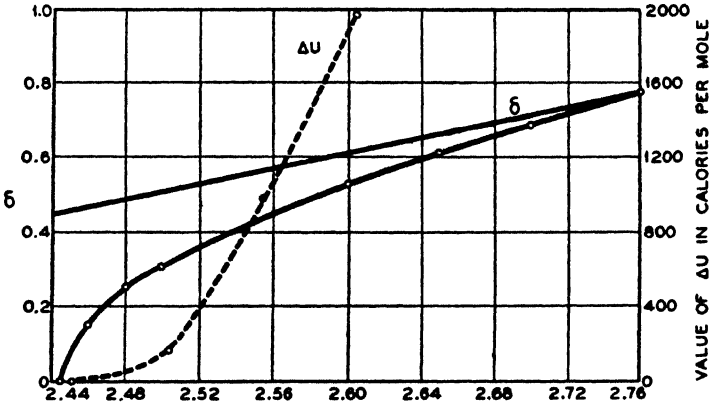

FIG. 11.4. Potential well separation δ and height of energy barrier ΔU as a function of the oxygen separation.

curve has recently been obtained by Landsberg and Baryshaskaya,[10] who observed the Raman spectrum of KDP and ADP. For KDP having a separation of 2.54Å between oxygens they observed a value of $\delta = 0.38$Å in close agreement with the value of 0.4Å shown by Fig. 11.4. Hence this curve will be taken as representing the relation between oxygen separations, the value of δ and the height of the energy barrier ΔU. For rochelle salt, the separation of oxygens is about 2.59Å which results in a value of $\delta =$ 0.51Å. The size of the unit cell is 14.3Å $\times$ 11.93A $\times$ 6.17Å, and there are four 1–10 bonds per unit cell. Hence $N = 3.81 \times 10^{21}$ dipoles per cubic centimeter. The polarizability γ is related to the dielectric constant for

[9] Huggins, M. L., *J. Phys. Chem.*, Vol. 40, p. 723, 1946.

[10] Landsberg, G. S., and F. S. Baryshaskaya, *Doklandy Akad. Nauk.*, SSSR, Vol. 61, 1027–30 (1948) and *Chem. Abst.*, Vol. 43, p. 495, Jan. 25, 1949. This reference shows also that for ADP at 150°K the NH band appears to split into a series of narrow maxima whereas the OH band preserves its aspect as in KH_2PO_4. This confirms that the transition in ADP is due to the ammonia hydrogen bond system.

atoms and electrons, ϵ_0, by the relation

$$\frac{4\pi}{3}\gamma = \frac{\epsilon_0 - 1}{\epsilon_0 + 2} \tag{11.19}$$

The dielectric constant at low temperatures, as shown by Fig. 7.7, flattens off at -160°C and remains constant at lower temperatures. According to the present theory, this is the temperature that the hydrogen nuclei freeze out into the low-potential well for each bond and hence we take ϵ_0 as 7.0. Substituting in equations (11.19)

$$0.159 = \gamma \tag{11.20}$$

The value of Δ or the value of Δ/kT at some fixed temperature (say the upper Curie temperature) principally determines how fast the dielectric constant disappears at low temperatures and to make this vanish suffi-

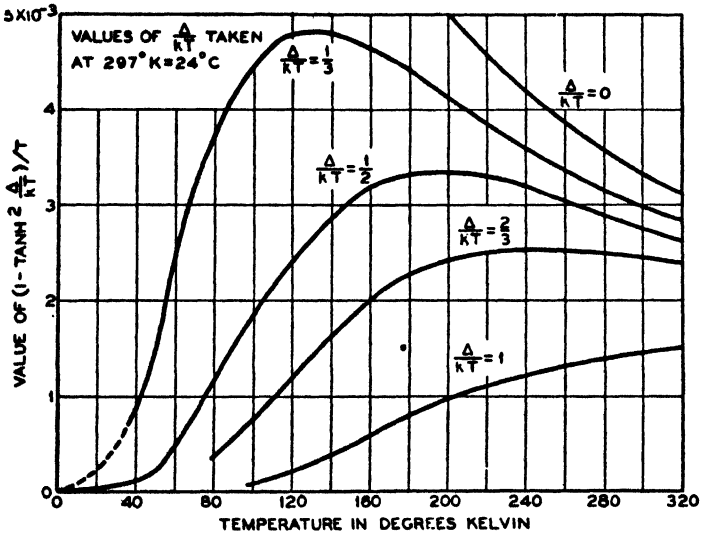

FIG. 11.5. Plot of function $\left(1 - \tanh^2 \frac{\Delta}{kT}\right)/T$.

ciently fast, (Δ/kT) is taken at $\frac{2}{3}$ at the upper Curie temperature. Figure 11.5 shows a plot of $[1 - \tanh^2 \Delta/kT]/T$ as a function of absolute temperature for various values of (Δ/kT) at 24°C, the upper Curie point. Over the ferroelectric region the factor rises by 4.5 per cent and since A' has to be 1 at -18°C the other Curie temperature, this has to be offset by the decrease in δ^2. If the hydrogen bonds expand in proportion to the rest of the structure (which amounts to 65 parts in 10^6 per °C), the oxygen

separation decreases from 2.59Å to 2.583Å and the value of δ^2 decreases by 7.0 per cent. Since N increases about $\frac{2}{3}$ of a per cent — due to the decrease in size of the unit cell — and $1/\left(1 - \frac{4\pi}{3}\gamma\right)$ about 2 per cent due to increase in the number of molecules at the lower temperatures, this is sufficient to bring A' back to unity at $-18°C$. Above and below the Curie points, the factor A' is less than unity and the crystal is not ferroelectric.

The measurements of Bancroft[11] on the effect of pressure on the Curie temperatures, also agree well with this amount of variation of δ with change in the oxygen positions. Bancroft's measurements — as can be seen from Fig. 7.4 — show that the upper Curie temperature $+24°C$ can be made the lower Curie temperature if 11,000 kilograms per square centimeter hydrostatic pressure is applied to the crystal. Taking the volume compressibility as 3.6×10^{-12} square centimeters per dyne and the compressibility along the x-axis as 2.0×10^{-12} square centimeters per dyne, this amount of pressure will change the volume by about 3.9 per cent and the x-axis by 2.1 per cent. Taking the separation of the 0's proportional to the total change in the x-dimension of the unit cell, the oxygen separation will decrease from 2.59 to 2.536Å and δ^2 will decrease by a factor of .62. Under this condition N increases 4 per cent and $1/\left(1 - \frac{4\pi}{3}\gamma\right)$ by 12 per cent. The dissymmetry may decrease some under high pressure so that the factor $\left[1 - \tanh^2\left(\frac{\Delta}{kT}\right)\right]$ also increases. Hence all factors are not far from balancing and the indicated change of δ with oxygen separation is not far from the curve shown.

All the factors are known reasonably well for A' except β. If we insert the values

$$A' = 1 = \frac{e^2\delta^2\beta N \cos^2 25°}{\frac{4kT}{3}}\left(1 - \tanh^2\frac{\Delta}{kT}\right) \tag{11.21}$$

with $e = 4.80 \times 10^{-10}$ esu, $\delta = 0.51 \times 10^{-8}$ cm; $N = 3.81 \times 10^{21}$; $\cos^2 25° = 0.821$; $\left(1 - \tanh^2\frac{\Delta}{kT}\right) = 0.66$, $k = 1.38 \times 10^{-16}$ ergs/degree; $T' = 297°K$, and solving for β we find

$$\beta = 4.4 \tag{11.22}$$

which is close to the theoretical value $4\pi/3 = 4.19$.

[11] Bancroft, D., "The Effect of Hydrostatic Pressure on the Susceptibility of Rochelle Salt," *Phys. Rev.*, Vol. 53, pp. 587–590, 1938.

11.11 *Coercive Force and Dielectric Constant at High Field Strength*

Equation (11.13) and the constants evaluated from the above considerations give methods for determining the properties of the crystal at large field strengths. This equation holds primarily for a single domain. Since in the ferroelectric region the difference between the symmetrical bond and the two dissymmetrical bonds is small, and the latter is considerably harder to discuss, the results of this and the next section are based on the symmetrical bond with the understanding that A refers to A' of equation (11.21).

Starting with the equation

$$\frac{P_d}{N\mu} = \tanh A\left(\frac{E}{\beta N\mu} + \frac{P_d}{N\mu}\right) \tag{11.23}$$

and noting that

$$N\mu = \frac{3.81 \times 10^{21} \times (4.8 \times 10^{-10}) \times 0.51 \times 10^{-8}}{2} = 4650 \text{ esu} \tag{11.24}$$

so that $A'/\beta N\mu$ has a value of about 4.9×10^{-5}, we can expand the equation into the form

$$\tanh A\left(\frac{E}{\beta N\mu} + \frac{P_d}{N\mu}\right) = \frac{\tanh \dfrac{AE}{\beta N\mu} + \tanh \dfrac{AP_d}{N\mu}}{1 + \tanh \dfrac{AE}{\beta N\mu} \tanh \dfrac{AP_d}{N\mu}} \tag{11.25}$$

$$\doteq 4.9 \times 10^{-5} E + \tanh \frac{AP_d}{N\mu}$$

The spontaneous polarization for rochelle salt and heavy water rochelle salt are shown by Fig. 11.6. The maximum polarization rises to 740 esu per square centimeter at 0°C. This however is the measured value P_d' which from equation (11.7) is larger than the internal dipole polarization P_d by the factor

$$1 + \beta\left(\frac{\epsilon_0 - 1}{4\pi}\right) = 3.1$$

Hence $AP_d/N\mu$ is of the order 0.05. We can then replace the hyperbolic tangent by the first two terms of the series and (11.25) can be written

$$\frac{AP_d}{N\mu} - \frac{A^3}{3}\left(\frac{P_d}{N\mu}\right)^3 = -4.9 \times 10^{-5} E + \frac{P_d}{N\mu} \tag{11.26}$$

The theoretical value of the coercive field required to reverse a single domain can be calculated from this equation. If we plot the curve on a graph, the shape is shown in an exaggerated form by Fig. 11.7. To deter-

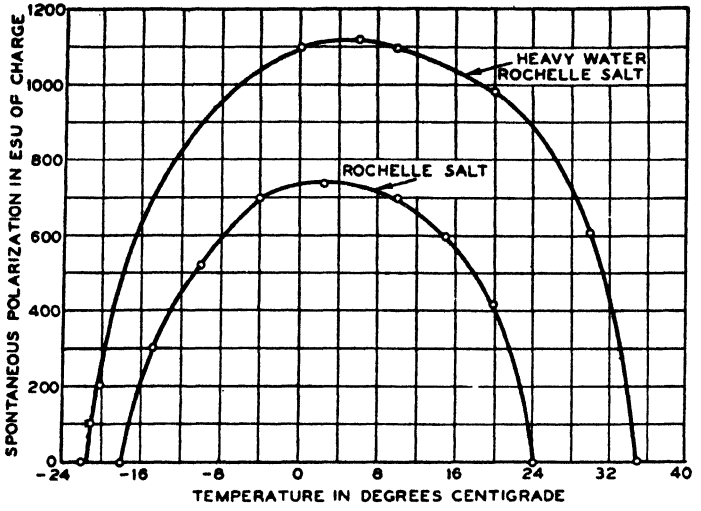

FIG. 11.6. Spontaneous polarization of rochelle salt and heavy water rochelle salt plotted as a function of temperature.

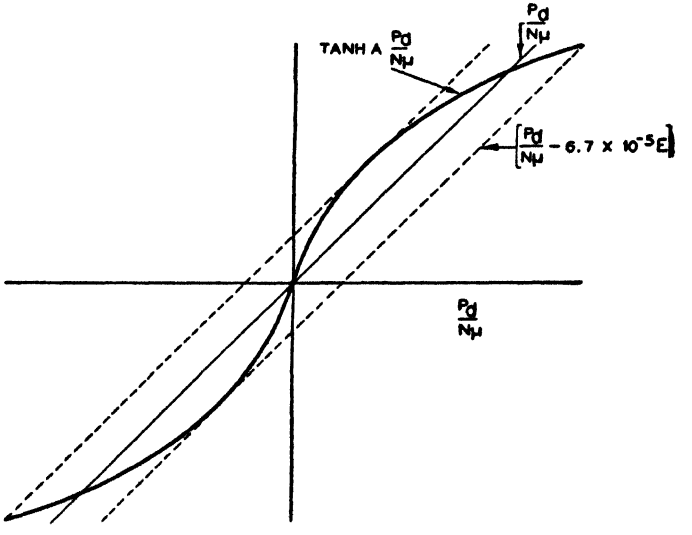

FIG. 11.7. Value of Equation (11.25) plotted as a function of $P_d/N\mu$.

mine the coercive field to change the polarization to the opposite sign, we have to raise E (negative) until $-4.9 \times 10^{-5}E$ equals the greatest deviation of the power series from the straight line going through zero and the value $P_d/N\mu$. By calculation this occurs when $P_d/N\mu = 0.035$ and $E = 0.33$ electrostatic units of potential or about 100 volts per centimeter. This is in the order of the experimental value shown by Fig. 7.5.

11.12 *Clamped Dielectric Constant at Low Field Strength*

A solution of equation (11.11) for small applied voltages also accounts quantitatively for the measured values of the clamped dielectric constant at low field strength over a frequency and temperature range. For simple harmonic motion, we let

$$E = E_0 e^{j\omega t}; \qquad P_d = P_s + P_0 e^{j\omega t} \tag{11.27}$$

where P_s is the spontaneous dipole polarization. Also, since the time variable field and polarization are small compared to the spontaneous effect, we can write

$$\sinh A\left(\frac{E_0 e^{j\omega t}}{\beta N\mu} + \frac{(P_s + P_0 e^{j\omega t})}{N\mu}\right) = \sinh A\left(\frac{E_0 + \beta P_0}{\beta N\mu}\right) e^{j\omega t} \times \cosh \frac{AP_s}{N\mu} + \cosh A\left(\frac{E_0 + \beta P_0}{\beta N\mu}\right) e^{j\omega t} \sinh \frac{AP_s}{N\mu}$$

and since the time variable parts are very small

$$\sinh A\left(\frac{E_0 + \beta P_0}{\beta N\mu}\right) e^{j\omega t} \doteq A\left(\frac{E_0 + \beta P_0}{\beta N\mu}\right) e^{j\omega t};$$

$$\cosh A\left(\frac{E_0 + \beta P_0}{\beta N\mu}\right) e^{j\omega t} \doteq 1$$

With these approximations, the two equations of (11.11) give the solutions

$$P_{s1} + P_{01} e^{j\omega t} = \frac{N\mu}{2}\left\{\tanh\left(\frac{\Delta}{kT} + \frac{AP_s}{N\mu}\right) + A\frac{(E_0 + \beta P_0)e^{j\omega t}}{\beta N\mu}\left[1 - \tanh^2\left(\frac{\Delta}{kT} + \frac{AP_s}{N\mu}\right)\right]\right\} - \frac{j\omega P_{01} e^{\Delta U/kT}}{\Gamma \cosh \frac{\Delta}{kT} \cosh \frac{AP_s}{N\mu}}$$

$$P_{s2} + P_{02} e^{j\omega t} = \frac{N\mu}{2}\left\{\tanh\left(\frac{-\Delta}{kT} + \frac{AP_s}{N\mu}\right) + A\left(\frac{E_0 + \beta P_0}{\beta N\mu}\right) e^{j\omega t} \times \left[1 - \tanh^2\left(\frac{-\Delta}{kT} + \frac{AP_s}{N\mu}\right)\right]\right\} - \frac{j\omega P_{02} e^{\Delta U/kT}}{\Gamma \cosh \frac{\Delta}{kT} \cosh \frac{AP_s}{N\mu}} \tag{11.28}$$

Adding these, we have the equations for spontaneous polarization and the equations

$$P_s = P_{s1} + P_{s2} = \frac{N\mu}{2}\left[\tanh\left(\frac{\Delta}{kT} + \frac{AP_s}{N\mu}\right) + \tanh\left(\frac{-\Delta}{kT} + \frac{AP_s}{N\mu}\right)\right] \quad (11.29)$$

$$P_0 e^{j\omega t} = A\left(\frac{E_0 + \beta P_0}{\beta}\right)\left\{1 - \left[\frac{\tanh^2\left(\frac{\Delta}{kT} + \frac{AP_s}{N\mu}\right) + \tanh^2\left(\frac{-\Delta}{kT} + \frac{AP_s}{N\mu}\right)}{2}\right]\right\} - \frac{j\omega P_0 e^{\Delta U/kT}}{\Gamma \cosh\frac{\Delta}{kT}\cosh\frac{AP_s}{N\mu}} \quad (11.30)$$

Discussing first the case for which the dissymmetry is zero, or $\Delta = 0$, we have

$$\frac{P_s}{N\mu} = \tanh\frac{AP_s}{N\mu}$$

$$P_0 = \frac{\frac{AE_0}{\beta}\left[1 - \left(\frac{P_s}{N\mu}\right)^2\right]}{1 - A\left[1 - \left(\frac{P_s}{N\mu}\right)^2\right] + \frac{j\omega e^{\Delta U/kT}}{\Gamma \cosh\frac{AP_s}{N\mu}}} \quad (11.31)$$

Inserting the time variable polarization of (11.31) in equation (11.8), we have

$$\epsilon = \epsilon_0 + \frac{\frac{4\pi A}{\beta}\left[1 - \left(\frac{P_s}{N\mu}\right)^2\right]\left[1 + \beta\left(\frac{\epsilon_0 - 1}{4\pi}\right)\right]}{1 - A\left[1 - \left(\frac{P_s}{N\mu}\right)^2\right] + \frac{j\omega e^{\Delta U/kT}}{\Gamma \cosh\frac{AP_s}{N\mu}}} \quad (11.32)$$

Outside of the Curie region the dielectric constant is given exactly by

$$\epsilon = \epsilon_0 + \frac{\frac{4\pi A}{\beta}\left[1 + \beta\left(\frac{\epsilon_0 - 1}{4\pi}\right)\right]}{1 - A + \frac{j\omega e^{\Delta U/kT}}{\Gamma}} \quad (11.33)$$

Inside the Curie region since when A is near unity, $(P_s/N\mu)^2 \doteq \frac{3(A-1)}{A^3}$,

the expression becomes

$$\epsilon \doteq \epsilon_0 + \frac{\frac{4\pi A}{\beta}\left[1 + \beta\left(\frac{\epsilon_0 - 1}{4\pi}\right)\right]}{2(A-1) + \frac{j\omega e^{\Delta U/kT}}{\Gamma \cosh \frac{AP_s}{N\mu}}} \tag{11.34}$$

For the dissymmetrical case outside the Curie region, the dielectric constant is given exactly by

$$\epsilon = \epsilon_0 + \frac{\frac{4\pi A'}{\beta}\left[1 + \beta\left(\frac{\epsilon_0 - 1}{4\pi}\right)\right]}{1 - A' + \frac{j\omega e^{\Delta U/kT}}{\Gamma \cosh \frac{\Delta}{kT}}} \quad \text{where } A' = A\left(1 - \tanh^2 \frac{\Delta}{kT}\right) \tag{11.35}$$

By expanding the terms in (11.29) and (11.30) in a power series it can be shown that equation (11.34) holds approximately in the Curie region with A replaced by A'.

The equations account in a general way for the observed value of the clamped dielectric constant. The exact values depend on the assumptions made for the dipole moment, the inhomogeneity, Δ, etc. The present theory does not account for the finite value of the clamped dielectric constant at the Curie points nor the hysteresis resistance at small amplitudes both inside and outside of the Curie temperatures, which is evidenced by the nearly constant values of Q versus frequency, shown by the curves of Fig. 7.8. These may be accounted for by the domain structure which broadens out the Curie temperature since different domains have different Curie temperatures due to the strains in them.

The equations for the dielectric constant account for some recent measurements of W. A. Yager on the dielectric constant of rochelle salt at a frequency of 2.5×10^{10} cycles. Yager finds that from $-40°$C to $+26°$C the dielectric constant and the Q of rochelle salt are practically independent of temperature and have the values

$$\epsilon = 8.0; \qquad Q = .25 \tag{11.36}$$

These measurements were made by a wave-guide technique. They indicate that the frequency is so high that the hydrogen bond dipoles cannot follow the field, and contribute little to the dielectric constant.

The impedance to be expected theoretically can be calculated from

equation (11.32). This results in

$$\frac{1}{Z} = \frac{1}{Z_d} + \frac{1}{Z_0} = \frac{j\omega\epsilon \times 1.11 \times 10^{-12}}{4\pi} = j\omega \times 1.11 \times 10^{-12}$$

$$\times \left\{ \frac{\frac{A}{\beta}\left[1 - \left(\frac{P_s}{N\mu}\right)^2\right]\left[1 + \beta\left(\frac{\epsilon_0 - 1}{4\pi}\right)\right]}{1 - A\left[1 - \left(\frac{P_s}{N\mu}\right)^2\right] + \frac{j\omega e^{\Delta U/kT}}{\Gamma \cosh \frac{\Delta}{kT} \cosh \frac{AP_s}{N\mu}}} + \frac{\epsilon_0}{4\pi} \right\} \tag{11.37}$$

This equation is the impedance of two parallel arms, one arm Z_d representing the impedance of the dipole term, and the other the impedance Z_0 is the impedance of a condenser with a dielectric constant ϵ_0 due to other types of polarization. The impedance of the dipole arm is per cubic centimeter

$$Z_d = 9 \times 10^{11} \left\{ \frac{\beta}{A\left[1 - \left(\frac{P_s}{N\mu}\right)^2\right]\left[1 + \beta\left(\frac{\epsilon_0 - 1}{4\pi}\right)\right]} \right\}$$

$$\times \left[\frac{\frac{1}{\Gamma} e^{\Delta U/kT}}{\cosh \frac{\Delta}{kT} \cosh \frac{AP_s}{N\mu}} - \frac{j}{\omega}\left\{1 - A\left[1 - \left(\frac{P_s}{N\mu}\right)^2\right]\right\} \right] \tag{11.38}$$

The impedance of the other arm with the dielectric constant ϵ_0 is

$$Z_0 = \frac{-j}{\omega C_0} = -j \frac{9 \times 10^{11} \times 4\pi}{\omega \epsilon_0} \tag{11.39}$$

In evaluating this equation we now assume the value Γ given by Eyring's reaction rate theory, namely $\Gamma = kT/h$. The value to take for ΔU is somewhat uncertain. If we take the value given by Huggins calculation for a value of $\delta = 0.51$Å and use classical statistics, the value of ΔU should be 1800 calories per mole. If, however, we use quantum statistics, we have to subtract from this the zero point energy. It is found from the high-frequency measurements of potassium dihydrogen phosphate discussed in the next section, that the potential barrier cannot be above 100 calories per mole. Since KDP has a value of δ equal to 0.40Å units and according to Fig. 11.4 should have a potential barrier of 700 calories per mole, we take the zero point energy as 600 calories per mole and $\Delta U = 1200$ calories per mole for rochelle salt. In making the calculations we assume $\beta = 4.4$; $(P_s/N\mu) = 0.051$; $A' = 1.00093$; $h = 6.62 \times 10^{-27}$; $k = 1.38 \times 10^{-16}$; $T = 273$; $\Delta U = 1200$ calories per mole, $\epsilon_0 = 7.0$

and we find at 2.5×10^{10} cycles that

$$Z_d = 1.64 - j.014; \qquad Z_0 = -j10.3 \tag{11.40}$$

Hence the resistance component of the dipole arm is larger than the reactance component. The indicated relaxation frequency is about 5×10^8 cycles at 0°C. The measured results of Yager, given by equation (11.36), indicate that the impedance per cubic centimeter at 2.5×10^{10} cycles, should be a reactance $-j9.0$ ohms in parallel with a resistance $\frac{1}{4}$ of this value or 2.25 ohms. This agrees within less than a factor of two with the calculated value.

11.13 *Application of Theory to Heavy Water Rochelle Salt*

When the hydrogens in the water molecules and the hydroxyl molecules are replaced by deuterium, a very considerable change occurs in the properties of the rochelle salt crystal. As shown[12] by Fig. 11.6, the lower Curie temperature is lowered to −22°C, the upper one raised to 35°C and a considerably larger spontaneous polarization occurs. Since the crystal unit cell dimensions have not changed appreciably, the potential well-distance distribution should be the same and the difference has to be accounted for by the lower zero point energy for the deuterium than exists for the hydrogens. The effect of this lower zero point energy is to make the molecules less mobile. This effect is approximated by letting k have a smaller value $k_d = k(1 - \epsilon)$ for the deuterium bond. If this is substituted in the factor

$$A' = \left(\frac{\beta N\mu^2}{1 - \frac{4\pi}{3}\gamma}\right)\left(\frac{1 - \tanh^2 \frac{\Delta}{kT}}{kT}\right) \tag{11.18}$$

the effect on the value of A' is given by the equation

$$A' = \frac{N\mu^2}{\left(1 - \frac{4\pi}{3}\gamma\right)}\left(\frac{1 - \tanh^2 \frac{\Delta}{kT}}{kT}\right)\left[1 + \epsilon\left(1 - \frac{2\Delta}{kT}\tanh\frac{\Delta}{kT}\right)\right]$$

The effect of the deuterium substitution on the Curie temperature then depends on the ratio of the potential energy difference Δ to kT at the Curie points. If Δ/kT is 0.775, the Curie temperature will not move. If Δ/kT is less than this, the Curie temperature will increase, while if it is greater than this, the Curie temperature will decrease. To agree with experiment, Δ/kT has to be 0.69 at the upper Curie temperature of

[12] Hablützel, J., *Helv. Phys. Acta*, Vol. 12, pp. 489–570, 1934.

24°C = 297°K, and hence will be 0.807 at the lower Curie temperature of −18°C = 255°K. Hence with these values the upper Curie temperature increases and the lower Curie temperature decreases. These values of Δ/kT agree very closely with the value of $\frac{2}{3}$ at the upper Curie point, assumed to make the dielectric constant disappear with sufficient rapidity at the low temperatures.

When the dissymmetry Δ disappears as it does for potassium dihydrogen phosphate (KDP), discussed in the next section, the effect of the lower zero point energy is to raise the Curie temperature by the factor $(1 + \epsilon)$. As can be seen from Fig. 8.6, this is quite a large factor for potassium deuterium phosphate. To determine the factor ϵ would require a quantum theory treatment of the hydrogen bond but so far this has not been possible.

11.2 *Ferroelectric Effect in Potassium Dihydrogen Phosphate (KDP)*

The distinguishing difference between the ferroelectric effect in rochelle salt and potassium dihydrogen phosphate is that the former has an upper and lower Curie point, whereas the latter has a single ferroelectric region extending from 0°K to 121°K and a non-ferroelectric region above this. On applying the theory developed in the last section, it appears that the reason for this difference is that the hydrogen bond in rochelle salt is a combination of two dissymmetrical bonds, while the hydrogen bond of potassium dihydrogen phosphate is a symmetrical bond and the positions of the hydrogen nuclei do not freeze out at low temperatures.

To show that the dipole moment is practically independent of temperature in potassium dihydrogen phosphate, we need the equations of the last section dealing with the dielectric constant. These are, for a symmetrical bond

$$\epsilon = \frac{\dfrac{4\pi A}{\beta}\left[1 - \left(\dfrac{P_s}{N\mu}\right)^2\right]\left[1 + \beta\left(\dfrac{\epsilon_0 - 1}{4\pi}\right)\right]}{1 - A\left[1 - \left(\dfrac{P_s}{N\mu}\right)^2\right] + \dfrac{j\omega e^{\Delta U/kT}}{\Gamma \cosh \dfrac{AP_s}{N\mu}}} + \epsilon_0; \qquad A = \frac{\beta N\mu^2}{\left(1 - \dfrac{4\pi}{3}\gamma\right)kT};$$

$$\frac{\epsilon_0 - 1}{\epsilon_0 + 2} = \frac{4\pi}{3}\gamma \tag{11.41}$$

Substituting for γ in A gives

$$A = \frac{\beta N\mu^2}{kT}\left[1 + \frac{(\epsilon_0 - 1)}{3}\right] = \frac{T_0}{T}.$$

Introducing this value of A in the first equation, the dielectric constant for temperatures above the Curie point (where $P_s = 0$), and at low frequencies (where the imaginary term can be neglected), can be written in the form

$$\epsilon = \frac{\frac{4\pi N\mu^2}{k}\left[1 + \frac{\beta(\epsilon_0 - 1)}{4\pi}\right]\left[1 + \frac{\epsilon_0 - 1}{3}\right]}{T - T_0} + \epsilon_0 \tag{11.42}$$

where

$$T_0 = \frac{\beta N\mu^2}{k}\left[1 + \frac{(\epsilon_0 - 1)}{3}\right]$$

Hence if the dipole moment μ is relatively independent of temperature, the clamped dielectric constant satisfies the Curie-Weiss law

$$\epsilon = \frac{C}{T - T_0} + \epsilon_0$$

where

$$C = \frac{4\pi N\mu^2}{k}\left[1 + \frac{\beta(\epsilon_0 - 1)}{4\pi}\right]\left[1 + \frac{\epsilon_0 - 1}{3}\right]; \tag{11.43}$$

$$T_0 = \frac{\beta N\mu^2}{k}\left[1 + \frac{(\epsilon_0 - 1)}{3}\right]$$

Therefore

$$\beta = \frac{\frac{4\pi T_0}{C}}{1 - \frac{T_0}{C}(\epsilon_0 - 1)}$$

The clamped dielectric constant of potassium dihydrogen phosphate (KDP), given in equation (8.11), Chapter VIII, satisfies the equation

$$\epsilon_3^s = 4.5 + \frac{3100}{T - 121°\text{K}} \tag{11.44}$$

quite well except at temperatures very close to the Curie temperature. Hence

$$C = 3100; \qquad \epsilon_0 = 4.5; \qquad T_0 = 121°\text{K} \tag{11.45}$$

The size of the unit cell from X-ray measurements[13] is 7.43Å × 7.43Å × 6.97Å and there are four molecules per unit cell. Since there are two hydrogen bonds per molecule which act as the dipoles, the number $N = 2.08 \times 10^{22}$ dipoles per cubic centimeter. All the other quantities

[13] West, J., *Zeits. F. Krist.*, Vol. 74, p. 306, 1930.

are known except μ and β, the Lorentz factor. Solving for these from the data of equation (11.45), we have

$$\mu = 0.81 \times 10^{-18}; \qquad \beta = .567 \tag{11.46}$$

where μ and β must be independent of the temperature to satisfy the Curie-Weiss law.

The conclusion that the dipole moment is independent of temperature is borne out in the ferroelectric region also by a study of the spontaneous polarization. If all the dipoles were lined up, the polarization should be

$$N\mu = 2.08 \times 10^{22} \times 0.81 \times 10^{-18} \times 1.159 = 19{,}500 \text{ esu of charge/cm}^2. \tag{11.47}$$

The spontaneous polarization as a function of temperature is shown by Fig. 8.6. According to equation (11.15), the ratio of spontaneous polarization P_d to the total dipole polarization $N\mu$ is given by the equation

$$\frac{P_d}{N\mu} = \tanh A \frac{P_d}{N\mu}$$

where (11.48)

$$A = \frac{\beta N\mu^2}{\left(1 - \frac{4\pi}{3}\gamma\right) kT} = \frac{T_0}{T}$$

if μ is independent of temperature. The theoretical value of P_d is shown plotted by the dashed line in Fig. 11.8 and compared with the experimental values shown by the solid line. Near the Curie temperature the agreement is good, but at lower temperatures the measured spontaneous polarization is less than the theoretical. The spontaneous polarization was measured by measuring the top of the hysteresis loop, and since $A \to \infty$ as $T \to 0$, the theory of section 11.11 would indicate that the coercive voltage becomes very large at low temperatures. Hence as the temperature decreases, the highest voltages that can be used are not sufficient to reverse all the domains. This is confirmed by the fact that below 58°K, the polarization, field loops lose hysteresis components and the dielectric constant becomes much smaller. This has been ascribed to an increase in the coercive field as the temperature decreases. The field of 3000 volts/cm was insufficient to reverse the domains. At higher temperatures, some domains probably could not be reversed and hence the measured spontaneous polarization was smaller than the theoretical value. This question has also been investigated by Barkla,[14] who used a static method in which a measured charge is supplied from a compensating condenser

[14] Barkla, H. M., *Nature*, Vol. 158, p. 340, Sept. 7, 1946.

of much larger capacitance in order to maintain a fixed potential difference across a crystal of potassium dihydrogen phosphate while its temperature is altered; it is possible by this means to show that in a constant field the

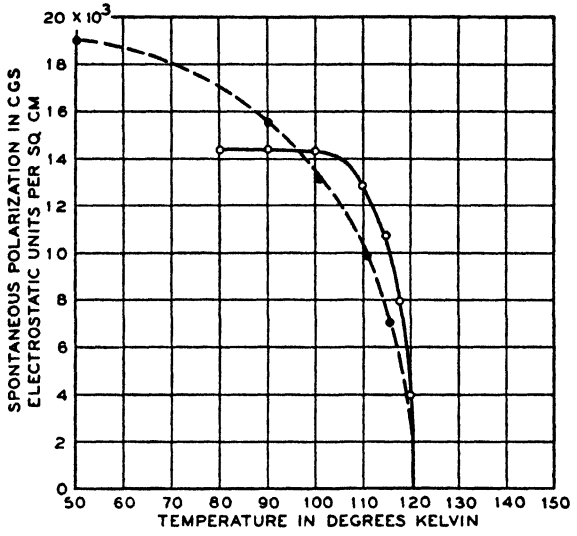

FIG. 11.8. Theoretical and experimental values of the spontaneous polarization of KDP.

electric moment of the salt is unchanged on passing through this " lower " transition point. Hence we conclude that all the evidence points to a dipole polarization independent (nearly) of the temperature with a value of about 0.81 Debye units.

11.21 *Slater's Theory*

The crystal structure of KDP has been worked out by West[13] and is shown in Fig. 11.9. The phosphate groups, PO_4, consist of a phosphorous tetrahedrally surrounded by four other phosphate groups. The positions of the hydrogen ions are not determined by X-ray analysis, but West has assumed that they lie between adjacent oxygens in neighboring PO_4 groups, a distance of 2.54Å at room temperature. A theory of the ferroelectric effect in KDP has been developed by Slater,[6] which is based on the change in direction of the dipole of each H_2PO_4 group due to the displacement of the hydrogen nucleus along the hydrogen bond. On this theory, when both nuclei are near the top oxygens, as shown in Fig. 11.9B, the dipole points in the z-direction. Other combinations can cause the dipole to point in directions perpendicular to z. Since the motions of the hydrogen nuclei are perpendicular to the z-axis, and hence will not them-

selves produce a moment along z, it has been pointed out by J. Bardeen that this theory will work only if the two hydrogen nuclei induce in the PO_4 groups a dipole pointing along z about equal to that due to the displacements of the hydrogen nuclei in the hydrogen bonds. The induced dipole will be directed along $-z$ for the two nuclei, as shown by Fig. 11.9B.

Estimates of the polarizability of the PO_4 groups indicate that the induced dipole can be as large or larger than the hydrogen bond dipole determined by the separation δ between potential minima. If we assume

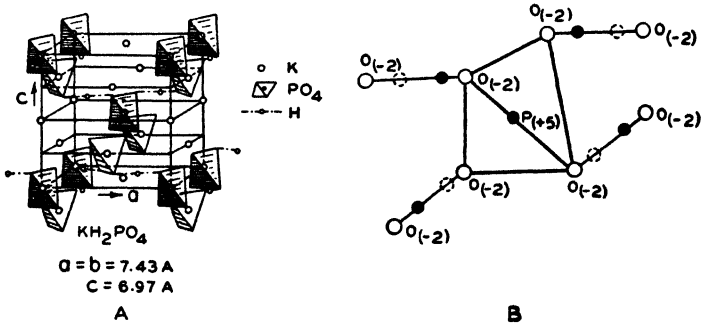

FIG. 11.9. Crystal structure of potassium dihydrogen phosphate (KDP).

that the induced dipole is equal to the hydrogen bond dipole, then in order to obtain a dipole of 0.81×10^{-18}, δ will be

$$\frac{e\delta}{} = 0.81 \times 10^{-18} \quad \text{or} \quad \delta = \frac{1.62 \times 10^{-18}}{4.8 \times 10^{-10}} = 0.34 \times 10^{-8} \text{ cm.} \quad (11.49)$$

This is a little smaller than the value of 0.4 shown by Fig. 11.4 for a separation of 2.54Å, which is the value measured by West. On this theory the change in dipole moment of KDP due to temperature changes, is quite small. To show this, the data of Fig. 8.14 show that the temperature expansion in the x or y direction is a linear function of the temperature equal to 26.7×10^{-6} per °C. Hence down to the Curie temperature -152°C, the unit cell will have contracted by .035Å. Since there are two hydrogen bonds in the x or y directions, the expansion across one of them cannot be more than .0175Å, and hence the separation 2.54Å at 25°C will not be reduced to less than 2.522, which corresponds to a very small change in the dipole.

At 25°C Yager finds that the dielectric constant along the z-axis is about 20 in agreement with the low-frequency measurements, and the Q is about 30 at 2.5×10^{10} cycles, or

$$\epsilon = 20.0; \quad Q = 30 \quad (11.50)$$

From equation (11.32), the impedance of the dipole arm, introducing the value of β and A from equation (11.48) and (11.45), should be

$$Z_d = 9 \times 10^{11} \left(\frac{.567}{1.159}\right)\left[\frac{h}{kT} e^{\Delta U/kT} - \frac{j}{\omega}(1 - .41)\right] \qquad (11.51)$$

In order to agree with the measured results of (11.50), ΔU cannot be over 100 calories per mole. With this value, equation (11.51) gives the numerical values of 2.5×10^{10} cycles

$$Z_d = .2 - j4.2; \qquad Z_0 = -j15.9 \qquad (11.52)$$

If we calculate the equivalent parallel circuit for the combination, we have a dielectric constant and Q equal to

$$\epsilon = 20; \qquad Q = 27 \qquad (11.53)$$

which agree well with the experimental values. This value of ΔU agrees with the ΔU values of Fig. 11.4 for a δ of 0.4Å if we subtract a zero point energy of 600 calories per mole.

11.3 *Ferroelectric Effect in Barium Titanate*

The theoretical model for the ferroelectric effect in rochelle salt and potassium dihydrogen phosphate has recently been extended[15] to the ferroelectric barium titanate crystal. It is the purpose of this section to describe a three-dimensional structure involving six equilibrium positions which accounts for the principal features of the barium titanate single domain crystal. The presentation given here is somewhat more general than the original theory since it accounts for the low temperature transitions that occur at +10°C and −80°C. It also incorporates recent measurements of the dielectric constants, which alter some of the constants presented in the original theory.

11.31 *Experimental Data*

Barium titanate above the transition temperature of 120°C has the cubic cell shown by Fig. 11.10. The top view A is a cross-section through one of the cell faces and the view B is a cross-section through the middle of the unit cell. The bariums which have a radius of about 1.33Å occupy the corners of the unit cell, while the oxygen, having a radius of about 1.35Å, occupies the face-centered position. In the 11.10B drawing, the titanium, which has a small radius, is usually pictured as being in the

[15] Mason, W. P., and B. T. Matthias, "Theoretical Model for Explaining Ferroelectric Effect in Barium Titanate," *Phys. Rev.*, Vol. 74, No. 11, pp. 1622–1637, Dec. 1, 1948.

center of the unit cell, but it probably makes a covalent bond with one of the oxygens at all times. When this happens the titanium may be displaced

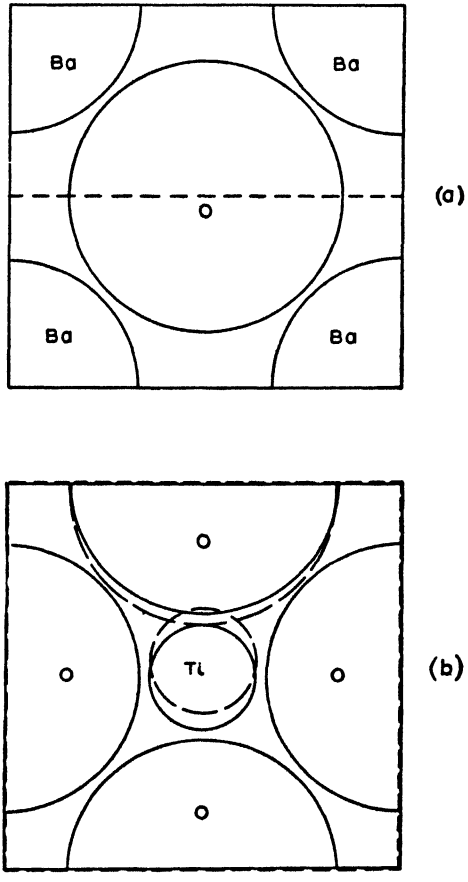

FIG. 11.10. Unit cell for barium titanate.

from the center of the unit cell, toward one of the oxygens.[16] Above 120°C, the thermal energy is sufficient to cause any one of the six positions to be equally probable and the cell appears to be cubic from X-ray measurements. Below 120°C, thermal energy is no longer sufficient to cause

[16] Danielson, G. C., *Phys. Rev.*, Vol. 74, 986 (1948), originally gave a value of 0.16Å but more recent measurements indicate the displacement is less than .09Å. "Recent studies by Devonshire (*Phil. Mag.*, Oct., 1949) show that the titanium is tightly bound while the oxygens may have stable positions in the directions of the titanium. This position shift could also form a dipole and to agree with the present theory, the separation of oxygen positions should be about 0.16Å."

any position to be equally probable, and most of the titaniums in a given region or domain line up along one of the six directions, a dipole moment develops in that direction and the crystal becomes ferroelectric. The axis along which the titanium has been displaced becomes larger than the other two, as shown by the X-ray measurements of Miss Megaw[2] (as

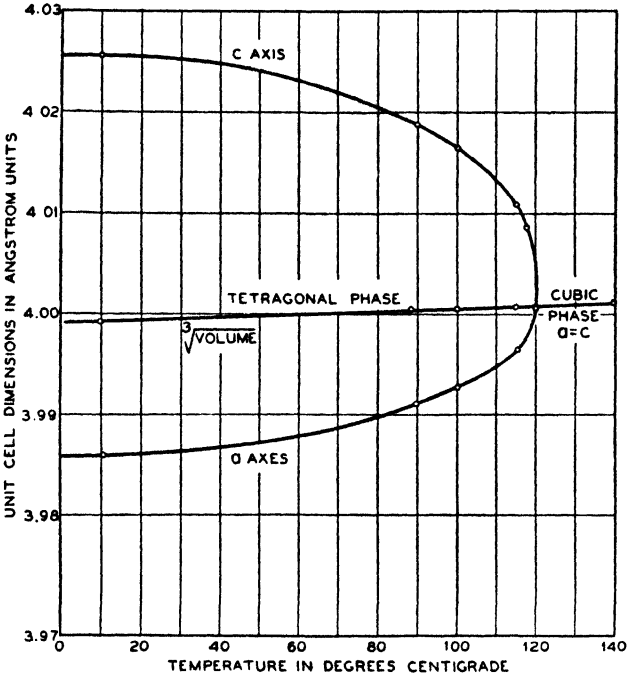

FIG. 11.11. Cell dimensions as a function of temperature.

shown by Fig. 11.11) and the crystal changes from cubic to tetragonal form.

The dielectric measurements of multi-crystalline ceramics, multi-domain crystals and single-domain crystals, all show the presence of a ferroelectric material below 120°C. Dielectric displacement — electric field curves occur in the form of hysteresis loops. The dielectric constant at low field strengths for multi-crystal ceramics,[17] as shown by Fig. 11.12 rises to a high value at the temperature of 120°C. Above 120 degrees, the dielectric constant follows a Curie-Weiss law approximately and the dielectric constant decreases inversely as the difference between the temper-

[17] Von Hipple, A., R. G. Breckinridge, F. G. Chesley, and L. Tisza, *Ind. Eng. Chem.*, Vol. 38, pp. 1097–1109, Nov., 1946.

ature and the Curie temperature, or

$$\epsilon = \epsilon_0 + C/(T - T_0) \tag{11.54}$$

where ϵ_0 is the constant dielectric constant for temperatures much higher than the Curie temperature, C is a constant, T the temperature, and T_0 the Curie temperature. Below the Curie temperature, the dielectric constant decreases from its high value to a value of about 90 near absolute zero.[18] The steady decrease is interrupted at two temperatures 10°C and −80°C. According to the theory presented here, the transition at 120°C is due to the crystal becoming ferroelectric along one axis, and occurs with a change of crystal structure from cubic to tetragonal. The transition at 10°C is due to the crystal becoming ferroelectric in two directions simultaneously, *i.e.* the titanium of Fig. 11.10B spends an equal percentage of time in covalent bonds with the oxygen along the $+z$ direction and the $+x$ direction. This occurs with a change of crystal structure from tetragonal to orthorhombic. Finally at −80°C, the crystal becomes ferroelectric along all three axes and the crystal structure becomes trigonal according to Forsbergh.[19]

The dielectric constant for multi-domain crystals is not too different from those for the multi-crystalline ceramics. Figure 11.13 shows the measurements of Matthias and Von Hippel[20] for the *a*- and *c*-axes. The dielectric constant along the *a*-axis is higher than that along the *c*-axis. The lowering of the Curie temperature is probably due to the impurities introduced and the failure to revert to a cubic structure above 120°C, as shown by the different dielectric constants along the two axes, is probably due to a distortion of the symmetry of the potential well distribution between the six oxygens due to the impurity strained structure. By introducing larger amounts of mineralizers, Matthias has recently grown single domain crystals of a relatively large size and these show a very marked difference between the dielectric constants along the two axes as shown by the measurements of Fig. 11.14. Here again the crystal fails

[18] Paper H-10, R. F. Blunt, W. F. Love and E. N. Skomal, *Amer. Physical Society Meeting*, Jan. 27, 1949.

[19] This interpretation of the transitions at 10°C and −80°C agrees with the recent measurements of P. W. Forsbergh, Jr., paper H-11, Amer. Phys. Soc. Meeting, Jan. 27, 1949. According to Forsbergh, the transition at 10°C is accompanied by a displacement of the titanium in the 101 direction. This agrees with the conception given here that the titanium nucleus spends most of its time in the $+x$ and $+z$ direction. The transition at −80°C corresponds to a displacement along the 111 direction which also can be described as a ferroelectric effect along three directions with the titanium spending most of its time along three perpendicular axes.

[20] Matthias, B., and A. Von Hippel, *Phys. Rev.*, Vol. 73, No. 11, pp. 1378–1384, June 1, 1948.

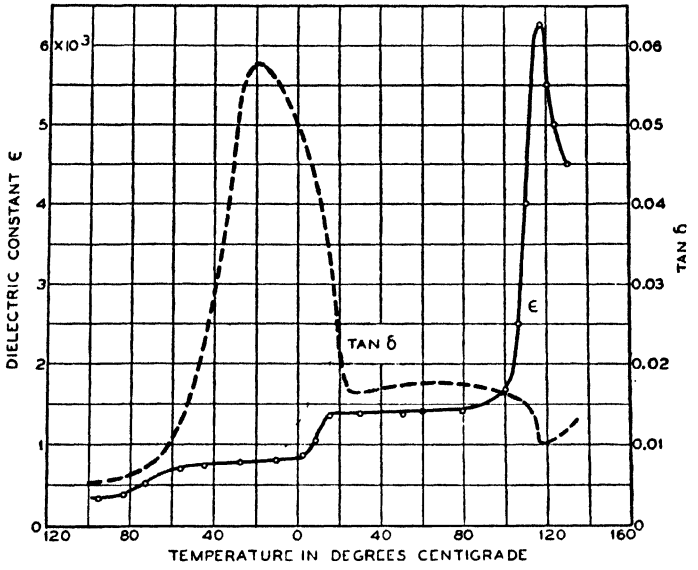

FIG. 11.12. Dielectric constant of barium titanate ceramic as a function of temperature.

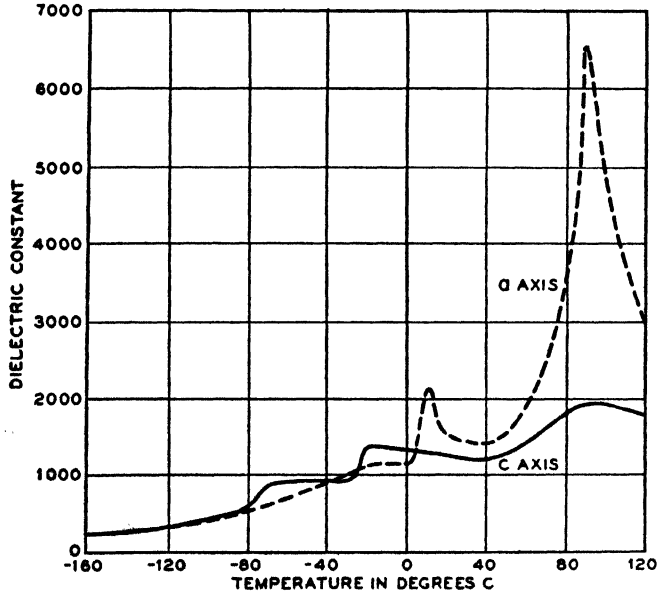

FIG. 11.13. Dielectric constants for the two crystallographic axes for multi-domain crystals of barium titanate.

to revert to a cubic structure above 120°C due to a permanent distortion of the lattice structure. More perfect crystals have recently been grown by Dr. W. J. Merz of the E.T.H. of Zurich and now of M.I.T.[21] by using an aluminum oxide crucible rather than a platinum crucible. These crystals revert to a cubic structure above 120°C showing that the permanently distorting element is the platinum absorbed from the crucible. The dielectric constant drops to 200 at 10°C for the *c*-axis and gets very large along the *a*-axis. Below the transition temperature of 5°C, the dielectric constant along *c* increases to 600 and gradually falls off with decreasing

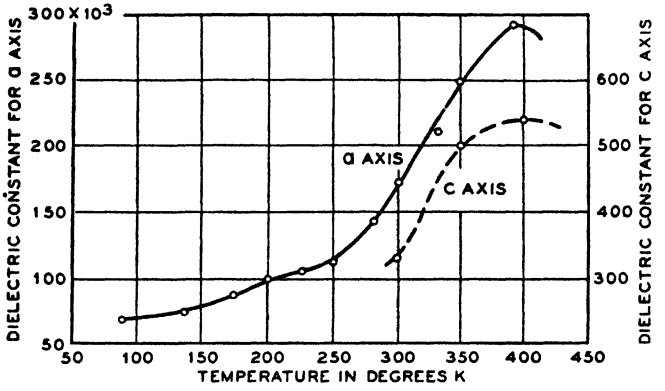

FIG. 11.14. Dielectric constants for a single domain crystal.

temperature until the transition at −80°C. It is evident from the measurements that the transitions at 5°C and −80°C are ferroelectric transitions.

When the dielectric constant along the *a*-axis for Matthias' single domain crystal was measured over a frequency range, a relaxation occurs at about 15 megacycles, and the dielectric constant drops to about 1200 or less, as shown by Fig. 11.15. A similar relaxation in the dielectric constant of the ceramic occurs at about 10^9 cycles, as shown by the measurements of Nash[22] and Yager (unpublished). At 23.7 centimeter wavelength, the former found a dielectric constant and tan δ of

$$\epsilon = 1250 \text{ to } 1420; \qquad \tan \delta \doteq 0.2 \tag{11.55}$$

[21] *Phys. Rev.*, Vol. 75, No. 4, p. 687, Feb. 15, 1949.

[22] Nash, D. E., Jr., *Exp. Theor. Phys.*, USSR, Vol. 17, p. 537, 1947. Recent Measurements by Powles, (*Nature*, Vol. 162, p. 614, Oct. 16, 1948) confirm this relaxation frequency. Since the measurements have been made over a temperature range, one can determine from the relaxation frequency that the activation energy is 3.65 kilocalories per mole in relatively good agreement with that of equation (11.107).

while at 1.25 centimeters, Yager found a dielectric constant of approximately

$$\epsilon = 250 \text{ to } 320, \qquad \tan \delta \doteq 0.70 \tag{11.56}$$

From these measurements, it can be calculated that the dielectric constant has a relaxation frequency of about 6.2×10^9 cycles.

The relaxation of the dielectric constant at these frequencies shows definitely that the high dielectric constant is due to a temperature movable

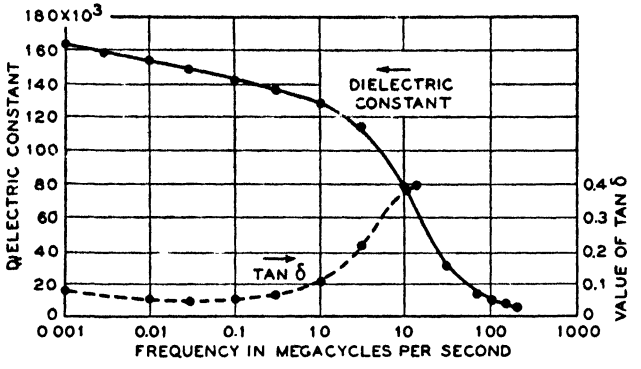

FIG. 11.15. Dielectric constant of *a* axis as a function of frequency.

dipole rather than a high dielectric constant of the type due to the near vanishing of the factor $\left(1 - \frac{4\pi}{3}\gamma\right)$ in the dielectric equation

$$\frac{\epsilon - 1}{4\pi} = \frac{\gamma}{1 - \frac{4\pi}{3}\gamma} \tag{11.57}$$

where γ is the polarizability and $\frac{4\pi}{3}$ the Lorentz factor, since the polarizability γ due to electrons, ions and atoms should not vary with frequency up to the infrared frequencies. Hence a temperature variable dipole of the type discussed in the next section is required to give a relaxation frequency as low as 15 megacycles.

11.32 *Spontaneous Polarization and Dielectric Constant Under Equilibrium Conditions*

The model considered here is the one shown by Fig. 11.16. Here there are six potential minima in the direction of the six oxygens which are displaced a distance δ from the center of the unit cell. If the titanium

nucleus is taken from a position such as 1 to position 2 directly across the unit cell, the form of the potential barrier may be as shown by Fig. 11.17 in which ΔU represents the height of the potential curve at the center with respect to that at the minima. If the nucleus went directly from

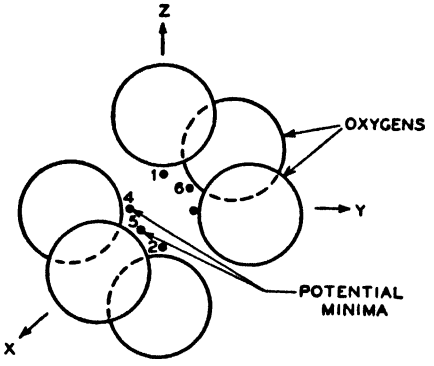

FIG. 11.16. Theoretical model for barium titanate showing positions of oxygens and potential minima for the titanium nucleus.

position 1 to position 3, it would in general have to cross a higher potential barrier than ΔU, but equilibrium between the two positions can be established by the nucleus jumping to a position slightly to one side of the

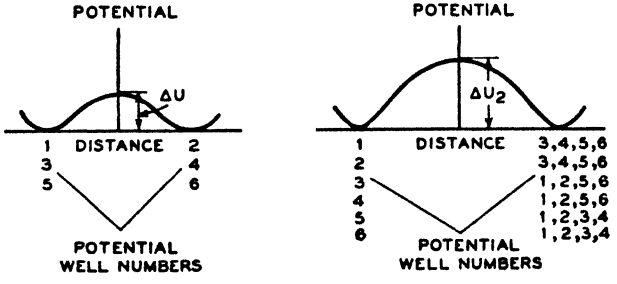

FIG. 11.17. Potential distribution as a function of distance from the center of the cell.

center in the direction 3; hence it is thought that the potential barrier determining the relaxation frequency for a 1 to 3 jump will not be much higher than for a 1 to 2 jump, namely ΔU.

For low frequencies, *i.e.* for frequencies well under the relaxation frequency, equilibrium values can be calculated by using Boltzmann's principle that the equilibrium ratios of numbers of nuclei in two potential

wells are in the ratio

$$\frac{N_1}{N_2} = e^{E/kT} \tag{11.58}$$

where E is the potential difference between well 2 and well 1, k is Boltzmann's constant and T the absolute temperature.

Suppose now that all the minima of Fig. 11.17 have initially the same potential, which is set equal to zero. Then if we apply a field E_z in the z direction, a polarization P_z in this direction results. This polarization causes an internal field F of the Lorentz type given by the equation

$$F = E + \frac{4\pi}{3} P_E + \beta P_d \tag{11.59}$$

where β may differ considerably from the theoretical value of $4\pi/3$ due to the shielding of the adjacent molecules. The inner dipole polarization is caused by the displacement of the titanium nucleus from the mid position of the unit cell. The dipole moment introduced by this change is

$$\mu = 4e\delta \tag{11.60}$$

since the valence of the titanium is 4 for the structure, e is the electronic charge, and δ the distance the titanium nucleus moves in going from the center of the unit cell to the equilibrium position. An addition to the dipole moment may also occur if the oxygen moves in toward the titanium. As shown by equation (11.7) the measured dipole polarization is enhanced by the shift of electronic charge and the measured value P_d' is related to the inner polarization by the equations

$$P_d' = P_d\left[1 + \beta\left(\frac{\epsilon_0 - 1}{4\pi}\right)\right] \tag{11.7}$$

The electronic and atomic polarization exerted will be proportional to the local field F, so that

$$F = E + \frac{4\pi}{3} P_e + \beta P_c = E + \frac{4\pi}{3}\gamma F + \beta P_d \quad \text{or} \quad F = \frac{E + \beta P_d}{1 - \frac{4\pi}{3}\gamma} \tag{11.61}$$

where γ is the polarizability per unit volume due to all polarization except that of the titanium dipoles. From equation (11.6)

$$\frac{\epsilon_0 - 1}{4\pi} = \frac{\gamma}{1 - \frac{4\pi}{3}\gamma} \quad \text{and} \quad \frac{4\pi}{3}\gamma = \frac{\epsilon_0 - 1}{\epsilon_0 + 2} \tag{11.62}$$

Hence the local field F is equal to

$$F = (E + \beta P_d)\left(1 + \frac{\epsilon_0 - 1}{3}\right) \tag{11.63}$$

The dielectric constant ϵ_0 near absolute zero is about 90, hence

$$\frac{1}{1 - \frac{4\pi}{3}\gamma} = 1 + \frac{(\epsilon_0 - 1)}{3} = 30.7 \tag{11.64}$$

This internal field caused by the applied field E_z, causes a decrease in the potential at the minima 1 and an increase in the potential at 2 equal respectively to

$$U_1 = -F(\mu) = -\left(\frac{E_z + \beta P_z}{1 - \frac{4\pi}{3}\gamma}\right)\mu; \qquad U_2 = +\left(\frac{E_z + \beta P_z}{1 - \frac{4\pi}{3}\gamma}\right)\mu \tag{11.65}$$

The potentials for the other four wells are unchanged by this field and hence

$$U_3 = U_4 = U_5 = U_6 = 0 \tag{11.66}$$

By Boltzmann's principle, equation (11.58), the relative number of nuclei in the six potential wells all expressed relative to N_5, are

$$N_1 = N_5 e^{\left(\frac{E_z + \beta P_z}{1 - (4\pi/3)\gamma}\right)\frac{\mu}{kT}}; \quad N_2 = N_5 e^{\left(\frac{E_z + \beta P_z}{1 - (4\pi/3)\gamma}\right)\frac{\mu}{kT}};$$
$$N_3 = N_4 = N_5 = N_6 \tag{11.67}$$

Then since the total number of nuclei is equal to N, where N is the number per cubic centimeter, we have

$$N = N_1 + N_2 + N_3 + N_4 + N_5 + N_6 \tag{11.68}$$

Substituting in the values from equations (11.67) we have

$$N_1 = \frac{Ne^{\left(\frac{E_z + \beta P_z}{1 - (4\pi/3)\gamma}\right)\frac{\mu}{kT}}}{2\left[2 + \cosh\left(\frac{E_z + \beta P_z}{1 - \frac{4\pi}{3}\gamma}\right)\frac{\mu}{kT}\right]}; \quad N_2 = \frac{Ne^{-\left(\frac{E_z + \beta P_z}{1 - (4\pi/3)\gamma}\right)\frac{\mu}{kT}}}{2\left[2 + \cosh\left(\frac{E_z + \beta P_z}{1 - \frac{4\pi}{3}\gamma}\right)\frac{\mu}{kT}\right]} \tag{11.69}$$

$$N_3 = N_4 = N_5 = N_6 = \frac{N}{2\left[2 + \cosh\left(\frac{E_z + \beta P_z}{1 - \frac{4\pi}{3}\gamma}\right)\frac{\mu}{kT}\right]}$$

The polarization of a dipole nature excited along the z-axis will then be

$$P_z = (N_1 - N_2)\mu = \frac{N\mu \sinh \left(\frac{E_z + \beta P_z}{1 - \frac{4\pi}{3}\gamma} \right) \frac{\mu}{kT}}{2 + \cosh \left(\frac{E_z + \beta P_z}{1 - \frac{4\pi}{3}\gamma} \right) \frac{\mu}{kT}} \tag{11.70}$$

All the equilibrium values of spontaneous polarization, coercive fields, dielectric constants, etc. can be determined from this equation.

Let us first consider the condition for spontaneous polarization and the ferroelectric effect. This can be obtained by setting E_z equal to zero and determining the conditions for which the polarization P_z is different from zero. Setting E_z equal to zero and introducing the substitution

$$A = \left(\frac{\beta N \mu^2}{1 - \frac{4\pi}{3}\gamma} \right) \frac{1}{kT} \tag{11.71}$$

equation (11.70) becomes

$$\frac{P_z}{N\mu} = \frac{\sinh \frac{AP_z}{N\mu}}{2 + \cosh \left(\frac{AP_z}{N\mu} \right)} \tag{11.72}$$

Examining this equation, we see that $P_z/N\mu$ will have a solution different from zero only if A is equal to 3 or greater. If A is greater than 3, $P_z/N\mu$ can have a positive or negative value lying between zero and 1. This represents a spontaneous polarization along the positive or negative z-axis due to the internal field generated by charge displacements of the titanium nuclei from the central position. In general, any one of the oxygen atoms can be considered as lying along the z-axis and only chance determines in which direction the spontaneous polarization occurs.

If we solve for $P_z/N\mu$ as a function of A, the relation shown by Fig 11.18, curve 1 results. This is a very much larger increase of $P_z/N\mu$ with increase in A than occurs for a single bond of the hydrogen bond type, which is determined by an equation of the type

$$\frac{P_z}{N\mu} = \tanh \frac{AP_z}{N\mu} \tag{11.73}$$

The relative increase for this type is shown by the dashed line of Fig. 11.18 for the same percentage increase in A. Some confirmation for this sudden

increase in polarization is obtained from the cell dimensions shown by Fig. 11.11. The changes in cell dimension, which are independent of the direction of polarization along the z-axis, can be regarded as due to the electrostrictive effect in barium titanate. The electrostrictive effect for the barium titanate ceramic has been investigated in Chapter XII and it is there shown that the ceramic has an increase in thickness and a decrease in radial dimension given by the strain equations

$$S_{33} = Q_{11}(P_z)^2; \qquad S_{11} = S_{22} = Q_{12}(P_z)^2 \tag{11.74}$$

where $Q_{11} = 3.6 \times 10^{-12} \left(\frac{\text{cm}^2}{\text{stat coulomb}}\right)^2$;

$$Q_{12} = -1.35 \times 10^{-12} \left(\frac{\text{cm}^2}{\text{stat coulomb}}\right)^2$$

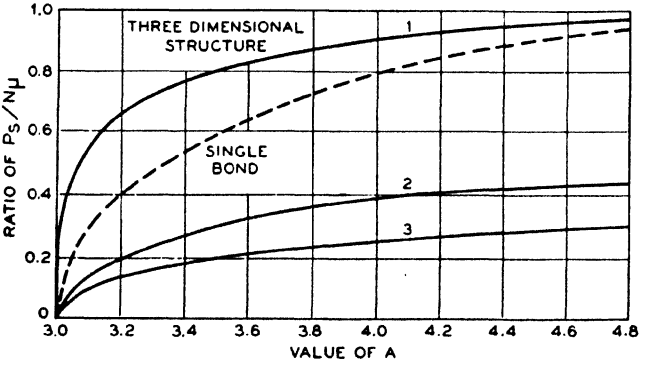

FIG. 11.18. Theoretical curve for ratio of spontaneous P_s to the total polarization $N\mu$ as a function of the factor A.

While the value of Q_{11}/Q_{12} is not exactly equal to -2 for the ceramic, a guide to the spontaneous polarization is obtained from these values. At 20°C, S_{33} the longitudinal thickness strain is equal to 6.7×10^{-3}, while the radial thickness strain is equal to $S_{11} = S_{22} = -3.3 \times 10^{-3}$ from the measurements of Fig. 11.11. With these values and the electrostrictive constants of (11.74), the indicated spontaneous polarization for the two effects is

$$P_s = 44{,}000 \frac{\text{stat coulomb}}{\text{cm}^2} = 14.6 \times 10^{-6} \frac{\text{coulomb}}{\text{cm}^2} \text{ (long.)} \tag{11.75}$$

$$P_s = 49{,}500 \frac{\text{stat coulomb}}{\text{cm}^2} = 16.4 \times 10^{-6} \frac{\text{coulomb}}{\text{cm}^2} \text{ (radial)}$$

The longitudinal mode gives the most likely value, so that

$$P_z = 44{,}000 \frac{\text{stat coulomb}}{\text{cm}^2} = 14.6 \times 10^{-6} \frac{\text{coulomb}}{\text{cm}^2} \tag{11.76}$$

This value agrees quite well with that measured electrically by means of the hysteresis loops. For this value Matthias and Von Hippel[20] find a value 12×10^{-6} coulomb per square centimeter, while Hulm[23] finds a

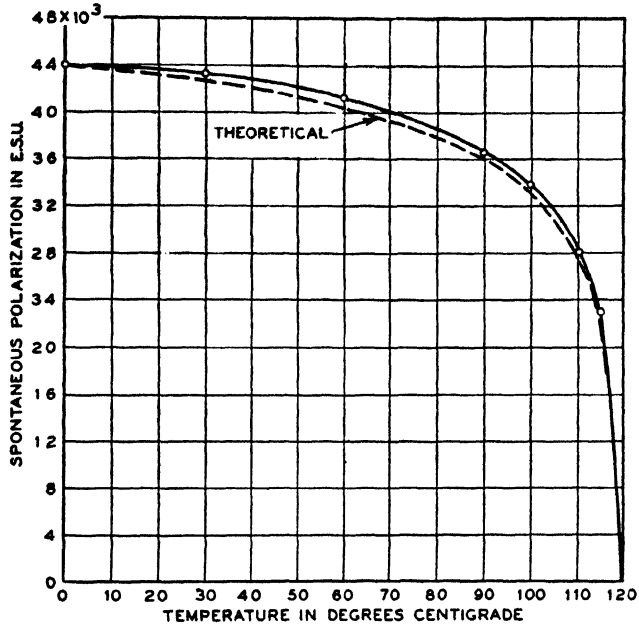

FIG. 11.19. Measured and theoretical spontaneous polarization as a function of the temperature.

value 16×10^{-6} coulomb per square centimeter. This calibration allows one to obtain the spontaneous polarization as a function of temperature, and this is shown plotted by Fig. 11.19. The very sudden rise in spontaneous polarization just below the Curie temperature, is evident and this agrees qualitatively with that shown by Fig. 11.18.

To find if the spontaneously generated polarization agrees quantitatively with that calculated from equation (11.72) we have to evaluate A and μ by other methods. One method for doing this is to measure the dielectric constants at low field strengths as a function of temperature. The cal-

[23] Hulm, F., *Nature*, Vol. 160, p. 126, 1947.

culated value can be obtained from equation (11.70) by dividing the polarization P_z into the spontaneous part P_S and a very small alternating part $P_0 e^{j\omega t}$. The applied field $E_z e^{j\omega t}$ is assumed very small and hence we have

$$\sinh\left[\frac{(E_z+\beta P_0)e^{j\omega t}+\beta P_S}{1-\frac{4\pi}{3}\gamma}\right]\frac{\mu}{kT}=\sinh\left[\frac{(E_z+\beta P_0)e^{j\omega t}}{1-\frac{4\pi}{3}\gamma}\right]\frac{\mu}{kT}$$

$$\cosh\left(\frac{\beta P_S}{1-\frac{4\pi}{3}\gamma}\right)\frac{\mu}{kT}+\cosh\left[\frac{(E_z+\beta P_0)e^{j\omega t}}{1-\frac{4\pi}{3}\gamma}\right]\frac{\mu}{kT}\sinh\left(\frac{\beta P_S}{1-\frac{4\pi}{3}\gamma}\right)\frac{\mu}{kT} \qquad (11.77)$$

$$\doteq\frac{(E_z+\beta P_0)e^{j\omega t}\mu}{\left(1-\frac{4\pi}{3}\gamma\right)kT}\cosh\frac{AP_S}{N\mu}+\sinh\frac{AP_S}{N\mu}$$

Similarly

$$\cosh\left[\frac{(E_z+\beta P_0)e^{j\omega t}+\beta P_S}{1-\frac{4\pi}{3}\gamma}\right]\frac{\mu}{kT}$$

$$\doteq\cosh\frac{AP_S}{N\mu}+\left[\frac{(E_z+\beta P_0)e^{j\omega t}}{1-\frac{4\pi}{3}\gamma}\right]\frac{\mu}{kT}\sinh\frac{AP_S}{N\mu} \qquad (11.78)$$

Inserting (11.77) and (11.78) in (11.70) and solving for the constant and time variable parts, we obtain equation (11.72) for the constant part and for the time variable part we have

$$\frac{P_0 e^{j\omega t}}{N\mu^2}=\frac{(E_z+\beta P_0)e^{j\omega t}}{\left(1-\frac{4\pi}{3}\gamma\right)kT}\left[\frac{2\cosh\frac{AP_S}{N\mu}+1}{\left(2+\cosh\frac{AP_S}{N\mu}\right)^2}\right] \qquad (11.79)$$

Solving for P_0, and substituting in equation (11.8)

$$\epsilon_z=\epsilon_0+\frac{\frac{4\pi A}{\beta}\left[\frac{2\cosh\frac{AP_S}{N\mu}+1}{2+\cosh\frac{AP_S}{N\mu}}\right]\left[1+\beta\frac{(\epsilon_0-1)}{4\pi}\right]}{2+\cosh\frac{AP_S}{N\mu}-A\left[\frac{2\cosh\frac{AP_S}{N\mu}+1}{2+\cosh\frac{AP_S}{N\mu}}\right]} \qquad (11.80)$$

Above the Curie point, the spontaneous polarization P_S disappears and this equation reduces to

$$\epsilon_z = \epsilon_0 + \frac{\frac{4\pi A}{\beta}}{3 - A}\left[1 + \beta\frac{(\epsilon_0 - 1)}{4\pi}\right] = \epsilon_0 + \frac{C}{T - T_0} \tag{11.81}$$

upon introducing the value of A from equations (11.71) and (11.64), where

$$C = \frac{4\pi N\mu^2\left[1 + \frac{\beta(\epsilon_0 - 1)}{4\pi}\right]\left[1 + \frac{\epsilon_0 - 1}{3}\right]}{3k}; \qquad T_0 = \frac{\beta N\mu^2}{3k}\left[1 + \frac{(\epsilon_0 - 1)}{3}\right] \tag{11.82}$$

Solving for β and μ from these equations we have

$$\beta = \frac{\frac{4\pi T_0}{C}}{1 - \frac{T_0}{C}(\epsilon_0 - 1)}; \qquad \mu = \sqrt{\frac{[C - T_0(\epsilon_0 - 1)]3k}{4\pi N\left[1 + \left(\frac{\epsilon_0 - 1}{3}\right)\right]}} \tag{11.83}$$

From the measurements of a number of dense ceramics above the Curie temperature and from the measurements of the single domain crystals of Merz,[22] one obtains a value of

$$C = 70{,}000; \qquad T_0 = 393°\text{K} \tag{11.84}$$

and from low temperature measurements[19]

$$\epsilon_0 = 90 \tag{11.85}$$

Hence from equation (11.83)

$$\beta = .142; \qquad \mu = 1.56 \times 10^{-18} \tag{11.86}$$

Since the number of dipoles per cubic centimeter is 1.56×10^{22}, the total measured polarization if all the dipoles were lined up would be

$$P_d' = N\mu\left[1 + \beta\left(\frac{\epsilon_0 - 1}{4\pi}\right)\right] = 49{,}000 \text{ esu} = 16.4 \times 10^{-6} \text{ coulombs/cm}^2 \tag{11.87}$$

If all the quantities entering into equation (11.71) for A were independent of temperature except T, the absolute temperature, the value of A for 10°C = 283°K would be 4.17 and the theoretical value of the polarization

$P_s/N\mu$ should be 0.92. This is close to the best estimated value but a slightly better value of $A = 3.95$ corresponding to $P_s/N\mu = 0.88$. With this value of A, the dielectric constant for the c axis is 202 at 10°C, a value agreeing well with the value measured by Merz.[22] In fact the dielectric constant above the transition temperature 10°C agrees well with that calculated from equation (11.80). A small variation in the components of the factor A is to be expected, for the residual dielectric constant ϵ_{c0} may vary with the electrostrictive effect, becoming smaller on account of the increase in the c dimension.

11.33 *Dielectric Constant along a-Axis and Low Temperature Transitions*

Measurements for the dielectric constants along the a-axis for single-domain crystals show that the dielectric constant along this axis is very much larger than that along the c-axis. To determine the dielectric along the a-axis, according to the model shown by Fig. 11.16, with a field applied along the x-axis, and a spontaneous polarization occurring along z, the potentials for all six wells are

$$U_1 = -\left(\frac{\beta_3 P_S \mu}{1 - \frac{4\pi}{3}\gamma}\right); \quad U_2 = \frac{\beta_3 P_S \mu}{1 - \frac{4\pi}{3}\gamma};$$
$$U_5 = -\frac{(E_x + \beta_1 P_x)\mu}{\left(1 - \frac{4\pi}{3}\gamma\right)}; \quad U_6 = \left(\frac{E_x + \beta_1 P_x}{1 - \frac{4\pi}{3}\gamma}\right)\mu; \quad U_3 = U_4 = 0 \tag{11.88}$$

We assume that β_1 along the x-axis may be different from β_3, along the z-axis. Applying the Boltzmann principle and relating N_1, N_2, N_5 and N_6 to $N_3 = N_4$ we find

$$N_1 = N_3 e^{\left[\frac{\beta_3 P_S}{1-(4\pi/3)\gamma}\right]\frac{\mu}{kT}}; \quad N_2 = N_3 e^{-\left[\frac{\beta_3 P_S}{1-(4\pi/3)\gamma}\right]\frac{\mu}{kT}}; \quad N_5 = N_3 e^{\left[\frac{E_x+\beta_1 P_x}{1-(4\pi/3)\gamma}\right]\frac{\mu}{kT}}$$
$$N_6 = N_3 e^{-\left[\frac{E_x+\beta_1 P_x}{1-(4\pi/3)\gamma}\right]\frac{\mu}{kT}}; \quad N_3 = N_4 \tag{11.89}$$

Since
$$N_1 + N_2 + N_3 + N_4 + N_5 + N_6 = N \tag{11.90}$$

we find for N_3, the value

$$N_3 = \frac{N}{2\left[1 + \cosh\left(\frac{\beta_3 P_S}{1 - \frac{4\pi}{3}\gamma}\right)\frac{\mu}{kT} + \cosh\left(\frac{E_x + \beta_1 P_x}{1 - \frac{4\pi}{3}\gamma}\right)\frac{\mu}{kT}\right]} \tag{11.91}$$

Inserting the value of N_3, N_5 and N_6 in the expression for the polarization along the x-axis, we have

$$P_x = (N_5 - N_6)\mu = \frac{N\mu \sinh\left(\frac{E_x + \beta_1 P_x}{1 - \frac{4\pi}{3}\gamma}\right)\frac{\mu}{kT}}{\left[1 + \cosh\left(\frac{\beta_3 P_S}{1 - \frac{4\pi}{3}\gamma}\right)\frac{\mu}{kT} + \cosh\left(\frac{E_x + \beta_1 P_x}{1 - \frac{4\pi}{3}\gamma}\right)\frac{\mu}{kT}\right]} \tag{11.92}$$

To determine the dielectric constant along x for small fields, we can replace

$$\sinh\left(\frac{E_x + \beta_1 P_x}{1 - \frac{4\pi}{3}\gamma}\right)\frac{\mu}{kT} \doteq \left(\frac{E_x + \beta_1 P_x}{1 - \frac{4\pi}{3}\gamma}\right)\frac{\mu}{kT}; \qquad \cosh\left(\frac{E_x + \beta_1 P_x}{1 - \frac{4\pi}{3}\gamma}\right)\frac{\mu}{kT} \doteq 1 \tag{11.93}$$

Then

$$P_x = \frac{\frac{N\mu^2}{kT}\left(\frac{E_x + \beta_1 P_x}{1 - \frac{4\pi}{3}\gamma}\right)}{2 + \cosh\left(\frac{\beta_3 P_S}{1 - \frac{4\pi}{3}\gamma}\right)\frac{\mu}{kT}} = \frac{\frac{N\mu^2}{kT}\left(\frac{E_x + \beta_1 P_x}{1 - \frac{4\pi}{3}\gamma}\right)}{2 + \cosh\frac{A_3 P_S}{N\mu}} \tag{11.94}$$

where

$$A_3 = \left(\frac{N\mu^2\beta_3}{1 - \frac{4\pi}{3}\gamma_3}\right)\frac{1}{kT} = \frac{N\mu^2\beta_3}{kT}\left[1 + \left(\frac{\epsilon_{03} - 1}{3}\right)\right] \tag{11.95}$$

Solving for the ratio of P_x to E_x, and substituting in equation (11.8) the dielectric constant along x becomes

$$\epsilon_x = \epsilon_{01} + \frac{\frac{4\pi N\mu^2}{kT\left(1 - \frac{4\pi}{3}\gamma_1\right)}\left[1 + \beta_1\left(\frac{\epsilon_{01} - 1}{4\pi}\right)\right]}{2 + \cosh\frac{A_3 P_S}{N\mu} - \frac{N\mu^2\beta_1}{\left(1 - \frac{4\pi}{3}\gamma_1\right)kT}} \tag{11.96}$$

Now since the crystal becomes tetragonal due to the distortion caused by

the electrostrictive effect, γ may increase along the a-axis and cause ϵ_{01} to become larger. Hence we can write

$$\frac{1}{1-\frac{4\pi}{3}\gamma_1} = 1 + \frac{(\epsilon_{01}-1)}{3} \tag{11.97}$$

Inserting this value and the abbreviation

$$A_1 = \frac{\beta_1 N\mu^2}{kT}\left[1 + \frac{(\epsilon_{01}-1)}{3}\right]$$

into equation (11.96) the dielectric constant along the $a = x$-axis becomes

$$\epsilon_x = \epsilon_{01} + \frac{\frac{4\pi A_1}{\beta_1}\left[1 + \beta_1\left(\frac{\epsilon_{01}-1}{4\pi}\right)\right]}{2 + \cosh\frac{A_3 P_s}{N\mu} - A_1} \tag{11.98}$$

At the Curie temperature where the crystal changes from tetragonal form to cubic form the value of the Lorentz factors for the x- and z-axes will be the same and hence the dielectric constant along the x-axis will have a Curie temperature at the same temperature as the one along the z-axis. For other temperatures the Lorentz factors along the two axes will not in general be equal on account of the shift in charge due to the electrostrictive effect. The same will also be true for the dielectric constants due to electrons and atoms. On account of the closer spacing along x than along z, ϵ_{01} will be larger than ϵ_{03}. Since no rational basis exists for calculating what the changes will be, all that can be said is that the value of A_1 for the x-axis is going to be larger than the value of A_3 for the z-axis.

To agree with experiment the values of A_1 and A_3 have to be as shown by the solid lines of Fig. 11.20. Since the dielectric constant for atoms and electrons is so large it is near the critical condition that a slight decrease in spacing may cause a large increase in dielectric constants. As shown by the X-ray data of Fig. 11.11 the spacing along a is approaching this condition. This explanation of the transition at 10°C as being due to the large increase in the dielectric constant along the a-axis due to electronic and atomic polarization receives some support from recent measurements on ceramic plates of lead zirconate. This material which has a cubic structure above 242°C, shows a ferroelectric transition at this temperature but does not have the two lower transitions observed in barium titanate. The lead zirconate has a dielectric constant less than 50 at low temperatures and hence the electrostrictive effect will not produce a large difference between ϵ_{01} and ϵ_{03}. A very slight change in A_1 to the dashed line above it will cause the dielectric constant along the a-axis to approach infinity. The

slight change in impurity content for the crystal whose dielectric constant is shown by Fig. 11.14 probably accounts for the increased dielectric con-

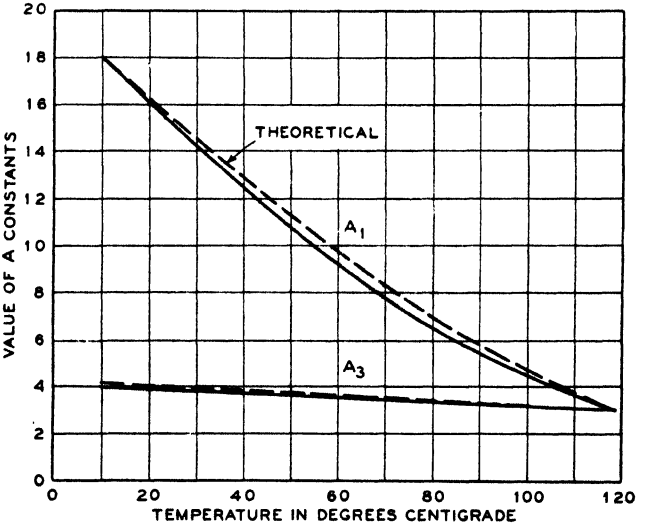

FIG. 11.20. Value of functions A_1 and A_3 plotted against temperature. Top dotted line, label theoretical, gives value of A_1 to cause the dielectric constant G_x to approach an infinite value.

stant along the a-axis over the one measured by Merz.[22] The following table shows the dielectric constant data for the a-axis as a function of temperature (as measured by Merz) and it is obvious that around 10°C the dielectric constant is becoming very large and approaching a transition temperature.

T in °K	393	360	340	320	300	288
ϵ_x	10,000	3400	3500	3800	4400	5400

This transition temperature is one for which all of the x-axes become ferroelectric. According to the present theory, the relative distribution of spontaneous charge along the x- and z-axes depends on a simultaneous solution of the two equations.

$$\frac{P_z}{N\mu} = \frac{\sinh \frac{A_3 P_z}{N\mu}}{1 + \cosh \frac{A_3 P_z}{N\mu} + \cosh \frac{A_1 P_x}{N\mu}}; \qquad \frac{P_x}{N\mu} = \frac{\sinh \frac{A_1 P_x}{N\mu}}{1 + \cosh \frac{A_3 P_z}{N\mu} + \cosh \frac{A_1 P_x}{N\mu}} \tag{11.99}$$

A solution can be arrived at by approximate methods for constant values of A_1 and A_3. The results indicate that $P_x/N\mu$ will be an appreciable fraction of $P_z/N\mu$ above the transition temperature while $P_z/N\mu$ below the transition temperature is less than $P_z/N\mu$ above this temperature. Since the difference between A_1 and A_3 was due to the shift in charge along z compared to x we should have to take new values of A_1 and A_3 closer together. The result of a series of such approximations is to show that finally $A_3 = A_1$ and the spontaneous polarization along x and z should be equal and given by the equation

$$\frac{P_s}{N\mu} = \frac{\sinh \dfrac{A_1 P_s}{N\mu}}{1 + 2\cosh \dfrac{A_1 P_s}{N\mu}} \tag{11.100}$$

A solution of this equation for spontaneous polarization is shown by the solid curve marked 2 of Fig. 11.18.

In the region between $-80°C$ and $+10°C$ the crystal is ferroelectric along two directions simultaneously which means that the titanium nucleus spends equal times for axes along x and z and very little time in the other four positions. This change is accompanied by a change in crystal structure from tetragonal to orthorhombic. This follows from the fact that if we draw a new z-axis along the 101 direction midway between the two favored positions, this is a two fold axis having a plane of symmetry coinciding with z and the two titanium positions and one coinciding with z and perpendicular to the titanium positions. Hence the symmetry is 2 mm as shown by the optical measurements of Forsbergh[19] and the crystal becomes orthorhombic. It is not possible to calculate the dielectric constants along the three axes without making assumptions as to the values of $A_1 = A_3$ and A_2. However, since the third axis y is going to be smaller than the other two, it is obvious that the value of A_2 will be larger than $A_1 = A_3$ and the dielectric constant in this direction will be larger. Eventually as the temperature becomes lower, the dielectric constant will approach a Curie transformation point and this axis will also become ferroelectric. By the same argument as given previously all three values of A will become equal and the titanium nucleus will spend equal times along three of the six positions and very little time in the other three. Taking the z-axis along the 111 direction, trigonal symmetry results since one can go from one preferred position to another by a 120° rotation. This results in the symmetry 3m class as observed by Forsbergh.[19]

For this condition the spontaneous polarization is determined by the

equation

$$\frac{P_s}{N\mu} = \frac{\sinh \dfrac{AP_S}{N\mu}}{3 \cosh \dfrac{AP_S}{N\mu}} \tag{11.101}$$

and the spontaneous polarization is plotted as a function of A by curve labeled 3 of Fig. 11.18.

11.34 *Coercive Fields Along a- and c-Axes*

The coercive fields along the a- and c-axes can be calculated from the fundamental equations

$$\frac{P_x}{N\mu} = \frac{\sinh \left[\dfrac{A_1(E_x/\beta_1 + P_x)}{N\mu}\right]}{1 + \cosh \left[\dfrac{A_3(E_z/\beta_3 + P_z)}{N\mu}\right] + \cosh \left[\dfrac{A_1(E_x/\beta_1 + P_x)}{N\mu}\right]} \tag{11.102}$$

$$\frac{P_z}{N\mu} = \frac{\sinh \left[\dfrac{A_3(E_z/\beta_3 + P_z)}{N\mu}\right]}{1 + \cosh \left[\dfrac{A_3(E_z/\beta_3 + P_z)}{N\mu}\right] + \cosh \left[\dfrac{A_1(E_x/\beta_1 + P_x)}{N\mu}\right]} \tag{11.103}$$

By employing the method for calculating the coercive field discussed in section 11.11 one can calculate that the coercive field to reverse a domain along the z-axis is given by the equation

$$\frac{\sinh \dfrac{A_3P_z}{N\mu}}{2 + \cosh \dfrac{A_3P_z}{N\mu}} - \frac{P_z}{N\mu} = \frac{A_3E_z}{\beta_3 N\mu}\left[\frac{2 \cosh \dfrac{A_3P_z}{N\mu} + 1}{\left(2 + \cosh \dfrac{A_3P_z}{N\mu}\right)^2}\right] \tag{11.104}$$

If we put a negative field along the z-axis, the ratio of $P_z/N\mu$ will decrease steadily until the value of the left-hand side is a maximum. For room temperature with $A_3 = 3.95$, $N\mu = 24{,}500$ esu, $\beta_3 = 0.142$, this occurs when $P_s/N\mu = 0.5$ giving a value of 0.120 for the left-hand side. Hence substituting in the values on the right-hand side, it requires a negative field of

$$E_z = 470 \text{ esu/cm} = 140{,}000 \text{ volts/cm} \tag{11.105}$$

to reverse the domain.

A true single domain crystal, however, will have a hysteresis loop for a considerably smaller field than this. To see that this is possible, one can

examine the conditions for spontaneous polarization along x given by equation (11.102). Here we set E_x equal to zero and solve for the conditions that will give a finite value of P_x in the presence of a field E_z, and a spontaneous polarization P_z. The onset of P_x will be determined when P_x approaches zero, and thus we can replace the hyperbolic sinh by the argument, and the hyperbolic cosh by unity. Then the equations to solve are

$$\frac{P_x}{N\mu} = \frac{\dfrac{A_1 P_x}{N\mu}}{2 + \cosh\left[\dfrac{A_3(E_z/\beta_3 + P_z)}{N\mu}\right]} \tag{11.106}$$

If $E_z = 0$, this reduces to the case

$$P_x\left[2 + \cosh\frac{A_3 P_z}{N\mu}\right] = A_1 P_x \tag{11.107}$$

The difference between the left-hand side and the right-hand side is the denominator of equation (11.98) for the dielectric constant along the x-axis. This denominator is small (about 1.9 for room temperature) but is always positive, and hence no spontaneous polarization can exist along x as long as there is no static field $-E_z$.

For the addition of a static field, equation (11.107) takes the form

$$P_x\left[2 + \cosh\left(\frac{A_3 E_z}{\beta_3 N\mu} + \frac{A_3 P_z}{N\mu}\right)\right] = A_1 P_x \tag{11.108}$$

A positive field E_z in the same direction as P_z makes the left-hand side still larger than the right, and no possibility exists for polarization along x. If, however, a negative field E_z is applied, the left-hand side can be made equal or less than the right-hand side, and spontaneous polarization can exist along x. To solve for the value of field, we separate the polarization P_z into the spontaneous polarization P_s plus a small charge ΔP_z. This is determined for small values of E_z by the dielectric constant ϵ_3 or

$$\Delta P_z = \left(\frac{\epsilon_3 - 1}{4\pi}\right) E_z \tag{11.109}$$

Hence since E_z/β_3 and ΔP_z are small compared to P_s, the equation for the coercive field is

$$\frac{A_3 E_z}{\beta_3 N\mu}\left[1 + \beta_3\left(\frac{\epsilon_3 - 1}{4\pi}\right)\right] = -\frac{\left[2 + \cosh\dfrac{A_3 P_s}{N\mu} - A_1\right]}{\sinh\dfrac{A_3 P_s}{N\mu}} \tag{11.110}$$

For values of $A_3 = 3.95$; $\beta_3 = 0.142$; $N\mu = 24{,}500$; $\epsilon_3 = 200$ and $P_s/N\mu = 0.88$; $A_1 = 16.3$ we find

$$-E_z = 6.5 \text{ esu} = 1950 \text{ volts/cm}^2 \tag{11.111}$$

This value is of the right order to agree with the observed hysteresis loops for single crystals and the hysteresis loops for ceramics as discussed in Chapter XII.

11.35 *Relaxation Frequencies for the Dielectric Constants*

A calculation[15] of the relaxation frequencies for the barium titanate crystal has been made along the lines of the calculation given in section 11.12. Since the method used is similar to that already discussed, only the final results will be given. For the dielectric constant in the first transition range between 10°C and 120°C, the dielectric constant along the z-axis becomes

$$\epsilon_z = \epsilon_{03} + \frac{\dfrac{4\pi A_3}{\beta_3}\left(\dfrac{2\cosh\dfrac{A_3P_s}{N\mu}+1}{2+\cosh\dfrac{A_3P_s}{N\mu}}\right)\left[1+\beta_3\left(\dfrac{\epsilon_{03}-1}{4\pi}\right)\right]}{\left\{\left(2+\cosh\dfrac{A_3P_s}{N\mu}\right)-A_3\left(\dfrac{2\cosh\dfrac{A_3P_s}{N\mu}+1}{2+\cosh\dfrac{A_3P_s}{N\mu}}\right)+\left(\dfrac{2+\cosh\dfrac{A_3P_s}{N\mu}}{\cosh\dfrac{A_3P_s}{N\mu}}\right)\dfrac{j\omega h e^{\Delta U/kT}}{6kT}\right\}} \tag{11.112}$$

When the last term in the denominator equals the sum of the other two, the dipole dielectric constant has equal resistance and reactance values and the corresponding frequency is the relaxation frequency. This frequency f_0 is given by

$$f_0 = \frac{6kTe^{-\Delta U/kT}}{2\pi h}\left\{\cosh\frac{A_3P_s}{N\mu}\left[\frac{1-A_3\left(2\cosh\dfrac{A_3P_s}{N\mu}+1\right)}{\left(2+\cosh\dfrac{A_3P_s}{N\mu}\right)^2}\right]\right\} \tag{11.113}$$

For 10°C = 283°K, we found $A_3 = 3.95$; $P_s/N\mu = 0.88$. Introducing these values and the values

$$k = 1.38 \times 10^{-16}; \qquad T = 300; \qquad h = 6.56 \times 10^{-27} \tag{11.114}$$

we find for f_0 the value

$$f_0 = 5.7 \times 10^{13} e^{-\Delta U/kT} \tag{11.115}$$

So far no measurements have been made for the relaxation frequency of the c-axis. For a ceramic a value of the activation energy is obtained from the dielectric measurements of Powles[22] where from the variation of the relaxation frequency with temperature one obtains a value of $\Delta U =$ 3.65 kilocalories per mole. This value represents the amount of energy required to remove the titanium nucleus from its equilibrium position to the center of the unit cell.

The dielectric data of Fig. 11.15 show that the dielectric constant for the a-axis of this crystal is relaxed at a frequency of about 15 megacycles at room temperature. Applying the same process to the calculation of the dielectric constant along the a-axis, one finds for the relaxation frequency

$$f_0 = \frac{6kT}{2\pi h} e^{-\Delta U/kT} \left[\frac{2 + \cosh \dfrac{A_3 P_s}{N\mu} - A_1}{2 + \cosh \dfrac{A_3 P_s}{N\mu}} \right] \cosh \frac{A_3 P_s}{N\mu} \tag{11.116}$$

For a dielectric constant of 150,000 at 27°C = 300°K, the numerator of the expression in brackets is 0.044. Introducing the other numerical values

$$e^{\Delta U/kT} = 15{,}500; \qquad \Delta U = 5.76 \text{ kilocalories per mole} \tag{11.117}$$

Hence the indicated activation energy for going from the 1 and 2 wells to the 3, 4, 5 or 6 wells is slightly higher than that between opposite wells such as 1 and 2. This calculation also checks the facts that it is the near vanishing of the denominator of equation (11.98) that causes the very high dielectric constant along the a-axis for this crystal. For the crystal grown by Merz,[21] the indicated relaxation frequency is about 6.5×10^8 cycles.

11.4 *Specific Heat Anomaly in Ferroelectric Crystals*

When a crystal becomes ferroelectric, some of the elements such as the hydrogen or titanium nuclei are not as free to move as they were in the non-ferroelectric state. Hence there is a specific heat anomaly in the neighborhood of the Curie temperature. As in the case of ferromagnetism, the increase above the normal value of the specific heat C_p is given by

$$\frac{d(\Delta C_p)}{dT} = \frac{\beta}{2} \frac{dP_s^2}{dT} \text{ erg cm}^{-3} \text{ deg}^{-1} \tag{11.118}$$

where β is the Lorentz factor and P_s the spontaneous polarization per square centimeter. Hence the specific heat anomaly between the two

temperatures T_2 and T_1 is equal to

$$\Delta C_p = \frac{\beta}{2}[P_{s2}^2 - P_{s1}^2] \tag{11.119}$$

In this equation, since β refers to the inner dipole polarization, P_s must also. Since the specific heat anomaly has been measured for rochelle salt,[24] potassium dihydrogen phosphate,[25] and barium titanate,[26] this gives an opportunity for comparing the Lorentz factor β determined from dielectric measurements with that determined from specific heat measurements.

The following table shows the best values of the specific heat measurements, the difference in the squares of the polarization at the temperature limits and the most probable value of β. The last column shows the value of β determined by dielectric measurements. As can be seen the two agree reasonably well.

Material	ΔC_p cal/gram	ΔC_p ergs/cc	$P_{s2}^2 - P_{s1}^2$	Value of β Specific Heat	Value of β Dielectric
Rochelle salt Upper Curie point	$<.0035$	$<2.6 \times 10^5$	7.5×10^4	<6.9	4.4
Rochelle salt Lower Curie point	$<.0035$	$<2.6 \times 10^5$	7.5×10^4	<6.9	4.4
KDP	0.75	7.2×10^7	2.0×10^8	0.72	0.567
Barium Titanate 120° Transition	0.2	5×10^7	5.8×10^8	0.172	0.142

11.5 *Elastic, Piezoelectric and Dielectric Properties of a Ferroelectric Crystal*

In order to bring out the fundamental mechanisms existing for the ferroelectric effect, only the clamped dielectric constant has been considered in the first four sections. It is possible, however, to include the modification in the elastic and piezoelectric constants caused by the ferroelectric effect in one unified theory. It is the purpose of this section to describe such a theory as applied to the simplest ferroelectric crystal potassium dihydrogen phosphate (KDP).

[24] Wilson, A. J. C., *Phys. Rev.*, Vol. 54, pp. 1103–1109, 1938.

[25] Stephenson, C. C., and J. G. Hooley, *Jour. Am. Chem. Soc.*, Vol. 66, pp. 1397–1401, 1944.

[26] Blattner, H., and W. Merz, *Helv. Phys. Acta*, Vol. 21, Fasciculus Tertius et Quartus, p. 210, 1948.

Although all four of the hydrogen bonds connected to each PO_4 group are at right angles to the z ferroelectric axis, on account of the polarization induced in the PO_4 group each bond can be treated as though a field were introduced along the bond length. In the absence of a field, the potential wells for the two symmetrical positions have an equal value U_0. On the application of an electrical field E, an internal field

$$F = E + \frac{4\pi}{3} P_E + \beta P_d \tag{11.120}$$

is generated which causes one potential well to be lowered while the other is raised by an amount

$$U_1 = U_0 - F\delta e/2; \qquad U_2 = U_0 + F\delta e/2 \tag{11.121}$$

where δ is the separation between potential wells.

If a piezoelectric effect exists in the crystal, then when a strain occurs in the crystal, the hydrogen bonds are stretched or compressed and also a dissymmetry must be introduced in the bond. The effect of the dissymmetry is similar to the introduction of an electric field E, so that the internal field can be written in the form

$$F = E + f_{36} S_6 + \frac{4\pi}{3} P_E + \beta P_d \tag{11.122}$$

where f_{36} is a fundamental constant of the crystal and S_6 the face-shear strain for a Z-cut crystal.

Now, since the potential well values U_1 and U_2 are known, the processes applied in sections 11.1, 11.2 and 11.3 can be used. For the present purpose we shall consider only the equilibrium values since an extension to high frequency values is obvious. Using the Boltzmann relation, the relative number of hydrogen nuclei in each of the types of potential wells is

$$\frac{N_1}{N_2} = e^{-\frac{F\delta e}{kT}} = e^{-[E + f_{36}S_6 + (4\pi/3)P_E + \beta P_d)]\delta e/kT}; \qquad N_1 + N_2 = N \tag{11.123}$$

Using the last relation that the sum of the number of nuclei in the two types of potential wells is equal to N, the number per cubic centimeter, the number in each type of well is

$$N_1 = \frac{N}{1 + e^{-F\delta e/kT}}; \qquad N_2 = \frac{Ne^{-F\delta e/kT}}{1 + e^{-F\delta e/kT}} \tag{11.124}$$

The expression for F can be simplified by substituting for the polarization for electrons and atoms, the factor

$$P_E = \gamma F$$

where γ is the polarizability per unit volume due to electrons and atoms. Then F becomes

$$F = \frac{E + f_{36}S_6 + \beta P_d}{1 - \frac{4\pi}{3}\gamma} \tag{11.125}$$

The dipole polarization P_d can now be evaluated as

$$P_d = (N_1 - N_2)\,\mu = N\mu \tanh\left[\frac{E + f_{36}S_6 + \beta P_d}{\left(1 - \frac{4\pi}{3}\gamma\right)kT}\right]\frac{\delta e}{2} \tag{11.126}$$

which contains the required solution. To separate the spontaneous polarization from that caused by the applied field or the strain we write

$$P_d = P_s + P_0 e^{j\omega t}; \qquad E = E_0 e^{j\omega t}; \qquad S_6 = S_6 e^{j\omega t} + S_{6s} \tag{11.127}$$

since a spontaneous polarization P_s and strain S_{6s} occur. Inserting these in equations (11.126), noting that the time-variable parts are very small compared to the constant parts, we have on separating the two parts

$$\frac{P_s}{N\mu} + \tanh A\frac{[f_{36}S_{6s}/\beta + P_s]}{N\mu}; \qquad \frac{P_0 e^{j\omega t}}{N\mu}$$

$$= e^{j\omega t}\frac{\left[\left(\frac{E_0 + \beta P_0}{1 - \frac{4\pi}{3}\gamma}\right)\frac{\mu}{kT} + \left(\frac{f_{36}S_6}{1 - \frac{4\pi}{3}\gamma}\right)\frac{\mu}{kT}\right]}{\cosh^2\frac{A[P_s + f_{36}S_{6s}/\beta]}{N\mu}} \tag{11.128}$$

where as before A is the constant

$$A = \left(\frac{\beta N\mu^2}{1 - \frac{4\pi}{3}\gamma}\right)\frac{1}{kT}$$

The first of equations (11.128) is the condition (11.13) for determining the spontaneous polarization for the clamped dielectric constant. Solving for the time variable polarization P_0, we have

$$P_0 = \frac{A}{\beta}\frac{(E_0 + f_{36}S_6)}{\cosh^2\frac{A[P_s + f_{36}S_{6s}/\beta]}{N\mu} - A} \tag{11.129}$$

From the first equation of (11.128) we have

$$\cosh^2 \frac{A[P_s + f_{36}S_{6s}/\beta]}{N\mu} = \frac{1}{\left[1 - \left(\frac{P_s}{N\mu}\right)^2\right]} \tag{11.130}$$

Introducing the value of A, noting that the clamped constant Curie temperature T_0 is

$$T_0 = \frac{\beta N\mu^2}{\left(1 - \frac{4\pi}{3}\gamma\right)k} \tag{11.131}$$

we have

$$P_0 = \frac{\frac{T_0}{\beta}(E_0 + f_{36}S_6)}{\frac{T}{\left[1 - \left(\frac{P_s}{N\mu}\right)^2\right]} - T_0} \tag{11.132}$$

The total polarization P is the sum of the alternating dipole polarization P_0, times the factor $\left[1 + \beta\left(\frac{\epsilon_0 - 1}{4\pi}\right)\right]$, plus the polarization P_E due to electrons and atoms. Hence we have for the dielectric displacement

$$\begin{aligned}\delta = \frac{D}{4\pi} &= P_0\left[1 + \beta\left(\frac{\epsilon_0 - 1}{4\pi}\right)\right] + P_E + \frac{E_0}{4\pi} \\ &= E_0\left\{\frac{\epsilon_0}{4\pi} + \frac{(T_0/\beta)\left[1 + \beta\left(\frac{\epsilon_0 - 1}{4\pi}\right)\right]}{\frac{T}{\left[1 - \left(\frac{P_s}{N\mu}\right)^2\right]} - T_0}\right\} \\ &\quad + \frac{f_{36}(T_0/\beta)\left[1 + \beta\left(\frac{\epsilon_0 - 1}{4\pi}\right)\right]S_6}{\frac{T}{\left[1 - \left(\frac{P_s}{N\mu}\right)^2\right]} - T_0}\end{aligned} \tag{11.133}$$

From the form of the potential function U, we can write the second equation as

$$T_6 = c_{66}^P S_6 - f_{36}P_s' = c_{66}^P S_6 - f_{36}\left[1 + \beta\left(\frac{\epsilon_0 - 1}{4\pi}\right)\right]P_0 \tag{11.134}$$

where P_s' is the measured dipole polarization.

For a free crystal $T_6 = 0$ and hence for a spontaneous polarization P_s there exists a spontaneous strain S_{6s} equal to

$$S_{6s} = f_{36}\left[1 + \left(\frac{\epsilon_0 - 1}{4\pi}\right)\right]P_s/c_{66}^P \tag{11.135}$$

Introducing this equation in the first of equations (11.128), we find that for the " free " dielectric constant, spontaneous polarization occurs at a higher temperature T_0' equal to

$$T_0' = T_0\left[1 + \frac{f_{36}^2\left(1 + \beta\dfrac{(\epsilon_0 - 1)}{4\pi}\right)}{\beta c_{66}^P}\right] \tag{11.136}$$

From the values derived previously it is found that T_0' is 3.5°K higher than T_0 for KDP.

The time variable stress, strain, field equation can be obtained by introducing the value of P_0 into equations (11.134), obtaining

$$\begin{aligned} T_6 = &\left\{c_{66}^P - \frac{(T_0/\beta)\left[1 + \beta\left(\dfrac{\epsilon_0 - 1}{4\pi}\right)\right]f_{36}^2}{\dfrac{T}{\left[1 - \left(\dfrac{P_s}{N\mu}\right)^2\right]} - T_0}\right\}S_6 \\ &- \frac{f_{36}(T_0/\beta)\left[1 + \beta\left(\dfrac{\epsilon_0 - 1}{4\pi}\right)\right]E_0}{\dfrac{T}{\left[1 - \left(\dfrac{P_s}{N\mu}\right)^2\right]} - T_0} \end{aligned} \tag{11.137}$$

Comparing these equations with the forms shown in equation (3.60) of Chapter III, we have

$$(\epsilon_{33}^S - \epsilon_{33_0}) = \frac{(4\pi T_0/\beta)\left[1 + \beta\left(\dfrac{\epsilon_0 - 1}{4\pi}\right)\right]}{\dfrac{T}{\left[1 - \left(\dfrac{P_s}{N\mu}\right)^2\right]} - T_0}; \tag{11.138}$$

$$e_{36} = \frac{f_{36}(\epsilon_{33}^S - \epsilon_{33_0})}{4\pi}; \qquad c_{66}^E = c_{66}^P - \frac{(\epsilon_{33}^S - \epsilon_{33_0})}{4\pi}f_{36}^2$$

Above the Curie temperature, since the spontaneous polarization $P_s = 0$,

the formulae for the three constants are

$$\epsilon_{33}^{S} = \epsilon_{330} + \frac{(4\pi T_0/\beta)\left[1 + \beta\left(\frac{\epsilon_0 - 1}{4\pi}\right)\right]}{T - T_0}$$

$$e_{36} = \frac{f_{36}(T_0/\beta)\left[1 + \beta\left(\frac{\epsilon_0 - 1}{4\pi}\right)\right]}{T - T_0} \qquad (11.139)$$

$$c_{66}^{E} = c_{66}^{P} - \frac{(T_0/\beta)f_{36}^2\left[1 + \beta\left(\frac{\epsilon_0 - 1}{4\pi}\right)\right]}{T - T_0}$$

Hence the clamped dielectric constant measured at frequencies high enough to eliminate the strain follows a Curie Weiss law with T_0 as the Curie temperature. A detailed calculation shows however that its value reaches a maximum when $T = T_0'$, the Curie temperature for the free dielectric constant. This follows from the fact that $(1 - (P_s/N\mu)^2)$ decreases faster with T than T does. Hence the damped dielectric constant reaches a finite maximum at T_0', in agreement with the data of Fig. 7.8, having a value for KDP of

$$\epsilon_{33}^{S} - \epsilon_0 = \frac{4\pi T_0 \beta}{T_0' - T_0}\left[1 + \beta\left(\frac{\epsilon_0 - 1}{4\pi}\right)\right] = 880 \qquad (11.140)$$

This agrees closely with the value of Table XIII, Chapter VIII. At the Curie temperature T_0', the value of the elastic constant c_{66}^{E} is

$$c_{66}^{E} = c_{66}^{P} - \frac{T_0 f_{36}^2\left[1 + \beta\left(\frac{\epsilon_0 - 1}{4\pi}\right)\right]}{\beta[T_0' - T_0]} = 0 \qquad (11.141)$$

by virtue of equation (11.136).

The present theory agrees with Mueller's interaction theory[27] in predicting an increase in the Curie temperature T_0' for a free dielectric constant over the value T_0 for a clamped crystal, but is based on an internal field theory rather than an interaction theory.

The last two equations of (11.138) will hold for any type of a ferroelectric crystal, for example rochelle salt, but on account of the bonds of the two types, the clamped dielectric constant is determined by a different equation as discussed in section 11.12.

[27] See *Phys. Rev.*, Vol. 58, pp. 805–811 or Cady's *Piezoelectricity*, Chapter XXIII.

CHAPTER XII

Electrostrictive Effect[1] in Rochelle Salt and Barium Titanate

12.1 *Introduction*

In addition to the first-order piezoelectric effect, all crystals have a second-order electrostrictive effect in which a distortion occurs which is proportional to the square of the electric displacement. While this effect exists for all crystals and indeed in all solid insulators, it is exceedingly small except in ferroelectric materials such as rochelle salt and barium titanate. The amount of motion generated in a barium titanate ceramic is larger than that in magnetostrictive materials, and it appears that barium titanate may be an important electromechanical transducing element.

The electrostrictive effect in rochelle salt is discussed in the appendix. The only constants measured are those for a polarization along the x-axis and the results are given in Fig. A.3. Here are plotted the strains in parts per million caused by the spontaneous polarization. The largest constant is the one that measures the contraction in the x-direction and this causes a contraction of 50 parts in a million when a spontaneous polarization of 740 esu of charge exists per square centimeter. In terms of equations (A.164), the strain along the thickness is given by

$$S_{11} = Q_{1111}\left(\frac{Dx}{4\pi}\right)^2 \tag{12.1}$$

[1] In the present book, a strain that is proportional to the square or the product of two fields or electric displacements is called an electrostrictive strain. This is contrary in some cases to a usage started by Mueller who calls the square term a "quadratic" piezoelectric effect, when it depends on a strain caused by a spontaneous polarization or an applied field acting on a piezoelectric constant. On this definition the electrostrictive effect in rochelle salt would be a "quadratic" piezoelectric effect because it depends on the orthorhombic crystal becoming monoclinic in the ferroelectric region and generating new piezoelectric constants, which give a strain proportional to the spontaneous polarization times the applied electric displacement. The electrostrictive effect in barium titanate[2] is not of this type and is in every way the analog of a magnetostrictive effect in a ferromagnetic material.

[2] Mason, W. P., "Piezoelectric or Electrostrictive Effect in Barium Titanate Ceramics," *Phys. Rev.*, Vol. 73, No. 11, p. 1398, June 1, 1948.

where $Q_{1111} = -86.5 \times 10^{-12}$. For the same electric displacement, the piezoelectric effect would cause a longitudinal strain about 5 times as large, so that the electrostrictive effect is approaching in size the piezoelectric effect.

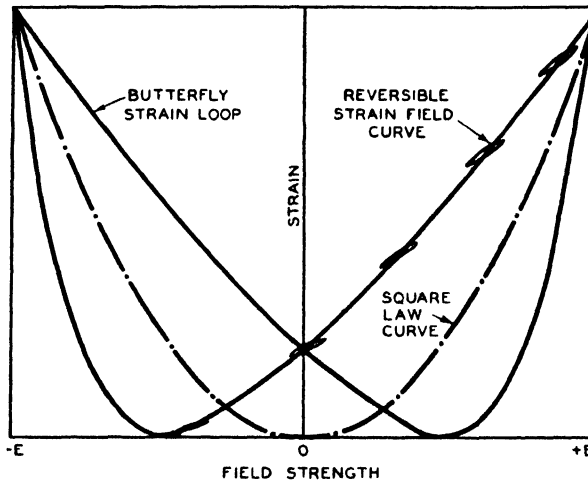

FIG. 12.1. Plot of displacement vs. voltage showing characteristic butterfly loop.

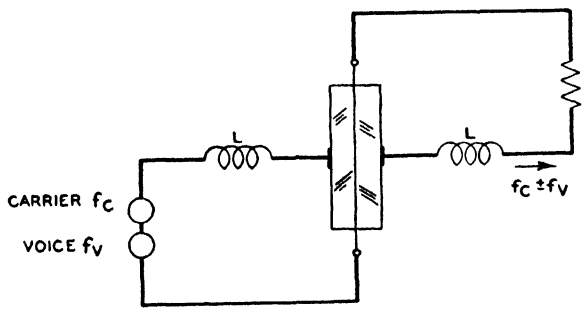

FIG. 12.2. Use of electrostrictive effect as a modulator.

Since the electrostrictive strain is proportional to the square of the electric displacement, if we plot it against the field, the characteristic butterfly loop of a hysteretic material results as shown in Fig. 12.1. For a large field, the vibration of the crystal surface will have twice the frequency of the applied field and such a crystal could be used as a modulator. A typical arrangement might be as shown by Fig. 12.2. Here a carrier and voice frequency are impressed on the crystal and the resulting vibration is picked up by a thickness vibrating crystal of the *L*-cut rochelle salt type.

The vibration picked up would have the two sideband frequencies and hence such a device could be used as a modulator.

A frequency equal to the applied frequency can be obtained by putting on a direct voltage bias or by bringing the polarization to saturation by a field and after taking off the field, using the remanent polarization to provide a bias. If the applied AC field is small, it will not reduce the remanent polarization and hence such a crystal will act as a thickness vibrating piezoelectric crystal.

It has been recently discovered[3,4,5] that another ferroelectric crystal, barium titanate in multicrystalline form, will act similarly. Here a ceramic made up of a number of crystals of barium titanate with their axes distributed in all directions and fused together with a small amount of binder can be made to change its dimensions when an electric field is applied to it. The thickness expansion is about as large as can be obtained by the direct piezoelectric effect in rochelle salt and is somewhat larger than can be obtained with magnetostrictive materials. Furthermore, the variations of the properties of barium titanate with temperature are not nearly as large as for rochelle salt. Hence such materials may be of use for various types of transducers. If the alternating variations are small compared to the DC polarization, a remanent polarization is sufficient to keep the device operative. By introducing small amounts of lead titanate in the ceramic, the coercive voltage becomes very large and power outputs have been obtained with this material as high as 100 watts per square centimeter without causing depolarization.

12.2 *Methods for Measuring the Fundamental Constants*

When a constant voltage bias is applied to a multicrystalline barium titanate ceramic, an alternating voltage can excite resonances in the ceramic. There are four effects that have been measured. These are radial vibrations of a disc of the material,[3] a length vibration of a bar cut from such a disc, a thickness vibration in the direction of the applied field[4] and a thickness-shear mode.[5] The first three motions are excited when the DC field is applied in the same direction as the AC field, while the fourth is excited when the DC polarization is at right angles to the AC field. Since, if there are two sets of plates at right angles to each other, the AC field cannot be made uniform through its direction of application,

[3] Roberts, Shepard, " Dielectric and Piezoelectric Properties of BariumTitanate," *Phys. Rev.*, Vol. 71, No. 13, pp. 890–895, June 15, 1947.

[4] Mason, W. P., " Electrostrictive Effect in Barium Titanate," *Phys. Rev.*, No. 1, p. 809, 1947.

[5] Cherry, W. L. Jr., and Robert Adler, " Piezoelectric Effect in Polycrystalline Barium Titanate," *Phys. Rev.*, p. 981, Nov. 15, 1947.

this mode has to be excited by exciting a remanent polarization by the DC field and then taking off the plating in this direction. In fact, for all of these modes, the DC biasing voltage can be applied and then taken off and the device will still operate by means of the remanent polarization.

A typical method for measuring such resonances is shown by Fig. 12.3. Here a source of high voltage, such as a high-voltage transformer and rectifying tube, with the output connected through high resistances is put directly on the ceramic piece, while the AC voltage is applied through two 4-microfarad condensers in series. At the resonant frequencies of the ceramic, which are usually above 100 kilocycles, the impedances of the condensers are less than 1 ohm, while the shunt impedance of the high-

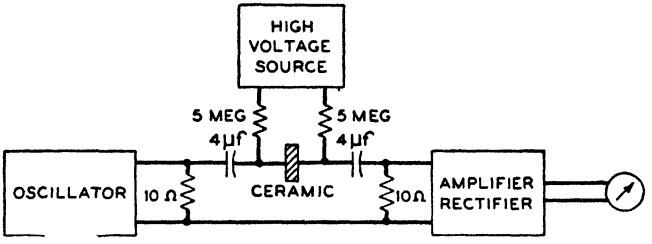

FIG. 12.3. Electrical circuit for investigating electrostrictive effect.

voltage source, being 10 megohms, is much higher than the impedance of the ceramic. Hence, by this method, one obtains a measure of the electrical impedance of the ceramic and can determine the effect of putting a high electrical bias on it.

If one measures the impedance of a freshly made ceramic on which no electrical bias has been placed, the impedance is that of a condenser and no resonances can be excited. However, if one puts a bias of 30,000 volts per centimeter on the ceramic disc of the material, for example, having the dimensions

$$\text{radius } a = 2.5 \text{ cm}; \qquad \text{thickness } t = 0.025 \text{ cm} \tag{12.2}$$

Fig. 12.4 shows a measurement of the resonant and anti-resonant frequencies as a function of the applied voltage, as the voltage bias is decreased to $-30{,}000$ volts per centimeter. Upon reversing the direction of the bias, the ascending curves shown are obtained. It is obvious that we are dealing with a hysteretic material for which the previous history determines the response. Since the electric displacement follows a similar hysteresis curve when plotted against the voltage, it is likely that the response is determined by the electric displacement rather than the electric field. When the field is reduced to zero a polarization remains and this determines the resonant and anti-resonant frequencies of the material.

From the data of Fig. 12.4 and the measured dielectric constant shown by Fig. 12.5, one can calculate the electromechanical coupling (which determines the percentage of energy stored in mechanical form to the total input electrical energy), the electrostrictive constant and the value of the elastic constant controlling the radial vibrations. The method for deriving the fundamental elastic, electrostrictive and electromechanical coupling

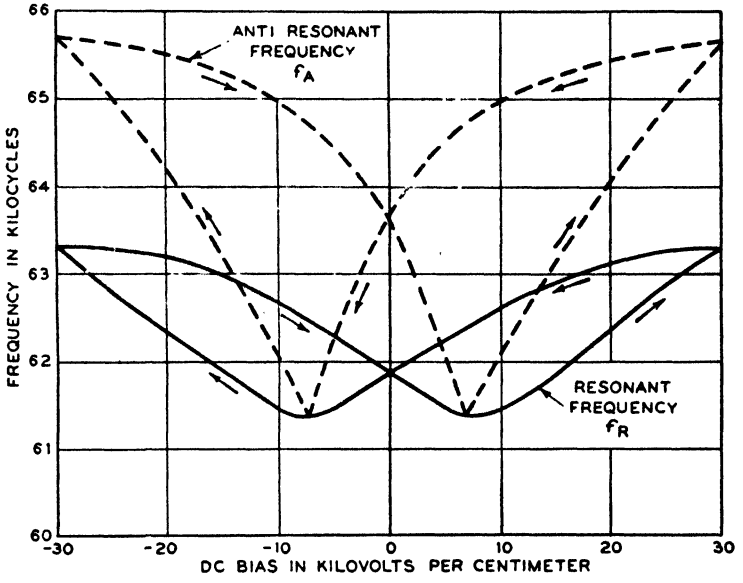

FIG. 12.4. Resonant and anti-resonant frequencies for a circular disc in radial vibration.

constants for radial vibrations is discussed in the Appendix A.9. It is shown that the resonant frequency for a material having a Poisson's ratio 0.27, which is near that for barium titanate, is given by the equation

$$f_r = \frac{2.03}{2\pi a}\sqrt{\frac{Y_0}{\rho(1-\sigma^2)}} \tag{12.3}$$

where a is the radius, Y_0 = Young's modulus, ρ = density and σ = Poisson's ratio. In the disc whose data are given by Fig. 12.4, a = 2.5 cm, ρ = 5.5 and σ = 0.27. Hence the value of Young's modulus for zero biasing field is 1.12×10^{12} dynes per square centimeter. The value of Young's modulus is increased slightly with bias, being 1.18×10^{12} at 30,000 volts per centimeter.

It is shown in the appendix that the electromechanical coupling factor

k is determined in terms of the separation of resonant and anti-resonant frequency, Δf, the resonant frequency f_R, the first root R, of the frequency determining equation, *i.e.* $R_1 = 2.03$, and the value of Poisson's ratio, by the equation

$$k^2 = \frac{\Delta f}{f_R}\left[\frac{R_1^2 - (1 - \sigma^2)}{1 + \sigma} + \cdots\right] \tag{12.4}$$

For $\sigma = 0.27$, the value of the factor multiplying $\Delta f/f_R$ is equal to 2.51. Hence, from the data of Fig. 12.4, the electromechanical coupling factor can be calculated and is shown plotted by Fig. 12.6. It follows a regular hysteresis loop, indicating that the remanent polarization is annulled

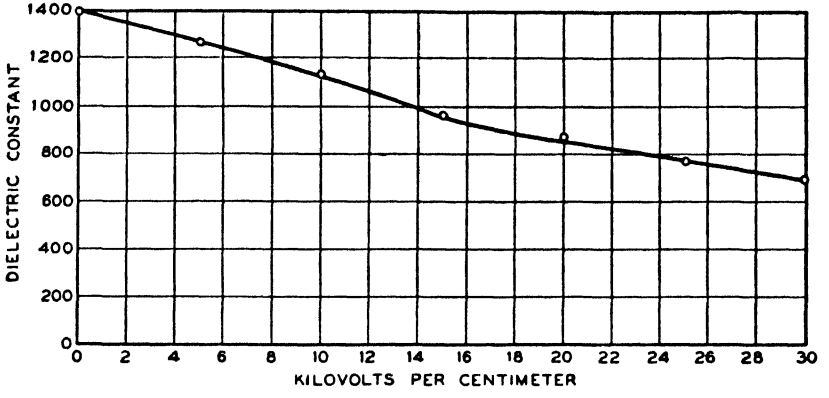

FIG. 12.5. Dielectric constant as a function of voltage.

when the voltage gradient is about 5,000 volts per centimeter negative. For a smaller initial polarizing field, the coercive field is less.

These results indicate that for an applied DC voltage, since the strain is proportional to the square of the electric displacement, if we plot it against the field, the characteristic butterfly loop of a hysteretic material will result, as shown by Fig. 12.1. Actual DC measurements, with a bimorph unit and the field applied to only one side, give values which follow this type of curve very well. The calculated constant comes very elose to that measured by AC measurements as discussed in the next section.

Similar AC measurements have been made for the thickness-longitudinal mode, the thickness-shear mode, the longitudinal-length mode and the coupling factors are shown plotted by Fig. 12.6. The frequency constant for the longitudinal-thickness mode for a zero bias is 2550 kilo-

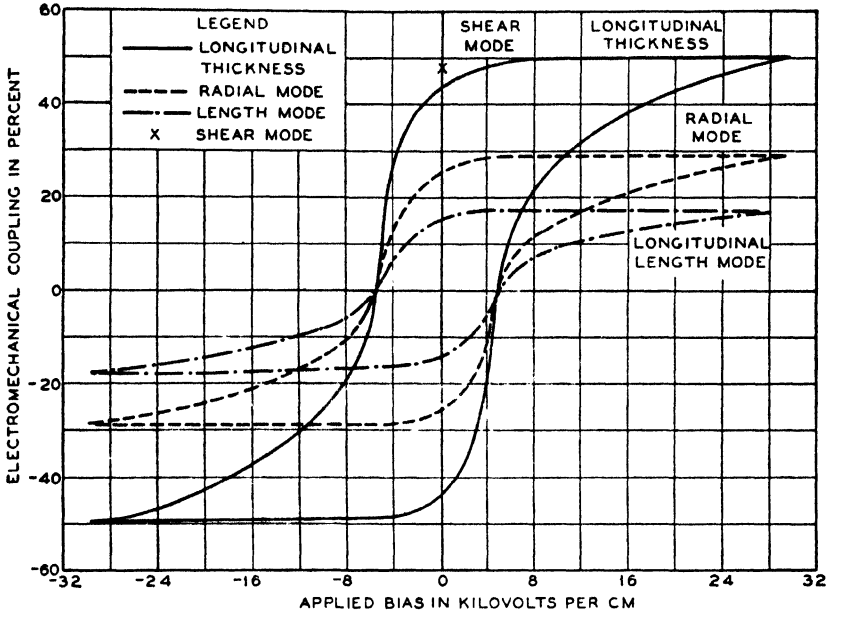

FIG. 12.6. Electrostrictive coupling for four modes of motion plotted as a function of the biasing field.

cycle-millimeters. From this, one obtains the elastic constant from the formula

$$f = \frac{1}{2t}\sqrt{\frac{\lambda + 2\mu}{\rho}} \tag{12.5}$$

as

$$(\lambda + 2\mu) = 1.42 \times 10^{12}\ \text{dynes/cm}^2 \tag{12.6}$$

This and the value of Young's modulus

$$Y_0 = 1.13 \times 10^{12}\ \text{dynes/cm}^2 = \mu\frac{(3\lambda + 2\mu)}{(\lambda + \mu)} \tag{12.7}$$

allow one to solve for the two Lamé elastic constants. These are

$$\lambda = 5.2 \times 10^{11}\ \text{dynes/cm}^2; \qquad \mu = 4.5 \times 10^{11}\ \text{dynes/cm}^2 \tag{12.8}$$

and from these the value of Poisson's ratio is

$$\sigma = \frac{\lambda}{2(\lambda + \mu)} = 0.27 \tag{12.9}$$

as quoted above.

To obtain the thickness-shear mode, one has to polarize the ceramic in one direction and then remove the plating. An AC field perpendicular to this will generate a thickness-shear mode with a coupling, shown by the single point of Fig. 12.6.

12.3 *Phenomenological Theory of Electrostrictive Effect In Barium Titanate Ceramics*

Since in a barium titanate ceramic, any crystal symmetry is lost by the distribution of crystal axes in all directions, any first-order piezoelectric effects are annulled and all the modes of motion must be due to second-order electrostrictive effects. In the experiments of section 12.2 it was shown that the electromechanical coupling was determined by the electric displacement rather than the electric field so that we take as the independent variables the stresses and the electric displacements. All the measurements were made under adiabatic conditions so that all constants can be considered as adiabatic.

In terms of a tensor notation the internal energy residing in the body can be expressed in the form

$$dU = T_{ij}\, dS_{ij} + E_m \frac{dD_m}{4\pi} + \Theta d\sigma \qquad \binom{i,j=1,2,3}{m=1,2,3} \qquad (12.10)$$

where T_{ij} are the six stress components, S_{ij} the six strain components, E_m the fields, D_m the electric displacements, Θ the absolute temperature, and σ the entropy. The strain components are defined in the usual tensor form

$$S_{ij} = \frac{1}{2}\left(\frac{\partial u_i}{\partial x_j} + \frac{\partial u_j}{\partial x_i}\right) \qquad (12.11)$$

where u_i are the displacements along the x_i-axes. In order to avoid using the factor $1/4\pi$, we made the substitution

$$\delta_m = D_m/4\pi \qquad (12.12)$$

δ_m is then measured in statcoulombs per square centimeter.

For the present purpose, since we are going to take T_{ij}, δ_m and σ as the fundamental variables, we introduce a potential H_1, called the elastic enthalpy, defined by the equation

$$H_1 = U - S_{ij}T_{ij} \qquad (12.13)$$

Hence

$$dH_1 = -S_{ij}\, dT_{ij} + E_m\, d\delta_m + \Theta\, d\sigma \qquad (12.14)$$

and

$$S_{ij} = -\frac{\partial H_1}{\partial T_{ij}}; \qquad E_m = \frac{\partial H_1}{\partial \delta_m}; \qquad \Theta = \frac{\partial H_1}{\partial \sigma} \qquad (12.15)$$

Since for adiabatic conditions σ does not vary, the dependent variables of interest, S_{ij} and E_m, can be written in the form

$$S_{ij}(T_{kl}, \delta_n); \qquad E_m(T_{kl}, \delta_n) \tag{12.16}$$

Expanding these functions about the position of zero strain and zero electric field, we have up to second-order terms

$$\begin{aligned} S_{ij} &= \frac{\partial S_{ij}}{\partial T_{kl}} dT_{kl} + \frac{\partial S_{ij}}{\partial \delta_n} d\delta_n + \frac{1}{2!}\left[\frac{\partial^2 S_{ij}}{\partial T_{kl}\, \partial T_{qr}} dT_{kl}\, dT_{qr}\right. \\ &\quad \left. + 2\frac{\partial^2 S_{ij}}{\partial T_{kl}\, \partial \delta_n} dT_{kl}\, d\delta_n + \frac{\partial^2 S_{ij}}{\partial \delta_n\, \partial \delta_0} d\delta_n\, d\delta_0\right] + \cdots \\ E_m &= \frac{\partial E_m}{\partial T_{kl}} dT_{kl} + \frac{\partial E_m}{\partial \delta_n} d\delta_n + \frac{1}{2!}\left[\frac{\partial^2 E_m}{\partial T_{kl}\, \partial T_{qr}} dT_{kl}\, dT_{qr}\right. \\ &\quad \left. + 2\frac{\partial^2 E_m}{\partial T_{kl}\, \partial \delta_n} dT_{kl}\, d\delta_n + \frac{\partial^2 E_m}{\partial \delta_n\, \partial \delta_0} d\delta_n\, d\delta_0\right] + \cdots \end{aligned} \tag{12.17}$$

For the present purpose some of these partial derivatives can be set equal to zero. Since there is no direct piezoelectric effect on account of the uniform distribution of the crystals in all directions,

$$\frac{\partial S_{ij}}{\partial \delta_n} = -\frac{\partial^2 H_1}{\partial \delta_n\, \partial T_{ij}} = -\frac{\partial^2 H_1}{\partial T_{ij}\, \partial \delta_n} = -\frac{\partial E_m}{\partial T_{ij}} = 0 \tag{12.18}$$

Furthermore, the ceramic can be described as soft electrically but not mechanically; hence, not much change in the elastic constants with stress will occur and $\partial^2 S_{ij}/\partial T_{kl}\, \partial T_{qr} = 0$. There is a slight change of elastic constants with electric displacement, as shown by Fig. 12.4, but it is small and is neglected here. Hence we can set

$$\frac{\partial^2 S_{ij}}{\partial T_{kl}\, \partial \delta_n} = -\frac{\partial^3 H_1}{\partial T_{kl}\, \partial \delta_n\, \partial T_{ij}} = -\frac{\partial^3 H_1}{\partial T_{ij}\, \partial T_{kl}\, \partial \delta_n} = -\frac{\partial E_m}{\partial T_{ij}\, \partial T_{kl}} = 0 \tag{12.19}$$

This leaves only three second-order partial derivatives, two of which are related, and these we designate as

$$\begin{aligned} &\frac{\partial^2 S_{ij}}{\partial \delta_n\, \partial \delta_0} = -\frac{\partial^3 H_1}{\partial \delta_n\, \partial \delta_0\, \partial T_{ij}} = -\frac{\partial^3 H_1}{\partial T_{ij}\, \partial \delta_n\, \partial \delta_0} = -\frac{\partial^2 E_0}{\partial T_{ij}\, \partial \delta_n} = 2Q_{ijno}; \\ &\frac{\partial^2 E_m}{\partial \delta_n\, \partial \delta_0} = 2O_{mno} \end{aligned} \tag{12.20}$$

The two remaining first-order derivatives of equation (12.17) determine the elastic compliances and dielectric impermeabilities according to the

equations

$$\frac{\partial S_{ij}}{\partial T_{kl}} = s^D_{ijkl}; \qquad \frac{\partial E_m}{\partial \delta_n} = 4\pi\beta^T_{mn} \tag{12.21}$$

where s^D_{ijkl} are the elastic compliance constants measured at constant electric displacement and β^T_{mn} are the dielectric "impermeability" constants (inverse of dielectric constants) measured at constant stress. For the most general case, there are 21 components of s^D_{ijkl} and 6 of the impermeability constants. For the isotropic case considered here, symmetry conditions insure that there are only two elastic compliances and one dielectric impermeability. For the most general case there are 36 components of the electrostrictive tensor Q_{ijno} and 18 for the correction O_{mno} to the dielectric constant. For the isotropic condition, the off-diagonal term of the type

$$Q_{1122} = \frac{\partial^2 S_{11}}{\partial \delta_2^2} \qquad \text{and} \qquad Q_{2211} = \frac{\partial^2 S_{22}}{\partial \delta_1^2} \tag{12.22}$$

are obviously equal since the expansion along x_1 for an electric field along x_2 is equal to an expansion along x_2 for a field along x_1. Hence the tensor is symmetrical and has the same number of components as the fourth-rank elastic compliance tensor s^D_{ijkl}. For the isotropic case, symmetry rules out all terms except those shown by the tensor on the opposite page.

The terms on the left are the strains generated by the products of the electric displacements shown by the top column. Since $S_{ij} = S_{ji}$ and $\delta_i\delta_j = \delta_j\delta_i$, three columns and three rows are redundant. The fourth-rank tensor for the elastic compliances will have the same terms with Q_{1111} replaced by s_{1111} and Q_{1122} replaced by s_{1122}. For the top variable line, δ_1^2 is replaced by T_{11}, $\delta_1\delta_2$ by T_{12}, etc.

To simplify the method of writing these equations, the usual one-index matrix symbols are used for the stresses and strains and the usual two-index compliance, electrostrictive, and impermeability constants are used, and the electrostrictive equations become

$$\begin{aligned}
S_1 &= s^D_{11}T_1 + s^D_{12}(T_2 + T_3) + Q_{11}\delta_1^2 + Q_{12}[\delta_2^2 + \delta_3^2] \\
S_2 &= s^D_{12}[T_1 + T_3] + s^D_{11}T_2 + Q_{11}\delta_2^2 + Q_{12}[\delta_1^2 + \delta_3^2] \\
S_3 &= s^D_{12}[T_1 + T_2] + s^D_{11}T_3 + Q_{11}\delta_3^2 + Q_{12}[\delta_1^2 + \delta_2^2] \qquad (12.23) \\
S_{12} &= \frac{S_6}{2} = (s^D_{11} - s^D_{12})T_6 + (Q_{11} - Q_{12})\delta_1\delta_2 \\
S_{13} &= \frac{S_5}{2} = (s^D_{11} - s^D_{12})T_5 + (Q_{11} - Q_{12})\delta_1\delta_3
\end{aligned}$$

	δ_1^2	$\delta_1\delta_2$	$\delta_2\delta_1$	$\delta_1\delta_3$	δ_2^2	$\delta_3\delta_1$	$\delta_2\delta_3$	$\delta_3\delta_2$	δ_3^2
S_{11}	Q_{1111}	0	0	0	Q_{1122}	0	0	0	Q_{1122}
S_{12}	0	$Q_{1111}-Q_{1122}$	$Q_{1111}-Q_{1122}$	0	0	0	0	0	0
S_{21}	0	$Q_{1111}-Q_{1122}$	$Q_{1111}-Q_{1122}$	0	0	0	0	0	0
S_{13}	0	0	0	$Q_{1111}-Q_{1122}$	0	$Q_{1111}-Q_{1122}$	0	0	0
S_{22}	Q_{1122}	0	0	0	Q_{1111}	0	0	0	Q_{1122}
S_{31}	0	0	0	$Q_{1111}-Q_{1122}$	0	$Q_{1111}-Q_{1122}$	0	0	0
S_{23}	0	0	0	0	0	0	$Q_{1111}-Q_{1122}$	$Q_{1111}-Q_{1122}$	0
S_{32}	0	0	0	0	0	0	$Q_{1111}-Q_{1122}$	$Q_{1111}-Q_{1122}$	0
S_{33}	Q_{1122}	0	0	0	Q_{1122}	0	0	0	Q_{1111}

$$S_{23} = \frac{S_4}{2} = (s_{11}^D - s_{12}^D)T_4 + (Q_{11} - Q_{12})\delta_2\delta_3$$

$$\begin{aligned}
E_1 &= \delta_1(4\pi\beta_{11}^T + O_{11}\delta_1) - 2\{Q_{11}(\delta_1 T_1 + \delta_2 T_6 + \delta_3 T_5) \\
&\quad + Q_{12}[\delta_1(T_2 + T_3) - (T_6\delta_2 + T_5\delta_3)]\} \\
E_2 &= \delta_2(4\pi\beta_{11}^T + O_{11}\delta_2) - 2\{Q_{11}(\delta_2 T_2 + \delta_1 T_6 + \delta_3 T_4) \\
&\quad + Q_{12}[\delta_2(T_1 + T_3) - (\delta_1 T_6 + \delta_3 T_4)]\} \\
E_3 &= \delta_3(4\pi\beta_{11}^T + O_{11}\delta_3) - 2\{Q_{11}(\delta_3 T_3 + \delta_1 T_5 + \delta_2 T_4) \\
&\quad + Q_{12}[\delta_3(T_1 + T_2) - (\delta_1 T_5 + \delta_2 T_4)]\}
\end{aligned} \tag{12.23}$$

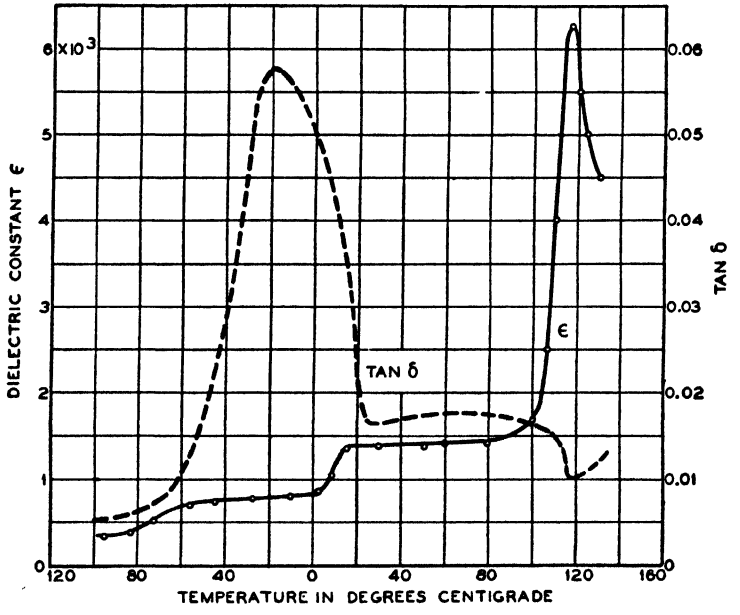

FIG. 12.7. Dielectric constant of barium titanate as a function of the temperature.

In this equation, an extra term O_{11} has been added to represent the decrease in dielectric constant with applied field, which, as shown by Fig. 12.5, is considerable.[6] Over a temperature range, the complex dielectric constant varies[7] as shown by Fig. 12.7. The equations for the various modes can be derived from equations (12.23).

[6] This measurement was made by Gordon Danielson formerly of the Bell Telephone Laboratories.

[7] Von Hippel, A., R. G. Breckinridge, F. G. Chesley and L. Tisza, *Ind. Eng. Chem.*, Vol. 38, pp. 1097–1109, Nov., 1946.

The simplest mode to consider is a longitudinal mode for a long, thin bar generated by a field perpendicular to the length. If we take the thickness as lying along z while the length is along x, the equations reduce to

$$S_1 = s_{11}^D T_1 + Q_{12}\delta_3^2 \qquad (12.24)$$
$$E_3 = \delta_3[4\pi\beta_{11}^T + O_{11}\delta_3] - 2Q_{12}\delta_3 T_1$$

For the case of interest here δ_3 consists of a part δ_{30} due to an applied field or a remanent polarization plus an alternating component, due to an applied AC voltage. As far as the alternating components go, we can write these two equations as

$$S_1 = s_{11}^D T_1 + Q_{12}(2\delta_{30}\delta_3); \quad E_3 = \delta_3[4\pi\beta_{11}^T + O_{11}\delta_{30}] - 2Q_{12}\delta_{30}T_1 \qquad (12.25)$$

To reduce this equation to the standard form[8] used in solving piezoelectric crystals, we have to express the stress T_1 in terms of the strain S_1 and field E_3. By eliminating δ_3, the alternating part of the electric displacement from the last equation and substituting in the first part of equations (12.25), we have

$$T_1 = \frac{S_1}{s_{11}^E} - \frac{2Q_{12}\delta_{30}E_3}{(4\pi\beta_{11}^T + O_{11}\delta_{30})s_{11}^E};$$
$$\delta_3 = \frac{E_3}{4\pi\beta_{11}^{S_1} + O_{11}\delta_{30}} + \frac{2Q_{12}\delta_{30}S_1}{s_{11}^D[4\pi\beta_{11}^{S_1} + O_{11}\delta_{30}]} \qquad (12.26)$$

where $s_{11}^D = s_{11}^E[1 - k^2]$ and $k^2 = \dfrac{4Q_{12}^2\delta_{30}^2}{[4\pi\beta_{11}^T + O_{11}\delta_{30}]s_{11}^E}$.

$$4\pi\beta_{11}^{S_1} + O_{11}\delta_{30} = 4\pi\beta_{11}^T + O_{11}\delta_{30} - \frac{4Q_{12}^2\delta_{30}^2}{s_{11}^D} = (4\pi\beta_{11}^T + O_{11}\delta_{30})(1 - k^2)$$

Substituting the last relation in the last of equations (12.26), the two equations become

$$T_1 = \frac{S_1}{s_{11}^E} - \frac{2Q_{12}\delta_{30}E_3}{(4\pi\beta_{11}^T + O_{11}\delta_{30})s_{11}^E};$$
$$\delta_3 = \frac{E_3}{4\pi\beta_{11}^{S_1} + O_{11}\delta_{30}} + \frac{2Q_{12}\delta_{30}S_1}{s_{11}^E[4\pi\beta_{11}^T + O_{11}\delta_{30}]} \qquad (12.27)$$

These have the same form as the piezoelectric equations (5.13) of Chapter V and hence the same considerations exist if we set the equivalent piezoelectric constant equal to

$$d_{31}' = \frac{2Q_{12}\delta_{30}}{4\pi\beta_{11}^T + O_{11}\delta_{30}} \qquad (12.28)$$

This can be evaluated as in the piezoelectric case by measuring the resonant

[8] See Chapter V, equation (5.18).

and anti-resonant frequencies of the device, the dielectric constant and the density. The coupling is given by equation (5.36) of Chapter V.

$$k^2 = \frac{\pi^2}{4}\frac{\Delta f}{f_R}\left[1 + \frac{(4-\pi^2)}{4}\frac{\Delta f}{f_R} + \cdots\right] \tag{12.29}$$

while the equivalent piezoelectric constant is given by

$$d'_{31} = \frac{2Q_{12}\delta_{30}}{4\pi\beta_{11}^T + O_{11}\delta_{30}} = k\sqrt{\frac{s_{11}^E}{4\pi\beta_{11}^T + O_{11}\delta_{30}}} \tag{12.30}$$

or

$$Q_{12} = \frac{k}{2\delta_{30}}\sqrt{s_{11}^E(4\pi\beta_{11}^T + O_{11}\delta_{30})}$$

Measurements have been made for the coupling of a long, thin bar as a function of the applied voltage and the results are shown by Fig. 12.6. The frequency constant for such a bar is 2.28×10^5 kilocycle centimeters. With a density of 5.5, this corresponds to a compliance constant (inverse of Young's modulus) of 0.88×10^{-12} cm^2/dyne. The remanent polarization was evaluated as 6,000 stat coulombs per sq. cm. and the remanent coupling for a number of bars was 18 per cent. Hence, one can calculate the value of Q_{12} and the value is approximately

$$Q_{12} = -1.35 \times 10^{-12} \text{ in cgs units.}$$

The negative sign is obtained from expansion measurements which show that the bar contracts in length when a voltage is applied normal to the length.

The same constant Q_{12} drives the radial mode of a disc, but since this requires a transformation to cylindrical coordinates, the equations are discussed in the Appendix A.9. It is there shown that the coupling is $\sqrt{2/(1-\sigma)}$ times as large as that for the longitudinal mode. This agrees well with the experimental curve of Fig. 12.6.

The coupling for the thickness mode is also shown by Fig. 12.6. The effective piezoelectric constant for a thickness mode can be evaluated from equation (12.23) by setting $S_1 = S_2 = 0$, since no sidewise motion occurs, and solving for T_3 and δ_3 in terms of S_3 and E_3. The resulting equations are

$$\begin{aligned} T_3 &= S_3 c_{11}^E - \frac{2\delta_{30}\left[Q_{11} - \dfrac{2s_{12}^D}{s_{11}^D + s_{12}^D}Q_{12}\right]c_{11}^E}{4\pi\beta_{11}^T + O_{11}\delta_{30}}E_3; \\ \delta_3 &= \frac{E_3}{4\pi\beta_{11}^S + O_{11}\delta_{30}} + \frac{2c_{11}^E\left[Q_{11} - \dfrac{2s_{12}^D}{s_{11}^D + s_{12}^D}Q_{12}\right]\delta_{30}S_3}{4\pi\beta_{11}^T + O_{11}\delta_{30}} \end{aligned} \tag{12.31}$$

where $c_{11}^E = \dfrac{c_{11}^D}{1-k^2}$; $k^2 = \dfrac{4\delta_{30}^2\left[Q_{11} - \dfrac{2s_{12}^D Q_{12}}{s_{11}^D + s_{12}^D}\right]^2 c_{11}^E}{4\pi\beta_{11}^T + O_{11}\delta_{30}}$ and $4\pi\beta_{11}^{S_2} + O_{11}\delta_{30}$ $= (4\pi\beta_{11}^T + O_{11}\delta_{30})(1-k^2)$. Hence the equivalent piezoelectric constant for this case is

$$d'_{33} = \frac{2\left[Q_{11} - \dfrac{2s_{12}^D}{s_{11}^D + s_{12}^D} Q_{12}\right]\delta_{30}}{4\pi\beta_{11}^T + O_{11}\delta_{30}} \tag{12.32}$$

From the remanent coupling measurements of a number of plates as 40%, one finds that

$$Q_{11} - \frac{2s_{12}^D}{s_{11}^D + s_{12}^D} Q_{12} = 2.7 \times 10^{-12} \tag{12.33}$$

Since s_{11} and s_{12} are given in terms of the c elastic constants by

$$\begin{aligned} s_{11} &= \frac{c_{11} + c_{12}}{c_{11}(c_{11} + c_{12}) - 2c_{12}^2} = \frac{\lambda + \mu}{\mu(3\lambda + 2\mu)}; \\ s_{12} &= \frac{-c_{12}}{c_{11}(c_{11} + c_{12}) - 2c_{12}^2} = \frac{-\lambda}{2\mu(3\lambda + 2\mu)} \end{aligned} \tag{12.34}$$

we have from the Lamé elastic constants of equation (12.8)

$$s_{11} = 0.88 \times 10^{-12}; \qquad s_{12} = -0.236 \times 10^{-12}. \tag{12.35}$$

Hence the value of Q_{11} becomes

$$Q_{11} = +3.6 \times 10^{-12} \tag{12.36}$$

which is of opposite sign and about 2.7 times as large as Q_{12}.

The fourth mode of motion that can be generated in a rectangular bar is the thickness-shear mode which occurs when the alternating voltage is applied at right angles to the DC electric displacement. This mode was tested by taking a bar 5 cm long, 0.5 cm wide and 0.25 cm thick, applying a voltage of 30,000 volts per cm and using the remanent polarization generated for this case. Since it is difficult to establish an electric displacement along the 0.5-cm direction with plates normal to the large faces, these were dissolved off and the AC field applied along the width (0.5-cm direction). The frequency of the measured resonance was 566 kilocycles, which agrees well with the shear-elastic constant of equation (12.8). The coupling for the shear mode is higher than that for the thickness-longitudinal mode. This is what one expects from equations (12.23), sixth equation, from which

one obtains the equation for a shear mode

$$T_4 = S_4\mu^E - \frac{2(Q_{11} - Q_{12})\delta_{30}\mu^E}{4\pi\beta_{11}^T + O_{11}\delta_{30}} E_2$$
$$\delta_2 = \frac{E_2}{4\pi\beta_{11}^S + O_{11}\delta_{30}} - \frac{2(Q_{11} - Q_{12})\delta_{30}\mu^E}{4\pi\beta_{11}^T + O_{11}\delta_{30}} S_4 \qquad (12.37)$$

where

$$\mu^E = \frac{c_{11}^E - c_{12}^E}{2} = \left(\frac{c_{11}^D - c_{12}^D}{2}\right)(1 - k^2); \qquad k^2 = \frac{4(Q_{11} - Q_{12})^2\delta_{30}\mu^E}{4\pi\beta_{11}^T + O_{11}\delta_{30}}$$

Inserting the values given previously for Q_{11}, Q_{12}, μ and δ_{30} (*i.e.* a remanent polarization equal to 0.85 times that for a 30,000 volt per centimeter field) one obtains a coupling of 48 per cent, which agrees well with experiment. Hence the phenomenological theory accounts quantitatively for all the modes of motion observed, and allows one to measure the electrostrictive, elastic and dielectric constants pertaining to the ceramic.

12.4 *Theoretical Explanation of Effect*

The ratio of about 2 to 1 between the thickness effect, and the fact that the radial effect is a contraction, allows one to obtain a mechanism for this effect. Barium titanate above 120°C has a cubic structure, having the

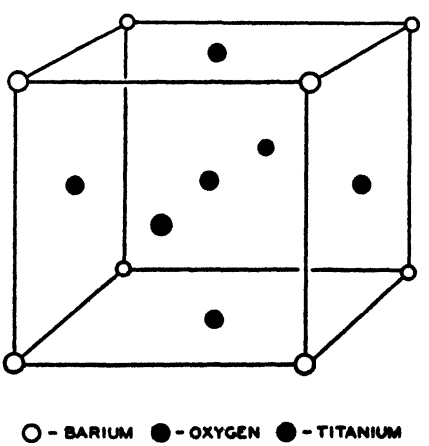

FIG. 12.8. Structure of barium titanate above 120° C.

form shown by Fig. 12.8. Here eight barium atoms form the corner of the cube. Since each barium atom is shared between eight adjacent cells, this gives a total of one barium atom per cell. Six oxygen atoms

occupy the face-centered position on the six sides, and since each is shared between two adjacent cells, this represents a total of three oxygen atoms per cell. Since the titanium atom is much smaller than the other atoms, it is relatively free to move between them.

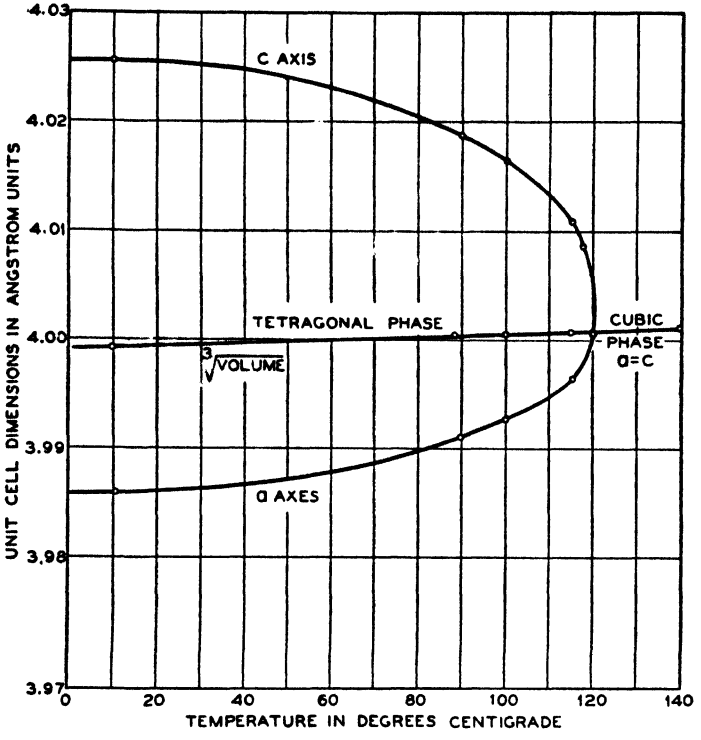

FIG. 12.9. Cell dimensions of barium titanate as a function of temperature.

As the temperature is lowered below 120°C, the titanium atom moves from the center to one of the six positions near the six oxygen atoms. Since the cell was neutral when the titanium was in the center, a dipole moment is introduced by the motion of the titanium, the cell acquires a permanent dipole and the domain in which the cell is situated becomes ferroelectric.

When the crystal becomes ferroelectric, the cubic form is lost and the crystal becomes tetragonal with the axis in the direction of the titanium motion 1 per cent longer than the other two axes. Figure 12.9 shows the cell dimensions as a function of temperature, as determined by Miss Megaw.[9] Along the ferroelectric axis, the cell dimension increases from

[9] Megaw, H. D., *Proc. Roy. Soc.*, Vol. 189, pp. 261–283, April, 1947.

4.0Å to 4.026Å at room temperature, while the other two axes decrease from 4.0Å to 3.86Å. The total volume of the unit cell remains unchanged for the crystal, but the axial ratio has changed to 1.01.

For a polycrystalline material the dominant mechanism for producing the electrostrictive effect is the following. As the ceramic material is prepared, all domains (which can exist below 120°C) are equally distributed in all directions and no residual polarization can occur. The effect of a large DC field is to change the direction of polarity so that more domains are lined up in the direction of the field rather than in other directions. This change in the direction of a domain occurs not by physically changing the orientation, but rather in changing the direction of the ferroelectric axis from one of the six oxygens to another of the six. When the field is taken off, the local field caused by the lining up of the domains remains and is sufficient to keep a large share of the domains lined up. Now, when domains are lined up in the direction of the field, the plate expands in this direction by $\frac{2}{3}$ per cent times the percentage of domains whose direction of polarization is changed. At the same time the radial dimensions contract. For the crystal, X-ray measurements show that the sidewise contraction is half as much as the thickness expansion. However, for the ceramic, since $-Q_{12}/Q_{11} = 1.35/3.6 = 0.37$, the amount of sidewise contraction is less and a volume electrostrictive effect exists. This is probably due to the fact that the crystal domains are not bonded at all points and a contraction of domains can occur without causing a corresponding contraction in the body, whereas an expansion along the c-axis carries the material with it whether it is bonded at all points or not. The two effects, the thickness effect and the radial effect, are both of a considerable magnitude.

When a small AC field is applied in the presence of a DC field or remanent polarization, the following process probably occurs. The AC field in itself is too small to reverse any complete domain, but it can cause molecules on the common planes of differently directed domains to change from one domain to another and hence cause one domain to grow at the expense of other domains. If the AC field is opposed to the DC field, some molecules of the domains directed along the thickness will be lost to other domains directed in different directions and the crystal will become thinner. When the AC field is added to the DC field, these molecules, and more too, will be directed in the direction of the field and the plate becomes thicker. Since the change in molecule direction will, in general, lag the applied field, a large dielectric hysteresis occurs just as for rochelle salt, and the mechanical resonances have a poor Q. The radial vibration is accounted for by the contraction of the domains in directions perpendicular to the ferroelectric

axis, and this process should generate a radial motion about half as large as the thickness motion, which agrees with experiment.

The value of the total increase in thickness, about 5 to 7 parts in 10^4 for 30,000 volts per cm applied, gives a method for estimating the number of domains lined up by the DC field. Since the plate could expand by $\frac{2}{3}$ per cent if all the domains were lined up, the per cent lined up is

$$\frac{5 \text{ to } 7 \times 10^{-4}}{6.6 \times 10^{-3}} = 7.6 \text{ to } 10.6\%. \tag{12.38}$$

over the average value for an isotropic condition.

12.5 *Method for Obtaining a Permanent Polarization*

Since for practical devices it is undesirable to have to supply a d.c. biasing voltage, use is made of the remanent polarization induced by polarizing the ceramic by a high voltage. There is some indication that this polarization may decrease with time as does the remanent magnetization of a soft magnet material. In order to obtain a remanent polarization that is really permanent, experiments have been made on the effect of introducing impurities into the barium titanate with the idea that the dipoles might be locked into position so that they would not change, as happens for the magnetic dipoles of a permanent magnet material. By introducing three or four per cent of lead in the form of lead titanate, the desired effect was found. When this mixed ceramic was poled at a high field strength at temperatures above the Curie temperature and cooled under the applied field, this remanent polarization and the concomittant electromechanical coupling could not be removed by any reversed field that could be applied up to a temperature of 70°C. As shown by Fig. 12.4 the remanent polarization of an ordinary barium titanate ceramic can be removed by a negative field of 5,000 volts per centimeter, but with 4 per cent lead titanate the coupling is only slightly diminished up to a negative voltage of 25,000 volts per centimeter. It is completely restored by cycling to 25,000 volts per centimeter positive. Hence the new material acts like a permanent magnet material and the remanent polarization should be stable with time.

It appears from the X-ray measurements of Rushman and Strivens (Faraday Society, Vol. XLII A p. 235, 1946) that lead goes in place of the barium. Since lead has a divalent radius of 1.21Å, *i.e.*, 0.14Å smaller than the barium, the lead may also act as a dipole, adding to that due to the titanium. This results in an increase in the Curie temperature of 10°C for the 4% mixture. Since lead has a smaller polarizability than barium, the value of ϵ_0 decreases, and the large rise in A_1 does not occur

until a lower temperature. The second transition temperature, as shown by the elastic data of Fig. 12.10 is lowered from 10°C to −20°C for a 4 per cent mixture and to −45°C for an 8 per cent mixture. Both the lowering of the dielectric constant and the lowering of the middle transition temperature are consistent with a decrease in A_1, while the increase in the Curie temperature indicates an increase in A_3 in the room temperature range. Hence the numerator of equation (11.110), determining the coercive voltage, may easily increase by a factor of five, resulting in five times the coercive voltage, as observed experimentally.

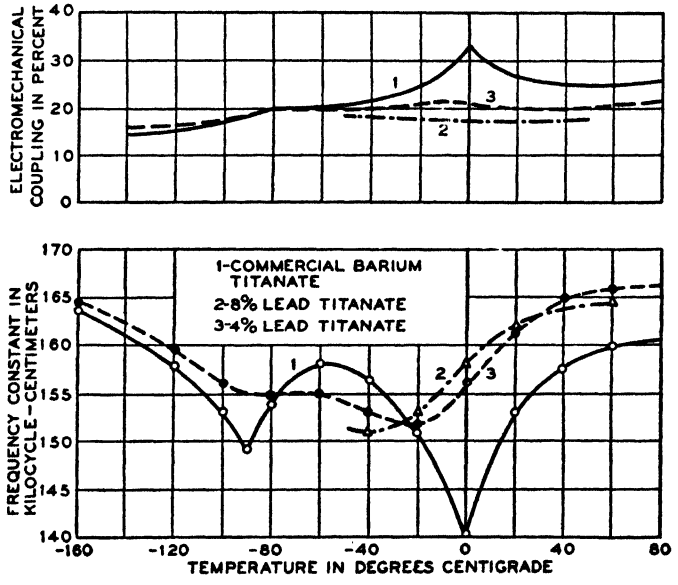

FIG. 12.10. Electromechanical coupling factor and frequency constant (frequency times radius) for a circular disc of commercial barium titanate, and barium titanate with two percentages of lead titanate added.

Using the 4 per cent lead mixture, acoustic powers as high as 100 watts per square centimeter have been continuously radiated without causing any loss of polarization as long as the surrounding medium is less than 70°C. This represents the highest power density obtained with any ultrasonic device.

While it is too early to tell for which application the ceramic type of transducer will give better results than other competing methods, several advantages are at once obvious. Figure 12.10 shows the electromechanical coupling factor and the frequency constant of a circular disc plotted as a function of temperature. The solid line is for an ordinary barium titanate

mixture while the dotted line is for a 4 per cent lead titanate mixture. The two transition temperatures of 0° and −90°C are evident from the data. According to the discussion in Chapter XI, these are temperatures for which the crystal becomes ferroelectric along two directions and three directions, respectively. The effects of these transition temperatures are somewhat curtailed for the lead titanate modifications. The intermediate transition temperature is lowered to −20°C. For an 8 per cent lead titanate mixture it is lowered even further. The constants of the transducer, as shown by Fig. 12.10, are far less temperature sensitive for example, than are those for rochelle salt.

Another definite advantage of the ceramic transducer is that it can be made of any size or shape. One possible use of this is in producing focusing radiators that can concentrate ultrasonic energy in a given region. This type of transducer can be made equally efficient at all points of the surface, which is not true for a quartz focusing radiator. In the form of a cylindrical radiator, a barium titanate transducer can produce a high ultrasonic intensity along the axis of the cylinder. This type may be of use in a continuous ultrasonic process for altering the properties of a liquid or solid.

CHAPTER XIII

Properties of Gases and Methods for Measuring Them by Crystal Transducers

Piezoelectric transducers have been used extensively in setting up vibrations in gases, liquids and solids and in measuring the elastic and dissipative properties of solids. Probably the first instrument of this kind was the acoustic interferometer of Pierce,[1] which has been used to measure velocities and attenuations in gases and liquids. While attempting to check the classical equations which predict an attenuation for a free wave proportional to the square of the frequency, Pierce found an attenuation maximum and an associated increase in velocity with frequency. This was soon explained by Herzfeld and Rice as a consequence of a coupling between the translational energy and internal modes of vibration which are excited on the average only after a large number of collisions. These internal modes could be excited only in polyatomic gases for which gases the adiabatic conditions may be modified through the effect of certain time constants that characterize the rate of exchange of thermal energy between the translational, rotational and vibrational states of the molecules. The phenomenon is known as thermal relaxation.

It is the purpose of this chapter to describe the methods of measurement and some of the results obtained for gases.

13.1 *Classical Equations for Sound Propagation and Application to Monatomic Gases*

The classical equations for sound absorption in gases arising from shear viscosity (Stokes, 1841) and heat conduction (Kirchoff, 1868) are derived in detail in the Appendix, Section A.7. It is there shown that a plane wave propagation takes place according to the equations

$$\begin{aligned} p &= p_o \cosh \Gamma x - \dot{\xi}_0 Z_0 \sinh \Gamma x \\ \dot{\xi} &= \dot{\xi}_0 \cosh \Gamma x - \frac{p_o}{Z_0} \sinh \Gamma x \end{aligned} \tag{13.1}$$

where p is the excess pressure at any point x from the origin, p_o the excess pressure at the origin, $\dot{\xi}$ the particle velocity in the plane wave, Γ the

[1] Pierce, G. W., *Proc. Am. Acad.*, Vol. 60, p. 269, Boston, 1925.

propagation constant, and Z_0 the image impedance, *i.e.* the impedance of an infinite medium. These two quantities are given in terms of the gas constants by

$$\Gamma = \frac{j\frac{\omega}{v}}{\sqrt{1+\frac{j\omega}{\rho v^2}\left[\chi+2\eta+\frac{(\gamma-1)K}{C_p}\right]}} \doteq \frac{2\pi^2 f^2}{\rho v^3}\left[\chi+2\eta+\frac{(\gamma-1)K}{C_p}\right]+\frac{j\omega}{v}$$

$$Z_0 = \rho v\sqrt{1+\frac{j\omega}{\rho v^2}\left[\chi+2\eta+\frac{(\gamma-1)K}{C_p}\right]} \doteq \rho v\left\{1+\frac{j\omega}{2\rho v^2}\left[\chi+2\eta+\frac{(\gamma-1)K}{C_p}\right]\right\} \tag{13.2}$$

In this equation ρ is the density, v the velocity $= \sqrt{\kappa/\rho}$ where κ is the constant of cubical elasticity, $\omega = 2\pi f$ where f is the frequency, η is the shearing viscosity and χ a compressional viscosity, γ = ratio of specific heats, K the constant of thermal conductivity, and C_p the specific heat at constant pressure. For gases, according to Stoke's assumption which appears justified at least for monatomic gases

$$\chi + 2\eta = \frac{4\eta}{3} \tag{13.3}$$

From gas theory

$$\frac{K}{C_p} = \frac{(9\gamma - 5)\eta}{4} \tag{13.4}$$

so that the effective attenuation is given by the formula

$$A = \frac{2\pi^2 f^2}{\rho v^3}\left[\frac{4\eta}{3} + \frac{(\gamma - 1)(9\gamma - 5)\eta}{4}\right] \tag{13.5}$$

For a monatomic gas $\gamma = 5/3$ and hence the attenuation is

$$A = \frac{2\pi^2 f^2}{\rho v^3}[2.96\eta] \tag{13.6}$$

Extensive measurements in argon at 4.25 megacycles by Keller[2] confirm the classical formula over a wide range of pressure up to 12 atmospheres. However, measurements made in helium by Von Itterbeck[3] and Thys (1938) and Von Itterbeck[4] and Mariens (1940) and in neon by Von Itterbeck[5] and Thys (1938), indicate that the absorption in these two

[2] Keller, H., *Phys. Zeits.*, Vol. 41, p. 386, 1940.
[3] Von Itterbeck and Thys, *Physica*, Vol. 5, p. 640, 1938.
[4] Von Itterbeck and Mariens, *Physica*, Vol. 7, p. 125, 1940.
[5] Von Itterbeck and Thys, *Physica*, Vol. 5, p. 889, 1938.

gases exceeds the theoretical value by a factor of the order of four. No explanation is forthcoming since no other factors should affect the absorption in monatomic gases. A more recent measurement[6] on helium gave results which agree with the complete thermodynamic equation (13.2) for pressures down to 5×10^2 dynes/cm^2.

An equivalent electrical circuit for representing the propagation of a wave according to the classical formula is of some interest, particularly in showing the attenuation due to several effects. Such a network can be obtained when the propagation constant Γ and the image impedance Z_0

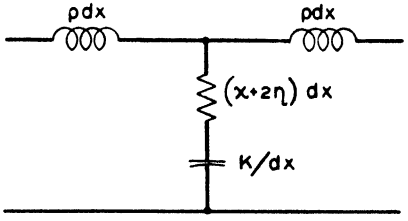

FIG. 13.1. Equivalent circuit representation for the propagation of a longitudinal wave in a gas or liquid.

are known. For a T network, the series impedance at low frequencies for a section of material of thickness dx, and the shunt impedance are given by the formulae

$$Z_1 = Z_0\Gamma\, dx; \qquad Z_2 = \frac{Z_0}{\Gamma\, dx} \tag{13.7}$$

Hence from equation (13.2)

$$Z_1 = j\omega\rho\, dx; \qquad Z_2 = \left[\left[\chi + 2\eta + \frac{(\gamma - 1)K}{C_p}\right] - \frac{j\kappa}{\omega}\right]\frac{1}{dx} \tag{13.8}$$

Figure 13.1 shows a drawing with a T network representing these impedances.

13.2 *Measurement of the Properties of Gases*

Measurements of the properties of gases at low frequencies are usually carried out by measuring the transmission properties in enclosed tubes or enclosed rooms. At ultrasonic frequencies, however, their properties are almost universally measured by an ultrasonic interferometer. Such interferometers, which were first devised and used by Pierce,[1] usually employ a quartz or other piezoelectric crystal to set up standing waves

[6] Greenspan, *Phys. Rev.*, Vol. 75, No. 1, p. 197, Jan. 1, 1949.

between the crystal surface and a movable reflecting plate. The cross-sectional area of the driving crystal is so large that very directive waves are set up and no account has to be taken of the divergence of the wave.

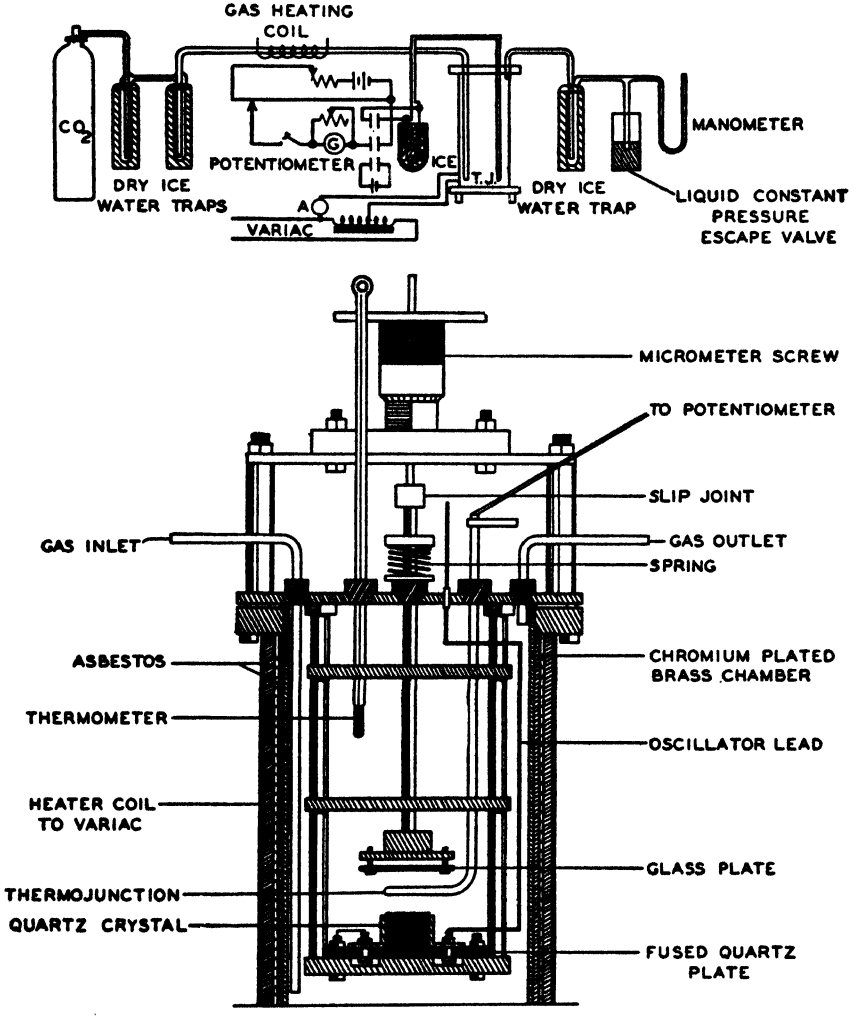

FIG. 13.2. Interferometer for measuring velocity and absorption in a gas or liquid.

13.21 *Theory of Operation of an Interferometer*

A typical interferometer for studying the velocity and absorption for a gas at various temperatures is shown by Fig. 13.2. A fixed quartz or ADP crystal of large cross-section is held rigidly in place between two electrodes.

A variable reflecting plate is connected to a micrometer screw which accurately measures the distance of the reflecting plate from the crystal surface. The reflecting plate is lined up to be accurately parallel with the crystal surface. The whole unit is placed in a thermostated heating coil for controlling the temperature of the unit. The outer chamber is gastight and provides arrangements for letting gases into and out of the chamber.

To operate the device an oscillator is connected to the crystal and tuned to the resonant frequency of the crystal. A thermocouple or amplifier in series with the crystal can be used to measure the variation in current through the crystal as a function of the position of the reflecting plate. As the position of the plate is varied with respect to the crystal surface,

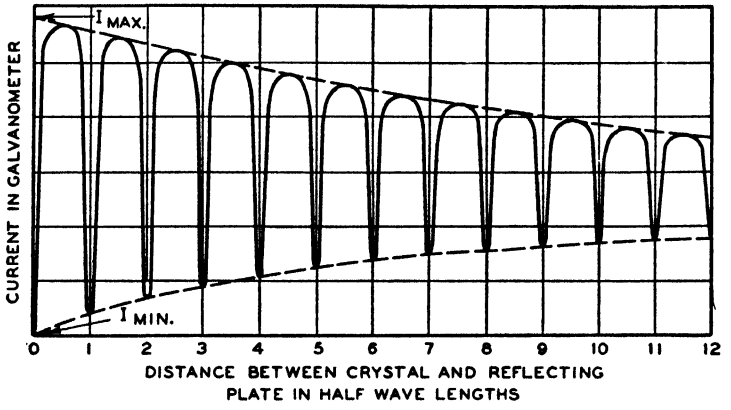

FIG. 13.3. Current through meter as a function of separation of crystal and reflector.

the current through the meter will be as shown in Fig. 13.3. At half-wavelength intervals, sharp dips occur in the received current, indicating that a high mechanical impedance is impressed on the end of the vibrating crystal by the standing-wave system between the crystal surface and the reflecting plate. By counting the number of half wavelengths occurring in a given displacement of the reflecting plate, and knowing accurately the frequency of vibration, the velocity of propagation of the gas is determined by the formula

$$v = \left(\frac{2 \times \text{displacement}}{\text{number of half wavelengths}}\right) \text{frequency} \qquad (13.9)$$

The maximum and minimum current points lie on lines labelled I_{max} and I_{min} and approach each other as the separation increases. The attenuation of the wave can be calculated from the shapes of these curves. The theoretical method of calculating the attenuation was first derived by

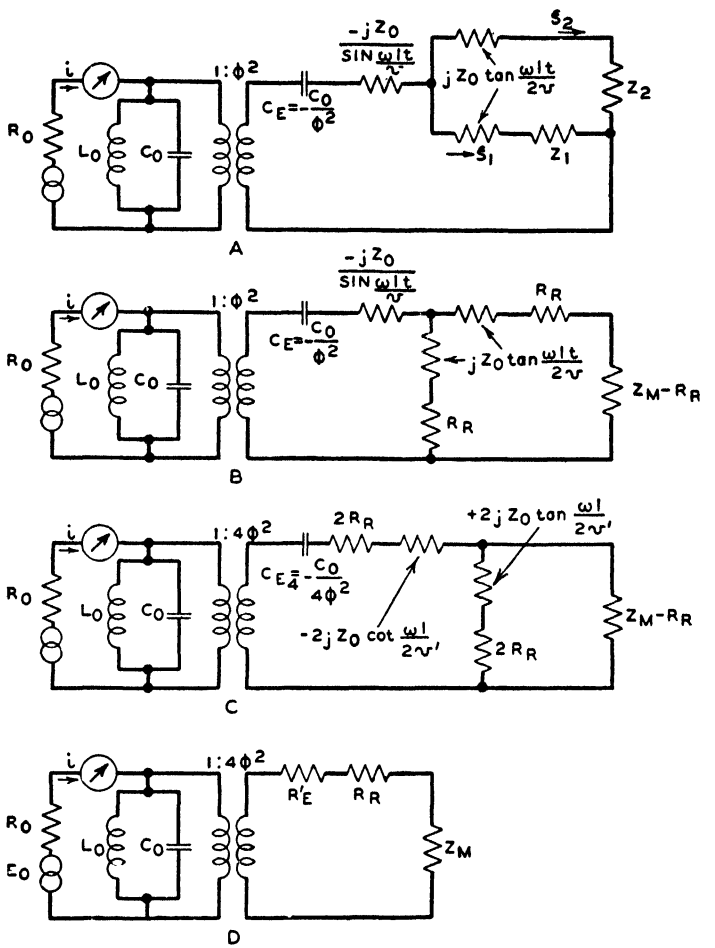

FIG. 13.4. Equivalent circuit of interferometer and gas column.

Hubbard,[7] but it can be simplified considerably by employing the equivalent circuit of a thickness vibrating crystal derived in the book *Electromechanical Traducers and Wave Filters*[8] Section 6.4. Figure 13.4A shows the equivalent circuit applicable for this case. If we tune out the

[7] "Acoustic Resonator Interferometer I: The Acoustic System and the Equivalent Electrical Network," *Phys. Rev.*, Vol. 38, No. 5, pp. 1011–1020, Sept. 1, 1931; "Acoustic Resonator Interferometer II: Ultrasonic Velocity and Absorption in Gases," *Phys. Rev.*, Vol. 41, p. 523, 1932.

[8] Mason, W. P., *Electromechanical Transducers and Wave Filters*, D. Van Nostrand Company, Inc., 1942, 2nd Edition, 1948.

static capacity of the crystal by a shunt inductance, the current at resonance in the meter is determined by the series electrical resistance R_1, the mechanical resistance of the crystal and the mechanical impedance imposed by the medium on the ends of the crystal. The end away from the reflecting plate can be assumed to have a constant impedance independent of the reflector plate. The most probable impedance is a resistance ρv times the area of the plate. Calling this R_R the equivalent circuit of Fig. 13.4A can be put into the form shown by Fig. 13.4B where Z_M is the mechanical impedance put on the crystal by the crystal reflector standing-wave system. By employing the equivalence shown by Fig. 6.16B,[8] Fig. 13.4B can be put into the form shown by Fig. 13.4C. But near the resonant frequency $2jZ_0 \tan \frac{\omega l}{2v'}$ is very large compared to $Z_M - R_R$ and can be neglected. Also at the resonance, the reactance of $C_E/4$ cancels that of $-2jZ_0 \cot \frac{\omega l}{2v'}$ and the circuit of Fig. 13.4D results. R'_E represents the resistance in the crystal caused by elastic hysteresis, mounting losses and any other sources of dissipation in the crystal. R_R represents the radiation resistance on the free side and Z_M the mechanical impedance on the crystal due to the standing-wave systems. If we combine R'_E and R_R into R_E, the current i flowing through the galvanometer at the resonant frequency of the crystal, is

$$i = \frac{E_0}{R_0 + \left(\frac{R_E + Z_M}{4\varphi^2}\right)} \tag{13.10}$$

If we consider that the radiator is so directive and the separation between crystal and reflecting plate so small that no diffraction has to be considered, the impedance can be calculated by the formula applicable for a plane wave, which is

$$\begin{aligned} p_2 &= p_1 \cosh \Gamma l - \dot{\xi}_1 Z_0 \sinh \Gamma l \\ \dot{\xi} &= \dot{\xi}_1 \cosh \Gamma l - \frac{p_1}{Z_0} \sinh \Gamma l \end{aligned} \tag{13.1}$$

where Γ is the propagation constant $A + jB$, Z_0 the characteristic impedance which very nearly equals ρv, p_1 and $\dot{\xi}_1$ the pressure and particle velocity at the crystal surface and p_2 and $\dot{\xi}_2$ the pressure and particle velocity at the reflector surface. The reflector in general will have a very high impedance compared to air. Calling this impedance Z_R per unit area, we have

$$\frac{p_2}{\dot{\xi}_2} = Z_R \tag{13.11}$$

Substituting this in equation (13.1), we have that the total mechanical impedances Z_M is equal to

$$\frac{Sp_1}{\dot{\xi}_1} = Z_M = Z_0 S \left[\frac{\coth \Gamma l + (Z_0/Z_R)}{1 + (Z_0/Z_R) \coth \Gamma l} \right] \tag{13.12}$$

where S is the effective cross-sectional area of the crystal. For any gases, the ratio of Z_0/Z_R is very small and can usually be set equal to zero. Even for a liquid Z_0/Z_R is small and can be set equal to a small quantity Δ. Then introducing this result in (13.10), we have

$$i = \frac{E_0}{R_0 + \dfrac{R_E}{4\varphi^2} + \dfrac{Z_0 S}{4\varphi^2} \left[\dfrac{\coth \Gamma l + \Delta}{1 + \Delta \coth \Gamma l} \right]} \tag{13.13}$$

Since Γ consists of a real part A (the attenuation in nepers per centimeter) and an imaginary part jB (where B is the phase constant in radians), coth Γl can be expanded into the form

$$\coth \Gamma l = \coth (A + jB) = \frac{\sinh 2Al - j \sin 2Bl}{\cosh 2Al - \cos 2Bl} \tag{13.14}$$

The maximum value of coth Γl comes when $\cos 2Bl = 1$ or $Bl = n\pi$. Hence for any integral number of half wavelengths, the impedance Z_M is high and the current reaches its minimum value as shown by Fig. 13.3. The value of coth Γl at these points is

$$\frac{\sinh 2Al}{\cosh 2Al - 1} = \coth Al \tag{13.15}$$

and the minimum current is

$$\begin{aligned} i_{\min} &= \frac{E_0}{R_0 + \dfrac{R_E}{4\varphi^2} + \dfrac{Z_0 S}{4\varphi^2} \left[\dfrac{\coth Al + \Delta}{1 + \Delta \coth Al} \right]} \\ &\doteq \frac{E_0}{R_0 + \dfrac{R_E}{4\varphi^2} + \dfrac{Z_0 S}{4\varphi^2} \left[\dfrac{1}{\tanh Al + \Delta} \right]} \end{aligned} \tag{13.16}$$

since Δ is small and can be neglected compared to the very large value of coth Al. If we extrapolate the value of current at the minimum points down to zero separation $l = 0$, the minimum current for zero length is

$$i_0 = \frac{E_0}{R_0 + \dfrac{R_E}{4\varphi^2} + \dfrac{Z_0 S}{4\varphi^2 \Delta}} \tag{13.17}$$

The maximum current will come at odd quarter wavelengths of the spacing between crystal and reflector where $\cos 2B = -1$. For this case

$$\coth \Gamma l = \frac{\sinh 2Al}{1 + \cosh 2Al} = \tanh Al \tag{13.18}$$

and the maximum current curve will be given by the equation

$$\begin{aligned} i_{\max} &= \frac{E_0}{R_0 + \dfrac{R_E}{4\varphi^2} + \dfrac{Z_0 S}{4\varphi^2}\left[\dfrac{\tanh Al + \Delta}{1 + \Delta \tanh Al}\right]} \\ &\doteq \frac{E_0}{R_0 + \dfrac{R_E}{4\varphi^2} + \dfrac{Z_0 S}{4\varphi^2}[\tanh Al + \Delta]} \end{aligned} \tag{13.19}$$

since $\tanh Al$ is always less than 1 and Δ is very small. If we extrapolate the maximum current curve down to zero length, the current is

$$i_M = \frac{E_0}{R_0 + \dfrac{R_E}{4\varphi^2} + \dfrac{Z_0 S}{4\varphi^2}\Delta} = \frac{E_0}{C} \tag{13.20}$$

where C is a constant for the interferometer. Taking the ratio of i_M to i_0 and calling it σ_0

$$\sigma_0 = \frac{R_0 + \dfrac{R_E}{4\varphi^2} + \dfrac{Z_0 S}{4\varphi^2 \Delta}}{R_0 + \dfrac{R_E}{4\varphi^2} + \dfrac{Z_0 S}{4\varphi^2}\Delta} = \frac{C + \dfrac{Z_0 S}{4\varphi^2}\left[\dfrac{1}{\Delta} - \Delta\right]}{C} \tag{13.21}$$

Since Δ is a very small quantity we have

$$\Delta = \frac{Z_0 S}{4\varphi^2 C(\sigma_0 - 1)} \tag{13.22}$$

We have two other equations (13.16) and (13.19) for solving for Δ and $\tanh Al$. If we write them as the ratios

$$\begin{aligned} \sigma_1 &= \frac{i_M}{i_{\max}} = \frac{1}{1 + \dfrac{Z_0 S}{4\varphi^2 C}\tanh Al} \\ \sigma_2 &= \frac{i_M}{i_{\min}} = \frac{1}{1 + \dfrac{Z_0 S}{4\varphi^2 C}\left[\dfrac{1}{\tanh Al + \Delta}\right]} \end{aligned} \tag{13.23}$$

we have three equations for solving for Δ and $\tanh Al$. The results are

$$\tanh Al = \sqrt{\frac{(\sigma_1 - 1)(\sigma_0 - \sigma_2)}{(\sigma_0 - 1)(\sigma_2 - 1)}}; \qquad \Delta = \sqrt{\frac{(\sigma_1 - 1)(\sigma_2 - 1)}{(\sigma_0 - 1)(\sigma_0 - \sigma_2)}} \tag{13.24}$$

Since Δ does not change with position, the last equation of (13.24) should be independent of the separation l. Hence curves of the form of Fig. 13.3 can be used to measure the velocity and attenuation existing in a gas.

An alternate method of measuring these quantities is to place the interferometer in an impedance bridge and measure the series resistance and reactance at the resonant frequency of the crystal as a function of the

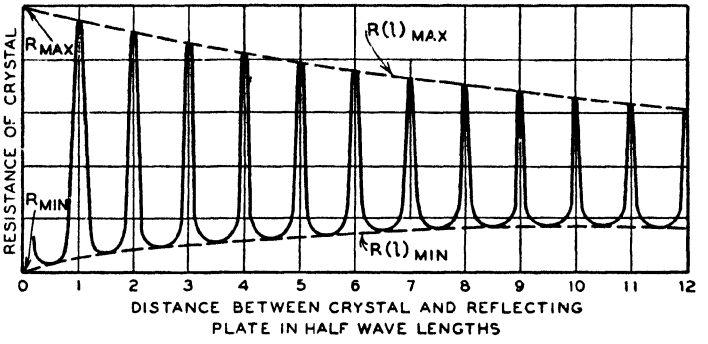

FIG. 13.5. Resistance of crystal as a function of separation.

interferometer spacing. From equation (13.13) the impedance is given by the equation

$$Z = R_0 + \frac{R_E}{4\varphi^2} + \frac{Z_0 S}{4\varphi^2}\left[\frac{\coth \Gamma l + \Delta}{1 + \Delta \coth \Gamma l}\right] \tag{13.25}$$

The resistance component will vary as shown by Fig. 13.5. It will vary between

$$R(l)_{\max} = R_0 + \frac{R_E}{4\varphi^2} + \frac{Z_0 S}{4\varphi^2}\left[\frac{1}{\tanh Al + \Delta}\right] \tag{13.26}$$

and

$$R(l)_{\min} = R_0 + \frac{R_E}{4\varphi^2} + \frac{Z_0 S}{4\varphi^2}[\tanh Al + \Delta]$$

Designating the minimum resistance at $l = 0$ as $R_{\min}$ and the minimum resistance at a distance l as $R(l)_{\min}$, the maximum resistance at $l = 0$ as $R_{\max}$ and the maximum resistance at a distance l as $R(l)_{\max}$ it can be shown

from equation (13.26) that the attenuation is given by the equation

$$\tanh Al = \sqrt{\left[\frac{R_{max} - R(l)_{max}}{R(l)_{max} - R_{min}}\right]\left[\frac{R(l)_{min} - R_{min}}{R_{max} - R_{min}}\right]}$$

and (13.27)

$$\Delta = \sqrt{\left[\frac{R(l)_{max} - R_{min}}{R_{max} - R_{min}}\right]\left[\frac{R(l)_{min} - R_{min}}{R_{max} - R(l)_{max}}\right]}$$

This provides an alternate method for obtaining the velocity and attenuation.

13.22 *Experimental Results*

Measurements made for the attenuations and velocities of air, oxygen, nitrogen, carbon dioxide and other gases show that the attenuations are considerably higher than can be accounted for by the classical viscous considerations such as discussed in Appendix A.7; furthermore, the velocity of such gases as carbon dioxide shows a dispersion with frequency. The first measurements for carbon dioxide were made by Pierce[1] in 1925. The first significant measurements for air were made by Knudsen.[9] By using a reverberation-time method in enclosed chambers of various sizes, the attenuation was measured at 3000 cycles, 6000 cycles and 10,000 cycles as a function of the percentage of water vapor molecules in the air. These curves, which are shown by Fig. 13.6, show a pronounced attenuation maximum at .2 to .4 per cent water vapor. For dry air, the attenuation is about 40 per cent higher than that calculated from viscosity and heat conduction considerations. With water vapor present the attenuation is over a hundred times the classical value. For carbon dioxide at certain frequencies the measured attenuation is over 340 times the classical value. Figure 13.7 shows the measured attenuation and velocity of carbon dioxide as a function of frequency.

The causes for this divergence from classical theory have been investigated by Herzfeld and Rice[10] and by Kneser.[11] The basic mechanism for this effect has been explained as follows: when a gas is compressed adiabatically, a certain amount of the energy is turned into internal energy of the molecules and a certain amount into rotational energy of the mole-

[9] "The Effect of Humidity Upon the Absorption of Sound in a Room, and a Determination of the Coefficient of Absorption of Sound in Air," *J.A.S.A.*, Vol. 3, pp. 126–133, 1931; "The Absorption of Sound in Air, in Oxygen, and in Nitrogen-Effects of Humidity and Temperature," *J.A.S.A.*, Vol. 5, pp. 112–121, 1933.

[10] "Dispersion and Absorption of High Frequency Sound Waves," *Phys. Rev. II*, Vol. 31, p. 691, 1928.

[11] "The Interpretation of the Anomalous Sound-Absorption in Air and Oxygen in Terms of Molecular Collision," *J.A.S.A.*, Vol. 5, pp. 122–126, 1933.

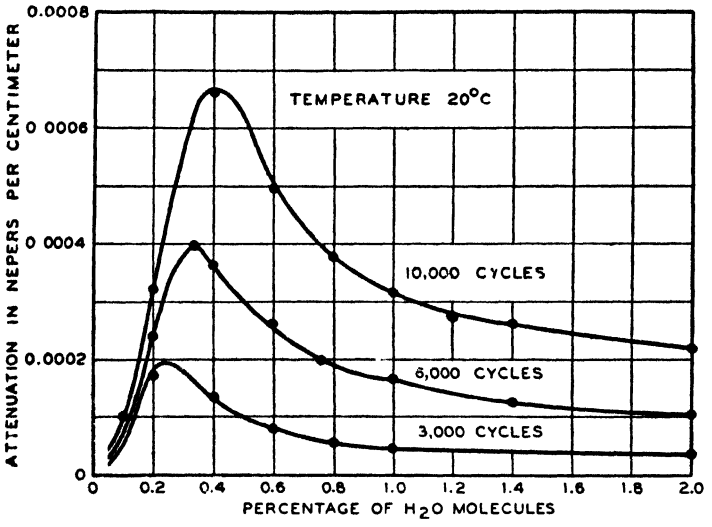

FIG. 13.6. Measured attenuation in air as a function of frequency and water vapor content.

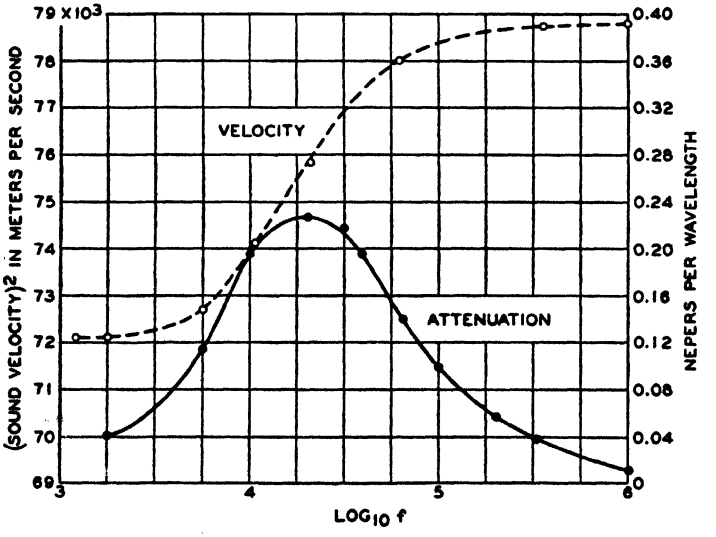

FIG. 13.7. Measured velocity and attenuation of carbon dioxide as a function of frequency.

cules. Calculations show that for most gases the interchange of energy between compressional and rotational energy is so rapid that for any of the frequencies used in measuring the effect, the interchange can be regarded as complete. However, for hydrogen, it appears that rotational modes can be excited which have a relaxation frequency of 10 mc. For certain vibrational modes of motion of the molecules the interchange is not nearly as rapid. For very low frequencies the amount of energy transferred into internal vibrations from compressional energy is regained, provided the compression and the expansion take place slow enough for the molecules to run through their states of equilibrium between the compressional and expansional stages. If, however, the gas is compressed and expanded within an interval of time, which is the order of the time required to establish thermal equilibrium between the quiescent and the vibrating molecules, then a certain fraction of the vibrational energy is not recovered but is turned into heat energy. Finally, if we carry out the process at a rate much faster than the rate of energy adjustment, very little energy is transferred into vibrational energy during the compression and hence little energy will be absorbed.

Over a frequency range then we would expect little energy to be lost at low frequencies, since most of it is returned to the wave. There should be an addition to the specific heat of the gas at low frequencies, since there are more modes of motion to be excited. Maximum absorption should occur when the frequency of the sound wave equals the rate of adjustment of thermal equilibrium. Finally at high frequencies, little energy gets into the vibrational modes and we should expect little loss of sound energy and a lower specific heat of the gas.

Calculations, based on these considerations, are given in the Appendix, section A.8, and formulae for the attenuation per wavelength A and the velocity v as a function of frequency are given by the equations

$$A_\lambda = \frac{\pi\left(\frac{\gamma-1}{\gamma}\right)\frac{C_{vi}}{C_v}\frac{v_0}{v_\infty}\left(\frac{\omega}{k_1}\right)}{1+\frac{\omega^2}{k_1^2}}$$

$$v = v_0\sqrt{\frac{k_1^2v_\infty^2+\omega^2v_0^2\left(1+\frac{\gamma-1}{\gamma}\frac{C_{vi}}{C_v}\right)}{k_1^2v_\infty^2+\omega^2v_0^2}} \qquad (13.28)$$

where C_v is the specific heat at constant volume, C_{vi} the specific heat at constant volume due to vibrational degrees of freedom, γ = ratio of specific heats = C_p/C_v, ω is 2π times the frequency and k_1 is the reaction

rate constant; that is, the number of transitions per molecule per second from the excited to the normal state. This is equal to $1/\tau'$, where τ' is the relaxation time. We note that when $\omega \to 0$ and $\omega \to \infty$, the velocities of propagation are

$$v = v_0 = \sqrt{\frac{p_0\gamma}{\rho}}; \qquad v_\infty = v_0\sqrt{1 + \frac{\gamma - 1}{\gamma}\frac{C_{vi}}{C_v}} \tag{13.29}$$

Hence $\dfrac{v_\infty^2}{v_0^2} = 1 + \dfrac{\gamma - 1}{\gamma}\dfrac{C_{vi}}{C_v}$ and $\dfrac{v_\infty^2 - v_0^2}{v_0 v_\infty} = \dfrac{\gamma - 1}{\gamma}\dfrac{C_{vi}}{C_v}\dfrac{v_0}{v_\infty} = \dfrac{2}{\pi}A_{\lambda m}$.

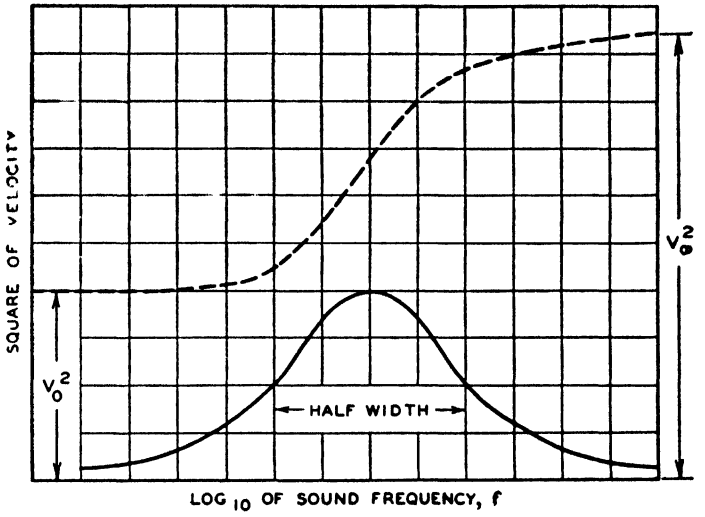

FIG. 13.8. Theoretical velocity and attenuation curves for a gas with an internal mode of vibration.

Hence when the velocities at very low and very high frequencies are evaluated, the heat of vibration C_{vi} can be evaluated as a certain fraction of the specific heat C_v. There is a relation between the maximum attenuation per wavelength $A_{\lambda m}$ and the velocities as shown by equation (13.29). Over a frequency range the square of the velocity is shown plotted by the dotted line of Fig. 13.8, while the solid line shows the attenuation as a function of frequency. The point of inflection of the velocity curve comes at the frequency of highest attenuation for the attenuation per wavelength, frequency curve. The frequency of maximum attenuation occurs at a different frequency for each gas or combination of gases. For carbon dioxide, the maximum occurs at about 20 kilocycles. From infrared spectroscopic investigation, it is known that there are three natural frequencies of vibration for the CO_2 molecule: two longitudinal and one

transverse or bending frequency. One of the longitudinal vibrations contributes little to the specific heat and the other about 0.308 calories per gram mole, while the bending oscillation contributes a value of 1.598 calories per gram mole. Taking the sum of these contributions, a good agreement is obtained with the value calculated from ultrasonic measurements. Hence this is a confirmation that the elimination of these frequencies from the specific heat gives rise to the increased velocity of sound at the high frequencies.

The effect of water vapor on the attenuation of sound in air is in acting as a catalytic agent for transferring the longitudinal vibrations into internal vibrational energy. In other words, the translational energy is rarely transformed into vibrational energy unless water vapor is present. If pure oxygen rather than air is used, the absorption is over 5 times as large, indicating that most of the internal vibrations reside in the oxygen molecule rather than in the nitrogen molecule. Experiments with nitrogen molecules indicate that the absorption is independent of the amount of water vapor and is nearly equal to the classical value determined by viscosity and heat conduction.

Relaxation phenomena have been observed in a number of gases including acetaldehyde, ammonia, carbon dioxide, nitric oxide, methane, carbon disulphide, propylene and various vapors. The relaxation frequencies depend upon the probability of exchanging energies between translational and internal modes and the probability ranges from 10^{-3} to 10^{-6}. Theoretical estimates of this probability are rather crude and it appears that further theoretical work would be profitable here.

Rotation relaxation (*i.e.* the excitation of a rotational mode by translational collisions) has recently been demonstrated for hydrogen. E. S. Stewart[12] reports a relaxation frequency of about 10 megacycles at standard temperatures and pressures. The probability of energy exchange is about 2×10^{-2} per collision. Vibrational relaxation is not possible here because the vibrational specific heat is not actuated at room temperature. Keller[13] suggested the possibility of rotational relaxation in nitrogen and ammonia gas.

For rotational and vibrational modes, the probabilities of interchange are within the ranges

Rotational translational	Vibrational translational	(13.30)
10^{-1} to 10^{-2}	10^{-3} to 10^{-6}	

[12] Stewart, E. S., *Phys. Rev.*, Vol. 69, p. 632, 1946.
[13] Keller, H., *Phys. Zeits.*, Vol. 41, p. 386, 1940.

CHAPTER XIV

Measurement of the Properties of Liquids

A large amount of work has been done in the last few years in measuring the velocity and attenuation of longitudinal waves in liquids. The measurement of the sound velocities in liquids is of interest for it provides a method for determining the adiabatic compressibility of the liquid. Given this and the isothermal compressibility obtained from static measurements, one is able to calculate the ratio of specific heats of the liquid. This gives the value of the specific heat at constant volume C_v which cannot be measured directly and is otherwise only calculable by complicated thermodynamic relations.

It is shown in Chapter III, section 3.14, that the difference in the specific heats of a solid body is equal to

$$\rho(C_p - C_v) = T_0(\alpha_1\lambda_1 + \alpha_2\lambda_2 \cdots + \alpha_6\lambda_6) \tag{14.1}$$

where

$$\lambda_1 = \alpha_1 c_{11} + \alpha_2 c_{12} \cdots + \alpha_6 c_{16}$$
$$\cdots\cdots\cdots\cdots\cdots\cdots\cdots$$
$$\lambda_6 = \alpha_1 c_{16} + \alpha_2 c_{26} \cdots + \alpha_6 c_{66}$$

ρ is the density, T_0 the absolute temperature, α_1 to α_6 the six linear temperature coefficients of expansion connecting the temperature and the six strains, and c_{11} to c_{66} the 21 elastic constants. For a liquid

$$\alpha_1 = \alpha_2 = \alpha_3 = \frac{\alpha}{3} \qquad \text{and} \qquad \alpha_4 = \alpha_5 = \alpha_6 = 0$$

where α is the temperature coefficient of cubical or volume expansion,

$$c_{11} = c_{12} = c_{13} = c_{22} = c_{23} = c_{33} = \frac{1}{\beta^I} \tag{14.2}$$

where β^I is the isothermal compressibility, and all the other elastic constants are zero. Hence for a liquid

$$C_p - C_v = \frac{T_0\alpha^2}{\rho\beta^I} \tag{14.3}$$

Now, since the velocity of propagation of a wave in a liquid is given by

$$v = \sqrt{\frac{\gamma}{\rho\beta^I}} = \sqrt{\frac{1}{\rho\beta^A}} \tag{14.4}$$

it follows that

$$\beta^I = \frac{C_p + T_0\alpha^2v^2}{v^2\rho C_p} = \beta^A + \frac{T_0\alpha^2}{\rho C_p} \tag{14.5}$$

where $\gamma = C_p/C_v$ is the ratio of the specific heats of the liquid. Hence, a measurement of the sound velocity v, the temperature coefficient of volume expansion α, the specific heat at constant pressure C_p, and the density ρ, all at the temperature T_0 will determine all the quantities.

Attenuation measurements throw considerable light on the molecular processes in liquids. According to classical theory the attenuation of a longitudinal wave in a liquid is caused by the same sources as in a gas, namely viscosity and heat conduction. For liquids, other than molten metals such as mercury, the heat conduction term is 1/20 or less than the viscosity term and can usually be neglected. The two monatomic liquids that have been measured are mercury and liquid argon, and these have values quite close to the theoretical values. Expressing the attenuation factor as

$$\frac{A_{(\text{nepers per cm})}}{f^2} \tag{14.6}$$

the calculated values from the classical theory are 5×10^{-17} for mercury and 3×10^{-17} for liquid argon. Recent measurements of mercury[1] taken up to 1,000 megacycles give a value for the attenuation factor of 6×10^{-17} while measurements of Galt,[2] give results in close agreement with the theoretical value for liquid argon.

For more complex liquids, however, the experimental results do not agree well with the classical theory and indicate that other sources of dissipation are required. For light liquids of low viscosity the experimental attenuation is invariably higher than the classical theoretical value. Highly associated liquids tend to show low, near-classical absorption. The alcohols and water are good examples of associated liquids, and they show the following values:

[1] Ringo, G. R., J. W. Fitzgerald and B. G. Hurdle, "Propagation of U.H.F. Sound in Mercury," *Phys. Rev.*, Vol. 72, No. 1, p. 87, July, 1947.

[2] Galt, J. K., "Sound Absorption and Velocity in Liquified Argon, Nitrogen and Hydrogen," *J. Chem. Phys.*, Vol. 16, No. 5, pp. 505–507, May, 1940.

Substance	A exp/A classical	
Methyl alcohol	3	
Ethyl alcohol	1	
Propyl alcohol	2	
Amyl alcohol	1.5	(14.7)
Butyl alcohol	1	
Water	3	

The three most absorbing liquids of the low-viscosity type are nonpolar, namely carbon disulphide, carbon tetrachloride and benzene, and these have the following ratio of experimental to classical absorption:

Substance	A exp/A classical	
Carbon disulphide	600	
Carbon tetrachloride	25	(14.8)
Benzene	90	

Other nonpolar liquids, such as heptane, hexane and toluene, are highly absorbing. One source for extra absorption is the interchange of energy between translational and vibrational modes similar to the process occurring in a gas. Considerable work[3] has been done in accounting for the velocity

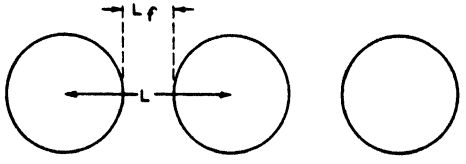

FIG. 14.1. Gas-like picture to account for the velocity and attenuation of a liquid.

of sound in liquids by employing the picture shown by Fig. 14.1. Here the sound wave is pictured as traveling with an infinite velocity within the molecule and with gas kinetic velocities through the space between the molecules of the liquid. This space is called the " available volume." The molecules effectively short-circuit a part of the path of the sound wave. If the intermolecular separation is L and the free path length is L_f, the molecules short circuit all but a fraction L_f/L of the path and the sound

[3] Eyring and Hirschfelder, *J. Chem. Phys.*, Vol. 41, p. 249, 1937; Kincaid and Eyring, *J. Chem. Phys.*, Vol. 5, p. 589, 1937, and Vol. 6, p. 620, 1938; Hirschfelder, Stevenson and Eyring, *J. Chem. Phys.*, Vol. 5, p. 896, 1937; Kittel, C., *J. Chem. Phys.*, Vol. 14, p. 614, 1946.

velocity in a liquid is then given by

$$v_{\text{liq.}} = (L/L_f)v_{\text{gas}} \tag{14.9}$$

where

$$v_{\text{gas}} = \gamma_0 \left(\frac{RT}{M}\right)$$

where γ_0 is the ratio of specific heats for the gas, R the gas constant, T the absolute temperature and M the molecular volume. By allowing the molecules to have internal modes of vibration, an absorption of the Herzfeld, Rice, Kneser type can be obtained.

Although the H, R, K mechanism probably operates in all types of liquids it is not the only one and is probably not the dominant one as has been shown by recent measurements[4, 5] of at least three liquids. These have shown that the H, R, K mechanism is not sufficient to account for the added attenuation. The measurements of Fox and Rock[4] on the absorption of water as a function of temperature show that the classical mechanisms and thermal relaxation cannot together account for all the absorption in water. The basis for this statement is that at 4°C the temperature-expansion coefficient of water vanishes; hence $(C_p - C_v)$ vanishes near 4°C in water and the wave proceeds isothermally without alternate heating or cooling. If the process is isothermal, there is no occasion for the population of the internal vibrational states of the molecule to change, so that there can be no attenuation caused by a delay in thermal equilibrium. The measured value of the absorption in water at 4°C is $A/f^2 = 50 \times 10^{-17}$ of which the classical mechanisms contribute about 15×10^{-17}. This leaves an unexplained term of 35×10^{-17}.

Another concept of the liquid state regards a liquid as a solid substance for which the long-range order between molecules has broken down. On this view, the extra loss can be accounted for by the Debye-Frenkel rearrangement theory. This process was first suggested by Debye,[6] and has been further developed by Frenkel.[7] On this theory the compressibility is due to two components: the increase in potential energy due to decreasing the distance between molecules, and a change in the degree of local

[4] Fox and Rock, *Phys. Rev.*, Vol. 70, p. 68, 1946; Hall, *Phys. Rev.*, Vol. 73, No. 7, pp. 775–781, April 1, 1948.

[5] Rupuano, R. A., "Ultrasonic Absorption from 75 to 250 mc/sec," *Phys. Rev.*, Vol. 72, No. 1, p. 79, July 1, 1947.

[6] Kneser, H. O., *Phys. Zeits.*, Vol. 39, p. 800, 1938; P. Debye, *Z. Elektrochem.*, Vol. 45, p. 174, 1939.

[7] Frenkel, J., *Kinetic Theory of Liquids*, p. 208, Oxford University Press.

order in the arrangement of the particles, in the sense of a more compact arrangement when the liquid is compressed, and a more open distribution when it is expanded. This change in the degree of local order must in general lag with respect to the variation of the pressure, since it is connected with a rearrangement of the particles or a redistribution of their mutual orientation, *i.e.*, with processes requiring a certain activation energy, and proceeding accordingly with a finite velocity only. This time lag of the arrangement with respect to the volume must coincide with the mean lifetime of vibrations about the same equilibrium positions which determine the shearing viscosities of the liquid. Hence a theoretical basis is laid for a compressional viscosity in a liquid which can add to the losses for longitudinal waves. When the frequency gets so high that the molecules do not have time to rearrange themselves in the course of a cycle, the rearrangement compliance disappears and the liquid becomes stiffer. So far no measurements have been made for light liquids which show a velocity dispersion. The measurements of Rupuano carried up to 250 megacycles, still show a loss proportional to the square of the frequency and a velocity independent of frequency. Calculations show that if an H, R, K mechanism were involved in the added loss, the velocity of benzene should have varied by a measurable amount and hence the measurements point to a Debye-Frenkel type of mechanism as the dominant cause for the increased attenuation. Hall[4] has recently explained the added attenuation in water by means of a Debye-Frenkel rearrangement process.

Recent measurements[8] have shown a velocity dispersion and associated attenuation dispersion in polyisobutylene. Associated shear measurements have shown that this dispersion is due to a high-frequency shear stiffness that causes the longitudinal velocity to increase according to a relaxation mechanism. The details of these measurements are discussed in Section 14.5.

The attenuation for longitudinal waves for very viscous liquids such as polyisobutylene, and silicone putty is considerably less than that calculated from the shear and compressional viscosities according to the classical formulae. This has been shown to be due to the fact that the low-frequency shear viscosities are relaxed by shear elasticities of the configuration type at relatively low frequencies and do not contribute to the attenuation of high-frequency longitudinal waves. Direct measurements of the shear viscosity and shear elasticity of liquids have been made by the

[8] Mason, W. P., W. O. Baker, H. J. McSkimin, and J. H. Heiss, "Mechanical Properties of Long Chain Polymer Liquids," *Phys. Rev.*, Vol. 73, No. 9, pp. 1074–1091, May 1, 1948.

writer[9] and the methods are discussed further in section 14.2. A liquid has a relaxation frequency f_0 equal to

$$f_0 = \frac{\mu}{2\mu\eta} \tag{14.10}$$

(μ = shear elasticity, η = shear viscosity) below which the liquid acts as a viscous medium and above which the liquid acts as an elastic medium. For rubber-like materials of the highly viscous polymer type, the configurational shear elasticity will be as low as 10^7 dynes per square centimeter, while the viscosity may range from 20 to 1,000 poises. Hence the relaxation frequency will vary from 10^5 to 10^3 cycles and shear elasticities are measurable by the torsional crystal method discussed in section 14.2. For light liquids which do not show configurational shear elasticity and with $\eta \doteq 10^{-2}$ poises, and shear moduli in the order of 10^{10} dynes/square centimeter (characteristic of ionic crystals), one would expect relaxation frequencies of 10^{11} cycles, which is far above the experimental range. Shear waves of these frequencies, however, may play a role in determining the heat capacity of liquids, as has been emphasized by Brillouin[10] and Lucas.[11]

The presence of shear elasticities in liquids has been demonstrated at hypersonic frequencies by Raman and Venkateswarm[12] using the thermal lattice vibrations of the Born-Debye waves. As predicted by Brillouin,[13] these waves cause light scattered by the molecules of the liquid through which a sound wave is traveling, to be modulated by the frequency of the sound wave. The scattered light will have frequencies $f \pm f_s$, where f_s is the frequency of the sound wave and will be visible at an angle φ, such that

$$2\lambda_s \sin\varphi = \lambda_l \tag{14.11}$$

where λ_s is the acoustic wavelength and λ_l the optical wavelength in the medium. Using this method, Raman and Venkateswarm found the longitudinal velocity of sound in glycerine to be v = 2,500 meters per second at a frequency of 1.53×10^4 megacycles as compared with an ultrasonic velocity of 1,910 meters per second. From these, the shear modulus $\mu = 2.4 \times 10^{10}$ dynes per square centimeter, while the bulk modulus $\kappa = \lambda + 2/3\mu$ was 4.6×10^{10} dynes per square centimeter.

[9] Mason, W. P., "Measurements of the Viscosity and Shear Elasticity of Liquids by Means of a Torsionally Vibrating Crystal," *Trans. Am. Soc. Mech. Eng.*, Vol. 69, pp. 359–370, May, 1947.

[10] Brillouin, L., *J. Phys. Radium*, [7], Vol. 7, p. 153, 1936.

[11] Lucas, R., *J. Phys. Radium*, [7], Vol. 8, p. 410, 1937.

[12] Raman, C. and C. S. Venkateswarm, *Nature*, pp. 143, 798, London, 1939.

[13] Brillouin, L., *Ann. Phys.*, [9], Vol. 17, p. 88, Paris, 1922.

From equation 14.10, since the viscosity of glycerine is about 5.8 poises, the relaxation frequency for shear waves is 6.5×10^2 megacycles which is much lower than the measuring frequency. Subsequent measurements suggest that velocity dispersion caused by shear elasticity does not occur below 1,000 mc in ordinary light liquids as it should not according to equation (14.10).

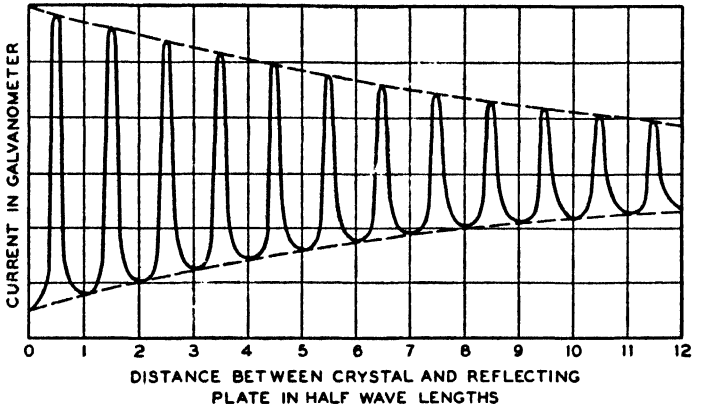

FIG. 14.2. Current in meter for an interferometer immersed in a liquid.

14.1 *Measurements of Velocities and Attenuations for Longitudinal Waves in Liquids*

For measurements of velocities and attenuations above 1 megacycle, acoustic interferometers, Debye-Sears cells and pulsing methods have all been used. An interferometer similar to that shown by Fig. 13.4 is ordinarily used except that the crystal is usually mounted in a sealed container with air backing. Since the crystal can be soldered, it is usually fastened to a machined cup by baking a coat of silver paste with a glass base to the edge of the crystal and soldering in place. Plating is baked on the outside surface and the inner surface is covered except for a small ring around the edge for insulating purposes. Since the mechanical impedances of liquids are much higher than those for gases, it is the low-resonant impedance that gives the sharp variations at odd quarter wavelengths. Figure 14.2 shows a typical current distance curve. The velocity and attenuation can be calculated from equations (13.9) and (13.24) as for gases. Since the attenuation in most liquids is small, it is difficult to obtain accurate results under frequencies of 5 to 8 megacycles by this method.

Other methods are also available for measuring velocities and attenu-

ations in liquids. One method widely used is an optical one employing the Debye-Sears effect for liquids. A crystal in liquids sets up acoustic waves consisting of regions of compression and regions of rarefaction in the liquid, which alternate at distances of half a wavelength. Hence, if a parallel beam of light shines through such a crystal tank with plate glass walls, the regions of density and rarefaction act like a phase light diffraction grating. If the parallel light from the cell is focused on a single spot when no sound waves are present, first and higher order diffraction spectra will appear on either side of the zero-order spot when sound waves are present. From the spacing of the diffraction orders, the sound wave-

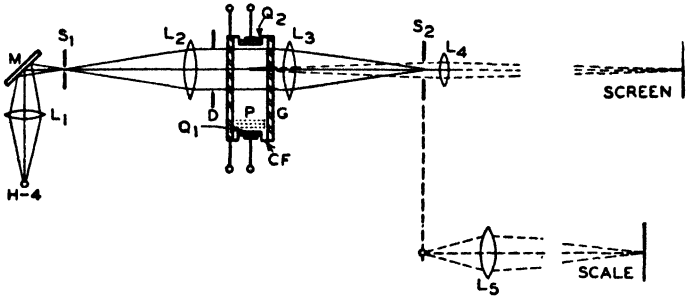

FIG. 14.3. Debye-Sears cell for measuring velocity and attenuation in a transparent liquid.

length λ can be determined, which, together with the frequency, gives the velocity of sound in the liquid. As the intensity of the sound waves is increased, more and more light is forced from the zero-order spot into the diffraction spectra and for one sound intensity all of the light can be removed from the zero-order spot. If either this zero-order spot, or all of the secondary spectra are eliminated by employing a bar or a slit respectively, the light that goes through can be controlled by the amplitude, and a light valve can be obtained. Such light valves have been used as the light modulating element for sound on film systems.[14]

Now, if another lens L4 of Fig. 14.3 is added, which focuses the central plane of the cell onto a screen through the slit S2, the shape of the sound beam can be made visible. Figure 14.3 is a typical arrangement taken from a paper by Willard.[15] Very clear photographs of interference, reflection and refraction phenomena can be obtained from such an arrangement. Figure 14.4A shows a photograph of a plane beam from a crystal and the diffraction lines which are similar to those occurring for a wide slit in optics. Figure 14.4C shows a photograph some distance away from a nar-

[14] U. S. Pat. No. 2,345,441, March 28, 1944, issued to G. W. Willard.

[15] Willard, G. W., *J.A.S.A.*, Vol. 12, p. 438, 1941.

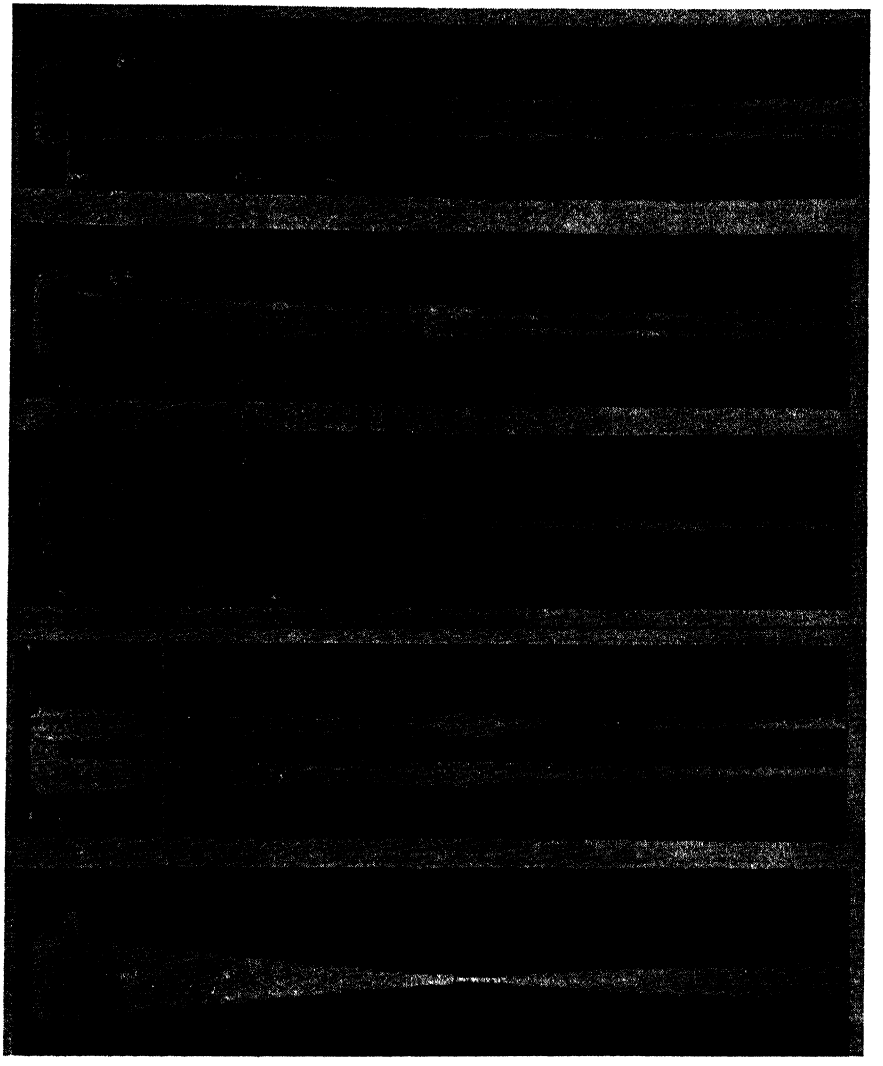

FIG. 14.4. Photographs of diffraction and focusing effects.

row slit and shows the side lobes from such a radiator which are similar to those from an acoustic transducer or a microwave radiator. Figure 14.4B shows an intermediate case. Figure 14.4E shows the transmission through a cylindrical lens made of lucite and shows the focusing effect that is caused by such a lens. Since the velocity of sound is greater in lucite at this frequency (10 megacycles) than the velocity of sound in water, it

requires a concave lens to focus the sound beam. Knowing the radius of curvature of the lens, the distance for focusing and the velocity of sound in water, the velocity of transmission in lucite can be obtained and was found to be 2,640 meters per second. Figure 14.4 was taken from a paper by Willard.[16]

By using a slit in the receiving system rather than a bar, Willard[15] has shown that there are color effects associated with the intensity of the wave, *i.e.* for a certain intensity a certain color appears. This has been made use of in measuring the attenuation of a wave in the liquid. For a certain applied voltage on the driving crystal, a color effect is noted at a distance l_1 from the crystal. The voltage on the crystal is then doubled and this color intensity pattern occurs at a distance l_2 from the crystal. Hence the attenuation expressed in db per centimeter is

$$A = \frac{6}{l_2 - l_1} \text{ db per cm} \tag{14.12}$$

since a voltage ratio of 2 corresponds to 6 db. In this way the attenuation of a large number of liquids was measured.[15]

Table XXII shows a measurement[17] of some or all of the properties of a number of liquids measured at the Bell Laboratories, sorted out in the order of decreasing velocities. In many cases the temperature coefficient of velocity has been measured and is shown in column 5. The attenuation expressed in the form

$$\frac{A_{(\text{nepers per cm})}}{f^2} \times 10^{15} \tag{14.13}$$

is shown in column 7. This form is used since theoretically the attenuation should increase proportional to the square of the frequency and experimentally this has been found to be the case. The eighth column shows the coefficient of viscosity, when this is known.

The data on the change in velocity with temperature shown by the fifth column show that all the liquids measured have a negative coefficient of velocity except water. Figure 14.5 shows the velocity of water as a function of temperature. The velocity increases up to a temperature of 75°C at which temperature the velocity has a zero temperature coefficient. Above this temperature, the velocity decreases with an increase in temperature. By dissolving any of the negative temperature coefficient liquids in water, the peak of the velocity-temperature curve can be brought to

[16] Willard, G. W., *Bell Lab. Rec.*, Vol. 25, No. 5, May, 1947.

[17] Some of these values have been measured by Willard.[15, 18] The rest have been measured with an acoustic interferometer by J. B. Johnson, H. J. McSkimin and the writer.

TABLE XXII

Substance	Form Index	Density	Velocity v at 25°C m/s	$-\Delta v$/C° m/s/C°	Impedance ρv at 25°C; ohms per Sq Cm	Absorp. $A\times10^{15}$ f^2	Viscosity $\eta\times10^3$
Glycerol	$C_3H_8O_3$	1.26	1904	2.2	2.40×10^5	24.00	5800
Ethanol Amide (2-Amino Ethanol)	C_2H_7NO	1.018	1724	3.4	1.755	—	—
Ethylene Glycol	$C_2H_6O_2$	1.113	1658	2 1	1.847	—	—
Analine	$C_6H_5NO_2$	1.022	1637	4.0	1.675	—	—
Formamide	CH_3NO	1.134	1622	2.2	1.842	0.57	—
Triethylene Glycol	$C_6H_{14}O_4$	1.123	1608	3.8	1.975	—	—
Diethylene Glycol	$C_4H_{10}O_3$	1.116	1586	2.4	1.770	—	—
Tetraethylene Glycol	$C_8H_{18}O_5$	1.123	1586	3.0	1.784	—	—
Cinnamaldehyde	C_9H_8O	1.112	1554	3.2	1.731	—	—
Sea Water	—	1.025	1531	−2.4	1.572	—	—
Lubricating Oil-X200	—	0.964	1530	3.7	1.475	—	—
α Methyl Napthalene	$C_{11}H_{10}$	1.090	1510	3.7	1.645	—	—
Distilled Water	H_2O	0.998	1498	−2.4	1.495	0.25	10.0
AA Gravity Fuel Oil	—	0.99	1485	3.7	1.472	—	—
2.3 Butylene Glycol	$C_4H_{10}O_2$	1.019	1484	—	1.511	20.0	—
Castor Oil	$C_{11}H_{10}O_{10}$	0.969	1477	3.6	1.430	61.0	6700
Nitrobenzene	$C_6H_5NO_2$	1.20	1463	3.6	1.758	0.9	20.0
Dimethyl Phthalate	$C_8H_{10}O_4$	1.20	1463	—	1.758	—	—
Peanut Oil	—	0.936	1458	—	1.365	—	—
Carbitol	$C_6H_{14}O_3$	0.988	1458	—	1.431	—	—
Cyclohexanol	$C_6H_{12}O$	0.962	1454	3.6	1.400	5.0	—
Furfuryl Alcohol	$C_5H_6O_2$	1.135	1450	3.4	1.645	—	—
Furfural	$C_5H_4O_2$	1.157	1444	3.7	1.670	—	—
Morpholine	C_4H_9NO	1.000	1442	3.8	1.442	—	—
Sperm Oil	—	0.88	1440	—	1.268	—	—
Olive Oil	—	0.912	1431	2.75	1.308	10.0	1000
Cyclohexanone	$C_6H_{10}O$	0.948	1423	4.0	1.391	—	—
Pyridine	C_6H_5N	0.982	1415	4.1	1.39	—	—
Dibutyl Phthalate	$C_8H_{22}O_4$	—	1408	—	—	—	—
Butyl Oleate	$C_{22}H_{42}O_2$	—	1404	3.0	—	—	—
3 Methyl Cyclohexanol	$C_7H_{14}O$	0.92	1400	—	1.29	3.5	—

TABLE XXII—*Continued*

Substance	Form Index	Density	Velocity v at 25°C m/s	$-\Delta v/C°$ m/s/C°	Impedance ρv at 25°C; ohms per Sq Cm	Absorp. $A\times10^{15}$ f^2	Viscosity $\eta\times10^{8}$
Acetonyl Acetone	$C_6H_{10}O_2$	0.729	1399	3.6	1.359×10^{5}	0.5	—
2, 3 Dichloro-dioxane	$C_2H_6Cl_2O_2$	—	1391	3.7	—	—	—
Oil of Camphor Sassafrassy	—	—	1390	3.8	—	—	—
Dioxane	$C_4H_8O_2$	1.033	1376	4.0	1.425	1.3	—
Solvesso #3	—	0.877	1370	3.7	1.201	—	—
Univis 800	—	0.870	1346	—	1.191	—	—
Nitromethane	CH_3NC_2	1.13	1330	4.0	1.504	0.9	—
M xylol	C_8H_{10}	0.864	1324	4.2	1.145	0.74	5.5
Kerosene	—	0.81	1324	3.6	1.072	1.1	—
d-Frenchone	$C_{10}H_{16}O$	0.94	1320	—	1.241	0.55	2.2
Alkazene-13	$C_{15}H_{24}$	0.86	1317	3.9	1.132	1.3	—
Mesityloxide	$C_6H_{16}O$	0.85	1310	—	1.115	3.3	—
Toluol	C_7H_8	0.866	1308	4.2	1.132	0.85	5.8
Alkazene-25	$C_{10}H_{12}Cl_2$	1.20	1307	3.4	1.568	0.6	—
Dichloro-t-butyl Alcohol	$C_4H_8Cl_2O$	—	1304	3.8	—	—	—
Chlorobenzene	C_6H_5Cl	1.10	1302	—	1.432	1.7	—
n-Hexanol	$C_6H_{14}O$	0.819	1300	3.8	1.065	—	—
Benzene	C_6H_6	0.870	1295	4.65	1.129	8.3	7.0
Acetonitrile	C_2H_3N	0.783	1290	4.1	1.01	0.8	—
Monochloro-benzene	C_6H_5Cl	1.107	1273	3.6	1.411	1.7	—
Diamylamine	$C_{10}H_{23}N$	—	1256	3.9	—	—	—
Turpentine	—	0.88	1255	—	1.105	1.5	14.0
Butylalcohol	$C_4H_{10}O$	0.810	1240	3.3	1.003	—	—
Diacetyl	$C_4H_6O_2$	0.99	1236	4.6	1.222	—	—
Naphtha	—	0.76	1225	—	1.08	1.0	—
1, 3 Dichloro-iso-butane	$C_4H_8Cl_2$	1.14	1220	3.4	1.390	0.9	—
Methyl Acetate	$C_3H_6O_2$	0.934	1211	—	1.131	1.09	3.8
Ethanol	C_2H_6O	0.79	1207	4.0	0.954	0.9	11.0
t-Amyl Alcohol	$C_5H_{12}O$	0.81	1204	—	0.976	3.3	—
Ethyl Acetate	$C_4H_8O_2$	0.90	1187	—	1.069	1.1	4.2
Acetone	C_3H_6O	0.79	1174	4.5	0.929	0.64	3.0
Octane	C_8H_{18}	—	1171	4.2	—	—	—
Carbon disulphide	CS_2	1.26	1149	—	1.449	74.0	3.5
Heptane	C_7H_{16}	—	1135	4.2	—	—	—
Hexane	C_6H_{14}	—	1112	—	—	—	—
Methanol	CH_4O	0.791	1103	3.2	0.872	0.9	5.5
Acetylen-dichloride	$C_2H_2Cl_2$	1.26	1015	3.8	1.280	4.0	4.0

TABLE XXII—*Continued*

Substance	Form Index	Density	Velocity v at 25°C m/s	$-\Delta v$/C° m/s/C°	Impedance ρv at 25°C; ohms per Sq Cm	Absorp. $A\times10^{15}$ f^2	Viscosity $\eta\times10^3$
Isopentane	C_5H_{12}	0.62	992	4.8	0.615×10^6	1.5	14.0
Silicone (30 centipoise)	—	0.993	990	—	0.985	—	300.0
Chloroform	$CHCl_3$	1.49	987	3.4	1.471	3.8	5.5
Ethyl Ether	$C_4H_{10}O$	0.713	985	4 87	0.702	—	—
tert Butyl Chloride	C_4H_9Cl	0.84	984	4.2	0.827	1.9	—
Methyl Iodide	CH_3I	—	978	—	—	—	—
Carbon Tetrachloride	CCl_4	1.595	926	2.7	1.478	5.7	10.0
Bromoform	$CHBr_3$	2.890	916	3.1	2.670	2.3	—
Xylene Hexafluoride	$C_8H_4F_6$	1.37	879	—	1.205	—	8.4

a lower temperature. Willard[18] finds that by adding 16 cubic centimeters of ethanol (C_2H_6O) to 100 cubic centimeters of water the peak of the velocity-temperature curve comes at 45°C, as shown by Fig. 14.5. Adding 22 cubic centimeters of ethanol to 100 cubic centimeters of water brings the peak down to 25°C. One surprising result is that although ethanol has a lower velocity (1207M/S) than water, a mixture of the two has a higher velocity than either. This appears to be true for the mixtures tried and suggests that the effect of the mixture is to change the position of the velocity parabola for water to a lower temperature and at the same time raise the effective stiffness at the highest velocity temperature. The zero coefficient property of a mixture of water and other liquids has been taken advantage of in constructing delay lines for measuring very short time intervals.[19] By using a thickness-vibrating crystal to set up acoustic waves in the liquid and another crystal for picking up these acoustic waves, short pulses of high frequency can be transmitted in the liquid. The time of arrival of such pulses can be compared with the time of arrival of radio pulses sent out simultaneously with the liquid pulse, and if a variable liquid path of known length is used, the time of the reflecting surface is accurately determined. For this purpose it is desirable to have the velocity of the liquid relatively constant with temperature.

[18] Willard, G. W., *J.A.S.A.*, Jan., 1947.

[19] U. S. Pat. No. 2,407,294, Sept. 10, 1946, issued to W. Shockley and G. W. Willard; U. S. Pat. No. 2,427,348, Sept. 16, 1947, issued to W. L. Bond and W. P. Mason.

If we consider only the classical viscosity and heat conduction as the source of dissipation of an acoustic wave, the attenuation of a plane wave in a liquid should be given by the formula

$$A_{(\text{nepers per cm})} = \frac{2\pi^2 f^2}{\rho v^3}\left[\chi + 2\eta + \frac{(\gamma - 1)K}{C_p}\right] \tag{13.2}$$

where f is the frequency, ρ the density, v the velocity, η the shear viscosity, χ the compressional viscosity, γ the ratio of specific heats, K the thermal conductivity, and C_p the specific heat at constant pressure for the liquid.

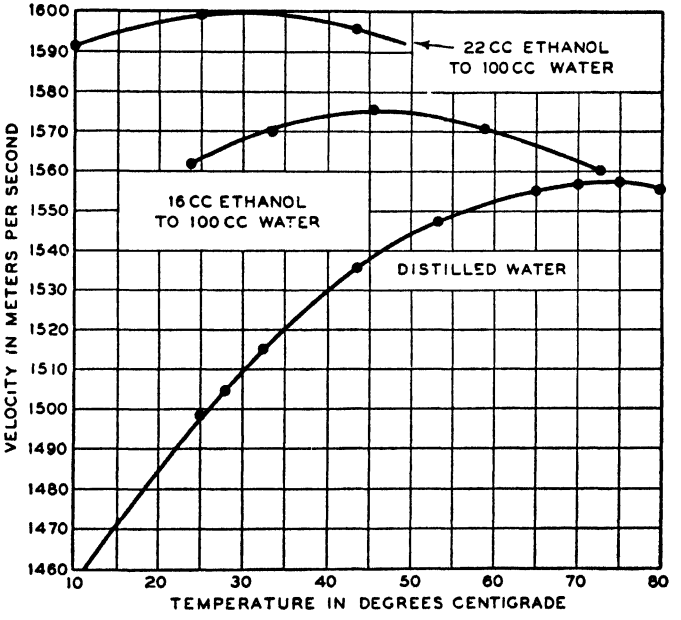

FIG. 14.5. Velocity of water and various mixtures as a function of temperature.

For non-metallic liquids, the heat conduction term is small and can usually be neglected. If we take Stokes's assumption that a liquid expanding radially will have no losses, $\chi + 2\eta = \frac{4\eta}{3}$ and this is the usual form given for the attenuation. The actual measurements for light liquids run from 2 to 900 times this formula as far as magnitude goes, although all the light liquids have a loss proportional to the square of the frequency, in agreement with (13.2), up to frequencies as high as 250 megacycles.[5]

A possible cause for this divergence is the existence of a compressional viscosity χ as well as a shear viscosity η. A theoretical basis for such a

viscosity is given by the Debye-Frenkel rearrangement theory. On this theory, as mentioned in the introduction, the compressibility is due to two components: the increase in potential energy due to decreasing the distance between molecules, and a rearrangement compliance due to a change in the local order in the rearrangement of particles in the sense of a more closely packed arrangement when the liquid is compressed and a more open distribution when it is expanded. This change in order takes place by molecules or parts of molecules jumping from one position to another across a potential barrier and hence a process is associated with a compression similar to the mechanism causing the shear viscosity of a liquid. For associated liquids which are built up into molecular groups, the amount of rearrangement that can take place due to a compression is small and hence only a small compressional viscosity is obtained. For non-polar groups a much larger rearrangement can take place and hence a higher compressional viscosity can be obtained. According to the Debye-Frenkel theory, the compressional viscosity will be relaxed at a frequency f_c for which

$$f_c = \frac{\kappa_1}{2\pi\chi} \tag{14.14}$$

where κ_1 is the rearrangement stiffness and χ the compressional viscosity. The shear viscosity can also be relaxed due to the shear stiffness of the liquid and this may occur at a lower frequency than the compressional relaxation frequency f_c.

When two liquids are mixed in various proportions, Willard,[15] Willis[20] and Burton[20] have shown that the loss of the combination sometimes is considerably larger than that of either component alone. Figure 14.6 shows the measured absorption of a water acetone mixture as a function of the percentage of acetone in water. At a percentage of 70, the absorption is over three times as high as that for either component alone. Since water is a highly associated liquid, it appears possible that the mixture destroys some of the association in water, decreases some of the structural compliance of the Debye-Frenkel type, and increases the rearrangement (compressional) viscosity. As shown in the first part of Fig. 14.6 when the non-associated liquids benzene and acetone are used, no such effect occurs.

14.2 *Measurement of Shear Viscosity and Elasticity of Liquids by Means of a Torsional Crystal*

If we set a crystal vibrating in a purely torsional mode, all the motion is tangential to the surface, and as discussed first by Stokes, highly attenu-

[20] Willis, F. H., Ph.D. Thesis, New York University, 1943; C. J. Burton, "A Study of Ultrasonic Absorption in Liquid Mixtures," *J.A.S.A.*, Vol. 20, No. 2, March, 1948.

ated viscous waves can be set up in the medium. The equations of propagation can be derived from the definition of viscosity and the equation of motion

$$T_5 = \eta \dot{S}_5 = \eta \left[\frac{\partial \dot{\zeta}}{\partial x} + \frac{\partial \dot{\xi}}{\partial z} \right]; \qquad \rho \frac{\partial \dot{\xi}}{\partial t} = \frac{\partial T_5}{\partial z} \tag{14.15}$$

where $\dot{\xi}$ is the velocity of the motion along x and $\dot{\zeta}$ along z. For a plane wave propagating along z, all the motion is tangential to the direction of

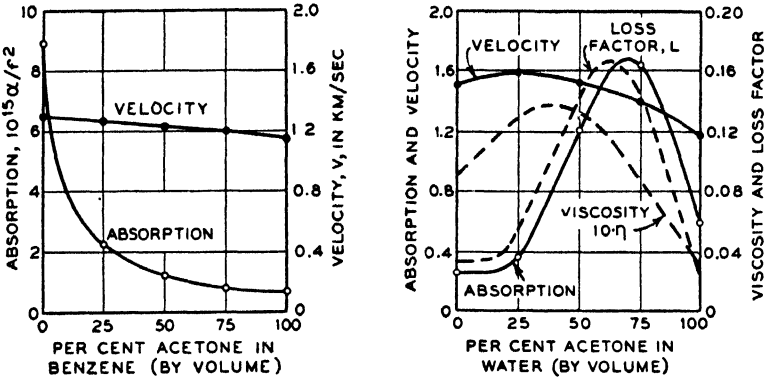

FIG. 14.6. Absorption of mixtures of liquids.

propagation on $\dot{\zeta} = 0$. Inserting the first equation of (14.15) (the definition of viscosity) in the second equation, the differential equation becomes

$$\rho \left(\frac{\partial \dot{\xi}}{\partial t} \right) = \eta \frac{\partial^2 \xi}{\partial z^2} \tag{14.16}$$

For simple harmonic motion, the plane viscous wave has the solution

$$\begin{aligned} T_5 &= T_{50} \cosh \Gamma z + \dot{\xi}_0 Z_0 \sinh \Gamma z \\ \dot{\xi} &= \dot{\xi}_0 \cosh \Gamma z + \frac{T_{50}}{Z_0} \sinh \Gamma z \end{aligned} \tag{14.17}$$

where Γ the propagation constant and Z_0 the image impedance, have the values

$$\Gamma = \sqrt{\frac{j\omega\rho}{\eta}} = \sqrt{\frac{\pi f \rho}{\eta}} (1 + j); \qquad Z_0 = \sqrt{j\omega\rho\eta} = \sqrt{\pi f \rho \eta} (1 + j) \tag{14.18}$$

For carbon tetrachloride, with a density $\rho = 1.595$ and a viscosity of .0098 poises, the attenuation is 2,660 nepers per centimeter at 14 kilocycles,

so that the shearing stress is appreciable for only a few thousandths of a centimeter from the crystal surface. Although the attenuation for such waves is too high to permit their wave propagation properties to be investigated, they do introduce a loading effect on the crystal which can be measured by the increase in the resonant resistance and the decrease of the resonant frequency of the crystal as it is changed from a vacuum to the medium under investigation.

The use of such a crystal for measuring viscosities was discussed in a former paper,[9] and it was there shown that the change in the measured electrical resistance ΔR_E and the lowering in frequency Δf, determined the mechanical resistance R_M per square centimeter, and the mechanical reactance X_M per square centimeter according to the formulae

$$R_M = \frac{\Delta R_E}{K_1}; \qquad X_M = -\frac{\Delta f}{K_2}$$

where

$$K_1 = \frac{r}{2\pi f_R^2 C_0 I}\left[R^3 + R_0^3 + \frac{(R^4 - R_0^4)}{l}\right]$$

$$K_2 = \frac{R^3 + R_0^3 + (R^4 - R_0^4)/l}{2I} \tag{14.19}$$

where r is the ratio of capacitances of the crystal determined by measuring the resonant frequency f_R, the anti-resonant frequency f_A, and setting $r = f_R/2(f_A - f_R)$, C_0 is the static capacitance of the crystal in farads, K the outside radius and R_0 the inside radius of the torsional crystal, l its length and I the moment of inertia per unit length, given by the formula

$$I = \frac{\pi}{2}\rho_c(R^4 - R_0^4) \tag{14.20}$$

where ρ_c is the density of the crystal.

The method for making a torsional crystal from ammonium dihydrogen phosphate ADP is shown by Fig. 14.7. Here a crystal is cut with its length along the x crystallographic axis, and a hole is bored along this axis. A cylinder is then turned, as shown in Fig. 14.7B. Since the mode of motion generated is a face-shear mode when the field is impressed along the z crystallographic axis, the plating is made continuous on the inside cylindrical surface and is divided into two 90° segments on the outside surface which are connected together electrically. The center lines of these two surfaces lie along the z-axis. As shown by Fig. 14.7C, the field in one segment produces a face shear in one direction, while the field in the other segment produces a face shear in the other direction. The result is a torsional motion of the crystal as a whole. As shown by Fig. 6.9, a torsional

vibration can also be produced in a quartz crystal and such crystals may be of use, especially if wide temperature ranges are to be covered.

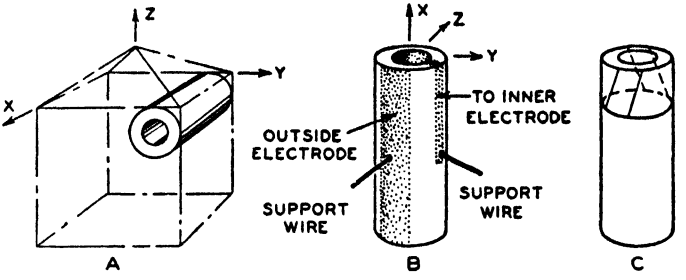

FIG. 14.7. Method for making a torsional crystal of ADP.

As discussed in the former paper (9), the viscosity of a number of light liquids was measured by using the experimental arrangement shown by Fig. 14.8. This consisted of an ADP crystal suspended from the three wires at its nodal points, mounted inside a container of small diameter. This container acts as a wave-guide tube and tends to attenuate highly any complicated vibrations of the longitudinal type which can be set up in the tube. The result is that if any such vibrations are set up by the fact that the motion of the crystal surface is not exactly tangential to the surface,

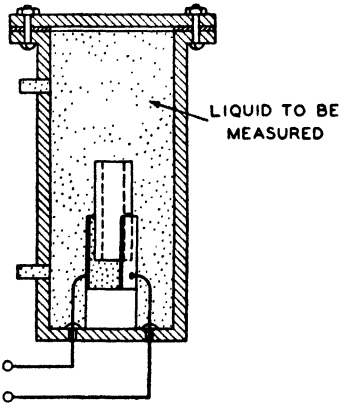

FIG. 14.8. Experimental arrangement for measuring viscosity of liquids.

the only effect that such waves have is to change the reactance loading on the crystal, and this is usually small. Measurements made of the loading due to nitrogen as a function of pressure, with the crystal inside and outside of wave-guide tubes, has shown that the longitudinal loading is negligible provided that the diameter of the crystal is a tenth or less of the length.

The outside container of Fig. 14.8 has two copper-to-glass seals for the

electrical wires to connect to the crystal. The chamber can be evacuated and filled with liquid through the two stopcocks. If desired, pressure can be put on the liquid by means of external gas pressure. The process of measurement consists in determining the resonant frequency f_{R0} and the resistance at resonance R_0 in a vacuum. Then, introducing the liquid, the new resonant frequency f_{R1} and the new resistance at resonance R_1 are determined. For liquids having a small viscosity, these values can be determined accurately by measuring the current through the crystal when a low impedance is connected on either side. The resonant frequency occurred at the frequency for which the current was a maximum, and the resonant resistance was measured by a substitution method. For very viscous liquids, however, this procedure does not accurately locate the resonant frequency, and measurements of resistance and reactance were made with a bridge circuit. A curve of the resistance for polymerized castor oil is shown by Fig. 14.9. The resonant frequency is determined as the lowest point of the resistance curve, or more accurately, by taking the average of two frequencies of equal resistance greater than the minimum, while the resistance used is the lowest value on the curve.

As an example, an ADP crystal, vibrating at nearly 14,000 cycles, and having the dimensions

$$L = 6.9 \text{ cm}; \qquad OD = 0.93 \text{ cm}; \qquad ID = 0.64 \text{ cm} \tag{14.21}$$

had a resonant frequency of 13,948 cycles, an anti-resonant frequency of 14,098.5, and a resistance at resonance of 1,300 ohms, all measured in a vacuum. The capacitance of the crystal was $C_0 = 140\mu\mu f$. The density of ADP is 1.804. From these values the constants K_1 and K_2 can be calculated as

$$K_1 = 366; \qquad K_2 = 0.673 \tag{14.22}$$

At 24°C, measurements were made of the viscosity of a number of light liquids. For dimethylphthalate, for example, the resonant resistance was 36,500 ohms. Hence the viscosity, with the density $\rho = 1.186$, is

$$\eta = \left(\frac{\Delta R_E}{K_1}\right)^2 \times \frac{1}{\pi f_R \rho} = 0.178 \text{ poises} \tag{14.23}$$

This compares with 0.176 measured by flow methods, which agrees within 1 per cent. By controlling the temperature accurately and using an accurate electrical bridge, this method is capable of precision. Measurements made over a range of viscosities from .01 poise to 6 poises were made and these agreed with those measured by flow methods within one per cent.

However, measurements made with very viscous liquids, such as poly-

merized castor oil, indicate that these liquids do not behave as simple viscous liquids since the reactance and resistance components are not equal, the resistance becoming progressively larger than the reactance at high

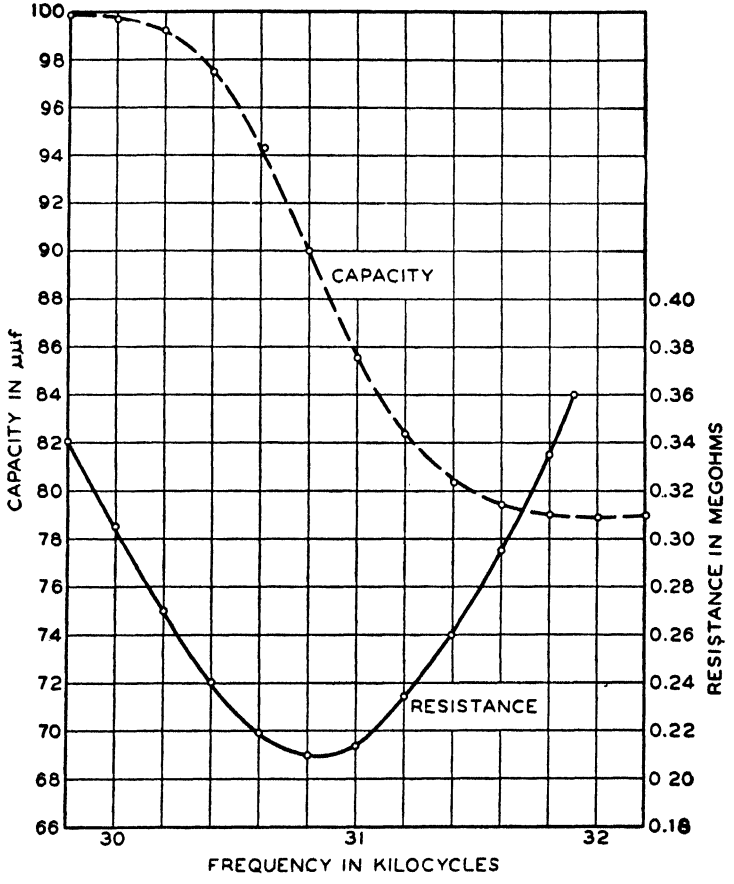

FIG. 14.9. Shunt resistance and capacity of crystal immersed in polymerized castor oil.

frequencies. This is illustrated by Fig. 14.10, the points of which represent the resistance and reactance values measured for polymerized castor oil as a function of frequency. The dot-dash line shows the resistance and reactance terms that would be obtained if the liquid were a viscous medium having a density of 0.967 and the viscosity of 18 poises measured by flow methods. The resistance is above this line and the reactance below.

This divergence and the shape of the curve are accounted for if the liquid is assumed to have a shear elasticity as well as a shear viscosity.

The impedance of such a wave is most easily calculated by means of an equivalent circuit, in which the stress corresponds to the voltage and the particle velocity to the current. For a purely viscous medium, the equivalent circuit is shown by the left side of Fig. 14.10. The series arm is an inductance equal to the density times the length dx, where dx is a length in the order of the mean free path. The shunt arm is a resistance equal to the viscosity η divided by the length dx. The equivalent circuit

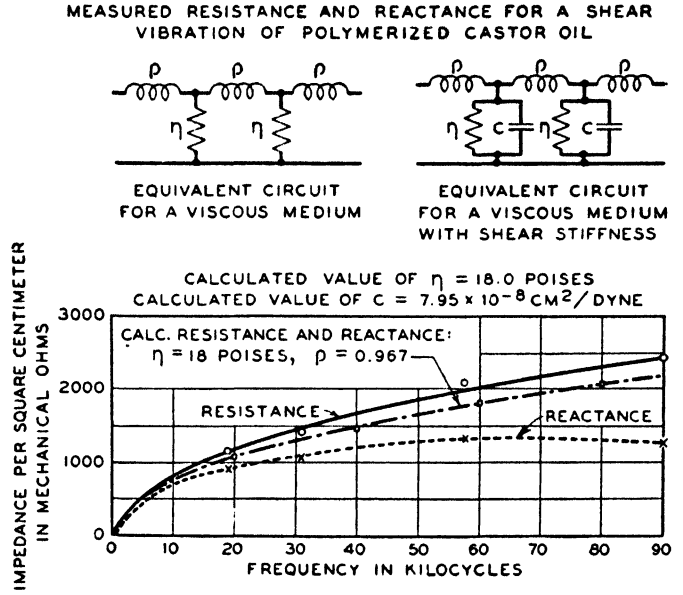

FIG. 14.10. Resistance and reactance of polymerized castor oil as a function of frequency.

is valid for a cross-section of 1 square centimeter. This circuit is repeated indefinitely for an infinite medium, or it may be terminated after a finite number of repetitions if it represents a finite path length. The characteristic impedance (impedance of an infinite line) and the propagation constant are given by the equations

$$Z_0 = \sqrt{Z_1 Z_2} = \sqrt{j\omega\rho\, dx \frac{\eta}{dx}} = \sqrt{j\omega\rho\eta} = \sqrt{\frac{\omega\rho\eta}{2}}\,(1+j)$$
$$\Gamma = \sqrt{\frac{Z_1}{Z_2}} = \sqrt{\frac{j\omega\rho\, dx}{\eta/dx}} = \sqrt{\frac{j\omega\rho}{\eta}}\,dx = \sqrt{\frac{\pi f\rho}{\eta}}\,(1+j)\,dx \qquad (14.24)$$

where Z_1 is the series impedance and Z_2 the shunt impedance of the net-

work. These equations agree with the same equations calculated from hydrodynamics, as shown by equation (14.18).

The effect of a shear elasticity can be represented by shunting the viscous resistance η/dx by a compliance (inverse of a stiffness) equal to $C_s\,dx$, where C_s is the modulus of compliance of the liquid. This network is the one shown by the right side of Fig. 14.10. Hence, at low frequencies, where the value of the resistance is much less than the reactance of the shunt compliance, the liquid behaves as a viscous liquid. On the other hand when the frequency is high enough so that the reactance of the compliance C_s equals the viscosity, a different reaction occurs. For very high frequencies, it should be possible to transmit a shear wave in such a medium. The propagation constant Γ and the characteristic impedance Z_0 can be calculated by using the series and shunt impedances

$$Z_1 = j\omega\rho\,dx; \qquad Z_2 = \frac{[(-j/\omega C_s)\eta]}{(\eta - j/\omega C_s)}\frac{1}{dx} \tag{14.25}$$

From these we find $Z_0 = R_M + jX_M$, where

$$\begin{aligned} R_M &= \sqrt{\frac{\omega^2\eta^2\rho C_s + \sqrt{\omega^4\eta^4\rho^2C_s^2 + \omega^2\eta^2\rho^2}}{2(1 + \omega^2\eta^2C_s^2)}} \\ X_M &= \sqrt{\frac{-\omega^2\eta^2\rho C_s + \sqrt{\omega^4\eta^4\rho^2C_s^2 + \omega^2\eta^2\rho^2}}{2(1 + \omega^2\eta^2C_s^2)}} \end{aligned} \tag{14.26}$$

and $\Gamma = A + jB$ where

$$\begin{aligned} A &= \sqrt{\frac{-\omega^2\rho C_s + \sqrt{\omega^4\rho^2C_s^2 + \omega^2\rho^2/\eta^2}}{2}} \\ B &= \sqrt{\frac{\omega^2\rho C_s + \sqrt{\omega^4\rho^2C_s^2 + \omega^2\rho^2/\eta^2}}{2}} \end{aligned} \tag{14.27}$$

where R_M is the resistance per square centimeter, X_M the reactance per square centimeter, A the attenuation of the wave in nepers per centimeter, and B the phase shift in radians per centimeter. Figure 14.11 shows a plot of the resistance and reactance terms plotted as a function of the ratio of the frequency to the relaxation frequency f_c. The resistance at low frequencies behaves like that of a viscous fluid, but at high frequencies it becomes asymptotic to the value $\sqrt{\rho/C_s}$. The reactance equals the resistance for low frequencies. For high frequencies it approaches zero. Figure 14.12 shows a plot of the attenuation and phase shift as a function

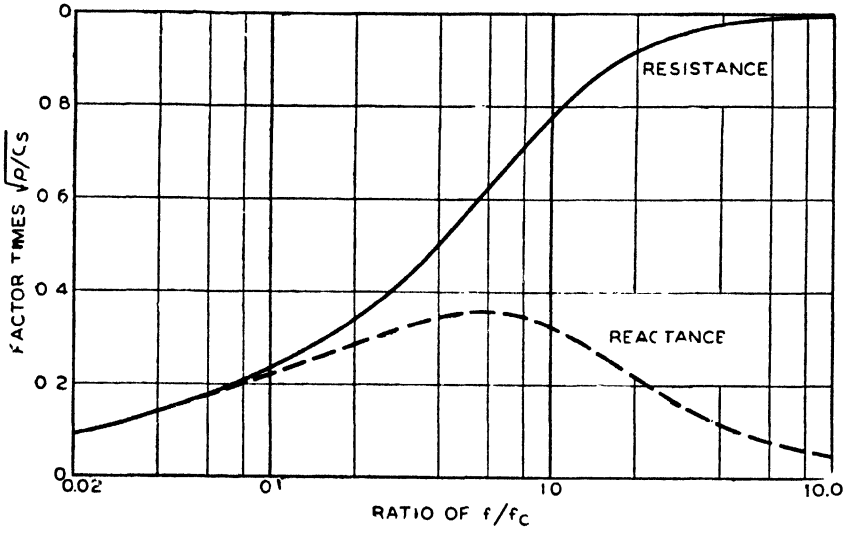

FIG. 14.11. Theoretical resistance and reactance of a liquid with shear elasticity.

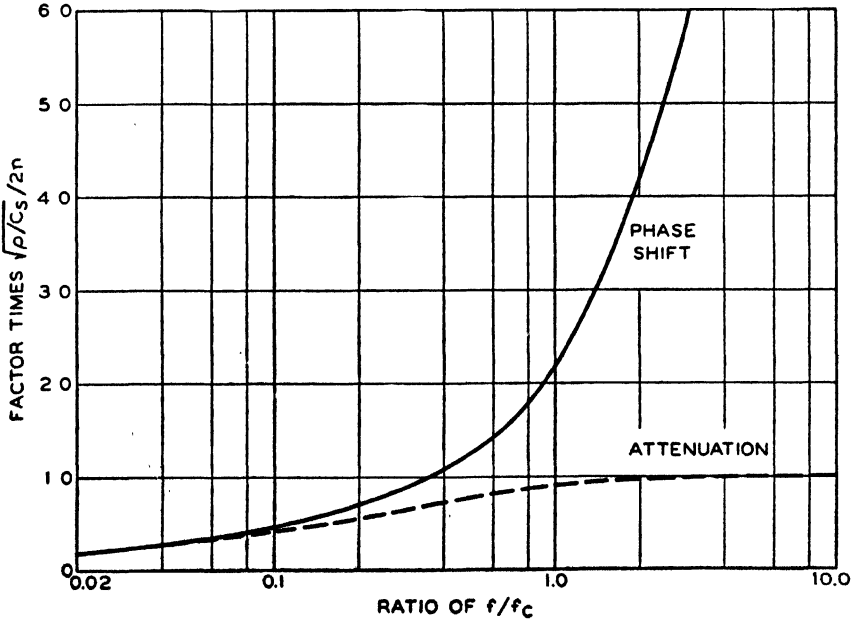

FIG. 14.12. Attenuation and phase shift of a liquid with shear elasticity.

of the frequency. The attenuation for large frequencies becomes constant and equal to

$$A_\infty = \frac{\sqrt{\rho/C_s}}{2\eta} \tag{14.28}$$

The phase shift for large frequencies becomes proportional to $\omega\sqrt{\rho C_s}$.

Solving equation (14.27) for the viscosity and the compliance, we find

$$\eta = \frac{(R_M^2 + X_M^2)^2}{2R_M X_M \omega\rho}; \qquad C_s = \frac{(R_M^2 - X_M^2)\rho}{(R_M^2 + X_M^2)^2} \tag{14.29}$$

Taking the value of R_M and X_M at 30,840 cycles, the values of η and C_s for polymerized castor oil become

$$\eta = 18 \text{ poises}; \qquad C_s = 7.95 \times 10^{-8} \text{ cm}^2/\text{dyne} \tag{14.30}$$

This value of shear elasticity is of the order to be expected from a configurational elasticity as discussed in section 14.31. Assuming these values, the calculated values of resistance and reactance are given by the full and dotted lines of Fig. 14.10. These agree well with the experimental values.

Since a viscous wave penetrates only a small fraction of a centimeter before it is attenuated by many nepers, a thin film will produce saturation effects. Hence this technique can be applied to measuring the viscosity of very small samples. The device might also be made into a continuous reading viscosimeter, since the crystal resistance and resonant frequency can be continuously measured and recorded.

The question arises as to whether this type of device can be used to study viscosity and shear elasticity of liquids at very high rates of shear. In the discussion of the previous paper,[9] it was shown that the shearing strain generated in a liquid adjacent to the torsional crystal was equal to the product of the maximum tangential displacement d_0 times the attenuation factor A, or

$$S = d_0 A = d_0 \sqrt{\frac{\pi f \rho}{\eta}} \tag{14.31}$$

In terms of the crystal strain S_5, the maximum displacement (which occurs on the two ends of the crystal) is

$$d_0 = \frac{l}{2} S_5 \tag{14.32}$$

where l is the total length of the crystal and S_5 the maximum shearing strain. For crystalline material the maximum strain is around 10^{-4}, although heavily etched crystals from which surface cracks are removed may be strained as high as 10^{-3}. This is multiplied by a factor A which may amount to 500 nepers per centimeter for light liquids so that very high strains are possible in the liquid adjacent to the surface. However, it would require a complicated differential equation solution to evaluate the effect of the strain, since it is going to vary along the length of the crystal and rapidly for positions in the liquid some distance from the crystal. So far no attempt has been made to evaluate these features, and no experimental results have been obtained.

The frequency limit for torsionally vibrating crystals is probably around 500 kilocycles on account of the small sizes of the cylinders that are required. The question arises as to whether thickness-shear vibrating crystals of the AT and BT type discussed in Chapter VI, can be used to produce viscous and shear-elastic waves in liquids. When the crystal is entirely surrounded by liquids, it was found that the shear coupling to flexural modes produced so high a loading due to longitudinal waves set up in the liquid that the shear loading could not be determined with certainty. However, by using the thin-film technique, it has been found possible to measure at least roughly the shear viscosity and elasticity of liquids that will wet the surface of the crystal. The film is so thin that it is only a small fraction of a wavelength for longitudinal waves and hence acts as a mass loading without appreciable resistance. For a viscous wave, however, the wavelength is so short that nearly complete saturation of the damping is obtained in less than 1/10,000 of a centimeter.

A few measurements have been made with a well-dimensioned BT quartz crystal vibrating at 3,527 kilocycles. The constant K_1 and K_2 relating the resistance loading per square centimeter to the change ΔR_E in electrical resistance, and the reactance loading to the change in frequency, can be derived from equations (14.19) by letting $R = R_0 + t$, where t is the crystal thickness and letting R_0 approach infinity. This would result in a shearing crystal of infinite radius (a flat crystal) and gives the formula

$$K_1 = \frac{r\left(1 + \frac{2t}{l}\right)}{2\pi^2 f_A^2 C_0 \rho_c t}; \qquad K_2 = \frac{-\left(1 + \frac{2t}{l}\right)}{2\pi\rho_c t} \tag{14.33}$$

However, it is known from the study of crystal surface motions that contoured crystals of these types do not have a uniform motion over the whole crystal surface and hence one would expect these formulae to be

only approximate. The BT crystal used had the constants

$$l = w = 12\,\text{mm}; \quad t = 0.7\,\text{mm}; \quad f_r = 3{,}527{,}000\,\text{cycles};$$

$$\Delta f = 3{,}450; \quad r = 510; \quad c_0 = 5\mu\mu f;$$

$$\text{resistance at resonance} = 180\,\text{ohms}; \quad \rho_c = 2.65.$$

Inserting these values in equations (14.33), we find $K_1 = 2.2$; $K_2 = 0.85$. Measurements with a number of light liquids into which the crystal had been dipped and the excess liquid had been shaken off, agreed within 20 per cent of their low-frequency values if K_1 was taken as 0.83. The decrease in frequency was several times larger than could be accounted for by the viscous reactance, indicating that the mass loading of the flexure modes was also lowering the frequency.

Another and probably better method for studying shear elasticities in liquids at high frequencies is the liquid terminated fused quartz rod transmitting shear pulses, discussed in section 15.31. By observing the amount of energy absorbed for each pulse, it has been shown that the shear elasticity of polyisobutylene (polymer D of section 14.3) was equal to 3.0×10^9 dynes per square centimeter at 10 megacycles and 5.5×10^9 dynes per square centimeter for 60 megacycles. The significance of this measurement is discussed in section 14.31.

14.21 *Use of Torsional Crystal in Measuring the Properties of Long Chain Polymers Dissolved in a Solvent*

Torsionally vibrating crystals have recently[21] been applied to measuring the properties of dilute solutions of long chain polymer molecules dissolved in a solvent. The mechanical properties of pure liquids are affected by interchain bonds and reactions as well as by the intra-chain interactions pertaining to the chain itself. In studying the possible motions occurring in the chains, it is desirable to be able to isolate the two effects. A simple method for accomplishing this is to use such a dilute solution of the polymer liquid that the molecules in their most probable curled-up form do not touch each other on the average. Then the mechanical properties of such liquids will be determined by the reactions of single chains and will not be determined by the interaction between chains. Calculations indicate that the concentrations to obtain non-interaction between chains should be less than 2 to 3 per cent and practically all the concentrations measured were from 0 to 1 per cent (*i.e.*, 0 to 1 gram per 100 cubic centimeters of solution).

[21] Baker, W. O., H. J. Heiss, and W. P. Mason, " Mechanical Properties of Long Chain Polymers Dissolved in a Solvent," presented before Am. Phys. Soc., Jan. 27, 1949.

When the shear mechanical impedance is measured for such a solution, it is found that the liquid does not act as a purely viscous liquid, but instead has a resistance that is larger than the reactance. Figure 14.13 shows measured curves for 20 kilocycles of the resistance and reactance for solutions of polyisobutylene of viscosity average molecular weight of 3,930,000 in cyclohexane. Four values of concentration were used and two temperatures were measured. For pure cyclohexane the resistance and reactance components are equal but as the percentage of polyisobutylene is increased, the resistance increases more rapidly than the reactance.

To obtain the effect of the chain structure alone, one has to be able to separate out the effect of the solvent from the effect of the chain structure on the resulting mechanical impedance of the solution. A suggestion on how to do this is obtained from considering the difference between the very low frequency behavior and the very high frequency behavior of the solution. At very low frequencies, the presence of 1 gram of the chain per 100 cubic centimeters of solution (molecular weight of the chain is 3.93×10^6) increases the static viscosity by a factor of over 30. On the other hand, at very high frequencies (at 14 megacycles made by the technique described in section 15.31), the indicated viscosity is only about 10 per cent higher than that for the pure solvent alone.

It appears that the difference in the behavior for the extreme frequency ranges is that at low frequency, the motion of the solvent molecules can cause a motion of the chain segments in the time of a single cycle and their motion abstracts energy from the motion of the solvent molecules and causes a smaller average displacement and hence a higher viscosity, whereas at very high frequencies, the motions of the solvent molecules cannot cause a chain segment motion from a favored position during the time of a single cycle and hence the solvent motion occurs as though the chain were not there and the resulting viscosity is nearly that of the solvent alone.

As the frequency increases from static or zero frequency to moderate frequencies the first motion that does not have time to be completed in the course of a single cycle is the configurational relaxation between all members of the chain. For a chain length of 3.93×10^6 molecular weight and a one gram per 100 cc concentration, this relaxation frequency is around 600 cycles for 25°C. This relaxation frequency is quite a function of temperature and chain length. Above this frequency the very large low frequency viscosity disappears. A second relaxation frequency was found at 80,000 cycles which has tentatively been identified as the relaxation frequency due to chain entanglements. This relaxation frequency varies inversely as the square root of the molecular weight, and its temperature variation is determined by the activation energy of the solvent. Finally by using the

high frequency technique of section 15.31 a third relaxation was found at about 3.3 megacycles. To analyze the conditions for this relaxation the motion of a segment from one position to another requires crossing a high potential barrier and the number of transitions per second is approximately the same as that given in equation (8.2) namely

$$\alpha_{12} \doteq \frac{kT}{h} e^{-W/kT}$$

With a relaxation frequency of 3.3 megacycles this corresponds to an activation energy of 8.7 kilocalories per mole. This activation energy is nearly that observed for a rotation from one preferred orientation to another, and hence the relaxation frequency probably corresponds to the motion of a single Eyring or Kuhn segment. The stiffness of about 80,000 dynes/cm^2 for a one per cent solution corresponds to the stiffness of the chain with all its joints frozen.

With the type of behavior discussed above, the viscous and stiffness properties of the solution can be represented by a stress-strain equation of the type

$$T = \eta_1 \frac{\partial S}{\partial t} + \sum_{n=1}^{N} \frac{1}{\dfrac{1}{\eta_{M_n} \dfrac{\partial S}{\partial t}} + \dfrac{1}{\mu_n S}} \tag{14.34}$$

where T is the shearing stress and S the shearing strain. In this equation η_1 represents nearly the viscosity of the solution and η_{M_n} represents a " molecular " viscosity of some particular motion of the chain which disappears when the reactance of μ_n of this motion is low enough so that the motion can follow the applied shearing stress at the frequency of measurement. In general, there may be more than one such mechanism and hence n varies from 1 to N. All the measurements made, however, were fitted by three relaxation mechanisms described above.

In analyzing the results of a single frequency measurement, it is simpler to consider only one molecular viscosity and one shear elasticity. If more than one mechanism exists, this viscosity and elasticity will be functions of the frequency. However, by suitable formulae, the variable viscosity and elasticity can be fitted to a curve involving two or more elements and hence the number of mechanisms and their relaxation frequencies can be determined.

If equation (14.34) with one relaxation mechanism, having the formula

$$T = \eta_1 \frac{\partial S}{\partial t} + \frac{1}{\dfrac{1}{\eta_M \dfrac{\partial S}{\partial t}} + \dfrac{1}{\mu S}}$$

is substituted in the equation of motion (14.15), a propagation constant and characteristic impedance are obtained equal to

$$\Gamma = A + jB = \sqrt{\frac{-\rho\mu\eta_M^2 + j\left[\omega\rho\eta_M^2\eta_1 + \frac{\rho\mu^2}{\omega}(\eta_1 + \eta_M)\right]}{\eta_1^2\eta_M^2 + \frac{\mu^2}{\omega^2}(\eta_1 + \eta_M)^2}}$$

$$Z_0 = R + jX = \sqrt{\frac{\rho\mu\eta_M^2 + j\left[\omega\rho\eta_1\eta_M^2 + \frac{\rho\mu^2}{\omega}(\eta_1 + \eta_M)\right]}{\eta_M^2 + \frac{\mu^2}{\omega^2}}} \tag{14.35}$$

As before, the torsional vibrating crystal can measure the resistance R and the reactance X. A third measurement of the viscosity at zero frequency gives the sum of $\eta_1 + \eta_M$. Solving these equations simultaneously for the values of η_1, η_M and μ we find

$$\eta_1 = \frac{2RX}{\omega\rho} - \frac{(R^2 - X^2)^2/\omega\rho}{\omega\rho(\eta_1 + \eta_M) - 2RX}; \qquad \eta_M = \eta_1 + \eta_M - \eta_1$$

$$\mu = \frac{(R^2 - X^2)\omega\eta_M}{\omega\rho(\eta_1 + \eta_M) - 2RX} \tag{14.36}$$

Since R, X and $\eta_1 + \eta_M$ are measured by the crystal and the zero frequency measurement of the viscosity, all the quantities can be determined.

Figure 14.13 shows some experimental data for a solution of polyisobutylene in cyclohexane. Polyisobutylene is a polymer molecule that occurs in a long chain. It has the formula shown by Fig. 14.14A and the zigzag form shown by Fig. 14.14B. This chain in an ordered, stretched state appears to rotate about the direction of its length once in every nine pair of CH_3 groups. Accordingly, non-planar zigzag segments can be expected in the liquid state. The data of Fig. 14.13 are for a molecular weight of 3,930,000.

Substituting the data of Fig. 14.13 in the formulae of equation (14.36), values are obtained for η_1, η_M and μ as a function of concentration and these are shown plotted by Fig. 14.15. The enhanced solvent viscosity η_1 increases slightly over that for the pure cyclohexane by a factor of from 1.0 to 2.2, depending on the temperature and the concentration. The shear elasticity μ is directly proportional to the concentration up to a concentration of 1 gram per 100 cubic centimeters of the solution. The molecular viscosity η_M plotted on Fig. 14.15 as a function of the concentration, shows markedly the effect of concentration since the viscosity increases much more than linearly with concentration. This shows that the viscosity

depends on much longer range forces than does the elasticity of the molecules.

Measurements have been made at 20 kilocycles of the effect of temperature and molecular weight on the variation of the three parameters η_1,

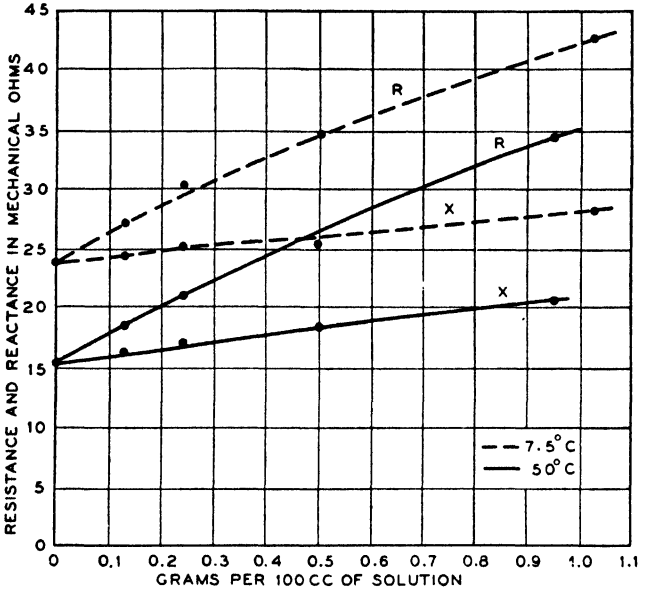

FIG. 14.13. Measured reactance and resistance for solution of polyisobutylene in cyclohexane.

η_M and μ for a one per cent concentration. The results are shown on Fig. 14.16. Within the experimental error, the shear elasticity does not change

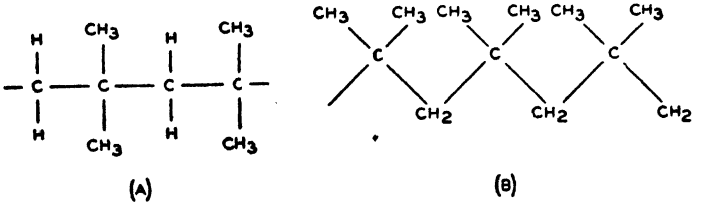

FIG. 14.14. Chemical structure of polyisobutylene.

much with molecular weight. The shear elasticity at 20 kilocycles appears to show a decrease with increasing temperature. However, when measurements were made at 20, 40 and 80 kilocycles, it was found that the elasticity was a function of frequency. This indicates the presence of two or more

relaxation phenomena and complicates the determination of the temperature relationships.

All the measured data were found to be fitted by a series viscosity η_1 in series with three relaxation mechanisms having the values η_2 in parallel with μ_2, η_3 in parallel with μ_3 and η_4 in parallel with μ_4. The configurational elasticity μ_2 varied in proportion to the absolute temperature and changed from 450 dynes/cm^2 for a one per cent solution to 900 dynes/cm^2

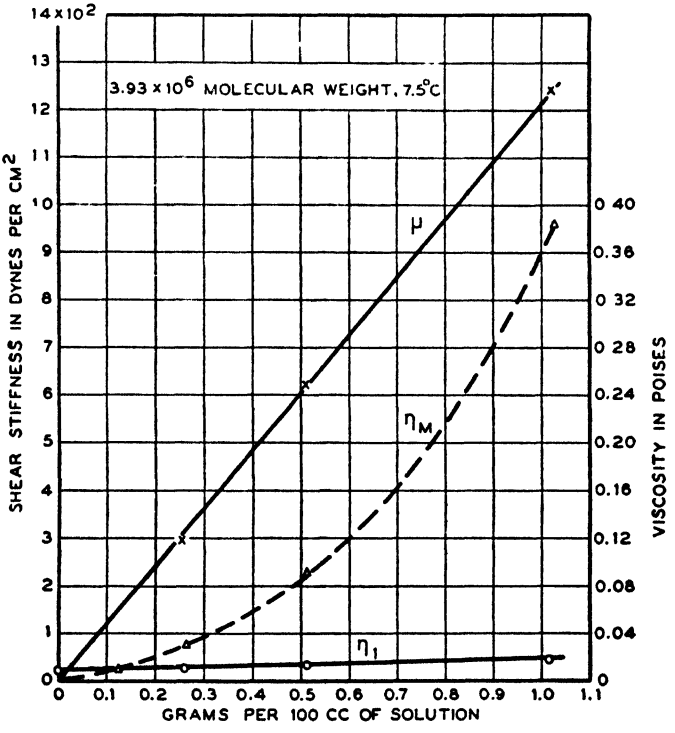

FIG. 14.15. η_1, η_M and μ plotted as a function of concentration at 7.5°C.

when the molecular weight changed from one million to four million. The viscosity η_2 comprises the main part of the low frequency viscosity and changed by a factor of 7 to 1 for a chain length change of 4 to 1. This confirms the interpretation that this relaxation is concerned with the configurational motion of the molecule as a whole. η_3 on the other hand is in the order of the solvent viscosity and increases about 50 per cent for a chain length decrease of 4 to 1. μ_3 is in the order of 2500 dynes per square centimeter and decreases somewhat with temperature. The value increases slightly with chain length. These facts indicate that this relaxation varies about inversely as the square root of the molecular weight, and is due to

inter-chain reaction. Finally the highest relaxation frequency has a stiffness of over 80,000 dynes/cm^2 for a one per cent solution, is independent of molecular weight, and has an associated viscosity of about half that of the solvent viscosity giving a relaxation frequency of 3.3×10^6 cycles at room temperature. As discussed above this appears to be associated with the motion of a single Eyring segment.

Measurements also show that there is a difference due to chains. Measurements of polystyrene in benzene showed values of μ_2 and μ_3 equal respec-

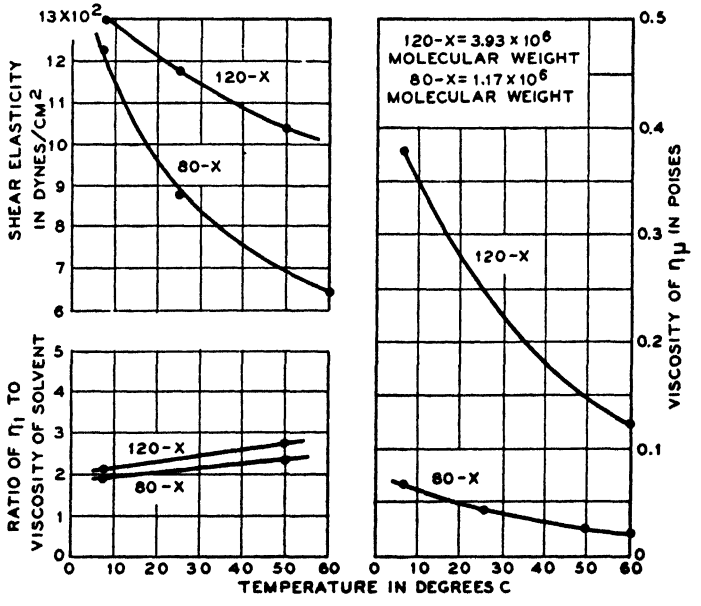

FIG. 14.16. η_1, η_M and μ for a 1 per cent solution plotted as a function of temperature and molecular weight.

tively to 100 dynes per square centimeter and 1,000 dynes per square centimeter. All the viscosities for the two substances varied with temperature in the same manner as the solvents, which confirms the interpretation of these viscosities as being due to the relative motion of the polymers and the solvent for the various relaxation mechanisms.

Some measurements were also made of the properties over a wide range of concentrations for a single molecular weight of 3.93 million. The shear elasticity, as shown by Fig. 14.17, is linear with concentration up to about 2 per cent. The elasticity as a function of concentration follows quite well the law

$$\mu = A_1 C + A_3 C^3$$

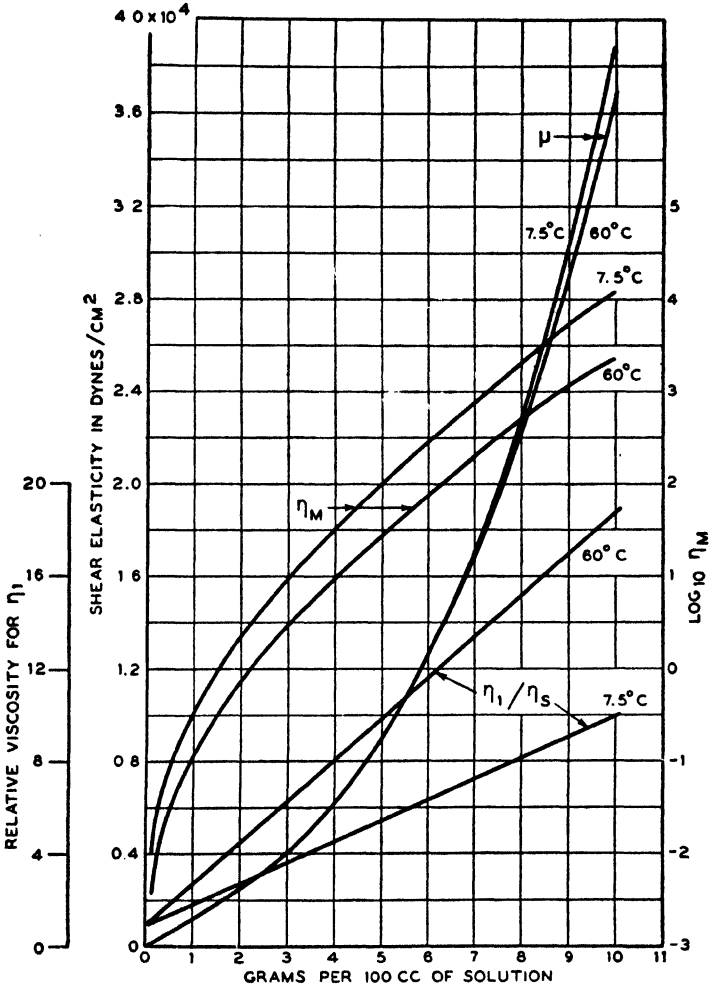

FIG. 14.17 Values of η_1, η_M and μ as a function of concentration.

where both A_1 and A_3 vary very little with temperature. The measurements for 20 kilocycles have the values

$$A_1 = 1.2 \times 10^5; \quad A_3 = 2.6 \times 10^7 \tag{14.37}$$

Farther measurements at 14 megacycles for this same molecular weight polymer at 25°C show the values

$$A_1 = 8.0 \times 10^6; \quad A_3 = 6.5 \times 10^8 \tag{14.38}$$

The term in A_1 represents the shear stiffness of isolated molecules whereas the term proportional to the cube of the concentration represents the effect of chain entanglements. Ferry[22] has observed the cube term for polyisobutylene (molecular weight of about 10^6) at much lower frequencies for 10 per cent solutions and higher concentrations, and gives the following explanation. The number of points for which the chains become entangled increases as the square of the concentration whereas the length between entanglement points varies inversely as the concentration. Since the stiffness of a portion of the chain between entanglement points varies inversely as the length, the entanglement stiffness should increase proportional to the cube of the concentration. The independence of stiffness on the temperature shows that the entanglement involves no activation energy. The measurements of equations (14.37) and (14.38) show that the chain entanglement stiffness increases with frequency due to the same causes as for the linear stiffness.

14.3 *Measurement of Shear Elasticity in Pure Liquids*

By employing the torsionally vibrating crystal, a study has been made of the shear elasticity and viscosity of pure liquid long chain polymers, which throw some light on the low shear stiffness of the polymer type. Ordinarily if a liquid behaved as a crystal, one would expect to find shear elasticities in the order of 10^8 to 10^{10} dynes per square centimeter, and indeed it is found that some liquids such as silicone putty and arochlor (pentachlordiphenyl) do have elasticities in the region. However, polymerized castor oil and polyisobutylene (vistanex) described in this section, have much lower shear elasticities in the order of 5×10^6 to 5×10^7 dynes per square centimeter in the frequency range up to 100 kilocycles. This type of elasticity is due to a distortion of the configuration of the molecule as discussed in Section 14.31.

The specimens of polyisobutylene used were designated *A*, *B*, *C* and *D* and had respectively average molecular weights of 903, 3,520, 4,550 and 5,590. Measurements of the viscosity of these four samples were made by the falling-ball method[23] over a range of temperatures and are shown plotted as the logarithm of the viscosity versus the inverse temperature by Fig. 14.18. All of these liquids have the same slope, which indicates, according to Eyring's[24] theory, that the element which moves from one

[22] Ferry, J. D., J. N. Ashworth, W. M. Sawyer, paper C3, *Amer. Phys. Soc.*, Jan. 27, 1949.

[23] These measurements and those of the density were made by J. H. Heiss, Jr., and this study and its interpretation has been carried out in cooperation with Dr. W. O. Baker.

[24] Kauzmann, W., and H. Eyring, "The Viscous Flow of Large Molecules," *J. Amer. Chem. Soc.*, Vol. 62, pp. 3113–3125, Nov., 1940.

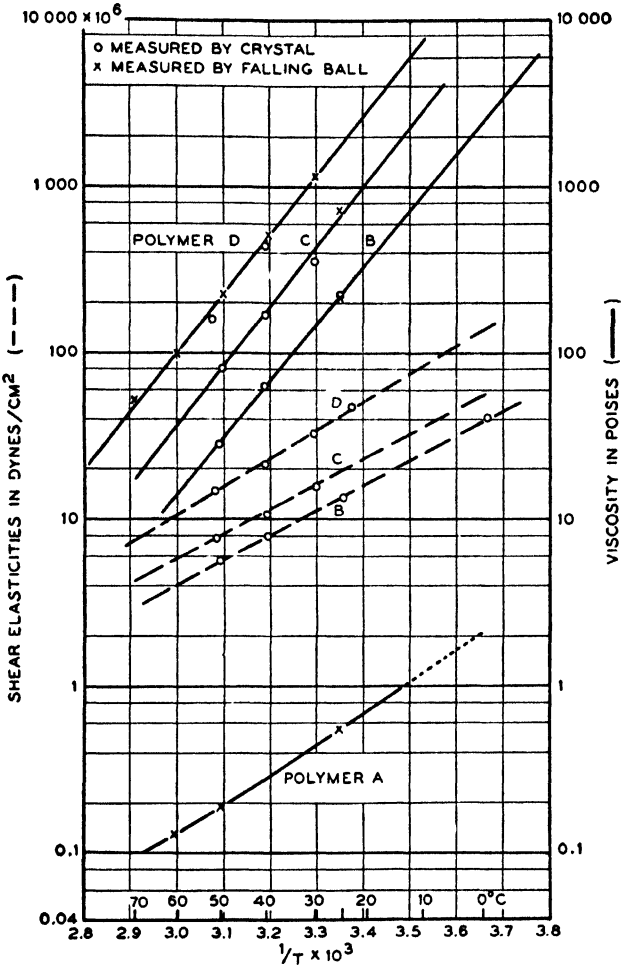

FIG. 14.18. Measurements of shear viscosity and shear elasticity of polyisobutylene as a function of temperature.

potential well to an adjacent one is a segment of the chain 20 molecules or so whose length is essentially independent of the total chain length. The large increase in viscosity for any one temperature as a function of chain length has been explained as the increased probability that the chain as a whole will jump to a new position as the chain length gets shorter. Measurements have also been made of the density of these liquids and the data are shown plotted on Fig. 14.19 as a function of temperature.

The experimental arrangement is that shown by Fig. 14.8. A torsional crystal of ADP was gold plated by the evaporation process and suspended

from its nodal plane by three wires glued to the surface by Bakelite cement. The measured constants of the crystal and the constants K_1 and K_2 of equation (14.19) are

length = 5.0 cm; $OD = 2R = 0.472$ cm; $ID = 2R_0 = 0.30$ cm;

$\rho = 1.804$; $f_R = 19{,}615$ cycles; $(f_A - f_R) = 220$ cycles;

$C_0 = 100\mu\mu f$; $R = 500$ ohms; $K_1 = 425$; $K_2 = 1.15$

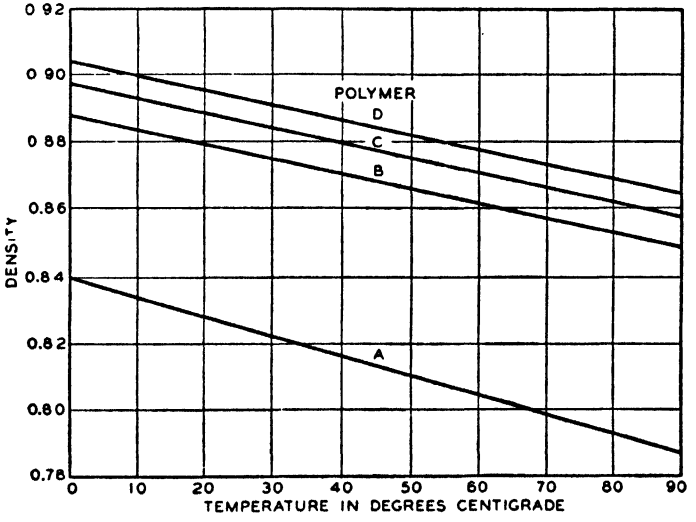

FIG. 14.19. Density of polyisobutylene as a function of temperature.

The value of K_1 changes slightly with temperature and at 50°C was evaluated as 455.

It was found that the resistance values at resonance gave the most reliable result since it was difficult to locate accurately the resonant frequency of the crystal in a viscous liquid. The measurements were made in a balanced electrical bridge and data similar to that of Fig. 14.9 were used to evaluate the resistance loading. Measurements were made at the first, third and fifth harmonic of the crystal. For the harmonics, the same values of K_1 hold as for the fundamental. Typical data for the resistance loading per square centimeter in terms of the frequency and temperature are shown for the polymer *B* liquid by Fig. 14.20. To interpret these data in terms of shear viscosity and shear elasticity, use is made of the calculation of the resistance and reactance loading for a liquid having shear elasticity and viscosity given by Fig. 14.11. Com-

paring this with the data of Fig. 14.20, we see, for example, that at 0°C, the loading is nearly independent of frequency, which means that the relaxation frequency is considerably below the lowest measuring frequency of 17.5 kilocycles. The curves of 24°, 40°, and 50°, however, show enough bending with frequency to allow one to fit them to the theoretical curve.

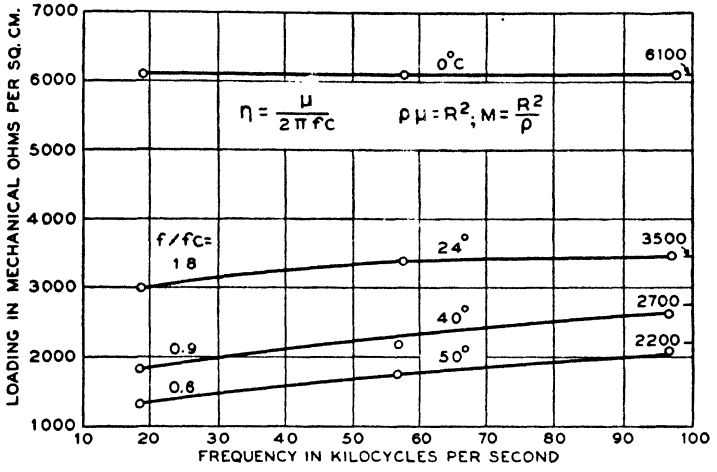

FIG. 14.20. Resistance loading of crystal in polymer *B* as a function of frequency and temperature.

From these data, one can find that the ratio of the lowest frequency (about 17.5 kc) to the relaxation frequency is given by the second column of Table XXIII, while the asymptotic value of the loading resistance at very high frequencies is given by the third column. Since the shear elasticity is related to the resistance loading at high frequencies by the formula

$$\sqrt{\rho\mu} = R \text{ or } \mu = R^2/\rho \tag{14.39}$$

the shear elasticity is shown by the fourth column. The fifth column shows the calculated relaxation frequency, while the sixth column shows the shear viscosity η which can be calculated from the formula

$$\eta = \frac{\mu}{2\pi f_c} \tag{14.40}$$

The values of viscosity measured by the crystal are shown plotted by the circles of Fig. 14.18 for all liquids, and, as is evident, they agree with the values measured by the falling-ball method within 10 per cent, which is probably the accuracy of measurement by the present method of curve fitting.

TABLE XXIII

POLYISOBUTYLENE "B"

Temperature	f/f_c	R at High Frequencies Mechanical Ohms	μ *dynes* cm^2	Relaxation Frequency f_c, *Cycles*	Value of Shear Viscosity in *Poises*, η
0°C	—	6,100	42×10^6	—	—
24°C	1.8	3,500	14×10^6	9,700	230.0
40°C	.9	2,650	8×10^6	19,400	68.8
50°C	.6	2,200	5.6×10^6	29,200	30.5

The values of shear elasticity measured for the three polymer liquids *B*, *C* and *D* are shown plotted by the dashed lines of Fig. 14.18. They lie nearly on straight lines of uniform slope when plotted as log μ versus $1/T$, at least within the temperature range shown. If we plot all of these shear elasticities as a function of density alone, which can be done by using the data of Figs. 14.18 and 14.19, the points of Fig. 14.21 result. It appears likely, that within the experimental error, all of these points can be represented by a single curve. This agrees with the measurements for polyisobutylene in a solvent which shows that the elasticity depends only on the amount of polymer per cubic centimeter.

Two other measurements made on other liquids appear to be significant. Measurements were made for Arochlor, which is a pentachlor diphenyl having the structure shown by Fig. 14.22. At 24°C it has a density of 1.535 and a viscosity of 150 poises. Over a frequency range the resistance and reactance values are shown by Fig. 14.22. The values cannot be fitted by a single relaxation frequency and indicate the presence of at least two relaxation frequencies and a much lower compliance — higher stiffness — of about 6×10^{-9} square centimeter per dyne. This stiffness approaches that of a crystal. In section 14.4 by a shear-wave method, the stiffness of silicone putty was measured at 50,000 cycles at a room temperature of 25°C. This had a compliance of 1.35×10^{-9} square centimeter per dyne, which is the stiffness of nearly 10^9 dynes per square centimeter and approaches that of a crystalline material.

14.31 *Discussion of the Origin of Shear Elasticity in Polymer Liquids*

The problem of structure, diffusion and stress biased diffusion (or viscosity) is fundamentally the same for long-chain polymers as for simple liquids. The long-chain structure of polymer molecules, however, introduces certain significant new effects. Long-chain molecules are flexible and can take up many different shapes. Certain coiled-up shapes are more probable than others and if a molecule is distorted from this shape, the

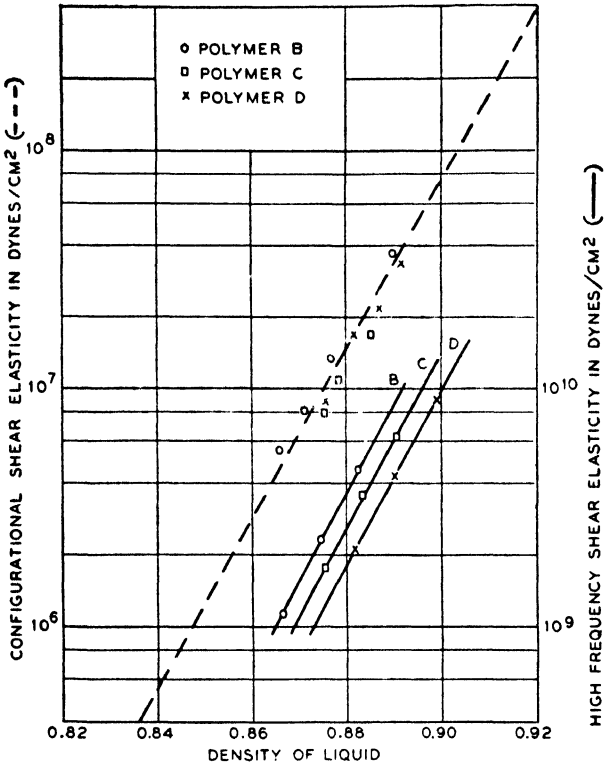

FIG. 14.21. Shear configurational and crystalline elasticities of polymer liquids plotted as a function of density.

molecule tends to return to it in a very short time when the stress is removed. This type of elasticity is called configurational elasticity and the rapidity with which it regains its most probable shape determines the relaxation time for such configurational elasticity.

When a shearing stress is put on such a molecule, segments of the molecule 20 to 30 chain atoms long are displaced from one configuration to another configuration, which coincides with an empty space or hole in the liquid. A single segmental jump will have two effects on the polymer molecule. First, the shape of the molecule will be slightly altered by the motion of the segment, and second, the center of gravity of the molecule will be slightly shifted. The result of a large number of successive segmental jumps will likewise be twofold. First, the molecule will wriggle about from one shape to another, and second, the center of gravity will undergo a slow wandering. When these segment jumps are caused by the application of a shearing stress, the wandering of the center of

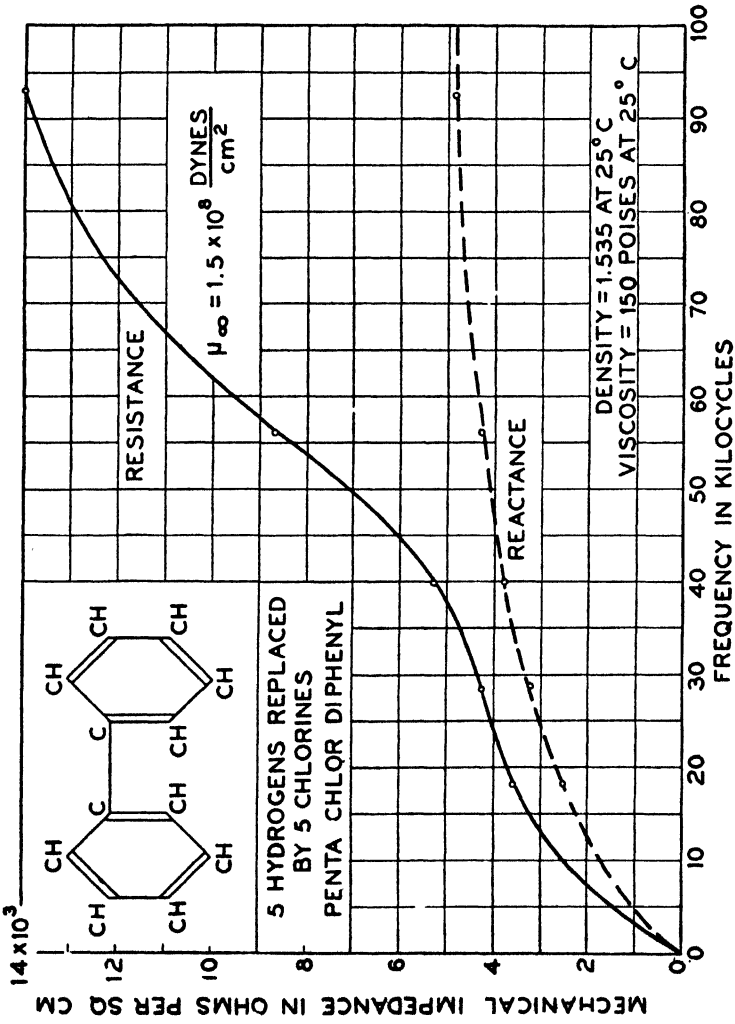

FIG. 14.22. Resistance and reactance values for Arochlor (pentachlor diphenyl).

gravity produces the viscous flow, while the change of shape from the most probable shape produces the shear configurational elasticity.

The flow of segments has to occur over certain energy barriers W and hence the temperature variations of the viscosity satisfies an equation of the type

$$\eta_1 = Ae^{BZ^{\frac{1}{2}}}e^{W/RT} \tag{14.41}$$

where W is the activation energy, R the gas constant (Nk) — where N is Avogadro's number and k Boltzmann's constant—and T the absolute temperature. The probability of the center of gravity of the molecule, as a whole, moving in a given direction depends on the probability of a number of successive segmental jumps occurring in the same direction and hence decreases with the chain molecular weight Z. Equation (14.41) is an equation proposed by Flory and justified on a theoretical basis by Eyring.[24] Equation (14.41) is strictly applicable only for linear polyesters. A more general equation which has a similar segmental flow justification[25] is

$$\log \eta = \log AZ + W/RT$$

and this equation holds for the polyisobutylene liquids.

When the stress is removed from the molecule, the molecule returns to its most probable position by a series of segmental jumps. The experimental data obtained from high-frequency shear-wave measurements show that the activation energy for this local distortion segmental jump is only about three quarters of that required for a flow viscosity segmental jump. Since the latter involves a change of the position of the center of gravity, it requires a higher activation energy.

Considerable study has been given to the configurational type of elasticity and it has been shown that under equilibrium conditions, the " kinetic theory " of elasticity describes the elastic retractive force, as[26] for example

$$F = -T\frac{\partial \sigma}{\partial L} = \frac{kT\nu}{L_0}\left[\alpha - \frac{1}{\alpha^2}\right]$$

where T = absolute temperature, L = length of sample, σ = entropy, L_0 = length of unstretched sample, ν = number of chains in the volume V, and $\alpha = L/L_0$. Here the theory accounts nicely for the widely observed shear modulus of 10^6 dynes per square centimeter and for its increase with temperature. It is, however, an equilibrium theory and requires time for equilibrium to be established before it is valid.

[25] Baker, Fuller and Heiss, *J. Amer. Chem. Soc.*, Vol. 63, p. 2142, 1941.

[26] Wall, *J. Chem. Phys.*, Vol. 10, p. 132, 485, 1942; Vol. 11, p. 1527, 1943; Flory, *Chem. Rev.*, Vol. 35, p. 51, 1944.

Most polymers show in addition to this " ideal " elasticity, several other elastic effects, portions of which have been extensively reported in earlier literature. For instance, at suitably low temperatures, ordinary supercooled organic liquids (glasses) become hard, as do also all kinds of rubbers and plastics. In this low-temperature range, however, rubbery materials usually exhibit a really high shear modulus, of the order of 10^8 to 10^{10} dynes per square centimeter. This is approximately the same whether chains are cross-linked into networks or not,[27, 28, 29] and does not depend

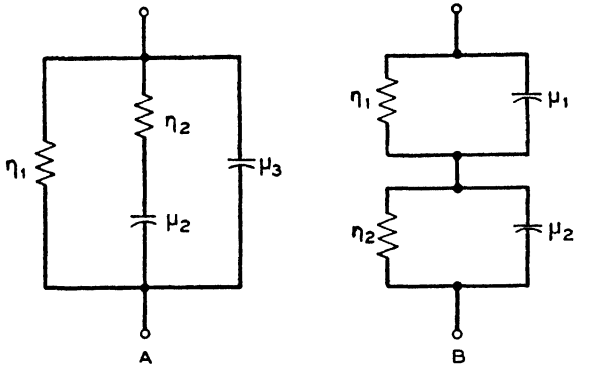

FIG. 14.23. Equivalent circuit for liquid having configurational and crystalline elasticity. A. Normal representation. B. Representation using two separated relaxation networks.

much on average lengths of chains or segments between cross links above a certain limit.[27] Accordingly the displacement process here can be imagined as the biasing of the position of small chain elements in potential wells defined by their interaction with neighboring chain elements. Thus, as expected, there is a steep decline in this modulus with increase in temperature, even for static measurements. The measurements for Arochlor and silicone putty indicate that the crystalline type of elasticity will also exist at frequencies so high that composite motions of the chains do not have time to take place. All of these various elements can be represented by the equivalent electrical circuit of Fig. 14.23A. Here η_1/dx represents the flow viscosity of a layer of thickness dx and the value over a temperature and molecular weight range is given by equation (14.41). The values η_2/dx and μ_2/dx determine the configurational shear stiffness and the rate at which it will become relaxed. Finally, μ_3/dx represents the stiffness due to moving the chain molecules closer together. This type of stiffness can be observed by lowering the temperature so that the viscosities η_1 and η_2

[27] Baker and Pape, Report to Rubber Reserve Co., May 27, 1943.
[28] Siska, *Ind. Eng. Chem.*, Vol. 36, p. 40, 1944.
[29] Siska and Conant, *J. Appl. Phys.*, Vol. 15, p. 767, 1944.

become so high that the material cannot flow. As we shall see presently this type of elasticity can also be observed by going to such high frequencies that the reactance of μ_3 is less than the flow viscosity η_1 and the relaxation viscosity η_2.

With increasing temperatures the potential wells separate farther, and for polymer chains composite motions, such as translations and hindered rotations, can take place. If sufficient time is given so that equilibrium can occur between all the various motions of the chains, true " kinetic theory " elasticity comes into play and an elasticity proportional to the absolute temperature results. If, however, the frequency is high enough so that equilibrium does not take place, the elasticity is controlled by the nearest neighbor and is of the type usually discussed by potential well theory. Under these conditions the elasticity decreases with an increase in temperature.

The nearest approach to " kinetic theory " elasticity for these high-frequency measurements, are the measurements of the polymer dissolved in a solvent discussed in section 14.21. Here the flow viscosity has an activation energy of only 3.9 kilocalories per mole, which is only slightly larger than that for the cyclohexane alone. The viscosity η_2 of the configurational elasticity has a similarly low activation energy and the value of η_2 is so low that the configurational elasticity relaxes so fast that equilibrium is established in times less than 1/600 second. The data of section 14.21 show that the shear elasticity increases nearly in proportion to the absolute temperature. Under these conditions, it is legitimate to neglect η_2 and μ_3 and in equation (14.34) η_M represents the flow viscosity of Fig. 14.23, while μ represents the configurational elasticity μ_2.

For the pure polymer liquids of section 14.3 the activation energy for the relaxing viscosity η_2 is around 12 kilocalories (as shown by the data of Fig. 14.33) and hence a considerable time is required for relaxing the configurational stiffness. Under these conditions equilibrium is not established in the time of a complete cycle and " kinetic theory " elasticity is no longer valid. No adequate treatment has been given for this case and the reason for the logarithm of the shear elasticity increasing proportionally to $1/T$ is not known.

The pulse measurements of section 15.31 show that the impedance of the liquid for shear is approximately that shown by Fig. 14.24. These curves show that at these frequencies the composite motion can no longer take place and the shear elasticity is that determined by single potential wells. From the data on the longitudinal measurements of section 14.5, this is in the order of 5.7×10^9 dynes per square centimeter which is over 100 times as high as that for the configurational elasticity shown by Fig. 14.18.

The shear impedance for the liquid is most easily calculated by using the equivalent circuit for the liquid shown by Fig. 14.23B. This is the equivalent of that shown by 14.23A if

$$\eta_1^A = \eta_1^B + \eta_2^B \qquad \eta_2^A = \frac{\eta_1^B \eta_2^B (\eta_1^B + \eta_2^B)(\mu_1^B + \mu_2^B)^2}{(\eta_1^B \mu_2^B - \eta_2^B \mu_1^B)^2}$$

$$\mu_2^A = \frac{(\eta_1^B \mu_2^B - \eta_2^B \mu_1^B)^2}{(\eta_1^B + \eta_2^B)^2(\mu_1^B + \mu_2^B)\mu_1^B \mu_2^B} \qquad \mu_3^A = \mu_1^B + \mu_2^B$$

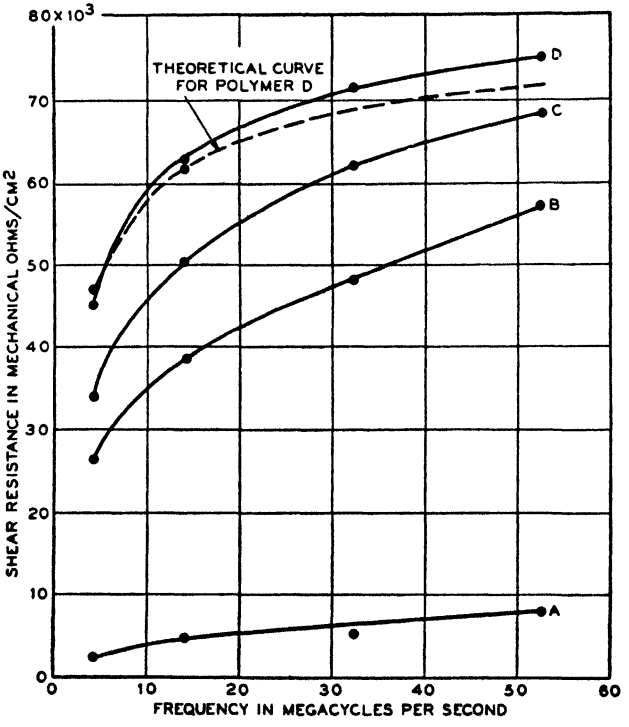

FIG. 14.24. High frequency resistance of polymer A, B, C, D polyisobutylene liquids as function of frequency for 25°C.

The model B gives two relaxation frequencies and a stress strain law

$$T_5 = \frac{1}{\frac{1}{\mu_1 S_5} + \frac{1}{\eta_1 \frac{\partial S_5}{\partial t}}} + \frac{1}{\frac{1}{\mu_2 S_5} + \frac{1}{\eta_2 \frac{\partial S_5}{\partial t}}} \tag{14.42}$$

The impedance and propagation constant can be obtained by substituting in equation (14.16) and solving for Γ and Z_0. An equivalent and shorter process from a numerical point of view is to employ the equivalent circuit of Fig. 14.25 and calculate the image impedance from the formula

$$Z_0 = \sqrt{Z_1 Z_2}$$

where $$Z_1 = j\omega\rho\, dx; \qquad Z_2 = \left[\frac{\frac{-j\mu_1\eta_1}{\omega} + \frac{-j\mu_2\eta_2}{\omega}}{\eta_1 \frac{-j\mu_1}{\omega} \quad \eta_2 - \frac{j\mu_2}{\omega}}\right]\frac{1}{dx} \tag{14.43}$$

The result of this computation can be expressed in the form

$$Z_0 = \sqrt{\frac{\left\{\rho(\mu_1+\mu_2)\left\{\left[\frac{f^4}{f_1^2 f_2^2} + f^2\left(\frac{\mu_2}{\mu_1+\mu_2}\times\frac{1}{f_2^2} + \frac{\mu_1}{\mu_1+\mu_2}\times\frac{1}{f_1^2}\right)\right] + jf\left[\frac{2\pi(\eta_1+\eta_2)}{\mu_1+\mu_2} + \frac{f^2}{f_1 f_2}\left(\frac{\mu_1}{\mu_1+\mu_2}\times\frac{1}{f_2} + \frac{\mu_2}{\mu_1+\mu_2}\times\frac{1}{f_1}\right)\right]\right\}\right\}}{(1+f^2/f_1^2)(1+f^2/f_2^2)}} \tag{14.44}$$

where f_1 and f_2 the two relaxation frequencies, are given by

$$f_1 = \frac{\mu_1}{2\pi\eta_1}; \qquad f_2 = \frac{\mu_2}{2\pi\eta_2}$$

Figure 14.25 shows a calculation of the shear reactance and resistance of the polymer D assuming

$$\begin{aligned} \mu_1 &= 4 \times 10^7 \text{ dynes/cm}^2 & \mu_2 &= 5.8 \times 10^9 \text{ dynes/cm}^2; \\ \eta_1 + \eta_2 &= 1600 \text{ poises} & \eta_2 &= 175 \text{ poises.} \end{aligned} \tag{14.45}$$

μ_1 and $\eta_1 + \eta_2$ are determined from the data of Fig. 14.18. η_2 and μ_2 are determined by the longitudinal measurements discussed in section 14.5. The impedance in the low-frequency region is determined mainly by the first relaxation frequency in agreement with the results of section 14.3. The high-frequency shear impedance agrees approximately with that shown by Fig. 14.24. However, a considerably better agreement is obtained by assuming that the high-frequency shear stiffness has a hysteresis component resulting in the impedance

$$\left[\frac{\mu_2' - j\mu_2}{\omega}\right]$$

The value of this constant μ_2' is evaluated in section 14.5 on the longitudinal measurements. By inserting this element in the network, as shown by

Fig. 14.24 and solving for the average impedance, we find:

$$Z_0 = \sqrt{\frac{\left\{\rho(\mu_1+\mu_2)\left[\left\{\frac{\mu_1}{\mu_1+\mu_2}\left(\frac{f^2}{f}\right)\left[1+\left(\frac{\mu_2'}{\mu_2}+\frac{f}{f_2}\right)^2\right]+\frac{\mu_2}{\mu_1+\mu_2}\left(\frac{f^2}{f_2^2}\right)\left(1+\frac{f^2}{f_1^2}\right)\right\}\right.\right.}{\left.\left.+jf\left\{\frac{\mu_1}{\mu_1+\mu_2}\left(\frac{1}{f_1}\right)\left[1+\left(\frac{\mu_2'}{\mu_2}+\frac{f}{f_2}\right)^2\right]+\frac{\mu_2}{\mu_1+\mu_2}\left(\frac{1}{f_2}\right)\left(1+\frac{f^2}{f_1^2}\right)\times\left[1+\frac{\mu_2'}{\mu_1}\left(\frac{\mu_2'}{\mu_1}+\frac{f}{f_2}\right)\right]\right\}\right]\right\}}{\left(1+\frac{f^2}{f_1^2}\right)\left[1+\left(\frac{\mu_2'}{\mu_2}+\frac{f}{f_2}\right)^2\right]}} \tag{14.46}$$

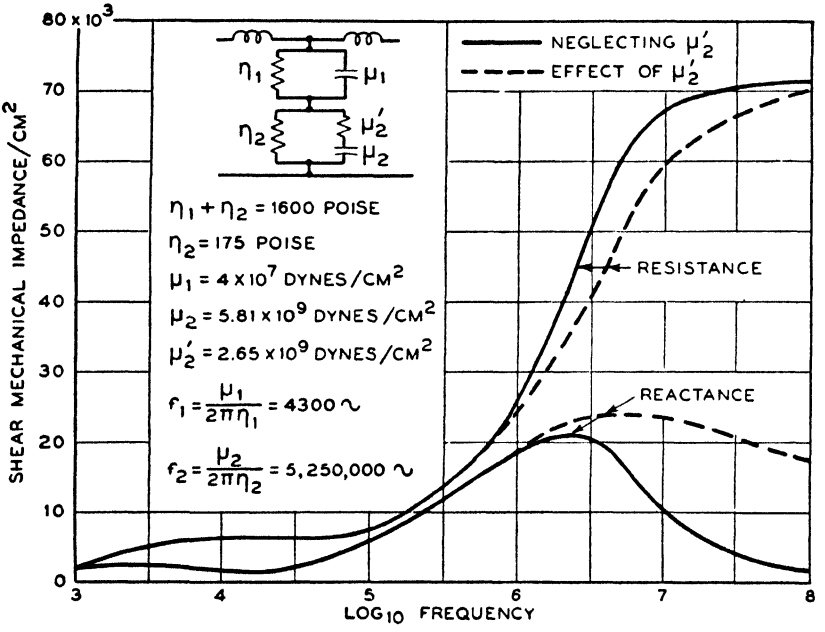

FIG. 14.25. Theoretical resistance and reactance curves for liquids having two relaxation frequencies. Dashed line represents effect of hysteresis term.

If $\mu_2' = 0$, this reduces to equation (14.44). Inserting the value of $\mu_2' = 2.65 \times 10^9$ dynes per square centimeter, determined by the longitudinal measurements of section 14.5, the modification is shown by the dot-dash line of Fig. 14.25. When the resistance component is plotted on Fig. 14.25, this agreement with the measured value is quite good.

Hence these measurements show definitely the presence of two relaxation mechanisms in the shear process, one connected with the configurational stiffness of chains and the other with the stiffness of the liquids in single

potential wells when the frequency is so high that configurational stiffness cannot be excited.

Since configurational and crystalline elasticities in all probability are determined by nearest neighbors, the action of any segment may be represented as due to the potential well distribution shown in Fig. 14.26. The viscous flow of the segment requires a translation and rotation and hence occurs over the free energy barrier ΔU_1. On the other hand, an extension or contraction of the chain as a whole, which results when configurational elasticity occurs, requires no change in the center of gravity of the chain and results in a lower free energy barrier ΔU_2. When a shearing stress is put on the liquid, one well is lowered compared to the other, as shown by the dotted line. At low frequencies, sufficient time is

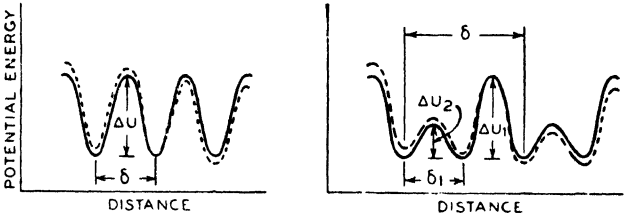

FIG. 14.26. Potential well distribution. A. Light liquid. B. Polymer liquid showing configurational elasticity.

given so that a viscous flow occurs over the high-energy barrier. As the frequency increases, there is not time for an actual transfer of the center of gravity in the time of a single cycle, but a local distortion still can occur across the lower energy barrier. This is a reversible process and results in the configurational elasticity. Since the motion that can occur is large, the configurational stiffness is small. At still higher frequencies, even the local distortion cannot occur and the only effect is the displacement of the segment from its equilibrium position. This results in a very high shear stiffness of the crystalline type. According to the measurements, the height of the flow viscosity energy barrier is 16 kilocalories per mole, whereas the local distortion energy barrier is 12 kilocalories per mole. As the chain length decreases, the distinction between a local distortion and true flow motion disappears, and for liquids having a chain length in the order of one Eyring unit, the two potential wells become equal and the potential well distribution is similar to that for a light liquid, as shown by Fig. 14.26A. Under these circumstances the configurational elasticity disappears, as shown for the low-density liquid of Fig. 14.21, and the shear viscosity equals the flow viscosity up to a frequency for which crystalline elasticity sets in, as shown in Fig. 14.24.

14.4 *Shear Waves in Liquids*

In addition to the viscous measurements indicating shear elasticity, measurements have also been made showing the presence of shear waves in very viscous liquids. The attenuation above the relaxation frequency of polymerized castor oil is

$$A = \frac{\sqrt{\rho/C_s}}{2\eta} = 97.2 \text{ nepers per cm} \tag{14.47}$$

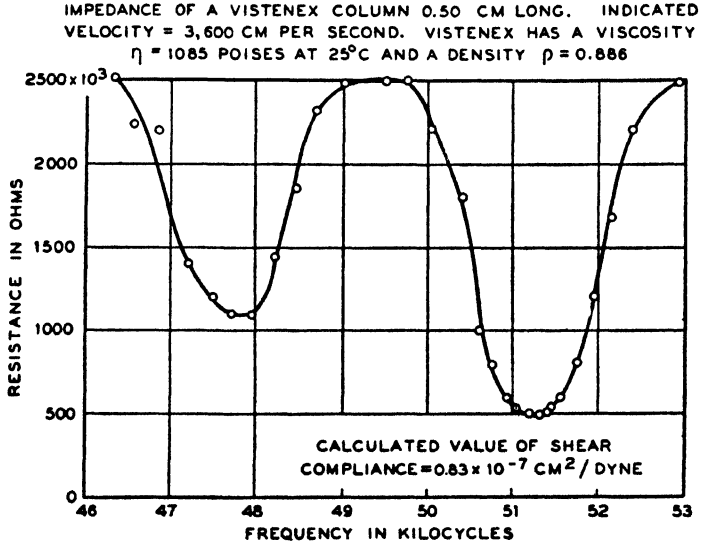

FIG. 14.27. Resistance of torsional crystal showing shear waves in polyisobutylene.

which is too high to demonstrate wave motion. However, if we use a liquid with a much higher viscosity, the limiting attenuation becomes lower. Such a liquid is the polyisobutylene of section 14.3, polymer *C* which has a viscosity of 900 poises at 25°C. This should have an attenuation of about 1.5 nepers per centimeter, if it has the same shear elasticity as does polymerized castor oil.

To demonstrate the presence of shear waves in polyisobutylene, a torsional crystal was used to set up a standing-wave system. On account of the large viscosity, since the separation between the reflector and the crystal could not easily be varied, a fixed distance between the crystal and the reflector plate was maintained and the frequency was varied. The measured resistance as a function of frequency is shown in Fig. 14.27. The separation between the crystal and reflector was 0.50 centimeter.

Since the minima occur at half-wavelength frequencies, the data are best fitted by assuming that the length is 14 half wavelengths at 47,800 cycles, and 15 half wavelengths at 51,300 cycles giving a velocity of 3,600 centimeters per second. Since the density of polymer *C* is 0.886 at 25°C, this gives a shear stiffness of 1.2×10^7 dynes per square centimeter, which agrees within the experimental error (since an interferometer with a single half wavelength change is not accurate) with that given in Fig. 14.18. The indicated attenuation, determined from the ratio of maximum resistance to minimum resistance, is 0.5 nepers for the column or 1.0 nepers per centimeter compared to the calculated value

$$A = \frac{\sqrt{0.886 \times 1.2 \times 10^7}}{2 \times 900} = 1.8 \text{ nepers per cm} \qquad (14.48)$$

This is within the experimental error.

Measurements were also made for silicone putty at 50,000 cycles and at 25°C the measurements were

$$\rho = 1.14; \qquad v = 2.55 \times 10^4 \text{ cm/sec}; \qquad A = 0.13 \text{ nepers per cm}$$

The shear viscosity, as measured by W. O. Baker by an extrusion process, was 3×10^5 poises. We note that the shear stiffness is much higher for this material than was the case with polyisobutylene. From the density and velocity, the value becomes

$$C_S = 1.35 \times 10^{-9} \text{ cm}^2/\text{dyne}; \qquad \mu = 7.4 \times 10^8 \text{ dynes/cm}^2 \quad (14.49)$$

which is only about 1/16 times the stiffness for the longitudinal mode for plane waves in this liquid and indicates that the stiffness is approaching that of a crystal. The calculated attenuation is 0.05 nepers per centimeter compared to a measured value of 0.13. While the accuracy is not high, it appears possible that another source of dissipation is involved.

It seems probable that all liquids may have shear elasticities but the relaxation frequency or frequencies are usually too high to produce observable effects for frequencies that have so far been used. This shear elasticity may have an important bearing on the specific heat of liquids.[10, 11]

14.5 *Propagation of Longitudinal Waves in Very Viscous Liquids and Demonstration of Velocity and Attenuation Dispersion in Liquids*

Since low-frequency shear viscosities of very viscous liquids are relaxed by the configurational shear elasticities, it appears likely that for longitudinal waves of frequencies much higher than those of the first shear relaxation frequencies, the shear component of the longitudinal distortion will occur elastically and this shear viscosity will not contribute to the

attenuation. This supposition is confirmed by a recent study[30] of longitudinal waves for the polyisobutylene liquids of section 14.3 and moreover velocity dispersion and associated attenuation dispersion due to molecular processes, has been observed for the first time in a liquid. Since this study throws considerable light on the mechanisms involved and the approach of a liquid at very high frequencies to the type of attenuation existing in solids, these measurements are discussed at some length.

The experimental method used was a combination of pulsing and steady-state methods and is shown schematically by Fig. 14.28. Here a source

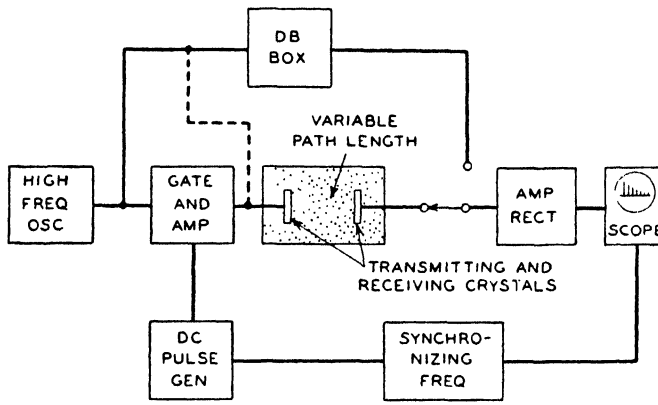

FIG. 14.28. Measuring equipment for measuring attenuation and velocity for longitudinal waves in a liquid.

of high frequency is fed to an amplifier through two parallel paths. One is through an amplifier that is gated by a direct-current pulse. The pulse of alternating current is impressed on a transmitting crystal, which sends a pulse of alternating longitudinal waves into the liquid. This wave is picked up by a second crystal, accurately parallel to the sending crystal and which is placed at a variable distance from the sending crystal. The voltage generated by the receiving crystal is sent through a wide-band amplifier, is rectified, and actuates the vertical set of electrodes of the oscilloscope. The sweep circuit of the horizontal set is controlled by the same synchronizing oscillator that controls the DC pulse generator so that the pulse received always occurs in the same position on the fluorescent screen. The second path from the high-frequency oscillator is a steady-state one through an attenuation box to the amplifier, rectifier and

[30] Mason, W. P., W. O. Baker, H. J. McSkimin, and J. H. Heiss "Mechanical Properties of Long Chain Molecule Liquids at Ultrasonic Frequencies," *Phys. Rev.*, Vol. 77, May, 1948.

oscilloscope. The attenuation box has carbon-film resistors that are stable in value up to a frequency of 10 megacycles. The process of attenuation measurement consists in comparing the amplitude of the pulse path with the amplitude through the attenuation path and adjusting the

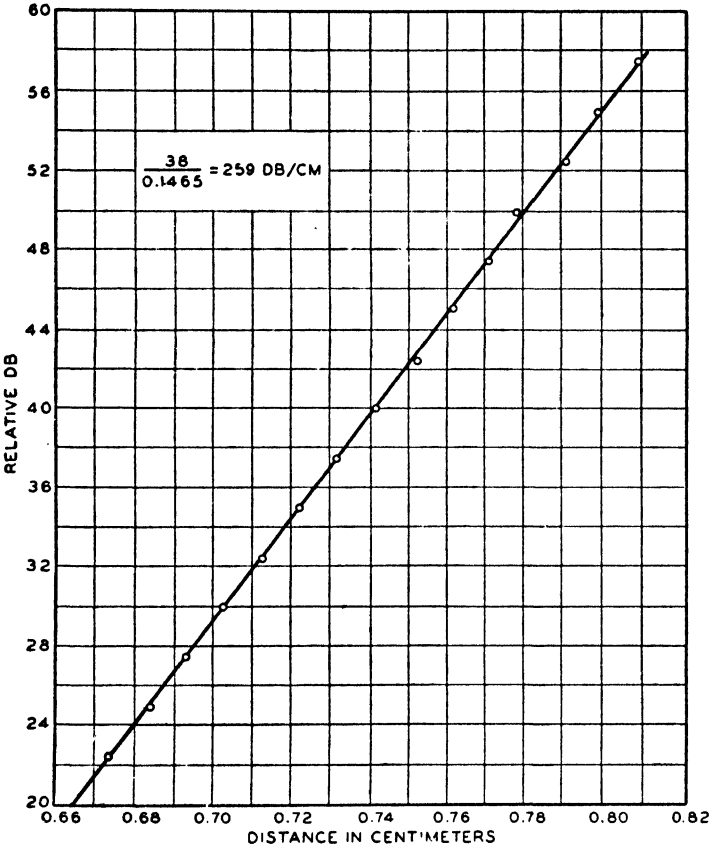

FIG. 14.29. Attenuation versus change in path length for polymer *D*.

box until they are equal. If the loss in the liquid is 15 db or more, the pulse length does not make any difference and comparisons can be made by steady-state methods. However, if the loss betweeen the two crystals is small, trouble is experienced with standing waves. To get around this difficulty a very short pulse length is used and the first received pulse, which is free from standing-wave complications, is compared with the steady-state amplitude. Figure 14.29 shows a typical measurement of attenuation versus change in path length for polymer *D*. A change of

38 db occurs in a path difference of 0.1465 centimeters, indicating an attenuation of 259 db per centimeter for a frequency of 8 megacycles and a temperature of 31°C. From the straightness of the attenuation-distance line, it appears likely that the attenuation can be measured within ±2% for a high-loss material and ±5% for a low-loss material.

A measurement of the velocity for such a high-loss material is more difficult by conventional methods. The path length is so short that a comparison of the position of received pulse with transmitted pulse does not give an accurate measurement of the velocity. On the other hand, the attenuation is too high to utilize the standing-wave properties of the

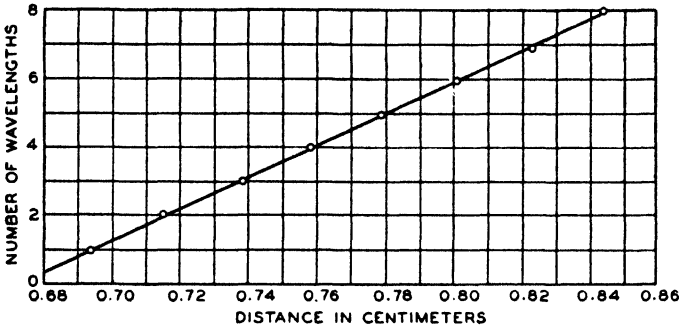

FIG. 14.30. Number of wavelength changes plotted against distance for polymer *D*.

liquid as is done with the acoustic interferometer. The method adopted was to compare the phase of the received pulse with the phase of the steady-state transmission. For this purpose both paths were connected simultaneously to the amplifier-rectifier and the attenuation in the db box was adjusted to be approximately equal to that through the liquid. As the path length was changed, the output from the pulse alternately added and subtracted from that through the box. By plotting the positions of the maxima, the wavelength in the liquid can be obtained. Figure 14.30 shows a typical measurement for the same liquid polyisobutylene polymer *D*, plotting the number of wavelengths change against the separation in centimeters. A very good straight line can be drawn through these points, and it is estimated that the velocity can be measured to about ±1 per cent. By this method velocities can be measured, even though the liquid path has 50 db or more attenuation.

Employing these methods, a series of measurements were made for these three liquids at the frequencies 2, 5 and 8 megacycles over a wide temperature range. The data on the attenuation for polymer *D* are shown plotted in Fig. 14.31, while the velocities for the same conditions are

plotted in Fig. 14.32. The attenuation is plotted in terms of nepers (1 neper equals 8.68 db) per wavelength, since the theoretical attenuation is most easily calculated for that quantity. It is obvious from the data that an attenuation and associated velocity dispersion are occurring for this liquid.

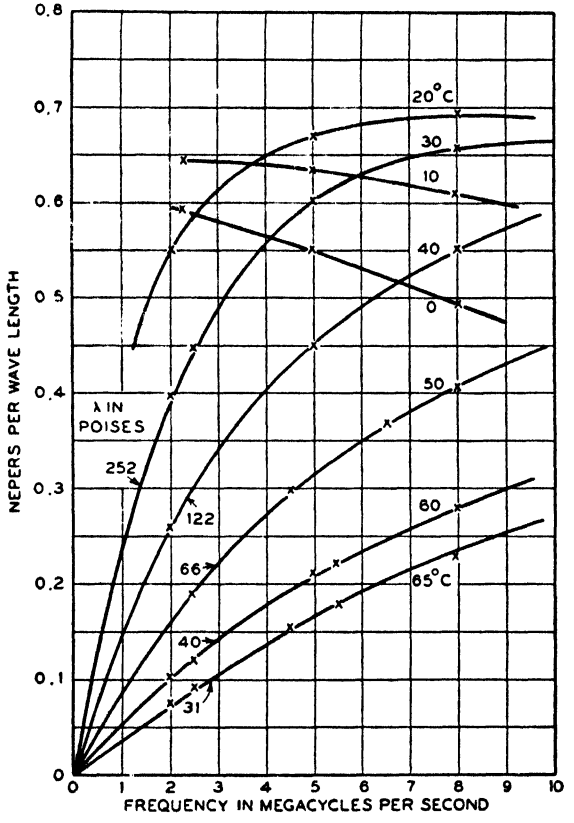

FIG. 14.31. Attenuation per wavelength of polymer *D* plotted as a function of frequency and temperature.

In order to classify the measured results and to obtain parameters in terms of which they can be expressed, use is made of the calculated value of the attenuation and phase shift due to a relaxation type of theory. Such a phenomenon can be represented by the equivalent circuit of Fig. 14.33, in which the series arm is the density times the length of the section dx considered, as the shunt arm consists of a stiffness κ_1/dx in parallel with a secondary viscosity divided by dx and the two in series with a second

stiffness κ_0/dx. At very low frequencies, this will reduce to the impedance of the stiffness κ_0, so that κ_0 represents the bulk stiffness of the liquid measured by static methods. At very high frequencies, the impedance of the shunt arm reduces to that of the two stiffnesses in series. Hence κ_0 = low-frequency bulk stiffness; κ_1 = difference between high-frequency

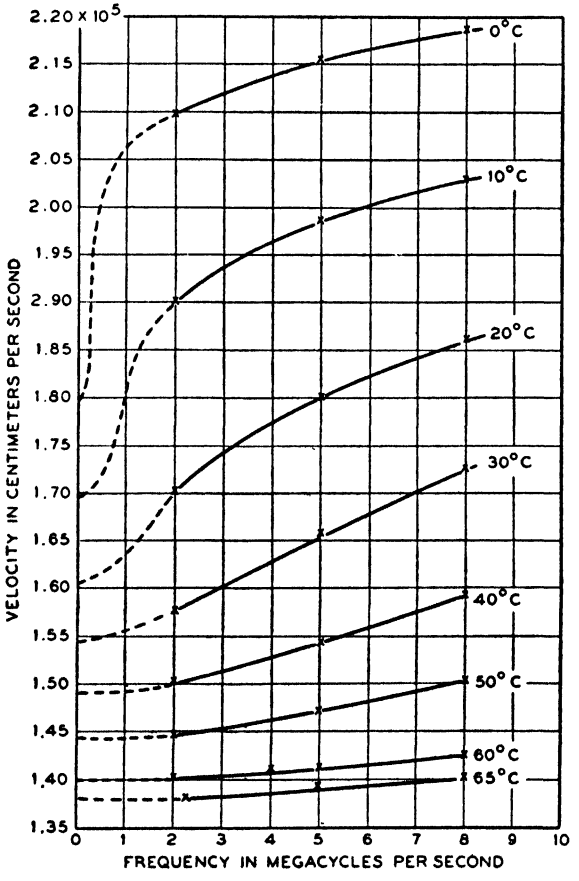

FIG. 14.32. Velocities of polymer *D* plotted as a function of frequency and temperature.

and low-frequency stiffness. From the measurement of the shear elasticity at high frequencies, discussed in section 14.31, it is evident that the dispersion in the longitudinal velocity is due to the dispersion in the shear elasticity. Since the longitudinal velocity is determined by the elastic constants $\lambda + 2\mu$, longitudinal measurements do not in themselves tell whether a change is due to the λ constant or the μ constant. At these high

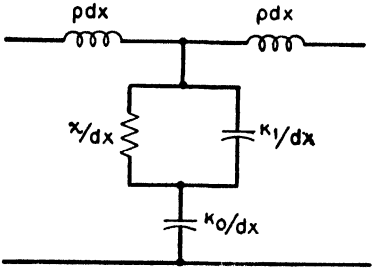

FIG. 14.33. Equivalent circuit for showing effect of secondary viscosity on a longitudinal wave.

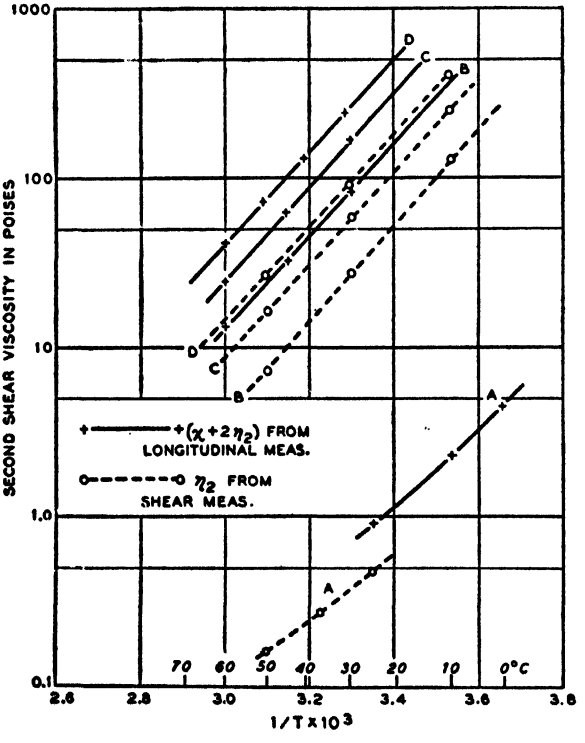

FIG. 14.34. Secondary shear viscosity plotted as a function of $1/T$. Solid lines represent the values $(\chi + 2\eta_2)$ determined from longitudinal measurements; dotted lines represent η_2 determined from shear measurements.

frequencies, the configurational elasticity μ_2 of Fig. 14.23A is relaxed by the configurational viscosity η_2, and since η_2 is much smaller than η_1 the flow viscosity, η_2 represents all of the shear viscosity at high frequencies. The values of η_2 for the *A*, *B*, *C* and *D* polyisobutylene polymers have recently been measured by the high-frequency pulsing methods of section 15.31 and are shown plotted on Fig. 14.34. In addition, there appears to be a compressional viscosity χ which is an appreciable fraction of η_2. The value of χ' introduced in Fig. 14.33 is then $\chi' = \chi + 2\eta_2$. κ_1 is closely equal to the shear stiffness $2\mu_3$, *i.e.* the high-frequency shear stiffness.

The attenuation and velocity can be calculated from the formula

$$\Gamma dx = (A + jB)\,dx = \sqrt{\frac{Z_1}{Z_2}} = \sqrt{\frac{j\omega\rho\,(dx)^2}{\dfrac{-j\kappa_0}{\omega} + \dfrac{\chi'\left(\dfrac{-j\kappa_1}{\omega}\right)}{\chi' - \dfrac{j\kappa_1}{\omega}}}} \tag{14.50}$$

where $Z_1 = j\omega\rho\,dx$ is the series arm and $Z_2 = \left[\dfrac{-j\kappa_0}{\omega} + \dfrac{\chi'\left(-\dfrac{j\kappa_1}{\omega}\right)}{\chi' - \dfrac{j\kappa_1}{\omega}}\right] x \dfrac{1}{dx}$

is the shunt arm.

If we solve for the attenuation *A* (expressed in nepers per centimeter) and *B* the phase shift (expressed in radians per centimeter), we have

$$B = \omega\sqrt{\frac{\rho}{\kappa_0}}\sqrt{\frac{1 + \chi'^2\omega^2\left(\dfrac{\kappa_0 + \kappa_1}{\kappa_0\kappa_1^2}\right)}{1 + \chi'^2\omega^2\left(\dfrac{\kappa_0 + \kappa_1}{\kappa_0\kappa_1}\right)^2}} = \frac{\omega}{\sqrt{\dfrac{k^2v_0^2 + \omega^2v_\infty^2}{k^2 + \omega^2}}}$$

$$\frac{A}{B} = \frac{1}{2}\frac{\omega\chi'/\kappa_0}{1 + \chi'^2\omega^2\left(\dfrac{\kappa_0 + \kappa_1}{\kappa_0\kappa_1^2}\right)} = \frac{1}{2}\left(\frac{v_\infty^2 - v_0^2}{v_0v_\infty}\right)\frac{k\omega}{k^2 + \omega^2} \tag{14.51}$$

where

$$v_0 = \sqrt{\frac{\kappa_0}{\rho}}; \qquad v_\infty = \sqrt{\frac{\kappa_0 + \kappa_1}{\rho}}; \qquad k = \frac{1}{\chi'\sqrt{\dfrac{\kappa_0 + \kappa_1}{\kappa_0\kappa_1^2}}} = \frac{(v_\infty^2 - v_0^2)\rho v_0}{\chi' v_\infty}$$

v_0 is the velocity at low frequencies, v_∞ the velocity at high frequencies and $k/2\pi$ is the relaxation frequency f_0. If we multiply the ratio A/B

by 2π, we obtain the attenuation A_w in nepers per wavelength, which is the quantity measured and expressed in Fig. 14.31. This becomes

$$A_w = \frac{\pi\omega\chi'}{\rho v_0^2} \times \frac{1}{1 + \chi'^2\omega^2\left[\dfrac{v_\infty^2}{\rho^2 v_0^2(v_\infty^2 - v_0^2)^2}\right]} \tag{14.52}$$

For very low frequencies this reduces to

$$A_w = \frac{2\pi^2 f\chi'}{\rho v_0^2} \tag{14.53}$$

and the attenuation should initially be proportional to the frequency. This agrees with the measurements of Fig. 14.31 for high temperatures, where the initial slopes of the attenuation frequency curves can be obtained. Equation (14.51) gives a method for determining the viscosity for

$$\chi' = \frac{A_w\rho v_0^2}{2\pi^2 f} \tag{14.54}$$

Since all these quantities are known, χ' can be determined and for polymer D is shown plotted as log χ' versus $1/T$ by Fig. 14.34. The points lie on a straight line having a slope 3/4 that of the low-frequency shear viscosity. The initial slopes have been determined for the other three liquids and are shown by Fig. 14.34. All the curves are parallel, as for the low-frequency shear viscosity, indicating, that the temperature dependent jump occurs by chain sections that are the same for all average molecular weights. The configurational viscosity increases with molecular weight although the spread is not nearly as large as that for low-frequency shear viscosity. For molecular weights above 10,000, no further increase with chain length has been observed. Comparing the value of $\chi' = (\chi + 2\eta_2)$ with the values of η_2 measured by shear measurements, we see that there is a compressional viscosity which varies from zero for the low-molecular-weight polymer A to nearly equal to the shear viscosity η_2 for the largest molecular weight. As nearly as can be judged from the relative slopes of the viscosities measured by longitudinal and shear waves, the activation energy of the compressional viscosity is equal to that of the second shear (configurational) viscosity.

To correlate all the measurements of Fig. 14.31 over temperature and frequency ranges, we plot the product

$$A_w\rho v_0^2/(\rho v_0^2)_s \tag{14.55}$$

against the product of frequency times χ' where $(\rho v_0^2)_s$ is the product of density times v_0^2 for polymer D at 20°C. All the values of χ' are shown

plotted on Fig. 14.34, while the zero frequency velocities can be obtained by extrapolating the data of Fig. 14.32 and are shown by Fig. 14.35. Within the experimental error all these points lie on one curve shown by Fig. 14.36. Also the measured attenuation per wavelength of the polymer C liquid and the polymer B liquid can be plotted on the same curve. From the equation for the phase shift, equation (14.51), since $B = \omega/v$,

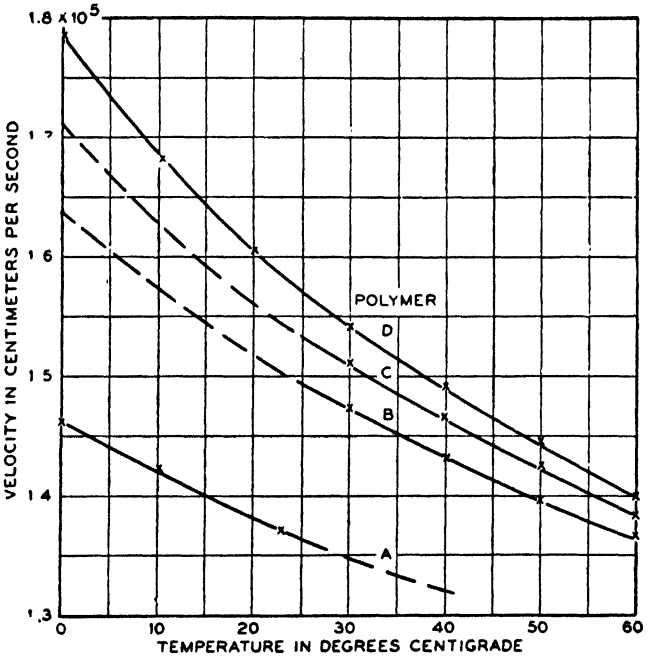

FIG. 14.35. Zero frequency velocities of polymers A to D of polyisobutylene.

we see that the ratio of v/v_0 should also be a function of the product of the frequency times $\chi' = \chi + 2\eta_2$. From the data of Fig. 14.32, showing the measured velocity, the data of Fig. 14.34 showing the value of χ', and the data of Fig. 14.35 for the zero frequency velocity, the ratio of v/v_0 can be evaluated and is shown plotted by Fig. 14.37 as a function of the product frequency times χ'. A single curve suffices for all the temperatures and for the other two polyisobutylene liquids.

Other measurements[9] made for silicone putty at room temperature indicate a much lower value of high-frequency viscosity than occurs for polyisobutylene. Silicone putty has a velocity of 1.03×10^5 centimeters per second, a density of 1.14 and an attenuation directly proportional to the square of the frequency equal to

$$A = 9.2 \times 10^{-14} f^2 \text{ nepers/cm} \qquad (14.56)$$

Since the low-frequency shear viscosity for this liquid is 300,000 poises, if the classical formula of equation (14.14) held, the attenuation would be $3 \times 10^{-10} f^2$ nepers and this shows that the low-frequency shear viscosity

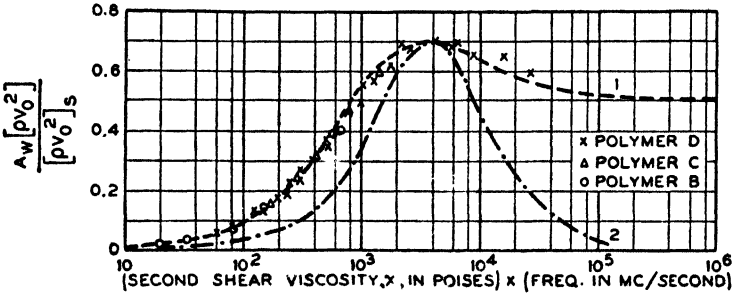

FIG. 14.36. Attenuation per wavelength as a function of secondary shear viscosity times frequency.

is been relaxed and is not contributing to the attenuation. The measur ents do not show whether the high-frequency viscosity $\chi' = 5.76$ pois a compressional viscosity or a relaxed second-shear viscosity. She

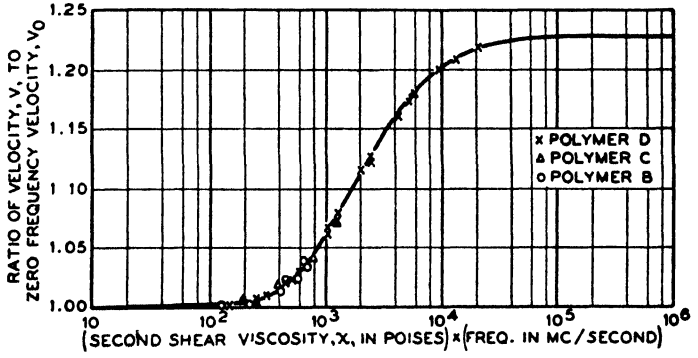

FIG. 14.37. Ratio of v/v_0 plotted as a function of secondary shear viscosity times frequency.

pulsing studies at high frequencies are inconclusive since the silicone putty does not wet the crystal and shear elasticities and losses cannot be measured.

14.51 *Discussion of Longitudinal Velocity and Attenuation Dispersion in Liquids*

The measurements of the velocity and attenuation of polyisobutylene for longitudinal waves provide material for testing the various mechanisms

proposed to account for added attenuation and velocity dispersion. Since the velocity of a longitudinal wave is controlled by the Lamé elastic constants $\lambda + 2\mu$, longitudinal measurements do not determine uniquely whether the dispersion is occurring in the compressibility constant λ or the shear constant μ.

Most theories developed for liquids assume that μ is equal to zero and the dispersion occurs in the elastic constant λ. The two mechanisms so far proposed are the Herzfeld, Rice, Kneser mechanism discussed in Chapter XIII and the Debye-Frenkel rearrangement mechanism discussed in the introduction to this chapter.

While these mechanisms are probably operative in light liquids, such as carbon disulphide where the attenuation is 900 times that calculated from measured shear viscosity, the measured values of the high-frequency shear impedances for these liquids, discussed in section 14.31, show definitely that the relaxation involved in this liquid is connected with the shear elasticity μ rather than with the compressional constant λ. It is suspected that most cases for which the attenuation is less than the classical attenuation, will be accounted for by a relaxation in μ rather than a relaxation in λ.

Whether the relaxation occurs in μ or λ, an equivalent circuit which represents the effect of this relaxation on the longitudinal wave is that shown by Fig. 14.33. The elasticity κ_0 is the low-frequency bulk modulus of the liquid and the sum of κ_1 and κ_0 is equal to the high-frequency modulus for the liquid. Since the high-frequency modulus is equal to $\lambda + 2\mu$ while the low-frequency modulus κ_0 is equal to the same elastic constant λ, we have the relation

$$\lambda = \kappa_0; \qquad 2\mu = \kappa_1 \tag{14.57}$$

The data of sections 14.30 and 14.31 show that there are two relaxation frequencies for shear. However, since the lower relaxation frequency is only 5,000 cycles, the high-frequency longitudinal measurements can be accounted for by a single relaxation mechanism. The relaxed low-frequency shear stiffness is added to λ but since $\lambda = 2.28 \times 10^{10}$ and $2\mu_1 = 8 \times 10^7$, the added amount to the compression stiffness is less than 0.4 per cent and can be neglected.

The high-frequency viscosity χ' is measured, as discussed, by finding the initial slope of the frequency attenuation curve and is plotted by Fig. 14.34. The ratio of 1.23 between the high-frequency and low-frequency velocity as given by Fig. 14.37, shows that the high-frequency shear stiffness is in the order of $1.17 \times 10^{10}/2 = 5.59 \times 10^9$ dynes per square centimeter in agreement with the measurement of Fig. 14.24.

However, this theory does not account entirely for the measured attenuation and velocity curves of Figs. 14.36 and 14.37. The calculated at-

tenuation per wavelength for a single relaxation frequency is shown by the dot-dash line of Fig. 14.36. The measured value is broader on a logarithmic scale than the curve for a single relaxation frequency, and moreover is dissymmetrical about the maximum. We could match this curve by a dissymmetrical distribution of relaxation frequencies.

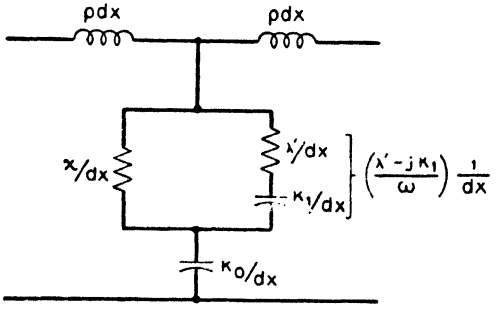

FIG. 14.38. Network taking account of hysteresis resistance as well as secondary shear viscosity.

However, a simpler explanation of this effect is that a hysteresis occurs in the stress-strain relationship which introduces a constant loss per cycle. In order to get an agreement with experiment, this hysteresis loss has to be introduced in series with the elastic stiffness κ_1, giving this arm the impedance, shown by Fig. 14.38, of

$$\frac{\chi' - j\kappa_1}{\omega} \tag{14.58}$$

Since this arm is shunted out at very low frequencies by the viscosity χ', this results in the following interpretation. At low frequencies, the local order change caused by the shearing of the liquid takes place by one segment of the chain jumping from one stable potential well to another with no appreciable tangling with other chains. There is even in this case a small amount of hysteresis loss, as is shown by Fig. 14.39, which shows the measured attenuation of the lightest liquid, the polymer *A* liquid. The attenuation values measured at 2, 5 and 8 megacycles, lie on straight lines that do not go through the origin at zero frequency but have intercepts of about .0025 nepers per wavelength, indicating the presence of a slight amount of hysteresis loss. As the frequency increases, fewer and fewer of the chains accumulate enough heat energy in the time of a single cycle to rearrange to adjacent stable potential wells and the liquid becomes less compressible. It appears, however, that they can be displaced to intermediate potential minima. The displacement probably consists of an internal twisting. The steric restrictions imposed by the closely packed

methyl groups on the flexibility of individual chains then tend to hold the new twisted position. The chain segments then are not released until a later part of the cycle and hence the strain lags behind the applied stress. It is supposed that the wave traveling through the polymer exerts such torque on certain portions of the convolved chains that an extreme biasing

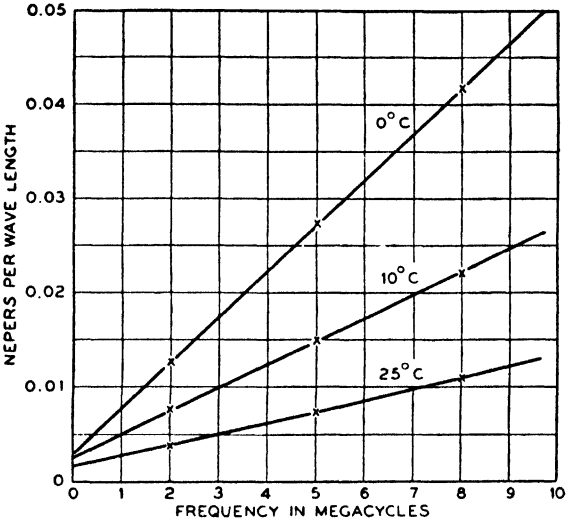

FIG. 14.39. Attenuation per wavelength for polymer *A* as a function of frequency.

force for pairs twisting occurs. Thus the normally considerable activation energy for internal rotation of pairs of methyl groups past each other, in polyisobutylene, is effectively reduced to zero. Also, accordingly, since this potential barrier that the chains have to surmount to reach the twisted positions is so small, compared, for instance, to that for proceeding to the next stable position (the latter process requires both twisting and translation), the hysteresis type of loss should continue to a very high frequency. This mechanism seems concordant with the general principles of hysteresis.

The network of Fig. 14.38 represents the effect of the hysteresis loss component. If we solve this network to obtain the velocity and attenuation, we have

$$P\,dx = (A + jB)\,dx = \sqrt{\frac{Z_1}{Z_2}} = \sqrt{\frac{j\omega\rho\,(dx)^2}{-\frac{j\kappa_0}{\omega} + \left[\frac{\chi'(\lambda' - j\kappa_1)}{\omega}\right]\left[\chi' + \frac{(\lambda' - j\kappa_1)}{\omega}\right]}} \tag{14.59}$$

where Z_1, the series arm, is $j\omega\rho\, dx$, and Z_2, the shunt arm, is

$$Z_2 = \frac{-j\kappa_0}{\omega} + \frac{\dfrac{\chi'[\lambda' - j\kappa_1]}{\omega}}{\chi' + \dfrac{\lambda' - j\kappa_1}{\omega}} \tag{14.60}$$

Solving for the attenuation A and the phase shift B, we find

$$A^2 = \frac{\omega^2\rho}{2\kappa_0}\left\{\frac{(\lambda'^2 + \kappa_1^2) + 2\omega\chi'\lambda' + \omega^2\chi'^2\left(\dfrac{\kappa_0 + \kappa_1}{\kappa_0}\right)}{\left[\lambda' + \omega\chi'\left(\dfrac{\kappa_0 + \kappa_1}{\kappa_0}\right)\right]^2 + \left[\dfrac{\omega\chi'\lambda'}{\kappa_0} - \kappa_1\right]}\right\}$$
$$\times\left[-1 + \sqrt{\frac{1 + \dfrac{\omega^2\chi'^2}{\kappa_0^2}[\lambda'^2 + \kappa_1^2 + \omega\lambda'\chi']^2}{\lambda'^2 + \kappa_1^2 + 2\omega\chi'\lambda' + \omega^2\chi'^2\left(\dfrac{\kappa_0 + \kappa_1}{\kappa_0}\right)^2}}\right] \tag{14.61}$$

$$B^2 = \frac{\omega^2\rho}{2\kappa_0}\left[\frac{(\lambda'^2 + \kappa_1^2) + 2\omega\chi'\lambda' + \omega^2\chi'^2\left(\dfrac{\kappa_0 + \kappa_1}{\kappa_0}\right)}{\left[\lambda' + \omega\chi'\left(\dfrac{\kappa_0 + \kappa_1}{\kappa_0}\right)\right]^2 + \left[\dfrac{\omega\chi'\lambda'}{\kappa_0} - \kappa_0\right]^2}\right]$$
$$\times\left[1 + \sqrt{1 + \frac{\dfrac{\omega^2\chi'^2}{\kappa_0^2}[\lambda'^2 + \kappa_1^2 + \omega\chi'\lambda']^2}{\lambda'^2 + \kappa_1^2 + 2\omega\lambda'\chi' + \omega^2\chi'^2\left(\dfrac{\kappa_0 + \kappa_1}{\kappa_0}\right)}}\right]$$

These can be written quite closely as

$$B = \omega\sqrt{\frac{\rho}{\kappa_0}}\sqrt{\frac{(\lambda'^2 + \kappa_1^2) + 4\pi\lambda'(f\chi') + \dfrac{4\pi^2}{\kappa_0^2}\left(\dfrac{\kappa_0 + \kappa_1}{\kappa_0}\right)(f\chi')^2}{(\lambda'^2 + \kappa_1^2) + 4\pi\lambda'(f\chi') + 4\pi^2\left(\dfrac{(\kappa_0 + \kappa_1)^2 + \lambda'^2}{\kappa_0^2}\right)(f\chi')^2}} \tag{14.62}$$

$$\frac{2\pi A}{B} = A_W = \frac{\dfrac{2\pi^2}{\kappa_0}(f\chi')[\lambda'^2 + \kappa_1^2 + 2\pi\lambda'(f\chi')]}{\left[\lambda'^2 + \kappa_1^2 + 4\pi\lambda'^2(f\chi') + 4\pi^2\left(\dfrac{\kappa_0 + \kappa_1}{\kappa_0}\right)(f\chi')^2\right]} \tag{14.63}$$

Several limiting cases are of interest. At low frequencies, the attenuation

per wavelength and velocity v_0 become

$$A_{W_0} = \frac{2\pi^2}{\kappa_0}(f\chi') = \frac{2\pi^2 f\chi'}{\rho v_0^2}$$
$$v_0 = \sqrt{\frac{\kappa_0}{\rho}} \tag{14.64}$$

For very high frequencies the attenuation per wavelength and the velocity become

$$A_{W_\infty} = \frac{\pi\lambda'}{\kappa_0 + \kappa_1} = \frac{\pi\lambda'}{\rho v_\infty^2} \tag{14.65}$$
$$v_\infty = \sqrt{\left(\frac{\kappa_0 + \kappa_1}{\rho}\right)\left[1 + \frac{\lambda'^2}{(\kappa_0 + \kappa_1)^2}\right]}$$

Hence with hysteresis type of loss, the attenuation per wavelength at high frequencies remains constant and independent of the frequency. This is the type of attenuation[31] found for solid bodies of the glass type, and it appears that the polyisobutylene liquids approach this condition at high frequencies.

Introducing these values in equation (14.61) the velocity, which is ω/B, and the attenuation per wavelength can be written in the form

$$v = v_0\sqrt{\frac{1 + 2C(f\chi') + D\frac{v_\infty^2}{v_0^2}(f\chi')^2}{1 + 2C(f\chi') + D(f\chi')^2}};$$
$$A_W = \frac{2\pi^2}{\kappa_0}\frac{(f\chi')[1 + C(f\chi')]}{1 + 2C(f\chi') + D(f\chi')^2} \tag{14.66}$$

where

$$C = \frac{2\pi\lambda'}{\lambda'^2 + \kappa_1^2}; \qquad D = \frac{4\pi^2(\kappa_0 + \kappa_1)}{\kappa_0(\lambda'^2 + \kappa_1^2)}$$

Hence, if C, D and v_∞^2/f_0^2 are relatively constant with temperature, the velocity and attenuation per wavelength are functions of the product frequency times viscosity χ'. As indicated by the data of Figs. 14.36 and 14.37 this assumption appears to be justified.

[31] Mason, W. P., and H. J. McSkimin, "Attenuation and Scattering of High Frequency Sound Waves in Metals and Glasses," *J.A.S.A.*, Vol. 19, No. 3, pp. 464–474, May, 1947 and Chapter XV of this volume.

The measured curves of Figs. 14.36 and 14.37 can be fitted quite closely by taking

$$\kappa_0 = 2.28 \times 10^{10} \text{ dynes/cm}^2; \qquad \kappa_1 = 1.17 \times 10^{10} \text{ dynes/cm}^2;$$

$$\lambda' = 0.53 \times 10^{10} \text{ dynes/cm}^2 \tag{14.67}$$

This gives a zero frequency velocity of 1.6×10^5 corresponding to a temperature of 20°C, the standard condition of Fig. 14.37. The dashed line shows the calculated attenuation per wavelength, which agrees very well with the measured points. The solid line of Fig. 14.37 is a plot of the ratio of velocity to zero frequency velocity, using equation (14.66) and the constants of equation (14.67). The agreement with the measured points is very good. The theoretical curve of Fig. 14.36 indicates that at high frequencies, polyisobutylene liquids should have an attenuation per wavelength of 0.5 nepers independent of frequency.

CHAPTER XV

Properties of Solids and Their Measurement by Ultrasonic Waves

Although most of the properties of solids have been measured by static means, during the last ten years considerable information has been obtained by means of ultrasonic waves in bars of solid materials. Most of the early work was done by a resonant method in which the resonant frequency and Q were measured for a definite length bar or tuning fork. From these data and their variation over frequency and temperature ranges considerable information was obtained regarding the properties of the materials and the mechanisms for absorbing energy. Among the first measurements were those of Wegel and Walther,[1] who measured the Q of various solid materials by exciting a bar of the material at its resonant frequency by means of a magnetic drive. They found that the Q of a large group of solid materials was practically independent of the frequency and suggested that the loss mechanism was a type of elastic hysteresis which produced a constant loss per cycle of the applied alternating stress.

Another method that has been widely used by Quimby and his students,[2] is the piezoelectric half-wave crystal which is used to drive a mechanical bar glued to the crystal. By adjusting the length of the bar until the resonant frequency of the combination is the same as the resonant frequency of the crystal alone, one knows that the length of the bar is an integral number of half wavelengths at the frequency of the crystal. By measuring the change in electrical resistance caused by the load, the Q of the mechanical bar can be measured. This process has been used in measuring the properties of single metal crystals[3] and the disappearance of the shear modulus near the melting point.

Other methods have also been used such as the transmission of sound from a liquid through a solid and into a liquid again. At normal incidence, good transmission is obtained when the solid is a half wavelength. By turning a solid at an angle to the sound beam, Bär and Walti[4] have shown

[1] Wegel, R. L. and H. Walther, *Physics*, Vol. 6, p. 141, 1935.

[2] Balamuth, L., *Phys. Rev.*, Vol. 45, p. 715, 1934.

[3] Read, T. A., *Phys. Rev.*, Vol. 58, p. 371, 1942; Hunter, L. P. and S. Seigel, *Phys. Rev.*, Vol. 61, p. 84, 1942.

[4] Bär and Walti, *Helv. Phys. Acta*, Vol. 7, pp. 113–139, 1938.

that a correlation can be obtained between the transmission and the properties of the solid. Solids whose impedance do not differ much from that of the liquid, can be measured by interferometric methods.

During World War II considerable effort was spent in sending short-sound pulses down columns of liquids. The same technique was applied in sending pulses through solid materials and quite acceptable delay lines were obtained with shear waves in fused quartz, which were used for reproducing the reflections from the radio wave at the proper time. This technique has recently been applied[5] to measuring the losses in solids of the metal and glass type and has resulted in establishing a connection between grain size of the metal crystallites and the Rayleigh fourth-power scattering law. A similar technique[6] has been used in locating flaws in metal castings and other solid materials.

The differences that exist between sound propagation in liquids and solids arise primarily from the rigidity of the solids, and secondarily from their anisotropy. The rigidity makes possible various kinds of wave motion while the anisotropy leads to two important types of loss, the thermal relaxation loss and the scattering loss. In an infinite solid and also in a finite solid for which the wave front is a large number of wavelengths, two types of waves can exist, the longitudinal wave and the shear wave. These have the velocities

$$v_{\text{long}} = \sqrt{\frac{\lambda + 2\mu}{\rho}}; \qquad v_{\text{shear}} = \sqrt{\frac{\mu}{\rho}} \tag{15.1}$$

where μ is the shearing constant and $\lambda + 2\mu$ the plate modulus. Values of v_{shear} to v_{long} are for fused quartz, steel and lead 0.65, 0.52, and 0.30 respectively. For a wire whose diameter is a small fraction of a wavelength, the velocity is controlled by Young's modulus

$$v_{\text{wire}} = \sqrt{\frac{Y_0}{\rho}} \qquad \text{where} \qquad Y_0 = \mu \frac{(3\lambda + 2\mu)}{\lambda + \mu} \tag{15.2}$$

For materials for which μ is small (rubber for example) Young's modulus is equal to 3μ.

The loss mechanisms that have been observed to cause loss in solids are thermal conductivity, thermoelastic relaxation, thermal or mechanical relaxation, plastic flow, elastic hysteresis and scattering. The thermo-

[5] Mason, W. P. and H. J. McSkimin, *J.A.S.A.*, Vol. 19, No. 3, pp. 464–474. May, 1947.

[6] Firestone, F. A., "The Supersonic Reflectoscope," *J.A.S.A.*, Vol. 17, p. 287, Jan., 1946; Firestone, F. A. and J. R. Frederick, "Polarized Sound," *J.A.S.A.*, Vol. 18, No. 1, p. 200, July, 1946.

elastic relaxation loss, which was first pointed out by Zener,[7] arises from the flow of heat from a hotter part of the medium to a cooler part. In this respect it is similar to the thermal losses discussed in Appendix A-7 but the losses are made much larger due to the polycrystalline nature of a metal. The Q due to this source has been shown to be[8]

$$\frac{1}{Q} = \left(\frac{C_p - C_v}{C_v}\right) R \frac{f_0 f}{f_0^2 + f^2} \tag{15.3}$$

where R is that fraction of the total strain energy which is associated with fluctuation in dilations. The relaxation frequency, f_0, is given approximately by

$$f_0 \doteq \frac{D}{L_c^2} \tag{15.4}$$

where D is the thermal diffusion constant and L_c is the mean diameter of the crystallites. R, the fluctuation constant, can be evaluated from the average variation of the elastic constant for the individual crystals, as discussed in section 15.33. Equation (15.5) shows values of the factor $(C_p - C_v)/C_v$, (C_p = specific heat at constant stress, C_v = specific heat at constant strain) and R for various metals.

	Metal						
	Pb	Ag	Cu	Au	Fe	Al	W
R	0.065	0.031	0.031	0.014	0.022	0.0009	10^{-6}
$(C_p-C_v)/C_v$	0.067	0.040	0.028	0.038	0.016	0.046	0.006
Product	4.4×10^{-3}	1.2×10^{-3}	8.7×10^{-4}	5.3×10^{-4}	3.5×10^{-4}	4×10^{-5}	6×10^{-9}

(15.5)

The last line gives an idea of the relative damping due to this source. The relaxation frequency is usually under 100 kc and the losses produced by this effect are too small to account for the losses measured in the high-frequency range.

The other sources of loss are discussed in more detail in the following sections.

[7] Zener, C., *Phys. Rev.*, Vol. 52, p. 230, 1937.

[8] Zener, C., *Phys. Rev.*, Vol. 53, p. 90, 1938. A complete discussion of thermal diffusion relaxation, grain boundary relaxation, twin boundary diffusion and atomic solution diffusion is given in a recent book "Elasticity and Anelasticity of Metals," C. Zener, Univ. of Chicago Press, 1948. Most of these effects take from seconds to weeks to occur at room temperature and are of interest principally in analyzing the physical processes occurring in metals.

15.1 *Low-Frequency Resonant Measurements*

A very extensive series of measurements of the dissipation in solid materials has been made by Wegel and Walther.[1] They used an electromagnetic drive and measured the dissipation in a frequency range from 2000 cycles to 100,000 cycles. The strain in every case varied from 10^{-8} to 10^{-5} and in this region the Q of the material was independent of ampli-

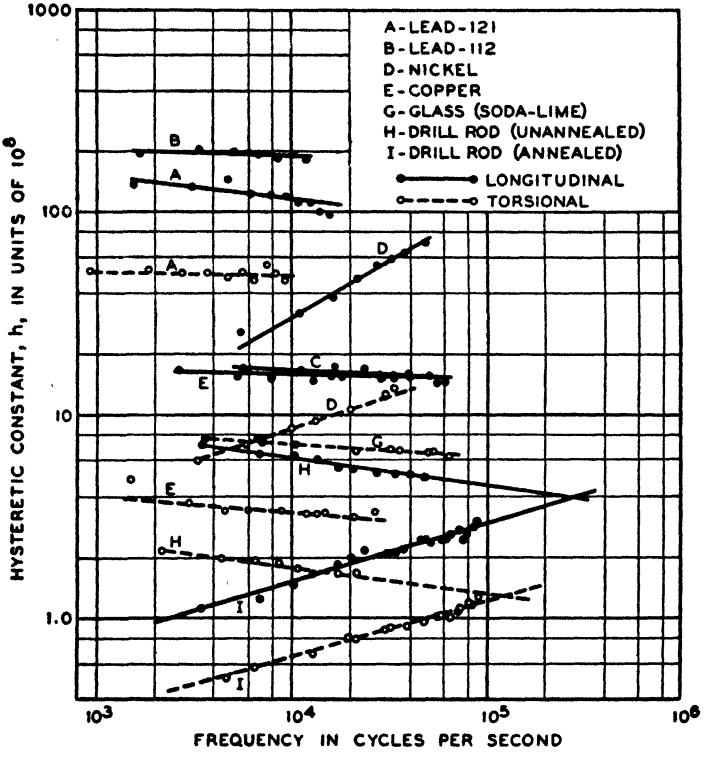

FIG. 15.1. Elastic hysteresis constant for a number of materials.

tude. They found that the Q of the solid materials was nearly independent of the frequency over the range used and concluded that the loss was due to an elastic hysteresis. Figure 15.1 shows a measurement of the elastic hysteresis constant, which is defined as the area in ergs of the stress strain loop for a unit volume per unit of strain squared. As discussed in the Appendix, Section A.7, the Q due to a hysteresis component is

$$Q = Y_0/H \tag{15.6}$$

where Y_0 is the elastic constant of interest, in this case Young's modulus.

According to the measurements of Fig. 15.1, a good share of the solid materials have a Q independent of frequency, and since

$$Q = B/2A \tag{15.7}$$

where B is the phase shift in radians per second per unit length (which is directly proportional to the frequency) and A the attenuation per unit length, then

$$A = B/2Q \tag{15.8}$$

and if Q is independent of the frequency, A is directly proportional to the frequency. As shown in section 15.32, the attenuation of fused quartz is proportional to frequency over a very wide frequency range and gives strong evidence for a hysteresis type of loss. The method of measuring the properties of a bar by attaching it to a crystal and adjusting the length until the combination resonance equals the crystal resonance has been discussed in detail by the writer.[9] It is there shown that the Q of the bar is equal to

$$Q_B = \frac{r}{2\pi f_R C_0 (R' - R)} \left(\frac{M_B}{M_C}\right) \tag{15.9}$$

where f_R is the resonant frequency, C_0 the capacitance of the crystal, r the ratio of capacitances of the crystal alone determined from $r = f_R/2\Delta f$ where Δf is the difference in frequency between the anti-resonant and the resonant frequency, R' is the measured electrical resistance of the combination, R that of the crystal alone, M_B the total mass of the bar and M_C the mass of the crystal. The velocity is determined from the fact that the bar is a known integral number of wavelengths at the resonant frequency and

$$v = f\lambda \tag{15.10}$$

where λ is the wavelength. Using this method the properties of a number of materials have been determined as shown in Table XXVI. The temperature coefficient was measured by observing the change in resonance of the combination with temperature compared to the change of the crystal alone.

For very low Q materials, another method was devised by the writer[9] which consisted in driving with one-half wave crystal and picking up with another. By adjusting the length until the maximum response coincided with that of the two crystals alone, the velocity could be measured and by measuring the transmission loss, the attenuation could be measured.

[9] Mason, W. P., *Electromechanical Transducers and Wave Filters*, D. Van Nostrand Company, Inc., 1942. Second Edition, 1948.

TABLE XXVI

PROPERTIES OF SOLID MATERIALS

Material	Density ρ	Velocity v in *cm per sec.*	Impedance ρv	Q	T_{f_B} in parts per million per °C
Aluminum	2.68	5.13×10^5	13.8×10^5	10,000	−215
Magnesium	1.705	5.10	8.7	5,700	−194
Tungsten Carbide Steel	8.52	4.72	41.0	8,180	−10.5
Molybdenum Steel	8.39	4.70	39.5	4,700	−16.0
Fused Quartz Rod (Milky)	2.2	5.11	11.3	5,000	+5.0
702 Pyrex	2.32	5.35	12.4	1,200	+25.0
Window Glass	2.42	5.44	13.5	910	−58.0
Lead Glass	2.48	5.13	12.8	1,910	+41.0
Micalex	3.34	5.35	17.9	2,890	−74.0
Ceramics	2.47 to 3.38	4.55 to 6.78	11.5 to 18.4	700 to 5,000	−45 to −215

When this method was applied to a number of plastics, it appeared that they were showing thermal or mechanical relaxation similar to that observed in polyisobutylene.

15.2 *Measurement of the Properties of Solid Materials by Means of Ultrasonic Waves in Liquids*

Ultrasonic waves in liquids have been used not only to measure the properties of liquids but also for measuring the properties of solids immersed in them. An example has already been given of the use of a plastic lens for focusing a sound beam in a liquid. From the radius of curvature of the lens, the velocity of sound in the liquid, and the distance of the point of focus from the lens, the velocity of propagation of sound waves in the plastic can be determined. By observing the change in the color index in going through a thin piece of plastic, the transmission loss can be determined.

Two other methods of measurement have also been used. One is an acoustic interferometer, in which a flat piece of rubber or plastic takes the place of the same thickness of water. By the change in the position of the resonance curve, the velocity of propagation of the sample can be determined. This method works well only when the normal impedance of the rubber does not differ much from that of the liquid, which is usually water. The second method consists in measuring the normal loss and the loss at

various angles through a sheet of solid material. From these transmission properties, the elastic constants and their associated dissipation can be calculated.

15.21 *Interferometer Measurements of the Velocities of Rubber*

If one measures the Young's modulus of a piece of rubber by stretching it, one obtains a value in the order of 10^7 dynes per square centimeter. If, however, one compresses the rubber by a hydrostatic pressure, a much higher elastic constant is obtained; in fact, it is of the same order of the modulus of compressibility for water, namely, 2.25×10^{10} dynes per square centimeter. The reason for this large difference is that the shearing modulus μ for rubber is very low while the dilation modulus λ is quite high. In this respect rubber is somewhat similar to a liquid which has a high value of λ and a zero value of μ at low frequencies. For this reason rubber has received some use as a medium for carrying sound waves from one liquid medium to another, for example, from castor oil to sea water, as used in some underwater transducers.

In order to measure the velocity of transmission of dilational waves in rubber, one of the simplest methods is to use an acoustic interferometer and to replace a certain thickness of the water path with the thickness of rubber. If the velocity in the rubber is the same as that in the liquid, usually water, the positions of the current maxima and minima will be unchanged. If the velocity in the rubber is higher than that in the liquid, the position of successive maxima and minima will be displaced in the direction of larger settings on the interferometer and the velocity is given by

$$v_R = \frac{tv}{t - d} \tag{15.11}$$

where v_R is the velocity in the rubber, t the thickness of the rubber, v the velocity in the liquid and d the displacement of the peaks from the position they occupied when the rubber was absent. When the velocity in the rubber is lower than that in water, the position of the peaks are displaced toward lower readings by a displacement d, and the velocity in the rubber is given by

$$v_R = \frac{tv}{t + d} \tag{15.12}$$

An example for a rubber measured for a low frequency is shown by Fig. 15.2.

A number of natural and synthetic rubbers were measured at a frequency of 1 megacycle in this way with the results shown by Table XXVII. All measurements were made at 25°C. The density and the impedance — product of ρv — per square centimeter are also shown.

TABLE XXVII

Type of Rubber	Velocity v at 1000 kc *cm/sec*	Density ρ grams per *cubic cm.*	Impedance ρv mechanical ohms *sq. cm.*
Gum rubber, Specimen No. 488–8	1.546×10^5	0.95	1.469×10^5
Butyl rubber, Specimen No. 488–3	1.83×10^5	1.065	1.95×10^5
Neoprene 1LS, Specimen No. 488–5	1.60×10^5	1.33	2.13×10^5
Hicar 488–2	2.04×10^5	1.14	2.32×10^5
Butyl rubber No. 488–6	1.630×10^5	0.96	1.565×10^5
Soft rubber No. 488–1	1.47×10^5	1.04	1.53×10^5
Soft rubber No. 2076–B	1.485×10^5	1.07	1.592×10^5

All of these measurements have been made at a relatively high frequency (1 megacycle), whereas these rubbers are usually used at considerably lower frequencies. The question arises as to whether the

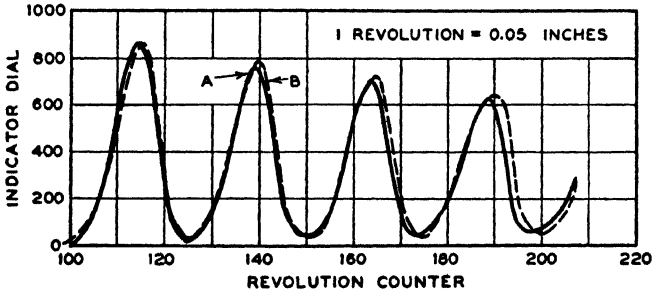

FIG. 15.2. Interferometer curves for water and water rubber path.

properties measured at high frequencies will also be the ones that are operative for lower frequencies. To settle these questions some work has been done in measuring the velocities for rubbers at frequencies around 25 kilocycles. For this purpose the usual type of interferometer cannot be used, because the transducer would have to be 40 times the diameter of the one used at one megacycle (1 inch) in order to obtain the same directivity and freedom from container resonances.

This problem was solved by using the " binomial " type hydrophone discussed in the book, *Electromechanical Transducers and Wave Filters*,

second edition in section 4.71 and the damped measuring tank discussed in section 4.31. This combination together with the interferometer used is shown by Fig. 15.3. The moving platform has a diameter of 8 inches and is moved relative to the hydrophone with a screw having an advance of 0.05 inches per revolution.

A typical current-distance curve for water alone is shown by the full line of Fig. 15.2. From this curve the velocity of propagation in the water

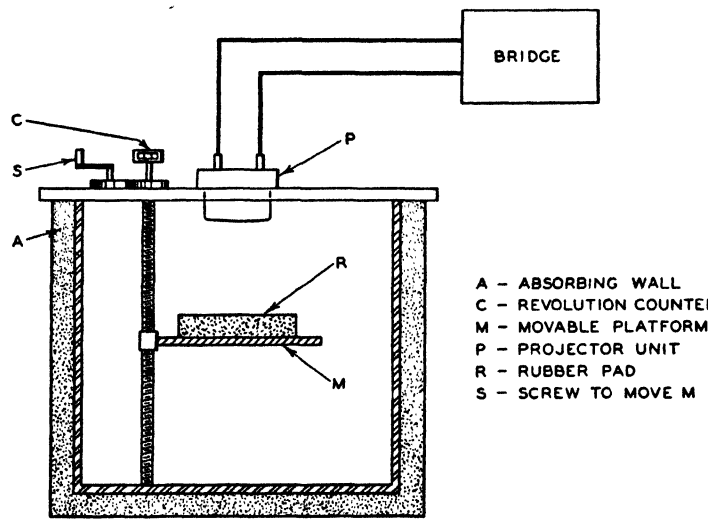

FIG. 15.3. Low frequency interferometer and measuring tank.

at 25°C is 1.54×10^5 centimeters per second. This is somewhat higher than the distilled water curve of Fig. 14.5, but since tap water with several per cent of dissolved salt was used, this increase is not surprising. The dotted curve shows the change occurring when one inch of Goodrich "ρc" gum rubber was substituted for the water. The peaks are displaced an average of about 1 revolution or .05 inches. Hence the velocity of the rubber was

$$v_R = \frac{1.54 \times 10^5 \times 1.0}{1 - .05} = 1.6 \times 10^5 \text{ cm/sec}$$

Fig. 15.4 shows a measurement of several specimens over a temperature range at a frequency of 24.5 kilocycles. All of the specimens had natural crepe rubber as the base, but specimen 163-3 and 163-4 had 50 and 100 parts of atomite respectively to 100 parts of crepe rubber. This resulted in a lowering of the velocities. Specimen 163-5 and 163-6 each had 110

parts of zinc oxide to 100 parts of crepe rubber, which lowered the velocities still farther. The densities of these samples were respectively

$$\rho c = 1.0; \quad \text{M-163} = 0.98; \quad \text{M-163-3} = 1.22;$$
$$\text{M-163-4} = 1.40; \quad \text{M-163-5 and -6} = 1.62.$$

All of these rubbers showed an increasing velocity at the lower temperatures. Specimen M-163 was the same as specimen 488-8 of Table XXVII so that there is no indication for this rubber of a change of velocity with frequency.

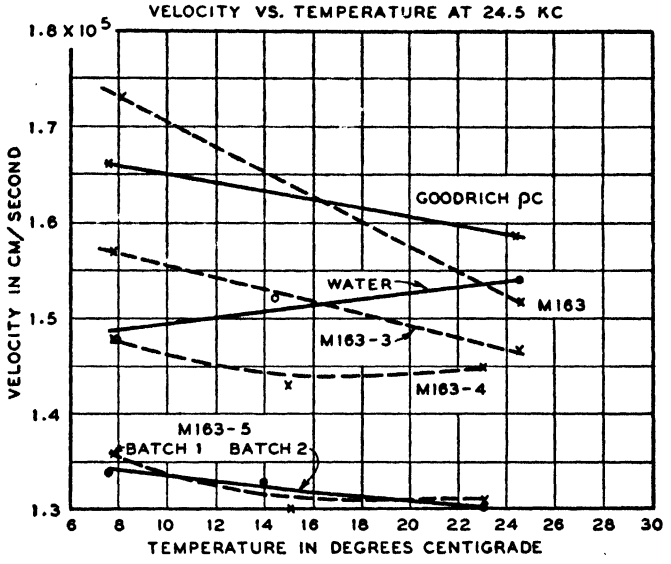

FIG. 15.4. Measurement of several rubbers over a temperature range.

15.22 *Measurement of the Properties of a Solid by Measuring the Transmission Loss through a Solid at Various Angles of Incidence*

When the velocity of propagation of a solid differs materially from that of the liquid in which it is immersed, the interferometer method cannot be used, for the reflections from the front of the specimen interfere with the standing-wave system from the back and prevent the location of the standing-wave system for the reflector. For such materials, however, another method is available, which was first devised by Bär and Walti.[4] This method consists in measuring the transmission loss through a sheet of the material as a function of the angle of incidence. Bär and Walti used the method in connection with a Debye-Sears cell of the type shown by Fig. 14.3 and hence were limited to frequencies above one megacycle. By using a damped measuring tank and hydrophones, the writer has applied

the method to frequencies as low as 20 kilocycles. A series of measurements on plastics has been made by this method.

Numerically this method depends on a theoretical solution obtained by Reissner[10] of the transmission of a sound wave through a plane sheet of a solid material from a liquid medium on one side to a liquid medium on the other side. The sheet may be at any angle θ with the incident sound wave. When a sound wave strikes a solid material at an angle θ, the wave is partly reflected and partly transformed into dilational and shear waves in the solid. These in turn are partly reflected in the solid and partly transmitted in the form of dilational waves to the liquid beyond. Reissner has shown that the transmission ratio T, *i.e.*, the ratio of the sound transmitted with the solid in the path to the sound transmitted with the solid removed, is given by the equation

$$T = \frac{4N^2}{(M^2 - N^2 - 1)^2 + 4M^2} \tag{15.13}$$

where

$$N = \frac{\rho \cos\theta}{\rho_1 v_1}\left[\frac{v_d \cos^2 2\theta_r}{\cos\theta_d \sin\varphi} + \frac{v_r \sin^2 2\theta_r}{\cos\theta_r \sin\psi}\right]$$

$$M = \frac{\rho \cos\theta}{\rho_1 v_1}\left[\frac{v_d \cos^2 2\theta_r}{\cos\theta_d \tan\varphi} + \frac{v_r \sin^2 2\theta_r}{\cos\theta_r \tan\psi}\right]$$

In the equation ρ = density of the plate; ρ_1 = density of liquid medium; v_1 = velocity of wave in the liquid medium; $v_d = \sqrt{\dfrac{\lambda + 2\mu}{\rho}}$ velocity of dilational wave in the plate; $v_r = \sqrt{\dfrac{\mu}{\rho}}$ = velocity of shear wave in the plate; θ = angle of incidence of the wave in the medium with regard to the plate normal. θ_d and θ_r are respectively the angles of refraction of the dilational and shear waves in the plate. These are determined by the usual formulae

$$\begin{aligned} \sin\theta_d &= \frac{v_d}{v_1}\sin\theta; \qquad \cos\theta_d = \sqrt{1 - \frac{v_d^2}{v_1^2}\sin^2\theta}\,; \\ \sin\theta_r &= \frac{v_r}{v_1}\sin\theta; \qquad \cos\theta_r = \sqrt{1 - \frac{v_r^2}{v_1^2}\sin^2\theta} \end{aligned} \tag{15.14}$$

As long as $(v_d/v_1)\sin\theta$ is less than unity, θ_d has real values; but when this quantity is greater than unity, θ_d is imaginary and the expression for $\cos\theta_d$ becomes

$$\cos\theta_d \sim j\cosh\theta_d \tag{15.15}$$

[10] Reissner, H., *Helv. Phys. Acta*, Vol., 7, p. 140, 1938.

φ and ψ in equation (15.13) are

$$\varphi = \frac{\omega d}{v_d} \cos \theta_d; \qquad \psi = \frac{\omega d}{v_r} \cos \theta_r \tag{15.16}$$

where d is the thickness of the plate. This equation has been derived assuming no dissipation in the plate.

Several limiting cases are of interest. When the shear velocity approaches zero, the value of the transmission reduces to the well-known equations familiar from light waves or transmission through a liquid layer

$$T = \frac{1}{1 + \frac{1}{4}\left(\frac{\rho_1 v_1 \cos \theta_d}{\rho v_d \cos \theta} - \frac{\rho v_d \cos \theta}{\rho_1 v_1 \cos \theta_d}\right)^2 \sin^2 \left(\frac{\omega d}{v_d} \cos \theta_d\right)} \tag{15.17}$$

This equation is applicable to the transmission through a sheet of rubber, for example, that has a very low shear velocity. An example is shown by Fig. 15.6.

Another limiting case of interest is the transmission at normal incidence. For this case $\theta = 0$ and

$$T = \frac{1}{1 + \frac{1}{4}\left(\frac{\rho_1 v_1}{\rho v_d} - \frac{\rho v_d}{\rho_1 v_1}\right)^2 \sin^2 \frac{\omega d}{v_d}} \tag{15.18}$$

Hence at every odd quarter wavelength of the dilational velocity v_d, an increased loss will occur. If the ratio $\rho v_d / \rho_1 v_1$ is large, a pronounced dip in the transmission occurs and Walti[4] has applied this method to measuring the velocity of a dilation wave in glasses. For plastics and rubber, however, the ratio is small and there are large losses at high frequencies so that no appreciable dips occur. Fig. 15.5 shows a measurement of the transmission T for a number of rubbers and plastics in the frequency range from 500 kilocycles to 3.5 megacycles. The loss is plotted as the number of db loss per centimeter as a function of frequency. In all cases no attenuation dips occur at the odd quarter wavelengths. The losses in plastics and rubbers are considerably higher than those occurring in metals, glasses, fused quartz and other solid bodies. The plastic having the least loss at high frequencies appears to be polystyrene. The presence of the square law terms in frequency probably indicate a relaxation phenomena.

When the transmission of a rubber or a plastic is measured at an angle to the acoustic wave, results similar to those shown by Fig. 15.6 are obtained. The dotted curve shows the transmission through a half-inch sheet of Hicar rubber, while the solid line shows the transmission through a half-inch sheet of lucite. The frequency for the rubber was 29.5 kilocycles, while that for the lucite was 20 kilocycles. The lucite shows a very sharp

dip at an angle of 44.5° from normal, while the rubber shows a gradual falling off with angle. From Table XXVII, the velocity and density of

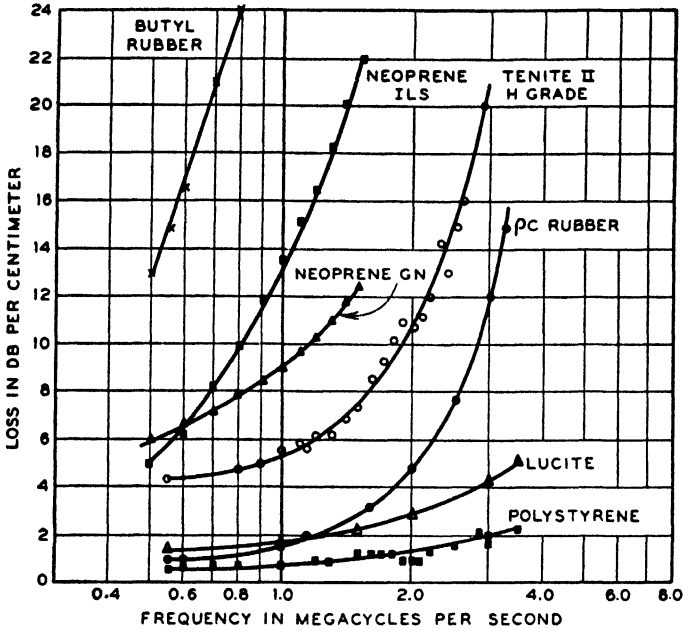

FIG. 15.5. Normal loss for rubbers and plastics.

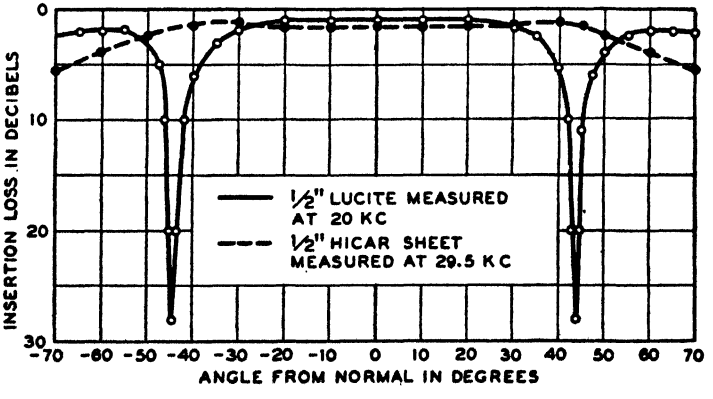

FIG. 15.6. Transmission at an angle through a rubber and a plastic.

Hicar rubber are 2.04×10^5 centimeters per second and 1.14 grams per cubic centimeter respectively. Inserting these values in equation (15.17),

the theoretical curve is obtained as shown by the dotted line of Fig. 15.7. This agrees well with the experimental value of Fig. 15.6.

The sharp dip in the transmission through the lucite is accounted for by equation (15.13); for at some angle obtained by setting $N = 0$, the dilation and shear waves react in such a manner as to cancel each other on the second surface and no wave is sent into the liquid. If the thickness of the plate is less than a half wavelength, this zero transmission angle occurs just beyond the critical angle θ_c for dilational waves. Figure 15.7 shows

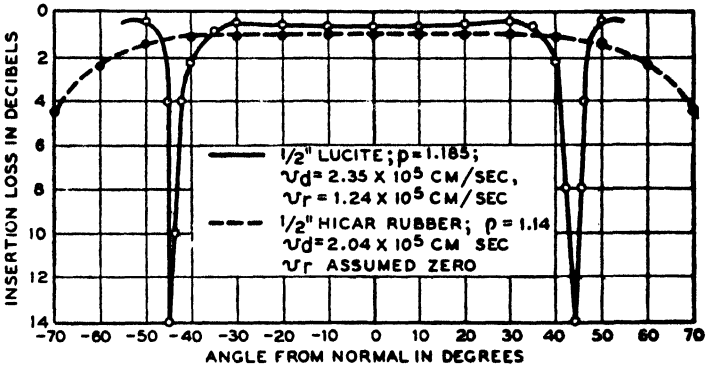

FIG. 15.7. Theoretical curve for transmission at an angle.

a plot of equation (15.13) for various angles of θ, when the frequency is 20,000 cycles, the thickness d is 1.27 centimeters and the velocities v_d, v_r and v_1 are taken as

$$v_d = 2.30 \times 10^5 \text{ cm/sec}; \qquad v_r = 1.24 \times 10^5 \text{ cm/sec};$$
$$v_1 = 1.49 \times 10^5 \text{ cm/sec} \tag{15.19}$$

Figure 15.7 shows that at 44.5° a very sharp dip occurs in the transmission. This angle is 4° above the critical angle for the dilational wave, given by

$$\sin \theta_c = \frac{v_1}{v_d} = \frac{1.49}{2.30} = .65; \qquad \theta_c = 40.5° \tag{15.20}$$

The values of v_d and v_r agree with this measurement and the value of Young's modulus measured separately, which was 4.75×10^{10} dynes per square centimeter. In fact, measurements of the angle of zero transmission and the value of Young's modulus provide enough data to calculate the two elastic constants λ and μ.

An examination of the expression obtained by setting N equal to zero

shows that

$$\frac{v_d}{v_r} = -\frac{\tan^2 2\theta_r \cos\theta_d \sin\left(\frac{\omega d}{v_d}\cos\theta_d\right)}{\cos\theta_r \sin\left(\frac{\omega d}{v_r}\cos\theta_r\right)} \tag{15.21}$$

Now, if v_d is larger than v_r, as is usually the case, and the thickness d is less than half a wavelength, then the only way the expression on the right can become negative is for θ_d to be imaginary or the angle θ to be larger than the critical angle for dilational waves. Under these conditions $\tan^2 2\theta_r$ is usually large and $\sin\left(\frac{\omega d}{v_1}\cos\theta_d\right)$ will be small. Replacing the sine by the angle, equation (15.21) becomes

$$\frac{v_d}{v_r} = -\frac{\tan^2 2\theta_r \frac{\omega d}{v_d}\cos^2\theta_d}{\cos\theta_r \sin\left(\frac{\omega d}{v_r}\cos\theta_r\right)} = \frac{\tan^2 2\theta_r \frac{\omega d}{v_d}\left(\frac{v_d^2}{v_1^2}\sin^2\theta - 1\right)}{\cos\theta_r \sin\left(\frac{\omega d}{v_r}\cos\theta_r\right)} \tag{15.22}$$

and this equation will be satisfied when θ is slightly larger than the critical angle θ_c.

15.23 *Ultra High-Frequency Measurements*

For very high-frequency measurements, the Debye-Sears type of optical cell provides a very simple method for measuring the properties of solids. Angles of transmission and reflection provide methods for evaluating the elastic constants, as discussed in the last section. A simple method for measuring the dilational velocity for a plastic is to form a lens and measure the distance of focus, as illustrated by Fig. 14.4. Using this method, G. W. Willard measured the velocities at 10 megacycles of the following plastics as shown by Table XXVIII. The lenses were cylindrical lenses, flat on one side and having a radius of curvature of 0.634 centimeter. The velocity in the plastic can be calculated from the formula

$$v_p = \frac{v_w}{1 - \frac{r}{d}} = \frac{1.5 \times 10^5}{1 - \frac{r}{d}} \tag{15.23}$$

where r is the radius of curvature of the lens, d the distance of focus and v_w the velocity of sound in water. All these plastics show a considerable dispersion of sound velocity with frequency and end up with a considerably higher velocity at 10 megacycles than they had at low frequencies. These

measurements agree with the attenuation measurements of Fig. 15.5 in showing the presence of a thermal or mechanical relaxation phenomena.

TABLE XXVIII

Material	d in *cm.*	Velocity of wave in plastic (*cm/sec*)
Lucite	1.48	2.64×10^5
Plioform	1.8	2.305
Polystyrene	1.75	2.35
Cellulose Acetate	1.67	2.405
Benzol Cellulose	1.58	2.495

15.3 *Pulse Methods for Measuring the Properties of Solids and for Locating Flaws in Materials*

During the last few years pulse methods and high-frequency attenuation methods have been widely applied in measuring the properties of liquids[11] and in locating flaws in metal castings and other solid bodies.[6] For liquids the method is described in Chapter XIV.

A similar method has recently been used by H. J. McSkimin and the writer[12] in determining the properties of solids by means of the technique of sending and receiving longitudinal and shear wave pulses. Although no very exact mathematical solutions have been obtained for the transmission of waves in finite solids, experimentally it has been found that a good replica of a longitudinal wave is obtained through a solid rod if the diameter is many wavelengths, the pulse traveling with the velocity for a free medium, namely

$$v_d = \sqrt{\frac{\lambda + 2\mu}{\rho}} \tag{15.24}$$

where λ and μ are the Lamé elastic constants of the solid and ρ the density. This main pulse is often followed by a series of pulses which are replicas of the main pulse of smaller amplitude and delayed in time by amounts that are proportional to the radius of the rod. It has been shown that these delayed pulses are due to the incident dilational wave, which travels nearly parallel to the rod surface, being reflected from the surface and breaking up into a reflected dilational wave and a generated shear wave

[11] Galt, J. K. and J. R. Pellam, "A Method of Measuring the Velocity and Absorption of Sound Waves in Liquids," *J.A.S.A.*, Vol. 18, No. 1, p. 251, July, 1946; *J. Chem. Phys.*, Vol. 14, No. 10, Oct., 1946.

[12] Mason, W. P. and H. J. McSkimin, "Attenuation and Scattering of High Frequency Sound Waves in Metals and Glasses," *J.A.S.A.*, April, 1947.

which makes a considerable angle with the periphery of the rod. This shear wave strikes the opposite side of the rod and is partially converted back into a dilational wave which proceeds with the dilational velocity. It will be delayed by an amount which depends on the diameter of the rod and the ratio of shear and dilational velocities. If, however, the diameter of the rod is a large number of wavelengths, these accompanying pulses are small compared to the main pulse and a measurement of the relative amplitudes of the main pulse as a function of distance can be used to determine the attenuation existing in the metal. By using a shear crystal to generate a shear wave in the rod, the velocity and attenuation of shear waves can be measured. These waves are not accompanied by the phenomenon of trailing pulses, since the shear waves, being nearly parallel to the surface, are incident on the side walls with angles greater than the critical angles for longitudinal waves. Hence, the properties of the solid are more easily measured with shear waves than with longitudinal.

15.31 *Experimental Methods*

In measuring the attenuation and velocity of a solid material, a rod of material several feet long is used, as straight as possible and surfaced off square on the ends in a lathe so that either X-cut and Y- or rotated Y'-cuts (AT and BT) quartz crystals can be attached to the surface. X-cut crystals are used for longitudinal waves and Y'-cuts for shear waves. Since the rod acts as a wave guide and will conduct a wave around a very small bend, the rod does not have to be accurately straight. For attenuation and velocity measurements, the crystals can be attached to the rod by such waxes as halowax or beeswax, which have a relatively high shear and longitudinal stiffness for a wax, although low compared to a crystal or metal. This small layer of low-stiffness material results in reducing the frequency range over which energy can be transferred from the crystal to the solid.

By using the equivalent circuit of the crystal, the loss of energy has been calculated in transferring from an electrical circuit of the most favorable impedance to the mechanical impedance of an aluminum bar when the crystal and bar are coupled with layers of wax of various stiffnesses. These losses expressed in db and plotted as a function of frequency are shown by Fig. 15.8. For a very stiff connection the loss is plotted by the solid line. The loss is least at the half-wave frequency of the crystal alone and amounts to about 14 db for either longitudinal or shear waves. Over quite a wide frequency range the loss does not change much. The effect of the compliance of the wax between the crystal and the bar is shown by the dashed and dot-dashed line of Fig. 15.8. As the ratio of the wax compliance to the crystal compliance gets larger, the device acts as a

transforming band-pass filter and increases the efficiency of conversion over a narrow frequency range just above the resonant frequency of the crystal. Since this characteristic occurs both at the input and output, the transmitted band is limited to about 10 per cent of the carrier frequency. This sets the minimum pulse length that can be employed, for the pulse will not build up to its full amplitude unless the length in seconds is as large as the inverse of the band width in cycles or approximately

$$\text{P.L.} \geqq \frac{1.2}{\text{B.W. in cycles}} \tag{15.25}$$

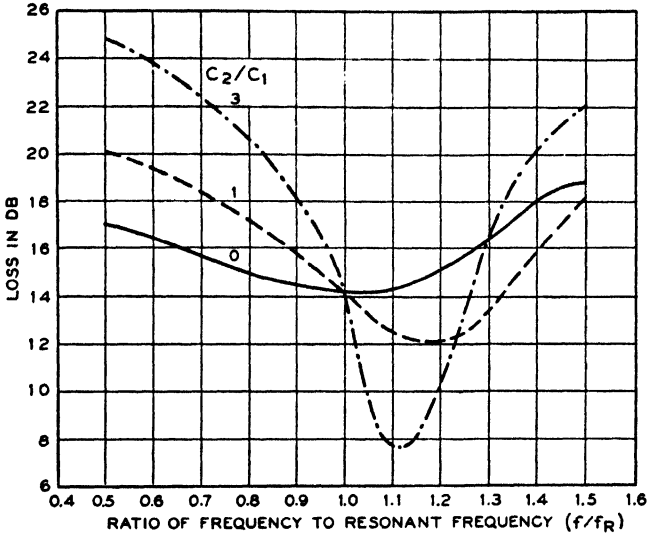

FIG. 15.8. Loss caused by inserting wax layers between crystal and rod. Numbers indicate the ratio of crystal stiffness to wax stiffness.

where 1.2 is an empirical constant and the band width, B.W., is determined by the frequency difference of the two band edges 3 db down from the maximum efficiency point. For a carrier of 3 megacycles, the pulse length had to be at least 4 microseconds in order to give a full amplitude.

The experimental arrangement is shown schematically in Fig. 15.9. A variable-frequency oscillator is the source of the carrier frequency. This is sent through a wide-band tuned amplifier that impressses about 10 volts at 100 ohms across the crystal. The bias on the input tube of the amplifier is controlled by the pulser. Normally a high negative bias is on the grid of the amplifier tube, and the pulser puts on a positive bias of a value to overcome the negative bias and allows the amplifier to amplify for the time duration that the biasing pulse is on. The firing of the pulse is controlled

by a sinusoidal wave of frequency from several hundred to 5,000 cycles, and this timing wave also controls the sweep circuit of the cathode-ray oscilloscope. The pulser is one of conventional design and puts a square-top pulse of positive voltage on the two balanced input tubes of the amplifier that are connected in push-pull arrangement. The DC pulse is then balanced out in the input and does not affect the succeeding tubes. The carrier frequency on the other hand is inserted on the suppressor grid of one of the tubes and is not balanced out in the output. When the grid is negative, the carrier output of the tube is neutralized and no steady-state output appears in the amplifier. When a gating pulse is impressed on the input, a pulse of alternating current of controllable time duration is impressed on the sending crystal.

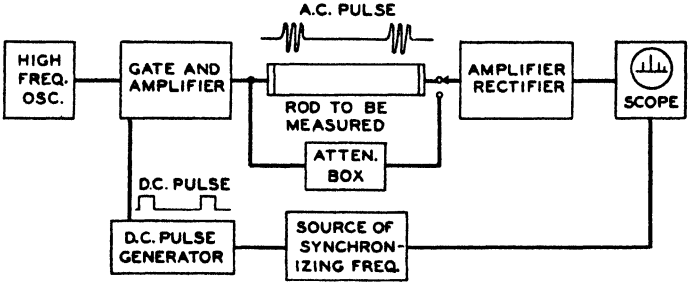

FIG. 15.9. Experimental arrangement for measuring losses.

The receiving crystal is terminated in a 100-ohm resistance and capacitance-annulling coil which are connected across the input of a wide-band untuned amplifier. This amplifier is terminated in a diode detector and the rectified output is impressed across the vertical plates of the cathode-ray oscilloscope. Since the horizontal sweep is controlled by the same sinusoidal wave that controls the pulses, the received pulse and reflected pulses appear in the same position on the cathode-ray tube for successive pulses and form a picture in time of the received pulse and its reflections. The position of the transmitted pulse can also be marked by establishing a slight coupling with the transmitting amplifier.

The method of measuring attenuation is as follows: the frequency of the pulse is set at the natural resonant frequency of the crystal alone and a pulse is used that is long enough to establish steady-state conditions. Hence as seen from Fig. 15.8, this effectively results in sending a single side band, the input of the pulse may be somewhat distorted, but the steady-state conditions correspond nearly to the steady-state output that would result if the carrier frequency were at the exact resonant frequency of the crystal. Furthermore, the reflections obtained at this frequency are

nearly perfect, because the termination impedance at the resonant frequency is effectively zero, since the mass and compliance of the crystal annul each other at this frequency. If the frequency had been set at the frequency of maximum conversion, the reflections would have been far from perfect on account of the transforming action of the wax joint. In order to evaluate the losses occurring in the wax joints, several lengths of rod were used, for example, 1.5 inches and 1 foot. By comparing the received pulses for a given total path length, the loss per reflection can be evaluated. For longitudinal waves this loss was quite small; for example, .07 db per reflection at 7.5 megacycles, but for shear waves it might amount to 0.5 db per reflection at 5 megacycles and had to be considered.

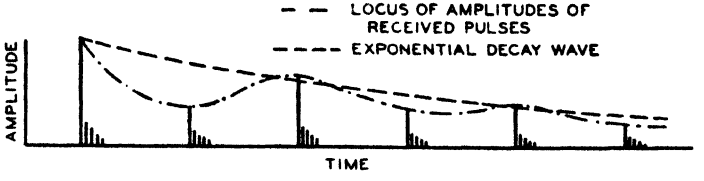

FIG. 15.10. Typical series of pulses for a longitudinal wave.

A typical series of received pulses for an aluminum rod 1 inch in diameter for a longitudinal wave, is shown in Fig. 15.10. The frequency of this pulse is 5 megacycles. The trailing pulses are of rather small magnitude but become larger with respect to the main pulse for greater distances. This figure shows another feature of the successive pulses, namely, that for a full electrode over both crystals; the successive pulses do not decrease exponentially but show an interference pattern between two or more normal modes, which causes successive pulses to first become smaller then larger as the phases between normal modes cause a cancellation or addition. This effect can be minimized by using electrodes of somewhat smaller diameter than the rod, or by shaping the back electrode of the crystal so that an air gap is produced between the crystal and electrode which becomes larger near the edges. This produces an approximation to a Bessel's function vanishing near the edge, which is the first normal mode for the rod.

With this arrangement the reflections are exponential and the trailing pulses are small enough to contain only a small portion of the total energy, and hence fairly accurate measurements can be made for frequencies above 5 megacycles for a rod 1 inch in diameter. The attenuation is measured by determining the number of db that has to be inserted in the db box, to make the height of the first received pulse equal to that for the first or higher order reflections. By comparing the db for successive reflected

pulses, the truth of the exponential law can be tested. By taking rods of different length, the loss due to the wax joints can be evaluated and deducted from the overall loss. The velocity of propagation can be measured by using a timing wave and measuring the time by which successive reflections are delayed with respect to each other. For a moderately long delay a very accurate method is to control the pulsing rate until two successive reflections are made to coincide on the scope pattern. For example, for a 2-foot aluminum rod, reflections were made to coincide when the pulsing rate was 5,184 cycles. The velocity was then

$$v = f \times l = 5{,}184 \times 2 \times (24 \times 2.54) = 6.32 \times 10^5 \text{ cm/sec} \qquad (15.26)$$

since the time between successive reflections is the time to travel twice the length of the rod.

Another method for measuring longitudinal waves in metals that has recently been employed by Roth[13] is to immerse the metal rod on one end in a water bath. The crystal generates a wave in the water, which in turn generates a longitudinal wave in the rod. A series of reflections is picked up by the receiving crystal due to the metal-water interface reflections and due to the reflections in the metal rod. By changing the water path, the reflections from the water and the reflections in the metal are easily separated and the series due to reflections within the metal can be determined. This series has to be corrected for the loss caused by the energy transmitted into the water, but this loss can be evaluated by calculations or by immersing the free end in a water bath. For aluminum this loss was 1.5 db per reflection. With this correction the attenuation in the metal can be evaluated. Losses by this method have been compared with those obtained by the wax-joint method described above and they come out quite accurately the same. The water-bath method is probably superior for very high frequencies but is limited to longitudinal waves.

For very high frequencies it is difficult to transmit shear waves through a wax joint. To get around this difficulty use is made of the fact (as discussed in Chapter XIV) that very viscous liquids have a shear elasticity. Since by heating the liquid and pressing the crystal on the metal surface a very thin layer of liquid can be obtained and the losses through such a joint are considerably less than through a wax joint. The liquid principally used for this purpose is polyisobutylene (polymer *D* of Chapter XIV having a molecular weight of 5,600). Measurements in the range from 20 to 100 kilocycles indicated that this liquid had a shear elasticity of about 4×10^7 dynes per square centimeter at room temperature. Some further measurements were made in the range from 10 to 53 megacycles by observing on a

[13] Roth, W., Quarterly Progress Report, Research Laboratory of Electronics, M.I.T., Oct. 15, 1947.

series of shear wave pulses in fused quartz the effect of terminating the rod in a layer of polyisobutylene. The result was uniformly to cause an added loss of 1.10 db per pulse and this was found to increase slightly with frequency from 10 to 53 megacycles. Water or any of the light liquids tried had no observable effect, showing that their shear viscosities had not been relaxed up to this frequency. Since the reflection coefficient goes from 0 to 1.10 db, the impedance of the liquid is

$$Z_L = \left(\frac{1 - .875}{1 + .875}\right) Z_Q = 5.4 \times 10^4 \text{ mechanical ohms per cm}^2$$

since Z_Q, the impedance of fused quartz, is $2.24 \times 3.76 \times 10^5 = 8.30 \times 10^5$ ohms per square centimeter. Since the density of polyisobutylene is 0.892, this corresponds to a shear elasticity of

$$\mu = 3.26 \times 10^9 \text{ dynes/cm}^2$$

at 10 megacycles, which is about 100 times as large as the value measured at 100 kilocycles for the same temperature. This confirms the existence of a composite motion and two potential barriers, as discussed in section 14.31. Using a thin layer of polyisobutylene, the junction loss up to 50 megacycles is very small.

This method for measuring the shear impedance of liquids has recently[14] been increased in sensitivity by using a fused quartz rod for which the shear wave strikes the reflecting surface at an angle from the normal of about 80 degrees. For this rod the crystals are lined up so that all the motion of the shear wave is tangential to the surface. The increased area, proportional to $1/\cos\theta$, where $\theta = 80°$, results in greatly increasing the reflection loss and reflection phase at the boundary and gives a more sensitive measure of the shear impedance. The resistance and reactance terms can be measured by using two identical rods, together with phase and attenuation shifters, and balancing out the two pulses from the rods. The procedure is to balance the pulse out when no liquid is on the surface, then introducing a liquid to rebalance in phase and amplitude until the pulse again disappears. This can be accomplished by using a capacitance and resistance network for phase shifts and changing the gain of the amplifier by using a bias on a suppressor grid. The details are discussed in a recent paper[14] and it is shown there that the shear impedance equals

$$Z_M = R_M + jX_M = \cos\theta Z_Q \left[\frac{1 - R^2 + 2jR\sin\theta}{1 + R^2 + 2R\cos\theta}\right]$$

[14] Mason, W. P., W. O. Baker, H. J. McSkimin, and J. H. Heiss, "Measurement of the Shear Elasticity and Viscosity of Liquids by Means of Ultrasonic Shear Waves," *Phys. Rev.*, Vol. 75, No. 6, pp. 936-946, March 15, 1949.

where R is the loss per reflection, expressed as a current ratio, and θ the phase angle required to rebalance the circuit. When this method was applied to light liquids such as water, the resistance and reactance components were equal to

$$R_M = X_M = \sqrt{\pi f \eta \rho}$$

where η the shear viscosity within the experimental error was equal to the static value. This shows that the enhanced loss for light liquids must be ascribed to a compressional viscosity as discussed in Chapter XIV. However for long chain polymers such as polyisobutylene, the two relaxation frequency ranges are confirmed in detail.

15.32 *Experimental Results*

These experimental methods have been applied in measuring the attenuation and velocities for shear and longitudinal waves for metal rods and for several types of glass rods. The only metals that gave any useful results were aluminum and magnesium. The reason for this, as discussed in the next section, is the large scattering effects in all metals except aluminum, magnesium, and tungsten, which causes the received pulses to be highly distorted and renders any accurate measurements not feasible. For glass rods the losses obtained were quite exactly proportional to the frequency. A glass is usually regarded as a liquid with a very high coefficient of viscosity, in the order of 10^{15} poises. Since the shear elastic constant found is in the order of 3×10^{11} dynes per square centimeter, the data of section 14.3 on shear waves in liquids, show that the relaxation frequency should be about 5×10^{-5} cycles and the loss due to shear viscosity about 10^{-8} nepers per centimeter independent of the frequency. This loss is much too small to observe experimentally at any frequency and hence the loss measured must be due to other sources. Since the losses measured for metals at low frequencies and for glasses at low and high frequencies are proportional to the frequency, it has become customary to ascribe them to an elastic hysteresis, since a hysteresis for a given strain cycle will cause a loss that is directly proportional to the number of cycles per second that the stress strain loop is traversed.

For high frequencies the data on the aluminum rods show another component of the attenuation that increases as the fourth power of the frequency. This has been found to be due to a scattering of energy by the finite grain size of the aluminum grains in the rod. The experimental data for two standard aluminum rods designated 17 S-T are shown for the shear and longitudinal waves by the data of Figs. 15.11 and 15.12. Data on attenuation for longitudinal waves above 5 megacycles should be reliable, while the data for shear waves should be good at all frequencies.

The velocity measurements gave the same result for both rods and for all frequencies, namely

$$v_d = 6.32 \times 10^5 \text{ cm/sec}; \qquad v_s = 3.13 \times 10^5 \text{ cm/sec} \tag{15.27}$$

These agree well with those calculated from the published values[15] of the elastic constants

$$\lambda = 5.44 \times 10^{11} \text{ dynes/cm}^2; \qquad \mu = 2.67 \times 10^{11} \text{ dynes/cm}^2; \qquad \rho = 2.71$$

resulting in

$$v_d = \sqrt{\frac{\lambda + 2\mu}{\rho}} = 6.32 \times 10^5 \text{ cm/sec}; \qquad v_s = \sqrt{\frac{\mu}{\rho}} = 3.14 \times 10^5 \text{ cm/sec}$$

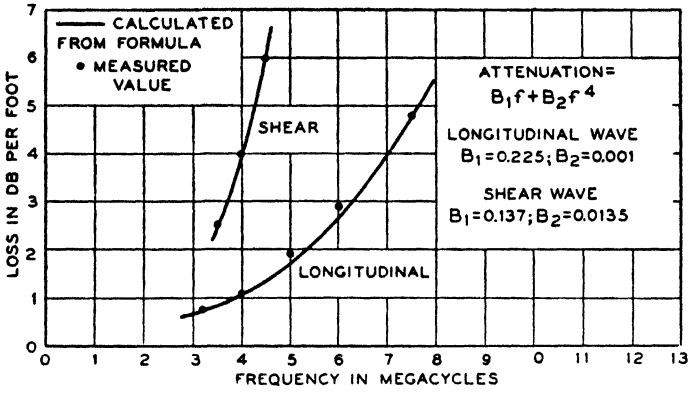

FIG. 15.11. Attenuation measurements for an aluminum rod having a grain size of 0.23 ± .01 mm.

These average elastic constants also agree reasonably well with the values[16] obtained for the aluminum single crystal. This is a face-centered cubic crystal which has the elastic constants

$$c_{11} = 10.76 \times 10^{11} \text{ dynes/cm}^2; \qquad c_{12} = 6.18 \times 10^{11};$$
$$c_{44} = 2.84 \times 10^{11} \tag{15.28}$$

To obtain the average elastic constant for longitudinal or shear motion, one should theoretically solve the cubic equation (6.14) for all possible orientations and average, considering every direction as equally probable. This is a very considerable problem and moreover would not give an exact result, for it neglects the effects of the grain boundary layers which have

[15] Kaye and Labe, *Physical and Chemical Constants*, p. 29, Longmans, Green & Co.

[16] Goens, E., "Elastic Constants for Aluminum Single Crystals," *Ann. d. Physik*, Vol. 17, p. 233, 1933.

recently been shown to act as a viscous medium.[17] An approximate method which should agree quite closely with the cubic equation method if the degree of anisotropy is not too large, is to average the constants c'_{11}

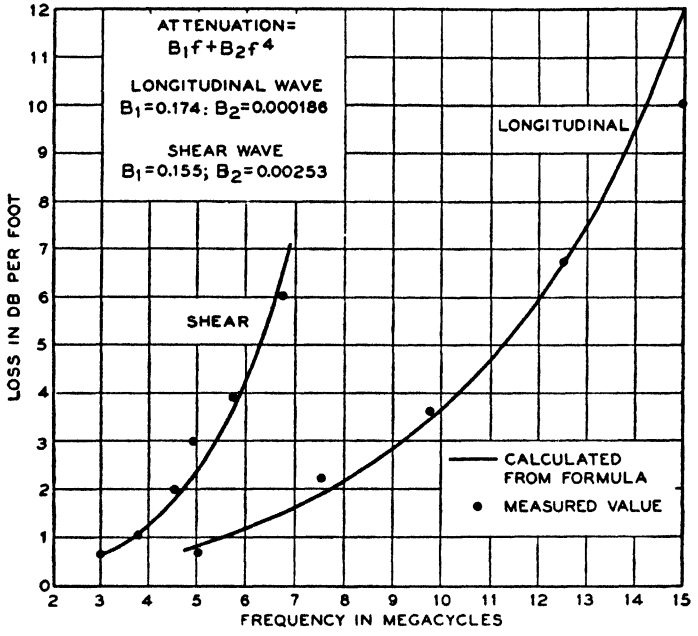

FIG. 15.12. Attenuation measurements for an aluminum rod having a grain size of 0.13 ± .01 mm.

and c'_{44} considering all directions as equally probable. These elastic constants for any orientation are given by the transformation equations

$$c'_{11} = c_{11}(l_1^4 + m_1^4 + n_1^4) + (2c_{12} + 4c_{44})(l_1^2m_1^2 + l_1^2n_1^2 + m_1^2n_1^2)$$

$$c'_{44} = c_{11}(l_1^2l_2^2 + m_1^2m_2^2 + n_1^2n_2^2) + 2c_{12}[l_1l_2m_1m_2 + n_1n_2(l_1l_2 + m_1m_2)] + c_{44}[(l_1l_2 + m_1m_2)^2 + (m_1m_2 + n_1n_2)^2] \quad (15.29)$$

where l_1 to n_3 are the direction cosines between the new set of axes and the old set

	x	y	z
x'	l_1	m_1	n_1
y'	l_2	m_2	n_2
z'	l_3	m_3	n_3

[17] Ting-Sui Ke, "Experimental Evidence of the Viscous Behavior of Grain Boundaries in Metals," *Phys. Rev.*, Vol. 71, No. 8, p. 533, April 15, 1947.

From these equations it can be shown that c'_{11} (which should correspond to $(\lambda + 2\mu)$ for an isotropic body) can vary from 10.76×10^{11} to 11.49×10^{11} dynes/cm, while the shear constant can vary from 2.84×10^{11} to 2.27×10^{11}.

The average value of c'_{11} can be determined from the equation

$$\begin{aligned} c'_{11} &= c_{11} + [2(c_{12} - c_{11}) + 4c_{44}][l_1^2 m_1^2 + l_1^2 n_1^2 + m_1^2 n_1^2] \\ &= 10.76 + 2.2[l_1^2 m_1^2 + l_1^2 n_1^2 + m_1^2 n_1^2] \end{aligned} \tag{15.30}$$

If we let the radius vector be in a plane through z making an angle φ from the x-axis, the vector making an angle θ from z, it is readily shown that the direction cosines are

$$l_1 = \sin\theta\cos\varphi; \qquad m_1 = \sin\theta\sin\varphi; \qquad n_1 = \cos\theta \tag{15.31}$$

Hence if all orientations are equally probable, the average space value of c'_{11} will be

$$\begin{aligned} \overline{c'_{11}} &= c_{11} + [2(c_{12} - c_{11}) + 4c_{44}] \times \\ &\qquad \frac{\int_0^{2\pi} d\varphi \int_0^{\pi} [\sin^4\theta \sin^2\varphi \cos^2\varphi + \sin^2\theta \cos^2\theta] \sin\theta \, d\theta}{} \\ &= c_{11} + \frac{[2(c_{12} - c_{11}) + 4c_{44}]}{5} \end{aligned} \tag{15.32}$$

For the values given above, this results in 11.20×10^{11}, which is somewhat high.

Since $l_1 l_2 + m_1 m_2 + n_1 n_2 = 0$ the shear modulus of equation (15.29) can be put into the form

$$\begin{aligned} c'_{44} &= 2(c_{12} - c_{11})[l_1 l_2 m_1 m_2 + l_1 l_2 n_1 n_2 + m_1 m_2 n_1 n_2] \\ &\quad + c_{44}[(m_1 n_2 + n_1 m_2)^2 + (n_1 l_2 + l_1 n_2)^2 \\ &\quad + (l_1 m_2 + m_1 l_2)^2] \end{aligned} \tag{15.33}$$

The shear modulus can be averaged in all directions by taking the direction cosines for a set of Euler coordinates

$$\begin{aligned} l_1 &= \cos\theta\cos\varphi\cos\psi - \sin\varphi\sin\psi; & m_1 &= \cos\theta\sin\varphi\cos\psi + \cos\varphi\sin\psi; \\ l_2 &= -\cos\theta\cos\varphi\sin\psi - \sin\varphi\cos\psi; & m_2 &= \cos\varphi\cos\psi - \sin\varphi\sin\psi\cos\theta; \\ l_3 &= \cos\varphi\sin\theta & m_3 &= \sin\varphi\sin\theta \end{aligned}$$

$$\begin{aligned} n_1 &= -\sin\theta\cos\psi; \\ n_2 &= \sin\theta\sin\psi; \\ n_3 &= \cos\theta \end{aligned} \tag{15.34}$$

where θ measures the angle of the normal z' with respect to z and φ is the angle of the zz' plane with respect to x. Inserting these values in (15.33) the average value of $\overline{c'_{44}}$ is

$$\overline{c'_{44}} = \int_0^{2\pi} \frac{d\psi}{2\pi} \int_0^{2\pi} \frac{d\varphi}{2\pi} \int_0^{\pi} \frac{c'_{44} \sin\theta \, d\theta}{2}$$

$$= c_{44} + \frac{[2(c_{11} - c_{12}) - 4c_{44}]}{5} \tag{15.35}$$

$$= \tfrac{3}{5}c_{44} + \frac{c_{11} - c_{12}}{5}$$

For aluminum this gives a value of $\overline{c'_{44}}$ of 2.62×10^{11} compared to the measured value of 2.67×10^{11}. Table XXIX gives the elastic constants of a number of cubic metals and their average $\overline{c'_{11}}$ and $\overline{c'_{44}}$ constants. In Table XXIX it is obvious that the materials that are the most isotropic are tungsten (W) and aluminum (Al).

The other metal of interest for high frequency ultrasonic work is magnesium which is a hexagonal crystal. For a hexagonal crystal there are five elastic constants as shown by equation (3.66) of Chapter III. For a hexagonal crystal the c'_{11} and c'_{66} elastic constants for any orientation take the form

$$c'_{11} = c_{11}(l_1^2 + m_1^2)^2 + c_{33}n_1^4 + (2c_{13} + 4c_{44})n_1^2(l_1^2 + m_1^2)$$

$$c'_{66} = c_{11}\left[(l_1l_2 + m_1m_2)^2 + \frac{(l_1m_2 - m_1l_2)^2}{2}\right] - \frac{c_{12}}{2}[l_1m_2 - m_1l_2]^2$$

$$+ 2c_{13}n_1n_2(l_1l_2 + m_1m_2) + c_{33}n_1^2n_2^2 + c_{44}[(m_1n_2 + n_1m_2)^2$$

$$+ (n_1l_2 + l_1n_2)^2] \tag{15.36}$$

Inserting the directional cosines of equations (15.31) and (15.34) and averaging over the sphere we find

$$\overline{c'_{11}} = \tfrac{8}{15}c_{11} + \tfrac{3}{15}c_{33} + \tfrac{2}{15}(2c_{13} + 4c_{44})$$

$$\overline{c'_{66}} = \tfrac{7}{30}c_{11} - \frac{c_{12}}{6} - \tfrac{2}{15}c_{13} + \frac{c_{33}}{15} + \tfrac{2}{5}c_{44} \tag{15.37}$$

Table XXX shows the elastic constants and average values of $\overline{c'_{11}}$ and $\overline{c'_{66}}$ for three hexagonal metals. In this table it is obvious that magnesium is quite isotropic, particularly for shear. The other two metals depart markedly from isotropy.

The attenuation measurements of Figs. 15.11 and 15.12 show a rapidly increasing attenuation with frequency that approaches the fourth power of

TABLE XXIX

ELASTIC CONSTANTS OF CUBIC METALS (s constants in cm²/dyne, c constants in dynes/cm²)

Metal	s_{11}	s_{12}	s_{44}	c_{11}	c_{12}	c_{44}	$\overline{c'_{11}}$	$\overline{c'_{44}}$
Face-Centered Cubic								
Al	1.59×10^{-12}	-0.58×10^{-12}	3.52×10^{-12}	10.76×10^{11}	6.18×10^{11}	2.84×10^{11}	11.20×10^{11}	2.62×10^{11}
Au	2.33	−1.07	2.38	19.6	16.45	4.20	21.7	3.15
Ag	2.32	−0.993	2.29	11.9	8.94	4.37	14.21	3.21
Cu	1.49	−0.625	1.33	17.02	12.3	7.51	21.14	5.46
Pb	9.30	−4.26	6.94	4.85	4.09	1.44	5.67	1.02
Ni*	0.80	−0.312	0.844	25.0	16.0	11.85	30.85	8.9
Ge*	0.964	−0.260	1.49	12.92	4.79	6.70	15.04	5.645
Body-Centered Cubic								
Fe	0.757	−0.282	0.862	23.7	14.1	11.6	29.15	8.86
Na	48.3	−20.9	16.85	0.615	0.469	0.592	1.03	0.384
K	83.3	−37.0	38.0	0.416	0.333	0.263	0.593	0.175
W	0.257	−0.073	0.660	50.2	19.9	15.15	50.2	15.15

* These two crystals have recently been measured by a pulsing method described by R. M. Bozorth, W. P. Mason, H. J. McSkimin and J. G. Walker, *Phys. Rev.*, Vol. 75, No. 12, pp. 195, 4–1955, June 15, 1949.

TABLE XXX

ELASTIC CONSTANTS OF HEXAGONAL METALS (s constants in $cm^2/dyne$; c constants in $dynes/cm^2$)

Metal	s_{11}	s_{12}	s_{13}	s_{33}	s_{44}	c_{11}	c_{12}	c_{13}
Mg	2.21×10^{-12}	-0.77×10^{-12}	-0.49×10^{-12}	1.97×10^{-12}	6.03×10^{-12}	5.86×10^{11}	2.49×10^{11}	2.08×10^{11}
Zn	0.84	+0.11	−0.78	2.87	2.64	16.35	2.64	5.17
Cd	1.23	−0.15	−0.93	3.55	5.40	12.12	4.81	4.42

	c_{33}	c_{44}	$\overline{c'_{11}}$	$\overline{c'_{66}}$
Mg	6.60×10^{11}	1.65×10^{11}	5.88×10^{11}	1.77×10^{11}
Zn	5.31	3.78	13.17	4.52
Cd	4.45	1.85	8.51	2.55

the frequency for high frequencies. In fact, if we express the attenuation according to the equation

$$A = B_1 f + B_2 f^4 \tag{15.38}$$

a good fit is obtained for both the shear and longitudinal curves for both rods. This indicates that we have a component of attenuation proportional to the frequency and another one proportional to the fourth power of the frequency. The component proportional to the frequency is the same as observed for most metals and solid materials at low frequencies[1] and indicates the presence of an elastic hysteresis. The term proportional to the fourth power is indicative of a scattering of energy similar to the scattering of sound by small particles, which, as Rayleigh[18] has shown, produce a scattered energy compared to the incident energy that increases as the fourth power of the frequency as long as the size of the scatterer is small compared to the wavelength.

The data of Fig. 15.11 for rod #1 are well-fitted at all frequencies for longitudinal waves if we take

$$B_1 = 0.225 \text{ db/foot/megacycle}; \quad B_2 = .001 \text{ db/foot/megacycle}^4 \tag{15.39}$$

For the theoretical values given in the next section, it is desirable to express these as nepers per centimeter per cycle. Since one neper = 8.68 db and one foot = 30.5 centimeter, these values become

$$\begin{aligned} B_1 &= 0.845 \times 10^{-9} \text{ nepers/cm/cycle}; \\ B_2 &= 3.74 \times 10^{-30} \text{ nepers/cm/cycle}^4 \quad \text{(long.)} \end{aligned} \tag{15.40}$$

Similarly the shear attenuation is well represented by the constants

$$\begin{aligned} B_1 &= 0.515 \times 10^{-9} \text{ nepers/cm/cycle}; \\ B_2 &= 50.2 \times 10^{-30} \text{ nepers/cm/cycle}^4 \quad \text{(shear)} \end{aligned} \tag{15.41}$$

For rod #2, the constants best fitting the curves are

$$\begin{aligned} B_1 &= 0.65 \times 10^{-9} \text{ nepers/cm/cycle}; \\ B_2 &= 0.695 \times 10^{-30} \text{ nepers/cm/cycle}^4 \quad \text{(long.)} \end{aligned} \tag{15.42}$$

and

$$\begin{aligned} B_1 &= 0.58 \times 10^{-9} \text{ nepers/cm/cycle}; \\ B_2 &= 9.4 \times 10^{-30} \text{ nepers/cm/cycle}^4 \quad \text{(shear)} \end{aligned} \tag{15.43}$$

Since rods 1 and 2 were supposed to be the same material but gave considerably different attenuation values, some effort was spent in trying

[18] Rayleigh, *Theory of Sound*, Vol. II, p. 152, Macmillan Co., 1924.

to determine the cause of the difference. Microphotographs were taken of the grain size and it was found that the average grain size[19] of rod #1 was .23 ± .01 mm while that of rod #2 was .130 ± .01 mm. This caused a larger scattering for rod #1, as discussed in the next section and resulted in a higher attenuation.

The elastic hysteresis losses proportional to the first power of the frequency are of some interest. The Q of a rod is equal to

$$Q = \frac{1}{2}\frac{B_0}{A_0} \tag{15.44}$$

where B_0 is the phase shift in radians and A_0 the attenuation in nepers. Since both B_0 and A_0 are proportional to the frequency for an elastic hysteresis alone, the Q should be independent of the frequency. The phase shift per cycle per centimeter is

$$B_0 = \frac{2\pi}{v} = .995 \times 10^{-5} \text{ for long. waves and } 2 \times 10^{-5} \text{ for shear waves in aluminum} \tag{15.45}$$

Dividing these values by twice the attenuation in nepers per centimeter per cycle given in equations (15.40), (15.41), (15.42) and (15.43), the Q's for the two rods are

Rod	Long.	Shear
1	5,900	19,400
2	7,650	17,200

(15.46)

These agree quite well with those previously found for longitudinal vibrations for low frequencies (see Table XXVI).

Figure 15.13 shows measurements of the losses in three glass rods and a fused quartz rod of optical quality for shear-wave transmission. Here any grain-size irregularities must be of a very small order and this is shown experimentally by the strict proportionality between the attenuation and the frequency. Clear fused quartz has the lowest loss of any material so far measured. The elastic hysteresis values for the glasses are

Material	A, *nepers/cm/cycle*	v in *cm/sec*	Q
1-C 1720 glass	4.37×10^{-9}	3.74×10^5 cm/sec	1,970
012 glass	2.67×10^{-9}	2.80×10^5	4,200
790 Vycor	1.03×10^{-9}	3.58×10^5	8,520
Fused quartz	1.88×10^{-10}	3.76×10^5	44,500

[19] This work was done by E. E. Thomas of Bell Telephone Laboratories.

15.33 *Calculation of Attenuation due to Scattered Energy*

A multicrystalline rod of aluminum or other metal is made up of a number of small-sized crystals that are not exactly lined up. The boundaries between these small crystals or grains can be determined by polishing and etching the surface and taking a microphotograph of the resulting etched surface. Sound scattering can occur due to a difference in density between adjacent elements of a medium or due to a difference in elasticity.

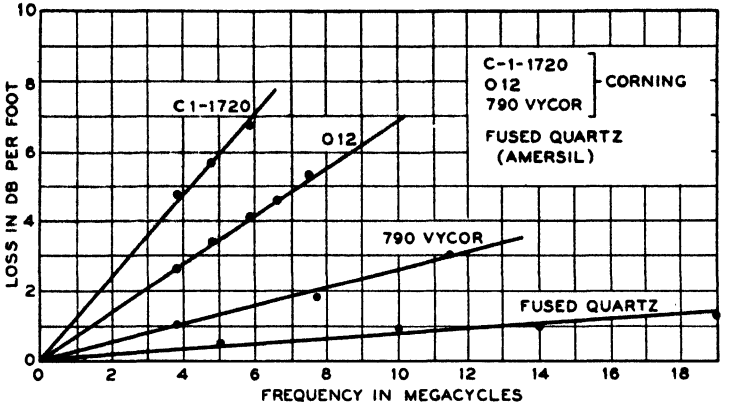

FIG. 15.13. Attenuation measurements for three glasses and fused quartz for shear waves.

It is probable that the difference in density between successive grains is negligible, but a difference in elasticity occurs since the grains are not all lined up and the elasticity depends on grain direction. Rayleigh's formula[18] for the scattering of energy of a single particle is

$$\frac{\text{S.A.}}{\text{I.A.}} = \frac{\pi T}{R\lambda^2}\left[\frac{\Delta\kappa}{\kappa} + \cos\theta\,\frac{\Delta\rho}{\rho}\right]$$

where T is the volume of the particle, λ the wavelength, κ the elasticity of the medium, $\Delta\kappa$ the difference in elasticity between the particle and the medium, ρ the density of the medium, θ the angle between the direction of observation and the direction of the incident wave, S.A. the scattered amplitude, I.A. the incident amplitude and R the distance of the particle from the point of observation. For the present case we can neglect $\frac{\Delta\rho}{\rho}$ since the density between successive particles does not vary.

The total energy scattered from the single particle is proportional to the square of the scattered amplitude integrated over a sphere of radius R.

Performing this integration, neglecting $\frac{\Delta\rho}{\rho}$, we find

$$\text{S.E.} = (\text{I.A.})^2 \frac{\pi^2 T^2}{\lambda^4 R^2} \times 2\pi R^2 \left(\frac{\Delta\kappa}{\kappa}\right)^2 \int_0^{2\pi} \sin\theta \, d\theta$$

$$= (\text{I.A.})^2 \frac{4\pi^3 T^2}{\lambda^4} \left(\frac{\Delta\kappa}{\kappa}\right)^2 \tag{15.47}$$

Now if we have a large number of grains concentrated in a volume whose cross sectional area is A and whose length is dx, and if we assume that the scattering from all the particles is random, the total scattered energy will be the sum of the scattered energy from each of the particles or

$$\text{Total S.E.} = (\text{I.A.})^2 \frac{4\pi^3}{\lambda^4} \sum_{k=1}^{N} \left[T_k^2 \left(\frac{\Delta\kappa}{\kappa}\right)_k^2 \right] \tag{15.48}$$

If there is no connection between the grain volume T and the inhomogeneity of the elasticity, so that the two can be summed independently, we have

$$\frac{\text{Total S.E.}}{(\text{I.A.})^2} = \frac{4\pi^3}{\lambda^4} \sum_{k=1}^{N} T_k^2 \sum_{k=1}^{N} \frac{\left(\frac{\Delta\kappa}{\kappa}\right)^2}{N} = \frac{4\pi^3}{\lambda^4} \sum_{k=1}^{N} T_k^2 \overline{\left(\frac{\Delta\kappa}{\kappa}\right)^2} \tag{15.49}$$

where $\overline{\left(\frac{\Delta\kappa}{\kappa}\right)^2}$ is the space average of the quantity $\left(\frac{\Delta\kappa}{\kappa}\right)^2$. For a distribution of particle sizes that does not differ much from the average, the first summation is

$$NT^2 = VT = A\,dx\,T \tag{15.50}$$

where V is the volume under consideration equal to $A\,dx$. But since $A(\text{I.A.})^2$ is proportional to the total incident energy, the ratio of the total scattered energy to the total incident energy becomes

$$\frac{\text{T.S.E.}}{\text{T.I.E.}} = \frac{4\pi^3\,dx\,T}{\lambda^4} \overline{\left(\frac{\Delta\kappa}{\kappa}\right)^2} \tag{15.51}$$

This determines an energy attenuation factor per unit length of material since

$$E_0 = E_I - E_S = E_I e^{-\alpha\,dx} = E_I(1 - \alpha\,dx) \tag{15.52}$$

where E_0 is the energy of the wave out of the sections, E_I the incident energy, and E_S the scattered energy which represents a total loss as far as the pickup crystal is concerned. Hence

$$\alpha = \frac{4\pi^3 T}{\lambda^4} \overline{\left(\frac{\Delta\kappa}{\kappa}\right)^2} \tag{15.53}$$

In the measurements it was the amplitude attenuation factor that was measured and this is half the energy attenuation factor. Then, since $1/\lambda = f/v$, the constant B_2 of equation (15.38) can be written in the form

$$B_2 = \frac{2\pi^3 T}{v^4}\overline{\left(\frac{\Delta\kappa}{\kappa}\right)^2} \tag{15.54}$$

If there is a range of particle sizes, the value of T tends to be larger than the average particle size obtained by counting the number in a given volume.

An approximate idea[20] of the value of the space average of $\overline{(\Delta\kappa/\kappa)^2}$ can be had from the variation of c'_{11} as a function of orientation. From equation (15.30) we have

$$c'_{11} = c_{11} + [2(c_{12} - c_{11}) + 4c_{44}][l_1^2 m_1^2 + l_1^2 n_1^2 + m_1^2 n_1^2]$$

and

$$\overline{c'_{11}} = c_{11} + \frac{[2(c_{12} - c_{11}) + 4c_{44}]}{5}$$

Hence

$$\overline{\left[\frac{c'_{11} - \overline{c'_{11}}}{\overline{c'_{11}}}\right]^2} = A - B[\sin^4\theta \sin^2\varphi \cos^2\varphi + \sin^2\theta \cos^2\theta] + C[\sin^4\theta \cos^2\varphi \sin^2\varphi + \sin^2\theta \cos^2\theta]^2$$

where

$$A = \left[\frac{[2(c_{12} - c_{11}) + 4c_{44}]}{5c_{11} + 2(c_{12} - c_{11}) + 4c_{44}}\right]^2; \qquad B = 10A, \quad C = 25A$$

Integrating this equation over all orientations, we have

$$\overline{\left(\frac{\Delta\kappa}{\kappa}\right)^2} = \overline{\left(\frac{c'_{11} - \overline{c'_{11}}}{\overline{c'_{11}}}\right)^2} = A\left(1 - 2 + \frac{25}{21}\right) = \frac{4}{21}A \tag{15.55}$$

For the values of equation (15.28) this gives a value of $\overline{\left(\frac{\Delta\kappa}{\kappa}\right)^2} = .0003$. Using this value of $\overline{\left(\frac{\Delta\kappa}{\kappa}\right)^2}$ and the particle diameter of .130 mm for the #2

[20] This method for evaluating the inhomogeneity factor was suggested to the writer by Dr. C. Kittel. It is related to the R function of Zener, used to calculate the thermoelastic losses in solids, see *Phys. Rev.*, Vol. 53, p. 90, 1938, and given for several metals by equation (15.5).

rod, the theoretical value of the attenuation should be

$$B_2 = 0.134 \times 10^{-30} \text{ nepers/cm/cycle}^4 \tag{15.56}$$

This compares with the measured value of $B_2 = 0.695 \times 10^{-30}$ which agrees as closely as could be expected, considering that the particles scatter shear as well as longitudinal waves and since the shear waves are shorter, they should be more efficient sources of scattering. For rod #1, the scattering loss should be in the ratio to rod #2, of

$$\left(\frac{.23}{.13}\right)^3 = 5.5 \tag{15.57}$$

and this agrees quite exactly with the experimental ratio of 5.4.

Since shear waves are polarized waves, the scattering formula should be somewhat different from that for longitudinal waves. The scattering formula should be the same as for light waves in which an irregularity occurs in the refractive index. This has been shown by Rayleigh[21] to be

$$\frac{\text{S.I.}}{\text{I.I.}} = \frac{N\pi T^2}{\lambda^4 R^2} \overline{\left(\frac{\Delta\mu'}{\mu'}\right)^2} (1 + \cos^2\theta) \tag{15.58}$$

where S.I. is the scattered intensity, I.I. the incident intensity and θ the angle between the direction of observation and the direction of the incident ray. With this value the amplitude attenuation factor becomes

$$B_2 = \frac{8}{3} \frac{\pi^2 T}{v^4} \overline{\left(\frac{\Delta\mu'}{\mu'}\right)^2}. \tag{15.59}$$

The value of $\overline{(\Delta\mu'/\mu')^2}$ can be obtained by integrating the expression

$$\overline{\left[\frac{c'_{44} - \overline{c'_{44}}}{\overline{c'_{44}}}\right]^2} = \frac{3}{175}\left[\frac{(c_{11} - c_{12}) - 2c_{44}}{\overline{c'_{44}}}\right]^2$$

For aluminum this constant is 3.3×10^{-3}, which is about 10 times larger than the scattering constant for longitudinal waves. Using this value the theoretical attenuation for rod #2 should be

$$B_2 = 10.3 \times 10^{-30} \text{ nepers/cm/cycle}^4 \tag{15.60}$$

compared to the measured value of $B_2 = 9.4 \times 10^{-30}$. The ratio between the shear scattering losses for the two rods is again 5.5 theoretically compared to the experimental value of 5.4.

The scattering factor $\overline{(\Delta c'_{11}/c'_{11})^2}$ and $\overline{(\Delta\mu'/\mu')^2}$ have been calculated for the metals of Tables XXIX and XXX and are shown by Table XXXI.

[21] *Phil. Mag.*, Vol. XLI, pp. 107–120, 274–279, 1871.

TABLE XXXI

SCATTERING FACTORS FOR LONGITUDINAL AND SHEAR WAVES

Metal	$\overline{(\Delta c'_{11}/\overline{c'_{11}})^2}$	$\overline{(\Delta\mu'/\overline{\mu'})^2}$
Al	3×10^{-4}	3.3×10^{-3}
Au	1.78×10^{-3}	5.2×10^{-2}
Ag	5×10^{-3}	6.1×10^{-2}
Cu	7.4×10^{-3}	6.7×10^{-2}
Pb	4.2×10^{-3}	7.2×10^{-2}
Fe	6.7×10^{-5}	4.0×10^{-2}
Na	2.9×10^{-2}	1.25×10^{-1}
K	1.7×10^{-2}	1.1×10^{-1}
W	0	0
Mg	2.2×10^{-4}	
Zn	5.6×10^{-2}	
Cd	2.8×10^{-2}	

The scattering factor for longitudinal waves has been calculated for hexagonal metals by introducing the direction cosines of equations 15.31 into equation (15.41) and averaging over the sphere. The result is

$$\overline{\left[\frac{c'_{11} - \overline{c'_{11}}}{\overline{c'_{11}}}\right]^2} = \frac{4}{1575}\left[\frac{\begin{array}{r}48c_{11}^2 - 64c_{11}c_{33} + 28c_{33}^2 - 16c_{11}(2c_{13} + 4c_{44}) \\ + 4c_{33}(2c_{13} + 4c_{44}) + 3(2c_{15} + 4c_{44})^2\end{array}}{\overline{c'_{11}}^2}\right] \tag{15.61}$$

While the shear scattering factor for hexagonal metals has not been calculated, it is obvious from Table XXX that since the average value of $\overline{c'_{66}} = 1.77 \times 10^{11}$ varies less from c_{44} and $c_{66} = \dfrac{c_{11} - c_{12}}{2}$ in a percentage value than $\overline{c'_{44}}$ does from c_{44} of aluminum that the scattering for shear waves will be less for magnesium than it is for aluminum. This has been shown experimentally by a measured curve which was taken for a grain-size material of 0.1 mm average diameter. Here the attenuation up to 11 megacycles can be represented by the equation

$$A_{\text{nepers/cm}} = 1.06 \times 10^{-10} f + 4.6 \times 10^{-31} f^4$$

and the shear scattering loss is considerably less than for aluminum. The first power hysteresis term is lower than that for aluminum and indicates a Q of 100,000 for low frequencies. For longitudinal waves the scattering in magnesium is higher and approaches that of aluminum.

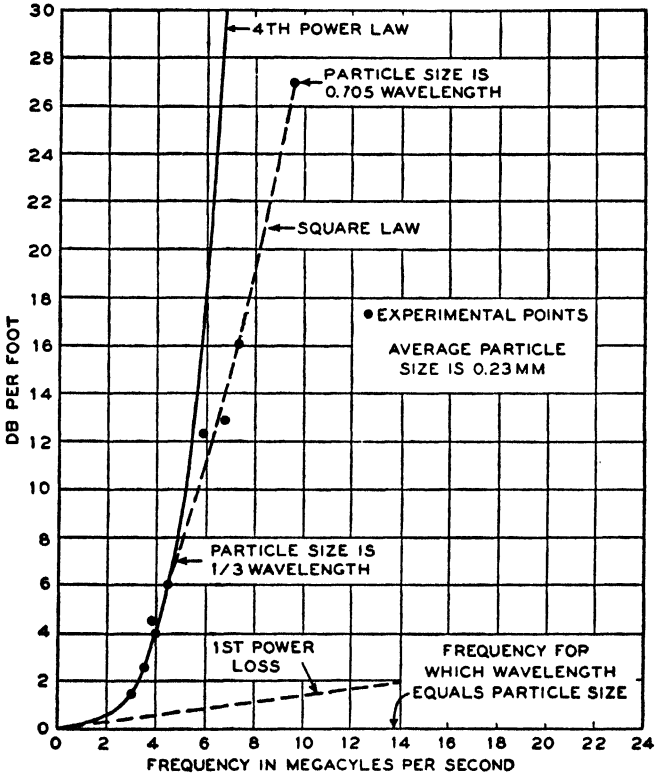

FIG. 15.14. Measured losses for aluminum rod No. 1 at high frequencies.

The fourth-power scattering law should hold as long as the wavelengths are considerably larger than the grain size. If, however, the wavelength becomes comparable to the grain size, the fourth-power law no longer holds and when the grain size gets large compared to the wavelength, the transmission of sound becomes similar to a diffusion process and the losses should be inversely proportional to the mean free path. If the grain diameter determines the mean free path, the losses should be inversely proportional to the grain diameter. Some experimental evidence has been obtained on the approach to the diffusion process. Fig. 15.14 shows measurements for shear waves for rod #1 having a grain diameter of

0.23 mm. The fourth-power law shown by the solid line is valid up to the frequency for which the grain size is about 0.33 of the wavelength. Above this point, a square law holds quite well up to a point where the particle size is 0.7 times the wavelength. Fig. 15.15 shows measurements for the two rods #1 and #2 for longitudinal waves. These measurements were made by using a water coupling between the crystal and the rod. Measurements were made from 5 to 34 megacycles. The lower frequency measurements checked very closely with those made by the wax-joint method. At high frequencies the loss of the small grain-size bar becomes larger than that of the large grain-size bar, indicating that the loss goes from a condition determined by scattering to a loss determined by diffusion.

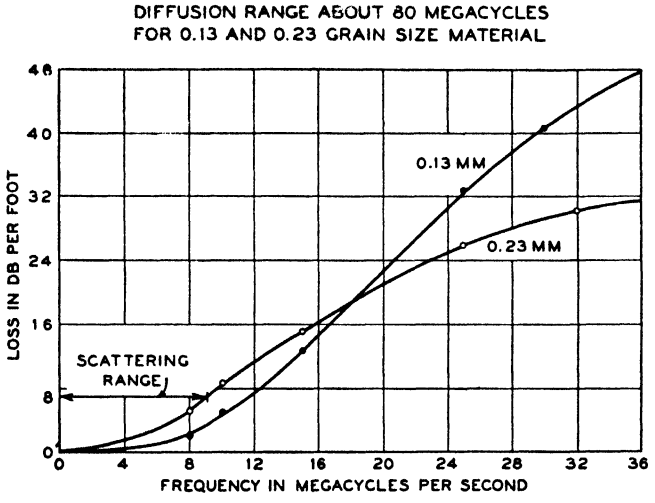

FIG. 15.15. Attenuation measurements for two aluminum rods at high frequencies.

Measurements for magnesium for longitudinal waves have been made by Roth[13] in the frequency range from 10 to 100 megacycles. Fig. 15.16 shows the loss in db per inch as a function of frequency for two different grain-size materials 0.21 mm and 2.0 mm. The losses are about 10 times as large for the small-grain-size materials as for the large and show that diffusion conditions are determining the loss in the high-frequency range. No measurements below 10 megacycles are given so that the scattering losses cannot be evaluated.

A rough estimate of diffusion losses can be made as follows: the receiving crystal is very directional and hence all that will be picked up are waves that are normal to the surface. When the frequency is so high that the wavelength is small compared to the grain size, the loss is caused

by reflection between grains and to the change of direction due to these reflections. These two losses, since they are both caused by reflections, are comparable and hence we calculate the losses by reflection at normal incidence, and assume the change in direction loss is of the same order of magnitude. If the wave goes from one grain to another at normal incidence across the boundary, one part is transmitted and the other reflected. Since the amount lost by reflection is small, the transmitted part is in terms of pressure

$$p = p_0[1 - R_1] \doteq p_0 e^{-R_1} \tag{15.62}$$

where R_1 is the reflection coefficient. For n such reflections in a length l, the terminal pressure becomes

$$p = p_0 e^{-[R_1 + R_2 \cdots + R_n]} = p_0 e^{-n\bar{R}} \tag{15.63}$$

where $\bar{R}$ is the average reflection coefficient. Now, if the average particle diameter is D, then

$$nD = l \qquad \text{or} \qquad n = l/D \tag{15.64}$$

where l is the total path length. Hence

$$p = p_0 e^{-\bar{R}l/D} \tag{15.65}$$

and the loss should be inversely as the grain diameter for a diffusion process. Multiplying the exponent by 2 to take account of the loss by change in direction (which should be the same order of magnitude as the reflection loss), the loss in nepers per centimeter should be in the order of

$$A = \frac{\overline{2R}}{D} \tag{15.66}$$

To evaluate the average reflection coefficient we have

$$R = \frac{Z_1 - Z_2}{Z_1 + Z_2} = \frac{\sqrt{\frac{c'_{11}}{\rho}} - \sqrt{\frac{\overline{c'_{11}}}{\rho}}}{\sqrt{\frac{c'_{11}}{\rho}} + \sqrt{\frac{\overline{c'_{11}}}{\rho}}} \tag{15.67}$$

where c'_{11} is the elastic constant in any direction and $\overline{c'_{11}}$ the elastic constant averaged over all directions. Since $(c'_{11} - \overline{c'_{11}})/\overline{c'_{11}}$ is a small quantity, this reduces to

$$R = \frac{1}{4}\left| \frac{c'_{11} - \overline{c'_{11}}}{\overline{c'_{11}}} \right| \tag{15.68}$$

In evaluating this, we have to take the absolute value since energy is lost

no matter what the sign of the reflection coefficient may be. This makes it a difficult integration and since only an approximate calculation has been made, it is sufficiently accurate to take one fourth the average of the two extremes of reflection coefficient. For magnesium the average value of $\overline{c'_{11}}$ is 5.88×10^{11}. The maximum value is $c_{33} = 6.60 \times 10^{11}$, while the minimum value is 5.75. Hence the average reflection coefficient is in the order of .0075. The indicated loss for the magnesium bar with 2-mm grain size, is .075 nepers per centimeter of 1.6 db per inch, which checks reasonably well with the data of Fig. 15.16 for the 2-mm grain-size magnesium.

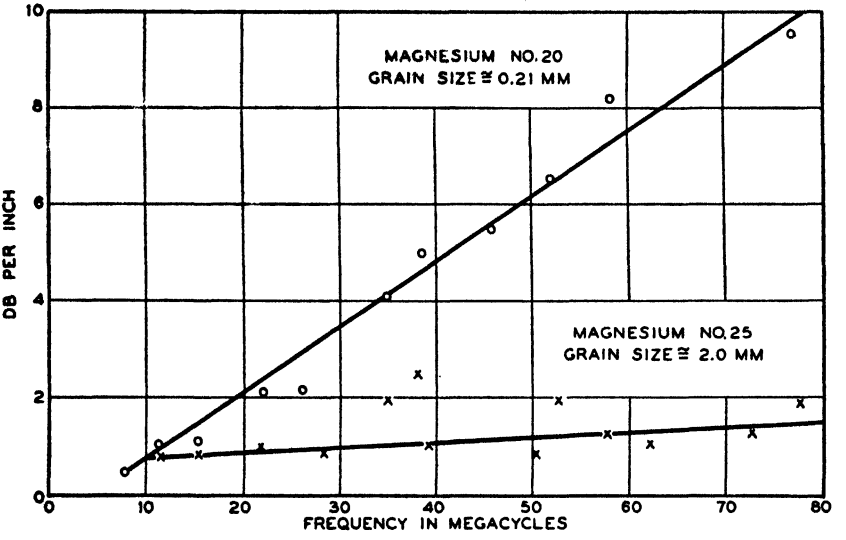

FIG. 15.16. Attenuation measurements of Roth for two magnesium rods for longitudinal waves.

Fourth-power scattering holds up to a frequency for which the grain size is about a third of a wavelength, while diffusion processes occur when the grain size is 3 wavelengths or larger. No adequate theory exists for the transition region.

15.34 *Sound Wave Transmission in a Granular Material and its Relation to Heat Wave Transmission*

Scattering and reflection are not true acoustic losses for they merely abstract energy from the main beam and send it off in other directions. Hence, due to multiple reflections of these beams with other grain boundaries, we might expect a trailing hash on the end of the received pulse which would last for some time. This is not particularly noticeable in the

nearly isotropic materials on account of the high directionality of the receiving crystal, but is very obvious in Fig. 15.17 which shows plotted as a function of time the received pulse from a one inch specimen of commercial brass for a 12 megacycle shear wave. Brass is the material having the least isotropic elastic constants. For this specimen the grain size is about 1.25 millimeters. The size of the active area of the receiving crystal is small in order that energy from a wide angular range can be received. The wave head, since it is attenuated exponentially, does not show up at all. What appears is a trailing component that gradually builds up to a maximum and then dies down.

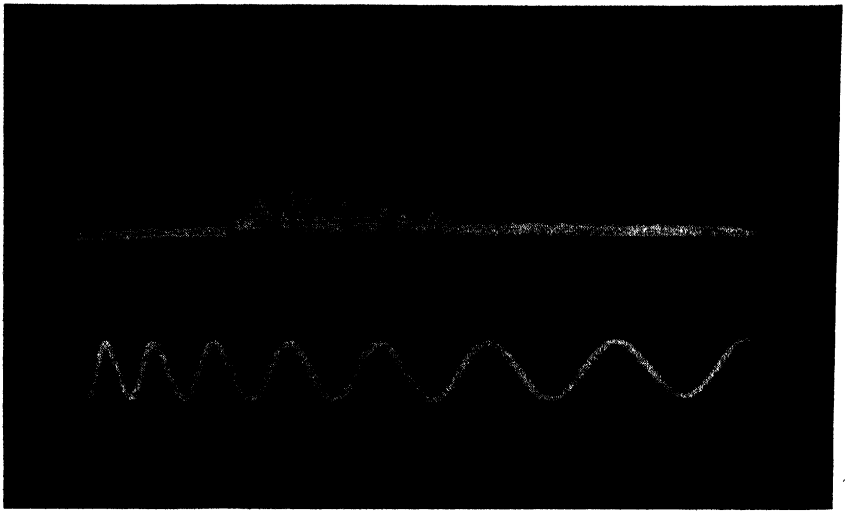

FIG. 15.17. Upper figure. Pulse received from a one inch specimen of commercial brass (grain size 1.5 mm) for a pulse of shear waves having a frequency of 12 megacycles. Lower curve shows a 10 kilocycle timing wave. Maximum response occurs 100 microseconds after pulse is sent. Velocity of sound for shear wave is 2.5×10^5 cm/sec.

If we deal with a three-dimensional rod extending in both directions, and neglect attenuation, one can show that when a pulse is sent out, the amplitude resulting from summing up all the energy reaching a plane at a distance l from the pulse position, is the same as the problem in the kinetic theory of gases which has the known solution

$$t = \frac{Bl^2}{v\Lambda} \tag{15.69}$$

where v is the velocity of sound propagation, B a constant equal to 2 and Λ, the mean free path for this case, is the distance required to attenuate the

wave by one neper, *i.e.*, $D/2\bar{R}$ from equation (15.66). The value of time for the maximum response obtained from Fig. 15.17 agrees fairly well with equation (15.69) if one allows for the attenuation occurring in the brass. From the rate for which the scattered energy dies down, one can calculate that the inherent attenuation is about 10 db per foot at 12 megacycles for shear waves in brass. This is one method for investigating high frequency attenuation in metals even in the scattering range.

The analogy is quite close between sound transmission in a granular medium and heat wave transmission in a liquid or solid except that no attenuation has to be considered for heat transmission. This follows from the fact that acoustic attenuation results in transferring vibrational energy into heat energy, *i.e.* a mechanical vibration of a considerably higher frequency. For heat transmission this loss does not occur since it would result in changing heat energy into heat energy. According to the present theories, heat is a mechanical vibration of the crystal lattice with most of the energy concentrated around a frequency range from 10^{12} to 10^{13} cycles for room temperature. Heat conduction is the process of transmitting acoustic energies of these frequencies from one place to another and this is controlled mostly by the mean free path for these frequencies. However, even though the heat energy in the ultrasonic range is very small, one has to make use of the observed attenuation to prevent the heat conductivity from becoming infinite.

If we put a temperature pulse at one point of a rod and calculate the temperature at a point distant l from the source as a function of time, the curve of Fig. 15.18 results. The temperature reaches its maximum value at a time t equal to

$$t = C\frac{l^2}{2K} \tag{15.70}$$

where K is the heat conductivity and C the specific heat per unit volume. The effect of attenuation in the low frequency acoustic case is to reduce the curve and shove the peak value to smaller times as shown by the dotted line. Since the two methods are different ways of describing the same phenomena, we can equate the times and have an expression for the heat conductivity

$$K = \tfrac{1}{4}Cv\Lambda \tag{15.71}$$

where Λ is the mean free path. Strictly speaking, since a solid will transmit two shear waves as well as a longitudinal wave, the equation should be

$$K = \tfrac{1}{4}[C_l v_l \Lambda + 2C_s v_s \Lambda] \tag{15.72}$$

where C_l and C_s and v_l and v_s are the specific heats and velocities of propagation for longitudinal and shear waves respectively.

There are two types of heat conductors that transmit heat by acoustic waves. These are the amorphous types such as the glasses and liquids that do not have a repeating structure, and the crystalline type. For the amorphous type the mean free path is in the order of the molecular separation since a change in spacing will cause a reflection. In fact if one puts in values of Λ of this order and the known values of the specific heats and sound velocities, one obtains a value of heat conductivity that agrees with experiment. As the temperature decreases the heat conductivity also decreases since Λ does not change much and C approaches zero. However, as pointed out by Kittel,[22] as the temperature approaches absolute zero the

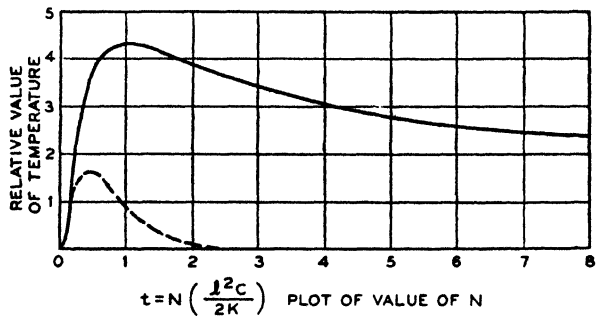

FIG. 15.18. Solid line shows temperature at distance l due to a heat pulse applied at end of rod, in terms of the thermal constants. Dotted line shows effect of attenuation in changing the time of maximum response.

frequency range of maximum energy decreases, the wavelength gets larger, the effect of a given sized irregularity in scattering the wave is less and the free path becomes larger. At 1°K heat transmission is similar to sound transmission in the frequency range of 10^{10} to 10^{11} cycles. For a crystalline medium no natural barriers exist to determine the mean free path. However, the thermal motion of the molecules, which causes them to be out of their regular spacing, produces a gradual scattering of the wave and limits the mean free path to around 10 to 100 atom spacings for room temperature. As the temperature is reduced, the mean free path increases at a more rapid rate than the specific heat decreases, and the thermal conductivity becomes very high at low temperatures. Experiments by de Haas and Biermasz,[22] show that the heat conductivity for several single crystals reaches a maximum in the liquid helium range, the temperature depending on the size of the specimen. At this temperature the mean free path equals the dimensions of the sample, *i.e.* in the order of a centimeter, and the fall off on the low temperature side is due to the decrease in specific heat.

[22] C. Kittel, *Phys. Rev.*, Vol. 75, No. 6, March 15, 1949.

15.4 *Use of Ultrasonic Methods in Observing Twinning in Metals*

The plastic properties of metals are usually explained on the basis of dislocations which are defects in the lattice in the order of a few atomic spacings in cross-section and extending through the crystal in the third direction. These are supposed to move with nearly the speed of sound through the metal and to be generated at the surface as a result of a shearing stress. While many of the properties of metals can be explained by assuming their existence, they have never been observed directly by any experiment.

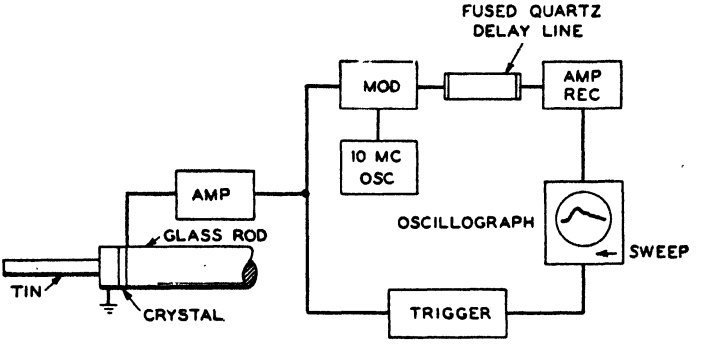

FIG. 15.19. Experimental arrangement for observing twinning in tin.

Recently[23] an attempt has been made to observe the presence and effects of such dislocations by means of the mechanical waves they generate in metals. If a dislocation moves across a test specimen with a speed approaching that of sound, a displacement of the order of the lattice constant d should occur in a time of the order of the diameter of the specimen divided by the speed of sound. This requires instruments capable of measuring displacements of about 10^{-8} centimeter occurring in times of 10^{-6} second, values which lie in ranges already exploited in connection with ultrasonic delay lines.

The first experimental arrangement employed, as shown by Fig. 15.19, was to solder a thin rod of the metal to be tested to the face of a plated quartz crystal, which in turn was soldered to a silver-paste coating baked on a long glass rod. The metal side of the crystal was connected to the ground side of the pre-amplifier which fed the modulator of a wide-band fused quartz delay line, having a delay of 15 microseconds and a band width of 4 megacycles. The demodulated output from the delay circuit

[23] Mason, W. P., H. J. McSkimin, and W. Shockley, "Ultrasonic Observation of Twinning in Tin," *Phys. Rev.*, Vol. 73, No. 10, p. 1213, May 15, 1948.

was amplified by a wide-band amplifier and impressed on the vertical plates of an oscilloscope. The sound pulse from the pre-amplifier was also impressed on a trigger circuit controlling the starting time of the sweep of a single-sweep oscilloscope. The rate of sweep was adjustable and for most tests was made about 10 microseconds for a one-inch travel.

When the tin specimen was bent, the noise of twinning tripped the sweep circuit and a straight line resulted for about the first inch and a half of travel. Fifteen microseconds later (as determined by the delay line) the output of the crystal actuated the vertical motion of the spot. With the experimental arrangement of Fig. 15.19, an irregular wave having about 100 kilocycles frequency, was observed. This died out very rapidly and could easily be discriminated from a mechanical noise caused by tapping, since the latter caused an end-to-end reflection along the whole system, which produced a 10-kilocycle vibration which lasted a considerable

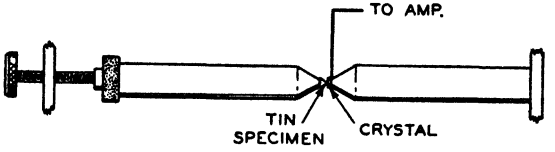

FIG. 15.20. Modification of stress applying mechanism to eliminate spurious reflections.

time. When an aluminum rod was substituted for tin, no twinning or slip noise was received. This indicated that the plastic deformation process in aluminum occurred in much smaller units than for the tin or else a different process is involved.

It was thought that the 100-kilocycle wave might have been generated by shock excitation of the resonances of the rod or crystal. To get around this difficulty, the arrangement of Fig. 15.20 was used. Here two glass rods, each 3 feet long, were tapered on the adjacent ends to a circle $\frac{1}{8}$ inch in diameter. On the end of one, a tin specimen $\frac{1}{8}$ inch in diameter on one end and tapered to a circle $\frac{1}{16}$ inch in diameter on the other end was soldered to a silver paste baked on the glass rod. The tin specimen was prepared from a 99.9 per cent pure tin having a crystal grain size in excess of $\frac{1}{16}$ inch. Hence the specimen approaches a single crystal. A quartz crystal 0.5 mm thick and $\frac{1}{8}$ inch in diameter, was soldered to the other glass rod. The sensitivity of this crystal was uniform from a few kilocycles to 5 megacycles and by calibration it was found that a total force of 1,000 dynes would produce a displacement of about $\frac{3}{8}$ inch on the oscilloscope. Pressure was exerted on these two rods lined up in a V block by turning a screw on one end which puts pressure on the combination through a rubber pad. With this arrangement, about fifteen photographs were taken of the

voltage generated by the twinning process. Since the light generated from a single trace moving at this rate is too small to produce a photograph that can be printed, the two curves of Fig. 15.21, which were typical of those measured, were reproduced from film by a pantograph tracing. Time variations in the order of 1 microsecond and decay rates up to 30 microseconds were observed. Various electrical and mechanical tests indicated that the crystal plus electrical circuits have an adequate band width for the effects observed.

During the time of observation, which amounts to about 30 microseconds, the ultrasonic disturbance does not have time to reach the ends of the glass rods and hence the rods act as infinite rods having characteristic impedances equal to the product of density ρ times velocity of propagation v times the area A. The transient voltage is always of a sign to indicate a relief of pressure on the crystal face and this transient pressure is less than 0.1 per cent of the applied load. Hence the deformation takes place essentially at constant load. Increasing the applied load by turning the screw provokes additional transient yielding. Since the crystal is terminated on both sides by mechanical impedances $Z = \rho v A$, the pressure difference, which is related to the voltage generated by the crystal, is caused by the velocity of yield of the tin specimen in a direction normal to the crystal surface. Calling this velocity of yield $\dot{\xi}$, the total force on the crystal is

$$F = \dot{\xi}\rho v A \qquad \text{and} \qquad \dot{\xi} = F/\rho v A \tag{15.73}$$

For the tin specimen used $\rho = 7.1$; $v = 2.6 \times 10^5$ cm/sec; $A = .02$ sq cm (corresponding to a circle $\frac{1}{16}$ inch in diameter). The impedance of the glasses are about 15×10^5 mechanical ohms per square centimeter, which matches that of the tin and quartz quite well. With these values of impedance, the velocity of yield for 1,000 dynes force is

$$\dot{\xi} = 3 \times 10^{-2} \text{ cm/sec} \tag{15.74}$$

Hence a velocity of yield scale can be put on Fig. 15.21 as shown. The time scale is shown by the 200-kilocycle trace at the bottom of Fig. 15.21. The (a) type curve rises to a velocity of yield of about 2×10^{-2} centimeters per second in about 2 microseconds and then dies off exponentially to a value $1/e$ in about 30 microseconds. The total volume change in the tin corresponds to the integral under this curve times the area A and amounts to about 1.2×10^{-8} cubic centimeters. The area under curve (b) is about half this amount.

The fine structure is not the same for any two traces, which suggests that it is characteristic of the twinning process rather than of some mechanical resonance of the specimen. The distance moved in one cycle of the

fine structure is about 2.5Å for (a) and about $\frac{1}{2}$Å for (b). The period of the fine structure corresponds to 2.5 microseconds for (a) and 1 microsecond for (b).

These results are in general agreement with passage at the speed of sound of twinning dislocations from side to side in the specimen. The most likely path for the twinning dislocations is at 45° to the applied stress, since this is the direction of greatest shearing stress. The distance across the specimen from one edge along a 45° path to the length is about 0.26 centimeters. Hence the time of travel across the specimen, if the speed of

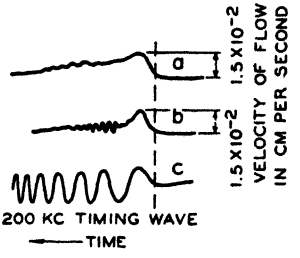

FIG. 15.21. Oscillograph traces showing voltages measured in the twinning process. Scale on right shows velocity of yield. Bottom curve shows timing wave.

travel is the speed of sound, is 1 microsecond. Hence the data of curve (a) indicate that dislocation proceeds from one corner across the specimen with nearly the speed of sound. When it reaches the other side, it starts a return dislocation which proceeds with the speed of sound. This would result in a slight variation in the sound picked up by the crystal since the sound picked up will be less when the dislocation is moving away from the crystal than when it is moving toward it. According to Barrett,[24] the twinning plane in tin is the 331 plane and the distance between adjacent twinning planes is 0.2Å. Since the displacement along the length from peak to peak is 2.5Å, it appears that a dislocation about 10 planes thick crosses the specimen at one time. Since the time between successive maxima appears to be about constant, the plastic flow dies out by having fewer planes in the dislocation toward the end of the deformation than occurs at the beginning. It appears that the material becomes strain hardened and it becomes more difficult to include as many planes in the dislocation at the end of the process.

The type of curve shown by (b) appears to be due to a path length that is less than the complete width of the specimen, which can occur if the crystal grain does not extend across the whole specimen. The time

[24] Barrett, Charles S., *Structure of Metals*, p. 312, McGraw-Hill Book Co., Inc., 1943.

between successive peaks is one microsecond and the displacement along the axis between maxima is about 0.5Å. This makes it appear that a grain about $\frac{1}{3}$ the maximum length is involved and a slight time elapses between the time a dislocation reaches the boundary and the return dislocation starts across the crystal.

It appears from these measurements that the evidence for the existence of dislocations is quite strong in the twinning process in tin.

APPENDIX

Applications of Tensors to the Equations of Liquids, Gases, and Solids

The equations for piezoelectric crystals have been developed in Chapter III in terms of the stresses, strains, electric fields and displacements, temperature and entropy. Two short-hand methods exist which greatly simplify the method of writing and manipulating the relations between fundamental quantities. These are the matrix method[1] and the tensor method. The tensor method is presented here on account of its greater generality which allows one to apply it to such second-order effects as electrostriction, for which matrix methods are not applicable.

In the first section, a brief discussion is given of tensor theory, after which tensor equations are developed for the elastic, piezoelectric, and dielectric equations of Chapter III. These tensor equations are applied to the transformation of piezoelectric equations from a fixed set of axes to a rotated set and the resulting constants for the various crystal classes are determined. The tensor equations are applied to pyroelectric effects and to second-order electrostrictive, piezo-optical, and electro-optical effects. In the sections A.7 and A.8, they are applied to calculating the classical losses in sound transmission in gases, liquids and solids due to viscosity, heat conduction and hysteresis, and to thermal relaxation effects.

The notation employed is that given by Jeffreys in his book *Cartesian Tensors*. In this notation, no distinction is made between covariant and contravariant tensors. The cartesian notation can also be applied to curvilinear coordinates if the basis vectors are taken as unit length vectors lying along the directions of the curvilinear coordinates. An example for cylindrical coordinates is given in section A.9. Hence it does not appear that the more general and more complicated covariant and contravariant notation is justified for any of the common applications for mechanics, electric field theory or for application with piezoelectric crystals.

On the other hand for such complex applications as the general theory of relativity the more complicated covariant and contravariant notation is a necessity. A general discussion of the notation as applied to mathematical physics will appear in a forthcoming book by J. A. Schouten *Tensor*

[1] The matrix method is well described by W. L. Bond, "The Mathematics of the Physical Properties of Crystals," *B.S.T.J.*, Vol. 22, pp. 1–72, 1943.

Calculus for Physicists, Clarendon Press, 1949. One chapter is devoted to piezoelectric crystals.

A.1 *General Properties of Tensors*

The expressions for the piezoelectric relations discussed in Chapter III can be considerably abbreviated by expressing them in tensor form. Furthermore, the calculation of elastic constants for rotated crystals is considerably simplified by the geometrical transformation laws established for tensors. Hence it has seemed worth-while to express the elastic, electric, and piezoelectric relations of a piezoelectric crystal in tensor form. It is the purpose of this section to discuss the general properties of tensors applicable to Cartesian coordinates.

If we have two sets of rectangular axes (Ox, Oy, Oz) and (Ox', Oy', Oz') having the same origin, the coordinates of any point P with respect to the second set are given in terms of the first set by the equations

$$\begin{aligned} x' &= l_1x + m_1y + n_1z \\ y' &= l_2x + m_2y + n_2z \\ z' &= l_3x + m_3y + n_3z. \end{aligned} \tag{A.1}$$

The quantities ($l_1, \cdots, n_3$) are the cosines of the angles between the various axes; thus l_1 is the cosine of the angle between the axes Ox', and Ox; n_3 the cosine of the angle between Oz' and Oz, and so on. By solving the equations (A.1) simultaneously, the coordinates x, y, z can be expressed in terms of x', y', z' by the equations

$$\begin{aligned} x &= l_1x' + l_2y' + l_3z' \\ y &= m_1x' + m_2y' + m_3z' \\ z &= n_1x' + n_2y' + n_3z'. \end{aligned} \tag{A.2}$$

We can shorten the writing of equations (A.1) and (A.2) considerably by changing the notation. Instead of x, y, z let us write x_1, x_2, x_3 and in place of x', y', z' we write x_1', x_2', x_3'. We can now say that the coordinates with respect to the first system are x_i, where i may be 1, 2, 3 while those with respect to the second system are x_j', where $j = 1$, 2 or 3. Then in (A.1) each coordinate x_j' is expressed as the sum of three terms depending on the three x_i. Each x_i is associated with the cosine of the angle between the direction of x_i increasing and that of x_j' increasing. Let us denote this cosine by a_{ij}. Then we have for all values of j,

$$x_j' = a_{1j}x_1 + a_{2j}x_2 + a_{3j}x_3 = \sum_{i=1}^{3} a_{ij}x_i. \tag{A.3}$$

Conversely, equation (A.2) can be written

$$x_i = \sum_{j=1}^{3} a_{ij} x_j' \tag{A.4}$$

where the a_{ij} have the same value as in (A.3), for the same values of i and j, since in both cases the cosine of the angle is between the values of x_i and x_j, increasing. Such a set of three quantities involving a relation between two coordinate systems is called a tensor of the first rank or a vector.

We note that each of the equations (A.3), (A.4) is really a set of three equations. Where the suffix i or j appears on the left it is to be given in turn all the values 1, 2, 3 and the resulting equation is one of the set. In each such equation the right side is the sum of three terms obtained by giving j or i the values 1, 2, 3 in turn and adding. Whenever such a summation occurs a suffix is repeated in the expression for the general term as $a_{ij}x_j'$. We make it a regular convention that whenever a suffix is repeated it is to be given all possible values and that the terms are to be added for all. Then (A.3) can be written simply as

$$x_j' = a_{ij} x_i$$

the summation being automatically understood by the convention.

There are single quantities such as mass and distance, that are the same for all systems of coordinates. These are called tensors of the zero rank or scalars.

Consider now two tensors of the first rank u_i and v_k. Suppose that each component of one is to be multiplied by each component of the other, then we obtain a set of nine quantities expressed by $u_i v_k$, where i and k are independently given all the values 1, 2, 3. The components of $u_i v_k$ with respect to the x_j' set of axes are $u_j' v_l'$, and

$$u_i' v_l' = (a_{ij} u_i)(a_{kl} v_k) = a_{ij} a_{kl} u_i v_k. \tag{A.5}$$

The suffixes i and k are repeated on the right. Hence (A.5) represents nine equations, each with nine terms. Each term on the right is the product of two factors, one of the form $a_{ij}a_{kl}$, depending only on the orientation of the axes, and the other of the form $u_i v_k$, representing the products of the components referred to the original axes. In this way the various $u_j' v_l'$ can be obtained in terms of the original $u_i v_k$. Products of vectors are not the only quantities satisfying the rule; in general a set of nine quantities w_{ik} referred to a set of axes, and transformed to another set by the rule

$$w_{jl}' = a_{ij} a_{kl} w_{ik} \tag{A.6}$$

is called a tensor of the second rank.

Higher order tensors can be formed by taking the products of more

vectors. Thus a set of n quantities that transforms like the vector product $x_i x_j \cdots x_p$ is called a tensor of rank n, where n is the number of factors.

On the right-hand side of (A.6) the i and k are dummy suffixes; that is, they are given the numbers 1 to 3 and summed. It, therefore, makes no difference which we call i and which k so that

$$w'_{jl} = a_{ij}a_{kl}w_{ik} = a_{kj}a_{il}w_{kl}. \tag{A.7}$$

Hence w_{kl} transforms by the same rule as w_{ik} and hence is a tensor of the second rank. The importance of this is that if we have a set of quantities

$$\begin{vmatrix} w_{11} & w_{12} & w_{13} \\ w_{21} & w_{22} & w_{23} \\ w_{31} & w_{32} & w_{33} \end{vmatrix} \tag{A.8}$$

which we know to be a tensor of the second rank, the set of quantities

$$\begin{vmatrix} w_{11} & w_{21} & w_{31} \\ w_{12} & w_{22} & w_{32} \\ w_{13} & w_{23} & w_{33} \end{vmatrix} \tag{A.9}$$

is another tensor of the second rank. Hence the sum $(w_{ik} + w_{ki})$ and the difference $(w_{ik} - w_{ki})$ are also tensors of the second rank. The first of these has the property that it is unaltered by interchanging i and k and therefore it is called a symmetrical tensor. The second has its components reversed in sign when i and k are interchanged. It is therefore an antisymmetrical tensor. Clearly in an antisymmetrical tensor all the leading diagonal components will be zero, *i.e.*, those with $i = k$ will be zero. Now since

$$w_{ik} = \tfrac{1}{2}(w_{ik} + w_{ki}) + \tfrac{1}{2}(w_{ik} - w_{ki}) \tag{A.10}$$

we can consider any tensor of the second rank as the sum of a symmetrical and an antisymmetrical tensor. Most tensors in the theory of elasticity are symmetrical tensors.

The operation of putting two suffixes in a tensor equal and adding the terms is known as contraction of the tensor. It gives a tensor two ranks lower than the original one. If, for instance, we contract the tensor $u_i v_k$ we obtain

$$u_i v_i = u_1 v_1 + u_2 v_2 + u_3 v_3 \tag{A.11}$$

which is the scalar product of u_i and v_k and hence is a tensor of zero rank.

We wish now to derive the formulae for tensor transformation to a new set of axes. For a tensor of the first rank (a vector) this has been given by equation (A.1). But the direction cosines l_1 to n_3 can be expressed in the form

$$l_1 = \frac{\partial x'}{\partial x} = \frac{\partial x'_1}{\partial x_1}; \qquad l_2 = \frac{\partial y'}{\partial x} = \frac{\partial x'_2}{\partial x_1}; \qquad l_3 = \frac{\partial z'}{\partial x} = \frac{\partial x'_3}{\partial x_1}$$

$$m_1 = \frac{\partial x'}{\partial y} = \frac{\partial x_1'}{\partial x_2}; \qquad m_2 = \frac{\partial y'}{\partial y} = \frac{\partial x_2'}{\partial x_2}; \qquad m_3 = \frac{\partial z'}{\partial y} = \frac{\partial x_3'}{\partial x_2} \tag{A.12}$$

$$n_1 = \frac{\partial x'}{\partial z} = \frac{\partial x_1'}{\partial x_3}; \qquad n_2 = \frac{\partial y'}{\partial z} = \frac{\partial x_2'}{\partial x_3}; \qquad n_3 = \frac{\partial z'}{\partial z} = \frac{\partial x_3'}{\partial x_3}.$$

Hence equation (A.1) can be expressed in the tensor form

$$x_j' = \frac{\partial x_j'}{\partial x_i} x_i = a_{ij} x_i. \tag{A.13}$$

Similarly since a tensor of the second rank can be regarded as the product of two vectors, it can be transformed according to the equation

$$x_j' x_l' = \left(\frac{\partial x_j'}{\partial x_i} x_i\right)\left(\frac{\partial x_l'}{\partial x_k} x_k\right) = \frac{\partial x_j'}{\partial x_i} \frac{\partial x_l'}{\partial x_k} x_i x_k \tag{A.14}$$

which can also be expressed in the generalized form

$$w_{jl}' = \frac{\partial x_j'}{\partial x_i} \frac{\partial x_l'}{\partial x_k} w_{ik}. \tag{A.15}$$

In general the transformation equation of a tensor of the nth rank can be written

$$X'_{k_1 \cdots k_n} = \frac{\partial x_{k_1}}{\partial x_{j_1}} \frac{\partial x_{k_2}}{\partial x_{j_2}} \cdots \frac{\partial x_{k_n}}{\partial x_{j_n}} X_{j_1 j_2 \cdots j_n}. \tag{A.16}$$

A.2 *Application of Tensor Notation to the Elastic, Piezoelectric and Dielectric Equations of a Crystal*

Let us consider the stress components of equation (3.7)

$$\begin{vmatrix} T_{xx} & T_{xy} & T_{xz} \\ T_{yx} & T_{yy} & T_{yz} \\ T_{zx} & T_{zy} & T_{zz} \end{vmatrix}$$

and equation (3.8) for a symmetrical tensor

$$T_{xy} = T_{yx}; \qquad T_{xz} = T_{zx}; \qquad T_{yz} = T_{zy}$$

We designate the components in the manner shown by equation (A. 17) to correspond with tensor notations

$$\begin{vmatrix} T_{11} & T_{12} & T_{13} \\ T_{21} & T_{22} & T_{23} \\ T_{31} & T_{32} & T_{33} \end{vmatrix} = \begin{vmatrix} T_{11} & T_{12} & T_{13} \\ T_{12} & T_{22} & T_{23} \\ T_{13} & T_{23} & T_{33} \end{vmatrix} \tag{A.17}$$

by virtue of the relations of (3.8). We wish to show now that the set of 9 elements of the equation constitutes a tensor, and by virtue of the relations of (3.8) a symmetrical tensor.

The transformation of the stress components to a new set of axes x', y', z' has been shown by Love[2] to take the form

$$T'_{xx} = l_1^2 T_{xx} + m_1^2 T_{yy} + n_1^2 T_{zz} + 2l_1 m_1 T_{xy} + 2l_2 n_1 T_{xz} + 2m_1 n_1 T_{yz}$$

$$\cdots\cdots\cdots\cdots\cdots\cdots\cdots\cdots\cdots\cdots\cdots\cdots\cdots\cdots\cdots\cdots\cdots\cdots \quad \text{(A.18)}$$

$$T'_{xy} = l_1 l_2 T_{xx} + m_1 m_2 T_{yy} + n_1 n_2 T_{zz} + (l_1 m_2 + l_2 m_1) T_{xy} + (l_1 n_2 + l_2 n_1) T_{xz} + (m_1 n_2 + n_1 m_2) T_{yz}$$

where l_1 to n_3 are the direction cosines between the axes as specified by equation (A.1). Noting that from (A.12)

$$l_1 = \frac{\partial x'_1}{\partial x_1}, \quad \cdots, \quad n_3 = \frac{\partial x'_3}{\partial x_3}$$

the first of these equations can be put in the form

$$\begin{aligned} T'_{11} = {} & \left(\frac{\partial x'_1}{\partial x_1}\right)^2 T_{11} + \frac{\partial x'_1}{\partial x_1}\frac{\partial x'_1}{\partial x_2} T_{12} + \frac{\partial x'_1}{\partial x_1}\frac{\partial x'_1}{\partial x_3} T_{13} \\ & + \frac{\partial x'_1}{\partial x_2}\frac{\partial x'_1}{\partial x_1} T_{21} + \left(\frac{\partial x'_1}{\partial x_2}\right)^2 T_{22} + \frac{\partial x'_1}{\partial x_2}\frac{\partial x'_1}{\partial x_3} T_{23} \\ & + \frac{\partial x'_1}{\partial x_3}\frac{\partial x'_1}{\partial x_1} T_{31} + \frac{\partial x'_1}{\partial x_3}\frac{\partial x'_1}{\partial x_2} T_{32} + \left(\frac{\partial x_1}{\partial x_3}\right)^2 T_{33} = \frac{\partial x'_1}{\partial x_k}\frac{\partial x'_1}{\partial x_l} T_{kl} \end{aligned} \quad \text{(A.19)}$$

while the last equation takes the form

$$\begin{aligned} T'_{12} = {} & \frac{\partial x'_1}{\partial x_1}\frac{\partial x'_2}{\partial x_1} T_{11} + \frac{\partial x'_1}{\partial x_1}\frac{\partial x'_2}{\partial x_2} T_{12} + \frac{\partial x'_1}{\partial x_1}\frac{\partial x'_2}{\partial x_3} T_{13} \\ & + \frac{\partial x'_1}{\partial x_2}\frac{\partial x'_2}{\partial x_1} T_{21} + \frac{\partial x'_1}{\partial x_2}\frac{\partial x'_2}{\partial x_2} T_{22} + \frac{\partial x'_1}{\partial x_2}\frac{\partial x'_2}{\partial x_3} T_{23} \\ & + \frac{\partial x'_1}{\partial x_3}\frac{\partial x'_2}{\partial x_1} T_{31} + \frac{\partial x'_1}{\partial x_3}\frac{\partial x'_2}{\partial x_2} T_{32} + \frac{\partial x'_1}{\partial x_3}\frac{\partial x'_2}{\partial x_3} T_{33} = \frac{\partial x'_1}{\partial x_k}\frac{\partial x'_2}{\partial x_l} T_{kl}. \end{aligned} \quad \text{(A.20)}$$

The general expression for any component then is

$$T'_{ij} = \frac{\partial x'_i}{\partial x_k}\frac{\partial x'_j}{\partial x_l} T_{kl} \quad \text{(A.21)}$$

which is the transformation equation of a tensor of the second rank. Hence the stress components satisfy the conditions for a second-rank tensor.

[2] Love, A. H., *Theory of Elasticity*, p. 80, Cambridge Univ. Press. 4th Edition, 1934.

The strain components

$$\begin{vmatrix} S_{xx} & S_{xy} & S_{xz} \\ S_{yx} & S_{yy} & S_{yz} \\ S_{zx} & S_{zy} & S_{zz} \end{vmatrix}$$

do not, however, satisfy the conditions for a second-rank tensor. This is shown by the transformation of strain components to a new set of axes, which have been shown by Love, to satisfy the equations

$$\begin{aligned} S'_{xx} &= l_1^2 S_{xx} + m_1^2 S_{yy} + n_1^2 S_{zz} + l_1 m_1 S_{xy} + l_1 n_1 S_{zx} + m_1 n_1 S_{yz} \\ &\cdots\cdots\cdots\cdots\cdots\cdots\cdots\cdots\cdots\cdots\cdots\cdots\cdots\cdots\cdots\cdots\cdots\cdots \quad \text{(A.22)} \\ S'_{xy} &= 2l_1 l_2 S_{xx} + 2m_1 m_2 S_{yy} + 2n_1 n_2 S_{zz} + (l_1 m_2 + l_2 m_1) S_{xy} \\ &\quad + (l_1 n_2 + n_1 l_2) S_{xz} + (m_1 n_2 + m_2 n_1) S_{xy}. \end{aligned}$$

If, however, we take the strain components as

$$\begin{aligned} S_{11} = S_{xx} &= \frac{\partial \xi}{\partial x}; \qquad S_{22} = S_{yy} = \frac{\partial \eta}{\partial y}; \qquad S_{33} = S_{zz} = \frac{\partial \zeta}{\partial z} \\ S_{12} = S_{21} &= \frac{S_{xy}}{2} = \frac{1}{2}\left(\frac{\partial \eta}{\partial x} + \frac{\partial \xi}{\partial y}\right); \qquad S_{13} = S_{31} = \frac{S_{xz}}{2} \qquad \text{(A.23)} \\ &= \frac{1}{2}\left(\frac{\partial \xi}{\partial z} + \frac{\partial \zeta}{\partial x}\right); \qquad S_{23} = S_{32} = \frac{S_{yz}}{2} = \frac{1}{2}\left(\frac{\partial \zeta}{\partial y} + \frac{\partial \eta}{\partial z}\right) \end{aligned}$$

the nine components

$$\begin{vmatrix} S_{11} & S_{12} & S_{13} \\ S_{21} & S_{22} & S_{23} \\ S_{31} & S_{32} & S_{33} \end{vmatrix}$$

will form a tensor of the second rank, as can be shown by the transformation-equations of (A.22).

The generalized Hooke's law given by equation (3.22) becomes

$$T_{ij} = c_{ijkl} S_{kl} \qquad \text{(A.24)}$$

c_{ijkl} is a fourth-rank tensor. The right-hand side of the equation being the product of a fourth-rank tensor by a second-rank tensor is a sixth-rank tensor, but since it has been contracted twice by having k and l in both terms the resultant of the right-hand side is a second-rank tensor. Since c_{ijkl} is a tensor of the fourth rank it will, in general, have 81 terms, but on account of the symmetry of the T_{ij} and S_{kl} tensors, there are many equivalences between the resulting elastic constants. These equivalences can be determined by expanding the terms of (A.24) and comparing with the

equivalent expressions of (3.22). For example

$$\begin{aligned} T_{11} = {} & c_{1111}S_{11} + c_{1112}S_{12} + c_{1113}S_{13} \\ & + c_{1121}S_{21} + c_{1122}S_{22} + c_{1123}S_{23} \\ & + c_{1131}S_{31} + c_{1132}S_{32} + c_{1133}S_{33}. \end{aligned} \tag{A.25}$$

Comparing this equation with the first of (3.22) noting that $S_{12} = S_{21} = \frac{S_{xy}}{2}$, etc., we have

$$\begin{aligned} & c_{1111} = c_{11}; \quad c_{1112} = c_{1121} = c_{16}; \quad c_{1133} = c_{13}; \\ & c_{1113} = c_{1131} = c_{15}; \quad c_{1122} = c_{12}; \quad c_{1123} = c_{1132} = c_{14}. \end{aligned} \tag{A.26}$$

In a similar manner it can be shown that the elastic constants of (3.22) correspond to the tensor elastic constants c_{ijkl} according to the relations

$$\begin{aligned} & c_{11} = c_{1111}; \quad c_{12} = c_{1122} = c_{2211}; \quad c_{13} = c_{1133} = c_{3311}; \\ & c_{14} = c_{1123} = c_{1132} = c_{2311} = c_{3211}; \quad c_{15} = c_{1113} = c_{1131} = c_{1311} = c_{3111}; \\ & c_{16} = c_{1112} = c_{1121} = c_{1211} = c_{2111}; \quad c_{22} = c_{2222}; \quad c_{23} = c_{2233} = c_{3322}; \\ & c_{24} = c_{2223} = c_{2232} = c_{2322} = c_{3222}; \quad c_{25} = c_{2213} = c_{2231} = c_{1322} = c_{3122}; \\ & c_{26} = c_{2212} = c_{2221} = c_{1222} = c_{2122}; \quad c_{33} = c_{3333}; \\ & c_{34} = c_{3323} = c_{3332} = c_{2333} = c_{3233}; \quad c_{35} = c_{3313} = c_{3331} = c_{1333} = c_{3133}; \\ & c_{36} = c_{3312} = c_{3321} = c_{1233} = c_{2133}; \quad c_{44} = c_{2323} = c_{2332} = c_{3223} = c_{3232}; \\ & c_{45} = c_{2313} = c_{2331} = c_{3213} = c_{3231} = c_{1323} = c_{1332} = c_{3132} = c_{3123}; \\ & c_{46} = c_{2312} = c_{2321} = c_{3212} = c_{3221} = c_{1223} = c_{1232} = c_{2123} = c_{2132}; \\ & c_{55} = c_{1313} = c_{1331} = c_{3113} = c_{3131}; \\ & c_{56} = c_{1312} = c_{1321} = c_{3112} = c_{3121} = c_{1213} = c_{1231} = c_{2113} = c_{2131}; \\ & c_{66} = c_{1212} = c_{1221} = c_{2112} = c_{2121}. \end{aligned} \tag{A.27}$$

Hence there are only 21 independent constants of the 81 c_{ijkl} constants which are determined from the ordinary elastic constants c_{ij} by replacing

1 by 11; 2 by 22; 3 by 33; 4 by 23; 5 by 13; 6 by 12 (A.28)

and taking all possible permutations of these constants by interchanging them in pairs.

The inverse elastic equations (3.26) can be written in the simplified form

$$S_{ij} = s_{ijkl}T_{kl}. \tag{A.29}$$

By expanding these equations and comparing with equations (3.26) we can establish the relationships

$$s_{11} = s_{1111}; \quad s_{12} = s_{1122} = s_{2211}; \quad s_{13} = s_{1133} = s_{3311};$$

$$\frac{s_{14}}{2} = s_{1123} = s_{1132} = s_{2311} = s_{3211}; \quad \frac{s_{15}}{2} = s_{1113} = s_{1131} =$$

$$s_{1311} = s_{3111}; \quad \frac{s_{16}}{2} = s_{1112} = s_{1121} = s_{1211} = s_{2111}; \quad s_{22} = s_{2222};$$

$$s_{23} = s_{2233} = s_{3322}; \quad \frac{s_{24}}{2} = s_{2223} = s_{2232} = s_{2322} = s_{3222};$$

$$\frac{s_{25}}{2} = s_{2213} = s_{2231} = s_{1322} = s_{3122}; \quad \frac{s_{26}}{2} = s_{2212} = s_{2221} =$$

$$s_{1222} = s_{2122}; \quad s_{33} = s_{3333}; \quad \frac{s_{34}}{2} = s_{3323} = s_{3332} = s_{2333} = s_{3233};$$

$$\frac{s_{35}}{2} = s_{3313} = s_{3331} = s_{1333} = s_{3133}; \quad \frac{s_{36}}{2} = s_{3312} = s_{3321} = \qquad \text{(A.30)}$$

$$s_{1233} = s_{2133}; \quad \frac{s_{44}}{4} = s_{2323} = s_{2332} = s_{3223} = s_{3232};$$

$$\frac{s_{45}}{4} = s_{2313} = s_{2331} = s_{3213} = s_{3231} = s_{1323} = s_{1332} = s_{3123} =$$

$$s_{3132}; \quad \frac{s_{46}}{4} = s_{2312} = s_{2321} = s_{3212} = s_{3221} = s_{1223} = s_{1232} =$$

$$s_{2123} = s_{2132}; \quad \frac{s_{55}}{4} = s_{1313} = s_{1331} = s_{3113} = s_{3131};$$

$$\frac{s_{56}}{4} = s_{1312} = s_{1321} = s_{3112} = s_{3121} = s_{1213} = s_{1231} = s_{2113} =$$

$$s_{2131}; \quad \frac{s_{66}}{4} = s_{1212} = s_{1221} = s_{2112} = s_{2121}.$$

Here again the s_{ijkl} elastic constants are determined from the ordinary elastic constants s_{ij} by replacing

1 by 11; 2 by 22; 3 by 33; 4 by 23; 5 by 13; 6 by 12.

However for any number 4, 5, or 6, the elastic compliance s_{ij} has to be divided by 2 to equal the corresponding s_{ijkl} compliance, and if 4, 5 or 6 occurs twice, the divisor has to be 4.

The isothermal elastic compliance of equations (3.35) can be expressed in tensor form

$$S_{ij} = s^{\Theta}_{ijkl} T_{kl} + \alpha_{ij}\, d\Theta \qquad \text{(A.31)}$$

where as before α_{ij} is a tensor of the second rank having the relations to the ordinary coefficients of expansion

$$\alpha_1 = \alpha_{11}; \quad \alpha_2 = \alpha_{22}; \quad \alpha_3 = \alpha_{33};$$

$$\frac{\alpha_4}{2} = \alpha_{23}; \quad \frac{\alpha_5}{2} = \alpha_{13}; \quad \frac{\alpha_6}{2} = \alpha_{12}.$$

The heat-temperature equation of (3.35) is written in the simple form

$$dQ = \alpha_{kl} T_{kl} \Theta + \rho C_p \, d\Theta. \tag{A.32}$$

By eliminating $d\Theta$ from (A.32) and substituting in (A.31), the adiabatic constants are given in the simple form

$$s^{\sigma}_{ijkl} = s^{\Theta}_{ijkl} - \frac{\alpha_{ij}\alpha_{kl}\Theta}{\rho C_p}. \tag{A.33}$$

The combination elastic and piezoelectric equations (3.58) can be written in the tensor form

$$S_{ij} = s^{E}_{ijkl} T_{kl} + d_{mij} E_m; \qquad \delta_n = \frac{\epsilon^{T}_{mn}}{4\pi} E_m + d_{nkl} T_{kl}. \tag{A.34}$$

Here d_{mij} is a tensor of third rank and ϵ^{T}_{mn} one of second rank. The d_{mij} constants are related to the eighteen ordinary constants d_{ij} by the equations

$$d_{11} = d_{111}; \quad d_{12} = d_{122}; \quad d_{13} = d_{133}; \quad \frac{d_{14}}{2} = d_{123} = d_{132};$$

$$\frac{d_{15}}{2} = d_{113} = d_{131}; \quad \frac{d_{16}}{2} = d_{112} = d_{121}; \quad d_{21} = d_{211}; \quad d_{22} = d_{222};$$

$$d_{23} = d_{233}; \quad \frac{d_{24}}{2} = d_{223} = d_{232}; \quad \frac{d_{25}}{2} = d_{213} = d_{231}; \tag{A.35}$$

$$\frac{d_{26}}{2} = d_{212} = d_{221}; \quad d_{31} = d_{311}; \quad d_{32} = d_{322}; \quad d_{33} = d_{333};$$

$$\frac{d_{34}}{2} = d_{323} = d_{332}; \quad \frac{d_{35}}{2} = d_{313} = d_{331}; \quad \frac{d_{36}}{2} = d_{312} = d_{321}.$$

The tensor equations (A.34) give a simple method of expressing the piezoelectric equations in an alternate form which is useful for some purposes. This involves relating the stress, strain and displacement, rather than the applied field strength as in (A.34). To do this let us multiply through the right-hand equation of (A.34) by the tensor $4\pi\beta^{T}_{mn}$, obtaining

$$4\pi\beta^{T}_{mn}\delta_n = \epsilon^{T}_{mn}\beta^{T}_{mn} E_m + 4\pi d_{nkl}\beta^{T}_{mn} T_{kl} \tag{A.36}$$

where β^{T}_{mn} is a tensor of the " free " dielectric impermeability obtained from

the determinant

$$\beta_{mn}^{T} = (-1)^{(m+n)} \frac{\Delta_{mn}^{\epsilon T}}{\Delta^{\epsilon T}} \tag{A.37}$$

where $\Delta^{\epsilon T}$ is the determinant

$$\Delta^{\epsilon T} = \begin{vmatrix} \epsilon_{11}^{T} & \epsilon_{12}^{T} & \epsilon_{13}^{T} \\ \epsilon_{12}^{T} & \epsilon_{22}^{T} & \epsilon_{23}^{T} \\ \epsilon_{13}^{T} & \epsilon_{23}^{T} & \epsilon_{33}^{T} \end{vmatrix} \tag{A.38}$$

and $\Delta_{mn}^{\epsilon T}$ the minor obtained from this by suppressing the mth row and nth column. If we take the product $\epsilon_{mn}^{T}\beta_{mn}^{T}$ for the three values of m, we have as multipliers of E_1, E_2, E_3, respectively

$$\begin{aligned} \epsilon_{11}^{T}\,\beta_{11}^{T} + \epsilon_{12}^{T}\,\beta_{12}^{T} + \epsilon_{13}^{T}\,\beta_{13}^{T} &= 1 \\ \epsilon_{21}^{T}\,\beta_{21}^{T} + \epsilon_{22}^{T}\,\beta_{22}^{T} + \epsilon_{23}^{T}\,\beta_{23}^{T} &= 1 \\ \epsilon_{31}^{T}\,\beta_{31}^{T} + \epsilon_{32}^{T}\,\beta_{32}^{T} + \epsilon_{33}^{T}\,\beta_{33}^{T} &= 1. \end{aligned} \tag{A.39}$$

But by virtue of equations (A.37) and (A.38) it is obvious that the value of each term of (A.39) is unity. Hence we have

$$E_m = 4\pi\beta_{mn}^{T}\,\delta_n - (4\pi\, d_{nkl}\,\beta_{mn}^{T})\,T_{kl}. \tag{A.40}$$

Since the dummy index n is summed for the values 1, 2, and 3, we can set the value of the terms in brackets equal to

$$g_{mkl} = 4\pi\, d_{nkl}\,\beta_{mn}^{T} = 4\pi[d_{1kl}\,\beta_{m1}^{T} + d_{2kl}\,\beta_{m2}^{T} + d_{3kl}\,\beta_{m3}^{T}] \tag{A.41}$$

and equation (A.40) becomes

$$E_m = 4\pi\,\beta_{mn}^{T}\,\delta_n - g_{mkl}\,T_{kl}. \tag{A.42}$$

Substituting this equation in the first equations of (A.34) we have

$$S_{ij} = s_{ijkl}^{D}\,T_{kl} + g_{nij}\,\delta_n \tag{A.43}$$

where

$$s_{ijkl}^{D} = s_{ijkl}^{E} - d_{mij}\,g_{mkl} = s_{ijkl}^{E} - 4\pi[\beta_{mn}^{T}\,d_{nkl}\,d_{mij}].$$

By substituting in the various values of i, j, k and l corresponding to the 21 elastic constants, the difference between the constant displacement and constant potential elastic constants can be calculated. If equations (A.42) and (A.43) are expressed in terms of the $S_1, \cdots, S_6$ strains and $T_1, \cdots, T_6$ stresses, the g_{nij} constants are related to the g_{ij} constants as are the corresponding d_{ij} constants to the d_{nij} constants of equation (A.35).

Another variation of the piezoelectric equations which is sometimes employed is one for which the stresses are expressed in terms of the strains

and field strength. This form can be derived directly from equations (A.34) by multiplying both sides of the first equation by the tensor c^E_{ijkl} for the elastic constants, where these are defined in terms of the corresponding s^E_{ij} elastic compliances by the equation

$$c^E_{ij} = (-1)^{(i+j)}\,\Delta^{sE}_{ij}/\Delta^{sE} \tag{A.44}$$

where Δ is the determinant

$$\Delta^{sE} = \begin{vmatrix} s^E_{11} & s^E_{12} & s^E_{13} & s^E_{14} & s^E_{15} & s^E_{16} \\ s^E_{12} & s^E_{22} & s^E_{23} & s^E_{24} & s^E_{25} & s^E_{26} \\ s^E_{13} & s^E_{23} & s^E_{33} & s^E_{34} & s^E_{35} & s^E_{36} \\ s^E_{14} & s^E_{24} & s^E_{34} & s^E_{44} & s^E_{45} & s^E_{46} \\ s^E_{15} & s^E_{25} & s^E_{35} & s^E_{45} & s^E_{55} & s^E_{56} \\ s^E_{16} & s^E_{26} & s^E_{36} & s^E_{46} & s^E_{56} & s^E_{66} \end{vmatrix}$$

and Δ^{sE}_{ij} in the minor obtained by suppressing the ith row and jth column. Carrying out the tensor multiplication we have

$$c^E_{ijkl}\,S_{ij} = c^E_{ijkl}\,s^E_{ijkl}\,T_{kl} + d_{mij}\,c^E_{ijkl}\,E_m. \tag{A.45}$$

As before we find that the tensor product of $c^E_{ijkl}\,s^E_{ijkl}$ is unity for all values of k and l. Hence equation (A.45) can be written in the form

$$T_{kl} = c^E_{ijkl}\,S_{ij} - e_{mkl}\,E_m \tag{A.46}$$

where e_{mkl} is the sum

$$e_{mkl} = d_{mij}\,c^E_{ijkl} \tag{A.47}$$

summed for all values of the dummy indices i and j. If we substitute the equation (A.46) in the last equation of (A.34), we find

$$\delta_n = \frac{\epsilon^S_{mn}}{4\pi}\,E_m + e_{nij}S_{ij} \tag{A.48}$$

where ϵ^S_{mn} the clamped dielectric constant is related to the free dielectric constant ϵ^T_{mn} by the equation

$$\epsilon^S_{mn} = \epsilon^T_{mn} - 4\pi[d_{nkl}\,e_{mkl}]. \tag{A.49}$$

Expressed in two-index piezoelectric constants involving the strains $S_1 \cdots S_6$ and stresses $T_1 \cdots T_6$ the relation between the two- and three-index piezoelectric constants is given by the equations

$$\begin{aligned}
&e_{11} = e_{111}; \quad e_{12} = e_{122}; \quad e_{13} = e_{133}; \quad e_{14} = e_{123} = e_{132}; \\
&e_{15} = e_{113} = e_{131}; \quad e_{16} = e_{112} = e_{121}; \quad e_{21} = e_{211}; \quad e_{22} = e_{222}; \\
&e_{23} = e_{233}; \quad e_{24} = e_{223} = e_{232}; \quad e_{25} = e_{213} = e_{231}; \\
&e_{26} = e_{212} = e_{221}; \quad e_{31} = e_{311}; \quad e_{32} = e_{322}; \quad e_{33} = e_{333}; \\
&e_{34} = e_{323} = e_{332}; \quad e_{35} = e_{313} = e_{331}; \quad e_{36} = e_{312} = e_{321}.
\end{aligned} \tag{A.50}$$

Finally, the fourth form for expressing the piezoelectric relation is the one given by equation (3.53). Expressed in tensor form, these equations become

$$T_{kl} = c^{D}_{ijkl} S_{ij} - h_{nkl}\,\delta_n; \qquad E_m = 4\pi\beta^{S}_{mn}\,\delta_n - h_{mij} S_{ij} \tag{A.51}$$

In this equation the three-index piezoelectric constants of equation (A.51) are related to the two-index constants of equation (3.53) as the e constants of (A.50). These equations can also be derived directly from (A.46) and (A.48) by eliminating E_m from the two equations. This substitution yields the additional relations

$$\begin{aligned} h_{nkl} &= 4\pi e_{mkl}\,\beta^{S}_{mn}; \qquad c^{D}_{ijkl} = c^{E}_{ijkl} + e_{mkl}\,h_{mij} \\ &= c^{E}_{ijkl} + 4\pi\, e_{mkl}\, e_{nij}\,\beta^{S}_{mn} \end{aligned} \tag{A.52}$$

where

$$\beta^{S}_{mn} = (-1)^{(m+n)}\,\Delta^{\epsilon S}_{mn}/\Delta^{\epsilon S}$$

in which

$$\Delta^{\epsilon S} = \begin{vmatrix} \epsilon^{S}_{11} & \epsilon^{S}_{12} & \epsilon^{S}_{13} \\ \epsilon^{S}_{12} & \epsilon^{S}_{22} & \epsilon^{S}_{23} \\ \epsilon^{S}_{13} & \epsilon^{S}_{23} & \epsilon^{S}_{33} \end{vmatrix}.$$

The four forms of the piezoelectric equations, and the relations between them are given in Table XXXII.

A.3 *Effect of Symmetry and Orientation on the Dielectric, Piezoelectric and Elastic Constants of Crystals*

All crystals can be divided into 32 classes depending on the type of symmetry. These groups can be divided into seven general classifications depending on how the axes are related and furthermore all 32 classes can be built out of symmetries based on twofold (binary) axes, threefold (trigonal) axes, fourfold axes of symmetry, sixfold axes of symmetry, planes of reflection symmetry and combinations of axis reflection symmetry besides a simple symmetry through the center. Each of these types of symmetry result in a reduction of the number of dielectric, piezoelectric, and elastic constants.

Since the tensor equation is easily transformed to a new set of axes by the transformation equations (A.16), this form is particularly advantageous for determining the reduction in elastic, piezoelectric and dielectric constants. For example, consider the second-rank tensors ϵ_{kl} and α_{kl} for the dielectric constant and the expansion coefficients. Ordinarily for the most general symmetry each tensor, since it is symmetrical, requires six independent coefficients. Suppose, however, that the x-axis is an axis of twofold or binary symmetry, *i.e.*, the properties along the positive z-axis are the same as those along the negative z-axis. If we rotate the axes

TABLE XXXII

FOUR FORMS OF THE ELASTIC, DIELECTRIC, AND PIEZOELECTRIC EQUATIONS AND THEIR INTERRELATIONS

Form	Elastic Relation	Electric Relation
1	$S_{ij} = s^E_{ijkl}T_{kl} + d_{mij}E_m$	$\delta_n = \frac{\epsilon^T_{mn}}{4\pi}E_n + d_{nkl}T_{kl}$
2	$S_{ij} = s^D_{ijkl}T_{kl} + g_{nij}\delta_n$	$E_m = 4\pi\beta^T_{mn}\delta_n - g_{mkl}T_{kl}$
3	$T_{kl} = c^E_{ijkl}S_{ij} - e_{mkl}E_m$	$\delta_n = \frac{\epsilon^S_{mn}}{4\pi}E_m + e_{nij}S_{ij}$
4	$T_{kl} = c^D_{ijkl}S_{ij} - h_{nkl}\delta_n$	$E_m = 4\pi\beta^S_{mn}\delta_n - h_{mij}S_{ij}$

Form	Relation Between Elastic Constants	Relation Between Piezoelectric Constants	Relation Between Dielectric Constants
1	$s^D_{ijkl} = s^E_{ijkl} - d_{mij}g_{mkl}$	$g_{mkl} = 4\pi\beta^T_{mn}d_{nkl}$	$\beta^T_{mn} = (-1)^{(m+n)}\Delta^{\epsilon T}_{mn}/\Delta^{\epsilon T}$
2	$c^E_{ij} = (-1)^{(i+j)}\Delta^{sE}_{ij}/\Delta^{sE}$	$e_{mkl} = d_{mij}c^E_{ijkl}$	$\epsilon^S_{mn} = \epsilon^T_{mn} - 4\pi(d_{nkl}e_{mkl})$
3	$c^D_{ijkl} = c^E_{ijkl} + e_{mkl}h_{mij}$	$h_{nkl} = 4\pi\beta^S_{mn}e_{mkl}$	$\beta^S_{mn} = \beta^T_{mn} + \frac{g_{nkl}h_{mkl}}{4\pi}$
4	$c^D_{ij} = (-1)^{(i+j)}\Delta^{sD}_{ij}/\Delta^{sD}$	$h_{nkl} = g_{nij}c^D_{ijkl}$	$\beta^S_{mn} = (-1)^{(m+n)}\Delta^{\epsilon S}_{mn}/\Delta^{\epsilon S}$

180° about the x-axis so that $+z$ is changed into $-z$, the direction cosines are

$$\begin{aligned} l_1 &= \frac{\partial x_1'}{\partial x_1} = 1; & m_1 &= \frac{\partial x_1'}{\partial x_2} = 0; & n_1 &= \frac{\partial x_1'}{\partial x_3} = 0 \\ l_2 &= \frac{\partial x_2'}{\partial x_1} = 0; & m_2 &= \frac{\partial x_2'}{\partial x_2} = -1; & n_2 &= \frac{\partial x_2'}{\partial x_3} = 0 \\ l_3 &= \frac{\partial x_3'}{\partial x_1} = 0; & m_3 &= \frac{\partial x_3'}{\partial x_2} = 0; & n_3 &= \frac{\partial x_3'}{\partial x_3} = -1. \end{aligned} \tag{A.53}$$

The tensor transformation equations for a second-rank tensor are

$$\epsilon'_{ij} = \frac{\partial x_i'}{\partial x_k}\frac{\partial x_j'}{\partial x_l}\epsilon_{kl}. \tag{A.54}$$

Applying (A.53) to (A.54) summing for all values of k and l for each value of i, and j we have the six components

$$\begin{aligned} \epsilon'_{11} &= \epsilon_{11}; & \epsilon'_{12} &= -\epsilon_{12}; & \epsilon'_{13} &= -\epsilon_{13}; \\ \epsilon'_{22} &= \epsilon_{22}; & \epsilon'_{23} &= \epsilon_{23}; & \epsilon'_{33} &= \epsilon_{33}. \end{aligned} \tag{A.55}$$

Since a crystal having the x-axis a binary axis of symmetry must have the same constants for a $+z$ direction as for a $-z$ direction, this condition can only be satisfied by

$$\epsilon_{12} = \epsilon_{13} = 0. \tag{A.56}$$

The same condition is true for the expansion coefficients since they form a second-rank tensor and hence

$$\alpha_{12} = \alpha_{13} = 0. \tag{A.57}$$

In a third-rank tensor such as d_{ijk}, e_{ijk}, g_{ijk}, h_{ijk}, we similarly find that of the eighteen independent constants

$$h_{112} = h_{16};\quad h_{113} = h_{15};\quad h_{211} = h_{21};\quad h_{222} = h_{22};\quad h_{223} = h_{24};$$

$$h_{233} = h_{23};\quad h_{311} = h_{31};\quad h_{322} = h_{32};\quad h_{323} = h_{34};\quad h_{333} = h_{33}. \tag{A.58}$$

are all zero. The same terms in the d_{ijk}, e_{ijk}, g_{ijk} tensors are also zero.

In a fourth-rank tensor such as c_{ijkl}, s_{ijkl}, applying the tensor transformation equation

$$c_{ijkl} = \frac{\partial x_i'}{\partial x_m}\frac{\partial x_j'}{\partial x_n}\frac{\partial x_k'}{\partial x_o}\frac{\partial x_l'}{\partial x_p}c_{mnop} \tag{A.59}$$

and the condition (A.53) we similarly find

$$c_{15} = c_{16} = c_{25} = c_{26} = c_{35} = c_{36} = c_{45} = c_{46} = 0. \tag{A.60}$$

If the binary axis had been the y-axis, the corresponding missing terms can be obtained by cyclically rotating the tensor indices. The missing terms are for the second-, third- and fourth-rank tensors, transformed to two index symbols,

$$\epsilon_{23}, \epsilon_{12};\qquad h_{11}, h_{12}, h_{13}, h_{15}, h_{24}, h_{26}, h_{31}, h_{32}, h_{33}, h_{35};$$

$$c_{14}, c_{16}, c_{24}, c_{26}, c_{34}, c_{36}, c_{45}, c_{56}. \tag{A.61}$$

Similarly if the z-axis is the binary axis, the missing constants are

$$\epsilon_{13}, \epsilon_{12};\qquad h_{11}, h_{12}, h_{13}, h_{16}, h_{21}, h_{22}, h_{23}, h_{26}, h_{34}, h_{35};$$

$$c_{14}, c_{15}, c_{24}, c_{25}, c_{34}, c_{35}, c_{46}, c_{56}. \tag{A.62}$$

Hence a crystal of the orthorhombic bisphenoidal class or class 6, which has three binary axes, the x, y and z directions, will have the remaining terms,

$$\epsilon_{11}, \epsilon_{22}, \epsilon_{33};\qquad h_{14}, h_{25}, h_{36};\qquad c_{11}, c_{12}, c_{13}, c_{22}, c_{23}, c_{33}, c_{44}, c_{55}, c_{66} \tag{A.63}$$

with similar terms for other tensors of the same rank. Rochelle salt is a crystal of this class.

If z is a threefold axis of symmetry, the direction cosines for a set of axes rotated 120° clockwise about z are,

$$\begin{aligned} l_1 &= \frac{\partial x_1'}{\partial x_1} = -.5; & m_1 &= \frac{\partial x_1'}{\partial x_2} = -.866; & n_1 &= \frac{\partial x_1'}{\partial x_3} = 0 \\ l_2 &= \frac{\partial x_2'}{\partial x_1} = .866; & m_2 &= \frac{\partial x_2'}{\partial x_2} = -.5; & n_2 &= \frac{\partial x_2'}{\partial x_3} = 0 \\ l_3 &= \frac{\partial x_3'}{\partial x_1} = 0; & m_3 &= \frac{\partial x_3'}{\partial x_2} = 0; & n_3 &= \frac{\partial x_3'}{\partial x_3} = 1. \end{aligned} \tag{A.64}$$

Applying these relations to equations (A.54) for a second-rank tensor, we find for the components

$$\begin{aligned} &\epsilon_{11}' = .25\epsilon_{11} + .866\epsilon_{12} + .75\epsilon_{22}; \quad \epsilon_{12}' = -.433\epsilon_{11} - .50\epsilon_{12} + .433\epsilon_{22} \\ &\epsilon_{13}' = -.5\epsilon_{13} - .866\epsilon_{23}; \qquad \epsilon_{22}' = .75\epsilon_{11} - .866\epsilon_{12} + .25\epsilon_{22} \\ &\qquad\qquad \epsilon_{23}' = .866\epsilon_{13} - .5\epsilon_{23}; \quad \epsilon_{33}' = \epsilon_{33}. \end{aligned} \tag{A.65}$$

For the third and fifth equations, since we must have $\epsilon_{13}' = \epsilon_{13}$; $\epsilon_{23}' = \epsilon_{23}$ in order to satisfy the symmetry relation, the equations can only be satisfied if

$$\epsilon_{13} = \epsilon_{23} = 0. \tag{A.66}$$

Similarly solving the first three equations simultaneously, we find

$$\epsilon_{12} = 0; \qquad \epsilon_{11} = \epsilon_{22}. \tag{A.67}$$

Hence the remaining constants are

$$\epsilon_{11} = \epsilon_{22}; \qquad \epsilon_{33}. \tag{A.68}$$

Similarly for third- and fourth-rank tensors, for a crystal having z a trigonal axis, the remaining terms are

$$\begin{aligned} &h_{11}, h_{12} = -h_{11}, h_{13} = 0; \qquad h_{14}, h_{15}, h_{16} = -h_{22} \\ &h_{21} = -h_{22}, h_{22}, h_{23} = 0, h_{24} = h_{15}; \qquad h_{25} = -h_{14}, h_{21} = -h_{11} \\ &h_{31}; \qquad h_{32} = h_{31}; \qquad h_{33}; \qquad h_{34} = 0; \qquad h_{35} = 0; \qquad h_{36} = 0 \end{aligned} \tag{A.69}$$

$$\begin{aligned} &c_{11}; \; c_{12}; \; c_{13}; \; c_{14}; \; c_{15} = -c_{25}; \; c_{16} = 0 \\ &c_{12}; \; c_{22} = c_{11}; \; c_{23} = c_{13}; \; c_{24} = -c_{14}; \; c_{25}; \; c_{26} = 0 \\ &c_{13}; \; c_{23} = c_{13}; \; c_{33}; \; c_{34} = 0; \; c_{35} = 0; \; c_{36} = 0 \\ &c_{14}; \; c_{24} = -c_{14}; \; c_{34} = 0; \; c_{44}; \; c_{45} = 0; \; c_{46} = c_{15} \\ &c_{15} = -c_{25}; \; c_{25}; \; c_{35} = 0; \; c_{45} = 0; \; c_{55} = c_{44}; \; c_{56} = c_{14} \\ &c_{16} = 0; \; c_{26} = 0; \; c_{36} = 0; \; c_{46} = c_{25}; \; c_{56} = c_{14}; \; c_{66} = \tfrac{1}{2}(c_{11} - c_{12}). \end{aligned} \tag{A.70}$$

If the z-axis is a trigonal axis and the x a binary axis, as it is in quartz, the resulting constants are obtained by combining the conditions (A.56), (A.58), (A.60) with conditions (A.68), (A.69), (A.70) respectively. The resulting second-, third- and fourth-rank tensors have the following terms

$$\begin{aligned} &\epsilon_{11}; \quad \epsilon_{12} = 0; \quad \epsilon_{13} = 0 \\ &\epsilon_{12} = 0; \quad \epsilon_{22} = \epsilon_{11}; \quad \epsilon_{23} = 0 \\ &\epsilon_{13} = 0; \quad \epsilon_{23} = 0; \quad \epsilon_{33} \end{aligned} \tag{A.71}$$

$$\begin{aligned} &h_{11};\ h_{12} = -h_{11};\ h_{13} = 0;\ h_{14};\ h_{15} = 0;\ h_{16} = 0 \\ &h_{21} = 0;\ h_{22} = 0;\ h_{23} = 0;\ h_{24} = 0;\ h_{25} = -h_{14};\ h_{26} = -h_{11} \\ &h_{31} = 0;\ h_{32} = 0;\ h_{33} = 0;\ h_{34} = 0;\ h_{35} = 0;\ h_{36} = 0 \end{aligned} \tag{A.72}$$

$$\begin{aligned} &c_{11};\ c_{12};\ c_{13};\ c_{14};\ c_{15} = 0;\ c_{16} = 0 \\ &c_{12};\ c_{22} = c_{11};\ c_{23} = c_{13};\ c_{24} = -c_{14};\ c_{25} = 0;\ c_{26} = 0 \\ &c_{13};\ c_{23} = c_{13};\ c_{33};\ c_{34} = 0;\ c_{35} = 0;\ c_{36} = 0 \\ &c_{14};\ c_{24} = -c_{14};\ c_{34} = 0;\ c_{44};\ c_{45} = 0;\ c_{46} = 0 \\ &c_{15} = 0;\ c_{25} = 0;\ c_{35} = 0;\ c_{45} = 0;\ c_{55} = c_{44};\ c_{56} = c_{14} \\ &c_{16} = 0;\ c_{26} = 0;\ c_{36} = 0;\ c_{46} = 0;\ c_{56} = c_{14};\ c_{66} = \tfrac{1}{2}(c_{11}-c_{12}). \end{aligned} \tag{A.73}$$

The results of the symmetries of the 32 classes on the elastic, piezoelectric and dielectric constants are given in Chapter III, equations (3.63), (3.64), (3.65) and (3.66).

A.4 *Piezoelectric Equations for Rotated Axes*

Another application of the tensor equations for rotated axes is in determining the piezoelectric equations of crystals whose length, width, and thickness do not coincide with the crystallographic axes of the crystal. Such oriented cuts are useful for they sometimes give properties that cannot be obtained with crystals lying along the crystallographic axes. Such properties may be higher electromechanical coupling, freedom from coupling to undesired modes of motion, or low temperature coefficients of frequency. Hence, in order to obtain the performance of such crystals, it is necessary to be able to express the piezoelectric equations in a form suitable for these orientations. In fact, in first measuring the properties of these crystals, a series of oriented cuts is commonly used, since by employing such cuts the resulting frequencies and impedances can be used to calculate all the primary constants of the crystal.

The piezoelectric equations (A.51) are

$$T_{kl} = c^D_{ijkl} S_{ij} - h_{nkl}\delta_n; \qquad E_m = 4\pi\beta^S_{mn}\delta_n - h_{mij}S_{ij}. \tag{A.51}$$

The first equation is a tensor of the second rank, while the second equation is a tensor of the first rank. If we wish to transform these equations to another set of axes x', y', z', we can employ the tensor transformation equations

$$\begin{aligned} T'_{kl} &= \frac{\partial x'_k}{\partial x_k}\frac{\partial x'_l}{\partial x_l} T_{kl} \\ &= \frac{\partial x'_k}{\partial x_k}\frac{\partial x'_l}{\partial x_l} \cdot [c^D_{11kl}S_{11} + 2c^D_{12kl}S_{12} + 2c^D_{13kl}S_{13} + c^D_{22kl}S_{22} \\ &\quad + 2c^D_{23kl}S_{23} + c^D_{33kl}S_{33}] - \frac{\partial x'_k}{\partial x_k}\frac{\partial x'_l}{\partial x_l}[h_{1kl}\delta_1 + h_{2kl}\delta_2 + h_{3kl}\delta_3] \\ E'_m &= 4\pi\frac{\partial x'_m}{\partial x_m}[\beta^S_{m1}\delta_1 + \beta^S_{m2}\delta_2 + \beta^S_{m3}\delta_3] - \frac{\partial x'_m}{\partial x_m} \times \\ &\quad [h_{m11}S_{11} + 2h_{m12}S_{12} + 2h_{m13}S_{13} + h_{m22}S_{22} + 2h_{m23}S_{23} + h_{m33}S_{33}]. \end{aligned} \tag{A.74}$$

These equations express the new stresses and fields in terms of the old strains and displacements. To complete the transformation we need to express all quantities in terms of the new axes. For this purpose we employ the tensor equations

$$S_{ij} = \frac{\partial x_i}{\partial x'_i}\frac{\partial x_j}{\partial x'_j} S'_{ij}; \qquad \delta_n = \frac{\partial x_n}{\partial x'_n}\delta'_n \tag{A.75}$$

where $\frac{\partial x_i}{\partial x'_i}$ are the direction cosines between the old and new axes. It is obvious that $\frac{\partial x'_i}{\partial x_i} = \frac{\partial x_i}{\partial x'_i}$ and the relations can be written

$$\begin{aligned} l_1 &= \frac{\partial x'_1}{\partial x_1} = \frac{\partial x_1}{\partial x'_1}; & l_2 &= \frac{\partial x_1}{\partial x'_2}; & l_3 &= \frac{\partial x_1}{\partial x'_3} \\ m_1 &= \frac{\partial x_2}{\partial x'_1}; & m_2 &= \frac{\partial x_2}{\partial x'_2}; & m_3 &= \frac{\partial x_2}{\partial x'_3} \\ n_1 &= \frac{\partial x_3}{\partial x'_1}; & n_2 &= \frac{\partial x_3}{\partial x'_2}; & n_3 &= \frac{\partial x_3}{\partial x'_3}. \end{aligned} \tag{A.76}$$

Hence, substituting equations (A.75) in equations (A.74), the transforma-

tion equations between the new and old axes become

$$T'_{kl} = c^D_{ijkl} \frac{\partial x'_k}{\partial x_k} \frac{\partial x'_l}{\partial x_l} \frac{\partial x_i}{\partial x'_i} \frac{\partial x_j}{\partial x'_j} S'_{ij} - h_{mkl} \frac{\partial x'_k}{\partial x_k} \frac{\partial x'_l}{\partial x_l} \frac{\partial x_n}{\partial x'_n} \delta'_n$$

$$E'_m = 4\pi\beta^S_{mn} \frac{\partial x'_m}{\partial x_m} \frac{\partial x_n}{\partial x'_n} \delta'_n - h_{mij} \frac{\partial x'_m}{\partial x_m} \frac{\partial x_i}{\partial x'_i} \frac{\partial x_j}{\partial x'_j} S'_{ij}. \tag{A.77}$$

These equations then provide means for determining the transformation of constants from one set of axes to another.

As an example let us consider the case of an ADP crystal, vibrating longitudinally with its length along the x'_1-axis, its width along the x'_2-axis and its thickness along the x'_3-axis, which is also the x_3-axis, and determine the elastic, piezoelectric and dielectric constants that apply for this cut when x'_1 is $\Theta = 45°$ from x_1. Under these conditions

$$l_1 = \frac{\partial x'_1}{\partial x_1} = \frac{\partial x_1}{\partial x'_1} = \cos\theta; \qquad l_2 = \frac{\partial x'_2}{\partial x_1} = \frac{\partial x_1}{\partial x'_2} = -\sin\theta;$$

$$l_3 = \frac{\partial x'_3}{\partial x_1} = \frac{\partial x_1}{\partial x'_3} = 0$$

$$m_1 = \frac{\partial x'_1}{\partial x_2} = \frac{\partial x_2}{\partial x'_1} = \sin\theta; \qquad m_2 = \frac{\partial x'_2}{\partial x_2} = \frac{\partial x_2}{\partial x'_2} = \cos\theta; \tag{A.78}$$

$$m_3 = \frac{\partial x'_3}{\partial x_2} = \frac{\partial x_2}{\partial x'_3} = 0$$

$$n_1 = \frac{\partial x'_1}{\partial x_3} = \frac{\partial x_3}{\partial x'_1} = 0; \qquad n_2 = \frac{\partial x'_2}{\partial x_3} = \frac{\partial x_3}{\partial x'_2} = 0;$$

$$n_3 = \frac{\partial x'_3}{\partial x_3} = \frac{\partial x_3}{\partial x'_3} = 1.$$

Since ADP belongs to the tetragonal scalenohedral (Class 11), it will have the dielectric, piezoelectric and elastic tensors shown by equations (3.63), (3.64), (3.66). Applying equations (A.78) and (A.79) to these tensors, it is readily shown that the stresses for $\Theta = 45°$ are given by the equations expressed in two index symbols

$$T'_1 = \frac{(c^D_{11} + c^D_{12} + 2c^D_{66})}{2} S'_1 + \frac{(c^D_{11} + c^D_{12} - 2c^D_{66})}{2} S'_2 + c^D_{13} S'_3 - h_{36}\delta'_3$$

$$T'_2 = \frac{(c^D_{11} + c^D_{12} - 2c^D_{66})}{2} S'_1 + \frac{(c^D_{11} + c^D_{12} + 2c^D_{66})}{2} S'_2 + c^D_{13} S'_3 + h_{36}\delta'_3 \tag{A.79}$$

$$
\begin{aligned}
T_3' &= c_{13}^D S_1' + c_{13}^D S_2' + c_{33} S_3' \\
T_4' &= c_{44}^D S_4' + h_{14}\delta_2'; \qquad E_1 = -h_{14} S_5' + 4\pi[\beta_{11}\delta_1'] \\
T_5' &= c_{44}^D S_5' - h_{14}\delta_1'; \qquad E_2 = h_{14} S_1' + 4\pi[\beta_{11}\delta_2'] \\
T_6' &= \frac{(c_{11}^D - c_{12}^D)}{2} S_6'; \qquad E_3 = -h_{36}[S_1' - S_2'] + 4\pi[\beta_{33}\delta_3'].
\end{aligned}
\tag{A.79}
$$

For a long, thin longitudinally vibrating crystal, all the stresses are zero except the stress T_1' along the length of the crystal. Hence it is more advantageous to use equations which express the strains in terms of the stresses, since all the stresses can be set equal to zero except T_1'. All the strains are then dependent functions of the strain S_1' and only this has to be determined. Furthermore, since plated crystals are usually used to determine the properties of crystals, and the field perpendicular to a plated surface is zero, the only field existing in a thin crystal will be E_3' if the thickness is taken along the x_3'- or z'-axis. Hence the equations that express the strains in terms of the stresses and fields are more advantageous for calculating the properties of longitudinally vibrating crystals. By orienting such crystals with respect to the crystallographic axis, all of the elastic constants except the shear-elastic constants can be determined. All of the piezoelectric and dielectric constants can be determined from measurements on oriented longitudinally vibrating crystals.

For such measurements it is necessary to determine the appropriate elastic, piezoelectric, and dielectric constants for a crystal oriented in any direction with respect to the crystallographic axes. We assume that the length lies along the x_1'-axis, the width along the x_2'-axis and the thickness along the x_3'-axis. Starting with equations of the form

$$
\begin{aligned}
S_{ij} &= s_{ijkl}^E T_{kl} + d_{ijm} E_m \\
\delta_n &= \frac{\epsilon_{mn}^T}{4\pi} E_m + d_{nkl} T_{kl}
\end{aligned}
\tag{A.80}
$$

and transforming to a rotated system of axes whose direction cosines are given by (A.76), the resulting equation becomes

$$
\begin{aligned}
S_{ij}' &= s_{ijkl}^E \frac{\partial x_i'}{\partial x_i}\frac{\partial x_j'}{\partial x_j}\frac{\partial x_k}{\partial x_k'}\frac{\partial x_l}{\partial x_l'} T_{kl}' + d_{ijm}\frac{\partial x_i'}{\partial x_i}\frac{\partial x_j'}{\partial x_j}\frac{\partial x_m}{\partial x_m'} E_m'; \\
\delta_n' &= \frac{\epsilon_{mn}^T}{4\pi}\frac{\partial x_n'}{\partial x_n}\frac{\partial x_m}{\partial x_m'} E_m' + d_{nkl}\frac{\partial x_n'}{\partial x_n}\frac{\partial x_k}{\partial x_k'}\frac{\partial x_l}{\partial x_l'} T_{kl}'.
\end{aligned}
\tag{A.81}
$$

All the stresses except T_{11}' can be set equal to zero and all the fields except E_3' vanish. Furthermore, all the strains are dependently related to S_{11}'.

Hence, for a thin longitudinal crystal, the equation of motion becomes

$$S'_{11} = s^E_{ijkl}\frac{\partial x'_1}{\partial x_i}\frac{\partial x'_1}{\partial x_j}\frac{\partial x_k}{\partial x'_1}\frac{\partial x_l}{\partial x'_1}T'_{11} + d_{ijm}\frac{\partial x'_1}{\partial x_i}\frac{\partial x'_1}{\partial x_j}\frac{\partial x_m}{\partial x'_3}E'_3,$$
$$\delta'_3 = \frac{\epsilon^T_{mn}}{4\pi}\frac{\partial x'_3}{\partial x_n}\frac{\partial x_m}{\partial x'_3}E'_3 + d_{nkl}\frac{\partial x'_3}{\partial x_n}\frac{\partial x_k}{\partial x'_1}\frac{\partial x_l}{\partial x'_1}T'_{11}. \tag{A.82}$$

In terms of the two index symbols for the most general type of crystal, we have

$$\begin{aligned} s'^{E}_{1111} = s'^{E}_{11} &= s^E_{11}l_1^4 + (2s^E_{12} + s^E_{66})l_1^2m_1^2 + (2s^E_{13} + s^E_{55})l_1^2n_1^2 \\ &+ 2(s^E_{14} + s^E_{56})l_1^2m_1n_1 + 2s^E_{15}l_1^3n_1 + 2s^E_{16}l_1^3m_1 + s^E_{22}m_1^4 \\ &+ (2s^E_{23} + s^E_{44})m_1^2n_1^2 + 2s^E_{24}m_1^3n_1 + 2(s^E_{25} + s^E_{46})m_1^2l_1n_1 \\ &+ 2s^E_{26}m_1^3l_1 + s^E_{33}n_1^4 + 2s^E_{34}n_1^3m_1 + 2s^E_{35}n_1^3l_1 \\ &+ 2(s^E_{36} + s^E_{45})n_1^2l_1m_1 \end{aligned} \tag{A.83}$$

$$\begin{aligned} d'_{311} = d'_{31} &= d_{11}l_3l_1^2 + d_{12}l_3m_1^2 + d_{13}l_3n_1^2 + d_{14}l_3m_1n_1 + d_{15}l_3l_1n_1 \\ &+ d_{16}l_3l_1m_1 + d_{21}m_3l_1^2 + d_{22}m_3m_1^2 + d_{23}m_3n_1^2 \\ &+ d_{24}m_3m_1n_1 + d_{25}n_3l_1n_1 + d_{26}m_3l_1m_1 + d_{31}n_3l_1^2 + d_{32}n_3m_1^2 \\ &+ d_{33}n_3n_1^2 + d_{34}n_3m_1n_1 + d_{35}n_3l_1n_1 + d_{36}n_3l_1m_1 \end{aligned}$$

$$\epsilon'^{T}_{33} = \epsilon^T_{11}l_3^2 + 2\epsilon^T_{12}l_3m_3 + 2\epsilon^T_{13}l_3n_3 + \epsilon^T_{22}m_3^2 + 2\epsilon^T_{23}m_3n_3 + \epsilon^T_{33}n_3^2$$

Hence, by cutting 18 crystals with independent direction cosines, 9 elastic constants and 6 relations between the remaining twelve constants can be determined. All of the piezoelectric constants and all of the dielectric constants can be determined from these measurements. These constants can be measured by measuring the resonant and anti-resonant frequencies and the capacitance at low frequencies. The resonant frequency f_R is determined by the formula

$$f_R = \frac{1}{2l}\sqrt{\frac{1}{\rho s'^{E}_{11}}} \tag{A.84}$$

for any long, thin crystal vibrating longitudinally. Hence, when the density is known, s'^{E}_{11} can be calculated from the resonant frequency and the length of the crystal. Using the values of s'^{E}_{11} obtained for 15 independent orientations, enough data are available to solve for the constants of the first of equations (A.83). The capacitances of the different crystal orientations measured at low frequencies determine the dielectric constant

$\epsilon_{33}^{T'}$ and six orientations are sufficient to determine the six independent dielectric constants ϵ_{mn}^{T}. The separation between resonance and antiresonance $\Delta f = f_A - f_R$ determines the piezoelectric constant d_{11}' according to the formula

$$d_{11}' \doteq \frac{\pi}{2}\sqrt{\frac{\Delta f}{f_R}}\sqrt{\frac{\epsilon_{33}^{T'}}{4\pi}\, s_{11}^{E'}}. \tag{A.85}$$

The values of d_{11}' measured for 18 independent orientations are sufficient to determine the eighteen independent piezoelectric constants.

The remaining six elastic constants can be determined by measuring long, thin crystals in a face-shear mode of motion. Since this is a contour mode of motion, the equations are considerably more complicated than for a longitudinal mode and involve elastic constants that are not constant field or constant displacement constants. It is shown[3] that the fundamental frequency of a crystal with its length along x_1, width (frequency determining direction) along x_2 and thickness (direction of applied field) along x_3, will be

$$f = \frac{1}{2l_w}\sqrt{\frac{c_{22}^{c,E} + c_{66}^{c,E} \pm \sqrt{(c_{22}^{c,E} - c_{66}^{c,E})^2 + 4c_{26}^{c,E2}}}{2\rho}} \tag{A.86}$$

where the contour elastic constants are given in terms of the fundamental elastic constants by

$$c_{22}^{c,E} = \frac{s_{11}^{E}s_{66}^{E} - s_{16}^{E2}}{\Delta}; \qquad c_{26}^{c,E} = \frac{s_{12}^{E}s_{16}^{E} - s_{11}^{E}s_{26}^{E}}{\Delta}; \tag{A.87}$$

$$c_{66}^{c,E} = \frac{s_{11}^{E}s_{22}^{E} - s_{12}^{E2}}{\Delta}$$

where Δ is the determinant

$$\Delta = \begin{vmatrix} s_{11}^{E}, & s_{12}^{E}, & s_{16}^{E} \\ s_{12}^{E}, & s_{22}^{E}, & s_{26}^{E} \\ s_{16}^{E}, & s_{26}^{E}, & s_{66}^{E} \end{vmatrix} \tag{A.88}$$

Since all of the constants except s_{12}^{E} and s_{66}^{E} can be determined by measurements on longitudinal crystals and the value of $(2s_{12}^{E} + s_{66}^{E})$ has been determined, the measurement of the lowest mode of the face-shear crystal gives one more relation and hence the values of s_{12}^{E} and s_{66}^{E} can be uniquely determined.

Similar measurements with crystals cut normal to x_1 and width along x_3 and with crystals cut normal to x_2 and width along x_1, determine the

[3] Chapter V, equation (5.62).

constants s_{44}^E, s_{23}^E and s_{55}^E, s_{13}^E respectively. The equivalent constants are obtained by adding 1 to each subscript 1, 2, 3 or 4, 5, 6 for the first crystal with the understanding that $3 + 1 = 1$ and $6 + 1 = 4$. For the second crystal 2 is added to each subscript.

Finally, the remaining three constants can be determined by measuring the face-shear mode of three crystals that have their lengths along one of the crystallographic axes and their width (frequency determining axis) 45° from the other two axes.

Any symmetry existing in the crystal will cut down on the number of constants and hence on the number of orientations to determine the fundamental constants.

A.5 *Temperature Effects in Crystals*

In Chapter III a general expression was developed for the effects of temperature and entropy on the constants of a crystal. Two methods were given: one which considers the stresses, field and temperature differentials as the independent variables, and the other which considers the strains, displacements and entropy as the independent variables. In tensor form the 10 equations for the second method take the form

$$\begin{aligned} T_{kl} &= c_{ijkl}^{D,\sigma} S_{ij} - h_{nkl}^{\sigma} \delta_n - \gamma_{kl}^{S,D}\, dQ \\ E_m &= -h_{mij}^{\sigma} S_{ij} + 4\pi\beta_{mn}^{S,\sigma} \delta_n - q_m^{S,D}\, dQ \\ d\Theta &= -\Theta\gamma_{ij}^{S,D} S_{ij} - \Theta q_n^{S,D}\, \delta_n + \frac{dQ}{\rho c_v^D} \end{aligned} \tag{A.89}$$

The piezoelectric relations have already been discussed for adiabatic conditions assuming that no increments of heat dQ have been added to the crystal.

If now an increment of heat dQ is suddenly added to any element of the crystal, the first equation shows that a sudden expansive stress is generated proportional to the constant $\gamma_{kl}^{S,D}$, which has to be balanced by a negative stress (a compression) in order that no strain or electric displacement shall be generated. This effect can be called the stress caloric effect. The second equation of (A.89) shows that if an increment of heat dQ is added to the crystal, an inverse field E_m has to be added if the strain and surface charge are to remain unchanged. This effect may be called the field caloric effect. Finally, the third equation of (A.89) shows that there is a reciprocal effect in which a stress or a displacement generates a change in temperature even in the absence of added heat dQ. These effects can be called the strain temperature and charge temperature effects.

The first form of the piezoelectric equations given by (3.56) are more

familiar. In tensor form these can be written

$$\begin{aligned} S_{ij} &= s^{E,\Theta}_{ijkl} T_{kl} + d^{\Theta}_{mij} E_m + \alpha^{E}_{ij}\, d\Theta \\ \delta_n &= d^{\Theta}_{nkl} T_{kl} + \frac{\epsilon^{T,\Theta}_{mn}}{4\pi} E_m + p^{T}_{n}\, d\Theta \\ dQ &= \Theta\, d\sigma = \Theta \alpha^{E}_{kl} T_{kl} + \Theta p^{T}_{m} E_m + \rho C^{E}_{p}\, d\Theta \end{aligned} \tag{A.90}$$

The α^{E}_{ij} are the temperature expansion coefficients measured at constant field. In general these are a tensor of the second rank having six components. The constants p^{T}_{n} are the pyroelectric constants measured at displacements which relate the increase in polarization or surface charge due to an increase in temperature. They are equal to the so-called " true " pyroelectric constants, which are the polarizations at constant volume caused by an increase in temperature plus the " false " pyroelectric effect of the first kind, which represents the polarization caused by a uniform temperature expansion of the crystal as its temperature increases by $d\Theta$. As mentioned previously it is more logical to call the two effects the pyroelectric effects at constant stress and constant strain. By eliminating the stresses from the first of equations (A.90) and substituting in the second equation, it is readily shown that

$$p^{S}_{n} = p^{T}_{n} - \alpha^{E}_{ij} e^{\Theta}_{nij} \tag{A.91}$$

Hence the difference between the pyroelectric effect at constant stress and the pyroelectric effect at constant strain is the so-called " false " pyroelectric effect of the first kind $\alpha^{E}_{ij} e^{\Theta}_{nij}$.

The first term on the right side of the last equation is called the heat of deformation, for it represents the heat generated by the application of the stresses T_{kl}. The second term is called the electrocaloric effect and it represents the heat generated by the application of a field. The last term is ρ times the specific heat at constant pressure and constant field.

The temperature expansion coefficients α^{E}_{ij} form a tensor of the second rank and hence have the same components for the various crystal classes as do the dielectric constants shown by equation (3.63).

The pyroelectric tensor p^{T}_{n} and p^{S}_{n} are tensors of the first rank and in general will have three components p_1, p_2, and p_3. In a similar manner to that used for second-, third- and fourth-rank tensors, it can be shown that the various crystal classes have the following components for the first rank tensor p_n.

Class 1: components p_1, p_2, p_3. (A.92)
Class 3: y-axis of binary symmetry, components 0, p_2, 0.
Class 4: components p_1, 0, p_3.
Classes 7, 10, 14, 16, 20, 23, and 26: components 0, 0, p_3; and Classes

2, 5, 6, 8, 9, 11, 12, 13, 15, 17, 18, 19, 21, 22, 24, 25, 27, 28, 29, 30, 31 and 32: components 0, 0, 0, *i.e.*, $p = 0$.

For a hydrostatic pressure, the stress tensor has the components

$$T_{11} = T_{22} = T_{33} = -p = \text{pressure}; \qquad T_{12} = T_{13} = T_{23} = 0 \quad \text{(A.93)}$$

Hence the displacement equations of (A.90) can be written in the form

$$\delta_n = \frac{\epsilon_{mn}^{T,\Theta}}{4\pi} E_m - d_{np}^{\Theta} p + p_n^T \, d\Theta \quad \text{(A.94)}$$

where

$$d_{np}^{\Theta} p = d_{n11}^{\Theta} T_{11} + d_{n22}^{\Theta} T_{22} + d_{n33}^{\Theta} T_{33}$$

that is the contracted tensor $d_{nkk} T_{kk}$. This is a tensor of the first rank which has the same components as the pyroelectric tensor p_n for the various crystal classes.

A.6 *Second Order Effects in Piezoelectric Crystals*

We have so far considered only the conditions for which the stresses and fields are linear functions of the strains and electric displacements. A number of second-order effects exist when we consider that the relations are not linear. Such relations are of some interest in ferroelectric crystals such as rochelle salt. A ferroelectric crystal is one in which a spontaneous polarization exists over certain temperature ranges due to a cooperative effect in the crystal which lines up all of the elementary dipoles in a given " domain " all in one direction. Since a spontaneous polarization occurs in such crystals, it is more advantageous to develop the equations in terms of the electric displacement rather than the external field. Also heat effects are not prominent in second-order effects so that we develop the strains and potentials in terms of the stresses and electric displacements D. By means of Maclaurin's theorem the first and second order terms are in tensor form

$$S_{ij} = \frac{\partial S_{ij}}{\partial T_{kl}} T_{kl} + \frac{\partial S_{ij}}{\partial \delta_n} \delta_n + \frac{1}{2!}\left[\frac{\partial^2 S_{ij}}{\partial T_{kl} \partial T_{qr}} T_{kl} T_{qr} + 2 \frac{\partial^2 S_{ij}}{\partial T_{kl} \partial \delta_n} T_{kl} \delta_n + \frac{\partial^2 S_{ij}}{\partial \delta_n \partial \delta_0} \delta_n \delta_0\right] + \cdots \text{higher terms} \quad \text{(A.95)}$$

$$E_m = \frac{\partial E_m}{\partial T_{kl}} T_{kl} + \frac{\partial E_m}{\partial \delta_n} \delta_n + \frac{1}{2!}\left[\frac{\partial^2 E_m}{\partial T_{kl} \partial T_{qr}} T_{kl} T_{qr} + 2 \frac{\partial^2 E_m}{\partial T_{kl} \partial \delta_n} T_{kl} \delta_n + \frac{\partial^2 E_m}{\partial \delta_n \partial \delta_0} \delta_n \delta_0\right] + \cdots \text{higher terms}$$

where as before $\delta = D/4\pi$.

Introducing the thermodynamic potential H_1, we have

$$dH_1 = -S_{ij}dT_{ij} + E_m\delta_m + \Theta\, d\sigma$$

and hence

$$S_{ij} = -\frac{\partial H_1}{\partial T_{ij}}; \qquad E_m = \frac{\partial H_1}{\partial \delta_m}; \qquad \Theta = \frac{\partial H_1}{\partial \sigma}$$

Hence there are relations between some of the partial derivatives by virtue of the fact that the order of differentiation makes no difference, namely

$$\frac{\partial S_{ij}}{\partial \delta_n} = \frac{\partial}{\partial \delta_n}\left(-\frac{\partial H_1}{\partial T_{ij}}\right) = -\frac{\partial^2 H_1}{\partial \delta_n \partial T_{ij}} = -\frac{\partial E_n}{\partial T_{ij}}$$

In this equation the linear partial differentials have already been discussed and are given by the equations

$$\frac{\partial S_{ij}}{\partial T_{kl}} = s^D_{ijkl}; \qquad \frac{\partial S_{ij}}{\partial \delta_n} = -\frac{\partial E_n}{\partial T_{ij}} = g_{ijn}; \qquad \frac{\partial E_m}{\partial \delta_n} = 4\pi\beta^T_{mn} \tag{A.96}$$

where s^D_{ijkl} are the elastic compliances of the crystal at constant displacement, g_{ijn} the piezoelectric constants relating strain to electric displacement $/4\pi$, and β^T_{mn} the dielectric " impermeability " tensor measured at constant stress. We designate the partial derivatives

$$\frac{\partial S_{ij}}{\partial T_{kl}\partial T_{qr}} = 2N^D_{ijklqr}; \qquad \frac{\partial^2 S_{ij}}{\partial T_{kl}\partial \delta_m} = -\frac{\partial^2 E_m}{\partial T_{kl}\partial T_{qr}} = 2M^D_{ijkln}$$

$$\frac{\partial^2 S_{ij}}{\partial \delta_n \partial \delta_0} = -\frac{\partial^2 E_n}{\partial T_{ij}\partial \delta_0} = 2Q^D_{ijno}; \qquad \frac{\partial^2 E_m}{\partial \delta_n \partial \delta_0} = 2O^D_{mno} \tag{A.97}$$

The tensors N, M, Q, and O are respectively tensors of rank 6, 5, 4 and 3 whose interpretation is discussed below. Introducing these definitions, equations (A.95) can be written in the form

$$\begin{aligned} S_{ij} &= T_{kl}[s^D_{ijkl} + N^D_{ijklqr}T_{qr} + 2M^D_{ijkln}\delta_n] + \delta_n[g_{ijn} + Q^D_{ijno}\delta_0] \\ E_m &= -T_{kl}[g_{mkl} + M^D_{ijkln}T_{qr} + 2Q^D_{klmn}\delta_n] + \delta_n[4\pi\beta^T_{mn} + O^D_{mno}\delta_0] \end{aligned} \tag{A.98}$$

Written in this form the interpretation of the second-order terms is obvious. N^D_{ijklqr} represents the nonlinear changes in the elastic compliances s^D_{ijkl} caused by the application of stress T_{qr}. Since the product of $N^D_{ijklqr}T_{qr}$ represents a contracted fourth-rank tensor, there is a correction term for each elastic compliance. The tensor M^D_{ijkln} can represent either the nonlinear correction to the elastic compliances due to an applied electric displacement D_n or it can represent the correction to the piezoelectric constant

g_{ijn} due to the stresses T_{kl}. By virtue of the second equation of (A.96) the second equivalence of (A.97) results. The fourth-rank tensor Q^D_{ijno} represents the electrostrictive effect in a crystal, for it determines the strains existing in a crystal which are proportional to the square of the electric displacement. Twice the value of the electrostrictive tensor Q^D_{ijno}, which appears in the second equation of (A.98), can be interpreted as the change in the inverse dielectric constant or " impermeability " constant. Since a change in dielectric constant with applied stress causes a double refraction of light through the crystal, this term is the source of the piezo-optical effect in crystals. The third-rank tensor O^D_{mno} represents the change in the " impermeability " constant due to an electric field and hence is the source of the electro-optical effect in crystals.

These equations can also be used to discuss the changes that occur in ferroelectric type crystals such as rochelle salt, when a spontaneous polarization occurs in the crystal. When spontaneous polarization occurs, the dipoles of the crystal are lined up in one direction in a given domain. For rochelle salt this direction is the $\pm x$-axis of the crystal. Now the electric displacement D_x is equal to

$$\delta_x = \frac{D_x}{4\pi} = \frac{E_x}{4\pi} + P_{x_0} + P_{x_D} = \frac{E_x \epsilon_0}{4\pi} + P_{x_D} \tag{A.99}$$

where P_{x_0} is the electronic and atomic polarization, and P_{x_D} the dipole polarization. The electronic and atomic polarization is determined by the field and hence can be combined with the field through the dielectric constant ϵ_0, which is the temperature independent part of the dielectric constant. When the crystal becomes spontaneously polarized, a field E_x will result, but this soon is neutralized by the flow of electrons through the surface and volume conductance of the crystal and in a short time $E_x = 0$. Hence, for any permanent changes occurring in the crystal, we can set

$$\delta_x = \frac{D_x}{4\pi} = P_{x_D} = \text{dipole polarization} \tag{A.100}$$

which we will write hereafter as P_1.

In the absence of external stresses the direct effects of spontaneous polarization are a spontaneous set of strains introduced by the product of the spontaneous polarization by the piezoelectric constant, and another set produced by the square of the polarization times the appropriate electrostrictive components. For example, rochelle salt has a spontaneous polarization P_1 along the x_1-axis between the temperatures $-18°C$ to $+24°C$. The curve for the spontaneous polarization as a function of

temperature is shown by Fig. A.1.[4] The only piezoelectric constant causing a spontaneous strain will be $g_{14/2} = g_{123}$. Hence the spontaneous polarization causes a spontaneous shearing strain

$$S_4 = g_{14}P_x = 63 \times 10^{-8} \times 760 = 4.8 \times 10^{-4} \qquad \text{(A.101)}$$

if we introduce the experimentally determined values. Since S_4 is the cosine of 90° plus the angle of distortion, this would indicate that the right-angled axes of a rhombic system would be distorted 1.6 minutes of arc. This is the value that should hold for any domain. For a crystal with

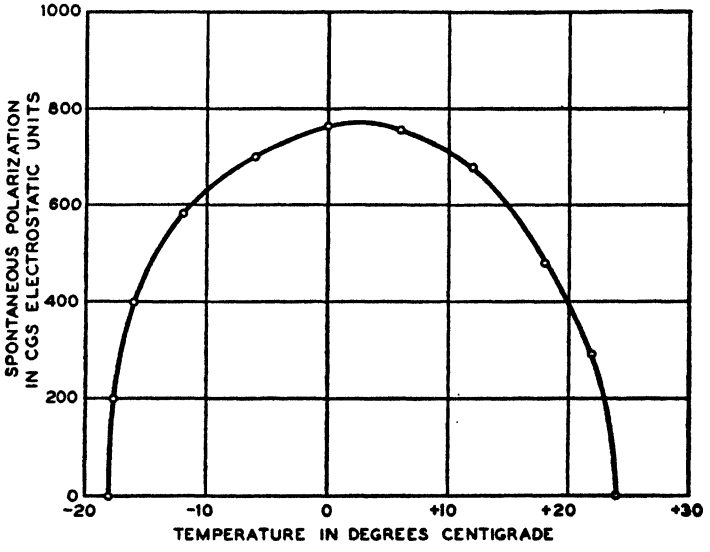

FIG. A.1 Spontaneous polarization in Rochelle Salt along the x-axis.

several domains, the resulting distortion will be partly annulled by the different signs of the polarization and should be smaller. Mueller[5] measured an angle of $3'45''$ at 0°C for one crystal. This question has also been investigated by Mrs. E. A. Wood and the writer by measuring the temperature expansion coefficients of the y- and z-axes and comparing their average with the expansion coefficient at 45° from these two axes. The difference between these two expansion coefficients measures the change

[4] This has been measured by measuring the remanent polarization, when all the domains are lined up. Mueller, H., "The Dielectric Anomalies of Rochelle Salt," *Ann. N. Y. Acad. Sci.*, Vol. 40, Art. 5, p. 338, Dec. 31, 1940.

[5] Mueller, H., "Properties of Rochelle Salt," *Phys. Rev.*, Vol. 57, No. 9, May 1, 1940.

in angle between the y- and z-axes caused by the spontaneous shearing strains. The results are shown by Fig. A.2. Above and below the ferroelectric region, the expansion of the 45° crystal coincides with the average expansion of the y- and z-axes measured from 25°C as a reference temperature. Between the Curie temperatures a difference occurs indicating that

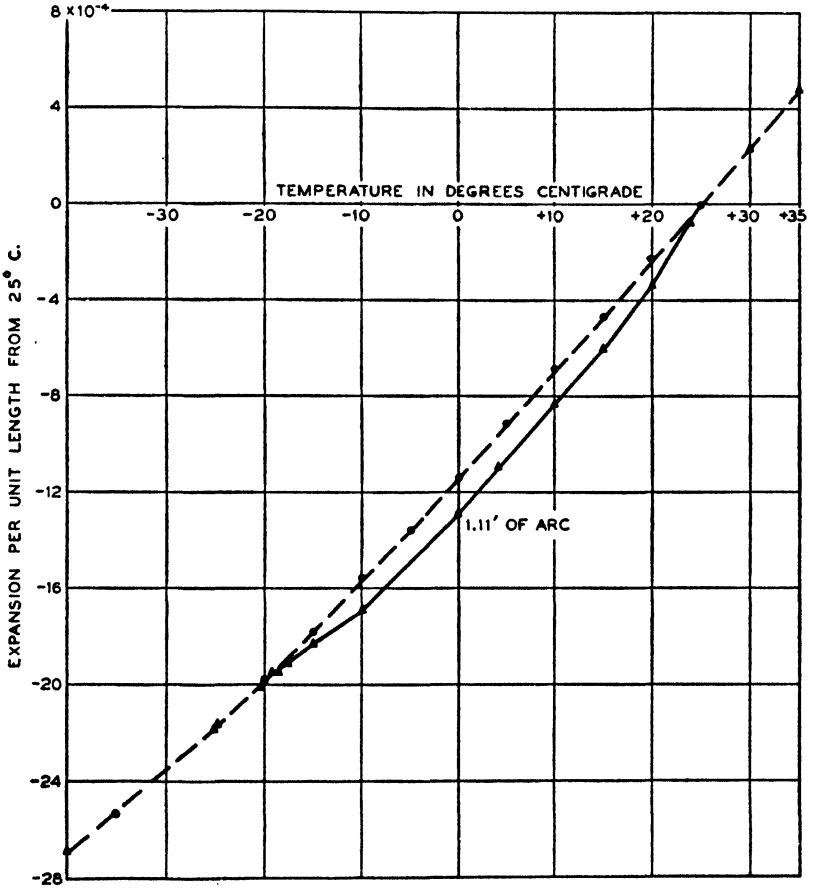

FIG. A.2. Temperature expansion curve along an axis 45° between Y and Z as a function of temperature.

the y- and z-crystallographic axes are no longer at right angles. The difference in expansion per unit length at 0°C (the maximum point) corresponds to 1.6×10^{-4} centimeter per centimeter. This represents an axis distortion of 1.1 minutes of arc. Correspondingly smaller values are found at other temperatures in agreement with the smaller spontaneous

polarization at other temperatures. It was also found that practically the same curve resulted for either 45° axis, indicating that the mechanical bias put on by the optometer used for measuring expansions introduced a bias determining the direction of the largest number of domains.

The second-order terms caused by the square of the spontaneous polarization, is given by the expression

$$S_{ij} = Q^D_{ij11}P_1^2 \tag{A.102}$$

Since Q is a fourth-rank tensor, the possible terms for an orthorhombic bisphenoidal crystal (the class for rochelle salt) are

$$S_{11} = Q^D_{1111}P_1^2; \qquad S_{22} = Q^D_{2211}P_1^2; \qquad S_{33} = Q^D_{3311}P_1^2 \tag{A.103}$$

In an effort to measure these effects, careful measurements have been made of the temperature expansions of the three axes x, y and z. The results are shown by Table XXXIII. On account of the small change in dimension from the standard curve it is difficult to pick out the spontaneous components by plotting a curve. By expressing the expansion in the form of the equation

$$\frac{\Delta L}{L} = a_1(T-25) + a_2(T-25)^2 + a_3(T-25)^3 \tag{A.104}$$

and evaluating the constants by employing temperatures outside of the ferroelectric range, a normal curve was established. For the x-, y-, and z-axes these relations are

$$\frac{\Delta L}{L} = 69.6\times 10^{-6}(T-25) + 7.4\times 10^{-8}(T-25)^2 - 3.13\times 10^{-10}(T-25)^3 \quad (x \text{ direction})$$

$$\frac{\Delta L}{L} = 43.7\times 10^{-6}(T-25) + 8.16\times 10^{-8}(T-25)^2 - 3.60\times 10^{-10}(T-25)^3 \quad (y \text{ direction}) \tag{A.105}$$

$$\frac{\Delta L}{L} = 49.4\times 10^{-6}(T-25) + 1.555\times 10^{-8}(T-25)^2 - 2.34\times 10^{-10}(T-25)^3 \quad (z \text{ direction})$$

The difference between the normal curves and the measured values in the Curie region is shown plotted by the points of Fig. A.3. The solid and dashed curves represent curves proportional to the square of the spontaneous polarization and with multiplying constants adjusted to give the best fits for the measured points. These give values of Q^D_{1111}, Q^D_{2211}, Q^D_{3311} equal to

$$Q^D_{1111} = -86.5\times 10^{-12}; \qquad Q^D_{2211} = +17.3\times 10^{-12}; \qquad Q^D_{3311} = -24.2\times 10^{-12} \tag{A.106}$$

TABLE XXXIII

MEASURED TEMPERATURE EXPANSIONS FOR THE THREE CRYSTALLOGRAPHIC AXES

Temperature Expansion		Temperature Expansion		Temperature Expansion	
in °C	$\times 10^{-4}$ x-axis	in °C	$\times 10^{-4}$ y-axis	in °C	$\times 10^{-4}$ z-axis
39.6	10.2	+35.0	4.45	+34.9	+4.9
38.7	9.46	30.3	2.5	29.9	2.5
35.2	6.96	25.25	0.2	25.05	+.05
30.2	3.63	23.9	−0.42	24.0	−.5
27.2	1.41	22.9	−0.88	19.95	−2.62
26.2	0.71	19.35	−2.4	14.95	−5.11
25.15	0.06	14.9	−4.25	+9.75	−7.55
24.0	−0.71	10.0	−6.25	+4.9	−9.9
23.0	−1.39	5.4	−8.18	0	−12.31
21.8	−2.37	+0.3	−10.15	−6.35	−15.3
16.0	−6.5	−9.7	−13.98	−10.5	−17.29
15.2	−7.05	−16.3	−16 41	−15.0	−19.42
4.9	−14.12	−20.85	−17.94	−18.0	−20.86
+0.3	−17.28	−25.1	−19.22	−23.2	−23.08
−4.7	−20.3	−30.3	−20.8	−25.1	−23.96
−10.7	−24.0	−35.0	−22.23	−31.1	−26.59
−15.3	−26.6	−39.7	−23.54	−35.0	−28.28
−20.7	−30.2	−53.2	−27.60	−40.0	−30.4
−25.7	−32.7				
−30.1	−35.2				
−34.7	−37.85				
−40.7	−41.25				
−45.0	−44.0				
−50.5	−47.0				

Another effect noted for rochelle salt is that some of the elastic constants suddenly change by small amounts at the Curie temperatures. This is a consequence of the tensor M^D_{ijkln}, for if a spontaneous polarization P occurs, a sudden change occurs in some of the elastic constants as can be seen from the first of equations (A.98). The second equation of (A.98) shows that this same tensor causes a nonlinear response in the piezoelectric constant. Since a change in the elastic constant is much more easily determined than a nonlinear change in the piezoelectric constant, the first effect is the only one definitely determined experimentally. Since all three crystallographic axes are binary axes in rochelle salt, it is easily shown that the only terms that can exist for a fifth-rank tensor are terms of the types

$$M^D_{11123}; \qquad M^D_{12223}; \qquad M^D_{12333} \tag{A.107}$$

with permutations and combinations of the indices. Hence, when a spon-

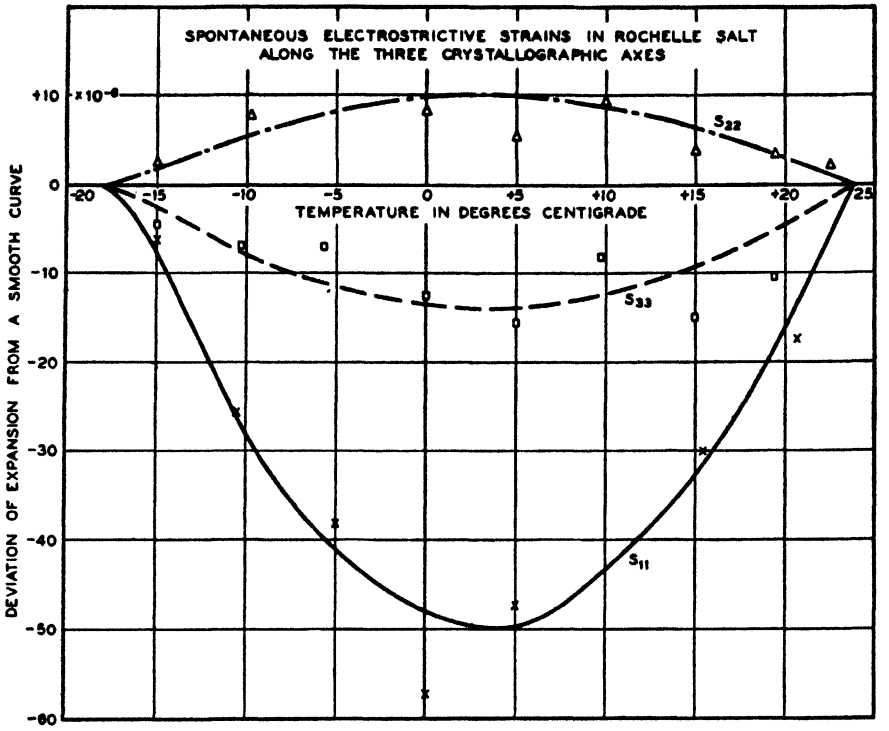

FIG. A.3. Spontaneous electrostrictive strain in Rochelle Salt along the three crystallographic axes, in parts per million.

taneous polarization P_1 occurs, the elastic constants become

$$s^D_{ijkl} - M^D_{ijkl}P_1 \tag{A.108}$$

Comparing these with the relation of (A.30), we see that the spontaneous polarization has added the elastic constants

$$\begin{aligned}
s^D_{14} &= \frac{(M^D_{11231} + M^D_{11321} + M^D_{23111} + M^D_{32111})P_1}{2} \\
s^D_{24} &= \frac{(M^D_{22231} + M^D_{22321} + M^D_{23221} + M^D_{32221})P_1}{2} \\
s^D_{34} &= \frac{(M^D_{23331} + M^D_{32331} + M^D_{33321} + M^D_{33231})P_1}{2} \\
s^D_{56} &= \frac{\begin{aligned}(M^D_{12131} + M^D_{13211} + M^D_{31121} + M^D_{31211} + M^D_{12131} \\ + M^D_{12311} + M^D_{21131} + M^D_{21311})P_1\end{aligned}}{2}
\end{aligned} \tag{A.109}$$

between the two Curie points. Hence while the spontaneous polarization P_1 exists, the resulting elastic constants are

$$\begin{vmatrix} s_{11}, & s_{12}, & s_{13}, & s_{14}, & 0, & 0 \\ s_{12}, & s_{22}, & s_{23}, & s_{24}, & 0, & 0 \\ s_{13}, & s_{23}, & s_{33}, & s_{34}, & 0, & 0 \\ s_{14}, & s_{24}, & s_{34}, & s_{44}, & 0, & 0 \\ 0, & 0, & 0, & 0, & s_{55}, & s_{56} \\ 0, & 0, & 0, & 0, & s_{56}, & s_{66} \end{vmatrix} \tag{A.110}$$

Comparing this to equation (3.66) which shows the possible elastic constants for the various crystal classes, we see that between the two Curie points, the crystal is equivalent to a monoclinic sphenoidal crystal (Class 3) with the x-axis the binary axis. Outside the Curie region the crystal becomes orthorhombic bisphenoidal. This interpretation agrees with the temperature expansion curves of Fig. A.2.

The sudden appearance of the polarization P_1 will affect the frequency of a 45° X-cut crystal, for with a crystal cut normal to the x-axis and with the length of the crystal at an angle Θ with the y-axis, the value of the elastic compliance s'_{22} along the length is

$$\begin{aligned} s'^{D}_{22} = {} & s^D_{22}\cos^4\Theta + 2s^D_{24}\cos^3\Theta\sin\Theta + (2s^D_{23} + s^D_{44})\sin^2\Theta\cos^2\Theta \\ & + 2s^D_{34}\sin^3\Theta\cos\Theta + s^D_{33}\sin^4\Theta \end{aligned} \tag{A.111}$$

Hence for a crystal with its length 45° between the y- and z-axes, the elastic compliance becomes

$$s'^{D}_{22} = \frac{s^D_{22} + 2(s^D_{24} + s^D_{23} + s^D_{34}) + s^D_{44} + s^D_{33}}{4} \tag{A.112}$$

For a 45° X-cut crystal we would expect a sudden change in the value of s'^{D}_{22} as the crystal becomes spontaneously polarized between the two Curie points due to the addition of the s^D_{24} and s^D_{34} elastic compliances. Such a change has been observed for rochelle salt[6] as shown by Fig. A.4, which shows the frequency constant of a nonplated crystal for which the elastic compliances s^D_{ij} should hold.

Hence the sudden change in the elastic constant is a result of the two second-order terms $s^D_{24} + s^D_{34}$, which are caused by the spontaneous polarization. The value of the sum of these two terms at the mean temperature of the Curie range, 3°C is

$$s^D_{24} + s^D_{34} = 4.1 \times 10^{-14}\ \text{cm}^2/\text{dyne} \tag{A.113}$$

Crystals cut normal to the y- and z-axes should not show a spontaneous

[6] Mason, W. P., "The Location of Hysteresis Phenomena in Rochelle Salt Crystals," *Phys. Rev.*, Vol. 50, p. 744–750, Oct. 15, 1940.

change in their frequency characteristic since the spontaneous terms s_{14}, s_{24}, s_{34} and s_{56} do not affect the value of Young's moduli in planes normal to y and z. Experiments on a 45° Y-cut rochelle salt crystal do not show a spontaneous change in frequency at the Curie temperature, although there is a large change in the temperature coefficient of the elastic compliance between the two Curie points. This is the result of a third-order term and is not considered here. The spontaneous s_{56} constant affects the shear constant s'_{66} for crystals rotated about the x-axis and could be detected experimentally. No experimental values have been obtained.

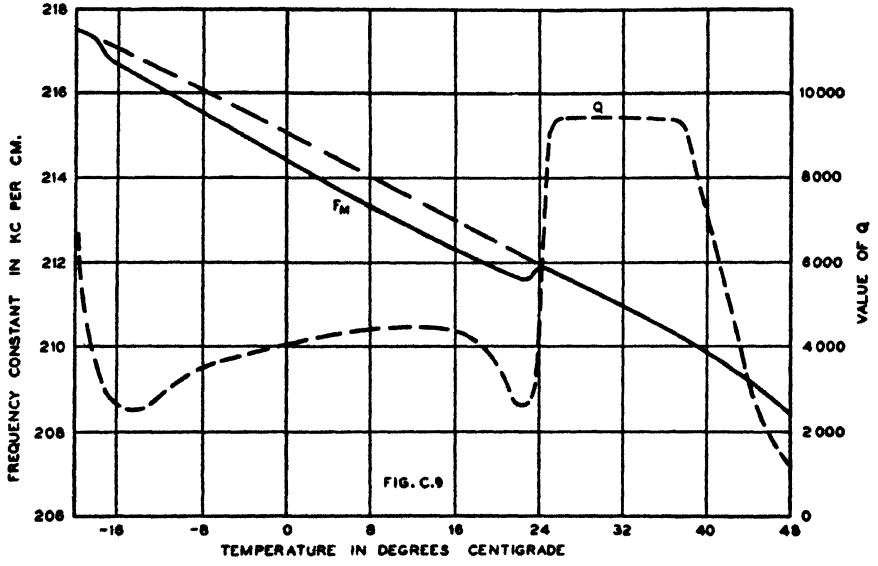

FIG. A.4. Frequency constant and Q of an unplated 45° X-cut Rochelle Salt crystal plotted as a function of temperature.

The effects of spontaneous polarization in the second equation of (A.98) are of two sorts. For an unplated crystal, a spontaneous voltage is generated on the surface, which, however, quickly leaks off due to the surface and volume leakage of the crystal. The other effects are that the spontaneous polarization introduces new piezoelectric constants through the tensor Q^D_{klmn}, changes the dielectric constants through the tensor O^D_{mno} and introduces a stress effect on the piezoelectric constants through the tensor M^D_{klmqr}. Since piezoelectric constants are not as accurately measured as elastic constants, the first effect has not been observed. The additional piezoelectric constants introduced by the tensor Q^D_{klmn} are shown by equa-

tion (A.114)

$$\begin{matrix} g_{11} & g_{12} & g_{13} & g_{14} & 0 & 0 \\ 0 & 0 & 0 & 0 & g_{25} & g_{26} \\ 0 & 0 & 0 & 0 & g_{35} & g_{36} \end{matrix} \qquad \text{(A.114)}$$

Since the only constants for the rochelle salt class, the orthorhombic bisphenoidal, are g_{14}, g_{25}, g_{36}, this shows that between the two Curie points the crystal becomes monoclinic sphenoidal, with the x-axis being the binary axis. The added constants are, however, so small that the accuracy of measurement is not sufficient to evaluate them. From the expansion measurements of equation (A.105) and the spontaneous polarization values, three of them should have maximum values of

$$g_{11} = -6.6 \times 10^{-8}; \quad g_{12} = +1.3 \times 10^{-8}; \quad g_{13} = -1.8 \times 10^{-8} \qquad \text{(A.115)}$$

These amount to only 6 per cent of the constant g_{14}, and hence they are not easily evaluated from piezoelectric measurements.

The effect of the tensor O^{D}_{mno} is to introduce a spontaneous dielectric constant ϵ_{23} between the Curie temperatures so that the dielectric tensor becomes

$$\begin{matrix} \epsilon_{11}, & 0 , & 0 \\ 0 , & \epsilon_{22}, & \epsilon_{23} \\ 0 , & \epsilon_{23}, & \epsilon_{33} \end{matrix} \qquad \text{(A.116)}$$

This introduces a birefringence for light in directions not along the crystallographic axes. To obtain the spontaneous quadratic effect observed by Mueller,[7] third order derivatives have to be taken.

A.7 *Losses in Gases, Liquids and Solids Due to Viscosity, Heat Conduction and Hysteresis*

According to the classical theory of wave propagation in liquids and gases, losses occur in a plane or other type of a wave due to frictional losses of the viscous type and losses due to the fact that the wave is not quite adiabatic but loses heat energy by heat transmission from the hot compressed parts to the cool rarified parts. The losses in solids and even in liquids for very high frequencies do not appear to be of this type but rather of the hysteresis type, caused by the fact that the stress-strain curve is not a straight line, but is a hysteresis loop in which the strain is a double valued function of the stress. This type of a hysteresis loop can be rep-

[7] "Properties of Rochelle Salt I and IV," *Phys. Rev.*, Vol. 47, p. 175, 1935; Vol. 58, p. 805, Nov. 1, 1940.

resented by giving the elastic constant an imaginary component whose magnitude represents the ratio of the breadth of the hysteresis loop to its length. Since the width will be proportional to the length, the total area is proportional to the square of the maximum strain and hence the loss introduced by it is independent of the amplitude. It is the purpose of this section to discuss the equations representing these effects. In the interests of simplicity, only non-piezoelectric materials will be discussed, although the extension to piezoelectric materials is straightforward.

The coefficient of shear viscosity of a liquid or gas is defined as equal to the tangential force exerted on a unit area of either of two horizontal planes placed a unit distance apart in the viscous substance, one of the planes being fixed and the other moving with a unit velocity. Hence, for a viscous substance, the stresses are functions not only of the strains and temperatures but also of the strain velocities. If we imagine a substance in which the viscosity is not uniform in all directions, the stresses and the entropy for a given volume can be developed in terms of the tensor equations

$$dT_{kl} = \frac{\partial T_{kl}}{\partial S_{ij}} dS_{ij} + \frac{\partial T_{kl}}{\partial \dot{S}_{ij}} d\dot{S}_{ij} + \frac{\partial T_{kl}}{\partial \Theta} d\Theta$$

$$d\sigma = \frac{\partial \sigma}{\partial S_{ij}} dS_{ij} + \frac{\partial \sigma}{\partial \dot{S}_{ij}} d\dot{S}_{ij} + \frac{\partial \sigma}{\partial \Theta} d\Theta \qquad \text{(A.117)}$$

where T_{kl} are the stresses, S_{ij} are the strains, $\dot{S}_{ij}$ are the time rates of change of strains, $d\Theta$ the increment of temperature and $d\sigma$ the increment of entropy. From the discussion in section 3.14, the partial derivatives are equal to the constants

$$\frac{\partial T_{kl}}{\partial S_{ij}} = c^{\Theta}_{ijkl}; \qquad -\frac{\partial T_{kl}}{\partial \Theta} = \frac{\partial \sigma}{\partial S_{ij}} = \lambda^{S}_{ij}; \qquad \frac{\partial \sigma}{\partial \Theta} = \frac{\rho C v}{\Theta} \qquad \text{(A.118)}$$

where c^{Θ}_{ijkl} are the isothermal elastic stiffnesses, λ^{S}_{ij} are the temperature coefficients of the stresses, when the strains are held constant, ρ the density, C_v the specific heat per gram at constant strain, and Θ the absolute temperature. In addition, we have two partial derivatives

$$\frac{\partial T_{kl}}{\partial \dot{S}_{ij}} = \eta_{ijkl}; \qquad \frac{\partial \sigma}{\partial \dot{S}_{ij}} = 0 \qquad \text{(A.119)}$$

of which the first is the generalized viscosities and the second is equal to zero, since energy cannot be stored in the element of volume due to a constant rate of change of strain. Introducing these values and also introducing the imaginary part of the elastic constants to represent the hysteresis effects, equations (A.117) can be written in the form, after

dropping the differential forms for T and S,

$$T_{kl} = [c^{\theta}_{ijkl} + jH_{ijkl}]S_{ij} + \eta^{\theta}_{ijkl}\dot{S}_{ij} - \lambda^{S}_{kl}\,d\Theta$$
$$d\sigma = \lambda^{S}_{ij}S_{ij} + \frac{\rho Cv}{\Theta}\,d\Theta \tag{A.120}$$

A7.1 *Viscous Losses in Liquids and Gases for Adiabatic Plane Waves*

If we neglect, for the time being, the losses due to heat conductivity and assume that the wave propagation is exactly adiabatic, we can set $d\sigma$ equal to zero in the last of equation (A.120) and eliminate $d\Theta$ from the first equation by employing the last equation. The resulting equation is

$$T_{kl} = [c^{\sigma}_{ijkl} + jH_{i,kl}]S_{ij} + \eta^{\sigma}_{ijkl}\dot{S}_{ij} \tag{A.121}$$

where

$$c^{\sigma}_{ijkl} = c^{\theta}_{ijkl} + \frac{\Theta\lambda_{ij}\lambda_{kl}}{\rho Cv}; \qquad \eta^{\sigma}_{ijkl} = \eta^{\theta}_{ijkl}$$

It is of some interest to point out the difference between the adiabatic and isothermal elastic constants for gases and for liquids at low frequencies. As shown below, the elastic constants for a gas or liquid reduce to $c_{11} = c_{12} = c_{13} = \kappa$, the constant of cubical elasticity, while all other constants are zero. Hence, we are interested only in the constant $c_{11} = c_{1111}$. From equation (3.38)

$$\lambda_1 = \alpha_1 c_{11} + \alpha_2 c_{12} + \alpha_3 c_{13} = \kappa(\alpha_1 + \alpha_2 + \alpha_3) = \kappa\alpha \tag{3.38}$$

where α is the thermal coefficient of cubic expansion, which is equal to the sum of the three linear expansions. Hence

$$\kappa^{\sigma} = \kappa^{\theta} + \frac{\Theta\alpha^2\kappa^{\theta 2}}{\rho Cv} = \kappa^{\theta}\left[1 + \frac{\Theta\alpha^2\kappa^{\theta}}{\rho Cv}\right] \tag{A.122}$$

A different form for this expression can be obtained by employing equation (3.40), which for a gas or liquid takes the form

$$\rho(C_p - C_v) = \Theta\alpha^2\kappa^{\theta} \tag{A.123}$$

Introducing this expression into (A.122), we find

$$\frac{\kappa^{\sigma}}{\kappa^{\theta}} = \frac{C_p}{C_v} \tag{A.124}$$

and the ratio of the elastic constants is equal to the ratio of the specific heats.

Now for liquids and gases, the hysteresis terms are not important and moreover liquids and gases are isotropic. Hence, by equations (3.66),

since both constants are fourth-rank tensors, they each reduce to two independent constants, which expressed in terms of two index symbols, are

$$\begin{vmatrix} c_{11} & c_{12} & c_{12} & 0 & 0 & 0 \\ c_{12} & c_{11} & c_{12} & 0 & 0 & 0 \\ c_{12} & c_{12} & c_{11} & 0 & 0 & 0 \\ 0 & 0 & 0 & \frac{c_{11}-c_{12}}{2} & 0 & 0 \\ 0 & 0 & 0 & 0 & \frac{c_{11}-c_{12}}{2} & 0 \\ 0 & 0 & 0 & 0 & 0 & \frac{c_{11}-c_{12}}{2} \end{vmatrix}$$

and (A.125)

$$\begin{vmatrix} \eta_{11} & \eta_{12} & \eta_{12} & 0 & 0 & 0 \\ \eta_{12} & \eta_{11} & \eta_{12} & 0 & 0 & 0 \\ \eta_{12} & \eta_{12} & \eta_{11} & 0 & 0 & 0 \\ 0 & 0 & 0 & \frac{\eta_{11}-\eta_{12}}{2} & 0 & 0 \\ 0 & 0 & 0 & 0 & \frac{\eta_{11}-\eta_{12}}{2} & 0 \\ 0 & 0 & 0 & 0 & 0 & \frac{\eta_{11}-\eta_{12}}{2} \end{vmatrix}$$

For liquids and gases (at least at low frequencies) there is no shearing stiffness and hence $c_{11} = c_{12} = \kappa$, where κ is the constant of cubical elasticity. We designate $\frac{\eta_{11}-\eta_{12}}{2} = \eta$ the shearing viscosity and denote $\eta_{12} = \chi$. Then $\eta_{11} = \chi + 2\eta$. With these designations, the six stress equations can be written in terms of the two index symbols:

$$\begin{aligned} T_{11} &= \kappa[S_{11}+S_{22}+S_{33}]+(\chi+2\eta)\dot{S}_{11}+\chi[\dot{S}_{22}+\dot{S}_{33}]; \quad T_{12} = \eta\dot{S}_{12} \\ T_{22} &= \kappa[S_{11}+S_{22}+S_{33}]+(\chi+2\eta)\dot{S}_{22}+\chi[\dot{S}_{11}+\dot{S}_{33}]; \quad T_{13} = \eta\dot{S}_{13} \\ T_{33} &= \kappa[S_{11}+S_{22}+S_{33}]+(\chi+2\eta)\dot{S}_{33}+\chi[\dot{S}_{11}+\dot{S}_{22}]; \quad T_{23} = \eta\dot{S}_{23} \end{aligned} \tag{A.126}$$

In this form there are two coefficients of viscosity, η the shearing viscosity and χ the compressional viscosity. It has been suggested by Stokes and is borne out experimentally for monatomic gases and liquids that a motion of dilation, in which an expansion or contraction occurs uniformly in all directions, will not give rise to viscous forces and will result in the actual

pressure being equal to the static pressure corresponding to the actual density. Such a motion will occur if

$$\dot{S}_{11} = \dot{S}_{22} = \dot{S}_{33} \qquad \text{and} \qquad \dot{S}_{12} = \dot{S}_{13} = \dot{S}_{23} = 0 \tag{A.127}$$

Under these conditions

$$T_{11} = T_{22} = T_{33} = 3\kappa S_{11} + (3\chi + 2\eta)\dot{S}_{11} \tag{A.128}$$

If the expansion is to occur with no frictional forces operative, we must have

$$(3\chi + 2\eta) = 0 \qquad \text{or} \qquad \chi = \frac{-2\eta}{3} \tag{A.129}$$

Since this relation is not generally true, we keep the form in equation (A.126) and apply the relation of (A.129) when it is justified.

To obtain the equation of a plane wave directed along the x-axis, we make use of equation (3.5) and set this equal to the mass reaction or

$$\frac{\rho\partial\dot{\xi}}{\partial t} = \frac{\partial T_{11}}{\partial x} + \frac{\partial T_{12}}{\partial y} + \frac{\partial T_{13}}{\partial z} \tag{A.130}$$

Now since the displacements and velocities $\eta = \zeta = \dot{\eta} = \dot{\zeta} = 0$ for a plane wave directed along x, and since there is no change in the y and z directions so that

$$\frac{\partial}{\partial y} = \frac{\partial}{\partial z} = 0 \tag{A.131}$$

the three stresses T_{11}, T_{12} and T_{13} of equation (A.126) reduce to

$$T_{11} = \kappa\frac{\partial\xi}{\partial x} + (\chi + 2\eta)\frac{\partial^2\xi}{\partial x\,\partial t}; \qquad T_{13} = T_{12} = 0 \tag{A.132}$$

Hence, differentiating T_{11} in (A.132) by x and inserting in (A.130), the equation of motion becomes

$$\frac{\rho\partial\dot{\xi}}{\partial t} = \kappa\frac{\partial^2\xi}{\partial x^2} + (\chi + 2\eta)\frac{\partial^3\xi}{\partial x^2\,\partial t} \tag{A.133}$$

The equation of motion for simple harmonic motion reduces to

$$\omega^2\rho\xi + [\kappa + j\omega(\chi + 2\eta)]\frac{d^2\xi}{dx^2} = 0 \tag{A.134}$$

A solution of this equation can be written in the form

$$\xi = A\cosh\Gamma x + B\sinh\Gamma x \tag{A.135}$$

where Γ, the propagation constant, is given by the equation

$$\omega^2\rho + \Gamma^2[\kappa + j\omega(\chi + 2\eta)] = 0 \quad \text{or} \quad \Gamma = \frac{\frac{j\omega}{v}}{\sqrt{1 + \frac{j\omega(\chi + 2\eta)}{\rho v^2}}} \tag{A.136}$$

since the velocity of propagation $v = \sqrt{\kappa/\rho}$. The constants of equation (A.135) can be evaluated as follows: when $x = 0$, $A = \xi_0$, the initial displacement at the beginning of the line and differentiating ξ by x, we have

$$\frac{\partial \xi}{\partial x} = \Gamma[A \sinh \Gamma x + B \cosh \Gamma x] = \frac{T}{\kappa + j\omega(\chi + 2\eta)} \tag{A.137}$$

Hence

$$B = \frac{T_0}{\Gamma[\kappa + j\omega(\chi + 2\eta)]} = \frac{T_0}{\frac{j\omega}{v}\kappa} \frac{\sqrt{1 + j\omega(\lambda + 2\eta)/\kappa}}{[1 + j\omega(\lambda + 2\eta)/\kappa]}$$

$$= \frac{T_0}{j\omega\rho v\sqrt{1 + \frac{j\omega(\chi + 2\eta)}{\rho v^2}}} \tag{A.138}$$

since $\kappa = \rho v^2$. The initial tension is T_0. Introducing these values in equations (A.135) and (A.137), the two equations for wave propagation become

$$\dot{\xi} = \dot{\xi}_0 \cosh \Gamma x + \frac{T_0}{Z_0} \sinh \Gamma x; \qquad T = T_0 \cosh \Gamma x + \dot{\xi}_0 Z_0 \sinh \Gamma x \tag{A.139}$$

where

$$\Gamma = \frac{\frac{j\omega}{v}}{\sqrt{1 + \frac{j\omega(\chi + 2\eta)}{\rho v^2}}} \doteq \frac{\omega^2}{2\rho v^3}(\chi + 2\eta) + \frac{j\omega}{v} = \frac{2\pi^2 f^2(\chi + 2\eta)}{\rho v^3} + \frac{j\omega}{v}$$

and Z_0 the image impedance of the wave is given by

$$Z_0 = \rho v\sqrt{1 + \frac{j\omega(\chi + 2\eta)}{\rho v^2}} \doteq \rho v\left[1 + \frac{j\omega(\chi + 2\eta)}{2\rho v^2}\right]$$

In discussing wave propagation in this and more complicated systems, it is often desirable to have an equivalent circuit which will give the same propagation constant and image impedance that are obtained from the differential equations. The network for an element of length dx is obtained by multiplying the image impedance by the propagation constant for the

element under consideration for the series element and taking the ratio for the shunt element. Hence

$$Z_1 = Z_0\Gamma\, dx = j\omega\rho\, dx; \qquad Z_2 = \frac{Z_0}{\Gamma\, dx} = \left[-\frac{j\kappa}{\omega} + (\chi + 2\eta)\right]\frac{1}{dx} \quad \text{(A.140)}$$

Such a representation is shown by Fig. 13.1.

A7.2 *Thermal Losses Due to Failure of Adiabatic Assumption*

The propagation of a plane wave in a gas or liquid does not quite satisfy the adiabatic assumption made in section A7.1, since some heat energy is propagated from the compressed hot regions of the gas to the rarified cool regions. This interchange of heat energy abstracts energy from the acoustic wave, and causes an added loss in wave propagation in gases, liquids and even solids. In fact, at very high frequencies, this source of loss is the largest one in a solid and eventually causes the velocity to decrease from the adiabatic velocity to the isothermal velocity. It is the purpose of this section to evaluate this source of loss.

The equation of heat conduction can be written in the form

$$C_v\rho\frac{\partial\Theta}{\partial t} = K\nabla^2\Theta - P \quad \text{(A.141)}$$

where K is the thermal conductivity and P the rate of production of heat, per unit volume, *i.e.* dQ/dt the heat added to the volume per unit of volume. From the last of equations (A.120) the heat added per unit volume by the mechanical wave is

$$dQ = \Theta\, d\sigma = \Theta\lambda_{ij}S_{ij}$$

and the rate of adding heat

$$P = \frac{dQ}{dt} = \Theta\lambda_{ij}\frac{dS_{ij}}{dt} \quad \text{(A.142)}$$

Introducing this in equation (A.141), the thermal equation becomes

$$C_v\rho\frac{\partial\Theta}{dt} = K\nabla^2\Theta - \Theta\lambda_{ij}\frac{dS_{ij}}{dt} \quad \text{(A.143)}$$

This reduces to the last of equations (A.120) with $d\sigma$ equal to zero if K, the heat conductivity, vanishes.

We now suppose that the deviation from the temperature Θ is small and is given by $\Theta = \Theta_0(1 + \theta)$. Also since we are dealing with simple harmonic motion, θ will also be harmonic and in equation (A.143) becomes

$$\left[j\omega\rho C_v - K\frac{\partial^2}{\partial x^2}\right]\theta = -j\omega\lambda_{ij}S_{ij} \quad \text{(A.144)}$$

Now the strain is going to be propagated as in equation (A.137) for a plane wave, and θ will have a similar variation for a plane wave. Hence writing

$$\theta = A' \cosh \Gamma x + B' \cosh \Gamma x$$

and

$$S_{11} = \frac{\partial \xi}{\partial x} = \Gamma[A \sinh \Gamma x + B \cosh \Gamma x]$$

a solution for θ is

$$\theta = \frac{-j\omega\lambda_{11}}{j\omega\rho C_v - K\Gamma^2}[\Gamma(B \cosh \Gamma x + A \sinh \Gamma x)]$$

$$= -\frac{j\omega\lambda_{11}S_{11}}{j\omega\rho C_v - K\Gamma^2} \tag{A.145}$$

Introducing this in the first equation of (A.120) and noting that $d\Theta = \Theta_0\theta$, we have

$$T_{kl} = \left[c^{\Theta}_{11kl} + jH_{11kl} + \frac{\Theta\lambda_{11}^2 j\omega}{j\omega C_v - K\Gamma^2}\right] S_{11} + \eta_{11kl}\dot{S}_{11} \tag{A.146}$$

For liquids and gases, neglecting the hysteresis terms, and assuming that

$$K\Gamma^2 \doteq -\frac{\omega^2 K}{v^2}$$

which gives the largest part of Γ if the attenuation is small, we can write the force equation (neglecting hysteresis) as

$$T_{11} = \kappa^{\theta}\left(1 + \frac{\Theta\alpha^2\kappa^{\theta}}{\rho C_v}\right) S_{11} + j\omega\left[\chi + 2\eta + \frac{(\gamma - 1)K}{C_p}\right] S_{11} \tag{A.147}$$

Hence, with these approximations, the velocity is the adiabatic velocity and a term is added to the viscosity equal to the product of the heat capacity K divided by the specific heat at constant pressure times $(\gamma - 1)$, where γ is the ratio of the specific heats.

It is obvious from (A.145) that at very high frequencies, *i.e.*

$$\omega \gg \frac{\rho C_v v^2}{K} \tag{A.148}$$

the expression for θ approaches zero, and the velocity reduces to the isothermal velocity. For most amorphous liquids or solids, since the heat conductivity is very small, this frequency is very high, and even for crystalline quartz, which has a high heat conductivity, it is about

$$f \gg \frac{1}{2\pi} \times \frac{2.65 \times 7.37 \times 10^6 \times (5.6 \times 10^5)^2}{6.66 \times 10^6} = 1.46 \times 10^{11} \text{ cycles} \tag{A.149}$$

since the specific heat for quartz is 7.37×10^6 ergs per gram, the heat conductivity perpendicular to the z-axis is 6.68×10^6 ergs per second per square centimeter per °C, and the velocity of propagation along the x-axis for a longitudinal wave is 5.6×10^5 centimeters per second. This is a frequency up near the cut-off frequency and hence one would not expect to observe this decrease in velocity experimentally.

From the kinetic theory of gases there is a relation between the viscosity and the ratio of specific heat to heat capacity, namely

$$\frac{K}{C_p} = \frac{(9\gamma - 5)}{4}\eta \tag{A.150}$$

Hence the ratio of thermal attenuation to viscous attenuation is

$$\frac{A_{tn}}{A\eta} = \frac{3}{4}\frac{\gamma - 1}{C_p}\frac{K}{\eta} = \frac{3}{4}(\gamma - 1)\left(\frac{9\gamma - 5}{4}\right) \tag{A.151}$$

which is about equal to 1.2 for a monatomic gas where $\gamma = \frac{5}{3}$, and less for more complex molecules.

For liquids the thermal term is much smaller than the viscous term and can usually be neglected except for mercury where the heat conductivity is high. Thermal losses should also occur in solids and are the controlling loss at very high frequencies, since thermal losses increase as the square of the frequency, while hysteresis losses increase only as the first power. For a solid material the thermal loss equals

$$A = \frac{2\pi^2 f^2}{\rho v^3}\left[\frac{K}{C_v}\frac{c_{11}^{\sigma} - c_{11}^{\theta}}{c_{11}^{\sigma}}\right] \tag{A.152}$$

As an example, for a quartz crystal vibrating along the x-axis, the constants of equation (A.152) are $\rho = 2.65$; $v = 5.6 \times 10^5$ cm/sec; $K = 6.66 \times 10^6$ ergs/sec/sq cm/C°; $C_p = 7.37 \times 10^6$ ergs per gram; $c_{11}^{\theta} = 86.02 \times 10^{10}$; $c_{11}^{\sigma} - c_{11}^{\theta} = 2.85 \times 10^9$, and the attenuation is

$$A = 12.8 \times 10^{-20} f^2 \text{ nepers/cm} \tag{A.153}$$

Since the Q of a bar is given by

$$Q = \frac{B}{2A} = \frac{2\pi}{2(12.8 \times 10^{-20})fv} = \frac{4.41 \times 10^{13}}{f} \tag{A.154}$$

where B is the phase shift in radians and A the attenuation in nepers and hence the Q at 1 megacycle due to this source should be about 10^8. This is considerably higher than has been measured indicating that most of the loss at this frequency should be due to hysteresis effects. At a frequency of 100 megacycles, however, the thermal loss is probably larger than the hysteresis loss.

A7.3 *Hysteresis Losses in Solid Materials*

The attenuation losses in fused quartz, copper and many solid materials varies directly as the frequency and hence cannot be accounted for by viscosity or thermal losses. Relaxation mechanisms introduce losses that are proportional to the square of the frequency below the relaxation frequency, and independent of the frequency above the relaxation frequency; hence such mechanisms cannot account for this type of loss.

Neglecting viscosity and thermal losses, the stress equations for adiabatic conditions can be written

$$T_{kl} = [c^{\sigma}_{ijkl} + jH_{ijkl}]S_{ij} \tag{A.155}$$

For a plane wave with a single stress S_{11} and assuming that the only elastic constant operative is $c_{11} = c_{1111}$, the equation of motion becomes

$$\rho \frac{\partial \dot{\xi}}{\partial t} = [c^{\sigma}_{11} + jH_{11}] \frac{\partial^2 \xi}{\partial x^2} \tag{A.156}$$

A solution of this equation for simple harmonic motion is

$$\xi = A \cosh \Gamma x + B \sinh \Gamma x$$

where

$$\Gamma^2 = \frac{-\omega^2 \rho}{c^{\sigma}_{11} + jH_{11}} \quad \text{or} \quad \Gamma = \frac{j\omega/v}{\sqrt{1 + \dfrac{jH_{11}}{c^{\sigma}_{11}}}} \doteq \frac{\pi f(H_{11}/c^{\sigma}_{11})}{v} + \frac{j\omega}{v} \tag{A.157}$$

Hence this type of dissipation produces a loss directly proportional to the frequency and does not affect the velocity to a first approximation. The Q of such a material, being

$$Q = \frac{B}{2A} = \frac{2\pi f/v}{\dfrac{2\pi f(H_{11}/c^{\sigma}_{11})}{v}} = \frac{c^{\sigma}_{11}}{H_{11}} \tag{A.158}$$

is independent of the frequency.

When all three effects exist, they are additive to a first approximation.

A.8 *Losses in Gases and Liquids due to Thermal Relaxation*

Thermal relaxation losses arise from the incomplete establishment of thermal equilibrium in the system and energy dissipation of a wave results whenever all parts of the system are not at the same temperature. The dissipation becomes particularly pronounced when the period of the heating and cooling cycle is comparable with the frequency of the applied wave. In polyatomic gases there are time lags in the order of 10^{-5} seconds

in establishing equilibrium between internal modes of motion in the molecules and the external translational degrees of freedom. This time lag produces velocity dispersions and anomalous absorption at frequencies of the order of 100 kilocycles. The absorption from this source is often very large and may produce attenuations hundreds of times larger than occur for the classical mechanisms of viscosity and heat conduction. The velocity is affected because the ratio of specific heats is involved in the velocity, and this ratio is a function of the completeness of the excitation of the internal degrees of freedom at a given frequency.

A phenomenological description of this process has been given by Herzfeld and Rice,[8] who treat the internal and external degrees of freedom as separate thermodynamic systems. The internal modes may be at a different temperature Θ' than the external translational system which has the temperature Θ. Neglecting viscosity, the stress and entropy equation (A.117) can then be written in the form

$$dT_{kl} = \frac{\partial T_{kl}}{\partial S_{ij}} dS_{ij} + \frac{\partial T_{kl}}{\partial \Theta} d\Theta$$

$$d\sigma = \frac{\partial \sigma}{\partial S_{ij}} dS_{ij} + \frac{\partial \sigma}{\partial \Theta} d\Theta + \frac{\partial \sigma}{\partial \Theta'} d\Theta' \qquad \text{(A.159)}$$

These equations state that the external stresses are affected only by the external temperature Θ, but the entropy consists in a term proportional to the external temperature Θ plus another term proportional to the internal temperature Θ'. Since Θ and Θ' differ by only very small amounts, we can write

$$\frac{\partial \sigma}{\partial \Theta} = \frac{\rho C_{va}}{\Theta}; \qquad \frac{\partial \sigma}{\partial \Theta'} = \frac{\rho C_{vi}}{\Theta} \qquad \text{(A.160)}$$

where C_{va} is the specific heat at constant strain due to translational and rotational modes, and C_{vi} the specific heat at constant volume due to internal vibrations. As before

$$\frac{\partial T_{kl}}{\partial S_{ij}} = c^{\theta}_{ijkl}; \qquad -\frac{\partial T_{kl}}{\partial \theta} = \frac{\partial \sigma}{\partial S_{ij}} = \lambda^{S}_{ij} \qquad \text{(A.161)}$$

where c^{θ}_{ijkl} are the isothermal elastic constants and λ^{S}_{ij} are the temperature coefficients of stress at constant strains.

The transfer of temperature between the internal and external systems will proceed at a rate that is proportional to the temperature difference of

[8] Herzfeld, K. F. and F. O. Rice, *Phys. Rev.*, Vol. 31, p. 691, 1928.

the two systems and hence we can write

$$\frac{\partial \Theta'}{\partial t} = \frac{(\Theta - \Theta')}{\tau} \tag{A.162}$$

where τ is a constant which turns out to be nearly the relaxation time. Since we are concerned with simple harmonic motion, both Θ and Θ' will have changes $d\Theta$ and $d\Theta'$ that are harmonic functions. Then from (A.162) we have

$$d\Theta'[1 + j\omega\tau] = d\Theta \tag{A.163}$$

Inserting these values in equations (A.159), these become on dropping the differential forms for T and S,

$$\begin{aligned} T_{kl} &= c^{\theta}_{ijkl} S_{ij} - \lambda^{S}_{ij}\, d\Theta \\ \Theta d\sigma &= \Theta\lambda_{ij} S_{ij} + \left[\rho C_{va} + \frac{\rho C_{vi}}{1 + j\omega\tau}\right] d\Theta \end{aligned} \tag{A.164}$$

Assuming that the wave progresses adiabatically, *i.e.* that all the heat energy of a given volume is divided between the internal and external motions and is not lost to cooler regions by heat propagation, we can set $d\sigma = 0$ and eliminate $d\Theta$ from the first equation. This results in one equation for the stresses

$$T_{kl} = \left[c^{\theta}_{ijkl} + \frac{\Theta\lambda^2_{ij}}{\rho\left(C_{va} + \dfrac{C_{vi}}{1 + j\omega\tau}\right)}\right] S_{ij} \tag{A.165}$$

Now, since liquids and solids are isotropic and moreover have no shear elastic constants, at least at low frequencies, these equations result in the stress strain equations

$$T_{11} = T_{22} = T_{33} = \kappa^{\theta}\left[1 + \frac{\kappa^{\theta}\Theta\alpha^2}{\rho\left(C_{va} + \dfrac{C_{vi}}{1 + j\omega\tau}\right)}\right][S_{11} + S_{22} + S_{33}] \tag{A.166}$$

For a plane wave along x, only S_{11} is different from zero and is equal to $\frac{\partial \xi}{\partial x}$. Inserting (A.166) in the equation of motion

$$\rho \frac{\partial \dot{\xi}}{\partial t} = \frac{\partial T_{11}}{\partial x}$$

we have
$$\rho\ddot{\xi} = \kappa^\theta\left[1 + \frac{\kappa^\theta\Theta\alpha^2}{\rho\left(C_{va} + \dfrac{C_{vi}}{1 + j\omega\tau}\right)}\right]\frac{\partial^2\xi}{\partial x^2} \tag{A.167}$$

This is satisfied for a plane progressive wave by the equation
$$\xi = \xi_0 e^{-\Gamma x} \tag{A.168}$$

where Γ the propagation constant has the value
$$\Gamma = A + jB = \sqrt{\frac{-\omega^2\rho}{\kappa^\theta\left[1 + \dfrac{\kappa^\theta\Theta\alpha^2}{\rho\left(C_{va} + \dfrac{C_{vi}}{1 + j\omega\tau}\right)}\right]}} \tag{A.169}$$

Solving for the attenuation constant A and the phase constant B, we have, after introducing the relations

$$\frac{\kappa^\theta\Theta\alpha^2}{\rho C_v} = \frac{C_p - C_v}{C_v} = \gamma - 1; \qquad \frac{\kappa^\sigma}{\kappa^\theta} = \frac{C_p}{C_v} = \gamma$$

$$B \doteq \sqrt{\frac{\omega^2\rho/\kappa^\sigma}{1 + \dfrac{\gamma - 1}{\gamma}\dfrac{C_{vi}}{C_v}\dfrac{\omega^2\tau^2}{1 + \omega^2\tau^2}}}; \qquad \frac{A}{B} = \frac{\dfrac{1}{2}\left(\dfrac{\gamma - 1}{\gamma}\right)\dfrac{C_{vi}}{C_v}\dfrac{\omega\tau}{1 + \omega^2\tau^2}}{1 + \dfrac{\gamma - 1}{\gamma}\dfrac{C_{vi}}{C_v}\left(\dfrac{\omega^2\tau^2}{1 + \omega^2\tau^2}\right)} \tag{A.170}$$

Since the velocity of propagation at any frequency f is $v = \omega/B$, we have
$$v = \frac{\omega}{B} = \sqrt{\frac{v_0^2\left[1 + \omega^2\tau^2\left(1 + \dfrac{\gamma - 1}{\gamma}\dfrac{C_{vi}}{C_v}\right)\right]}{1 + \omega^2\tau^2}} = \sqrt{\frac{v_0^2 + \omega^2\tau^2 v_\infty^2}{1 + \omega^2\tau^2}} \tag{A.171}$$

where the low-frequency velocity v_0 and the high-frequency velocities are
$$v_0 = \sqrt{\frac{\kappa^\sigma}{\rho}}; \qquad v_\infty = v_0\sqrt{1 + \frac{\gamma - 1}{\gamma}\frac{C_{vi}}{C_v}} \tag{A.172}$$

Since the attenuation per wavelength is 2π times the ratio A/B, we have
$$A_\lambda = \frac{\pi\left(\dfrac{\gamma - 1}{\gamma}\right)\dfrac{C_{vi}}{C_v}\omega\tau}{1 + \omega^2\tau^2\left(1 + \dfrac{\gamma - 1}{\gamma}\dfrac{C_{vi}}{C_v}\right)} = \frac{\pi\left(\dfrac{\gamma - 1}{\gamma}\right)\dfrac{C_{vi}}{C_v}\omega\tau}{1 + \omega^2\tau^2\left(\dfrac{v_\infty^2}{v_0^2}\right)} \tag{A.173}$$

Now if we define τ' as

$$\tau' = \tau\left(\frac{v_\infty}{v_0}\right) \tag{A.174}$$

the attenuation formula becomes

$$A_\lambda = \frac{\pi\left(\frac{\gamma-1}{\gamma}\right)\left(\frac{v_0}{v_\infty}\right)\frac{C_{vi}}{C_v}[\omega\tau']}{1+\omega^2\tau'^2} \tag{A.175}$$

The velocity becomes

$$v = v_0\sqrt{\frac{\frac{v_\infty^2}{\tau'^2}+v_0^2\omega^2\left[1+\left(\frac{\gamma-1}{\gamma}\right)\frac{C_{vi}}{C_v}\right]}{\frac{v_\infty^2}{\tau'^2}+\omega^2 v_0^2}} \tag{A.176}$$

These are the formulae given in equation (13.28).

A.9 *Application of Tensor Equations to Cylindrical Coordinates*

In Chapter XII resonant frequencies of a disc of barium titanate driven by the electrostrictive effect are of interest. To obtain such equations one has to transform the stress strain and field equations into cylindrical coordinates. It is the purpose of this section to discuss the use of tensor equations in cylindrical coordinates.

In cylindrical coordinates, the variables are the radius vector r, the angle θ and the dimension along the cylinder designated by z. In terms of the x, y, z rectangular coordinates

$$r^2 = x^2 + y^2; \qquad \tan\theta = \frac{y}{x}, z = z \tag{A.177}$$

The direction cosines between the r, θ and z directions, and the x, y, z directions are given by the equation

	x	y	z
r	$\cos\theta$	$\sin\theta$	0
θ	$-\sin\theta$	$\cos\theta$	0
z	0	0	1

(A.178)

Making use of the formula for the transformation of a tensor from one coordinate system to another

$$T_{a,b} = \frac{\partial x_a}{\partial x_k}\frac{\partial x_b}{\partial x_l}T_{kl} \tag{A.179}$$

where a, b are associated with the r, θ, z coordinates, and noting that the partial derivatives are the direction cosines of equation (A.178), the stress tensor becomes in cylindrical coordinates

$$\begin{aligned}
T_{rr} &= \cos^2\theta T_{11} + 2\sin\theta\cos\theta T_{12} + \sin^2\theta T_{22} \\
T_{\theta\theta} &= \sin^2\theta T_{11} - 2\sin\theta\cos\theta T_{12} + \cos^2\theta T_{22} \\
T_{r\theta} &= \sin\theta\cos\theta[T_{22} - T_{11}] + [\cos^2\theta - \sin^2\theta]T_{12} \\
T_{rz} &= \cos\theta T_{13} + \sin\theta T_{23} \\
T_{\theta z} &= -\sin\theta T_{13} + \cos\theta T_{23} \\
T_{zz} &= T_{33}
\end{aligned} \tag{A.180}$$

The strain tensor transforms in a similar manner.

Conversely, the rectangular stress and strain components are related to the cylindrical components by equations of the type

$$S_{ij} = \frac{\partial x_i}{\partial x_a}\frac{\partial x_j}{\partial x_b} S_{ab} \tag{A.181}$$

and

$$\begin{aligned}
S_{11} &= \cos^2\theta S_{rr} - 2\sin\theta\cos\theta S_{r\theta} + \sin^2\theta S_{\theta\theta} \\
S_{22} &= \sin^2\theta S_{rr} + 2\sin\theta\cos\theta S_{r\theta} + \cos^2\theta S_{\theta\theta} \\
S_{33} &= S_{zz} \\
S_{12} &= \sin\theta\cos\theta(S_{rr} - S_{\theta\theta}) + (\cos^2\theta - \sin^2\theta)S_{r\theta} \\
S_{13} &= \cos\theta S_{rz} - \sin\theta S_{\theta z} \\
S_{23} &= \sin\theta S_{rz} + \cos\theta S_{\theta z}
\end{aligned} \tag{A.182}$$

In solving the equations of motion it is necessary to know the values of the strains in terms of the displacements in the r, θ and z directions. Denoting these by

$$u_r, \quad u_\theta \quad \text{and} \quad u_z \tag{A.183}$$

these relations can be obtained from the transformation equations for strains which are similar to equations (A.180). For example:

$$\begin{aligned}
S_{rr} &= \cos^2\theta S_{11} + 2\sin\theta\cos\theta S_{12} + \sin^2\theta S_{22} \\
&= \cos^2\theta\frac{\partial u_x}{\partial x} + \sin\theta\cos\theta\left(\frac{\partial u_y}{\partial x} + \frac{\partial u_x}{\partial y}\right) + \sin^2\theta\frac{\partial u_y}{\partial y}
\end{aligned} \tag{A.184}$$

Making use of the relations

$$\frac{\partial u_x}{\partial x} = \frac{\partial u_x}{\partial r}\frac{\partial r}{\partial x} + \frac{\partial u_x}{\partial(r\theta)}\frac{\partial(r\theta)}{\partial x} + \frac{\partial u_x}{\partial z}\frac{\partial z}{\partial x} \tag{A.185}$$

and noting that

$$u_x = u_r \cos\theta - u_\theta \sin\theta; \qquad u_y = u_r \sin\theta + u_\theta \cos\theta$$

the various terms of (A.184) become

$$\begin{aligned} S_{rr} = {} & \cos^2\theta \left[\frac{\partial u_r}{\partial r} \cos^2\theta - \frac{u_r}{r} \sin^2\theta - \left(\frac{1}{r} \frac{\partial u_\theta}{\partial \theta} \sin\theta + \frac{u_\theta}{r} \cos\theta \right) \sin\theta \right] \\ & + \sin\theta \cos\theta \left[2 \frac{\partial u_r}{\partial r} \sin\theta \cos\theta + 2 \frac{u_r}{r} \sin\theta \cos\theta + \frac{2}{r} \frac{\partial u_\theta}{\partial \theta} \sin\theta \cos\theta \right. \\ & \qquad \left. + \frac{u_\theta}{r} (\cos^2\theta - \sin^2\theta) \right] \\ & + \sin^2\theta \left[\frac{\partial u_r}{\partial r} \sin^2\theta - \frac{u_r}{r} \cos^2\theta - \cos\theta \left(\frac{1}{r} \frac{\partial u_\theta}{\partial \theta} \cos\theta - \frac{u_\theta}{r} \sin\theta \right) \right] \\ = {} & \frac{\partial u_r}{\partial r} \end{aligned} \tag{A.186}$$

In a similar manner it can be shown that

$$\begin{aligned} S_{\theta\theta} &= \frac{1}{r} \frac{\partial u_\theta}{\partial \theta} + \frac{u_r}{r} \\ S_{zz} &= \frac{\partial u_z}{\partial z} \\ S_{r\theta} &= \frac{\partial u_\theta}{\partial r} - \frac{u_\theta}{r} + \frac{1}{r} \frac{\partial u_r}{\partial \theta} \\ S_{rz} &= \frac{\partial u_r}{\partial z} + \frac{\partial u_z}{\partial r} \\ S_{\theta z} &= \frac{1}{r} \frac{\partial u_z}{\partial \theta} + \frac{\partial u_\theta}{\partial z} \end{aligned} \tag{A.187}$$

The final equation to be transformed into cylindrical coordinates is the Newton's law equation, which in rectangular coordinates is

$$\rho \frac{d^2 u_k}{dt^2} = \frac{\partial T_{kl}}{\partial x_k} \tag{A.188}$$

This is a vector equation and can be transferred according to the law

$$\ddot{u}_a = \frac{\partial x_a}{\partial x_k} \ddot{u}_k \tag{A.189}$$

where a denotes the variables r, $(r\theta)$ and z. For example:

$$\begin{aligned}\rho\ddot{u}_r &= \frac{\partial r}{\partial x}\rho\ddot{u}_x + \frac{\partial r}{\partial y}\rho\ddot{u}_y + \frac{\partial r}{\partial z}\rho\ddot{u}_z \\ &= \cos\theta\left[\frac{\partial T_{11}}{\partial x} + \frac{\partial T_{12}}{\partial y} + \frac{\partial T_{13}}{\partial z}\right] + \sin\theta\left[\frac{\partial T_{21}}{\partial x} + \frac{\partial T_{22}}{\partial y} + \frac{\partial T_{23}}{\partial z}\right]\end{aligned} \tag{A.190}$$

Inserting the values of T_{11} etc. which are related to T_{rr} etc. as the cartesian and cylindrical strains of equation (A.182) and introducing relations of the type

$$\frac{\partial T_{11}}{\partial x} = \frac{\partial T_{11}}{\partial r}\frac{dr}{dx} + \frac{\partial T_{11}}{\partial(r\theta)}\frac{d(r\theta)}{dx} + \frac{\partial T_{11}}{\partial z}\frac{dz}{dx} \tag{A.191}$$

One finds that equation (A.190) becomes

$$\rho\ddot{u}_r = \frac{\partial T_{rr}}{\partial r} + \frac{1}{r}\frac{\partial T_{r\theta}}{\partial\theta} + \frac{\partial T_{rz}}{\partial z} + \frac{(T_{rr} - T_{\theta\theta})}{r} \tag{A.192}$$

Similarly the other acceleration equations become

$$\begin{aligned}\rho\ddot{u}_\theta &= \frac{\partial T_{r\theta}}{\partial r} + \frac{1}{r}\frac{\partial T_{\theta\theta}}{\partial\theta} + \frac{\partial T_{\theta z}}{\partial z} + \frac{2T_{r\theta}}{r} \\ \rho\ddot{u}_z &= \frac{\partial T_{rz}}{\partial r} + \frac{1}{r}\frac{\partial T_{\theta z}}{\partial\theta} + \frac{\partial T_{zz}}{\partial z} + \frac{T_{rz}}{r}\end{aligned} \tag{A.193}$$

These equations give enough relations to solve the case of the electrostrictive disc of barium titanate in radial vibration. Equations (12.23) of Chapter XII give the electrostrictive and elastic equations in rectangular coordinates. Transferring these to cylindrical coordinates by means of the tensor relations of equations (A.180) and (A.182) we find

$$\begin{aligned}S_{rr} &= s^D_{1111}T_{rr} + s^D_{1122}(T_{\theta\theta} + T_{zz}) + [Q_{1111}\delta_r^2 + Q_{1122}(\delta_\theta^2 + \delta_z^2)] \\ S_{\theta\theta} &= s^D_{1122}(T_{rr} + T_{zz}) + s^D_{1111}T_{\theta\theta} + [Q_{1122}(\delta_r^2 + \delta_z^2) + Q_{1111}\delta_\theta^2] \\ S_{zz} &= s^D_{1111}T_{zz} + s^D_{1122}(T_{rr} + T_{\theta\theta}) + [Q_{1111}\delta_z^2 + Q_{1122}(\delta_r^2 + \delta_\theta^2)] \\ S_{rz} &= (s^D_{1111} - s^D_{1122})T_{rz} + (Q_{1111} - Q_{1122})\delta_r\delta_z \\ S_{r\theta} &= (s^D_{1111} - s^D_{1122})T_{r\theta} + (Q_{1111} - Q_{1122})\delta_r\delta_\theta \\ S_{\theta z} &= (s^D_{1111} - s^D_{1122})T_{\theta z} + [Q_{1111} - Q_{1122}]\delta_\theta\delta_z\end{aligned} \tag{A.194}$$

where δ_r, δ_θ, δ_z are the electric displacements along the r, θ and z directions.

The electrical relations become

$$\begin{aligned}
E_r &= \delta_r(4\pi\beta_{11}^T + O_{111}\delta_r) - 2\{Q_{1111}(\delta_r T_{rr} + \delta_\theta T_{r\theta} + \delta_z T_{rz}) \\
&\quad + Q_{1122}[\delta_r(T_{\theta\theta} + T_{zz}) - (\delta_\theta T_{r\theta} + \delta_z T_{rz})]\} \\
E_\theta &= \delta_\theta(4\pi\beta_{11}^T + O_{111}\delta_\theta) - 2\{Q_{1111}(\delta_\theta T_{\theta\theta} + \delta_r T_{r\theta} + \delta_z T_{\theta z}) \\
&\quad + Q_{1122}[\delta_\theta(T_{rr} + T_{zz}) - (\delta_r T_{r\theta} + \delta_z T_{\theta z})]\} \\
E_z &= \delta_z(4\pi\beta_{11}^T + O_{111}\delta_z) - 2\{Q_{1111}(\delta_z T_{zz} + \delta_r T_{rz} + \delta_\theta T_{\theta z}) \\
&\quad + Q_{1122}[\delta_z(T_{rr} + T_{\theta\theta}) - (\delta_r T_{rz} + \delta_\theta T_{\theta z})]\}
\end{aligned} \tag{A.195}$$

where E_r, E_θ and E_z are the three fields along the r, θ and z directions.

For the radially vibrating disc, we assume the thickness to be so small that the change of stress is negligible along the z direction. Since the stresses are zero on the surface, we can set

$$T_{zz} = T_{rz} = T_{\theta z} = 0 \tag{A.196}$$

Furthermore, since the motion is entirely radial, $u_\theta = u_z = 0$, and

$$T_{r\theta} = 0 \tag{A.197}$$

Since a field is applied only along the z direction, $\delta_r = \delta_\theta = 0$. The remaining equations then become

$$\begin{aligned}
S_{rr} &= s_{1111}^D T_{rr} + s_{1122}^D T_{\theta\theta} + Q_{1122}\delta_z^2 \\
S_{\theta\theta} &= s_{1122}^D T_{rr} + s_{1111}^D T_{\theta\theta} + Q_{1122}\delta_z^2 \\
E_z &= \delta_z[4\pi\beta_{11}^T + O_{111}\delta_z] - 2Q_{1122}\delta_z(T_{rr} + T_{\theta\theta})
\end{aligned} \tag{A.198}$$

To insert in the equation of motion (A.192) we need to have the stresses expressed in terms of the strains and for the electrical boundary conditions it is better to use the fields rather than the electric displacements. Furthermore, for small alternating fields superposed on a large DC electric displacement, which may be caused by an applied field or a remanent polarization, we can replace δ_z by

$$\delta_z = \delta_{z0} + \delta_z e^{j\omega t} \tag{A.199}$$

where δ_{z0} is the remanent electric displacement and δ_z the alternating component. Then solving these three equations simultaneously the alternating components of stress, strain and displacement are given by the equations

$$\begin{aligned}
T_{rr} &= S_{rr}\left(\frac{s_{1111}^E}{s_{1111}^E - s_{1122}^E}\right) - S_{\theta\theta}\left(\frac{s_{1122}^E}{s_{1111}^E - s_{1122}^E}\right) \\
&\quad - \left(\frac{2Q_{1122}\delta_{z0}E_z}{4\pi\beta_{11}^T + O_{111}\delta_{z0}}\right)\left(\frac{1}{s_{1111}^E + s_{1122}^E}\right).
\end{aligned}$$

$$T_{\theta\theta} = S_{\theta\theta}\left(\frac{s^E_{1111}}{s^{E^2}_{1111} - s^{E^2}_{1122}}\right) - S_{rr}\left(\frac{s^E_{1122}}{s^{E^2}_{1111} - s^{E^2}_{1122}}\right) - \left(\frac{2Q_{1122}\delta_{z0}E_z}{4\pi\beta^T_{11} + O_{111}\delta_{z0}}\right)\left(\frac{1}{s^E_{1111} + s^E_{1122}}\right) \quad \text{(A.200)}$$

$$\delta_z = \frac{E_z}{4\pi\beta^T_{11} + O_{111}\delta_{z0}} + \left(\frac{2Q_{1122}\delta_{z0}}{4\pi\beta^T_{11} + O_{111}\delta_{z0}}\right)(T_{rr} + T_{\theta\theta})$$

Where $s^E_{1111} = \dfrac{s^D_{1111}}{1 - \dfrac{4Q^2_{1122}\delta^2_{z0}}{(4\pi\beta^T_{11} + O_{111}\delta_{z0})s^E_{1111}}} = \dfrac{s^D_{1111}}{1 - k_l^2}$

$$s^E_{1122} = \frac{s^D_{1122}}{1 - \dfrac{s^D_{1111}}{s^D_{1122}}\left(\dfrac{4Q_{1122}{}^2\delta^2_{z0}}{(4\pi\beta^T_{11} + O_{111}\delta_{z0})s^E_{1111}}\right)} = \frac{s^D_{1122}}{1 - \dfrac{s^D_{1111}k_l{}^2}{s^D_{1122}}}$$

where k_l is the electromechanical coupling for a longitudinal mode and is defined by equation (12.5). We note that since $1/s^E_{1111} = Y^E_0$, the Young's modulus, and $-s^E_{1122}/s^E_{1111} = \sigma$, the Poisson's ratio, that these equations can be simplified to

$$\begin{aligned} T_{rr} &= \left(\frac{Y^E_0}{1 - \sigma^2}\right)(S_{rr} + \sigma S_{\theta\theta}) - \frac{2Q_{1122}\delta_{z0}E_zY^E_0}{(4\pi\beta^T_{11} + O_{111}\delta_{z0})(1 - \sigma)} \\ T_{\theta\theta} &= \left(\frac{Y^E_0}{1 - \sigma^2}\right)(S_{\theta\theta} + \sigma S_{rr}) - \frac{2Q_{1122}\delta_{z0}E_zY^E_0}{(4\pi\beta^T_{11} + O_{111}\delta_{z0})(1 - \sigma)} \quad \text{(A.201)} \\ \delta_z &= \frac{E_z}{4\pi\beta^T_{11} + O_{111}\delta_{z0}} + \frac{2Q_{1122}\delta_{z0}}{(4\pi\beta^T_{11} + O_{111}\delta_{z0})}(T_{rr} + T_{\theta\theta}) \end{aligned}$$

Noting that since the plating on the surface is an equipotential surface, E_z is not a function of r, then when equations (A.201) are inserted in the equation of motion (A.192), and using the relations for a radial motion

$$S_{rr} = \frac{\partial u_r}{\partial r}; \qquad S_{\theta\theta} = \frac{u_r}{r} \quad \text{(A.202)}$$

the equation of motion becomes

$$\frac{Y^E_0}{1 - \sigma^2}\left[\frac{\partial^2 u_r}{\partial r^2} + \frac{1}{r}\frac{\partial u_r}{\partial r} - \frac{u_r}{r^2}\right] = \rho\frac{\partial^2 u_r}{\partial t^2} = -\omega^2\rho u_r \quad \text{(A.203)}$$

for simple harmonic motion.

Since this is a Bessel's equation of the first order, a solution is

$$u_r = AJ_1\left(\frac{\omega r}{v}\right); \qquad v^2 = \frac{Y^E_0}{(1 - \sigma^2)\rho} \quad \text{(A.204)}$$

No Bessel's function of the second kind is required since the displacement u_r vanishes at the center of the disc. At the boundary when $r = a$ the radius of the disc, the stress $T_{rr} = 0$. From (A.201) and (A.202)

$$T_{rr} = \frac{Y_0^E}{1-\sigma^2}\left[\frac{\partial u_r}{\partial r} + \frac{\sigma u_r}{r}\right] - \frac{2Q_{1122}\delta_{z0}E_z Y_0^E}{(4\pi\beta_{11}^T + O_{111}\delta_{z0})(1-\sigma)} \tag{A.205}$$

Since

$$\frac{\partial u_r}{\partial r} = A\left[\frac{\omega}{v}J_0\left(\frac{\omega r}{v}\right) - J_1\frac{\left(\frac{\omega r}{v}\right)}{r}\right] \tag{A.206}$$

then setting $T_{rr} = 0$ when $r = a$, we have

$$0 = \left(\frac{Y_0^E A}{1-\sigma^2}\right)\left[\frac{\omega}{v}J_0\left(\frac{\omega a}{v}\right) - \frac{(1-\sigma)J_1\left(\frac{\omega a}{v}\right)}{a}\right] - \frac{2Q_{1122}\delta_{z0}E_z Y_0^E}{(4\pi\beta_{11}^T + O_{111}\delta_{z0})(1-\sigma)} \tag{A.207}$$

Hence

$$A = +\frac{2Q_{1122}\delta_{z0}(1+\sigma)E_z}{\left[\frac{\omega}{v}J_0\left(\frac{\omega a}{v}\right) - \frac{(1-\sigma)}{a}J_1\left(\frac{\omega a}{v}\right)\right](4\pi\beta_{11}^T + O_{11}\delta_{z0})} \tag{A.208}$$

and

$$T_{rr} = -\frac{2Q_{1122}\delta_{z0}Y_0^E E_z}{(4\pi\beta_{11}^T + O_{111}\delta_{z0})(1-\sigma)} \times \left\{1 - \left[\frac{\frac{\omega}{v}J_0\left(\frac{\omega r}{v}\right) - \frac{(1-\sigma)J_1\left(\frac{\omega r}{v}\right)}{r}}{\frac{\omega}{v}J_0\left(\frac{\omega a}{v}\right) - \frac{(1-\sigma)}{a}J_1\left(\frac{\omega a}{v}\right)}\right]\right\} \tag{A.209}$$

$$T_{\theta\theta} = -\frac{2Q_{1122}\delta_{z0}E_z Y_0^E}{(4\pi\beta_{11}^T + O_{111}\delta_{z0})(1-\sigma)} \times \left\{1 - \left[\frac{\frac{\sigma\omega}{v}J_0\left(\frac{\omega r}{v}\right) + \frac{(1-\sigma)J_1\left(\frac{\omega r}{v}\right)}{r}}{\frac{\omega}{v}J_0\left(\frac{\omega a}{v}\right) - \frac{(1-\sigma)}{a}J_1\left(\frac{\omega a}{v}\right)}\right]\right\} \tag{A.210}$$

The next step in the solution is to obtain the electrical impedance as measured by A.C. methods. This can be obtained by substituting the values of T_{rr} and $T_{\theta\theta}$ in the last of equations (A.201) and integrating over the surface of the crystal. Since the value of δ_z at the surface is equal to the surface charge, this will evaluate the total charge Q and we have

$$Q = \int_0^{2\pi} d\theta \int_0^a \delta_z r\, dr = \frac{E_z \pi a^2}{(4\pi\beta_{11}^T + O_{111}\delta_{z0})} + \left(\frac{2Q_{1122}\delta_{z0}}{4\pi\beta_{11}^T + O_{111}\delta_{z0}}\right) \int_0^{2\pi} d\theta \int_0^a r[T_{rr} + T_{\theta\theta}]\, dr \tag{A.211}$$

Introducing the value of T_{rr} and $T_{\theta\theta}$ from equation (A.209) and (A.210), this integral becomes

$$Q = \frac{E_z \pi a^2}{(4\pi\beta_{11}^T + O_{111}\delta_{z0})} \left\{ 1 - \frac{8Q_{1122}^2 \delta_{z0}^2 Y_0^E (1+\sigma)}{(4\pi\beta_{11}^T + O_{111}\delta_{z0})(1-\sigma^2)} \times \left[1 - \frac{(1+\sigma)\int_0^a r \frac{\omega}{v} J_0\left(\frac{\omega r}{v}\right) dr}{a^2\left[\frac{\omega}{v} J_0\left(\frac{\omega a}{v}\right) - \frac{(1-\sigma)}{a} J_1\left(\frac{\omega a}{v}\right)\right]} \right] \right\} \tag{A.212}$$

Performing the integration and employing the substitution

$$\frac{1}{4\pi\beta_{11}^T + O_{111}\delta_{z0}} \left[1 - \frac{8Q_{1122}^2 \delta_{z0}^2 Y_0^E (1+\sigma)}{(4\pi\beta_{11}^T + O_{111}\delta_{z0})(1-\sigma^2)} \right] = \frac{1}{4\pi\beta_{11}^{RC} + O_{111}\delta_{z0}} \tag{A.213}$$

where β_{11}^{RC} is the radially clamped impermeability constant, we have

$$Q = \frac{E_z \pi a^2}{4\pi\beta_{11}^{RC} + C_{111}\delta_{z0}} \times \left\{ 1 + \left(\frac{k^2}{1-k^2}\right) \frac{(1+\sigma) J_1\left(\frac{\omega a}{v}\right)}{\left[\left(\frac{\omega a}{v}\right) J_0\left(\frac{\omega a}{v}\right) - (1-\sigma) J_1\left(\frac{\omega a}{v}\right)\right]} \right\} \tag{A.214}$$

where the coefficient of coupling for a radial mode becomes

$$k^2 = \frac{8Q_{1122}^2 \delta_{z0}^2 Y_0^E}{(4\pi\beta_{11}^T + O_{111}\delta_{z0})(1-\sigma)} \tag{A.215}$$

Comparing this with the longitudinal mode driven by the same constant, we see that the radial mode has a higher coupling by a factor

$$\sqrt{\frac{2}{1-\sigma}} \tag{A.216}$$

Since the admittance of the plate is equal to the current into the plate divided by the voltage across the plate, and for simple harmonic motion

$$i = \frac{dQ}{dt} = j\omega Q \tag{A.217}$$

the impedance of the electrostrictive plate is given by

$$\frac{1}{Z} = \frac{i}{E} = \frac{j\omega\pi a^2}{(4\pi\beta_{11}^{RC} + O_{111}\delta_{z_0})l_t} \times \left\{1 + \left(\frac{k^2}{1-k^2}\right)\frac{(1+\sigma)J_1\left(\frac{\omega a}{v}\right)}{\left[\left(\frac{\omega a}{v}\right)J_0\left(\frac{\omega a}{v}\right) - (1-\sigma)J_1\left(\frac{\omega a}{v}\right)\right]}\right\} \tag{A.218}$$

The resonant frequency occurs when

$$\left(\frac{\omega a}{v}\right)J_0\left(\frac{\omega a}{v}\right) - (1-\sigma)J_1\left(\frac{\omega a}{v}\right) = 0$$

or

$$\frac{\left(\frac{\omega a}{v}\right)J_0\left(\frac{\omega a}{v}\right)}{J_1\left(\frac{\omega a}{v}\right)} = (1-\sigma) \tag{A.219}$$

For a value of $\sigma = 0.27$ as found in Chapter XII, this equation has the lowest root

$$\left(\frac{\omega a}{v}\right) = 2.03 = R_1 \tag{A.220}$$

Hence the frequency is given by the equation

$$f_R = \frac{2.03}{2\pi a}\sqrt{\frac{Y_0^E}{\rho(1-\sigma^2)}} \tag{A.221}$$

The anti-resonant frequency occurs when the expression in brackets in equation (A.218) reduces to zero. This occurs at a frequency somewhat above the resonant frequency. To determine the frequency separa-

tion Δf between resonance and anti-resonance we develop the function $J_0\left(\frac{\omega a}{v}\right)$ and $J_1\left(\frac{\omega a}{v}\right)$ in a Maclaurin's series about the root R_1. This gives

$$J_0\left(\frac{\omega a}{v}\right) = J_0(R_1) + \frac{\partial}{\partial f}\left[J_0\left(\frac{\omega a}{v}\right)\right]_{\left(\frac{\omega a}{v}\right)=R_1} \Delta f + \cdots$$

$$= J_0(R_1) - \frac{2\pi a}{v} J_1(R_1)\,\Delta f + \cdots \tag{A.222}$$

$$J_1\left(\frac{\omega a}{v}\right) = J_1(R_1) + \frac{\partial}{\partial f}\left[J_1\left(\frac{\omega a}{v}\right)\right]_{\left(\frac{\omega a}{v}\right)=R_1} \Delta f + \cdots$$

$$= J_1(R_1) + \frac{2\pi a}{v}\left[J_0(R_1) - \frac{J_1(R_1)}{R_1}\right]\Delta f + \cdots$$

Inserting these values in equation (A.218) and setting the numerator equal to zero, the frequency separation Δf becomes

$$\frac{\Delta f}{f_R} = \frac{\left(\frac{k^2}{1-k^2}\right)(1+\sigma)}{R_1^2 - (1-\sigma^2)} \tag{A.223}$$

Hence, solving for the coupling factor k^2, we find to a first approximation

$$k^2 = \frac{\Delta f}{f_R}\left[\frac{R_1^2 - (1-\sigma^2)}{1+\sigma} + \cdots\right] \tag{A.224}$$

For $\sigma = 0.27$ the value of the factor multiplying $\frac{\Delta f}{f_R}$ is equal to 2.51. Comparing this to the factor for a longitudinal crystal given by equation (5.36) which is $\pi^2/4 = 2.47$, it is seen that the same equations are very nearly applicable and hence the coupling can be evaluated by measuring the separation of resonant and anti-resonant frequencies and using equation (A.224) to determine the coupling.

A.10 *Second Order Effects in Wave Propagation*[9]

When waves of high amplitude are propagated in liquids and gases, several non-linear effects of interest take place. These are the slow secular currents and pressures, such as crystal "wind" and radiation pressure that are due to the non-linear terms in the wave propagation. Among other examples are the forces on Rayleigh discs, the sorting of

[9] This treatment follows one given recently by Dr. J. M. Richardson.

components and the acceleration of chemical reactions in an ultrasonic field. It is the purpose of this section to discuss how tensors can be applied in the solution of such equations.

Newton's equation of motion, in the form given by equation (5.9), is exact if it refers to an element of volume which always encloses a given mass of material and can be written in the form

$$\rho \frac{D}{Dt}(\dot{x}_k) = \frac{\partial T_{kl}}{\partial x_l} \tag{A.225}$$

where D/Dt refers to the time variation of the velocity in the enclosed volume, and this is set equal to the applied force. Now if we fix our attention on an element of space $dxdydz$, moving in the fluid, the rate of change of velocity in this element of space is equal to

$$\frac{D}{Dt}(\dot{x}_k) = \frac{\partial \dot{x}_k}{\partial t} + \dot{x}_l \frac{\partial}{\partial x_l}(\dot{x}_k) \tag{A.226}$$

a well-known formula from fluid dynamics.[10] Hence Newton's equation for a fixed volume becomes

$$\rho \frac{\partial \dot{x}_k}{\partial t} = \frac{\partial T_{kl}}{\partial x_l} - \rho \dot{x}_l \frac{\partial}{\partial x_l}(\dot{x}_k) \tag{A.227}$$

The other necessary equation is the continuity equation which can be written in the form

$$\frac{\partial \rho}{\partial t} + \frac{\partial}{\partial x_l}(\rho \dot{x}_l) = 0 \tag{A.228}$$

and states that the amount of material flowing into the elementary volume is equal to the rate of change of the density of the volume. In the following treatment it is much simpler to use the mass current or transport of momentum

$$M_l = \rho \dot{x}_l \tag{A.229}$$

This results in simpler equations and simpler boundary conditions since for an impermeable boundary such as a thin membrane of plastic $\overline{M_l}$ must vanish for boundaries that are stationary whereas no such statement can be made about the corresponding quantities $\overline{\dot{x}_l}$. This situation is easily seen from the fact that on the average no mass should be transported through a surface representing the average positions of an impermeable boundary. The vanishing of $\overline{\dot{x}_l}$ does not imply this, since the density during the forward motion of the fluid may be different from the density during the backward motion resulting in a net transport of mass.

[10] Rayleigh, Lord, *Theory of Sound*, Vol. II, Chapter I; H. Lamb, *Hydrodynamics*, Chapter I.

To put the fundamental equation (A.227) in a form involving the mass current M_l, we multiply equation (A.228) by $\dot{x}_k$ and add to equation (A.225) obtaining

$$\rho \frac{\partial \dot{x}_k}{\partial t} + \dot{x}_k \frac{\partial \rho}{\partial t} = \frac{\partial T_{kl}}{\partial x_l} - \left[\rho \dot{x}_l \frac{\partial}{\partial x_l} (\dot{x}_k) + \dot{x}_k \frac{\partial}{\partial x_l} (\rho \dot{x}_l) \right]$$

or

$$\frac{\partial}{\partial t} (M_k) = \frac{\partial T_{kl}}{\partial x_l} - \frac{\partial}{\partial x_l} \left[\frac{M_k M_l}{\rho} \right] \tag{A.230}$$

which together with (A.228) expresses the transport of mass and momentum. If we wish to take account of body forces F_l, the two fundamental equations can be written in the form

$$\frac{\partial}{\partial t} (M_l) = \frac{\partial T_{kl}}{\partial x_l} - \frac{\partial}{\partial x_l} \left[\frac{M_k M_l}{\rho} \right] + \rho F_l$$

$$\frac{\partial \rho}{\partial t} + \frac{\partial}{\partial x_l} (M_l) = 0 \tag{A.231}$$

As in the theory of turbulence, the quantity $M_k M_l / \rho$ is often called the Reynold's stress since it satisfies the same law as an ordinary stress T_{kl}. For a plane progressive wave the Reynold's stress reduces to the value

$$\frac{M_k M_l}{\rho} = \rho \dot{\xi}_0^2 \cos^2 \omega t. \tag{A.232}$$

Averaged over a long period this produces a constant stress or pressure

$$p_R = \tfrac{1}{2} \rho \dot{\xi}_0^2 \tag{A.233}$$

which is equal to the energy density of the wave and the radiation pressure. The negative sign in equation (A.231) shows that the term is a pressure rather than a tension.

The method for solving (A.231) is one of successive approximations based on an expansion of all pertinent quantities in terms of a characteristic amplitude α. Hence

$$\begin{aligned} \rho &= \rho^{(0)} + \rho^{(1)} \alpha + \cdots \\ M_l &= M_l^{(1)} \alpha + M_l^{(2)} \alpha^2 + \cdots \\ T_{kl} &= T_{kl}^0 + T_{kl}^{(1)} \alpha + T_{kl}^{(2)} \alpha^2 + \cdots \\ F_l &= F_l^0. \end{aligned} \tag{A.234}$$

Here we have assumed the body force F_l to be a given function of position and hence independent of α. We have also assumed that M_l vanishes when $\alpha = 0$, that is, all disturbances are excited by a force whose amplitude

is proportional to α. Introducing the above expansions into equations (A.231) and equating to zero the coefficients of each power of α, we get the following set of equations:

$$\frac{\partial \rho^0}{\partial t} = 0; \qquad \frac{\partial T_{kl}}{\partial x_l} + \rho^0 F_l = 0 \tag{A.235}$$

$$\frac{\partial \rho^{(1)}}{\partial t} + \frac{\partial}{\partial x_l}[M_l^{(1)}] = 0; \qquad \frac{\partial M_l}{\partial t} = \frac{\partial}{\partial x_l}[T_{kl}^{(1)}] - \rho^{(1)} F_l; \tag{A.236}$$

$$\frac{\partial}{\partial t}[M_l^{(2)}] = \frac{\partial}{\partial x_l}\left[T_{kl}^{(2)} - \frac{M_k^{(1)} M_l^{(1)}}{\rho^0}\right] + \rho^{(2)} F_l;$$

$$\frac{\partial \rho^{(2)}}{\partial t} + \frac{\partial}{\partial x_l}[M_l^{(2)}] = 0 \tag{A.237}$$

The first equations (A.235) are the conditions for static equilibrium, the second (A.236) are the ordinary linearized equations for acoustics, while equations (A.237) give the quadratic corrections for non-linear effects.

So far we have not limited the equations to any particular type of medium, but since the greatest application is in connection with gases and liquids we shall consider only these cases. For these cases the stress strain relations reduce to those given by equation (A.126) as a linear effect. Second-order terms in the stress can also occur, but these are usually small compared to the effect of the Reynold's stress ($M_k M_l/\rho^0$) and are usually neglected.

The method for solving equations (A.237) is first to find the exact solutions of equation (A.236). The second equation of (A.237) does not contain any quantities from the previous approximation. Substituting in the solution for M_l from equation (A.236), the value for the Reynold's stress becomes

$$R_{kl} = \frac{M_k M_l}{\rho_0} \cos^2 \omega t = \frac{1}{2}\left(\frac{M_k M_l}{\rho_0}\right)(1 + \cos 2\omega t) \tag{A.238}$$

Hence the Reynold's stress R_{kl} consists of two parts, the first term which is time independent and the second which oscillates with twice the frequency.

For most purposes we are interested only in the secular variation of the quantities with the superscript (2), not the high-frequency behavior which represents a distortion of the main wave. Hence we are interested only in the first term of (A.238). Introducing this value in (A.237), the secular

behavior of a fluid is controlled by the equation

$$\frac{\partial \rho^{(2)}}{\partial t} + \frac{\partial}{\partial x_l}[M_l^{(2)}] = 0$$

$$\frac{\partial}{\partial t}[M_l^{(2)}] = \frac{\partial}{\partial x_l}[T_{kl}^{(2)} - R_{kl}] + \rho^{(2)} F_l \tag{A.239}$$

where R_{kl} is the constant term of (A.238). Thus the secular behavior of a liquid or gas through which waves are propagated is the same as the behavior of the unperturbed system subject to an additional constant stress R_{kl}.

A10.1 *Special Cases*

Let us consider the forms that R_{kl} may take for various kinds of wave motions. In the case of a general running plane wave, the form is given by

$$M_l^{(1)} = M_{l0}^{(1)} e^{-(A_l + jB_l)x_l} \cos \omega t \tag{A.240}$$

where $M_{l0}^{(1)}$ are the amplitudes of the mass currents in the various directions and A_l and B_l the attenuation and phase constants of the wave propagation. Inserting these values in (A.238), the secular part of the Reynold's stress is

$$R_{kl} = \frac{M_{k0}^{(1)} M_{l0}^{(1)}}{2\rho_0} e^{-(A_k x_k + A_l x_l)} \tag{A.241}$$

and the gradient of R_{kl} is

$$\frac{\partial}{\partial x_l}(R_{kl}) = -\frac{M_{k0}^{(1)} M_{l0}^{(1)} A_l}{2\rho_0} e^{-(A_k x_k + A_l x_l)} \tag{A.242}$$

Examining equation (A.242) we see several things about the gradient of the Reynold's stress

(1) It vanishes when the propagation constant $A + jB$ has no real part A
(2) It vanishes when the momentum M_{l0} is at right angles to the direction of propagation, as in a shear wave
(3) It is non-vanishing when the propagation vector has a real part parallel to the momentum vector as in the case of an attenuated longitudinal wave. The attenuation may be due either to loss or to the existence of a completely real part parallel to the momentum vector, such as in the case of total reflection.
(4) When several wave systems are superposed there are Reynold's stresses due to the cross products of the terms even when there is no attenuation.

(5) Any non-uniform field, such as that from a focusing radiator, gives rise to Reynold's stresses even when there is no attenuation of the wave.

A10.2 *Convection of Medium Caused by Sound Waves*

Second-order equations of the type of (A.239) have been used by Eckart[11] to explain crystal " winds " which are the secular flow of fluids or gases from a vibrating crystal surface. Eckart considers the case of a plane beam of sound waves of radius r_1 inside a tube of diameter r_0 and shows that when the attenuation in the medium is neglected, a flow of liquid runs along the sound beam while a reverse flow runs in a tube outside of the sound beam of such a value that the total flow across any cross-section is zero. The distribution of flow velocity across the tube is given by the equation

$$g = G[\tfrac{1}{2}(1 - x^2/y^2) - (1 - \tfrac{1}{2}y^2)(1 - x^2) - \log y] \qquad 0 \leq x \leq y$$
$$= -G[(1 - \tfrac{1}{2}y^2)(1 - x^2) + \log x] \qquad y \leq x \leq 1 \tag{A.243}$$

where $x = r/r_0$; $y = r_1/r_0$ and G is the fraction

$$G = \frac{k^2 p_0^2 r_1^2 \left(\dfrac{\chi + 2\eta}{\eta}\right)}{4\rho_0^2 v_0^3} \tag{A.244}$$

where $k = \omega/v_0 = 2\pi f/v_0$ where f is the frequency, v_0 the velocity of propagation in the medium, p_0 the maximum acoustic pressure in dynes per square centimeter, r_1 the radius of the sound beam, ρ_0 the density of the medium, η the shear viscosity, and χ the compressional viscosity of the medium. For a pressure of 10^5 dynes per square centimeter (0.1 atmosphere) and a frequency of 24 megacycles and using the constants for water $\rho_0 = 1.0$; $v_0 = 1.5 \times 10^5$ centimeters per second, the value of G is for a beam of 1.5 centimeter radius

$$G = 1.5\left(\frac{\chi + 2\eta}{\eta}\right) \text{cm/sec} \tag{A.245}$$

Since the velocity increases proportionally to the square of the frequency, the velocity of such streams becomes negligible below 1 megacycle for liquids. However, for air, on account of the low density and velocity, the effect is appreciable for frequencies as low as 1 kilocycle and becomes very large for high frequencies. Since the compressional viscosity χ

[11] Eckart, Carl, " Vortices and Streams Caused by Sound Waves," *Phys. Rev.*, Vol. 73, No. 1, pp. 68, 76, Jan. 1, 1948.

appears in the expression for G, Eckart suggests that the measurement of convection currents may be a method for evaluating the compressional viscosity.

This idea has recently been tested out by Liebermann,[12] who finds that the compressional viscosity measured by flow methods agrees well with that required to explain the high measured acoustic losses in light liquids.

[12] *Phys. Rev.*, Vol. 75, No. 9, pp. 1415, 1422, May 1, 1949.

INDEX